

UNCLASSIFIED

AD NUMBER

AD905201

LIMITATION CHANGES

TO:

Approved for public release; distribution is unlimited. Document partially illegible.

FROM:

Distribution authorized to U.S. Gov't. agencies only; Test and Evaluation; MAR 1972. Other requests shall be referred to Air Force Flight Dynamics Laboratory, Attn: FBC, Wright-Patterson AFB, OH 45433.

AUTHORITY

AFFDL ltr, 24 Oct 1973

THIS PAGE IS UNCLASSIFIED

AD905201

AFFDL-TR-72-97

THE DEVELOPMENT OF NONLINEAR ANALYSIS METHODS FOR BONDED JOINTS IN ADVANCED FILAMENTARY COMPOSITE STRUCTURES

G. C. Grimes

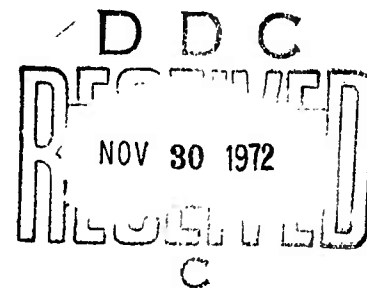
L. F. Greimann

T. Wah

G. E. Commerford

W. R. Blackstone

G. K. Wolfe



Southwest Research Institute

TECHNICAL REPORT AFFDL-TR-72-97

September 1972

Distribution limited to U.S. Government Agencies only; test and evaluation statement applied March 1972. Other requests for this document must be referred to the Air Force Flight Dynamics Laboratory (FBC), Wright-Patterson Air Force Base, Ohio 45433.

Air Force Flight Dynamics Laboratory

Air Force Systems Command

Wright-Patterson Air Force Base, Ohio

**Best
Available
Copy**

NOTICES

When Government drawings, specifications, or other data are used for any purpose other than in connection with a definitely related Government procurement operation, the United States Government thereby incurs no responsibility nor any obligation whatsoever, and the fact that the Government may have formulated, furnished, or in any way supplied the said drawings, specifications, or other data, is not to be regarded by implication or otherwise as in any manner licensing the holder or any other person or corporation, or conveying any rights or permission to manufacture, use, or sell any patented invention that may in any way be related thereto.

Copies of this report should not be returned to the Research and Technology Division unless return is required by security considerations, contractual obligations, or notice on a specific document.

AFFDL-TR-72-97

THE DEVELOPMENT OF NONLINEAR ANALYSIS METHODS FOR BONDED JOINTS IN ADVANCED FILAMENTARY COMPOSITE STRUCTURES

G. C. Grimes
L. F. Greimann
T. Wah
G. E. Commerford
W. R. Blackstone
G. K. Wolfe

Distribution limited to U.S. Government Agencies only; test and evaluation statement applied March 1972. Other requests for this document must be referred to the Air Force Flight Dynamics Laboratory (FBC), Wright-Patterson Air Force Base, Ohio 45433.

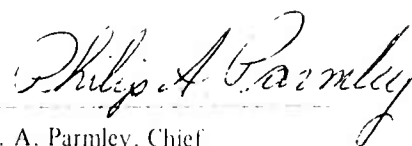
FOREWORD

The research reported herein was performed by Southwest Research Institute, 8500 Culebra Road, Box 28510, San Antonio, Texas 78284 in the Department of Structural Research under Air Force Contract No. F33615-69-C-1641. The contract was initiated under Project No. 436403 by the Air Force Flight Dynamics Laboratory, Air Force Systems Command, Wright-Patterson Air Force Base, Ohio 45433. Dr. Edvins Demuts, Air Force Project Engineer administered the program.

This report covers the research work conducted at SwRI between 14 April 1969 and 30 October 1971 under the management of Mr. Glenn C. Grimes, Project Leader in the Department of Structural Research headed by Dr. Robert C. DeHart, Director and Mr. L. U. Rastrelli, Assistant Director. Principal Investigators in this effort were Dr. L. F. Greimann, Dr. T. Wah,* Mr. G. E. Commerford, Mr. W. R. Blackstone, and Mr. G. K. Wolfe.

The authors gratefully acknowledge the fine laboratory work of Senior Technician Mr. William Keith and Technician Mr. Albert Reichert under the direction of Mr. B. C. Irbey, Laboratory Manager.

This technical report has been reviewed and is approved.



P. A. Parmley, Chief
Advanced Composites Branch
Structures Division
AFFDL

*Associate Professor, School of Engineering, Texas A & I University, Kingsville, Texas.

ABSTRACT

Development of analysis methods for orthotropic adherend bonded lap joints which account for material nonlinearities at room temperature was the primary objective of the research reported herein. The use of these methods in predicting mechanical behavior, ultimate loads, and failure modes was the goal. In order to accomplish this, new analytical procedures were developed and successfully checked with discrete element techniques for single, double, and step lap adhesively bonded attachment configurations. Experimental verification of these nonlinear analyses was accomplished by the fabrication and evaluation of a variety of simple joint specimens under static monotonically increasing load. Failure loads and modes were used as the primary substantiation characteristics but the mechanical behavior of a small number of these simple joint specimens was observed at intermediate loadings and found to compare favorably with the analytically predicted behavior. Larger, more complex bonded joints were designed, fabricated, and evaluated under static monotonically increasing loads at room temperature utilizing these methods. Ultimate load, failure mode, and detailed strain behavior at any intermediate load were accurately predicted with the new analyses, as substantiated by experimental observations. These techniques were put into a computerized design/analysis program for structural application use and the program was used to generate bonded joint design allowable curves.

CONTENTS

Section	Page
I. INTRODUCTION	1
II. THEORETICAL METHODS DEVELOPMENT	2
II.1. GENERAL	2
II.2. SINGLE LAP JOINT	2
II.3. DOUBLE LAP JOINT	5
II.4. STEP LAP JOINT	7
II.5. SOLUTION TO DIFFERENTIAL EQUATIONS	21
III. DISCRETE ELEMENT ANALYSIS (DEVELOPMENT)	35
III.1. GENERAL	35
III.2. CONSTITUTIVE EQUATIONS	35
III.3. ELEMENT STIFFNESS MATRIX AND PLASTIC FORCES	39
IV. COMPARISON OF THEORETICAL AND DISCRETE ELEMENT RESULTS	41
IV.1. JOINT CONFIGURATIONS AND MATERIAL PROPERTIES	41
IV.2. JOINT ANALYSIS	42
V. EXPERIMENTAL DESIGN	46
V.1. GENERAL	46
V.2. LITERATURE SURVEY	46
V.3. TRIAL EFFECTIVE PROPERTIES PREDICTION	49
V.4. DESIGN OF THE EXPERIMENTAL PROGRAM	59
VI. LAMINATE PROCESSING	68
VI.1. GENERAL	68
VI.2. PROCESSING FACILITIES	68
VI.3. PROCESS DEVELOPMENT	68
VI.4. ADHEREND PANEL FABRICATION AND QUALITY CONTROL	76
VII. LAMINATE AND TITANIUM ADHEREND TEST RESULTS	87
VII.1. GENERAL	87
VII.2. LAMINATE ADHEREND EXPERIMENTAL RESULTS	87
VII.3. TITANIUM ADHEREND EXPERIMENTAL RESULTS	92
VIII. BONDED JOINT PROCESSING	95
VIII.1. GENERAL	95
VIII.2. ADHESIVE ACCEPTANCE TEST RESULTS	95
VIII.3. SIMPLE SPECIMEN JOINT FABRICATION	95

CONTENTS (Cont'd)

Section	Page
IX. BONDED JOINT TEST RESULTS	108
IX.1. GENERAL	108
IX.2. SIMPLE SPECIMEN DATA SUMMARY	108
IX.3. SPECIAL JOINT INVESTIGATION DATA SUMMARY	127
X. THEORETICAL/EXPERIMENTAL BEHAVIOR COMPARISONS AND "EFFECTIVE" PROPERTIES	146
X.1. GENERAL	146
X.2. ADDITION OF EFFECTIVE BENDING	146
X.3. ANALYTICAL/EXPERIMENTAL BEHAVIOR COMPARISON ON SIMPLE AND SPECIAL JOINTS	148
X.4. DESIGN ANALYSIS OF COMPLEX JOINTS	157
X.5. COMPLEX JOINT TEST DATA CORRELATION WITH PREDICTIVE METHODS	165
XI. BONDED JOINT DESIGN CURVES	173
XI.1. GENERAL	173
XI.2. DISCUSSION OF APPROACH	173
XI.3. DESIGN CURVES	173
XII. RESULTS, CONCLUSIONS AND RECOMMENDATIONS	177
XII.1. GENERAL	177
XII.2. RESULTS AND CONCLUSIONS	177
XII.3. RECOMMENDATIONS	178
LIST OF REFERENCES	180
APPENDICES	182

ILLUSTRATIONS

<u>Figure</u>		<u>Page</u>
1	DIMENSIONS AND COORDINATE SYSTEM	2
2	FORCES AND DISPLACEMENTS FOR AN ELEMENT OF INFINITESIMAL LENGTH OF A SINGLE LAP BONDED JOINT	3
3	MATERIAL COORDINATES x, y AND STRESS-STRAIN CURVES FROM UNIAXIAL STRESS TESTS IN PRINCIPAL DIRECTIONS	9
4	FREE BODY OF AN ELEMENT OF INFINITESIMAL LENGTH OF A BONDED DOUBLE LAP JOINT	15
5	FORCES AND DISPLACEMENTS OF r th RISER	19
6	ORTHOTROPIC LAMINA COORDINATES x, y AND STRESS-STRAIN CURVES FROM UNIAXIAL TEST IN PRINCIPAL DIRECTIONS	37
7	PLANE STRAIN DISCRETE ELEMENT USED FOR NONLINEAR JOINT ANALYSIS	39
8	JOINT CONFIGURATIONS FOR COMPARISON OF ANALYSIS METHODS	41
9	DISCRETE ELEMENT LAYOUT FOR SINGLE LAP JOINT	43
10	DISCRETE ELEMENT LAYOUT FOR DOUBLE LAP JOINT	43
11	DISCRETE ELEMENT LAYOUT FOR STEP LAP JOINT	43
12	ADHESIVE STRESS, SINGLE LAP JOINT	44
13	ADHESIVE STRESS, DOUBLE LAP JOINT	44
14	ADHESIVE STRESS, STEP LAP JOINT	44
15	STANDARD DEVIATION VS MEAN ADHESIVE FAILURE STRESS COMPARISON	48
16	STANDARD DEVIATION VS MEAN ADHESIVE FAILURE STRESS COMPARISON	48
17	BE/BE DOUGLAS SINGLE LAP/SHELL 951	50
18	BE/AL DOUGLAS SINGLE LAP/SHELL 951	50
19	BE/AL DOUGLAS DOUBLE LAP/SHELL 951	50
20	NGE/NGE DOUGLAS SINGLE LAP/SHELL 951	50
21	NGE/AL DOUGLAS SINGLE LAP/SHELL 951	51
22	NGE/AL DOUGLAS SINGLE LAP/SHELL 951	51
23	NGE/NGE SwRI DOUBLE LAP/3M AF 126	51

ILLUSTRATIONS (Cont'd)

Figure		Page
24	NGE/AL AND NGE/WGE SwRI DOUBLE LAP/3M AF 126	51
25	NGE/AL, NGE/WGE, AND NGE/TI SwRI DOUBLE LAP/3M AF 126	52
26	NGE/AL DOUGLAS DOUBLE LAP/SHELL 951	52
27	NGE/NGE ITRI DOUBLE LAP/FM-1000	52
28	NGE/NGE ITRI DOUBLE LAP/METLBOND 400	52
29	COMPARISON OF GROUP STANDARD DEVIATION ESTIMATES	53
30	COMPARISON OF STANDARD DEVIATIONS SwRI DOUBLE LAP DATA	53
31	COMPARISON OF STANDARD DEVIATIONS DOUGLAS SINGLE LAP DATA	54
32	COMPARISON OF STANDARD DEVIATIONS DOUGLAS DOUBLE LAP DATA	54
33	COMPARISON OF STANDARD DEVIATIONS GRUMMAN SINGLE LAP DATA	55
34	COEFFICIENT OF VARIATION AND STANDARD DEVIATION VS MEAN FAILURE STRESS, SwRI DOUBLE LAP DATA	55
35	CONFIDENCE LIMIT STRESS VS GROUP SURFACE TREATMENT MARTIN (AL/E)	56
36	CONFIDENCE LIMITS ITRI DOUBLE LAP DATA	56
37	CONFIDENCE LIMITS SwRI DOUBLE LAP DATA	57
38	CONFIDENCE LIMITS DOUGLAS SINGLE LAP DATA	57
39	CONFIDENCE LIMITS DOUGLAS DOUBLE LAP DATA	58
40	CONFIDENCE LIMITS GRUMMAN SINGLE LAP DATA	58
41	ORTHO-/ISO-ELASTIC SHEAR STRESS DISTRIBUTION FOR $G = 160,000$ PSI	60
2	ORTHO-/ISO-ELASTIC SHEAR STRESS DISTRIBUTION FOR $G = 90,000$ PSI	60
43	ORTHO-/ISO-ELASTIC SHEAR STRESSES DISTRIBUTION FOR $G = 40,000$ PSI	61
44	VARIATION OF SHEAR STRESS WITH ASSUMED SHEAR MODULUS	61
45	AF-126 (LS-HE) ESTIMATED ADHESIVE FAILING STRESSES (τ_u)	63
46	MB-329 (HS-LE) ESTIMATED ADHESIVE FAILING STRESSES (τ_u)	63
47	$[0]_c$ ADHEREND TENSILE STRESS VS OVERLAP LENGTH, LS-HE (EMPIRICAL)	64
48	$[0/90]_c$ ADHEREND TENSILE STRESS VS OVERLAP LENGTH, LS-HE (EMPIRICAL)	64

ILLUSTRATIONS (Cont'd)

Figure		Page
49	$[0/\pm 45]_c$ ADHEREND TENSILE STRESS VS OVERLAP LENGTH, LS-HE (EMPIRICAL) . . .	65
50	$[0]_c$ ADHEREND TENSILE STRESS VS OVERLAP LENGTH, HS-LE (EMPIRICAL) . . .	65
51	$[0/90]_c$ ADHEREND TENSILE STRESS VS OVERLAP LENGTH, HS-LE (EMPIRICAL) . . .	66
52	$[0/\pm 45]_c$ ADHEREND TENSILE STRESS VS OVERLAP LENGTH, HS-LE (EMPIRICAL) . . .	66
53	COMPOSITE LABORATORY AND EQUIPMENT	69
54	1581 GLASS FABRIC/5505 EPOXY HEAT SURVEY PANEL POSITIONS OF THERMO- COUPLE	71
55	HEAT SURVEY PANEL BACK-LIGHTED PHOTOGRAPH	71
56	PANEL NO. G-6 WITH TEFLON-COATED GLASS FABRIC AND GLASS CLOTH ELECTRICAL TAPE INCLUSIONS FOR ULTRASONIC TEST CALIBRATION	73
57	PANEL NO. G-6 BACK-LIGHTED PHOTOGRAPH	73
58	PANEL NO. G-6 ULTRASONIC TEST CHART INDICATING INCLUSIONS IN PANEL . . .	75
59	CHART OF ULTRASONIC TEST OF PANEL B-8	75
60	CHART OF ULTRASONIC TEST OF PANEL B-2	75
61	CHART OF ULTRASONIC TEST OF PANEL B-7	75
62	AVERAGE FLEXURE TEST RESULTS PANEL G-11 NO FLAWS INDICATED BY ULTRASONIC INSPECTION	77
63	AVERAGE FLEXURE TEST RESULTS PANEL G-11 FLAWS INDICATED BY ULTRA- SONIC INSPECTION	77
64	CUTTING PATTERN FOR PANEL G-11	78
65	ULTRASONIC THRU-SCAN RECORD PANEL G-11	78
66	X-RAY OF PANEL B-4	79
67	X-RAY OF PANEL B-8	79
68	X-RAY OF PANEL B-7	79
69	MATERIAL ACCEPTANCE TEST SPECIMENS	80
70	PANEL DRAWING BONDED JOINT STUDY	81
71	ULTRASONIC INSPECTION RECORD FOR PANEL B-20	82

ILLUSTRATIONS (Cont'd)

<u>Figure</u>		<u>Page</u>
72	POSITIVE PRINT OF X-RAY OF PANEL B-20 USED FOR ACCEPTANCE TESTING . . .	83
73	BORON REINFORCED ULTRASONIC TEST PANELS	84
74	ULTRASONIC INSPECTION OF VOID PANEL B-29	85
75	ULTRASONIC INSPECTION OF VOID PANEL B-30	85
76	QUALITY CONTROL AND TENSILE STRENGTH TEST SPECIMENS	86
77	TYPICAL FAILED COMPOSITE TENSILE SPECIMENS, MATERIAL BATCH 373	89
78	TYPICAL FAILED COMPOSITE TENSILE SPECIMENS, MATERIAL BATCH 381	89
79	TYPICAL FAILED Ti 6Al-4V ANNEALED TENSILE SPECIMENS	94
80	LAP SHEAR ASSEMBLY SINGLE LAP JOINT	98
81	LAP SHEAR ASSEMBLY DOUBLE LAP JOINT	99
82	LAP SHEAR ASSEMBLY STEP LAP JOINT	102
83	LAP SHEAR ASSEMBLY MACHINED STEP LAP JOINT	103
84	MULTIPLE-LAMINATE SINGLE STEP LAP JOINT	104
85	MULTIPLE-LAMINATE TWO-STEP LAP JOINT	105
86	MULTIPLE-LAMINATE TRIPLE STEP LAP JOINT	106
87	LAP SHEAR ASSEMBLY SCARF JOINT	107
88	LSA-28 FAILED SPECIMENS	114
89	LSA-29 FAILED SPECIMENS	114
90	LSA-30 FAILED SPECIMENS	114
91	LSA-40 FAILED SPECIMENS	115
92	LSA-66 FAILED SPECIMENS	115
93	LSA-57 FAILED SPECIMENS	115
94	LSA-6 FAILED SPECIMENS	116
95	LSA-19 FAILED SPECIMENS	116
96	LSA-8 FAILED SPECIMENS	116

ILLUSTRATIONS (Cont'd)

<u>Figure</u>		<u>Page</u>
97	LSA-22 FAILED SPECIMENS	117
98	LSA-10 FAILED SPECIMENS	117
99	LSA-71 FAILED SPECIMENS	118
100	LSA-46 FAILED SPECIMENS	118
101	LSA-72 FAILED SPECIMENS	118
102	LSA-47 FAILED SPECIMENS	119
103	LSA-74 FAILED SPECIMENS	119
104	SINGLE LAP COMPOSITE/COMPOSITE JOINTS LOAD TRANSFER CAPABILITY	120
105	DOUBLE LAP COMPOSITE/COMPOSITE JOINTS LOAD TRANSFER CAPABILITY	121
106	SINGLE LAP COMPOSITE/TITANIUM JOINTS LOAD TRANSFER CAPABILITY	122
107	DOUBLE LAP COMPOSITE/TITANIUM JOINTS LOAD TRANSFER CAPABILITY	123
108	STEP LAP COMPOSITE/TITANIUM JOINTS LOAD TRANSFER CAPABILITY	125
109	LOAD/STRAIN CURVE FOR DOUBLE LAP AF-126-2 BONDED JOINT	126
110	LOAD/STRAIN CURVE FOR MB-329 BONDED JOINT	126
111	SINGLE LAP COMPOSITE/TITANIUM JOINT WITH NITRILE EPOXY ADHESIVE (LS-HE)	129
112	SINGLE LAP C/T-LSHE JOINT, COMPOSITE ADHEREND STRAIN DISTRIBUTION	130
113	DOUBLE LAP COMPOSITE/TITANIUM JOINT WITH NITRILE EPOXY ADHESIVE (LS-HE)	131
114	LSA-23 FAILURE PHOTOGRAPHS	132
115	DOUBLE LAP C/T-LSHE JOINT, COMPOSITE AND TITANIUM ADHEREND STRAIN DISTRIBUTION	133
116	SINGLE LAP COMPOSITE/TITANIUM JOINT WITH EPOXY NOVOLAK ADHESIVE (HS-LE)	134
117	LSA-59 FAILURE PHOTOGRAPHS	135
118	SINGLE LAP C/T-HSLE JOINT, COMPOSITE ADHEREND STRAIN DISTRIBUTION	136
119	DOUBLE LAP COMPOSITE/TITANIUM JOINT WITH EPOXY NOVOLAK ADHESIVE (HS-LE)	137
120	LSA-62 FAILURE PHOTOGRAPHS	138

ILLUSTRATIONS (Cont'd)

<u>Figure</u>		<u>Page</u>
121	DOUBLE LAP C/T-HSLE JOINT, COMPOSITE AND TITANIUM ADHEREND STRAIN DISTRIBUTION	139
122	ONE-STEP LAP COMPOSITE/TITANIUM JOINT WITH EPOXY NOVOLAK ADHESIVE (HS-LE)	140
123	ONE-STEP LAP C/T-HSLE JOINT, COMPOSITE ADHEREND STRAIN DISTRIBUTION	141
124	TWO-STEP LAP COMPOSITE/TITANIUM JOINT WITH NITRILE EPOXY ADHESIVE (LS-HE)	143
125	TWO-STEP LAP C/T-LSHE JOINT, COMPOSITE ADHEREND STRAIN DISTRIBUTION	144
126	SHEAR STRESS-STRAIN CURVE OF AF126-2 ADHESIVE, SPECIMEN 3A11-126-1	145
127	TYPICAL SHEAR STRESS-STRAIN CURVE OF METLBOND 329 ADHESIVE	145
128	JOINT LOAD/DEFLECTION CURVES FOR LSA-56 (D.L-HSLE)	152
129	CORRELATION CURVE ON BONDED JOINTS FOR BF/JT	153
130	CORRELATION CURVE ON BONDED JOINTS FOR BF/JT-AT-FT	154
131	LSA-31 FAILURE	155
132	LSA-33 FAILURE	155
133	LSA-36 FAILURE	155
134	LSA-56 FAILURE	156
135	LSA-58 FAILURE	156
136	LSA-61 FAILURE	157
137	THEORETICAL/EXPERIMENTAL CORRELATION OF SINGLE LAP JOINT SURFACE STRAINS	158
138	THEORETICAL/EXPERIMENTAL CORRELATION OF DOUBLE LAP JOINT SURFACE STRAINS	159
139	COMPLEX JOINT PANELS	160
140	BONDLINE SHEAR STRESS VS L/l FOR COMPOSITE/TITANIUM DOUBLE LAP JOINTS	162
141	LOAD INTRODUCTION FIXTURE FOR COMPLEX JOINT	163
142	COMPLEX JOINT STRAIN GAGE LOCATIONS	165
143	COMPLEX JOINT -501 TEST SET-UP	166

ILLUSTRATIONS (Cont'd)

<u>Figure</u>		<u>Page</u>
144	COMPLEX JOINT -509 TEST SET-UP	166
145	C/T COMPLEX JOINT-PREDICTED VS EXPERIMENTAL ADHEREND SURFACE STRAINS. LS-HE ADHESIVE	170
146	C/T COMPLEX JOINT-PREDICTED VS EXPERIMENTAL ADHEREND SURFACE STRAINS. HS-LE ADHESIVE	170
147	COMPLEX JOINT -501 AFTER FAILURE	171
148	FAILURE MODE OF -501 COMPLEX JOINT	171
149	COMPLEX JOINT -509 AFTER FAILURE	172
150	FAILURE MODE OF -509 COMPLEX JOINT	172
151	DESIGN CURVES FOR SINGLE, DOUBLE, AND STEP-LAP JOINTS	175

TABLES

<u>Table</u>		<u>Page</u>
I	MATERIAL CONSTANTS FOR RAMBERG-OSGOOD APPROXIMATION	41
II	SIMPLE AND "SPECIAL" SPECIMEN TEST PLAN	67
III	PRELIMINARY EVALUATION PANELS	72
IV	TENSILE STRENGTH TESTS OF PANEL G-2	74
V	PANEL DATA SUMMARY PACKAGE, PANEL NO. G-11	76
VI	MATERIAL ACCEPTANCE TESTS	80
VII	PANEL FABRICATION FOR SIMPLE BONDED JOINT EVALUATION	82
VIII	MATERIAL ACCEPTANCE TEST	83
IX	LAMINATE MECHANICAL/PHYSICAL PROPERTIES DATA SUMMARY	88
X	UNIDIRECTIONAL LAMINATE PERFORMANCE	90
XI	6AL-4V TITANIUM SHEET PROPERTIES SUMMARY	93
XII	ACCEPTANCE TEST RESULTS ON AF-126 ADHESIVE (LS-HE)	96
XIII	ACCEPTANCE TEST RESULTS ON MB-329 ADHESIVE (HS-LE)	96
XIV	SINGLE AND DOUBLE LAP SHEAR ASSEMBLIES BORON/BORON	100
XV	SINGLE AND DOUBLE LAP SHEAR ASSEMBLIES BORON/TITANIUM	101
XVI	COMPOSITE/COMPOSITE SINGLE LAP JOINT DATA SUMMARY (LS-HE)	109
XVII	COMPOSITE/COMPOSITE DOUBLE LAP JOINT DATA SUMMARY (LS-HE)	109
XVIII	COMPOSITE/COMPOSITE SINGLE LAP JOINT DATA SUMMARY (HS-LE)	110
XIX	COMPOSITE/COMPOSITE DOUBLE LAP JOINT DATA SUMMARY (HS-LE)	110
XX	COMPOSITE/TITANIUM SINGLE LAP JOINT DATA SUMMARY (LS-HE)	111
XXI	COMPOSITE/TITANIUM DOUBLE LAP JOINT DATA SUMMARY (LS-HE)	111
XXII	COMPOSITE/TITANIUM SINGLE LAP JOINT DATA SUMMARY (HS-LE)	112
XXIII	COMPOSITE/TITANIUM DOUBLE LAP JOINT DATA SUMMARY (HS-LE)	112
XXIV	STEP LAP JOINT DATA SUMMARY	113
XXV	AVERAGE ADHESIVE MECHANICAL PROPERTIES	149

TABLES (Cont'd)

<u>Table</u>		<u>Page</u>
XXVI	THREE PARAMETER STRESS-STRAIN CURVE VALUES	150
XXVII	SUMMARY OF EXPERIMENTAL/THEORETICAL CORRELATION	151
XXVIII	VARIABLE BENDING FACTOR SELECTIONS: BF/JT	153
XXIX	BEST BENDING FACTOR SELECTIONS: BF/JT-AT-FT	154
XXX	COMPLEX JOINT ANALYSIS	161
XXXI	COMPLEX JOINT EXPERIMENTAL DATA WITH LSHE ADHESIVE	167
XXXII	COMPLEX JOINT EXPERIMENTAL DATA WITH HSLE ADHESIVE	168
XXXIII	LARGE JOINT ANALYSIS/TEST COMPARISON	169
XXXIV	BONDED JOINT ANALYTICAL/EXPERIMENTAL DESIGN DATA SUMMARY FOR 0/±45 COMPOSITE ADHERENDS	174

SECTION I

INTRODUCTION

This research program had three objectives as defined in Exhibit "A" of the Statement of Work of Contract F33615-69-C-1641. The first one was to develop new static structural analysis methods for bonded joints which account for the adhesive and composite (or metal) adherend nonlinear behavior under stress. Prediction of static failure in all principal modes was to be the goal of the analytical techniques developed under this first objective. Objective number two was to develop a method of determining "effective" adhesive properties for use in the analytical methods since true properties data are seldom available and not generally obtained from simple tests. In the third objective, useful static design curves were to be developed based on the new analysis techniques. The accomplishment of these objectives was the primary goal of the research, reported herein.

The "how, what, and why" results obtained in accomplishing these objectives make up the contents of this report. Work and results in completing the requirements of the first objective are given in Section II—Theoretical Methods Development, III—Discrete Element Analysis (Development), and IV—Comparison of Theoretical and Discrete Element Results. In Section V—Experimental Design, literature data were surveyed, analyzed, and used in test program development on adherend materials and bonded joints. Manufacturing and quality control of the composite materials is covered in Section VI—Laminate Processing, whereas Section VII—Laminate and Titanium Adherend Test Results, reports the experimental characterization values obtained. Lap shear assembly manufacture and postbond fabrication are covered in Section VIII—Bonded Joint Processing, while the experimental data obtained in the program are reported in Section IX—Bonded Joint Test Results. With the completion of the work reported in the previous Sections it was possible to satisfy the second objective as covered in Section X—Theoretical/Experimental Behavior Comparisons and "Effective" Properties. Satisfaction of the first two objectives made possible the accomplishment of the third objective reported in Section XI—Bonded Joint Design Curves. Section XII—Results, Conclusions, and Recommendations, covers the meaning and impact of the research effort with suggestions for related, pertinent future study of bonded joint structures.

After the List of References, the Appendices, except Appendix A, present the detailed information utilized in the program and are included for the reader's perusal if more data are needed.

In summary, the three objectives outlined above have been satisfied and the method developed can be used in R. T. static nonlinear design/analysis of adhesive bonded single, double, and step lap joints. With the publication of this report, computer programs based on this analytical method are available through the Air Force Flight Dynamics Laboratory, Wright-Patterson AFB, Ohio.

SECTION II

THEORETICAL METHODS DEVELOPMENT

II.1. GENERAL

This section contains the mathematical development of nonlinear analysis methods* for bonded single, double, and step lap joints subjected to static loads at R.T. These three joints are shown in Figure 1, along with the coordinate systems, dimensions, and applied loads which will be utilized in the following developments. The joints are assumed to be sufficiently wide in the z direction (perpendicular to the plane of the paper) such that the material under load is in a state of plane strain; i.e., the normal strain ϵ_z and the shear strains γ_{xz} and γ_{yz} are assumed to be zero. In general, the adherends may be either orthotropic (laminates) or isotropic, and may have different thicknesses which are constant for each adherend. The adhesive is assumed to be isotropic and of a constant thickness which is much smaller than the adherend thickness. The adherends are assumed to be flat plates in bending; i.e., normal stresses through the thicknesses (σ_y) are neglected. Interlaminar shear is neglected. Laminates are assumed to be

symmetrical about their middle surface. Further assumptions involving material behavior and assumptions peculiar to each joint will be discussed as they occur.

II.2. SINGLE LAP JOINT

II.2.a. Equilibrium Equations

The differential equations of equilibrium governing the behavior of a segment of a bonded single lap joint can be developed from the free bodies in Figure 2. (The joint is assumed to have a unit width in the z direction.) Summing forces in the x and y directions and moments in the x - y plane for adherends 1 and 2 gives

$$\frac{dV_1}{dx} - \tau = 0 \quad \frac{dV_2}{dx} + \tau = 0 \quad (1a)$$

$$\frac{dV_1}{dx} - \sigma = 0 \quad \frac{dV_2}{dx} - \sigma = 0 \quad (1b)$$

$$\frac{dM_1}{dx} - V_1 + \tau \frac{t_1}{2} = 0 \quad \frac{dM_2}{dx} - V_2 - \tau \frac{t_2}{2} = 0 \quad (1c)$$

where σ and τ are the normal stress and shear stress in the adhesive, respectively, which are assumed constant through the thickness of the adhesive, and N_i , V_i , and M_i are the stress resultants for adherend i . Subtracting Equations (1a) gives:

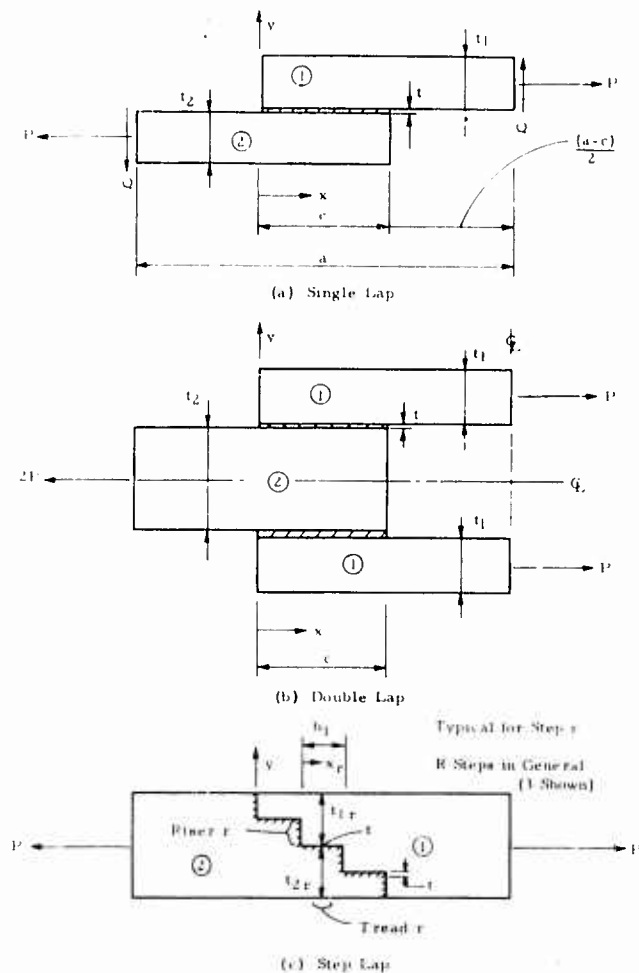
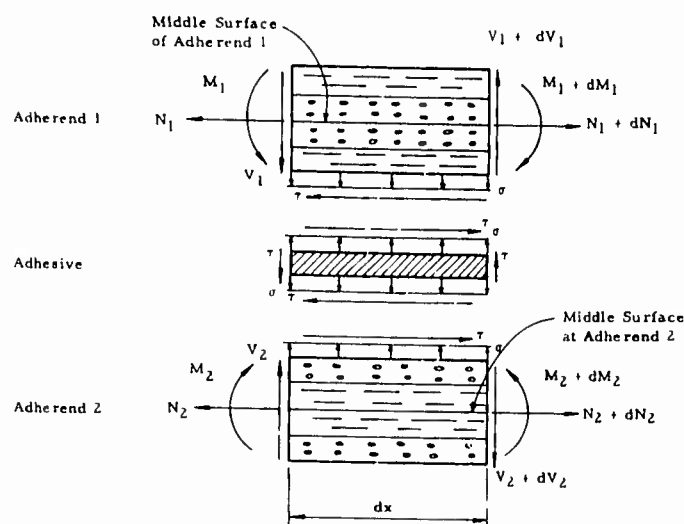
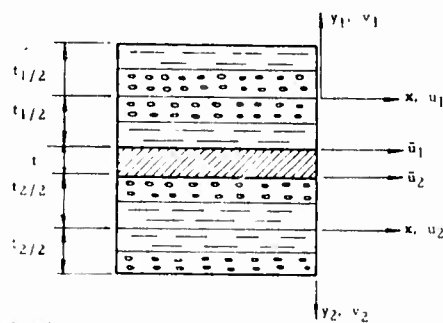


FIGURE 1. DIMENSIONS AND COORDINATE SYSTEM

*The differential equations governing the behavior of a scarf joint are presented in Appendix A. No solution was obtained, however.



a) Force Free Body



b) Displacements

FIGURE 2. FORCES AND DISPLACEMENTS FOR AN ELEMENT OF INFINITESIMAL LENGTH OF A SINGLE LAP BONDED JOINT

$$\tau = \frac{1}{2} \phi' \quad (2)$$

where

$$\phi = N_1 - N_2 \quad (3)$$

and the prime denotes differentiation with respect to x . Adding Equations (1b) and solving for σ yields

$$\sigma = \frac{1}{2} \frac{d}{dx} (V_1 + V_2) \quad (4)$$

or, by substitution of (1c), and (1a),

$$\sigma = \frac{1}{2} \theta'' \quad (5)$$

where

$$\theta = M_1 + M_2 + \frac{t_1 - t_2}{4} (N_1 - N_2) \quad (6)$$

Equilibrium of the overall joint, as deduced from Figure 1a, requires that

$$N_1 + N_2 - P = 0 \quad (7)$$

and, by summing moments about the centerline of the adhesive,

$$M_1 - M_2 + \frac{N_1 t_1}{2} - \frac{N_2 t_2}{2} + P \left(\frac{\bar{t}c}{2a} - \frac{\bar{t}x}{a} - \frac{t_1}{4} + \frac{t_2}{4} \right) = 0 \quad (8)$$

By Equation (7), this can be written as

$$M_1 - M_2 - Q \left(x - \frac{c}{2} \right) + \frac{\bar{t}}{2} (N_1 - N_2) = 0 \quad (9)$$

where Q is taken as

$$Q = \frac{P\bar{t}}{a} \quad (10)$$

and

$$\bar{t} = \frac{t_1 + t_2}{2} \quad (11)$$

and P is the joint load per unit width of joint. The quantity \bar{t} has been neglected with respect to t_i (the adherend thicknesses). Note that the "a" dimension is the distance between points of zero moment.

The variables ϕ and θ will be taken as the primary unknown functions. By solving Equations (3), (6), (7), (9), and (1c) simultaneously, the stress resultants are found in terms of ϕ and θ as:

$$\begin{aligned} N_1 &= \frac{1}{2}(P + \phi) \\ N_2 &= \frac{1}{2}(P - \phi) \\ M_1 &= \frac{1}{2} \left[\theta + \frac{P\bar{t}}{a} \left(x - \frac{c}{2} \right) - \frac{t_1}{2} \phi \right] \\ M_2 &= \frac{1}{2} \left[\theta - \frac{P\bar{t}}{a} \left(x - \frac{c}{2} \right) + \frac{t_2}{2} \phi \right] \\ V_1 &= \frac{1}{2} \left(\theta' + \frac{P\bar{t}}{a} \right) \\ V_2 &= \frac{1}{2} \left(\theta' - \frac{P\bar{t}}{a} \right) \end{aligned} \quad (12)$$

The adhesive stresses τ and σ are also determined from ϕ and θ by Equations (2) and (5).

H.2.b. Compatibility Equations

Another set of equations, namely the compatibility equations, must be brought into play. The shear strain γ and normal strain ϵ which are assumed constant through the adhesive are given by

$$\begin{aligned} \gamma &= \frac{\bar{u}_1 - \bar{u}_2}{t} \\ \epsilon &= \frac{v_1 + v_2}{t} \end{aligned} \quad (13)$$

where \bar{u}_1 and \bar{u}_2 are the x displacements of the upper adherend lower face and the lower adherend upper face, respectively (Fig. 2b).

$$\begin{aligned} \bar{u}_1 &= u_1 + \frac{t_1}{2} v_1' \\ \bar{u}_2 &= u_2 + \frac{t_2}{2} v_2' \end{aligned} \quad (14)$$

The quantities u_i and v_i are the axial and lateral displacements of the midplane of adherend i , respectively, as shown in Figure 2b. The middle surface normal strain e_i and curvature X_i in the adherends are given by

$$\begin{aligned} e_i &= u_i' \\ X_i &= -v_i'' \end{aligned} \quad (15)$$

where i refers to adherend number.

11.2.c. Constitutive Equations

Constitutive equations must now be introduced to relate material deformations to stresses. The bonded joints are composed of both isotropic and orthotropic materials: isotropic and/or orthotropic adherends and an isotropic adhesive.

11.2.c.(1) Isotropic Adherend

The adherends are assumed to be in a state of plane stress in the x - z plane (Fig. 1), i.e., $\sigma_y = \tau_{xy} = \tau_{yz} = 0$. (The additional assumption of plane strain in the x - y plane, i.e., $\epsilon_z = \gamma_{xz} = \gamma_{yz} = 0$ will be introduced later.) Two basic theories of plasticity are available for the description of the nonlinear behavior of isotropic materials: deformation (total strain) theory and flow (incremental strain) theory. Deformation theory is independent of the loading path whereas flow theory depends upon the loading path. Deformation theory will be assumed here. For an isotropic material in plane stress, the deformation theory of plasticity states that the relationship between stresses and strains in the inelastic regime is^{(1)*}

$$\begin{Bmatrix} \epsilon_x \\ \epsilon_z \\ \gamma_{xz} \end{Bmatrix} = \left(\frac{1}{E} \begin{bmatrix} 1 & -\nu & 0 \\ -\nu & 1 & 0 \\ 0 & 0 & 2(1+\nu) \end{bmatrix} + \frac{\bar{\epsilon}_p}{\bar{\sigma}} \begin{bmatrix} 1 & -1/2 & 0 \\ -1/2 & 1 & 0 \\ 0 & 0 & 3 \end{bmatrix} \right) \begin{Bmatrix} \sigma_x \\ \sigma_z \\ \tau_{xz} \end{Bmatrix} \quad (16)$$

where $\epsilon_x, \epsilon_z, \gamma_{xz}$ are the plane stress strains; $\sigma_x, \sigma_z, \tau_{xz}$ are the plane stresses in the x - z plane of Figure 1; E, ν , are elastic constants; $\bar{\sigma}$, the equivalent stress, is⁽¹⁾

$$\bar{\sigma} = (\sigma_x^2 + \sigma_z^2 - \sigma_x \sigma_z + 3\tau_{xz}^2)^{1/2} \quad (17)$$

and $\bar{\epsilon}_p$ is the corresponding equivalent plastic strain. Deformation theory assumes that $\bar{\epsilon}_p$ for the plane stress case can be obtained from the uniaxial stress-strain curve at a stress level $\bar{\sigma}$. (The $\bar{\sigma}$ vs $\bar{\epsilon}_p$ curve is identical to the σ_x vs ϵ_{xp} curve for uniaxial stress.) Since the plastic strain is the difference between the total strain and the elastic component, one has

$$\bar{\epsilon}_p = \bar{\epsilon} - \frac{\bar{\sigma}}{E} \quad (18)$$

where $\bar{\epsilon}$ is equivalent total strain at a stress level $\bar{\sigma}$. If the Ramberg-Osgood⁽²⁾ approximation to the stress-strain curve is used, the relationship between $\bar{\sigma}$ and $\bar{\epsilon}$ can be expressed by:

$$\bar{\epsilon} = \frac{\bar{\sigma}}{E} + \frac{3}{7} \frac{\sigma_0}{E} \left(\frac{\bar{\sigma}}{\sigma_0} \right)^n \quad (19)$$

where σ_0 and n are material constants selected such that Equation (19) fits the nonlinear portion of the uniaxial stress-strain curve. (See Discrete Element Analysis, Section III.)

By combining Equations (16) and (18), one obtains

$$\begin{Bmatrix} \epsilon_x \\ \epsilon_z \\ \gamma_{xz} \end{Bmatrix} = \frac{1}{E_s} \begin{bmatrix} 1 & -\nu_p & 0 \\ -\nu_p & 1 & 0 \\ 0 & 0 & 2(1+\nu_p) \end{bmatrix} \begin{Bmatrix} \sigma_x \\ \sigma_z \\ \tau_{xz} \end{Bmatrix} \quad (20)$$

*Raised numbers in parentheses refer to entries in the List of References.

in which E_s , the secant modulus, is

$$E_s = \frac{\bar{\sigma}}{\bar{\epsilon}} \quad (21)$$

and ν_p , the plastic Poisson's ratio, is

$$\nu_p = \frac{1}{2} \left[1 - \frac{E_s}{E} (1 - 2\nu) \right] \quad (22)$$

Inversion of Equation (20) yields the stresses in terms of strain as

$$\begin{Bmatrix} \sigma_x \\ \sigma_z \\ \tau_{xz} \end{Bmatrix} = \frac{E_s}{(1 - \nu_p^2)} \begin{bmatrix} 1 & \nu_p & 0 \\ \nu_p & 1 & 0 \\ 0 & 0 & \frac{(1 - \nu_p)}{2} \end{bmatrix} \begin{Bmatrix} \epsilon_x \\ \epsilon_z \\ \gamma_{xz} \end{Bmatrix} \quad (23)$$

in which, now, the equivalent stress $\bar{\sigma}$ is found from the uniaxial stress-strain curve at an equivalent strain of

$$\bar{\epsilon} = \frac{1}{(1 - \nu_p^2)} \left[(1 - \nu_p + \nu_p^2)(\epsilon_x^2 + \epsilon_z^2) + (4\nu_p - 1 - \nu_p^2)\epsilon_x\epsilon_z + \frac{3}{4}(1 - \nu_p)^2\gamma_{xz}^2 \right]^{1/2} \quad (24)$$

which applies to the plane stress case in the x - z plane. The additional assumption of zero strain in the z direction can now be conveniently introduced ($\epsilon_z = \gamma_{xz} = 0$) so that Equations (23) and (24) specialize to

$$\begin{aligned} \sigma_x &= \frac{E_s}{(1 - \nu_p^2)} \epsilon_x \\ \sigma_z &= \nu_p \frac{E_s}{(1 - \nu_p^2)} \epsilon_x \\ \tau_{xz} &= 0 \end{aligned} \quad (25)$$

and

$$\bar{\epsilon} = \frac{(1 - \nu_p + \nu_p^2)^{1/2}}{(1 - \nu_p^2)} \epsilon_x \quad (26)$$

It will be convenient, for later developments, to separate the stress into two components - the stresses which would be present if the strains were totally elastic and the stresses which must be subtracted from these stresses to account for plasticity, i.e.,

$$\begin{aligned} \sigma_x &= \frac{E}{(1 - \nu^2)} \epsilon_x - \sigma_{xp} \\ \sigma_z &= \frac{\nu E}{(1 - \nu^2)} \epsilon_x - \sigma_{zp} \end{aligned} \quad (27)$$

where the fictitious stresses σ_{xp} and σ_{zp} , herein termed plastic stresses, are given by:

$$\begin{aligned}\sigma_{xp} &= \left[\frac{E}{(1-\nu^2)} - \frac{E_s}{(1-\nu_p^2)} \right] \epsilon_x = \frac{E}{(1-\nu^2)} [1-\eta] \epsilon_x \\ \sigma_{zp} &= \left[\frac{\nu E}{(1-\nu^2)} - \frac{\nu_p E_s}{(1-\nu_p^2)} \right] \epsilon_x = \frac{\nu E}{(1-\nu^2)} \left[1 - \frac{\nu_p}{\nu} \eta \right] \epsilon_x\end{aligned}\quad (28)$$

in which:

$$\eta = \frac{E_s(1-\nu^2)}{E(1-\nu_p^2)} \quad (29)$$

In the analysis of the adherend, the relationship between the stress resultant in the x direction and middle surface strains is desired. In the customary fashion, one defines the stress-resultant normal force in the x direction of the adherend as:

$$N = \int_{-t/2}^{t/2} \sigma_x dy \quad (30)$$

and the stress resultant moment as

$$M = \int_{-t/2}^{t/2} \sigma_x y dy \quad (31)$$

where t is the adherend thickness. Employing the assumption that plane sections remain plane, one has

$$\epsilon_x = e + yX \quad (32)$$

where e is the middle surface normal strain and X is the middle surface curvature.

For an isotropic plate, one employs Equations (27), (30), (31), and (32) to arrive at the following plate constitutive equations:

$$\begin{aligned}N &= Ae - N_p \\ M &= DX - M_p\end{aligned}\quad (33)$$

where

$$\begin{aligned}A &= \frac{Et}{(1-\nu^2)} \\ D &= \frac{Et^3}{12(1-\nu^2)}\end{aligned}\quad (34)$$

and the plastic stress resultants are:

$$\begin{aligned}N_p &= \int_{-t/2}^{t/2} \sigma_{xp} dy \\ M_p &= \int_{-t/2}^{t/2} \sigma_{xp} y dy\end{aligned}\quad (35)$$

For purposes of numerical integration, the isotropic plate thickness will be divided into nine equal layers so that the plastic stress resultants can be written as

$$N_p = \frac{t}{9} \sum_{k=1}^9 \sigma_{xp}^k \quad (36)$$

$$M_p = \frac{t}{9} \sum_{k=1}^9 \sigma_{xp}^k y^k$$

where k refers to the layer number and y^k is the distance to the center of the layer from the middle surface. Introducing the strain-displacement relationships of Equation (15), Equation (33) can be written as

$$\begin{aligned} u_i' &= \frac{N_i + N_{ip}}{A_i} \\ v_i'' &= -\frac{M_i + M_{ip}}{D_i} \end{aligned} \quad (37)$$

where the subscript i has been added to denote adherend number.

II.2.c.(2) Orthotropic Adherend

An appropriate modification of the deformation theory of plasticity for orthotropic materials which has been suggested by Reference (1) is a generalization of Equation (16) as

$$\begin{pmatrix} \epsilon_\ell \\ \epsilon_t \\ \gamma_{\ell t} \end{pmatrix} = \begin{pmatrix} S_{11} & S_{12} & 0 \\ S_{12} & S_{22} & 0 \\ 0 & 0 & S_{66} \end{pmatrix} + \frac{\bar{\epsilon}_p}{\bar{\sigma}} \begin{pmatrix} \alpha_{11} & \alpha_{12} & 0 \\ \alpha_{12} & \alpha_{22} & 0 \\ 0 & 0 & 3\alpha_{66} \end{pmatrix} \begin{pmatrix} \sigma_\ell \\ \sigma_t \\ \tau_{\ell t} \end{pmatrix} \quad (38)$$

where the subscripts ℓ and t correspond to the principal material directions. The ℓ -axis is along the fibers and the t -axis is perpendicular to the fibers in the plane of a typical lamina (see Fig. 3). The quantities S_{11} , S_{12} , S_{22} , and S_{66} are elastic constants in the principal material directions:

$$\begin{aligned} S_{11} &= 1/E_\ell \\ S_{12} &= -\nu_{\ell t}/E_\ell = -\nu_{t\ell}/E_t \\ S_{22} &= 1/E_t \\ S_{66} &= 1/G_{\ell t} \end{aligned} \quad (39)$$

where E_ℓ , E_t , and $G_{\ell t}$ are the elastic orthotropic moduli and $\nu_{\ell t}$ is the orthotropic Poisson's ratio. The equivalent stress corresponding to Equation (38) is:

$$\bar{\sigma} = (\alpha_{11} \sigma_\ell^2 + \alpha_{22} \sigma_t^2 + 2\alpha_{12} \sigma_\ell \sigma_t + 3\alpha_{66} \tau_{\ell t}^2)^{1/2} \quad (40)$$

The quantities α_{ij} are, in general, variables dependent upon the state of stress. Their values will be discussed shortly. It is apparent that, for isotropic materials (isotropic strain-hardening), one has $\alpha_{11} = \alpha_{22} = \alpha_{66} = 1$ and $\alpha_{12} = -1/2$; i.e., the α_{ij} are constant, and $\bar{\epsilon}_p$ is determined from a single uniaxial stress-strain curve. This will not be the case for orthotropic materials.

Note: Right Hand Coordinate System for:
 $x(1), z(2), y(3)$
 $\ell(1), t(2), y(3)$

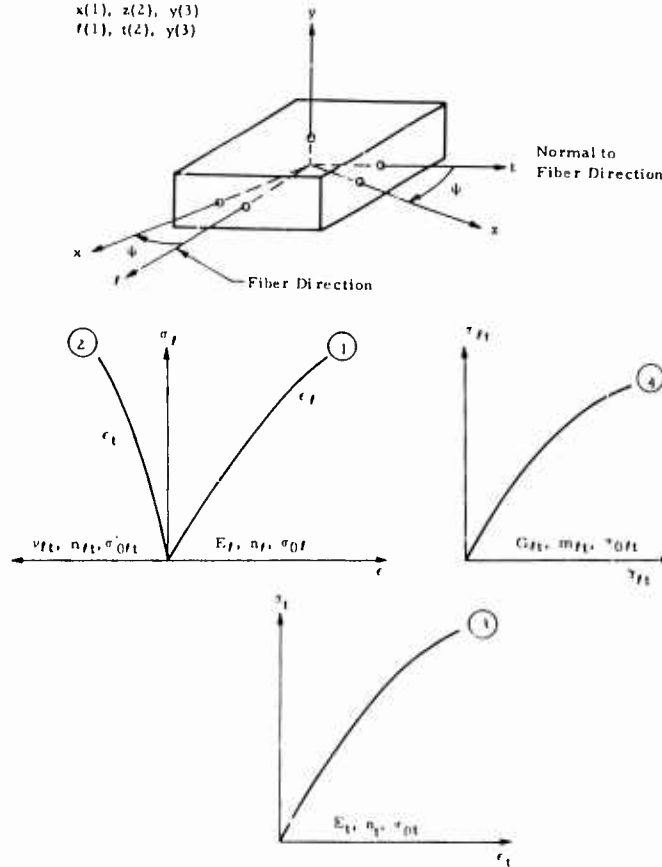


FIGURE 3. MATERIAL COORDINATES ℓ, t, y AND STRESS-STRAIN CURVES FROM UNIAXIAL STRESS TESTS IN PRINCIPAL DIRECTIONS

where the n 's, $m_{\ell t}$, and σ_0 's, and $\tau_{0\ell t}$ are material constants selected such that Equations (41a), (41b), (41c), and (41d) fit the curves in Figure 3. The elastic constants are the same as those given in Equation (38).

For a uniaxial test in the ℓ direction, Equations (38) and (40) give the strain in the ℓ direction as

$$\epsilon_\ell = S_{11} \sigma_\ell + \sqrt{\alpha_{11}} \bar{\epsilon}_p \quad ; \quad \sigma_\ell = \frac{\bar{\sigma}}{\sqrt{\alpha_{11}}} \quad (42)$$

By comparison with Equation (41a), it is apparent that both α_{11} and $\bar{\epsilon}_p$ cannot be determined uniquely; i.e., either α_{11} or $\bar{\epsilon}_p$ is arbitrary. It is convenient to select

$$\alpha_{11} = 1 \quad (43)$$

so that, from (41a) and (42),

$$\bar{\epsilon}_p = \frac{3}{7} S_{11} \sigma_{0\ell} \left(\frac{\bar{\sigma}}{\sigma_{0\ell}} \right)^{n_\ell} \quad (44)$$

In other words, we have defined the uniaxial stress-strain curve in the ℓ direction [Eq. (41a)] to be the equivalent stress-strain curve,

The values of $\alpha_{11}, \alpha_{12}, \alpha_{22}, \alpha_{66}$, and $\bar{\epsilon}_p$ are determined such that Equations (38) and (40) are satisfied for the conditions of uniaxial (normal and shear) stress in the principal directions. Suppose that the orthotropic material is characterized by the four uniaxial curves shown in Figure 3, which are obtained by uniaxial tests of a typical lamina, i.e., uniaxial normal stress tests in the ℓ and t directions and a pure shear stress test in the ℓt -plane. Each curve is to be approximated by a Ramberg-Osgood law, so that, for the uniaxial tests, one has

Uniaxial Stress σ_ℓ

$$\epsilon_\ell = S_{11} \sigma_\ell + \frac{3}{7} S_{11} \sigma_{0\ell} \left(\frac{\sigma_\ell}{\sigma_{0\ell}} \right)^{n_\ell} \quad (41a)$$

$$\epsilon_t = S_{12} \sigma_\ell + \frac{3}{7} S_{12} \sigma_{0\ell t} \left(\frac{\sigma_\ell}{\sigma_{0\ell t}} \right)^{n_{\ell t}} \quad (41b)$$

Uniaxial Stress σ_t

$$\epsilon_t = S_{22} \sigma_t + \frac{3}{7} S_{22} \sigma_{0t} \left(\frac{\sigma_t}{\sigma_{0t}} \right)^{n_t} \quad (41c)$$

In-Plane Shear $\tau_{\ell t}$

$$\gamma_{\ell t} = S_{66} \tau_{\ell t} + \frac{3}{7} S_{66} \tau_{0\ell t} \left(\frac{\tau_{\ell t}}{\tau_{0\ell t}} \right)^{m_{\ell t}} \quad (41d)$$

$$\bar{\epsilon} = S_{11} \bar{\sigma} + \frac{3}{7} S_{11} \sigma_{0\ell} \left(\frac{\bar{\sigma}}{\sigma_{0\ell}} \right)^{n\ell} \quad (45)$$

Using the remaining three equations (41b, c, d) in a similar manner, one finds [note that $\bar{\epsilon}_p$ is now defined by Equation (44)]

$$\begin{aligned} \alpha_{12} &= \frac{S_{12} \sigma_{0\ell}}{S_{11} \sigma_{0\ell}} \left(\frac{\bar{\sigma}}{\sigma_{0\ell}} \right)^{n\ell} \left(\frac{\sigma_{0\ell}}{\bar{\sigma}} \right)^{n\ell} \\ \alpha_{22} &= \left[\frac{S_{22} \sigma_{0\ell}}{S_{11} \sigma_{0\ell}} \left(\frac{\bar{\sigma}}{\sigma_{0\ell}} \right)^{n\ell} \left(\frac{\sigma_{0\ell}}{\bar{\sigma}} \right)^{n\ell} \right]^{\frac{2}{n\ell + 1}} \\ \alpha_{66} &= \frac{1}{3} \left[\frac{S_{66} \tau_{0\ell}}{S_{11} \sigma_{0\ell}} \left(\frac{\bar{\sigma}}{\tau_{0\ell}} \right)^{m\ell} \left(\frac{\sigma_{0\ell}}{\bar{\sigma}} \right)^{n\ell} \right]^{\frac{2}{m\ell + 1}} \end{aligned} \quad (46)$$

Replacing $\bar{\epsilon}_p$ by

$$\bar{\epsilon}_p = \bar{\epsilon} - S_{11} \bar{\sigma} \quad (47)$$

in Equation (38), and letting α_{11} be unity in Equation (40), gives

$$\begin{pmatrix} \epsilon_\ell \\ \epsilon_t \\ \gamma_{\ell t} \end{pmatrix} = \begin{bmatrix} S_{11\ell} & S_{12s} & 0 \\ S_{12s} & S_{22s} & 0 \\ 0 & 0 & S_{66s} \end{bmatrix} \begin{pmatrix} \sigma_\ell \\ \sigma_t \\ \tau_{\ell t} \end{pmatrix} \quad (48)$$

and

$$\bar{\sigma} = (\sigma_\ell^2 + \alpha_{22} \sigma_t^2 + 2\alpha_{12} \sigma_\ell \sigma_t + 3\alpha_{66} \tau_{\ell t}^2)^{1/2} \quad (49)$$

where the orthotropic secant compliance elements are given by:

$$\begin{aligned} S_{11s} &= \frac{\bar{\epsilon}}{\bar{\sigma}} \\ S_{12s} &= S_{12} + \alpha_{12} (S_{11s} - S_{11}) \\ S_{22s} &= S_{22} + \alpha_{22} (S_{11s} - S_{11}) \\ S_{66s} &= S_{66} + 3\alpha_{66} (S_{11s} - S_{11}) \end{aligned} \quad (50)$$

which corresponds to Equation (20) for isotropic materials. For a given stress state σ_ℓ , σ_t , $\tau_{\ell t}$ and given material constants, Equations (45), (46), (48), and (49) completely define the state of strain. However, the definition is not explicit since Equations (45), (46), and (49) represent five nonlinear equations in the five unknowns $\bar{\sigma}$, $\bar{\epsilon}$, α_{12} , α_{22} , and α_{66} .

Inversion of Equation (48) yields the stresses in terms of the strains as

$$\begin{Bmatrix} \sigma_{\ell} \\ \sigma_t \\ \tau_{\ell t} \end{Bmatrix} = \begin{bmatrix} Q_{11s} & Q_{12s} & 0 \\ Q_{12s} & Q_{22s} & 0 \\ 0 & 0 & Q_{66s} \end{bmatrix} \begin{Bmatrix} \epsilon_{\ell} \\ \epsilon_t \\ \gamma_{\ell t} \end{Bmatrix} \quad (51)$$

where the secant stiffness elements $Q_{ij s}$, are given by

$$\begin{aligned} Q_{11s} &= S_{22s} / (S_{11s} S_{22s} - S_{12s}^2) \\ Q_{12s} &= -S_{12s} / (S_{11s} S_{22s} - S_{12s}^2) \\ Q_{22s} &= S_{11s} / (S_{11s} S_{22s} - S_{12s}^2) \\ Q_{66s} &= 1 / S_{66s} \end{aligned} \quad (52)$$

The equivalent strain, obtained by combining Equations (50), (49) and (51), is found as:

$$\bar{\epsilon} = (\beta_{11} \epsilon_{\ell}^2 + \beta_{22} \epsilon_t^2 + 2\beta_{12} \epsilon_{\ell} \epsilon_t + 3\beta_{66} \gamma_{\ell t}^2)^{1/2} \quad (53)$$

in which

$$\begin{aligned} \beta_{11} &= (Q_{11s}^2 + \alpha_{22} Q_{12s}^2 + 2\alpha_{12} Q_{11s} Q_{12s}) S_{11s}^2 \\ \beta_{12} &= [Q_{11s} Q_{12s} + \alpha_{22} Q_{22s} Q_{12s} + \alpha_{12} (Q_{11s} Q_{22s} + Q_{12s}^2)] S_{11s}^2 \\ \beta_{22} &= (Q_{12s}^2 + \alpha_{22} Q_{22s}^2 + 2\alpha_{12} Q_{11s} Q_{22s}) S_{11s}^2 \\ \beta_{66} &= \alpha_{66} Q_{66s}^2 S_{11s}^2 \end{aligned} \quad (54)$$

Separating the stresses into two components, as for isotropic materials in Equation (27), gives

$$\begin{Bmatrix} \sigma_{\ell} \\ \sigma_t \\ \tau_{\ell t} \end{Bmatrix} = \begin{bmatrix} Q_{11} & Q_{12} & 0 \\ Q_{12} & Q_{22} & 0 \\ 0 & 0 & Q_{66} \end{bmatrix} \begin{Bmatrix} \epsilon_{\ell} \\ \epsilon_t \\ \gamma_{\ell t} \end{Bmatrix} - \begin{Bmatrix} \sigma_{\ell p} \\ \sigma_{tp} \\ \tau_{\ell tp} \end{Bmatrix} \quad (55)$$

in which the elastic stiffness elements Q_{ij} are as given in Equation (52) without the subscript s , i.e., in terms of the elastic compliance elements in Equation (39), and

$$\begin{Bmatrix} \sigma_{\ell p} \\ \sigma_{tp} \\ \tau_{\ell tp} \end{Bmatrix} = \begin{bmatrix} Q_{11} - Q_{11s} & Q_{12} - Q_{12s} & 0 \\ Q_{12} - Q_{12s} & Q_{22} - Q_{22s} & 0 \\ 0 & 0 & Q_{66} - Q_{66s} \end{bmatrix} \begin{Bmatrix} \epsilon_{\ell} \\ \epsilon_t \\ \gamma_{\ell t} \end{Bmatrix} \quad (56)$$

When dealing with orthotropic materials, it is necessary to transform stresses and strains from the x - z coordinate system to the principal material directions (ℓ - t) and vice versa (see Fig. 3). The stresses in the x - z coordinate system are given in terms of the stresses in the ℓ - t coordinate system by

$$\begin{Bmatrix} \sigma_x \\ \sigma_z \\ \tau_{xz} \end{Bmatrix} = \begin{bmatrix} c^2 & s^2 & -2sc \\ s^2 & c^2 & 2sc \\ sc & -sc & c^2 - s^2 \end{bmatrix} \begin{Bmatrix} \sigma_\ell \\ \sigma_t \\ \tau_{\ell t} \end{Bmatrix} \quad (57)$$

where

$$\begin{aligned} s &= \sin \psi \\ c &= \cos \psi \end{aligned} \quad (58)$$

and ψ is shown in Figure 3. Similarly, the strains in the ℓ - t plane, due to strains in the x direction, are (note, by the plane strain assumption in the x - y plane, $\epsilon_z = \gamma_{xz} = 0$)

$$\begin{Bmatrix} \epsilon_\ell \\ \epsilon_t \\ \gamma_{\ell t} \end{Bmatrix} = \epsilon_x \begin{Bmatrix} c^2 \\ s^2 \\ -2cs \end{Bmatrix} \quad (59)$$

In a manner similar to that used for isotropic adherends, Equations (55), (30), (31), and (32) and the transformation Equation (57) are used to obtain the constitutive equations for a laminated plate composed of different layers of an orthotropic material. Assuming symmetry of the laminated adherend plate about its midplane, one again arrives at Equation (33) for the plate constitutive equations, except in this case the constants A and D are defined as:

$$\begin{aligned} A &= \sum_k \bar{Q}_{11}^k t^k \\ D &= \sum_k \bar{Q}_{11}^k \left[t^k (y^k)^2 + \frac{(t^k)^3}{12} \right] \end{aligned} \quad (60)$$

where t^k is the thickness of layer k ,

$$\bar{Q}_{11}^k = [Q_{11}c^4 + 2(Q_{12} + 2Q_{66})c^2s^2 + Q_{22}s^4]_k \quad (61)$$

and s and c are defined in Equation (58). In Equation (60), the sum on k is taken over all the layers in the laminate. The plastic stress resultants for the laminate are found as

$$\begin{aligned} N_p &= \sum_k \sigma_{xp}^k t^k \\ M_p &= \sum_k \sigma_{xp}^k t^k y^k \end{aligned} \quad (62)$$

II.2.c.(3) Isotropic Adhesive

The adhesive is assumed to be an isotropic material and the constitutive equations of Reference (1) are utilized. The relations for the three-dimensional stress state will now be specialized for the adhesive. The normal stress in the x direction is neglected, $\sigma_x = 0$. Since the joint is assumed to be in a state of plane strain in the x - y plane, one has $\gamma_{xz} = \gamma_{yz} = 0$. Hence, the equations of Reference (1) apply to the adhesive in the following form

$$\begin{Bmatrix} \epsilon_y \\ \epsilon_z \\ \gamma_{xy} \end{Bmatrix} = \frac{1}{E_s} \begin{bmatrix} 1 & -\nu_p & 0 \\ -\nu_p & 1 & 0 \\ 0 & 0 & 2(1 + \nu_p) \end{bmatrix} \begin{Bmatrix} \sigma_y \\ \sigma_z \\ \tau_{xy} \end{Bmatrix} \quad (63)$$

where now

$$\bar{\sigma} = (\sigma_y^2 + \sigma_z^2 - \sigma_y \sigma_z + 3\tau_{xy}^2)^{1/2} \quad (64)$$

is the equivalent stress. E_s and ν_p are defined by Equations (21) and (22) respectively. Inversion of Equation (63) and introduction of the other zero strain for the plane strain assumption, $\epsilon_z = 0$, gives

$$\begin{aligned} \sigma_y &= \frac{E_s}{(1 - \nu_p^2)} \epsilon_y \\ \sigma_z &= \frac{\nu_p E_s}{(1 - \nu_p^2)} \epsilon_y \\ \tau_{xy} &= \frac{E_s}{2(1 + \nu_p)} \gamma_{xy} \end{aligned} \quad (65)$$

Now the equivalent stress $\bar{\sigma}$ is found from the uniaxial stress strain curve at an equivalent strain of

$$\bar{\epsilon} = \frac{1}{(1 - \nu_p^2)} \left[(1 - \nu_p + \nu_p^2) \epsilon_y^2 + \frac{3}{4} (1 - \nu_p)^2 \gamma_{xy}^2 \right]^{1/2} \quad (66)$$

Separating the elastic and inelastic portions of the stress, as was done for the adherends, one finds the total stresses

$$\begin{aligned} \sigma &= \frac{E\epsilon}{(1 - \nu^2)} - \sigma_p \\ \tau &= G\gamma - \tau_p \end{aligned} \quad (67)$$

in which the subscripts on the adhesive stresses and strains have been removed, i.e., σ has replaced σ_y , τ replaced τ_{xy} , ϵ replaced ϵ_y , and γ replaced γ_{xy} . The plastic stresses are given by

$$\begin{aligned} \sigma_p &= \left[\frac{E}{(1 - \nu^2)} - \frac{E_s}{(1 - \nu_p^2)} \right] \epsilon \\ \tau_p &= \left[G - \frac{E_s}{2(1 + \nu_p)} \right] \gamma \end{aligned} \quad (68)$$

Introducing the compatibility equations for the adhesive [Equation (13)], the stress-displacement relationship for the adhesive is

$$\tau = \frac{G}{l} (u_1 - u_2) + \frac{G}{2l} (t_1 \nu'_1 - t_2 \nu'_2) - \tau_p \quad (69a)$$

$$\sigma = \frac{E}{(1 - \nu^2)l} (\nu_1 + \nu_2) - \sigma_p \quad (69b)$$

The constitutive equations for the adhesive and adherends are now complete.

11.2.d. Governing Differential Equation

The equilibrium, compatibility, and constitutive equations are combined to develop the governing differential equations for the single lap joint. In particular, by substituting Equations (2), (5), and (37) into (69) and employing (12) gives

$$\begin{aligned}\theta'''' + p_1\theta - p_2\phi &= q_1 + q_2'' \\ \phi'' - p_3\phi + p_4\theta &= q_3 + q_4'\end{aligned}\quad (70)$$

where

$$\begin{aligned}p_1 &= \frac{E}{t(1-\nu^2)} \left(\frac{1}{D_1} + \frac{1}{D_2} \right) \\ p_2 &= \frac{F}{2t(1-\nu^2)} \left(\frac{t_1}{D_1} - \frac{t_2}{D_2} \right) \\ p_3 &= \frac{G}{t} \left(\frac{1}{A_1} + \frac{1}{A_2} + \frac{t_1^2}{4D_1} + \frac{t_2^2}{4D_2} \right) \\ p_4 &= \frac{G}{2t} \left(\frac{t_1}{D_1} - \frac{t_2}{D_2} \right) \\ q_1 &= \frac{PE\bar{I}}{at(1-\nu^2)} \left(\frac{1}{D_1} - \frac{1}{D_2} \right) \left(x - \frac{c}{2} \right) - \frac{2E}{t(1-\nu^2)} \left(\frac{M_{1p}}{D_1} + \frac{M_{2p}}{D_2} \right) \\ q_2 &= -2\sigma_p \\ q_3 &= \frac{PG}{t} \left[\frac{1}{A_1} - \frac{1}{A_2} + \frac{\bar{I}}{2a} \left(\frac{t_1}{D_1} + \frac{t_2}{D_2} \right) \left(\frac{c}{2} - x \right) \right] + \frac{G}{t} \left[\frac{2N_{1p}}{A_1} - \frac{2N_{2p}}{A_2} - \frac{t_1 M_{1p}}{D_1} + \frac{t_2 M_{2p}}{D_2} \right] \\ q_4 &= -2\tau_p\end{aligned}\quad (71)$$

Equations (70) represent the governing differential equations for the single lap joint. It will be noted that they are nonlinear equations since the plastic quantities N_{ip} , M_{ip} , σ_p , and τ_p are nonlinear functions of the displacements. However, as the equations are written, the portions on the left are linear differential equations with constant coefficients (p_i are constants). The portions on the right (q_i) which contain the plastic portions are nonlinear. Equations (70) are, thus, in proper form for an iterative solution to be discussed in Section 11.5. It is apparent that the equations become uncoupled if both adherends are identical; i.e., $p_2 = p_4 = 0$.

From Figure 1a, the boundary conditions for the single lap joint are developed by requiring that the stress resultants in the upper adherend must be zero at $x = 0$ and the stress resultants in the lower adherend be zero at $x = c$:

$$\begin{aligned}N_1 = M_1 = V_1 &= 0 \quad \text{at} \quad x = 0 \\ N_2 = M_2 = V_2 &= 0 \quad \text{at} \quad x = c\end{aligned}\quad (72)$$

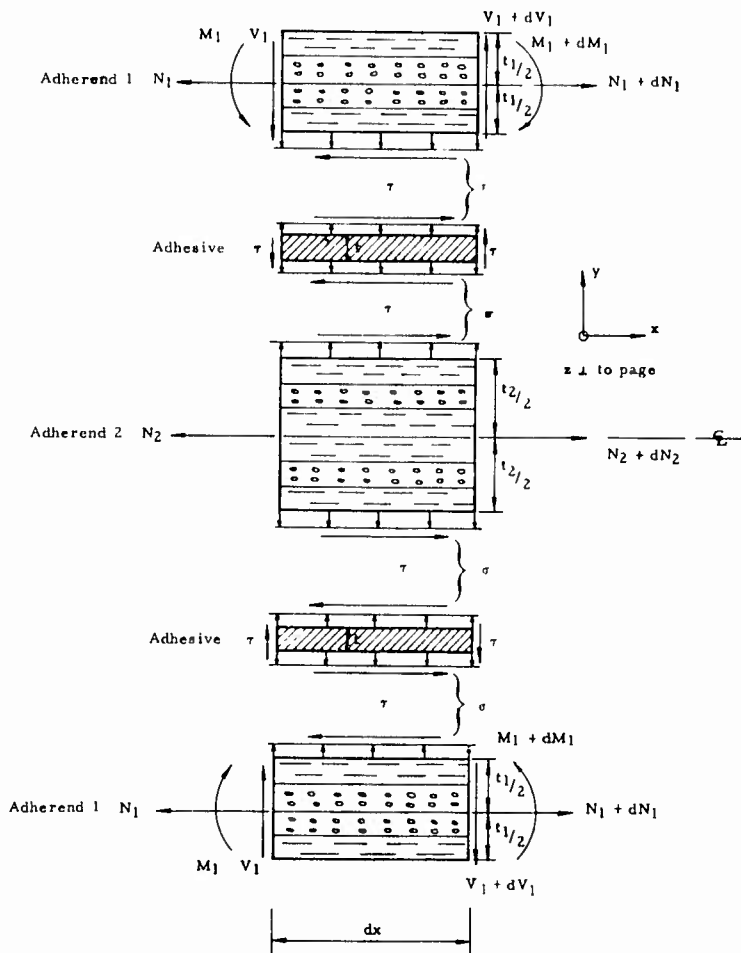
By substituting Equations (12) into (72), one arrives at the boundary conditions in terms of ϕ and θ as

$$\begin{array}{ll}
 \underline{x = 0} & \underline{x = c} \\
 \phi_0 = -P & \phi_c = P \\
 \theta_0 = \frac{P}{2} \left(\frac{c\bar{t}}{a} - t_1 \right) & \theta_c = \frac{P}{2} \left(\frac{c\bar{t}}{a} - t_2 \right) \\
 \theta'_0 = -\frac{P\bar{t}}{a} & \theta'_c = \frac{P\bar{t}}{a}
 \end{array} \quad (73)$$

These boundary conditions, along with Equations (70) and the constitutive equations of Section II.2.c, are the governing equations for the bonded single lap joint.

II.3. DOUBLE LAP JOINT

The free body in Figure 4 is used to develop the governing equations for the bonded double lap joint. Since the joint is assumed to be symmetrical about the midplane of adherend 2, the moment M_2 and shear V_2 vanish everywhere. Equating the total forces and moments on adherends 1 and 2 to zero gives the equilibrium equations as



$$\left. \begin{array}{l} \frac{dN_1}{dx} - \tau = 0 \\ \frac{dN_2}{dx} + 2\tau = 0 \end{array} \right\} \quad (74a)$$

$$\left. \begin{array}{l} \frac{dV_1}{dx} - \sigma = 0 \\ V_2 = 0 \end{array} \right\} \quad (74b)$$

$$\left. \begin{array}{l} \frac{dM_1}{dx} - V_1 + \frac{\tau t_1}{2} = 0 \\ M_2 = 0 \end{array} \right\} \quad (74c)$$

where the notation is as defined previously in accordance with Figures 1 and 4. Subtracting Equations (74a) and solving for τ yields

$$\tau = \frac{1}{2} \phi' \quad (75)$$

where

$$\phi = N_1 - \frac{N_2}{2} \quad (76)$$

FIGURE 4. FREE BODY OF AN ELEMENT OF INFINITESIMAL LENGTH OF A BONDED DOUBLE LAP JOINT

The normal stress is given by the first of Equations (74b) as

$$\sigma = \frac{dV_1}{dx} \quad (77)$$

or, introducing Equations (74a) and (74c),

$$\sigma = \frac{1}{2} \theta'' \quad (78)$$

where

$$\theta = 2 \left[M_1 + \frac{t_1}{4} \left(N_1 - \frac{N_2}{2} \right) \right] \quad (79)$$

Equilibrium of the overall joint requires that (see Fig. 1b)

$$N_1 + \frac{N_2}{2} - P = 0 \quad (80)$$

Solving for the stress resultants from Equations (74c), (76), (79), and (80) gives the stress resultants in terms of the unknown functions ϕ and θ as

$$N_1 = \frac{1}{2} (P + \phi)$$

$$N_2 = P - \phi$$

$$M_1 = \frac{1}{2} \left(\theta - \frac{t_1}{2} \phi \right) \quad (81)$$

$$V_1 = \frac{\theta'}{2}$$

One now proceeds to introduce the compatibility and constitutive equations, (69) and (37), in a manner almost identical to that followed for the single lap joint. Noting that, by symmetry, the lateral displacement of Adherend 2 is zero, one finds the governing differential equations to be:

$$\theta'''' + p_1 \theta - p_2 \phi = q_1 + q_2'' \quad (82)$$

$$\phi'' - p_3 \phi + p_4 \theta = q_3 + q_4'$$

where now the quantities p_i and q_i are defined by

$$\begin{aligned} p_1 &= \frac{E}{(1-\nu^2)tD_1} & p_2 &= \frac{Et_1}{2(1-\nu^2)tD_1} \\ p_3 &= \frac{G}{t} \left(\frac{1}{A_1} + \frac{2}{A_2} + \frac{t_1^2}{4D_1} \right) & p_4 &= \frac{Gt_1}{2tD_1} \\ q_1 &= -\frac{2EM_1p}{tD_1(1-\nu^2)} & q_2 &= -2\sigma_p \\ q_3 &= \frac{PG}{t} \left(\frac{1}{A_1} - \frac{2}{A_2} \right) + \frac{G}{t} \left(\frac{2N_1p}{A_1} - \frac{2N_2p}{A_2} - \frac{t_1M_1p}{D_1} \right) & q_4 &= -2\tau_p \end{aligned} \quad (83)$$

The reader will note the obvious similarity between these equations and those for the single lap joints. In fact, by replacing N_2 with $N_2/2$, A_2 with $A_2/2$, and i/D_2 with zero, and dropping the $x - c/2$ term (letting $\bar{t} = 0$, which accounts for the shear Q) in Equations (71), one arrives at Equation (83). Similarly, one may deduce Equations (81) from (12).

The boundary conditions for the double lap are also only slightly different from those for the single lap. Equations (72) also apply to the double lap, but the equations $M_2 = V_2 = 0$ at $x = c$ are redundant since this has already been used as a symmetry condition. Hence, two additional equations are required at $x = c$. By symmetry of the joint about the vertical centerline in Figure 1, the shear V_1 must be zero at $x = c$. It is now assumed that M_1 is also zero at $x = c$. The boundary conditions then become, by Equations (81),

$$\begin{array}{ll} \underline{x = 0} & \underline{x = c} \\ \phi_0 = -P & \phi_c = P \\ \theta_0 = -\frac{Pt_1}{2} & \theta_c = \frac{Pt_1}{2} \\ \theta'_0 = 0 & \theta'_c = 0 \end{array} \quad (84)$$

The solution of the nonlinear Equation (82) with the boundary conditions (84) and the constitutive equations will be discussed in Section II.5.

II.4. STEP LAP JOINT

Figure 1c shows schematically a step lap bonded joint under an axial tension, P . The total number of horizontal sections or "treads" is R , the number of risers being $R + 1$. The notation remains the same as for the single and double lap, except that it now becomes necessary, at times, to identify the particular step under consideration by a subscript r . For example, t_{1r} is the thickness of the upper adherend (adherend 1 in Fig. 1c) at the r th tread. The subscript r will be omitted unless it is necessary for clarity.

The derivation of the governing differential equations for the step lap follows the development for the single lap very closely. Using the free body in Figure 2, the shear stress and normal stress in the adhesive are found as in Equations (2) and (5) to be

$$\tau = \frac{1}{2} \phi' \quad (85)$$

where

$$\phi = N_1 - N_2 \quad (86)$$

and

$$\sigma = \frac{1}{2} \theta'' \quad (87)$$

where

$$\theta = M_1 + M_2 + \frac{t_1 - t_2}{4} (N_1 - N_2) \quad (88)$$

Equilibrium of the overall joint, as found from Figure 1c, requires that

$$N_1 + N_2 - P = 0 \quad (89)$$

and

$$M_1 - M_2 + \frac{\bar{t}}{2}(N_1 - N_2) - \frac{P}{4}(t_1 - t_2) = 0 \quad (90)$$

The adherend stress resultants are found in terms of the unknown functions ϕ and θ by solving Equations (86), (88), (89), and (90) simultaneously:

$$\begin{aligned} N_1 &= \frac{1}{2}(P + \phi) & M_1 &= \frac{1}{2} \left[\theta + \frac{P}{4}(t_1 - t_2) - \frac{t_1}{2} \phi \right] & V_1 &= \frac{\theta'}{2} \\ N_2 &= \frac{1}{2}(P - \phi) & M_2 &= \frac{1}{2} \left[\theta - \frac{P}{4}(t_1 - t_2) + \frac{t_2}{2} \phi \right] & V_2 &= \frac{\theta'}{2} \end{aligned} \quad (91)$$

The constitutive and compatibility conditions, (69) and (37)*, are now introduced in a manner similar to that used for the single lap. The governing differential equation is found to be

$$\begin{aligned} \theta'''' + p_1 \theta - p_2 \phi &= q_1 + q_2'' \\ \phi'' - p_3 \phi + p_4 \theta &= q_3 + q_4' \end{aligned} \quad (92)$$

in which, except for q_1 and q_3 , the p_i and q_i are identical to those listed for the single lap; i.e.:

$$\begin{aligned} p_1 &= \frac{E}{t(1-\nu^2)} \left(\frac{1}{D_1} + \frac{1}{D_2} \right) \\ p_2 &= \frac{E}{2t(1-\nu^2)} \left(\frac{t_1}{D_1} - \frac{t_2}{D_2} \right) \\ p_3 &= \frac{G}{t} \left(\frac{1}{A_1} + \frac{1}{A_2} + \frac{t_1^2}{4D_1} + \frac{t_2^2}{4D_2} \right) \\ p_4 &= \frac{G}{2t} \left(\frac{t_1}{D_1} - \frac{t_2}{D_2} \right) \\ q_1 &= -\frac{PE}{t(1-\nu^2)} \left(\frac{t_1 - t_2}{4} \right) \left(\frac{1}{D_1} - \frac{1}{D_2} \right) - \frac{2E}{t(1-\nu^2)} \left(\frac{M_1 p}{D_1} + \frac{M_2 p}{D_2} \right) \\ q_2 &= -2\sigma_p \\ q_3 &= \frac{PG}{t} \left[\frac{1}{A_1} - \frac{1}{A_2} - \left(\frac{t_1 - t_2}{8} \right) \left(\frac{t_1}{D_1} + \frac{t_2}{D_2} \right) \right] + \frac{G}{t} \left[\frac{2N_1 p}{A_1} - \frac{2N_2 p}{A_2} - \frac{t_1 M_1 p}{D_1} + \frac{t_2 M_2 p}{D_2} \right] \\ q_4 &= -2\tau_p \end{aligned} \quad (93)$$

*By use of Equation (37), it has been tacitly assumed that the adherends are symmetrical at each step. This may not be the typical case for the real problem but, considering the other assumptions involved in this analysis, it will be assumed that the stretch/bending coupling induced by asymmetry can be neglected.

The reader is reminded that Equation (92) applies only for one tread of the step lap, and that, in fact, each quantity should have a subscript r to refer it to the r th tread.

When Equation (92) has been written and its general solution found for each of the R treads, the individual solutions must be connected by a set of continuity conditions at each riser. The general solution of Equations (92) for each tread has six arbitrary constants or a total of $6R$ constants if there are R steps. Thus, we need six continuity conditions at each intermediate riser, giving $6(R - 1)$ equations. With three boundary conditions at each end riser, there are $6R$ equations.

The continuity and boundary conditions will now be derived by the use of Figure 5 which shows a segment of the joint at riser number r . The length of the segment, δ , goes to zero in the limit. The continuity conditions for the

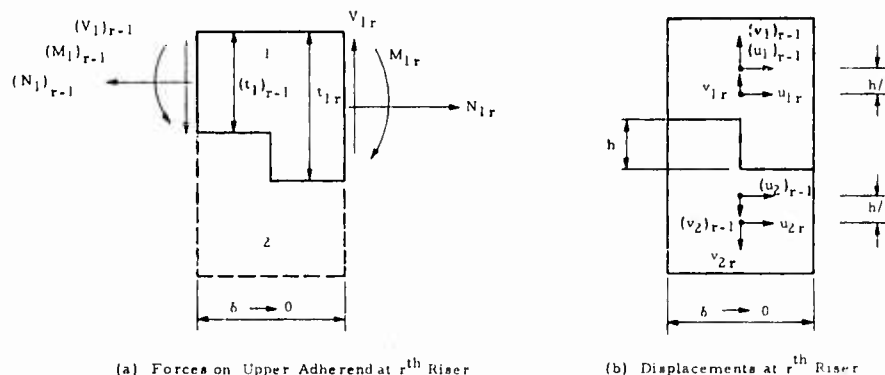


FIGURE 5. FORCES AND DISPLACEMENTS OF r th RISER

stress resultants are obtained by satisfying equilibrium of the free body of the upper adherend in Figure 5a. Assuming that no force is transmitted by the adhesive in the riser, one has

$$(M_1)_{r-1} - M_{1r} + N_{1r} \left[\frac{t_{1r}}{2} - \frac{(t_1)_{r-1}}{2} \right] = 0 \quad (94a)$$

$$(N_1)_{r-1} - N_{1r} = 0 \quad (94b)$$

$$(V_1)_{r-1} - V_{1r} = 0 \quad (94c)$$

where now the subscripts r and $r - 1$ are required to refer to a particular tread. According to Figure 1c, the quantities for tread $r - 1$ are evaluated at $x_{r-1} = b_{r-1}$ and for tread r at $x_r = 0$.

From Figure 5b, continuity of the lateral displacements and rotations requires that

$$(v_1)_{r-1} = v_{1r} \quad (v_2)_{r-1} = v_{2r} \quad (95a)$$

$$(v'_1)_{r-1} = v'_{1r} \quad (v'_2)_{r-1} = v'_{2r} \quad (95b)$$

Continuity of longitudinal displacements is satisfied if

$$u_{1r} = (u_1)_{r-1} + \frac{h}{2} (v'_1)_{r-1} \quad (95c)$$

$$u_{2r} = (u_2)_{r-1} - \frac{h}{2} (v'_2)_{r-1}$$

where

$$h = t_{1r} - (t_1)_{r-1} = (t_2)_{r-1} - t_{2r}$$

By subtracting Equations (95c), we obtain

$$u_{1r} - u_{2r} = (u_1)_{r-1} - (u_2)_{r-1} + \frac{h}{2} [(v'_1)_{r-1} + (v'_2)_{r-1}] \quad (96)$$

Now, from Equation (69a), one finds

$$u_{1r} - u_{2r} = \frac{t}{G} (\tau_r + \tau_{pr}) - \frac{1}{2} (t_{1r} v'_{1r} - t_{2r} v'_{2r}) \quad (97)$$

and, similarly, for tread $r-1$. Introducing Equation (97) for treads r and $r-1$ into Equation (96) and using Equation (95b) gives

$$\tau_r + \tau_{pr} - \frac{Gh}{2t} (v'_{1r} + v'_{2r}) = \tau_{r-1} + (\tau_p)_{r-1} + \frac{Gh}{2t} [(v'_1)_{r-1} + (v'_2)_{r-1}] \quad (98)$$

By Equation (69b), this becomes

$$\tau_r + \tau_{pr} - \frac{Gh(1-\nu^2)}{2E} (\sigma'_r + \sigma'_{pr}) = \tau_{r-1} + (\tau_p)_{r-1} + \frac{Gh(1-\nu^2)}{2E} [\sigma'_{r-1} + (\sigma'_p)_{r-1}] \quad (99)$$

which represents the continuity equation for longitudinal displacements. The continuity equation for lateral displacements is obtained by adding Equations (95a) to obtain:

$$(v_1)_{r-1} + (v_2)_{r-1} = v_{1r} + v_{2r} \quad (100)$$

which, by Equation (69b), becomes

$$\sigma_{r-1} + (\sigma_p)_{r-1} = \sigma_r + \sigma_{pr} \quad (101)$$

Similarly, the equation for continuity of rotations becomes

$$\sigma'_{r-1} + (\sigma'_p)_{r-1} = \sigma'_r + \sigma'_{pr} \quad (102)$$

Equations (94a), (94b), (94c), (99), (101), and (102) are the six required continuity conditions to be employed at each riser. By introducing Equations (85), (87), and (91) and the definitions of q_i in Equations (93), these continuity conditions become, respectively,

$$\begin{aligned} \theta_{r-1} + \frac{h}{2} \phi_{r-1} &= \theta_r - \frac{h}{2} \phi_r \\ \phi_{r-1} &= \phi_r \\ \theta'_{r-1} &= \theta'_r \\ \phi'_{r-1} - (q_4)_{r-1} + \frac{Gh(1-\nu^2)}{2E} [\theta'''_{r-1} - (q'_2)_{r-1}] &= \phi'_r - q_{4r} - \frac{Gh(1-\nu^2)}{2E} [\theta'''_r - q'_{2r}] \\ \theta''_{r-1} - (q_2)_{r-1} &= \theta''_r - q_{2r} \\ \theta'''_{r-1} - (q'_2)_{r-1} &= \theta'''_r - q'_{2r} \end{aligned} \quad (103)$$

where again the subscript $r - 1$ refers to a quantity for tread $r - 1$ evaluated at $x_{r-1} = b_{r-1}$, and the subscript r to a quantity for tread r evaluated at $x_r = \text{zero}$.

The boundary conditions at the two end risers, $r = 1$ and $r = R + 1$, are obtained from equilibrium considerations. At the first riser, one has

$$N_{11} = M_{11} = V_{11} = 0 \quad (104)$$

and, at the $R + 1$ riser,

$$N_{2R} = M_{2R} = V_{2R} = 0 \quad (105)$$

In terms of ϕ and θ , the boundary conditions become, respectively,

$$\begin{array}{ll} \underline{x_1 = 0} & \underline{x_R = b_R} \\ \phi_1 = -P & \phi_R = P \\ \theta_1 = \frac{P}{4}(t_{21} - 3t_{11}) & \theta_R = \frac{P}{4}(t_{1R} - 3t_{2R}) \\ \theta'_1 = 0 & \theta'_R = 0 \end{array} \quad (106)$$

where the second subscript again refers to the tread number. The solution of the nonlinear Equations (92) with the compatibility Equations (103), boundary conditions (106), and constitutive equations for the step lap joint will be discussed in Section II.5.

II.5. SOLUTION TO DIFFERENTIAL EQUATIONS

II.5.a. General Procedure

The differential equations governing the behavior of single lap (70), double lap (82), and step lap (92) bonded joints are all of the same general form:

$$\begin{aligned} \theta'''' + p_1\theta - p_2\phi &= q_1 + q_2'' \\ \phi'' - p_3\phi + p_4\theta &= q_3 + q_4' \end{aligned} \quad (107)$$

where the p_i are constants and the q_i are functions of the applied load P , the plastic stress resultants in the adherends, and the plastic stresses in the adhesive. The quantities p_i and q_i are given in Sections II.2, II.3 and II.4 for each of the respective joints. It is apparent that this set of equations is actually two nonlinear coupled differential equations since the q_i are nonlinear functions of the stress resultants and stresses and, hence, of ϕ and θ . The general approach will be to solve this set of nonlinear equations by iteration. Equation (107) is written as

$$\begin{aligned} (\theta'''')^j + p_1\theta^j - p_2\phi^j &= q_1^{j-1} + (q_2'')^{j-1} \\ (\phi'')^j - p_3\phi^j + p_4\theta^j &= q_3^{j-1} + (q_4')^{j-1} \end{aligned} \quad (108)$$

where j refers to the current iteration. The portions on the left-hand side of the equations are linear differential equations with constant coefficients for which a solution can be found. Thus, supposing at iteration j we have the q_i from the previous iteration ($j - 1$), then the functions θ and ϕ for the current iteration j are obtained by solving

Equations (108) subject to the boundary (and continuity for the step lap) conditions. Symbolically, this may be written as

$$\begin{aligned}\theta^j &= \theta^j(q_i^{j-1}, x) \\ \phi^j &= \phi^j(q_i^{j-1}, x)\end{aligned}\tag{109}$$

With these functions of θ and ϕ , the adhesive stresses and adherend stress resultants may be obtained by equations presented in Section II.2, II.3, or II.4, e.g., Equations (2), (5), and (12):

$$\begin{aligned}\tau^j &= \tau^j(\phi^j) \\ \sigma^j &= \sigma^j(\theta^j) \\ N_i^j &= N_i^j(\theta^j, \phi^j, x) \\ M_i^j &= M_i^j(\theta^j, \phi^j, x)\end{aligned}\tag{110}$$

where i refers to the adherend number. Using these new values of the stresses and the previous values of the plastic stresses (contained in q_i^{j-1}), the pertinent strains can be computed by the constitutive equations of Section II.2, e.g., Equation (20). These strains are then employed to compute new values of the plastic stress, e.g., by Equation (28), and, hence, new values of q_i :

$$q_i^j = q_i^j(\tau^j, \sigma^j, N_i^j, M_i^j, P, x)\tag{111}$$

This completes iteration j . The solution process now returns to Equation (109) to begin iteration $j + 1$. Iteration continues until there is an insignificant change in the plastic stresses. This solution will be discussed in more detail in the remainder of this section.

II.5.b. Homogeneous Solution

The homogeneous equation corresponding to Equations (107) is

$$\begin{aligned}\theta'''' + p_1\theta - p_2\phi &= 0 \\ \phi'' - p_3\phi + p_4\theta &= 0\end{aligned}\tag{112}$$

The superscript j 's have been eliminated here as well as in the following developments since they are not needed for clarity. The reader should remember, however, that the solution is not in closed form and that an iterative procedure is involved. Following the standard procedure for the solution of linear differential equations with constant coefficients, one assumes a solution of the form

$$\begin{aligned}\phi &= C_1 e^{\rho x} \\ \theta &= C_2 e^{\rho x}\end{aligned}\tag{113}$$

Substituting Equations (113) into (112) and setting the determinate of the coefficients C_1 and C_2 equal to zero, one finds the characteristic equation for ρ to be

$$\Gamma^3 - p_3\Gamma^2 + p_1\Gamma - p_1p_3 + p_2p_4 = 0\tag{114}$$

where

$$\Gamma = \rho^2\tag{115}$$

Equation (114) has one real, positive root, Γ_1 , which can be found numerically. (Note that for equal adherends in the single lap, $p_2 = p_4 = 0$, and the real, positive root is given by $\Gamma_1 = p_3$.)*

$$\Gamma_1 = \text{real, positive root of Equation (114)} \quad (116)$$

Then the other two roots are the complex conjugates:

$$\Gamma_2, \Gamma_3 = \xi_1 \pm i\xi_2 \quad (117)$$

where

$$\begin{aligned} \xi_1 &= \frac{p_3 - \Gamma_1}{2} \\ \xi_2 &= \left[\frac{p_1 p_3 - p_2 p_4}{\Gamma_1} - \left(\frac{\Gamma_1 - p_3}{2} \right)^2 \right]^{1/2} \\ i &= \sqrt{-1} \end{aligned} \quad (118)$$

The complete set of six roots for p can now be written using Equations (115) and (117) as

$$\begin{aligned} \rho_1 &= \lambda \\ \rho_2 &= -\lambda \\ \rho_3 &= \alpha + i\beta \\ \rho_4 &= -\alpha - i\beta \\ \rho_5 &= \alpha - i\beta \\ \rho_6 &= -\alpha + i\beta \end{aligned} \quad (119)$$

where

$$\begin{aligned} \lambda &= \sqrt{\Gamma_1} \\ \alpha &= \left[\frac{p_3 - \Gamma_1}{4} + \sqrt{\frac{p_1 p_3 - p_2 p_4}{4\Gamma_1}} \right]^{1/2} \\ \beta &= \left[\frac{\Gamma_1 - p_3}{4} + \sqrt{\frac{p_1 p_3 - p_2 p_4}{4\Gamma_1}} \right]^{1/2} \end{aligned} \quad (120)$$

*Equation (114) will have one real root and two complex conjugate roots if

$$27 p_2^2 p_4^2 + 4 p_1^3 + 4 p_3^3 (p_1 p_3 - p_2 p_4) + p_1 p_3 (8 p_1 p_3 - 36 p_2 p_4) > 0$$

This will generally be true since $p_1 p_3 \gg p_2 p_4$.

The homogeneous solution to Equation (112) can, thus, be written in matrix notation as

$$\begin{aligned}\phi &= \{f(x)\}^T \{C_1\} \\ \theta &= \{f(x)\}^T \{C_2\}\end{aligned}\quad (121)$$

in which

$$\{f(x)\} = \begin{Bmatrix} e^{\lambda x} \\ e^{-\lambda x} \\ e^{\alpha x} \cos \beta x \\ e^{\alpha x} \sin \beta x \\ e^{-\alpha x} \cos \beta x \\ e^{-\alpha x} \sin \beta x \end{Bmatrix} \quad (122)$$

and the arbitrary constants are

$$\{C_1\} = \begin{Bmatrix} C_{11} \\ C_{12} \\ C_{13} \\ C_{14} \\ C_{15} \\ C_{16} \end{Bmatrix} ; \quad \{C_2\} = \begin{Bmatrix} C_{21} \\ C_{22} \\ C_{23} \\ C_{24} \\ C_{25} \\ C_{26} \end{Bmatrix} \quad (123)$$

Only six of the twelve constants C_{1i} and C_{2i} are arbitrary; the other six are determined by substitution into Equation (112). After some lengthy algebraic manipulations, one obtains:

$$\begin{aligned}\{C_1\} &= [T_1] \{C\} \\ \{C_2\} &= [T_2] \{C\}\end{aligned}\quad (124)$$

where $\{C\}$ is another vector of arbitrary constants and

$$[T_1] = \begin{bmatrix} 1 & 0 & 0 & 0 & 0 & 0 \\ 0 & 1 & 0 & 0 & 0 & 0 \\ 0 & 0 & \delta_2 & -\delta_3 & 0 & 0 \\ 0 & 0 & \delta_3 & \delta_2 & 0 & 0 \\ 0 & 0 & 0 & 0 & \delta_2 & \delta_3 \\ 0 & 0 & 0 & 0 & -\delta_3 & \delta_2 \end{bmatrix} \quad (125)$$

$$[T_2] = \begin{bmatrix} \delta_1 & 0 & 0 & 0 & 0 & 0 \\ 0 & \delta_1 & 0 & 0 & 0 & 0 \\ 0 & 0 & 1 & 0 & 0 & 0 \\ 0 & 0 & 0 & 1 & 0 & 0 \\ 0 & 0 & 0 & 0 & 1 & 0 \\ 0 & 0 & 0 & 0 & 0 & 1 \end{bmatrix} \quad (125)$$

in which

$$\begin{aligned} \delta_1 &= \frac{p_2}{p_1 + \lambda^4} \\ \delta_2 &= \frac{-(\alpha^2 - \beta^2 - p_3)p_4}{(\alpha^2 - \beta^2 - p_3)^2 + 4\alpha^2\beta^2} \\ \delta_3 &= \frac{-2\alpha\beta p_4}{(\alpha^2 - \beta^2 - p_3)^2 + 4\alpha^2\beta^2} \end{aligned} \quad (126)$$

Substituting Equations (124) into Equation (121) gives the homogeneous solution as

$$\begin{aligned} \phi &= \{f\}^T [T_1] \{C\} \\ \theta &= \{f\}^T [T_2] \{C\} \end{aligned} \quad (127)$$

It will be convenient, for computation purposes, to determine the derivatives of $\{f\}^T$ as

$$\{f'\}^T = \{f\}^T [d] \quad (128)$$

where

$$[d] = \begin{bmatrix} \lambda & 0 & 0 & 0 & 0 & 0 \\ 0 & -\lambda & 0 & 0 & 0 & 0 \\ 0 & 0 & \alpha & \beta & 0 & 0 \\ 0 & 0 & -\beta & \alpha & 0 & 0 \\ 0 & 0 & 0 & 0 & -\alpha & \beta \\ 0 & 0 & 0 & 0 & -\beta & -\alpha \end{bmatrix} \quad (129)$$

The reader will note that, for the special case of equal adherends in the single lap, one has

Special Case—Equal Adherends in a Single Lap

$$p_2 = p_4 = 0$$

$$\Gamma_1 = p_3$$

$$\lambda = \sqrt{p_3}$$

$$\alpha = \beta = \sqrt[4]{\frac{p_1}{4}}$$

$$\delta_1 = \delta_2 = \delta_3 = 0$$

and, hence, the homogeneous differential equations uncouple.

II.5.c. General Solution

The general solution (homogeneous plus particular) to Equations (107) will be obtained by the method of variation of parameters.⁽³⁾ According to this method, one supposes that the arbitrary constants $\{C\}$ in the homogenous solution [Equation (127)] are functions of x ; i.e.,

$$\begin{aligned}\phi &= \{f(x)\}^T [T_1] \{C(x)\} \\ \theta &= \{f(x)\}^T [T_2] \{C(x)\}\end{aligned}\tag{130}$$

Successive differentiations of Equations (130) are made and conditions employed on these derivatives to ensure satisfaction of the differential Equations (107):

$$\begin{aligned}\phi' &= \{f'\}^T [T_1] \{C\} + \{f\}^T [T_1] \{C'\} \\ \text{Condition 1: } \{f\}^T [T_1] \{C'\} &= q_4 \\ \theta' &= \{f'\}^T [T_2] \{C\} + \{f\}^T [T_2] \{C'\} \\ \text{Condition 2: } \{f\}^T [T_2] \{C'\} &= 0 \\ \phi'' &= \{f''\}^T [T_1] \{C\} + \{f'\}^T [T_1] \{C'\} + q_4' \\ \text{Condition 3: } \{f'\}^T [T_1] \{C'\} &= q_3 \\ \theta'' &= \{f''\}^T [T_2] \{C\} + \{f'\}^T [T_2] \{C'\} \\ \text{Condition 4: } \{f'\}^T [T_2] \{C'\} &= q_2 \\ \phi''' &= \{f'''\}^T [T_1] \{C\} + \{f''\}^T [T_1] \{C'\} + q_3' \\ \text{Condition 5: } \{f''\}^T [T_1] \{C'\} &= 0 \\ \theta''' &= \{f'''\}^T [T_2] \{C\} + \{f''\}^T [T_2] \{C'\} + q_2' \\ \text{Condition 6: } \{f''\}^T [T_2] \{C'\} &= q_1\end{aligned}\tag{131}$$

In summary, the six conditions on $\{C'\}$ are

$$[h(x)] \{C'(x)\} = \{q(x)\}\tag{132}$$

where

$$\{q(x)\} = \begin{Bmatrix} q_4 \\ 0 \\ q_3 \\ q_2 \\ 0 \\ q_1 \end{Bmatrix} \quad (133)$$

and $[h(x)]$ is the 6×6 matrix

$$[h(x)] = \begin{Bmatrix} \{f\}^T [T_1] \\ \{f\}^T [T_2] \\ \{f'\}^T [T_1] \\ \{f'\}^T [T_2] \\ \{f''\}^T [T_2] \\ \{f'''\}^T [T_2] \end{Bmatrix} \quad (134)$$

Solving for $\{C(x)\}$ from Equation (132) gives

$$\{C(x)\} = \{C_0\} + \int_0^x [h(v)]^{-1} \{q(v)\} dv \quad (135)$$

where C_0 is a vector of arbitrary constants and v is a variable of integration. (It is a consequence of this application of the method of variation of parameters that it is not necessary to evaluate derivatives of q_2 and q_4 .) Thus, the complete general solution is given by Equations (130) and (135):

$$\begin{aligned} \phi &= \{f(x)\}^T [T_1] \left(\{C_0\} + \int_0^x [h(v)]^{-1} \{q(v)\} dv \right) \\ \theta &= \{f(x)\}^T [T_2] \left(\{C_0\} + \int_0^x [h(v)]^{-1} \{q(v)\} dv \right) \end{aligned} \quad (136)$$

The reader can satisfy himself that Equation (136) indeed satisfies Equation (107) by substitution and use of the conditions (131).

II.5 d. Boundary Conditions for Single, Double, and Step Lap Joints

According to the developments of Section II.2, II.3, and II.4, the boundary conditions are specified as

$$\begin{array}{cc} \underline{x = 0} & \underline{x = c} \\ \phi = \phi_0 & \phi = \phi_c \\ \theta = \theta_0 & \theta = \theta_c \\ \theta' = \theta'_0 & \theta' = \theta'_c \end{array} \quad (137)$$

where ϕ_0, θ_0 , etc., are specified values of ϕ and θ at the boundaries. Substituting these conditions into Equations (136) and solving for the arbitrary constants $\{C_0\}$ gives:

$$C_0 = [H]^{-1} \left\{ \begin{array}{c} 0 \\ 0 \\ 0 \\ \{f(c)\}^T [T_1] \int_0^c [h]^{-1} \{q\} dy \\ \{f(c)\}^T [T_2] \int_0^c [h]^{-1} \{q\} dy \\ \{f'(c)\}^T [T_2] \int_0^c [h]^{-1} \{q\} dy \end{array} \right\} \quad (138)$$

in which

$$\{ \phi_0 \} = \left\{ \begin{array}{c} \phi_0 \\ \theta_0 \\ \theta'_0 \\ \phi_c \\ \theta_c \\ \theta'_c \end{array} \right\} \quad (139)$$

and $[H]$ is the 6×6 matrix

$$[H] = \begin{bmatrix} \{f(0)\}^T [T_1] \\ \{f(0)\}^T [T_2] \\ \{f'(0)\}^T [T_2] \\ \{f(c)\}^T [T_1] \\ \{f(c)\}^T [T_2] \\ \{f'(c)\}^T [T_2] \end{bmatrix} \quad (140)$$

By substituting Equation (138) into (136), one obtains the particular solution of Equations (107). By defining the matrix $[F]$ by

$$[F(x)] = [h(x)] [H]^{-1} \quad (141)$$

this solution can be written as

$$\begin{Bmatrix} \phi \\ \theta \end{Bmatrix} = \begin{bmatrix} 1 & 0 & 0 & 0 & 0 & 0 \\ 0 & 1 & 0 & 0 & 0 & 0 \end{bmatrix} [F(x)] \left(\{\phi_0\} + \{\phi_p(x)\} \right) \quad (142)$$

where

$$\{\phi_p(x)\} = \left\{ \begin{array}{l} \int_0^x Q_1(y) dy \\ \int_0^x Q_2(y) dy \\ \int_0^x Q_3(y) dy \\ \int_c^x Q_4(y) dy \\ \int_c^x Q_5(y) dy \\ \int_c^x Q_6(y) dy \end{array} \right\} \quad (143)$$

and the quantities $Q_i(y)$ are elements of the vector $\{Q(y)\}$:

$$\{Q(y)\} = [F(y)]^{-1} \{q(y)\} \quad (144)$$

The integrals in $\{\phi_p(x)\}$ will be evaluated numerically by a standard IBM integration subroutine. The adhesive shear and normal stresses are obtained as derivatives of ϕ and θ , e.g., Equations (2) and (5). Using the conditions in Equation (131), the complete solution can be summarized as

$$\begin{Bmatrix} \phi \\ \theta \\ 2\tau \\ \theta' \\ 2\sigma \\ 2\sigma' \end{Bmatrix} = [F(x)] \left(\{\phi_0\} + \{\phi_p(x)\} \right) + \begin{Bmatrix} 0 \\ 0 \\ q_4 \\ 0 \\ q_2 \\ q_2' \end{Bmatrix} \quad (145)$$

The application of these equations to the solution of the joint problems will be discussed in Section II.5.e.

II.5.d.(1) Single Lap Joint

Equation (145) applies directly to the single lap joint with the quantities p_i and q_i appropriately defined as in Section II.2.a. From Equation (73), the vector $\{\phi_0\}$ is given by:

$$\{\phi_0\} = P \begin{Bmatrix} -1 \\ \frac{1}{2} \frac{c\bar{l}}{a} - t_1 \\ -\frac{\bar{l}}{a} \\ 1 \\ \frac{1}{2} \frac{c\bar{l}}{a} - t_2 \\ \frac{\bar{l}}{a} \end{Bmatrix} \quad (146)$$

II.5.d.(2) Double Lap Joint

For the double lap joint, Equation (145) is used in conjunction with the boundary condition vector

$$\{\phi_0\} = P \begin{Bmatrix} -1 \\ -\frac{t_1}{2} \\ 0 \\ 1 \\ \frac{t_1}{2} \\ 0 \end{Bmatrix} \quad (147)$$

II.5.d.(3) Step Lap Joint

For the step lap joint, Equation (145) applies to each of the R treads. The continuity conditions [Equation (103)] which are to be applied at each intermediate riser, r , can be written by employing Equation (145) as:

$$[R_{r-1}] [F_{r-1}(b_{r-1})] [\{\phi_0\}_{r-1} + \{\phi_p(b_{r-1})\}_{r-1}] = [S_r] [F_r(0)] [\{\phi_0\}_r + \{\phi_p(0)\}_r] \quad (148)$$

where

$$[R_{r-1}] = \begin{bmatrix} 1 & 0 & 0 & 0 & 0 & 0 \\ \frac{h}{2} & 1 & 0 & 0 & 0 & 0 \\ 0 & 0 & 1 & 0 & 0 & \frac{hG(1-\nu^2)}{2E} \\ 0 & 0 & 0 & 1 & 0 & 0 \\ 0 & 0 & 0 & 0 & 1 & 0 \\ 0 & 0 & 0 & 0 & 0 & 1 \end{bmatrix} \quad (149)$$

$$[S_r] = \begin{bmatrix} 1 & 0 & 0 & 0 & 0 & 0 \\ -\frac{h}{2} & 1 & 0 & 0 & 0 & 0 \\ 0 & 0 & 1 & 0 & 0 & \frac{-hG(1-\nu^2)}{2E} \\ 0 & 0 & 0 & 1 & 0 & 0 \\ 0 & 0 & 0 & 0 & 1 & 0 \\ 0 & 0 & 0 & 0 & 0 & 1 \end{bmatrix}$$

This provides a set of $6(R-1)$ equations for determining the six elements in the R vectors $\{\phi_0\}_r$. The additional six equations are obtained from the boundary conditions in Equation (106) which specify ϕ , θ , and θ' at the end risers.

II.5.e. Iteration Procedure

The iteration procedure which will be used to solve the system of nonlinear equations was outlined briefly in Section II.5.a. A more detailed description is given here. The computer program which performs the calculations is organized along these lines. The process given on the following page refers specifically to the single lap solution. The double lap solution is almost identical. Comments regarding the step lap solution are enclosed in parenthesis.

(A) Input parameters

- (1) Geometry (Steps).
- (2) Loads.
- (3) Material constants.
- (4) Laminate layup.

(B) Compute appropriate constants:

- (1) Adherend stiffnesses [Eq. (60)].
- (2) Differential equation constants p_i [Eq. (71)].
- (3) Characteristic roots [Eq. (119)].
- (4) Coupling coefficients [Eq. (126)].

(This is done for each tread of the step lap.)

(C) Subdivide the joint into a number of stations and set up the $[F(x)]$ and $[F(x)]^{-1}$ matrix at each station:

- (1) Set up $\{f(x)\}$ at each station [Eq. (122)].
- (2) Compute the derivatives at each station [Eq. (128)].
- (3) Set up $[h(x)]$ at each station [Eq. (134)].
- (4) Set up $[H]$ [Eq. (140)] and invert.
- (5) Obtain $[F(x)]$ at each station [Eq. (141)].
- (6) Invert $[F(x)]$ at each station.

(This is done for each tread of the step lap.)

(D) Set up the boundary condition vector [Eq. (146)]:

(For the step lap, set up the continuity condition matrix at each of the intermediate risers [Eq. (148)]. Invert the coefficient matrix. Introduce the boundary conditions [Eq. (106)].)

(E) Initialize all iteration quantities—plastic stresses, plastic stress resultants, equivalent plastic strain, β_{ij} coefficients, and ν_p .

(F) Compute the particular integrals in the differential equation solution:

- (1) Compute the q_i at each station [Eq. (71)].
- (2) Find the vector $\{Q\}$ at each station [Eq. (144)].

- (3) By numerical integration, obtain the particular integrals $\{\phi_p\}$ [Eq. (143)]. This integration is performed by the *QSF* subroutine which is based on Simpson's rule together with Newton's 3/8 rule (see listing for details). Truncation error is of order h^4 , where h is the distance between stations.

(This is done for each tread of the step lap.)

- (G) Compute the adhesive stresses and adherend stress resultants [Eqs. (145) and (12)]:

(For the step lap, insert the computed $\{\phi_p\}$ into the continuity conditions [Eq. (148)]. By matrix multiplication, obtain the unknown elements in the *R* boundary condition vectors $\{\psi_0\}$. Note that the coefficient matrix was inverted in Step (D).)

- (H) Find new values of the plastic stresses and stress resultants at each station:

Adhesive Plastic Stresses

- (1) Obtain the adhesive strains using the previous plastic stresses [Eq. (20)].
- (2) Compute the equivalent strain using the previous ν_p [Eq. (26)].
- (3) Using the constant strain method⁽¹⁾, determine the equivalent stress [Eq. (17)] and, hence, the new E_s and ν_p [Eqs. (21) and (22)].
- (4) Determine the new plastic stresses [Eq. (28)].
- (5) Compute the iteration error as

$$e = \text{Max} \frac{|\sigma_p^k - \sigma_p^{k-1}|}{\sigma}, \quad \sigma \neq 0$$

Adherend Plastic Stress Resultants

- (1) Obtain the strain in each layer using the previous plastic stress resultants [Eqs. (32) and (33)]. For an orthotropic adherend, transform the strain to the principal material directions [Eq. (59)].
- (2) Compute the equivalent strain using the previous β_{ij} [Eq. (53)].
- (3) Using the constant strain method, determine the equivalent stress [Eq. (40)] and, hence, new α_{ij} [Eq. (46)].
- (4) Determine the secant compliance S_{ijS} and stiffness Q_{ijS} elements [Eqs. (50) and (52)].
- (5) Compute the stresses in this layer [Eq. (51)].
- (6) Compute new values for β_{ij} [Eq. (54)].
- (7) Find the plastic stresses [Eq. (56)]. For orthotropic materials, transform plastic stresses to the joint plane [Eq. (57)].

(8) Compute the iteration error as

$$e = \text{Max} \frac{|N_p^k - N_p^{k-1}|}{N_p}, \quad N_p \neq 0$$

(9) Determine the plastic stress resultants [Eq. (62)].

(1) If the maximum error is greater than prescribed, return to Step (F) and continue iteration. Otherwise, iteration is complete and the current stresses are the final values for the prescribed load.

SECTION III

DISCRETE ELEMENT ANALYSIS (DEVELOPMENT)

III.1. GENERAL

To solve the nonlinear composite joint problem by the discrete element method, several assumptions are made:

- (1) The joint is assumed to be in a state of plane strain in the x - y plane (see Fig. 1). This assumption, or that of plane stress, is a practical necessity if any real problem is to be worked with a reasonable computer cost. A three-dimensional analysis is theoretically possible but the number of nodal points increases so rapidly that external storage devices, with a significant increase in cost, would have to be used with the digital computer. It is felt that the plane strain assumption more closely approximates the conditions along the centerline of the joint than the plane stress assumption.
- (2) The adhesive is assumed to be an isotropic material which obeys the Von Mises yield condition and the associated flow rule. The composite material is assumed to be orthotropic with transverse isotropy, i.e., isotropic in a plane perpendicular to the fibers. Superposition of plastic strains is assumed valid so that, for example, the plastic strain in the z direction resulting from a stress in the x direction is independent of the other stress levels.
- (3) Deformation theory of plasticity is assumed valid.

III.2. CONSTITUTIVE EQUATIONS

III.2.a. Isotropic Material, Plane Strain

The adhesive material is considered to be an isotropic material in a state of plane strain in the x - y plane. Stresses and strains in the adhesive are represented by

$$\begin{aligned} \{\sigma_x\}^T &= \{\sigma_x \quad \sigma_y \quad \sigma_z \quad \tau_{xz} \quad \tau_{zy} \quad \tau_{xy}\} \\ \{\epsilon_x\}^T &= \{\epsilon_x \quad \epsilon_y \quad \epsilon_z \quad \gamma_{xz} \quad \gamma_{zy} \quad \gamma_{xy}\} \end{aligned} \quad (150)$$

where x - y is the longitudinal cross-section plane of the joint so that $\epsilon_z = \gamma_{xz} = \gamma_{zy} = 0$ for plane strain. One can write the total strains $\{\epsilon_x\}$ as the sum of the elastic and plastic strains, i.e.,

$$\{\epsilon_x\} = \{\epsilon_x\}_e + \{\epsilon_x\}_p \quad (151)$$

It will be noted that, in order to write (151), ϵ_z , the strain perpendicular to the longitudinal cross-section plane of the joint, must be included. Thus,

$$\{\epsilon_x\}_e^T = \{\epsilon_{xe} \quad \epsilon_{ye} \quad \epsilon_{ze} \quad \gamma_{xze} \quad \gamma_{zye} \quad \gamma_{xye}\} \quad (152)$$

and, similarly, for $\{\epsilon_x\}_p^T$. Therefore, though the total strains vanish

$$\epsilon_z = \gamma_{xz} = \gamma_{zy} = 0 \quad (153)$$

for plane strain, this does *not* imply that the elastic and plastic strains, separately, vanish

$$\left. \begin{aligned} \epsilon_{ze} = \gamma_{xze} = \gamma_{zye} &= 0 \\ \epsilon_{zp} = \gamma_{xzp} = \gamma_{zyp} &= 0 \end{aligned} \right\} \text{NOT TRUE}$$

For the isotropic material, since there is no shear coupling, it happens that the elastic and plastic shear strains are zero, although ϵ_{ze} and ϵ_{zp} are, in general, not zero. For the orthotropic material which has shear coupling, the elastic and plastic shear strains will not, in general, be zero.

By Hooke's law, the stresses can be found as

$$\{\sigma_x\} = [C] \{\epsilon_x\}_e \quad (154)$$

in which

$$[C] = \frac{E}{(1+\nu)(1-2\nu)} \begin{bmatrix} 1-\nu & \nu & \nu & 0 & 0 & 0 \\ & 1-\nu & \nu & 0 & 0 & 0 \\ & & 1-\nu & 0 & 0 & 0 \\ & & & \frac{(1-2\nu)}{2} & 0 & 0 \\ & & & & \frac{(1-2\nu)}{2} & 0 \\ \text{Symmetric} & & & & & \frac{(1-2\nu)}{2} \end{bmatrix}$$

where E and ν are the elastic modulus and Poisson's ratio, respectively. The material is assumed to obey the Von Mises yield condition. By the deformation theory of plasticity,

$$\{\epsilon_x\}_p = [S]_p \{\sigma_x\} \quad (155)$$

in which

$$[S]_p = \frac{\bar{\epsilon}_p}{\bar{\sigma}} \begin{bmatrix} 1 & -\frac{1}{2} & -\frac{1}{2} & 0 & 0 & 0 \\ & 1 & -\frac{1}{2} & 0 & 0 & 0 \\ & & 1 & 0 & 0 & 0 \\ & & & 3 & 0 & 0 \\ \text{Symmetric} & & & & 3 & 0 \\ & & & & & 3 \end{bmatrix}$$

where

$$\bar{\sigma} = \left\{ \frac{1}{2} [(\sigma_x - \sigma_z)^2 + (\sigma_z - \sigma_y)^2 + (\sigma_y - \sigma_x)^2] + 3[\tau_{xz}^2 + \tau_{zy}^2 + \tau_{xy}^2] \right\}^{1/2}$$

is the effective stress and $\bar{\epsilon}_p$ is the effective plastic strain which may be found from the material stress-strain curve in uniaxial stress. If the Ramberg-Osgood law⁽²⁾ is used to approximate the stress-strain curve, one has

$$\bar{\epsilon} = \frac{\bar{\sigma}}{E} + \frac{3\sigma_0}{7E} \left(\frac{\bar{\sigma}}{\sigma_0} \right)^n \quad (156)$$

in which

σ_0 = secant yield stress (stress at which the secant modulus = $0.7E$)

$$n = \text{shape factor} = 1 + \frac{\log\left(\frac{17}{7}\right)}{\log\left(\frac{\sigma_0}{\sigma_1}\right)}$$

where

σ_1 = stress at secant modulus at $0.85E$

According to the constant strain method⁽²⁾, the effective plastic strain $\bar{\epsilon}_p$ for a given total effective strain $\bar{\epsilon}$ can be found from Equation (156) if it is rewritten as

$$\bar{\epsilon} = \left(\frac{7\bar{\epsilon}_p}{3}\right)^{1/n} \left(\frac{\sigma_0}{E}\right)^{1 - \frac{1}{n}} + \bar{\epsilon}_p \quad (157)$$

The above expressions could be simplified slightly by eliminating the elastic and plastic shearing strains γ_{xz} and γ_{zy} since this is an isotropic material. However, in order to keep the development parallel to the orthotropic case, they are included.

III.2.b. Orthotropic Material, Plane Strain

One ply (or lamina) of the adherend composite material, Figure 6, is assumed to be orthotropic. The principal material directions are ℓ - t - y where ℓ is parallel to the fiber direction. Stress and strains in the principal material directions are

$$\begin{aligned} \{\sigma_\ell\}^T &= \{\sigma_\ell \quad \sigma_t \quad \sigma_y \quad \tau_{\ell t} \quad \tau_{\ell y} \quad \tau_{ty}\} \\ \{\epsilon_\ell\}^T &= \{\epsilon_\ell \quad \epsilon_t \quad \epsilon_y \quad \gamma_{\ell t} \quad \gamma_{\ell y} \quad \gamma_{ty}\} \end{aligned} \quad (158)$$

The composite is assumed to be isotropic in the t - y plane.

Separating the total strain into its elastic and plastic components, one can write

$$\{\epsilon_\ell\} = \{\epsilon_\ell\}_e + \{\epsilon_\ell\}_p \quad (159)$$

Using Hooke's law, one obtains the stresses as

$$\{\sigma_\ell\} = [C] \{\epsilon_\ell\}_e \quad (160)$$

Note: Right-Hand Coordinate System for: $x(1), z(2), y(3)$, and $t(1), u(2), v(3)$

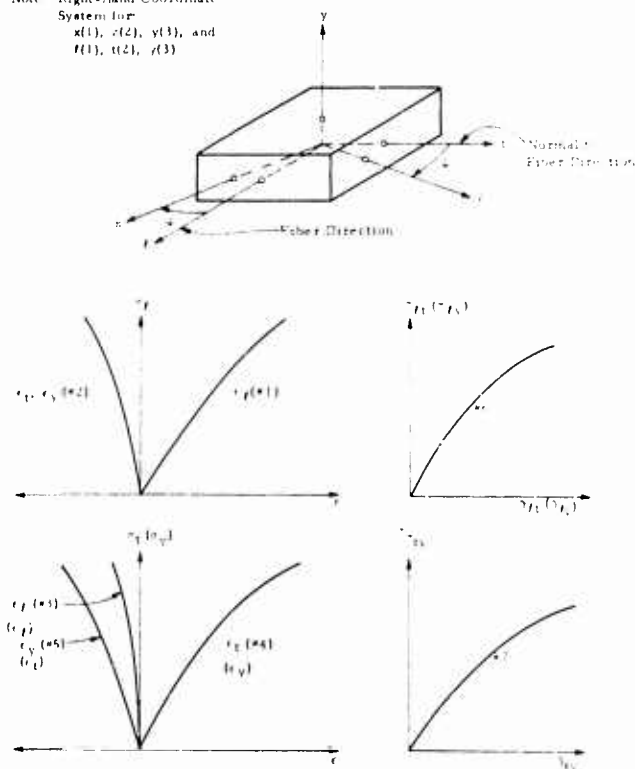


FIGURE 6. ORTHOTROPIC LAMINA COORDINATES ℓ, t, y AND STRESS-STRAIN CURVES FROM UNI-AXIAL TEST IN PRINCIPAL DIRECTIONS

where

$$[C] = \begin{bmatrix} \frac{1}{E_1} & \frac{1}{E_1} & \frac{1}{E_1} & 0 & 0 & 0 \\ & \frac{1}{E_2} & \frac{1}{E_2} & 0 & 0 & 0 \\ & & \frac{1}{E_3} & 0 & 0 & 0 \\ & & & \frac{1}{E_4} & 0 & 0 \\ & & & & \frac{1}{E_5} & 0 \\ \text{Symmetric} & & & & & \frac{1}{E_6} \end{bmatrix}$$

All the E_i values are lamina elastic constants (some negative) which are obtained as the initial slope of the i th curve in Figure 6.

According to assumption (2) in Section III.1, it is assumed that the plastic strains can be found by superposition, e.g.:

$$\epsilon_{\psi p} = \epsilon_{\psi p} + \epsilon_{\psi tp} + \epsilon_{\psi yp}$$

where $\epsilon_{\psi tp}$ is the longitudinal plastic strain corresponding to the stress σ_t as found from the simple uniaxial test. Let the stress-strain relations from uniaxial tests of a typical lamina be as given in Figure 6. Each of the seven curves can be approximated by a Ramberg-Osgood relation of the form

$$\epsilon = \frac{\sigma}{E_i} + \frac{3\sigma_{0i}}{7E_i} \left(\frac{\sigma}{\sigma_{0i}} \right)^{n_i} \quad (161)$$

where ϵ and σ are the appropriate stress and strain for each curve, E_i is the initial slope of the curve, σ_{0i} and n_i are the quantities corresponding to those given in Equation (156) and i refers to the curve number as given in Figure 6. The plastic strains can now be written as*

$$\begin{Bmatrix} \epsilon_{\psi p} \\ \epsilon_{tp} \\ \epsilon_{yp} \\ \gamma_{\psi tp} \\ \gamma_{ty p} \\ \gamma_{y\psi p} \end{Bmatrix} = \frac{3}{7} \begin{Bmatrix} \frac{\sigma_{01}}{E_1} \left(\frac{\sigma_t}{\sigma_{01}} \right)^{n_1} + \frac{\sigma_{03}}{E_1} \left(\frac{\sigma_t}{\sigma_{03}} \right)^{n_3} + \frac{\sigma_{05}}{E_1} \left(\frac{\sigma_t}{\sigma_{05}} \right)^{n_5} \\ \frac{\sigma_{02}}{E_2} \left(\frac{\sigma_t}{\sigma_{02}} \right)^{n_2} + \frac{\sigma_{04}}{E_2} \left(\frac{\sigma_t}{\sigma_{04}} \right)^{n_4} + \frac{\sigma_{06}}{E_2} \left(\frac{\sigma_t}{\sigma_{06}} \right)^{n_6} \\ \frac{\sigma_{03}}{E_3} \left(\frac{\sigma_t}{\sigma_{03}} \right)^{n_3} + \frac{\sigma_{05}}{E_3} \left(\frac{\sigma_t}{\sigma_{05}} \right)^{n_5} + \frac{\sigma_{07}}{E_3} \left(\frac{\sigma_t}{\sigma_{07}} \right)^{n_7} \\ \frac{\sigma_{06}}{E_6} \left(\frac{\tau_{\psi t}}{\sigma_{06}} \right)^{n_6} \\ \frac{\sigma_{07}}{E_7} \left(\frac{\tau_{ty}}{\sigma_{07}} \right)^{n_7} \\ \frac{\sigma_{08}}{E_8} \left(\frac{\tau_{y\psi}}{\sigma_{08}} \right)^{n_8} \end{Bmatrix} \quad (162)$$

*The plasticity theory used here for orthotropic materials is different than that employed in the theoretical methods. The "best" theory has not yet been established by experiments. As the results from the two theories show (see the following section), the difference is insignificant.

The transformation relating the plane strain strains in the x - y plane to the strains in the principal material directions x - y can be written as

$$\{\epsilon_q\} = [T] \{\epsilon_x\} \quad (163)$$

where $\{\epsilon_q\}$ and $\{\epsilon_x\}$ are given in Equations (153) and (150), respectively, and $[T]$ is a 6×3 matrix:

$$[T] = \begin{bmatrix} \cos^2 \psi & 0 & 0 \\ \sin^2 \psi & 0 & 0 \\ 0 & 1 & 0 \\ -2 \sin \psi \cos \psi & 0 & 0 \\ 0 & 0 & -\sin \psi \\ 0 & 0 & \cos \psi \end{bmatrix}$$

in which ψ is the angle of fiber orientation as shown in Figure 6.

III.3. ELEMENT STIFFNESS MATRIX AND PLASTIC FORCES

After the constitutive equations have been defined in the above manner, the solution of the discrete element problem follows very closely the procedure outlined for ELPLAN⁽⁴⁾, a computer program for the inelastic analysis of plane stress problems. A typical finite element is taken to be a triangle in the longitudinal cross-section plane of the joint (x - y plane) with a unit thickness, Figure 7. The following expressions are obtained for the element stiffness matrix $[k]$ and the plastic nodal forces $\{f_p\}$ for the composite material:

$$[k] = \bar{A} [B]^T [T]^T [C] [T] [B] \quad (164)$$

$$\{f_p\} = [D] \{\epsilon_q\}_p \quad (165)$$

$$[D] = \bar{A} [B]^T [T]^T [C] \quad (166)$$

in which $[T]$ is given in Equation (163), $[C]$ in Equation (160), $\{\epsilon_q\}_p$ in Equation (162) and \bar{A} is the element area in the x - y plane. The matrix $[B]$ relates the element strains to the nodal displacements $\{X\}^{(4)}$, i.e.,

$$\{\epsilon_x\} = [B] \{X\} \quad (167)$$

The stresses in a composite element in the principal material directions are

$$\{\sigma_q\} = [C] ([T] [B] \{X\} - \{\epsilon_q\}_p) \quad (168)$$

The above expressions apply also to the isotropic adhesive material although they can be slightly simplified. For programming purposes, it is convenient to use the same algorithm for the isotropic and orthotropic materials. In this regard, Equations (164), (165), (166), (167), and (168) are valid for the

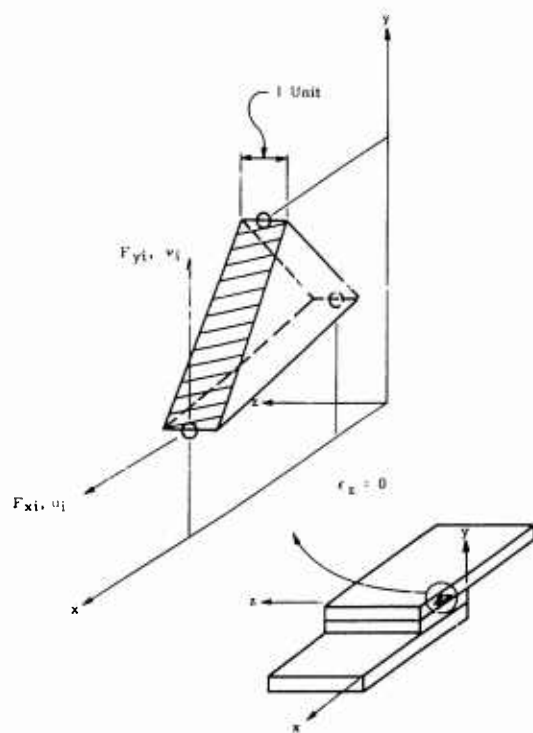


FIGURE 7. PLANE STRAIN DISCRETE ELEMENT USED FOR NONLINEAR JOINT ANALYSIS

adhesive if ψ is taken equal to zero in $[T]$. Then $[C]$ is found in Equation (154), and Equation (155) is used for the plastic strains.

The solution of the discrete element problem proceeds, according to deformation theory, in the following manner:

- (1) Formulate the structural stiffness matrix $[K]$ by assembling the element stiffness matrices in (164) and the applied nodal load matrix $\{F\}$ as specified by the loading.
- (2) Perform an elastic analysis with the current values of $\{F_p\}$ to obtain the nodal displacements $\{X\}$:

$$\{F\} + \{F_p\} = [K] \{X\}$$

For the initial iteration, $\{F_p\} = \{O\}$.

- (3) Calculate the stresses via Equation (168) with the current values of $\{\epsilon_q\}_p$, $\{\epsilon_q\}_p = 0$ for the first iteration.
- (4) Calculate the new plastic strains via Equation (162) for the composite or (155), (156), and (157) for the adhesive.
- (5) Consider the new plastic strains as initial strains and compute new values of the element plastic forces $\{f_p\}$ by Equation (165). Assemble the element plastic forces into the structural plastic forces $\{F_p\}$.
- (6) If the maximum change in plastic strain from the previous iteration is sufficiently small, the solution is complete. If not, return to Step 2.

This process was incorporated into ELPLAN. The application of the resulting program is discussed in a later section.

SECTION IV

COMPARISON OF THEORETICAL AND DISCRETE ELEMENT RESULTS

IV.1. JOINT CONFIGURATIONS AND MATERIAL PROPERTIES

In order to compare the theoretical and discrete element analysis methods, the three particular joint configurations shown in Figure 8, i.e., single lap, double lap, and step lap, were analyzed by both methods. The Narmco 5505 Boron/Epoxy System was taken as the adherend and AF-126-2 as the adhesive. The adherend was a

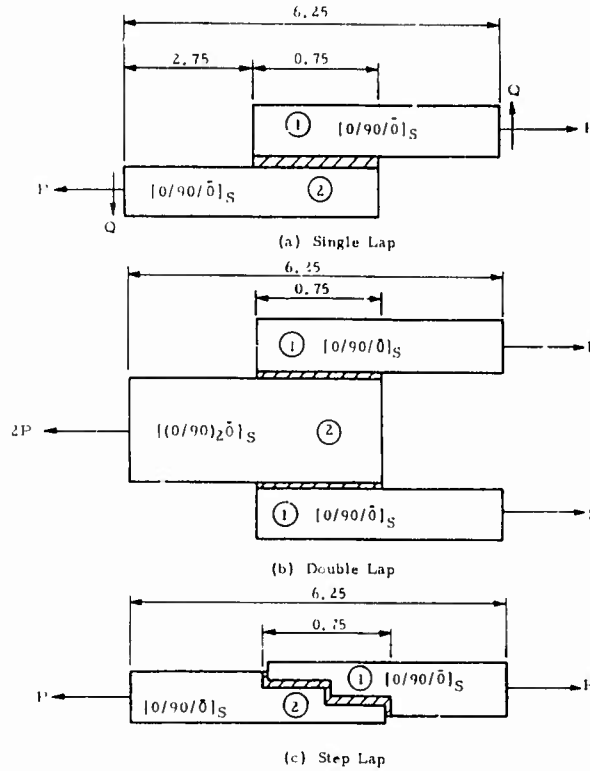


FIGURE 8. JOINT CONFIGURATIONS FOR
COMPARISON OF ANALYSIS METHODS

five-ply laminate (nominal ply thickness 0.0052 in.) with 0° , 90° , 0° , 90° , 0° orientations, except for the inner laminate of the double lap which had nine plies with $0/90$ orientations. In each case, the joint length, c , was 0.75 in., and the total length, a , was 6.25 inches. The adhesive thickness was 0.005 inch.

The material properties used in the Ramberg-Osgood approximation [Eq. (156)] of the adhesive *shear* stress-strain curve are shown in Table I. Poisson's ratio of the adhesive was taken as 0.3. The material constants for the characterization of a typical lamina of an adherend are also given in Table I. They represent the Ramberg-Osgood constants in Equation (161) for the uniaxial stress-strain curves in Figure 6. The stress-strain curve for AF-126-2 was not available at the time of the comparison, but those values shown in Table I were thought to be appropriate.⁽⁵⁾ More recent work shows that the shear modulus is about 80 ksi⁽⁶⁾ instead of the 175 ksi value shown in Table I and used in the analysis. Since consistent material properties were used in both analysis methods, the results of the comparison study will remain valid, however. Stress-strain curves for the Narmco 5505 were obtained from Reference 7. Curves 5 and 7 for lamina characterization in a plane perpendicular to the fibers were not available. These curves were assumed to be identical to those of the transverse unidirectional lamina. Many of the curves for the lamina were quite linear to failure, and, thus, do not reach the stress σ_0 which corresponds to a secant modulus of $0.7E$. In these cases, the value of σ_0 and n were determined such that the Ramberg-Osgood approximation passed

TABLE I.

MATERIAL CONSTANTS FOR RAMBERG-
OSGOOD APPROXIMATION

Adhesive (AF-126-2)			
	G (ksi)	τ_0 (ksi)	n
τ vs γ	175	3.32	2.684
Adherend (Narmco 5505)			
Curve (i) of Figure 6	E_i (ksi)	σ_{0i} (ksi)	n_i
1 σ_x vs ϵ_x	29,600	312.7	4.463
2 σ_x vs ϵ_y (ϵ_y)	-130,000	285.5	5.129
3 σ_y vs ϵ_y	-130,000	285.5	5.129
4 σ_y vs ϵ_x (ϵ_x)	2,750	11.91	2.541
5 σ_y vs ϵ_y (ϵ_y)	-8,876	10.52	3.350
6 τ_{xy} vs γ_{xy}	933	7.95	2.991
7 τ_{xy} vs γ_{yx}	191	68.44	2.031

through two points on the upper nonlinear portion of the stress-strain curves. For an isotropic material, the solution for n and σ_0 is

$$n = \frac{\left(\frac{E\epsilon' - \sigma'}{E\epsilon'' - \sigma''} \right)}{\left(\frac{\sigma'}{\sigma''} \right)}$$

$$\sigma_0 = \left[\frac{7}{3} (E\epsilon'' - \sigma'') (\sigma')^n \right]^{\frac{1}{1-n}}$$

where (σ', ϵ') and (σ'', ϵ'') are two points on nonlinear portion of the stress-strain curve.

IV.2. JOINT ANALYSIS

IV.2.a. Discrete Element Analysis

The three joints shown in Figure 8 were analyzed by the discrete element computer program discussed in Section III. The finite element idealization of the single, double, and step lap joint are shown in Figures 9, 10, and 11, respectively. Joint boundary conditions are illustrated schematically in these figures. Material properties listed in Table I were used.

Results from the discrete element analysis for the shear and normal stress in the adhesive are presented as circled points in Figures 12, 13, and 14 for the single, double, and step lap joints, respectively. The discrete element program evaluates the stresses at the centroid of each triangular element. Hence, the stresses are evaluated at 1/3 and 2/3 thickness levels in the adhesive. In order to compare results with the theoretical method, these stresses were averaged to obtain the stress at midthickness. The discrete element program did not converge to the specified error tolerance of 0.01 within 20 iterations for step lap joint loads greater than 1000 lb/inch. This was caused by large plastic laminate strains developing in the stress concentration area at the juncture of a tread and a riser. (Note the change in the stress scale for the step lap joint as compared to that of the single and double lap joints.)

IV.2.b. Theoretical Analysis

The theoretical analysis technique outlined in Section II and programmed for the CDC 6400 computer was also used to analyze the joints in Figure 8. In addition to the geometric quantities, the adhesive material constants and the adherend material constants for Curves 1, 2, 4, and 6 from Table I were input into the program. These four curves for the adherend correspond to the four curves in Figure 3 and the four Equations (41a, b, c, and d). For the numerical integration involved in this solution, the single lap and double lap were subdivided into 20 equal segments (21 stations) along the joint. Each tread of the step lap was subdivided into 30 equal segments. The results of the theoretical analysis are presented as the curves in Figures 12, 13, and 14 for the three joints.

IV.2.c. Discussion

Despite the different assumptions involved in the finite element method and the analytical method, i.e., plastic strain superposition for the finite element method versus deformation theory for the analytical method and three dimensional stresses in the finite element method versus negligible shear deformation in the adherends for the analytical method, the comparison of the results in Figures 12 and 13 is quite good for the adhesive shear stress in the single and double lap joint. The difference in the two methods for the step lap joint adhesive shear (Fig. 14) is probably due to both of the following two causes:

- Shear deformation is neglected in the adherends for the theoretical method. For the step, the adhesive is attached to the 90-degree oriented layers. The shear modulus of these layers in the plane of the joint is only 191 ksi (see Table I), which is about equal to that of the adhesive itself.
- Transmission of force through the step risers is neglected in the theoretical method. Hence, the total force is transmitted by shear along the treads. Thus, the average shear stress for the theoretical method is about $1000/0.75$ or 1333 psi, whereas it is lower for the discrete element method since some force is transmitted through the risers.

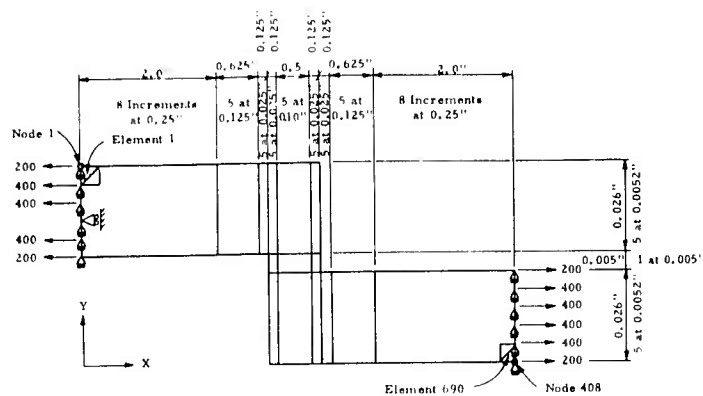


FIGURE 9. DISCRETE ELEMENT LAYOUT FOR SINGLE LAP JOINT

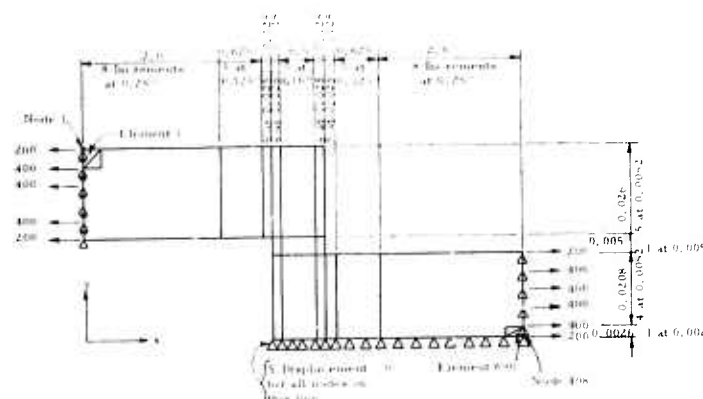


FIGURE 10. DISCRETE ELEMENT LAYOUT FOR DOUBLE LAP JOINT

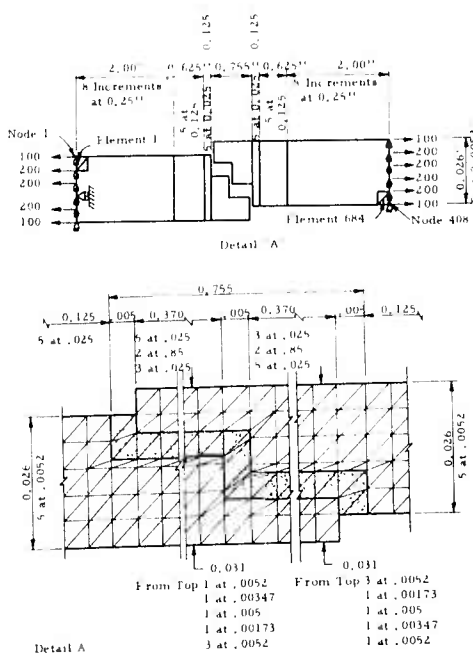


FIGURE 11. DISCRETE ELEMENT LAYOUT FOR STEP LAP JOINT

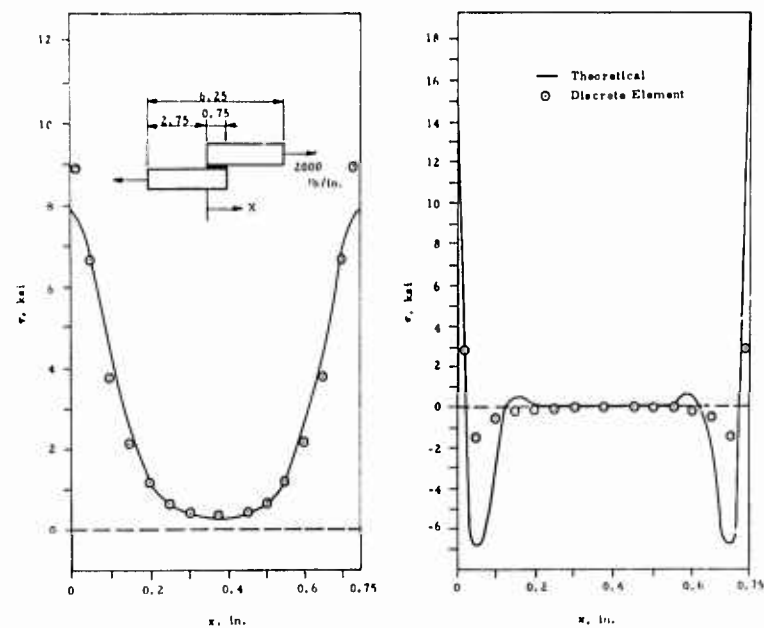


FIGURE 12. ADHESIVE STRESS, SINGLE LAP JOINT

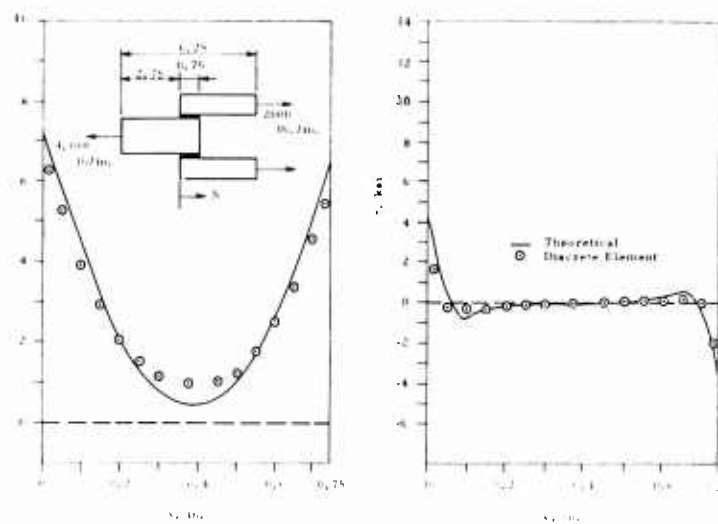


FIGURE 13. ADHESIVE STRESS, DOUBLE LAP JOINT

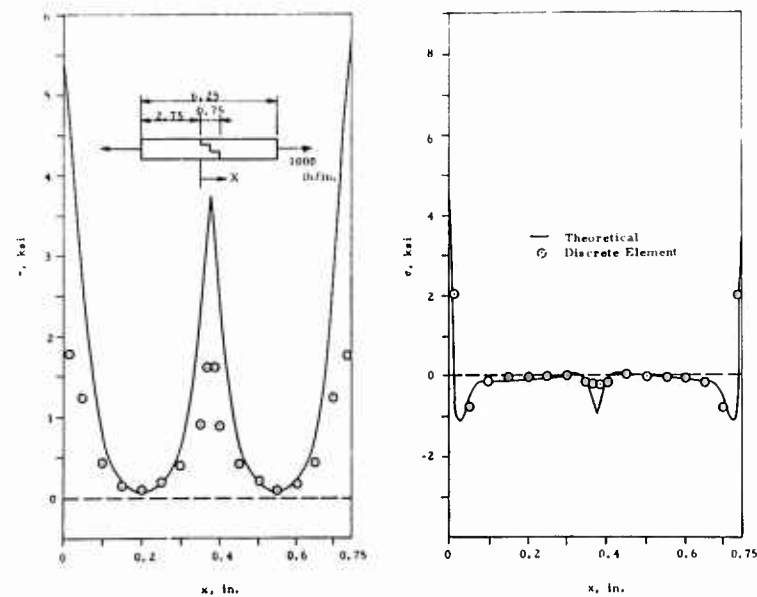


FIGURE 14. ADHESIVE STRESS, STEP LAP JOINT

According to Equation (122), the normal stress varies approximately as a damped cosine (and sine) curve with a period of length

$$L = \frac{2\pi}{\omega} \quad (169)$$

where, approximately,

$$\omega = \left[\frac{E}{4t(1-\nu^2)} \left(\frac{1}{D_1} + \frac{1}{D_2} \right) \right]^{1/4} \quad (170)$$

These conditions are exact for the special case of equal adherends in the single lap—see Section II.2. For the single, double, and step lap joints, the cyclic period, L , of the normal stress is 0.189 in., 0.224 in., and 0.084 in., respectively. (Note that $1/D_2 = 0$ for the double lap.) The discrete elements in the region of the adhesive were 0.025 in. long. These were not sufficiently small to pick up the rapid variation of the normal stress since the method is based on an assumed constant stress in each element. The theoretical method is somewhat limited in this regard also because of the numerical integration involved. However, the integration is performed according to Simpson's rule which is based on a parabolic approximation to the integrand. The error for the discrete element method is about h^2 and about h^5 for the theoretical method where h is the interval spacing. Thus, the normal stresses obtained by the theoretical method are probably more reliable than those from the discrete element method.

Although extensive calculations were not conducted for verification, it is thought that the interval for the numerical integration in the theoretical method should be no greater than about $L/2\pi$ or $1/\omega$. (For the examples above, the intervals were $L/5.0$, $L/6.0$, and $L/6.8$ for the single, double, and step lap, respectively.

SECTION V

EXPERIMENTAL DESIGN

V.1. GENERAL

This section presents the study of bonded joint data taken from the literature followed by the design of the experimental program to verify the theory of Sections II, III, and IV. Section V.2 presents the Literature Study covering six information data sources to establish statistical techniques for experimental data analysis and provide experimental design information. Section V.3 presents Trial Effective Properties Prediction for the elastic case utilizing the methods developed in the previous three sections. Design of the Experimental Program presented in Section V.4 provides the detailed history of the specimen selection and design which were used for verification of the new analytical methods in subsequent sections.

V.2. LITERATURE SURVEY

An example development of single and double lap joint experimental data analysis is presented in this section. It was accomplished by the study and analysis of test data from three sources: Douglas, IITRI, and SwRI. Preliminary analysis of the more limited data from two additional sources, Martin-Orlando and Grumman is also included. Two composite materials, boron/epoxy and S-glass/epoxy of several orientations were utilized as the primary adherend materials in the data studied in detail and they were bonded to the same materials or to aluminum, titanium or woven E-glass/epoxy secondary adherends. For the two sources of data studied in preliminary fashion, Grumman used composite and metal adherends while Martin-Orlando used only metal.

The data collection and analysis effort had two primary objectives: a gross characterization of the "effective" properties of the various adhesives, and a meaningful estimate of the general test precision in order to establish guidelines for the experimental effort. Pertinent data from all five sources [i.e., Dastin of Grumman⁽⁸⁾, Lehman of McDonnell-Douglas⁽⁹⁾, Chessin and Curran of Martin-Orlando⁽¹⁰⁾, Kutsche of IITRI⁽¹¹⁾, and Grimes of SwRI⁽¹²⁾] yielded lap joint test data in quantities sufficient for meaningful analysis. The Martin-Orlando data on metal adherend-bonded lap joints were included for comparative purposes. It should be noted that the Martin-Orlando data covered only one type of variable in their tests, the adherend surface preparation. While this variation caused a larger range of failure stress magnitudes than would be expected with one chosen surface preparation, the standard deviation was comparable to that of the Douglas, IITRI, and SwRI data which had variable overlap lengths and the Grumman data which used several different adhesives.

The data analysis consisted of two sequential steps: the generation of reliable precision estimates in order that confidence intervals might be established for the various mean failure stress measurements, and the subsequent use of these intervals to establish a reasonable range of apparent material properties as a function of the joint configuration for experimental design and data analysis purposes. The analysis work concentrated on the average apparent adhesive shear stress failure measurement, the average adherend tensile failure stresses, and on the running loads transferred in lb/in./ply. The generation of precision estimates was complicated generally by the scarcity of such estimates in the literature and specifically by the wide variance in test parameters among the five major data sources. As an example, it can be seen that, for the various parameters by which the data were tabulated, not a single instance can be found in which two different sources ran an identical test. This, of course, means that interlaboratory reproducibility could not be estimated.

On the other hand, the data collected did prove sufficient for estimating the intralaboratory repeatability, provided that analysis was approached via a method now under study for publication by ASTM Committee D2. This procedure is designed specifically for the generation of precision estimates from data in which

- (1) the standard deviation appears to vary with the mean rating of the various samples, and
- (2) only relatively small amounts of data are available on any one sample.

This is precisely the case with the lap joint data collected. The first step in the process was to calculate the standard deviations for the individual samples. Following this, a decision had to be made concerning grouping of the data, e.g., of the various parameters in the tabulation; how many should one group together? In this case, the decision was fairly easy, since groups broken down any further than source and test type would be too small to be useful. Hence, the data were divided into these six groups:

Single Lap	Douglas—(adherend materials and overlap length variations)
	Grumman—(adherend material and adhesive type variations)
	Martin-Orlando—(adherend material surface preparation variation)
Double Lap	Douglas—(adherend material and overlap length variation)
	SwRI—(adherend material and overlap length variation)
	IITRI—(adherend material, adhesive, and overlap length variation)

Linear regression lines resulting from plots of standard deviation vs mean adhesive shear stress failure for each of these six groups* are presented in Figures 15 and 16. These straight lines were fitted to the data points by linear regression techniques which represent the best estimates of the overall test (or population) standard deviations for each of the six groups. The advantage of the above approach is that a large number of degrees of freedom can be utilized in the estimating procedure rather than the small number available in the few data points actually falling at a given level. This gives a much more realistic calculation for confidence intervals and provides a means of looking at data trends with respect to the variables encountered.

The difference between Figures 15 and 16 is the inclusion and exclusion, respectively, of the Metalbond 400 data in those analyzed from IITRI. When the Metalbond 400 data is removed from the balance of the IITRI data, the standard deviation vs mean line falls on top of all the rest of the data except for the Douglas single lap data. These two groups of data were obviously out of control in some fashion. It could have been the material, processing or testing; however, the important point is that the statistical technique picked it up.

Before dealing with confidence intervals, a study of the trends is shown in Figure 16 with the standard deviation estimates for all six data groups given on the same plot. Here it can be seen that, at mean adhesive shear stress failure levels in the area of 3,000 psi, the standard deviations for all but one are approximately equal. Considering that the experimental parameters varied a great deal in these tests, and that the double lap data behaved (statistically) much like two of the three single lap groups the general variance to be expected for both groups appears to be about the same at any mean level, regardless of the adhesive type, adherend combination, overlap length, etc.

Calculation of the confidence intervals for the population mean adhesive shear stress failure levels consists of using the regression line standard deviation estimate in the following formula:

$$95\% \text{ Confidence Limits at } f_s = \bar{f}_s \pm \frac{ts}{\sqrt{n}} \quad (171)$$

where \bar{f}_s is the average of these experimentally determined mean adhesive failure stresses, n is the number of determinations, s is standard deviation, and t is the t -deviate corresponding to the number of degrees of freedom involved in the regression line estimate of the standard deviation (not n). These limits define the interval within which the mean of a very large number of tests would probably lie relative to the mean of this experimental data.

With the confidence limits established, it is possible to calculate 95% confidence design allowables in the following manner:

$$DA_{95} = LCL - ts \left(\frac{1}{\sqrt{n}} + 1 \right) \quad (172)$$

*Using ASTM E-178 (Ref 13) for the deletion of "outlier points."

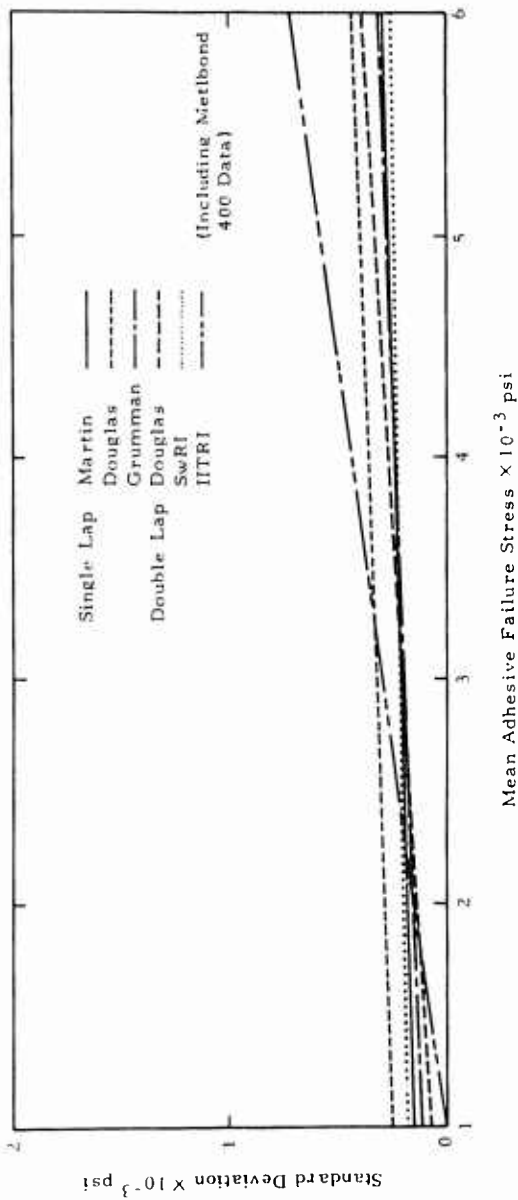


FIGURE 15. STANDARD DEVIATION VS MEAN ADHESIVE FAILURE STRESS—COMPARISON

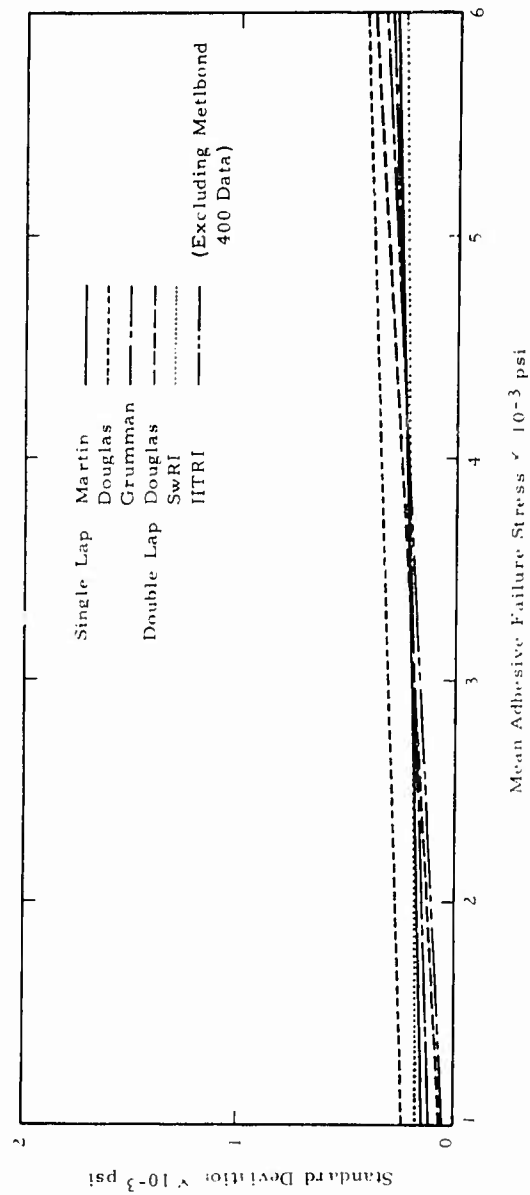


FIGURE 16. STANDARD DEVIATION VS MEAN ADHESIVE FAILURE STRESS—COMPARISON

where $LCL = \bar{f}_s - (ts/\sqrt{n})$ is the lower confidence limit and t , n and s have the same definitions as above. In essence, this calculation says that, if the population mean \bar{f}_s did turn out to be at the lower confidence level, then about 5 of 100 specimens would fail at the design allowable stress level or lower. This is a conservative estimate; the real failure probabilities should be more favorable.

In the Douglas, IITRI and SwRI data groups, overlap lengths were varied, hence, it was possible to plot mean failure stress (or unit load) vs overlap lengths for various composite materials and joint types. These mean experimental plots are presented in Figures 17 through 28.

The data analyses performed on the unit running loads per ply transferred were essentially a reiteration of those described above for adhesive failure stresses. Linear regression lines based on plots of standard deviation vs mean running load transferred in lb/in./ply for four of the five groups mentioned (the Martin-Orlando tests being on metal adherends were omitted) are presented in Figure 29. Because the adhesive failure stress and the running load are both calculated at the failure point and thus have a proportional relationship, it should be noted that their linear regressions look much alike. Only the Douglas single lap data regressions showed any appreciable difference in slope, and this is most probably due to the following related factors:

- (1) These data generally showed a significantly higher variance than did the other groups
- (2) The accuracy of the regression line slope as an estimator of the corresponding population statistic is inversely proportional to the average magnitude of the sample variance involved.

Thus, the different slope indicated for the Douglas single lap data may well be apparent rather than real, although Figure 29 shows that the standard deviations for all but the Douglas single lap data are approximately equal at a loading of 500 lb/in./ply.

Several interesting phenomena can be seen from study of this data. The lower curves in Figure 25 showed that a weak interface region is detrimental to composite bonded joints. The cause of this could be high adhesive viscosity at flow temperature (occurring during cure), i.e., a material quality problem, probably aging. Also, it can be seen from Figures 30 through 33 that a comparison of the plots of mean vs standard deviations for shear stress and load/ply transferred are very similar (as would be expected) except for the Douglas single lap data. In Figure 34 the coefficient of variation line slope and location are considerably different from that of the standard deviation. Because of this the coefficient of variation is less desirable as a design tool than is the standard deviation. Finally, a plot of the 95% confidence limits of the failure stresses for the Martin-Orlando data showing controlled variations in processing are significant is presented in Figure 35. This is because all the data are shown to be consistent (under control) even though the difference in the magnitude of the mean stresses is quite large as a result of different processing techniques. It illustrates that the right processing technique should be chosen and kept under close control.

Illustrations of plots of 95% confidence limits vs mean failure magnitudes are shown in Figures 36 through 40. In Figure 36 the shear stresses for the IITRI data are presented in this fashion while Figures 37 through 40 present the SwRI, Douglas, and Grumman data in terms of lb/in./ply of running load transferred.

From the study of these data from the literature, techniques have been established to analyze similar experimental information on bonded joints for acceptable scatter limits (confidence limits) for the 95% confidence level when the number of like test points are limited.

V.3. TRIAL EFFECTIVE PROPERTIES PREDICTION⁽¹⁴⁾

Utilizing the mean data from Figure 23 on a 1/2-inch overlap double lap joint with a 14-ply $[0]_c$ adherend made of Scotchply XP-251S the shear stress distribution was calculated for three assumed bondline shear moduli values. The G values for which τ_x distribution will be computed are 160, 90, and 40 ksi.

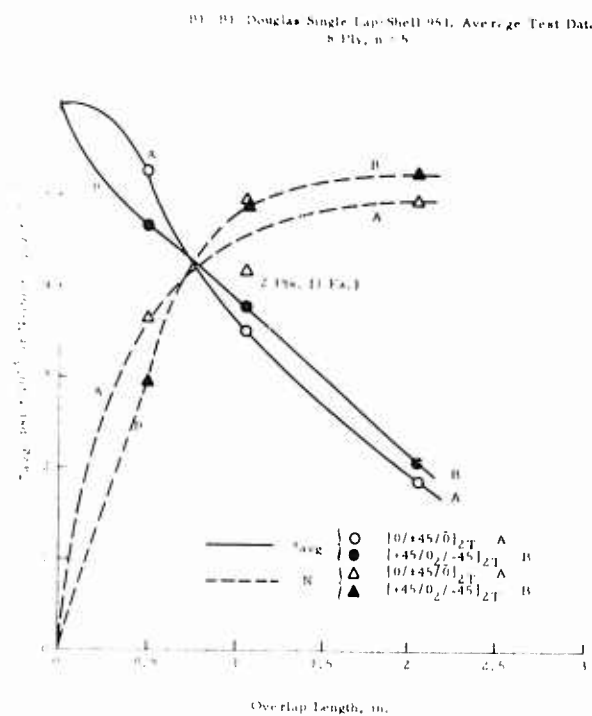


FIGURE 17. BE/BE DOUGLAS SINGLE LAP/SHELL 951

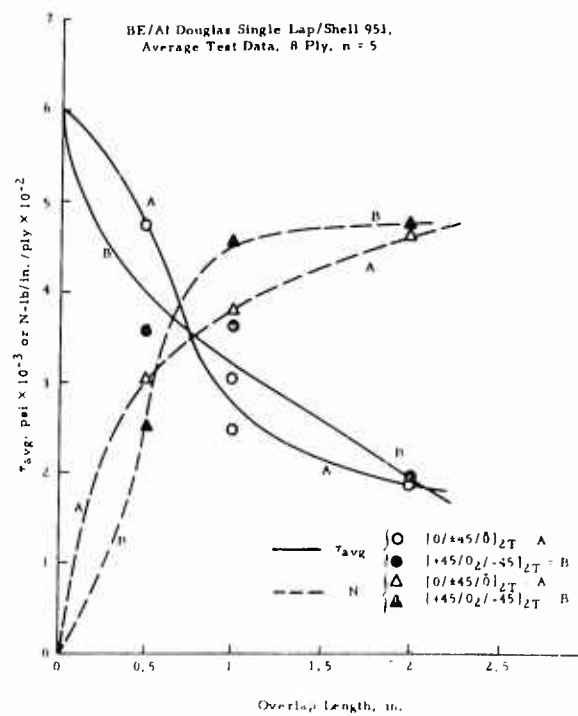


FIGURE 18. BE/AL DOUGLAS SINGLE LAP/SHELL 951

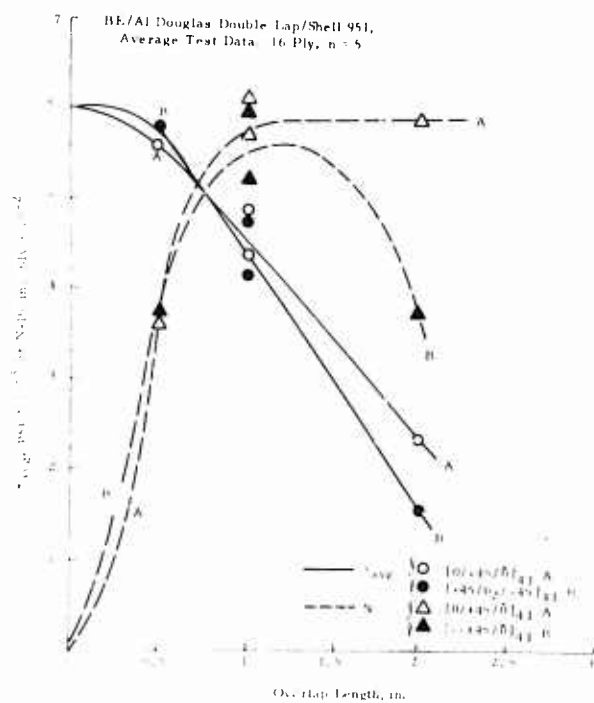


FIGURE 19. BE/AL DOUGLAS DOUBLE LAP/SHELL 951

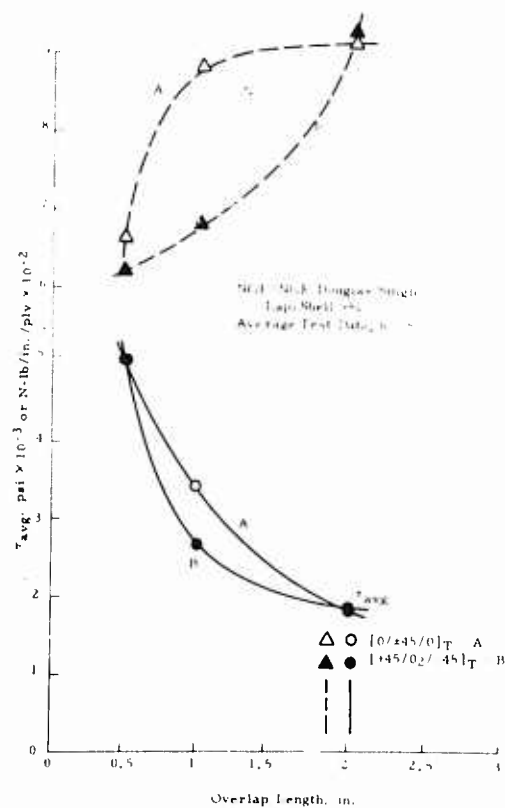


FIGURE 20. NGE/NGE DOUGLAS SINGLE LAP/SHELL 951

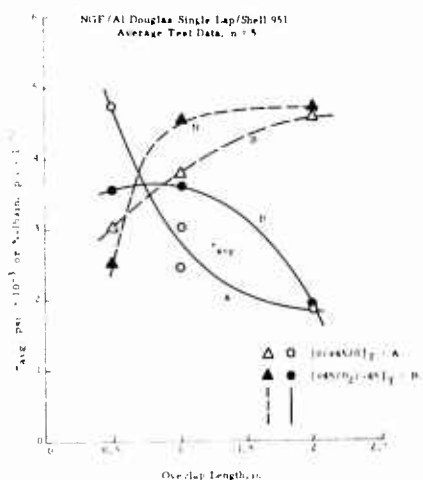


FIGURE 21 NGE/AL DOUGLAS
SINGLE LAP/SHIEL 951

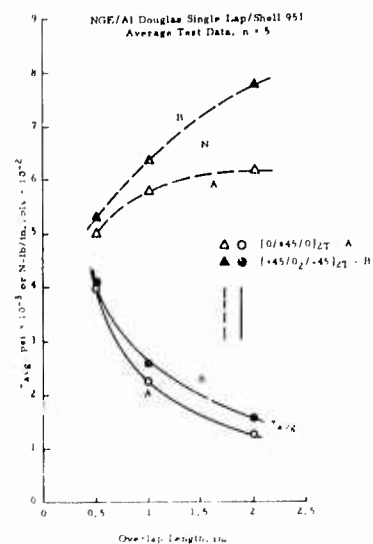


FIGURE 22. NGE/AL DOUGLAS
SINGLE LAP/SHIEL 951

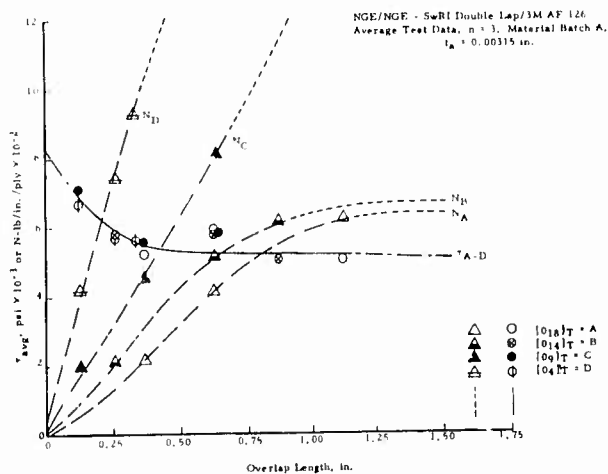


FIGURE 23. NGE/NGE SwRI DOUBLE
LAP/3M AF 126

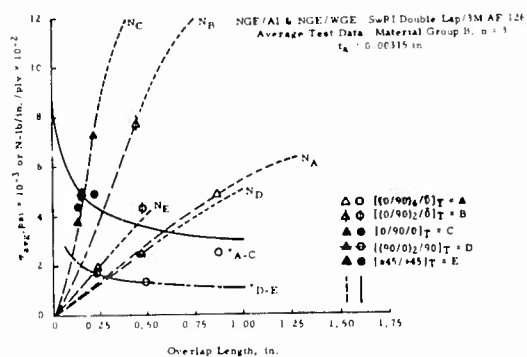


FIGURE 24. NGE/AL AND NGE/WGE SwRI
DOUBLE LAP/3M AF 126

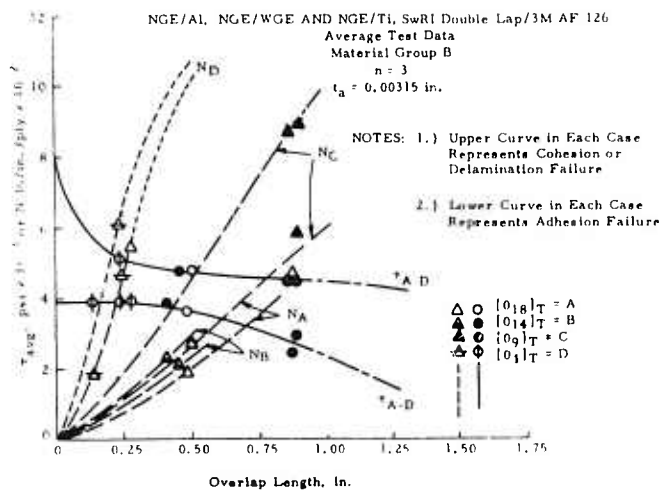


FIGURE 25. NGE/AL, NGE/WGE, AND NGE/TI SwRI DOUBLE LAP/3M AF 126

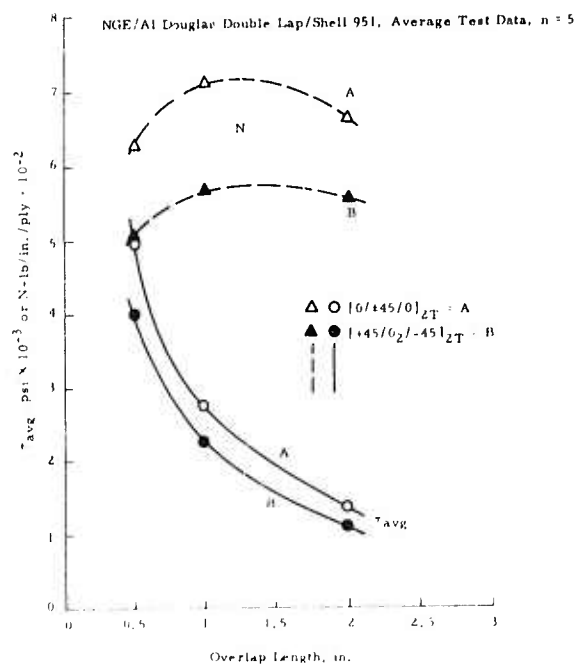


FIGURE 26. NGE/AL DOUGLAS DOUBLE LAP/SHELL 951

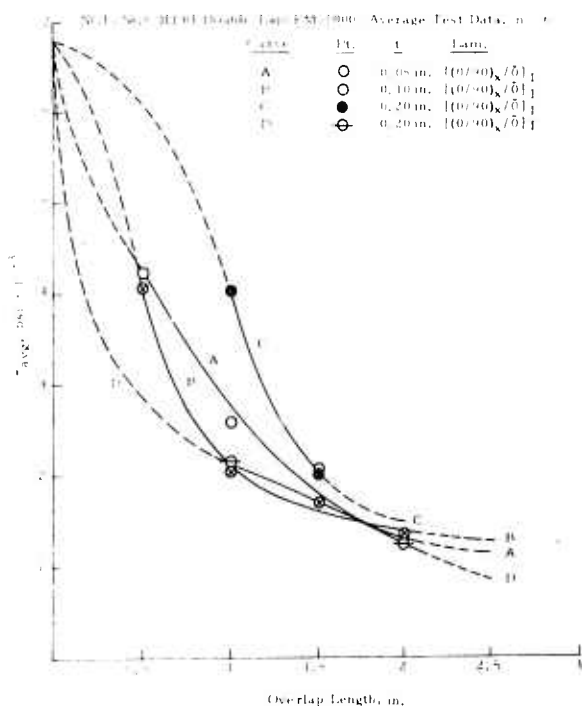


FIGURE 27. NGE/NGE IITRI DOUBLE LAP/FM-1000

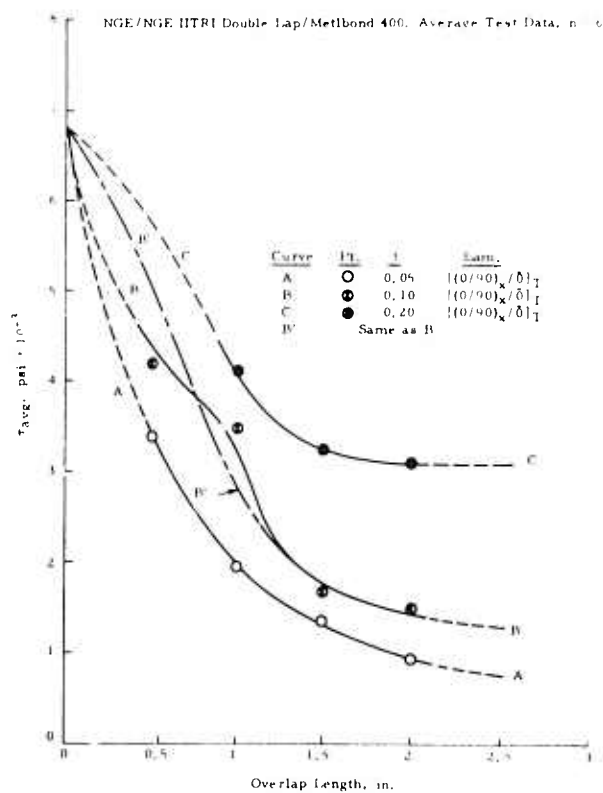


FIGURE 28. NGE/NGE IITRI DOUBLE LAP/METLBOND 400

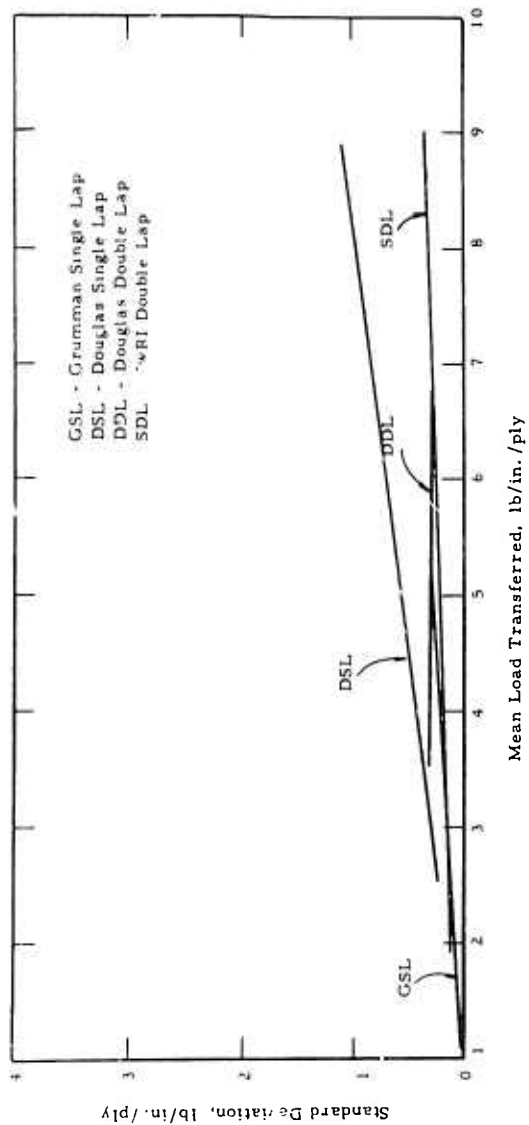


FIGURE 29. COMPARISON OF GROUP STANDARD DEVIATION ESTIMATES

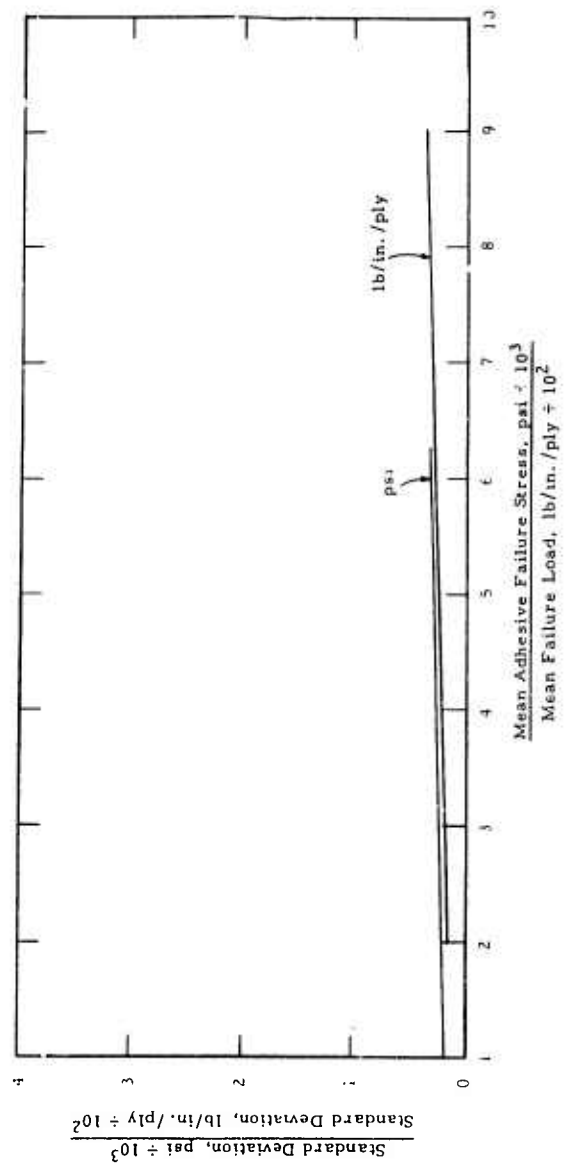


FIGURE 30. COMPARISON OF STANDARD DEVIATIONS SwRI DOUBLE LAP DATA

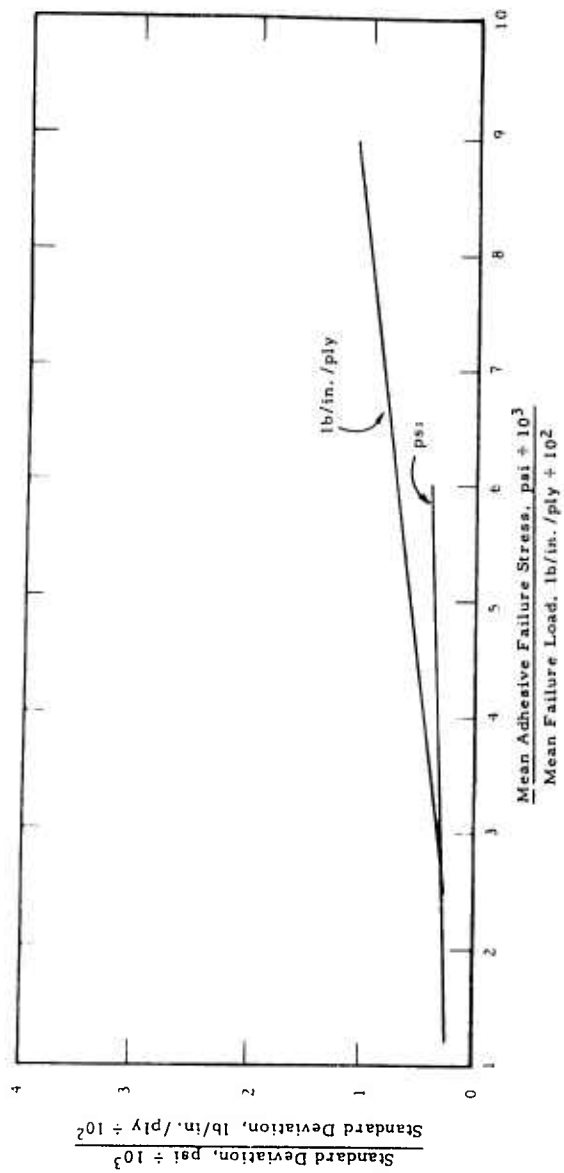


FIGURE 31. COMPARISON OF STANDARD DEVIATIONS—DOUGLAS SINGLE LAP DATA

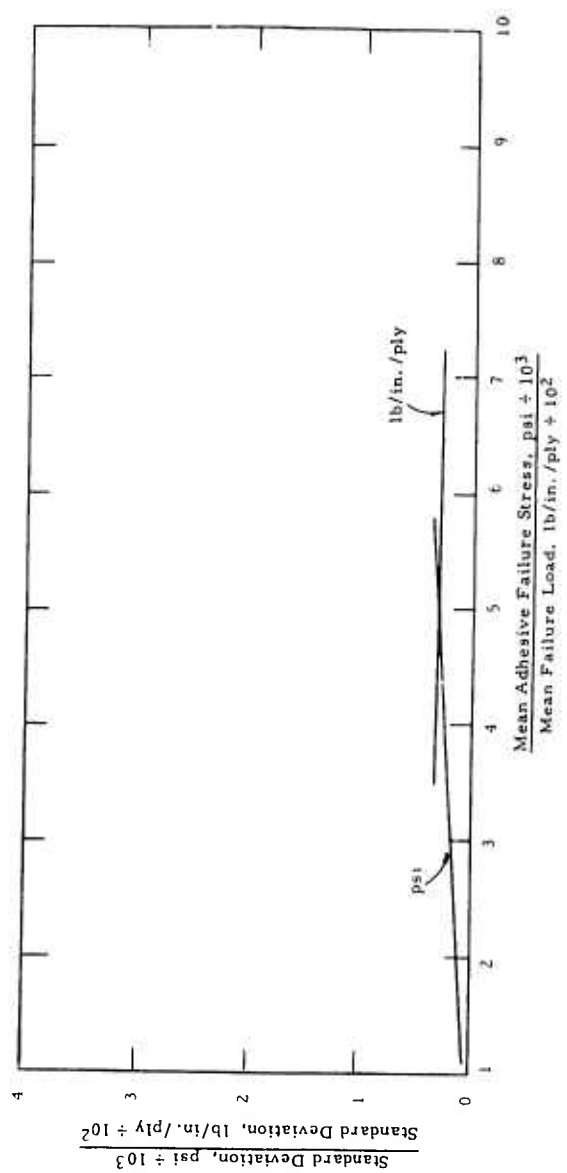


FIGURE 32. COMPARISON OF STANDARD DEVIATIONS—DOUGLAS DOUBLE LAP DATA

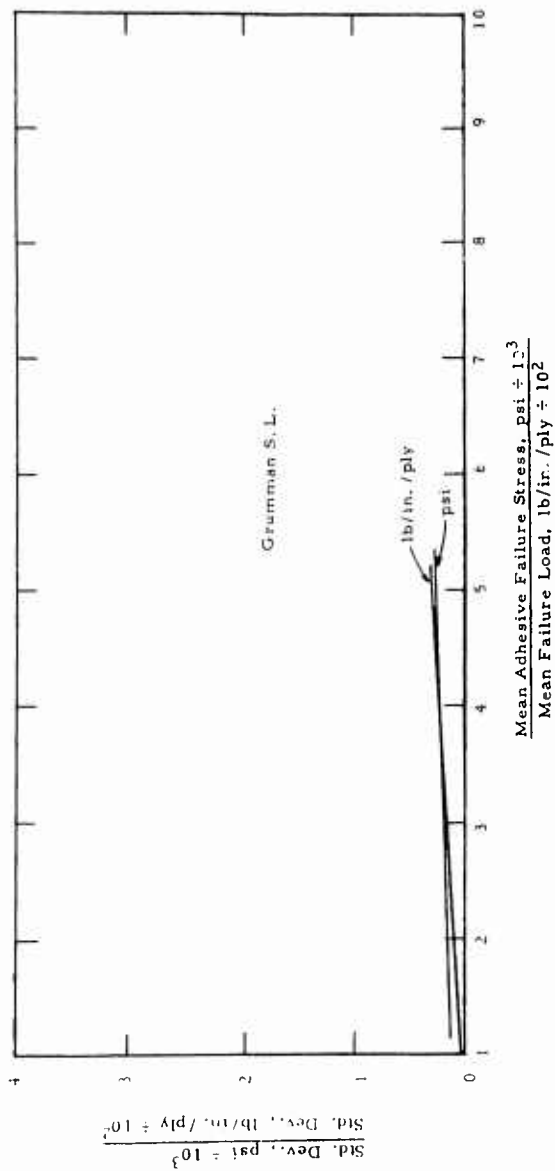


FIGURE 33. COMPARISON OF STANDARD DEVIATIONS—GRUMMAN SINGLE LAP DATA

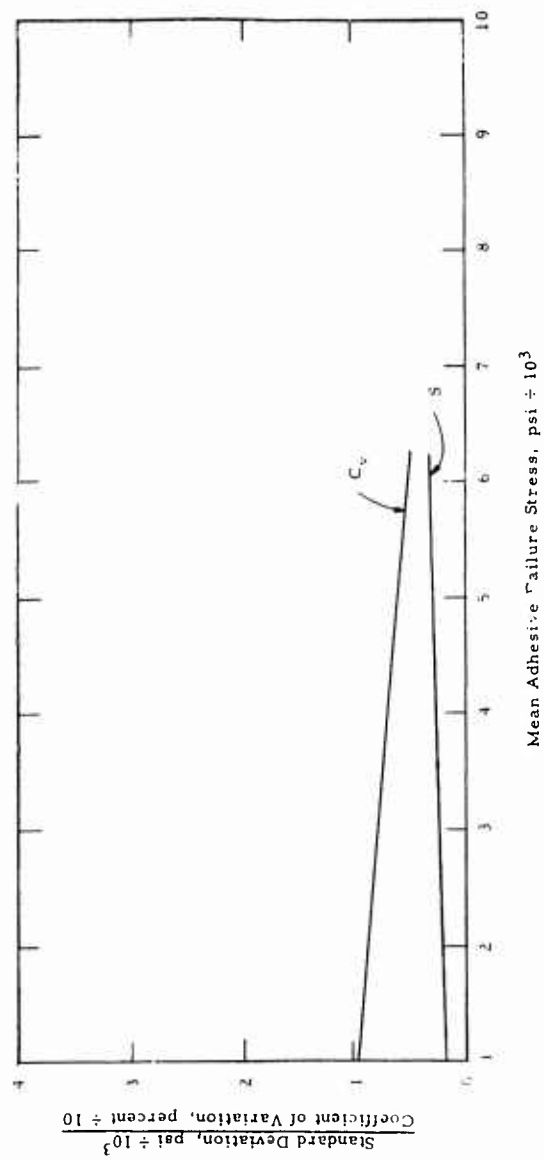


FIGURE 34. COEFFICIENT OF VARIATION AND STANDARD DEVIATION VS MEAN FAILURE STRESS, SWRI DOUBLE LAP DATA

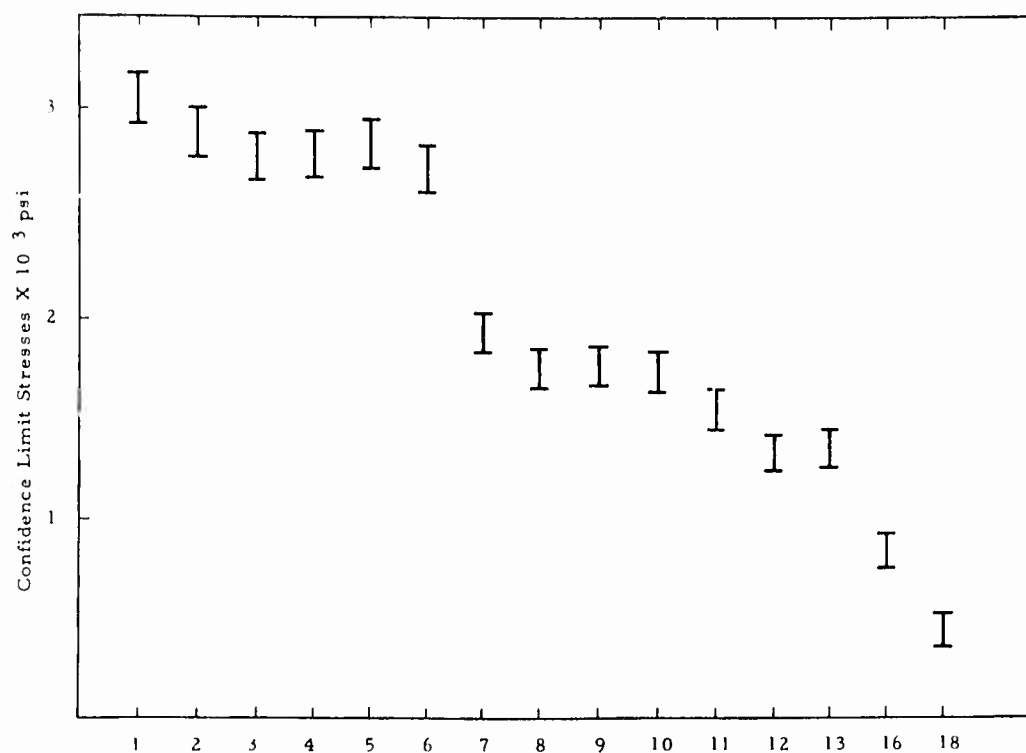


FIGURE 35. CONFIDENCE LIMIT STRESS VS GROUP SURFACE TREATMENT—MARTIN (AL/E)

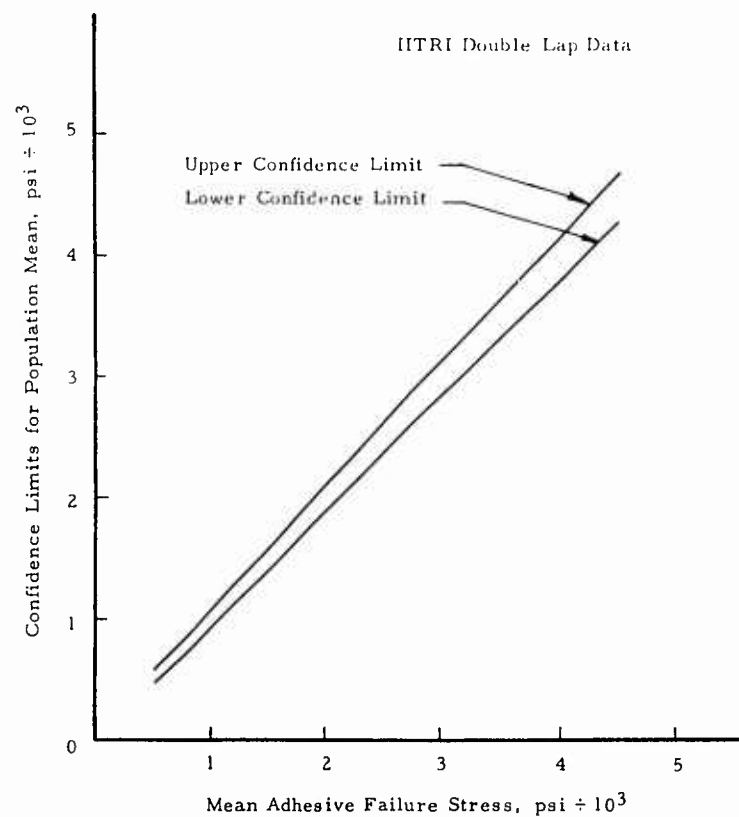


FIGURE 36. CONFIDENCE LIMITS—IITRI DOUBLE LAP DATA

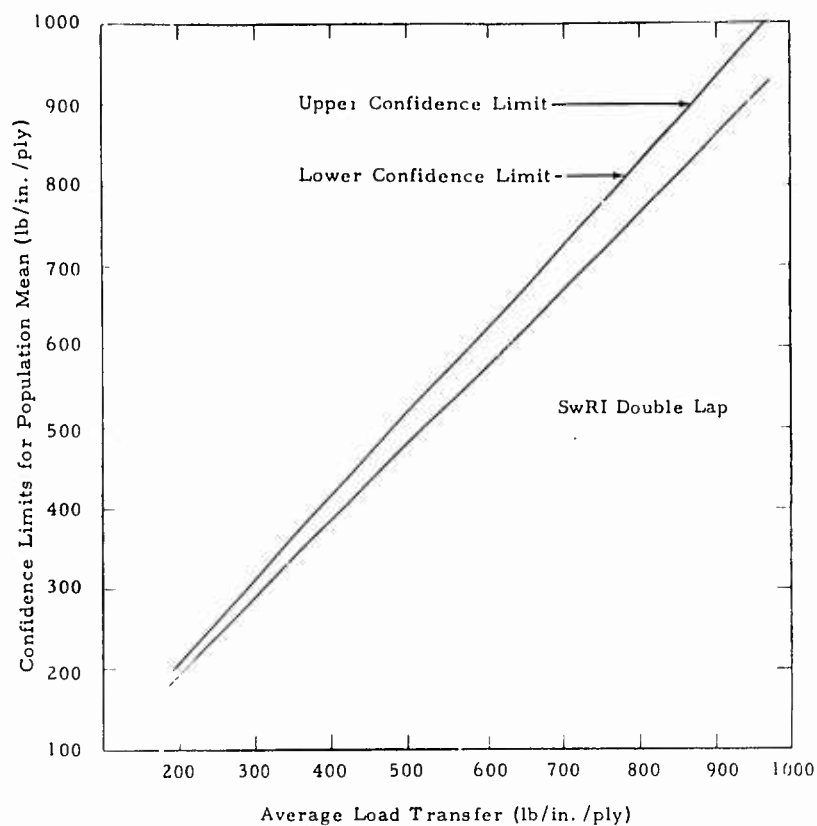


FIGURE 37. CONFIDENCE LIMITS—SwRI DOUBLE LAP DATA

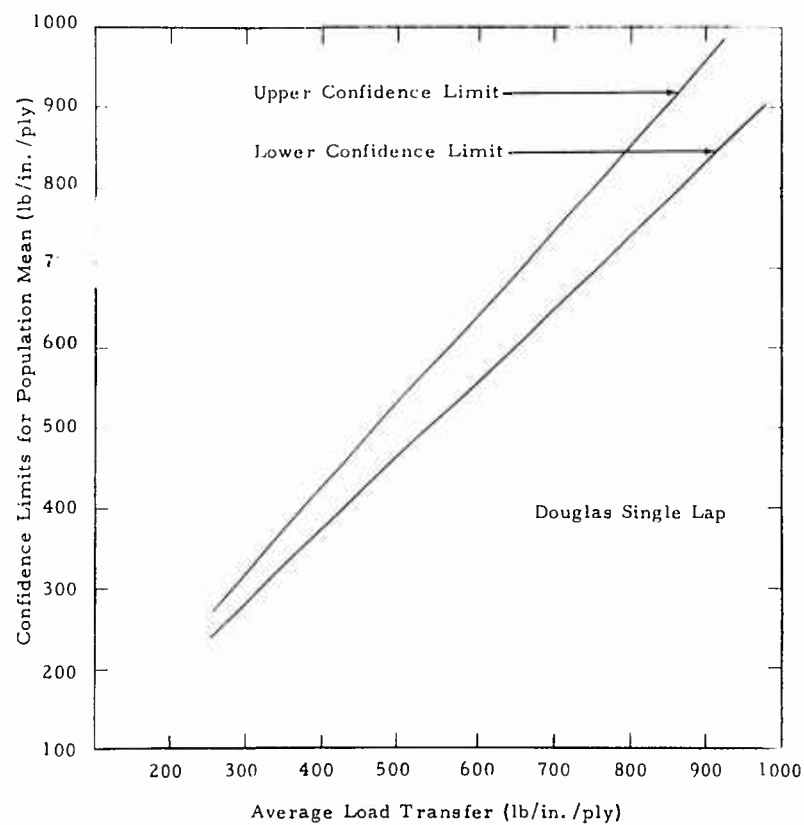


FIGURE 38. CONFIDENCE LIMITS—DOUGLAS SINGLE LAP DATA

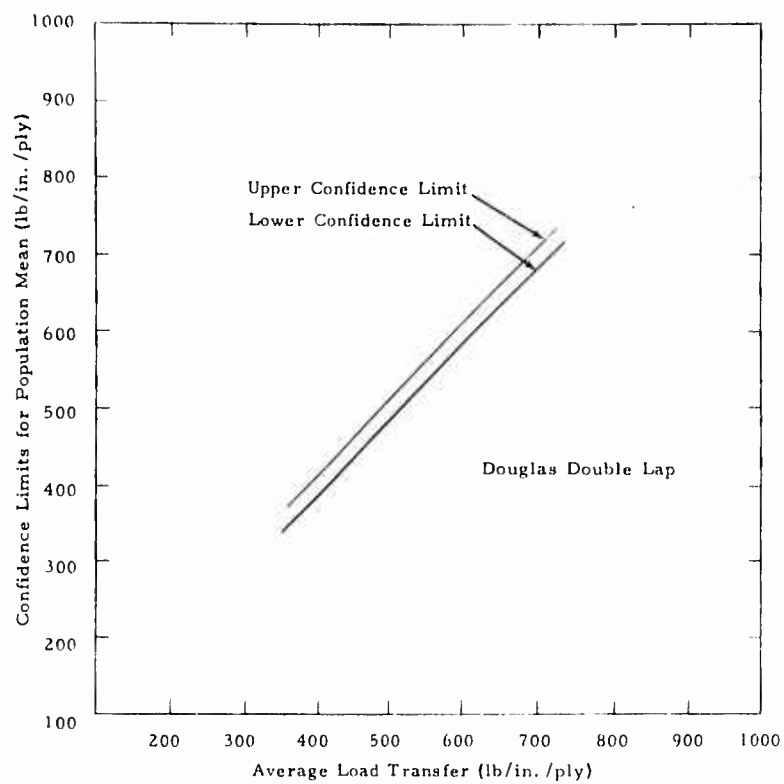


FIGURE 39. CONFIDENCE LIMITS DOUGLAS DOUBLE LAP DATA

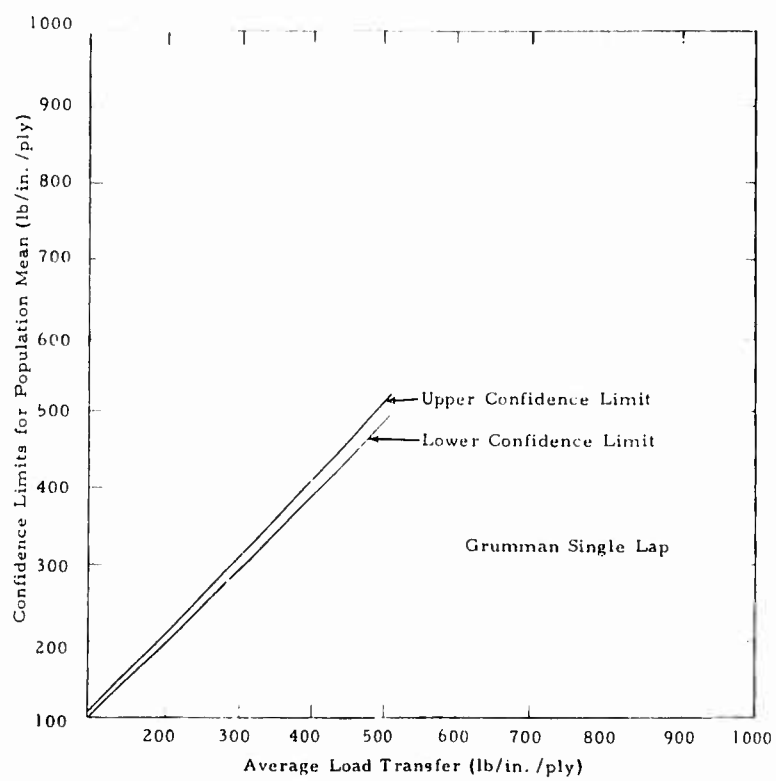


FIGURE 40. CONFIDENCE LIMITS-GRUMMAN SINGLE LAP DATA

Figure 41 shows the distribution for the $G = 160$ -ksi value. It is assumed that the end point τ_{\max} and τ_c values are found at one bondline thickness (0.00315 in.) away from the end of the joint (via St. Venant's principle), for the shear stress must go to zero at both ends at the free surface. However, the τ_{\max} value of 21,600 psi shown is, in the authors' judgment, too high. If the elastic G of the adhesive is actually close to the assumed 160 ksi, the end points would have to be cut off at some lower τ_{\max} value which would make the area under the τ_x curve the same as the area under the τ_{avg} line (i.e., $A_1 + A_3 = A_2$ on Fig. 41).

Figure 42 looks to be a more reasonable assumption for an assumed $G = 90,000$ psi with theoretical τ_{\max} being closer to the estimated τ_{\max} . It should be noted that lowering the modulus lowers the maximum shear stresses in the cement and raises the minimum stresses.

One additional computation for a $G = 40,000$ psi is shown in Figure 43. This is made to establish the relationship between adhesive shear stresses and the assumed G for the specific composite adherend combination, joint geometry, and experimentally measured average failing shear stress utilized. When the results from Figures 41, 42, and 43 are plotted, the variation of τ with the assumed G is shown in Figure 44. This shows the "effective" G to be 12,500 psi for $\tau_{\max} = 8,400$ psi and $\tau_{\text{avg}} = 5,250$ psi, assuming elastic conditions to failure.

From this initial preliminary study the technique of using an effective G to determine bondline shear stress distribution was deemed feasible for the elastic condition.

V.4. DESIGN OF THE EXPERIMENTAL PROGRAM

An experimental program designed to verify the analytical techniques developed herein requires the complete evaluation of the mechanical properties of (1) the adhesives, (2) the adherend materials, and (3) joints made from these materials. Since the first item was being evaluated by at least two other programs, effort in this contract was concentrated on Items 2 and 3.

Because of the wealth of data available on N-5505 boron/epoxy composites and 6Al-4V titanium it was decided to evaluate only the longitudinal properties of these adherend materials. Three study areas on joints were decided upon to satisfy the verification objective and those of the contract Statement of Work. These were (1) a large number of simple specimen bonded joints tested primarily to determine ultimate strength, (2) a small number of special bonded joints to evaluate the strain distribution under a monotonically increasing load to failure, and (3) a very small number of complex (larger) joints to evaluate size effects on both ultimate strength and strain distribution.

V.4.a. Adherend Materials

It was decided to test four longitudinal tensile specimens from the two 0.938 in. wide, 20 in. long strips taken from each composite adherend panel made. In addition, two similar configuration tensile specimens were to be taken from each of the four gages of 6Al-4V titanium sheet. Specimen and test details are given in specification SwRI 03-401, Test Standard for Fibrous Composite Tensile Specimens published in Appendix C of this report. Complete uniaxial tension stress/biaxial strain curves to failure were to be recorded on each static test specimen. These data were then to be used in the nonlinear methods developed in this program for bonded joint analysis.

For purposes of experimental design, properties based on average test data were taken from the literature as follows:

Property	N-5505 Boron/Epoxy ⁽¹⁵⁾ (50% F.V. Fraction)*			Sheet ⁽¹⁶⁾
	0	0/90	0/±45	Titanium (6Al-4V) Ann.
σ_{ult}	191.0 ksi	72.0 ksi	103.0 ksi	147.0 ksi
σ_{ave}	134.0 ksi	29.0 ksi	36.7 ksi	120.0 ksi

*0.0052 in./ply

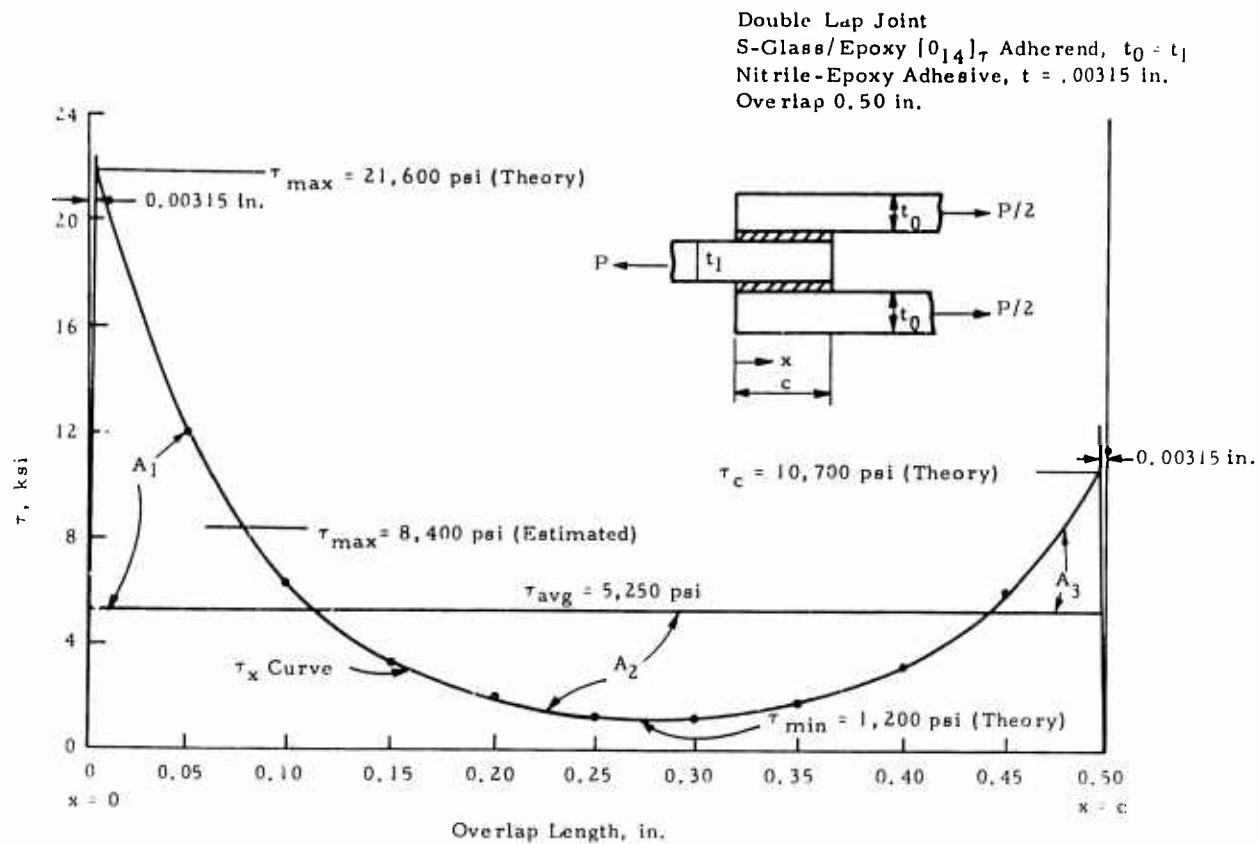


FIGURE 41. ORTHO-/ISO-ELASTIC SHEAR STRESS DISTRIBUTION FOR $G = 160,000$ PSI

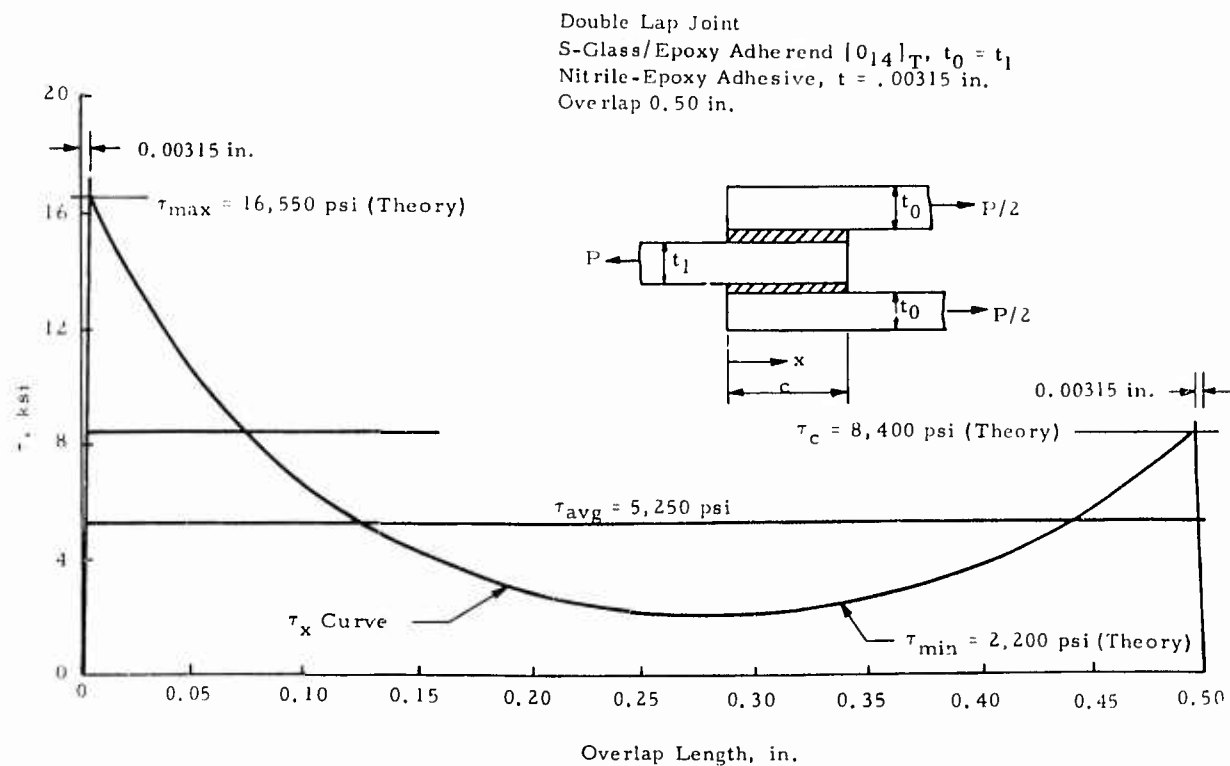


FIGURE 42. ORTHO-/ISO-ELASTIC SHEAR STRESS DISTRIBUTION FOR $G = 90,000$ PSI

Double Lap Joint
 S-Glass/Epoxy Adherend, $[0]_4 T$, $t_0 = t_1$
 Nitrile-Epoxy Adhesive, $t = 0.00315$ in.
 Overlap 0.50 in.

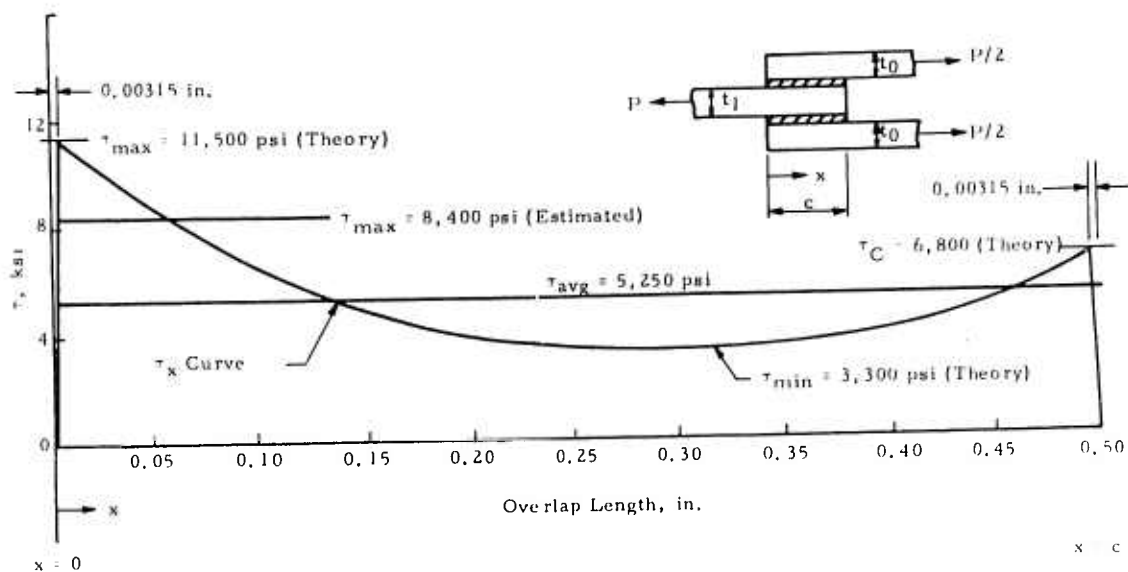


FIGURE 43. ORTHO-/ISO-ELASTIC SHEAR STRESSES DISTRIBUTION FOR $G = 40,000$ PSI

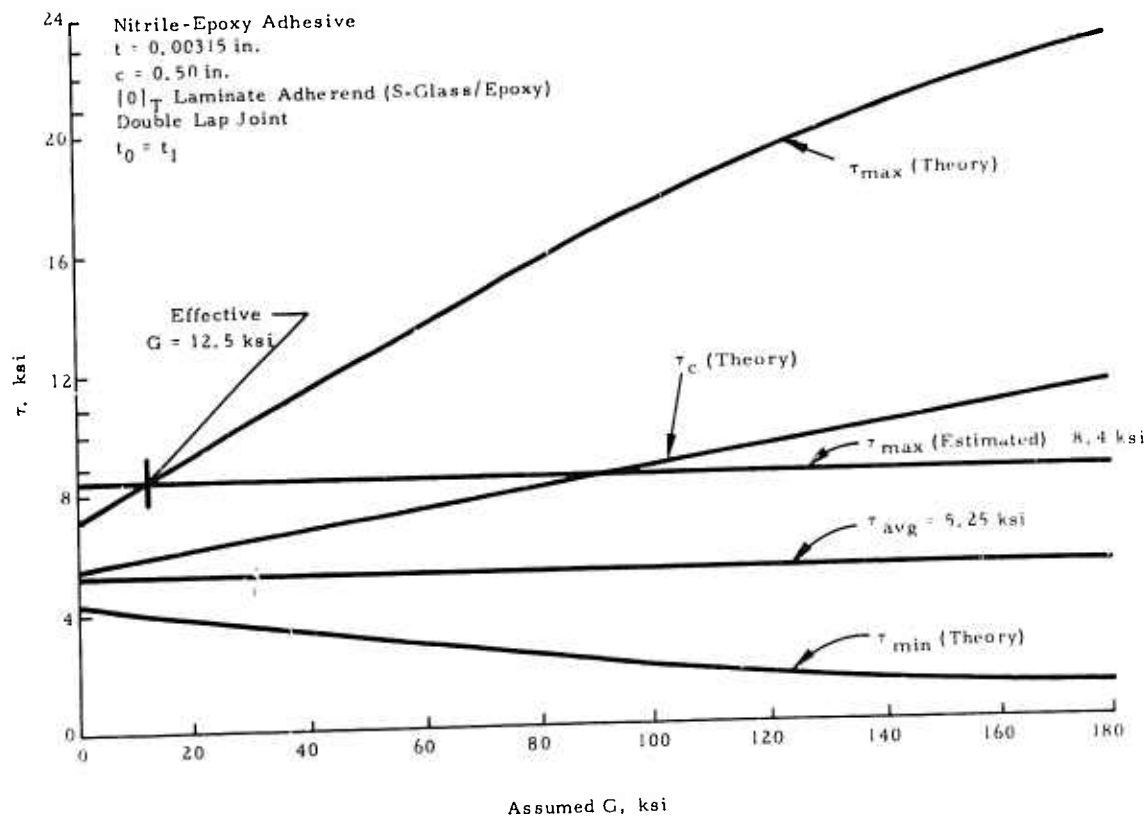


FIGURE 44. VARIATION OF SHEAR STRESS WITH ASSUMED SHEAR MODULUS

V.4.b. Adhesive Properties

Since little data were available on the empirical strength of AF-126-2 and MB-329 adhesives used in single, double, step lap and scarf joints with variable overlap lengths, the data which were available were used to develop extrapolated curves. Those for AF-126-2 nitrile epoxy, low stiffness-high elongation (LSHE) adhesive are shown in Figure 45. Figure 46 presents similar type curves on MB-329 epoxy novolak high stiffness-low elongation (HSLE) adhesive. These estimated ultimate shear strength values were used in the design of the joint specimens.

V.4.c. Simple and Special Joint Specimen Design

Using the properties presented in the previous sub-sections, joint design curves were calculated and plotted which would cover both the linear and nonlinear ranges of both the adherend and the adhesive. In other words, some joints were designed to fail in the adhesive with the adherend tensile stresses in either the linear or nonlinear range but below failure. Others were designed to fail in the adherend while the adhesive shear stress was either in the linear or nonlinear range. Additionally, some were designed to cause failure to occur simultaneously in the adhesive and the adherend.

For the three fiber orientations selected and the four types (3 lap and 1 scarf) of joints to be studied, the empirical design curves using the AF-126-2 (LSHE) adhesive are given in Figures 47 through 49. Similar curves are presented for the MB-329 (HSLE) adhesive in Figures 50 through 52. With these empirical design curves based on average test properties, the overlap lengths were designed for a given stress level in the adherend for a given type adhesive and orientation of the composite. This information was then used to generate the required number of plies of a balanced symmetric laminate. Where titanium was used as the other adherend materials it was matched as closely as possible to the total composite adherend thickness. With this information, the simple and special specimen test plan could be completed and is shown in Table II

V.4.d. Complex Joint Design

General requirements established for the complex joints (C.J.) were:

- (1) One (1) C.J. test panel for each adhesive, i.e., two (2) C.J. test panels, total
- (2) Each C.J. test panel: approximately 5 in. wide X 15 in. long
- (3) Each C.J. test panel: double lap type
- (4) Each C.J. test panel: instrumented to determine load/strain distribution, concentrations, failure initiation locations, and ultimates.

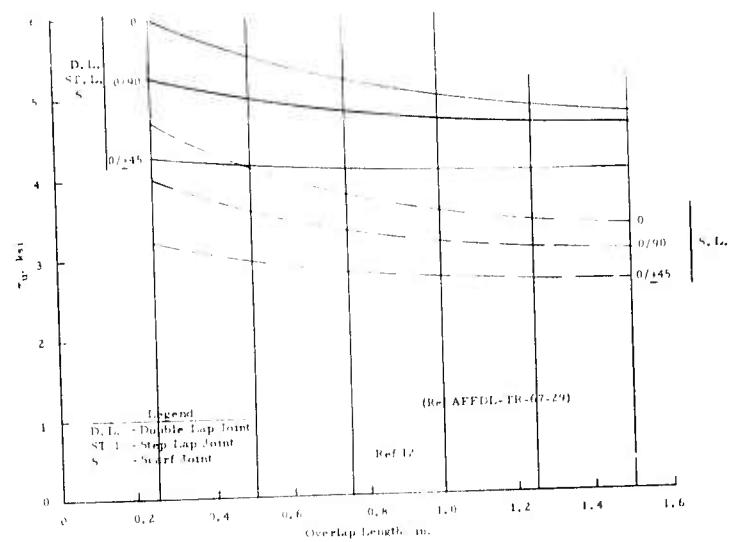


FIGURE 45. AF-126 (LS-HE) ESTIMATED ADHESIVE FAILING STRESSES

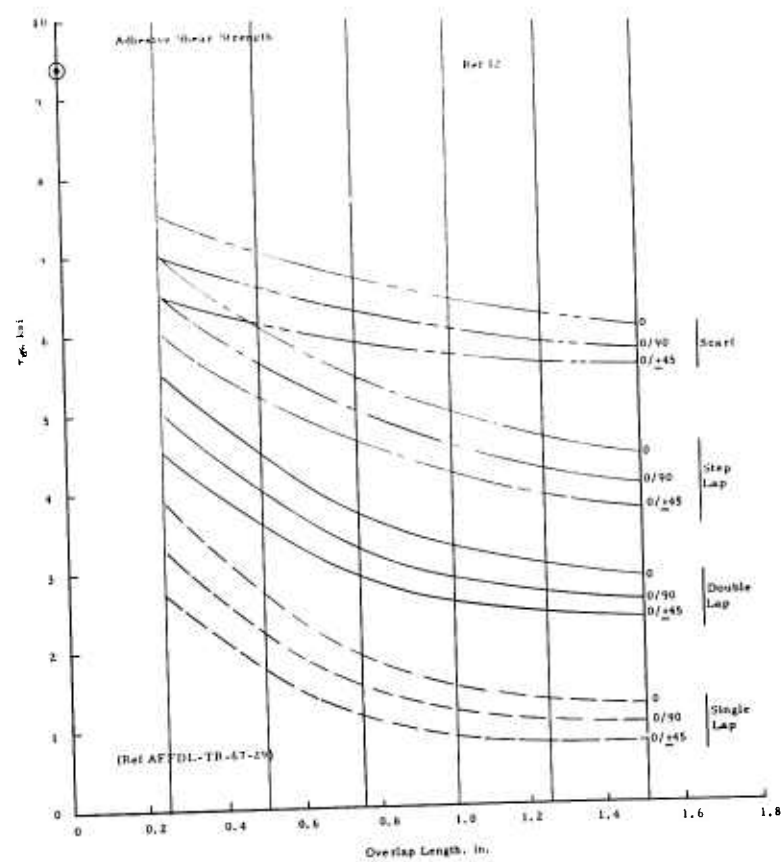


FIGURE 46. MB-329 (HS-LE) ESTIMATED ADHESIVE FAILING STRESSES

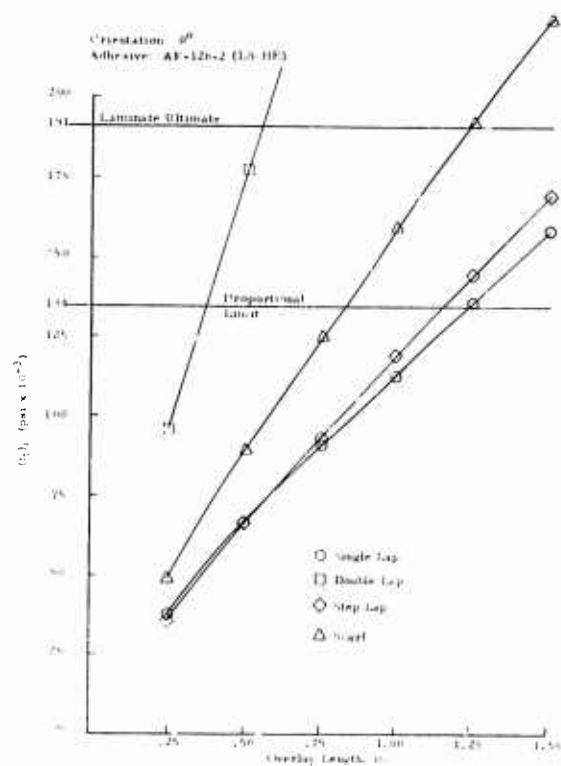


FIGURE 47. $[0]_c$ ADHEREND TENSILE STRESS VS OVERLAP LENGTH, LS HE (EMPIRICAL)

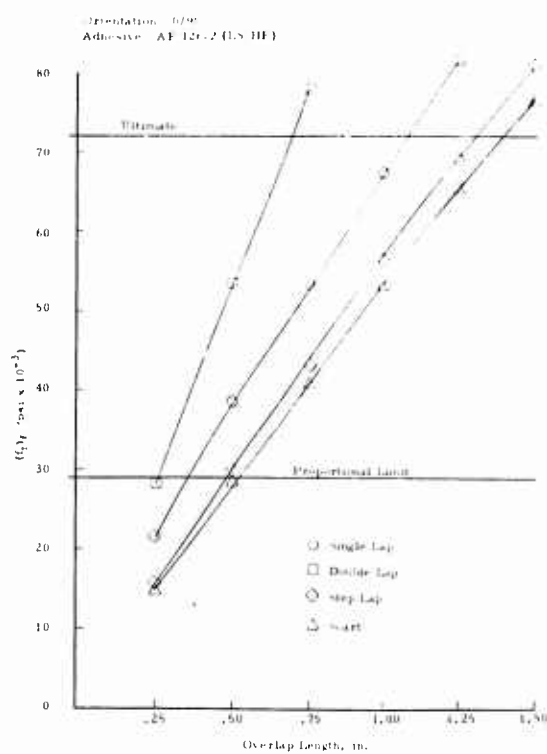


FIGURE 48. $[0/90]_c$ ADHEREND TENSILE STRESS VS OVERLAP LENGTH, LS-HE (EMPIRICAL)

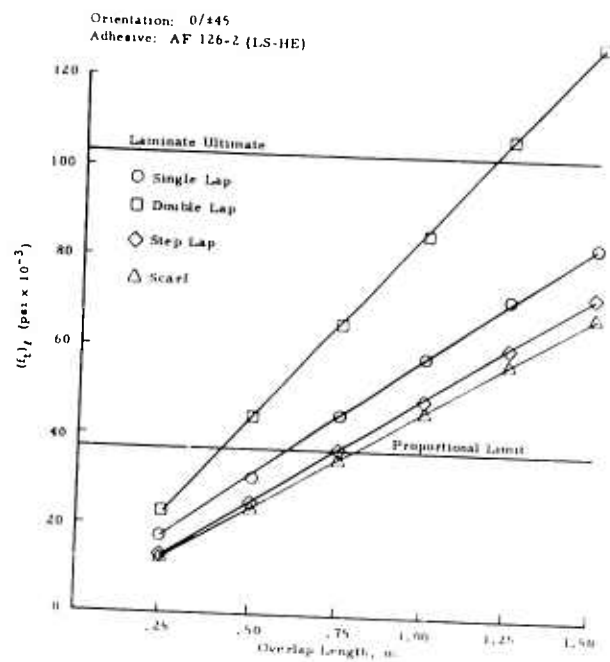


FIGURE 49. $[0/\pm 45]_c$ ADHEREND TENSILE STRESS VS OVERLAP LENGTH, LS-HE (EMPIRICAL)

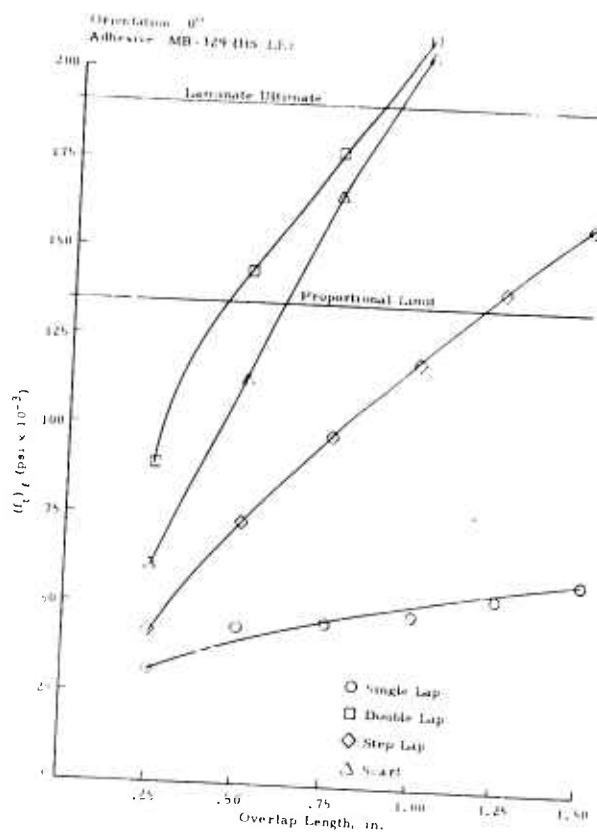


FIGURE 50. $[0]_c$ ADHEREND TENSILE STRESS VS OVERLAP LENGTH, HS-LE (EMPIRICAL)

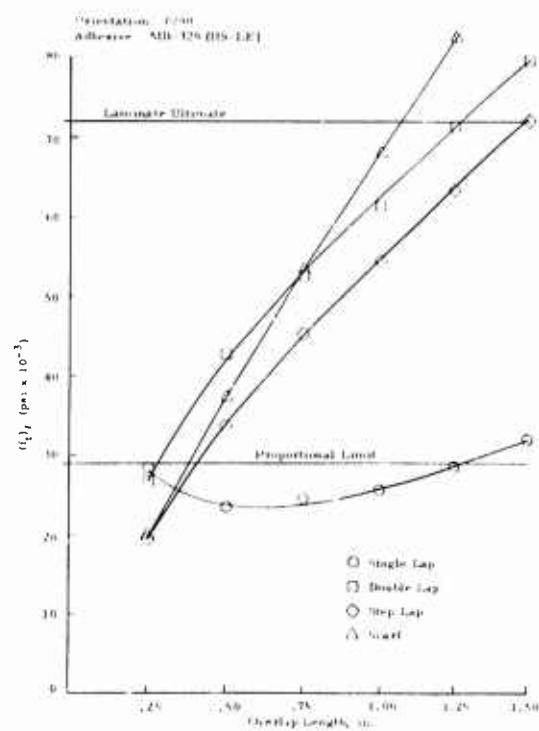


FIGURE 51. $[0/90]_c$ ADHEREND TENSILE STRESS VS OVERLAP LENGTH, HS-LE (EMPIRICAL)

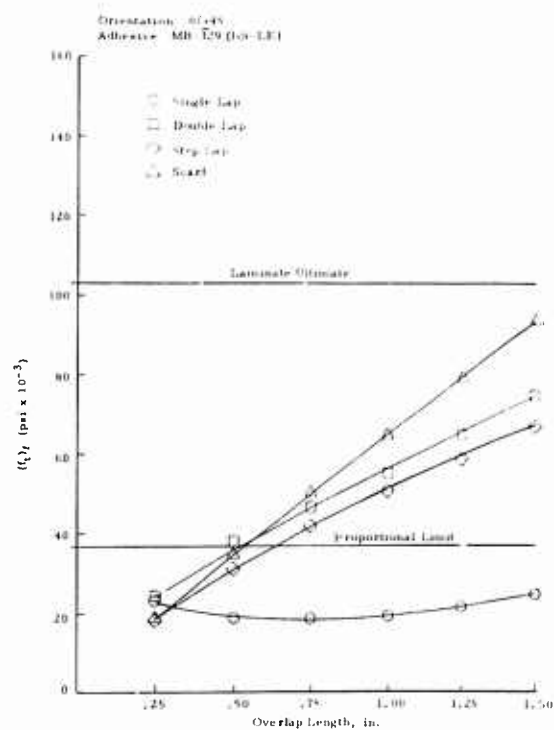


FIGURE 52. $[0/\pm 45]_c$ ADHEREND TENSILE STRESS VS OVERLAP LENGTH, HS-LE (EMPIRICAL)

TABLE II

SIMPLE AND "SPECIAL" SPECIMEN TEST PLAN
(Monotonically Increasing Load to Failure)

Type of Joint	General Fiber Orientation Category	Overlap Segments*												Line Total N		
		Number 1				Number 2				Number 3						
		B-B		B-T		B-B		B-T		B-B		B-T				
		N	O.L.	N	O.L.	N	O.L.	N†	O.L.	N	O.L.	N	O.L.			
Single Lap	$[0]_c$	3	1/4	3	1/4	3	1-1/4	3	1-1/4	3	1-3/4	3	1-3/4	18	AF-126-2(LS-HE) adhesive	
	$[0/90]_c$	—	—	—	—	—	—	—	—	—	—	—	—	0		
	$[0/\pm 45]_c$	3	1/4	3	1/4	3	1-1/4	3 + 1	1-1/4	3	2	3	2	18 + 1		
Double Lap	$[0]_c$	3	1/4	3	1/4	3	1/2	3	1/2	3	3/4	3	3/4	18		
	$[0/90]_c$	3	1/4	3	1/4	3	1/2	3	1/2	3	3/4	3	3/4	18		
	$[0/\pm 45]_c$	3	1/4	3	1/4	3	3/4	3 + 1	3/4	3	1-1/4	3	1-1/4	18 + 1		
Step Lap	$[0]_c$	—	—	3	1/4	—	—	3	1-1/4	—	—	3	2	9		
	$[0/90]_c$	—	—	3	1/4	—	—	3	1	—	—	3	1-1/2	9		
	$[0/\pm 45]_c$	—	—	3	1/4	—	—	3 + 1	1-1/2	—	—	3	2-1/4	9 + 1		
First Group Totals														117 + 3		
Single Lap	$[0]_c$	3	1/4	3	1/4	3	1-1/4	3	1-1/4	3	2-1/4	3	2-1/4	18		MB-329(HS-LE) adhesive
	$[0/90]_c$	—	—	—	—	—	—	—	—	—	—	—	—	0		
	$[0/\pm 45]_c$	3	1/2	3	1/2	3	1-1/2	3 + 1	1-1/2	3	2-1/2	3	2-1/2	18 + 1		
Double Lap	$[0]_c$	3	1/4	3	1/4	3	1/2	3	1/2	3	1	3	1	18		
	$[0/90]_c$	3	1/4	3	1/4	3	3/4	3	3/4	3	1-1/2	3	1-1/2	18		
	$[0/\pm 45]_c$	3	1/4	3	1/4	3	1	3 + 1	1	3	1-3/4	3	1-3/4	18 + 1		
Step Lap	$[0]_c$	—	—	3	1/2	—	—	3	1-1/2	—	—	3	2-1/4	9		
	$[0/90]_c$	—	—	3	1/4	—	—	3	3/4	—	—	3	1-1/2	9		
	$[0/\pm 45]_c$	—	—	3	1/4	—	—	3 + 1	1-1/4	—	—	3	2-1/2	9 + 1		
Second Group Totals														117 + 3		
GROUP TOTALS														234 + 6		
* Adherend Material: B-B is boron-to-boron; B-T is boron-to-titanium; N = Number of Specimens; O.L. = Overlap Length in inches.																
† (a) All simple specimens in this column will have clamp-on (2-in. gage length) extensometer used to record deformation during loading.																
(b) All "special" specimens in this column will be used to determine load deformation behavior of joint (e.g., strain gage instrumentation).																

SECTION VI

LAMINATE PROCESSING

VI.1. GENERAL

The purpose of this section is to describe the processing, fabrication and quality control activities in making composite laminate panels during this research program. These are presented in Sections VI.2, VI.3 and VI.4. Processing Facilities described in Section VI.2 give detailed information about the type of buildings and equipment used, while Section VI.3 on Process Development provides the reader with a brief summary of the developmental aspects of the materials processing. Adherend Panel Fabrication and Quality Control are presented in Section VI.4 and cover the processing and inspection details of panels used in the experimental program.

VI.2. PROCESSING FACILITIES

Special facilities and equipment are required for composite fabrication and quality control. This section describes these areas.

The processing laboratory* in which cleaning and layup of the boron/epoxy and fiber glass/epoxy laminates and the bonded joints was accomplished is 19 X 20 feet with air conditioning supplied by the zone-controlled central building unit. During a normal week, the temperature in the laboratory varies between 72° and 74°F while relative humidity varies from 51 to 57 percent. Temperature and humidity in the laboratory were recorded continuously by a Honeywell two-pen recorder actuated by a mercury-filled temperature sensor and a hair humidity sensor. Extremes recorded during the period of this research were 65° to 75°F in temperature and 40 to 65 percent relative humidity.

Equipment in the laboratory included a work bench, several work tables (two with Formica® tops for cleaning operations and layup), a Formica®-topped wash basin made of special chemical resistant molded epoxy reinforced plastic, storage cabinets, an air circulating Blue M oven capable of controlled temperatures up to 500°F ± 2°F, and a chest-type deep freeze for storage of preimpregnated materials at 0°F.

The 50-ton M and N press is located in an adjacent laboratory (same building) which is also air conditioned, but the temperature and humidity may vary more widely since it is a large open area with direct access to the outside. Figure 5.3 consists of photographs of the laboratory and associated equipment.

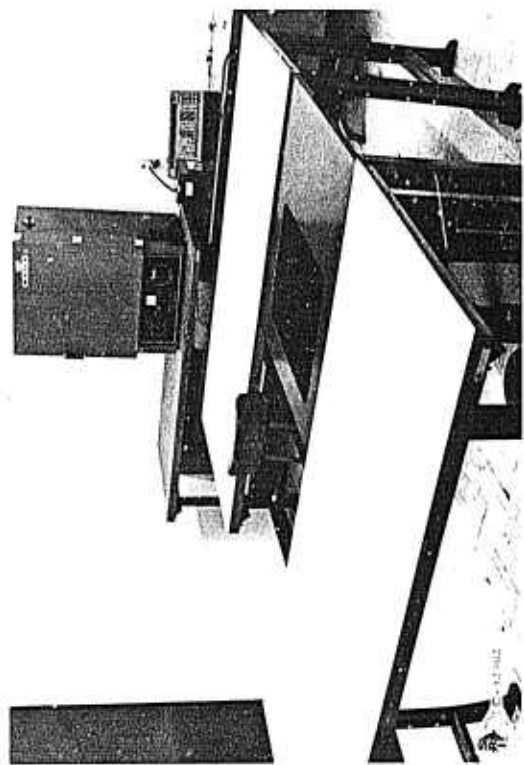
VI.3. PROCESS DEVELOPMENT

The development of a standard process (see Appendix C) for making laminates and inspecting them was required to provide the necessary consistency and control for the adherend materials to be used in the experimental effort. While the processing and laminating variations were investigated, so was equipment functioning. Besides the hand layup process, the two main areas of concern were the laminating press and the thru-scan ultrasonic inspection system.

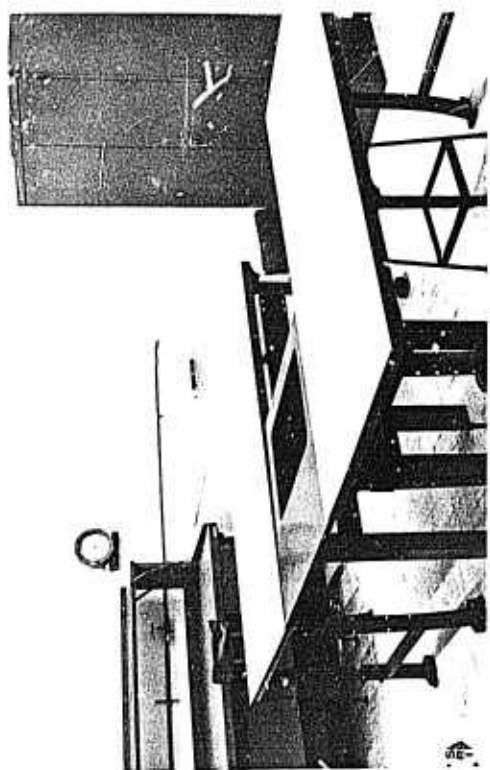
Providing a laminating press which had closely controlled temperatures was the first order of business. After considerable overhaul and modification of the 50-ton M and N press with 20 X 24-inch electrically heated platens the following heat survey/adjustment procedure was begun.

Separate recorder-controllers were connected to the contactors of the top and bottom platens. Four 20 X 24-inch plates were cut from 0.125-inch aluminum. A slot from the center to one side was cut in the back side of each plate and a 26-gage iron-constantin thermocouple cemented into the slot with the hot junction at the center of

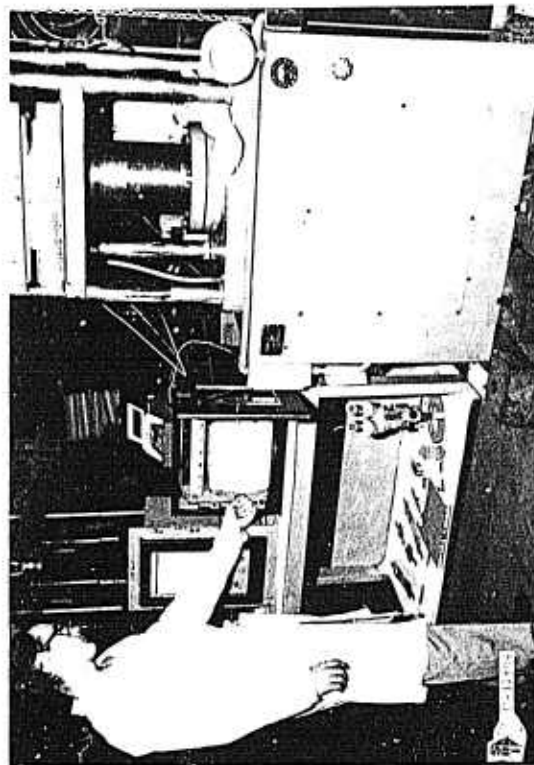
*Located in the Department of Structural Research.



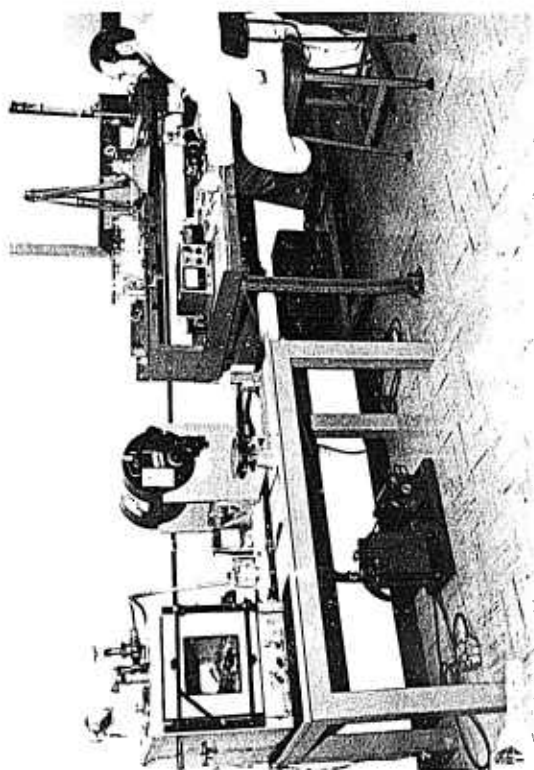
B. Composite Layup Laboratory



A. Composite Layup Laboratory



D. 50-Ton M&N Press



C. Strain Gage Work Area

FIGURE 53. COMPOSITE LABORATORY AND EQUIPMENT

the plate. These thermocouples serve as the control input to the platen temperature recorder-controllers. The face of each tool plate was sanded to remove scratches and given two coats of a wax base mold release agent.

An eight-ply, 16 X 20-inch heat survey panel (made from 1581 glass/5505 epoxy) was laid up with eighteen thermocouples arranged in a triangular pattern (see Figure 54) embedded between the fourth and fifth plies. Layup and cure of this panel was accomplished in accordance with the SwRI 03-301 Process Standard for Boron/Resin Composite Laminate Fabrication*. During the cure cycle, the temperature at these thermocouples was monitored at frequent intervals. During the 200°F portion of the cycle, there was not more than 6°F difference between the highest and lowest thermocouple readings. There was an initial overrun of temperature on heat-up to 214°F which dropped within 15 min to 210°F, and was under control at 200° to 206°F during most of the remainder of the 2 hours. No overrun occurred at 300°F and control was maintained between 296°F and 302°F with a maximum difference of 12°F between the highest and lowest temperature readings. Control was maintained at 344° to 348°F with a maximum temperature difference of 14°F during the final 2 hours of cure. Figure 55 is a back-lighted photograph of the cured heat survey panel. The dark patches across the thermocouple wires are Scotch® Brand glass cloth electrical tape, No. 27, which was required to hold the thermocouples in place during layup and cure. The wires are 26-gage iron-constantin with enamel and glass fiber wrap on each wire and glass braid over all. Quality of the panel was visually good with a generally uniform light yellow translucent appearance.

Fifteen panels were fabricated using the 1581 glass fabric/5505 epoxy material and eleven panels were fabricated from Narmco 5505 boron/epoxy Lot No. 297, Roll 13 (twisted fiber) and Lot No. 373, Roll 1, which was the first production lot of material received. These panels are listed in Table III.

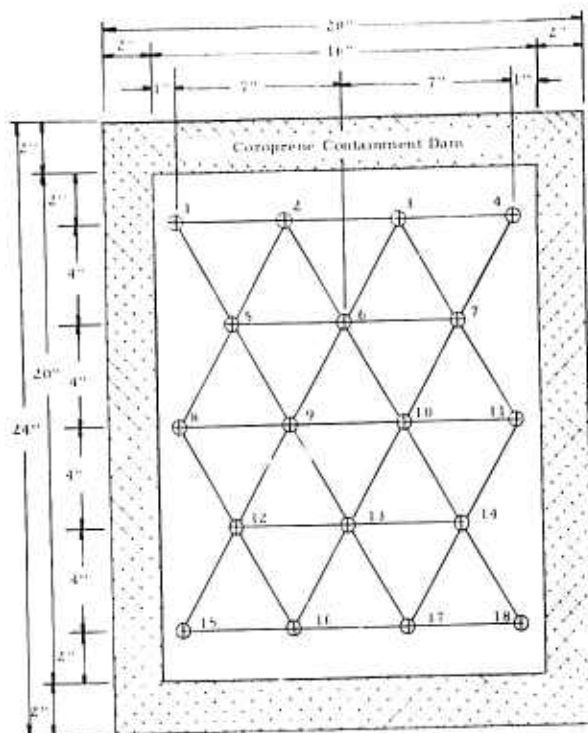
Panel No. 6 has pieces of Teflon®-coated glass fabric and Scotch® Brand glass cloth electrical tape, No. 27, embedded between the fourth and fifth plies as shown in Figure 56. Figure 57 is a back-lighted photograph of this panel. This was used to develop the ultrasonic test technique for voids and inclusions.

Initial laminates using the boron prepreg had rather poor appearance. The top surface was resin-starved. Panels B-1 and B-2 were cured at a higher total pressure than had been used on an equivalent size of glass fabric reinforced panels, but the increased pressure was evidently not sufficient to accomplish the greater compression of the Coroprene boundary support required by the thinner boron layup. A 0.020-in. aluminum shim was placed under the layup for Panel B-3, and the press was adjusted to the load used previously for the glass fabric/epoxy panels. This also resulted in a resin-starved surface. An increased load was then used for panels B-4 and B-5. This improved the resin flow and, except for a few loose fibers in one location on the surface of B-4, the appearance was good. The later boron laminates all had good appearance, except Panel B-9 which had some loose fibers on the top surface.

Tensile strength specimens were prepared from Panel G-2 and were tested on the Instron machine at a constant deflection rate of 0.05 in./min. The average ultimate tensile strength of nine specimens was 56,700 psi, with a proportional limit of 30,030 psi. The average modulus was 4.78×10^6 psi initially and 3.17×10^6 psi above the proportional limit. Complete data on these tests are presented in Table IV. While these tests were performed for the IRAD Creep Program†, they provide an indication of the quality of the fabrication technique.

A through transmission ultrasonic inspection facility was completed and all glass/epoxy panels, except G-1, 2 and 5 and boron/epoxy panels through B-8, were subjected to ultrasonic inspection. Panel G-1 is the heat survey panel with thermocouples imbedded as shown in Figures 54 and 55. Panels G-2 and G-5 had already been cut for test specimens; however, the larger remaining pieces of these panels were inspected. The recording of the ultrasonic test of Panel G-6 is shown in Figure 58. Plastic tape was placed on all edges and the whole panels were sprayed with clear lacquer to prevent water absorption while immersed in the water bath. The edge tape shows as pips along each end of the panel and solid lines along one side. Each line on the chart represents a 1/8-inch interval on the panel.

*Appendix C, Page C-9.



⊕ Survey Thermocouples

FIGURE 54. 1581 GLASS FABRIC/5505 EPOXY
HEAT SURVEY PANEL POSITIONS OF
THERMOCOUPLE

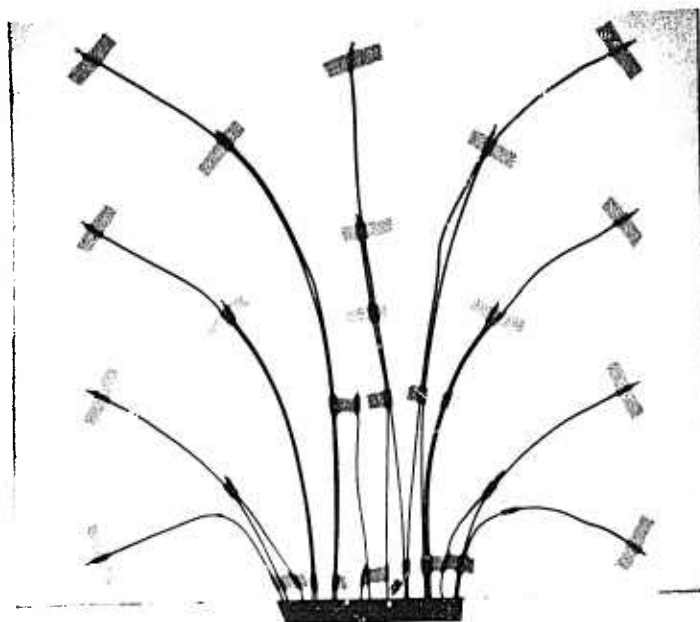


FIGURE 55. HEAT SURVEY PANEL—
BACK-LIGHTED PHOTOGRAPH

TABLE III

A. 1581 Glass Fabric/N-5505 Epoxy Panels					
Panel No.	Size, in.	No. of Plies	Thickness, in.	Fiber Orientation	Remarks
G-1	16 x 20	8		0°	Heat Survey Panel-18 Thermocouples at Center
G-2*	16 x 20	8	0.072	0°	To be used for Tensile Test Specimens
G-3*	16 x 20	12	0.103	0°	To be used for Flexural Test Specimens
G-4*	6 x 10	8	0.067	0°	Void and Inclusion Test Panel
G-5*	6 x 10	12		0°	
G-6*	6 x 10	8		0°	
G-7*	16 x 20	10	0.090	0°	
G-8*	16 x 20	9		0°, 90°, ..., 0°	
G-9*	6 x 10	11		±45°	
G-10*	6 x 10	19		0°, ±45°, ..., 0°	
G-11*	16 x 20	11	0.0975	0°	
G-12*	16 x 20	11	0.0960	90° to long axis of panel	
G-13*	16 x 20	11	0.0940	±45°	
G-14*	16 x 20	11	0.0930	0°, 90°, ..., 0°	
G-15*	16 x 20	13	0.115	0°, ±45°, ..., 0°	
B. Boron Fiber/N-5505 Epoxy Panels					
B-1*	6 x 9	9	0.0493	0°	Surface is resin starved
B-2*	6 x 9	8	0.0450	0°	Surface is resin starved
B-3*	6 x 10	8	0.0357	0°	Surface is resin starved
B-4*	6 x 9	9	0.0458	0°, 90°, ..., 0°	Loose fiber on one surface
B-5*	6 x 10	9	0.0465	±45°	Good appearance
B-6	6 x 9	9	0.0474	0°	Used new material from Lot 373
B-7	6 x 10	15	0.0791	0°	Used for acceptance tests of Narmco 5505 Lot 373, Roll No. 1
B-8	6 x 9	17	0.0784	0°, 90°, ..., 0°	From Lot 373, Roll No. 1
B-9*	6 x 10	8	0.0447	0°, ±45°, ..., 0°	Loose fibers on one surface
B-10*	6 x 9	15	0.0757	90° to long axis of panel	
B-11*	6 x 9	17	0.0803	0°, 90°, ..., 0°	
*IRAD Panels for Creep Program.					

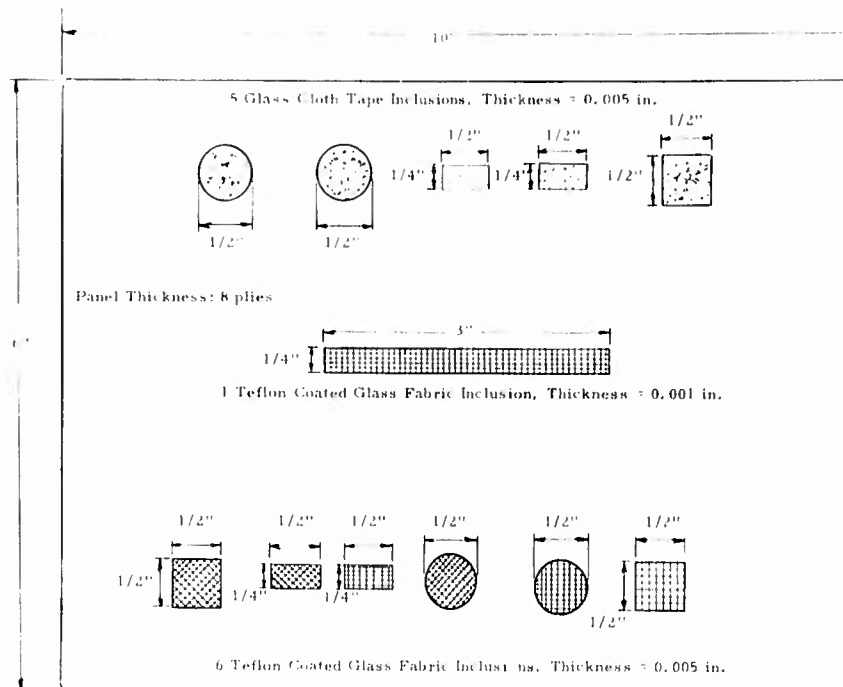


FIGURE 56. PANEL NO. G-6 WITH TEFLON-COATED GLASS FABRIC AND GLASS CLOTH ELECTRICAL TAPE INCLUSIONS FOR ULTRASONIC TEST CALIBRATION

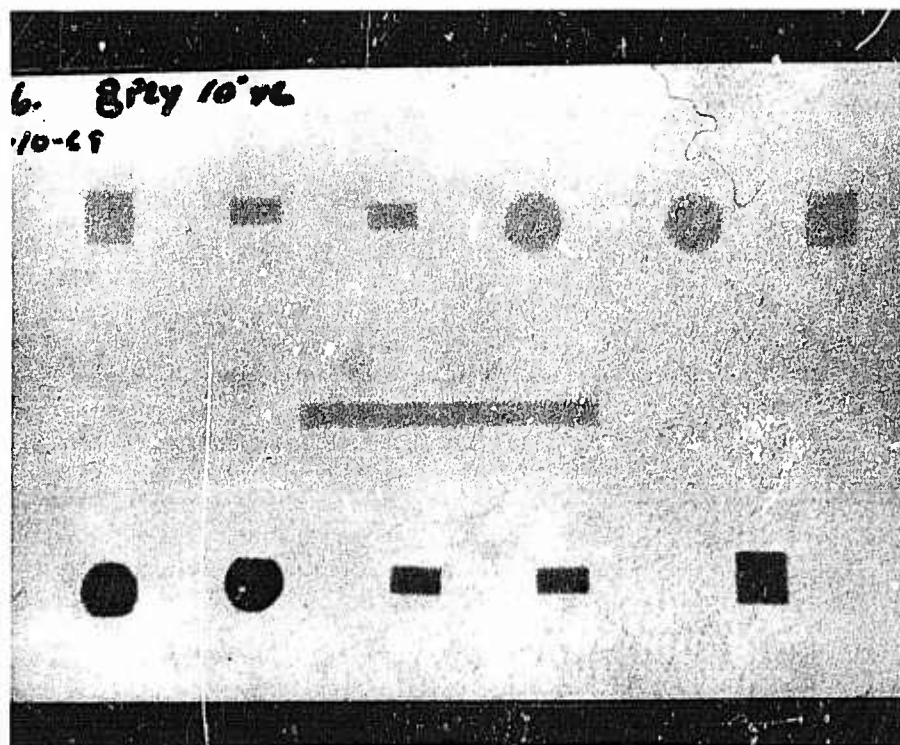


FIGURE 57. PANEL NO. G-6 - BACK-LIGHTED PHOTOGRAPH

TABLE IV
TENSILE STRENGTH TESTS* OF PANEL G-2

Dimension or Property	Specimen Numbers									Average
	-1-1	-1-2	-1-3	-2-1	-2-2	-2-3	-3-1	-3-2	-3-3	
Gage Dimensions: Length (in.)	2.00	2.00	2.00	2.00	2.00	2.00	2.00	2.00	2.00	
Width (in.)	0.501	0.501	0.501	0.502	0.502	0.500	0.501	0.500	0.497	
Thickness (in.)	0.070	0.069	0.068	0.069	0.069	0.069	0.069	0.069	0.070	
Proportional Limit Load (lb)	1,010	950	980	940	1,140	1,090	1,050	1,120	1,080	
Maximum Load (Failure) (lb)	2,050	2,025	1,950	1,860	1,775	2,000	2,115	1,940	1,950	
Ultimate Tensile Strength (psi)	58,300	58,600	57,200	53,800	51,200	57,900	61,200	56,200	56,100	56,720
P. L. Strength (psi)	28,750	27,400	28,700	27,100	32,900	31,600	30,300	32,500	31,000	30,030
Initial Modulus ($\times 10^{-6}$ psi)	4.08	4.74	4.88	4.92	4.48	4.78	4.55	5.81	4.78	4.78
Final Modulus ($\times 10^{-6}$ psi)	3.12	3.14	3.44	3.68	3.04	2.82	2.88	2.75	3.65	3.17
*Performed for IRAD Creep Program by SwRI										

The tape inclusions in the panel are shown distinctly but are not very well defined by size or shape. Ultrasonic tests of Panels B-2 and B-8 show extensive areas of reduced ultrasonic transmission. Panel B-8 is a $0/90^\circ$ layup, and the tape pattern is apparent in the chart (Fig. 59). Panel B-2 is a 0° layup, and no particular pattern is presented on the chart (Fig. 60). These two results indicate that the recording system's sensitivity was too high during this test. Panel B-7 was an acceptance test panel and is shown in Figure 61 at a lower sensitivity.

Areas of reduced transmission also appear in one corner of Panels G-7, G-11, G-12, G-13, G-14 and G-15. It was possible to determine the significance of these areas by cutting flexure specimens which included these areas of reduced ultrasonic transmission. A more detailed study of Panel No. G-11 will reveal this.

Typical and reduced performance of such flexure specimens is illustrated by the results of tests on glass fabric/epoxy composite (Panel No. G-11). A data summary package is included here as Table V and Figures 62, 63, 64 and 65. Table V gives general information on the prepreg material and the cured laminated panel. The fiber orientation indicates the warp direction of the 1581 style woven glass fabric. The 2387 epoxy resin system is the same that is used in Narmco's Rigidite 5505 boron/epoxy materials which were used as the primary adherend materials in this program. The material was 2 months beyond the warranty expiration date when cured, but it does not appear to have deteriorated to any significant extent.

Figures 62 and 63 represent the average results of flexure tests on three specimens each from adjacent areas of the panel in which the ultrasonic inspection indicated no flaws and extensive flaws, respectively. The flawed area flexure strength and modulus were slightly lower than in the area with no flaws. Figure 64 is the cutting pattern for Panel G-11 in approximately true proportion. Figure 65 is the ultrasonic inspection record for Panel G-11. This is not in true proportion to the panel. The long dimension of the chart represents the 16-in. width of the panel. Each line across the chart represents $1/4$ in. in $18-1/2$ in. of the 20-in. length of the panel (approximately $1-1/2$ in. at the end of the panel, area 11-3 in Fig. 64, was not inspected). The portions of the panel used in these flexure tests are outlined in Figure 65. The other specimens cut were for the IRAD* program only.

*Ibid. († on page 70)

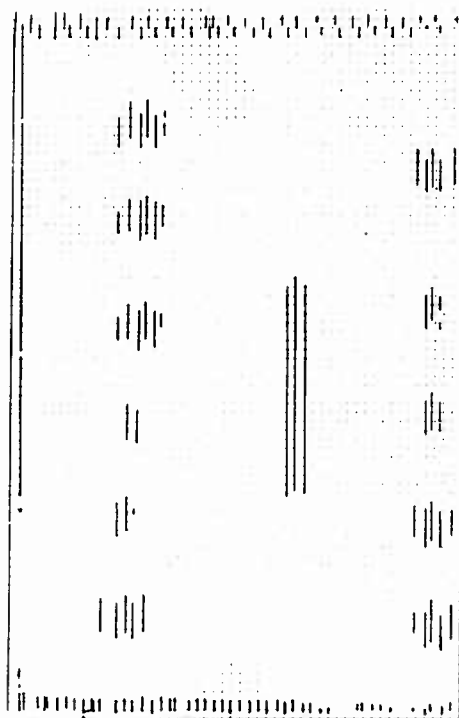


FIGURE 58. PANEL NO. G-6 - ULTRASONIC TEST CHART
INDICATING INCLUSIONS IN PANEL

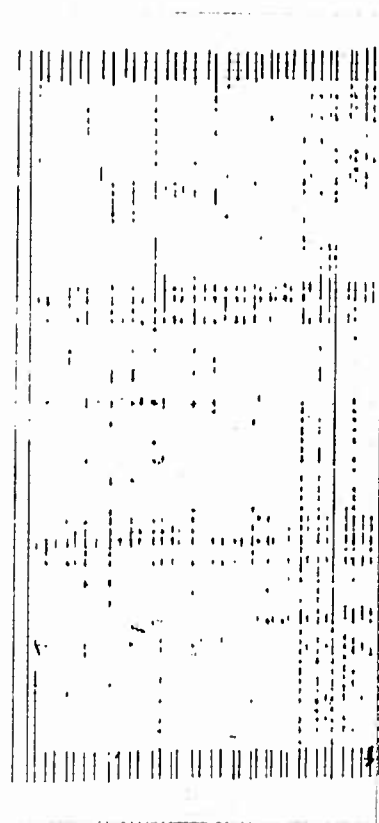


FIGURE 59. CHART OF ULTRASONIC TEST
OF PANEL B-8

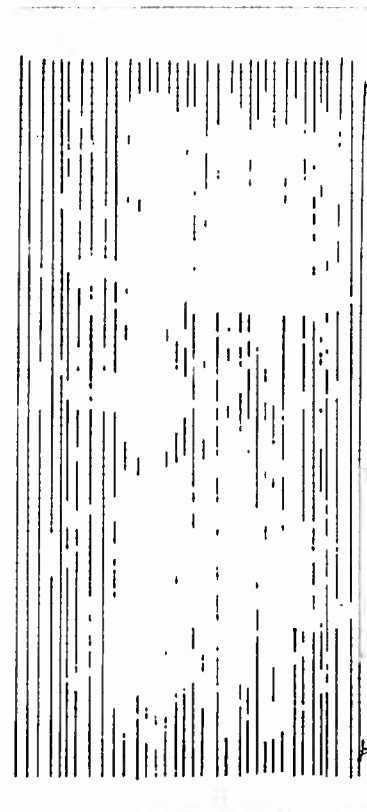


FIGURE 60. CHART OF ULTRASONIC TEST
OF PANEL B-2

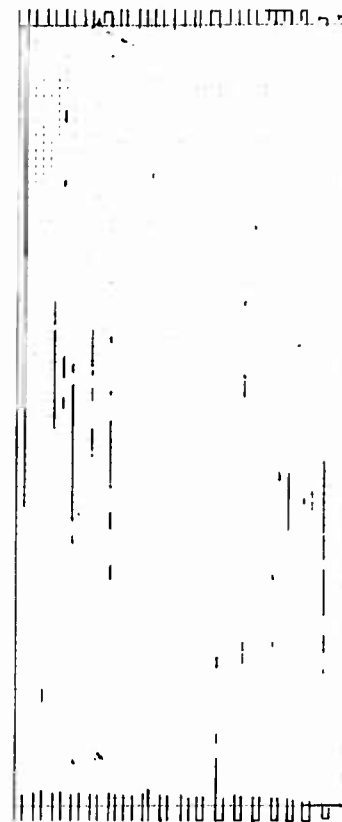


FIGURE 61. CHART OF ULTRASONIC TEST
OF PANEL B-7

TABLE V
PANEL DATA SUMMARY PACKAGE
PANEL NO. G-11

I.	MATERIAL INFORMATION
A.	Material Type: <u>Narmco 2387-1581-38</u>
B.	Date of Manufacture: <u>6-10-69</u>
C.	Material Confirms to Specification: _____
D.	Prepreg Resin Content (Volume %): <u>34.0</u>
E.	Batch No.: <u>11</u>
F.	Roll No.: <u>1</u>
G.	Warranty Expiration: <u>9-11-69</u>
II.	LAMINATE INFORMATION:
A.	Orientation: <u>[0] 11T</u>
B.	Process Record No.: <u>G-11</u>
C.	Process Conforms to Specification: _____
D.	Cure Date: <u>11-14-69</u>
E.	Number of Plies: <u>11</u>
F.	Average Panel Thickness (in.): <u>0.0975</u>
G.	Average Ply Thickness (in.): <u>0.00886</u>
H.	Fiber Content (wt %): <u>70.810</u>
I.	Resin Content (wt %): <u>29.190</u>
J.	Void Volume (Volume %): <u>3.87</u>
K.	Panel Density (lb/in. ³): <u>0.0671</u>
L.	Panel Size: <u>16" X 20"</u>

The boron panels were also X-rayed. A positive print of Panel B-4 is shown in Figure 66 and Panel B-8 in Figure 67. These are both 0°/90° layups, but B-4 was prepared with material from Lot 297, Roll 13 and is nine plies thick, while B-8 was made from Lot 373, Roll 1 and is seventeen plies thick. Spaces are quite evident between the 1/8-in. tapes used in preparing the 3-in. wide tapes in each of these panels. Panel B-8 shows evidence of poor spacing between the 3-in. tapes during layup of the panel which also corresponds to the pattern found in the ultrasonic inspection. The fiber-poor (light) areas on Panel B-4 running parallel to the long axis of the panel (along the edges) are the areas where surface fibers were loose and peeled off when the panel was removed from the tool plate. Panel B-7, the material acceptance test panel, is shown in Figure 68.

Rolls 1, 2 and 3 of Lot 373, Narmco 5505 boron/epoxy prepreg were received on December 16, 1969. Panel B-7 was prepared from Roll 1 on December 23, 1969, for acceptance testing. This was first subjected to ultrasonic and X-ray examination (see Figs. 61 and 68). The panel was then cut into specimens for longitudinal and transverse flexure strength tests and horizontal shear strength test. The results of these tests are given in Table VI along with the results from Narmco. The specimens after test are shown in Figure 69. The test results all satisfy the General Dynamics specification FMS-2001 except the flexural modulus which is slightly (5%) low.

VI.4. ADHEREND PANEL FABRICATION AND QUALITY CONTROL

All composite adherend material panels were fabricated in accordance with Figure 70. These panels and one acceptance test panel (B-20) are listed in Table VII with the ply thickness and fiber orientation. The panel thicknesses shown represent the average of a number of measurements taken 1 in. from the edge around the perimeter of the panel. Except for Panel B-20, these measurements indicate a ply thickness value of 0.0053 ± 0.0004 in. average for the boron/epoxy composites. Panel B-20 is indicated to have a ply thickness of 0.00486 in.; however, measurement of the ply thickness in a microphotograph gave a value of 0.00518 inch.

Panel B-20 was a 6 X 10-in. panel which was prepared for acceptance testing of the Narmco 5505 material from Batch No. 381. This shipment was comprised of Roll Nos. 30, 31, 32, 33 and 73, which were received on March 5, 1970. The ultrasonic test chart of this panel is shown in Figure 71, and a positive print of the X-ray is shown in Figure 72. The results of the longitudinal and transverse flexure strength and modulus and horizontal shear strength tests are given in Table VIII along with the qualification test results from Narmco and the General Dynamics FMS-2001 specification requirements. All acceptance test results were substantially in excess of this specification's requirements and also exceeded the Narmco qualification flexure values.

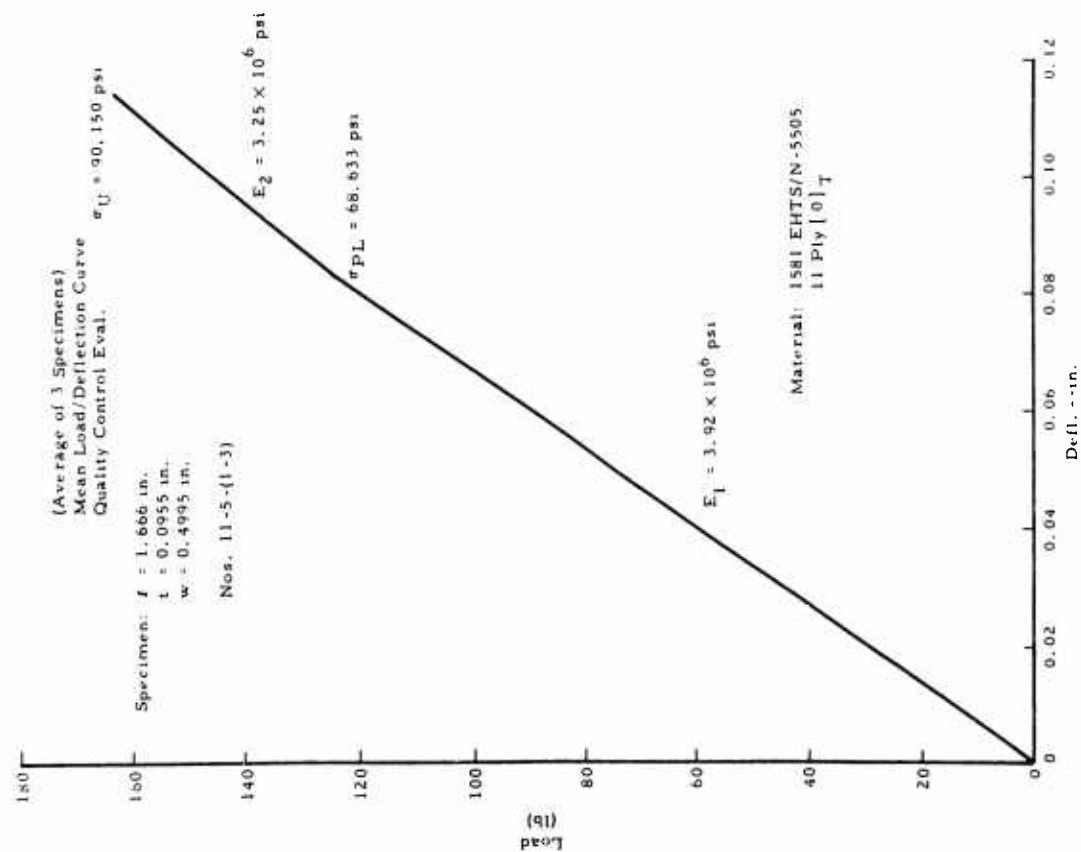


FIGURE 62. AVERAGE FLEXURE TEST RESULTS—PANEL G-11—NO FLAWS INDICATED BY ULTRASONIC INSPECTION

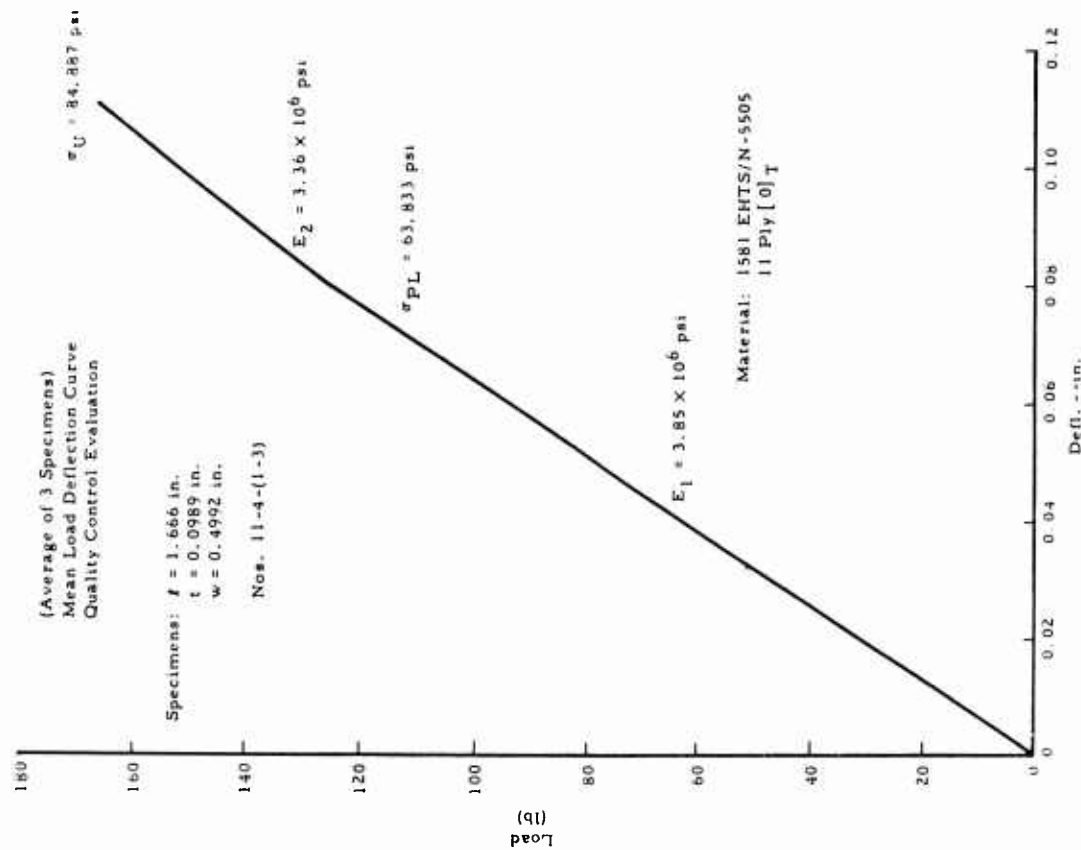


FIGURE 63. AVERAGE FLEXURE TEST RESULTS—PANEL G-11—FLAWS INDICATED BY ULTRASONIC INSPECTION



FIGURE 65. ULTRASONIC THRU-SCAN RECORD--PANEL G-11

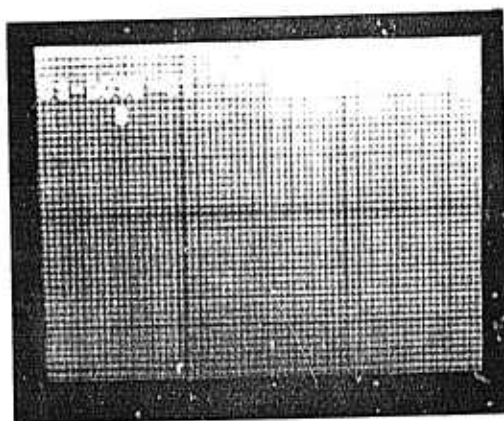


FIGURE 66. X-RAY OF PANEL B-4

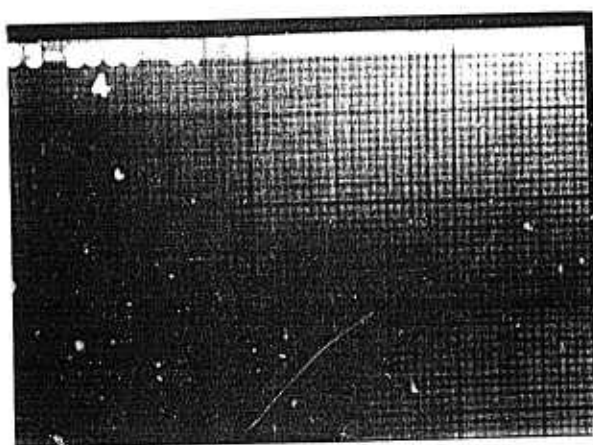


FIGURE 67. X-RAY OF PANEL B-8

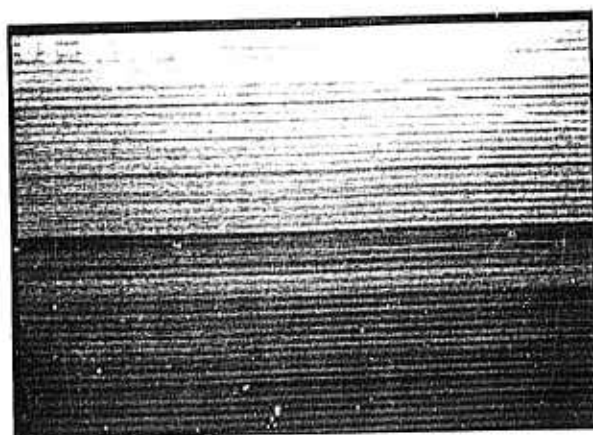


FIGURE 68. X-RAY OF PANEL B-7

TABLE VI
MATERIAL ACCEPTANCE TESTS

Narmco 5505 Boron/Epoxy Prepreg Lot 373, Roll 1					
Laminate Fiber Orientation: 0°					
Load Orientation: 0° and 90°					
Laminate Thickness: 15 plies - 0.080 inch					
Physical Property	Test Temp, ° F	SwRI Acceptance Tests		Narmco QC Report	G.D.'s Spec. FMS-2001
		Spec. No.	Results		
Flexural Strength— Longitudinal (psi)	RT	B-7-1	233,260	225,900	225,000
	RT	B-7-2	268,130		
	RT	B-7-3	234,490		
		Average	245,290		
Flexural Modulus— Longitudinal (psi)	RT	B-7-1	29.85×10^6		30×10^6
	RT	B-7-2	27.65×10^6		
	RT	B-7-3	27.85×10^6		
		Average	28.45×10^6		
Flexural Strength— Transverse (psi)	RT	B-7-4	14,770	14,200	10,000
	RT	B-7-5	9,375		
	RT	B-7-6	12,300		
		Average	12,150		
Horizontal Shear Strength (psi)	RT	B-7-7	15,390	13,400	13,000
	RT	B-7-8	15,510		
	RT	B-7-9	15,330		
	RT	B-7-10	15,340		
		Average	15,390		

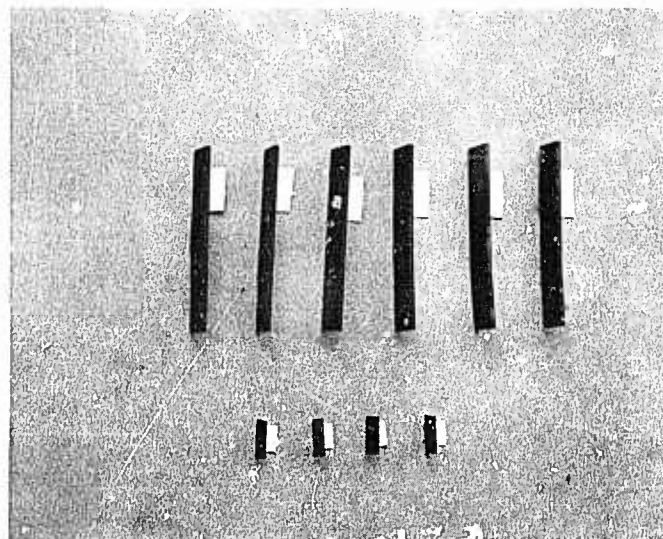


FIGURE 69. MATERIAL ACCEPTANCE TEST SPECIMENS

TABLE VII
PANEL FABRICATION FOR SIMPLE BONDED
JOINT EVALUATION

Panel No.	Nominal Size, in.	No. of Plys	Measured Average Panel Thickness, in.	Fiber Orientation*	Material Narmco 5505		Remarks
					Batch No.	Roll No.	
B-12	16 x 20	3	0.01655	$[0]_{3T}$	373	1	
B-13	16 x 20	6	0.03325	$[0]_{6T}$	373	1	
B-14	16 x 20	9	0.04918	$[(0/90)_6/0]_T$	373	1	
B-15	16 x 20	17	0.09098	$[(0/90)_8/0]_T$	373	1, 2	
B-16	16 x 20	9	0.04925	$[0/+45/0/-45/0]_S$	373	2	
B-17	16 x 20	17	0.09150	$[0/+45/0/-45/0]_S$	373	3	
B-18	16 x 20	6	0.03167	$[0]_{6T}$	373	3	
B-19	16 x 20	17	0.09077	$[(0/90)_8/0]_T$	373	3	
B-20	6 x 10	15	0.07290	$[0]_{15T}$	381	30	Acceptance Test Panel
B-21	16 x 20	9	0.04760	$[0]_{9T}$	381	30	
B-22	16 x 20	17	0.09117	$[(0/+45/0/-45/0]_S$	381	30, 31	
B-23	16 x 20	16	0.08306	$[(0/90)_2/0]_{4T}$	381	30, 31	
B-24	16 x 20	9	0.04835	$[0/+45/0/-45/0]_S$	381	30, 31	
B-25	16 x 20	8	0.04126	$[0]_{8T}$	381	31	
B-26	16 x 20	16	0.08385	$[(0/+45/0]_2]_S$	381	31, 32	
B-27	16 x 20	16	0.08460	$[(0/+45/0]_2]_S$	381	32, 33, 34	
B-28	16 x 20	9	0.04494	$[(0/+45/0/-45/0]_S$	381	34	
B-29	6 x 9	8	0.03610	$[(0/90)_2/0]_{1T}$	381	34	Void Standard Panel
B-30	6 x 9	16	0.07230	$[(0/90)_2/0]_{4T}$	381	34	Void Standard Panel

*See Appendix C for the General Specifications on the Laminate Orientation Code

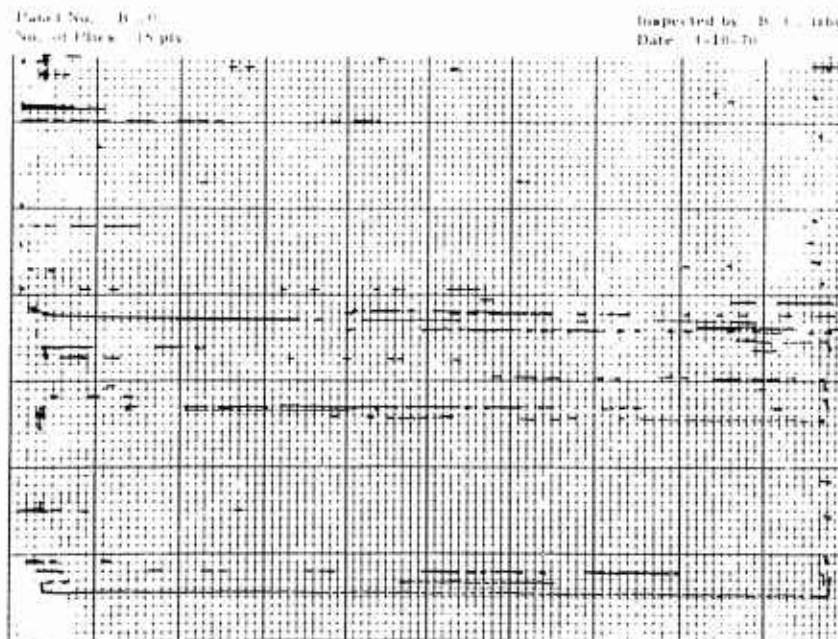


FIGURE 71. ULTRASONIC INSPECTION RECORD FOR PANEL B-20

TABLE VIII
MATERIAL ACCEPTANCE TEST

March 20, 1970

by
R. E. Tuck

Narmco 5505 Boron-Epoxy Prepreg Lot 381, Roll 30
Laminate Fiber Orientation 0
Laminate Thickness .15 plys. 0.073 in

Physical Property	Test Temp., °F	SWRI Spec. No.	Results	Narmco QC Report	G.D.'s Spec. 1MS, 2001
Flexural Strength Longitudinal (psi)	RT	B-20-4	258,772	245,700	225,000
	RT	B-20-5	280,430		
	RT	B-20-6	277,181		
		Average	272,428		
Flexural Modulus Longitudinal (psi)	RT	B-20-4	30.76×10^6		30×10^6
	RT	B-20-5	31.49×10^6		
	RT	B-20-6	32.57×10^6		
		Average	31.60×10^6		
Flexural Strength Transverse (psi)	RT	B-20-1	13,148	14,100	10,000
	RT	B-20-2	15,157		
	RT	B-20-3	14,604		
		Average	14,303		
Flexural Modulus Transverse (psi)	RT	B-20-1	7.90×10^6		
	RT	B-20-2	7.61×10^6		
	RT	B-20-3	7.61×10^6		
		Average	7.72×10^6		
Horizontal Shear Strength (psi)	RT	B-20-1	14,228	13,600	13,000
	RT	B-20-2	14,162		
	RT	B-20-3	14,938		
	RT	B-20-4	14,411		
		Average	14,436		

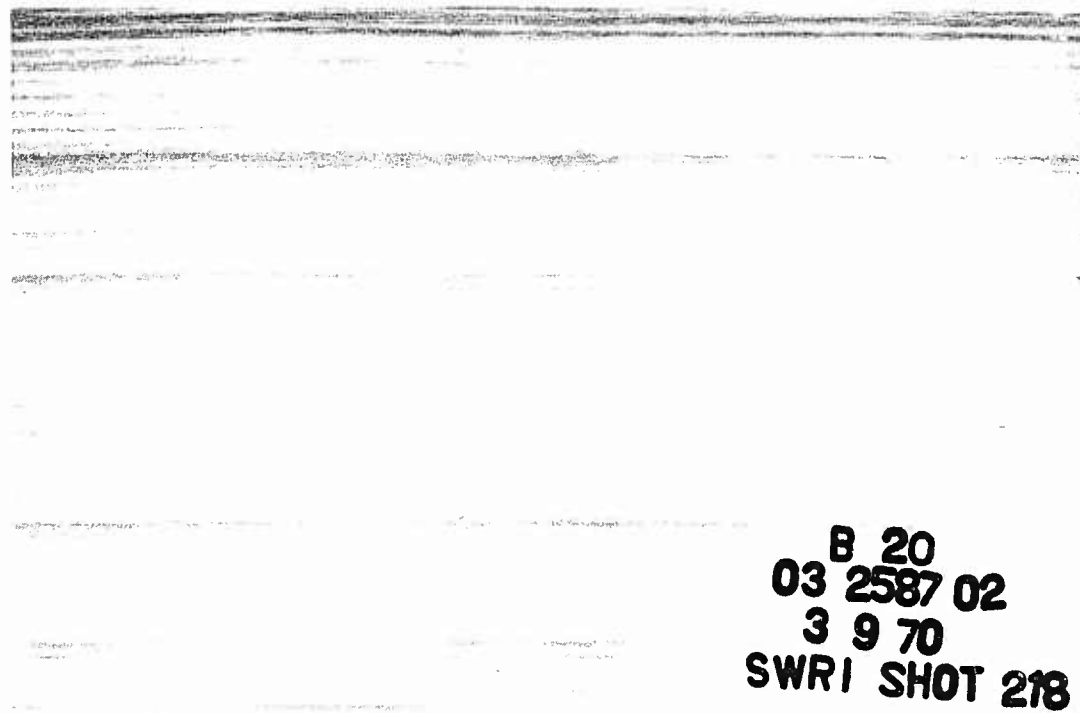


FIGURE 72. POSITIVE PRINT OF X-RAY OF PANEL B-20 USED FOR ACCEPTANCE TESTING

Panels B-29 and B-30 were manufactured with known void inclusions for use as void standards in comparisons with the actual panels. A scale drawing of the void inclusion panels is shown in Figure 73, locating and describing

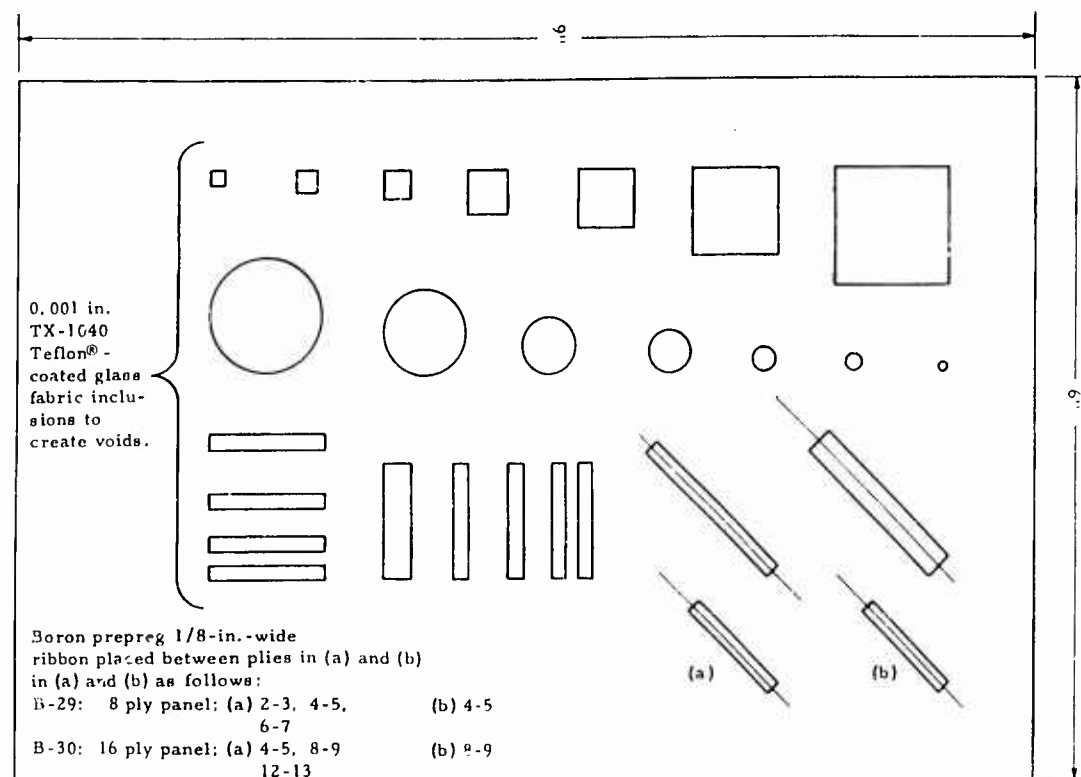


FIGURE 73. BORON REINFORCED ULTRASONIC TEST PANELS

them precisely. The ultrasonic record of void panel B-29 is shown in Figure 74, and that of void panel B-30, in Figure 75. Two void panels, one 8-ply and one 16-ply, were necessary to adjust the ultrasonic inspection system. Most of the panels used in the program are close to these numbers of plies.

The ultrasonic inspection recorder charts (see Figs. 74 and 75) for the 6- X 9-in. panels, B-29 (8 plies) and B-30 (16 plies), contain the following built-in voids. Pieces of TX-1040 Teflon®-treated glass fabric, 0.001-in. thick, were placed between the center plies. The top row is composed of square shapes ranging from 1/8 to 1 in. in size. The second row is composed of circles of the same diameters. The third row, from left to right, contains 1/8- X 1-in. long strips spaced 1/8, 1/4 and 3/8 in. apart, oriented at 0° to the direction of the ultrasonic scan. Next are strips oriented at 90° to the scan direction. The first strip is 1/4 in. wide and the others are 1/8 in. wide and again spaced at intervals of 3/8, 1/4 and 1/8 inch. These are followed by a 1/8- and a 1/4-in. wide strip at a 45° angle. Below the 1/4-in. wide, 45° strip, a 1/8-in. wide X 1-in. long strip of boron/epoxy prepreg was placed between the center plies. Below the 1/8-in., 45° strip, three strips of boron/epoxy were placed between plies 2 and 3, 4 and 5, and 6 and 7. The boron/epoxy strips were also oriented at 45° to the scan direction. A 0/90 cross-ply fiber orientation was used for both panels.

The 1/8-in. diameter circle was lost at the 6-dB sensitivity level required to minimize extraneous signals in the 16-ply panel (B-30). Some other areas of apparent thickness discontinuity are present in addition to the TX-1040 fabric. The extra layer of boron/epoxy also is detected by the ultrasonic test. In the 8-ply panel (B-29) the 1/8-in. square and circle are barely detectable at a 4-dB sensitivity. The single extra ply of boron/epoxy shows up more

*Registered trademark, E. I. DuPont de Nemours.

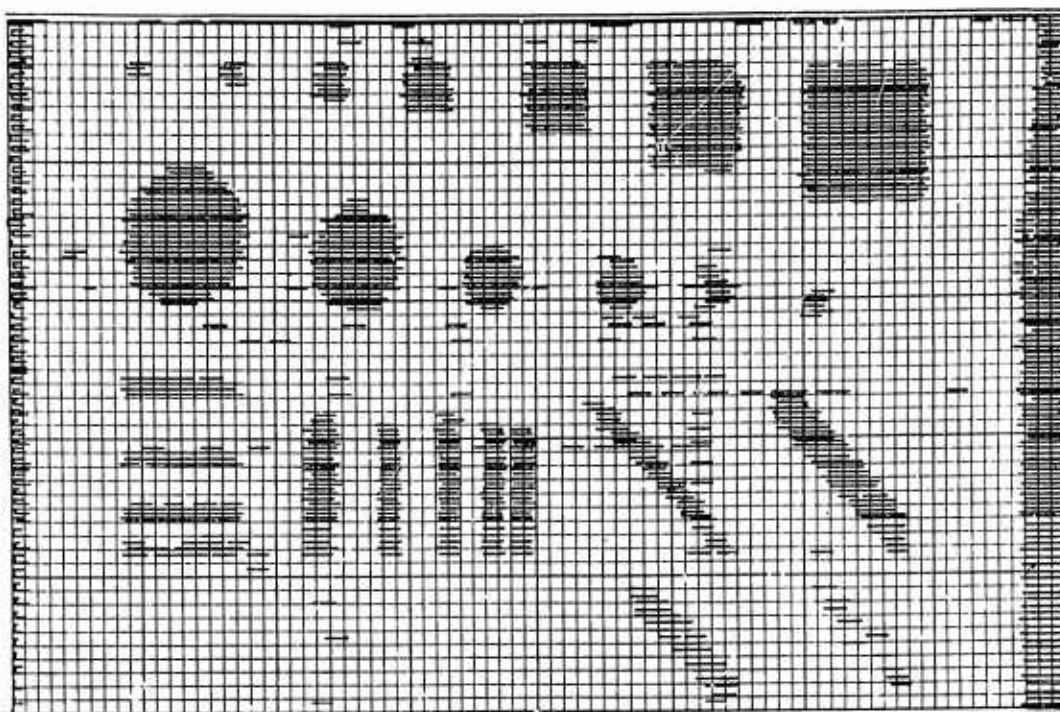


FIGURE 74. ULTRASONIC INSPECTION OF
VOID PANEL B-29

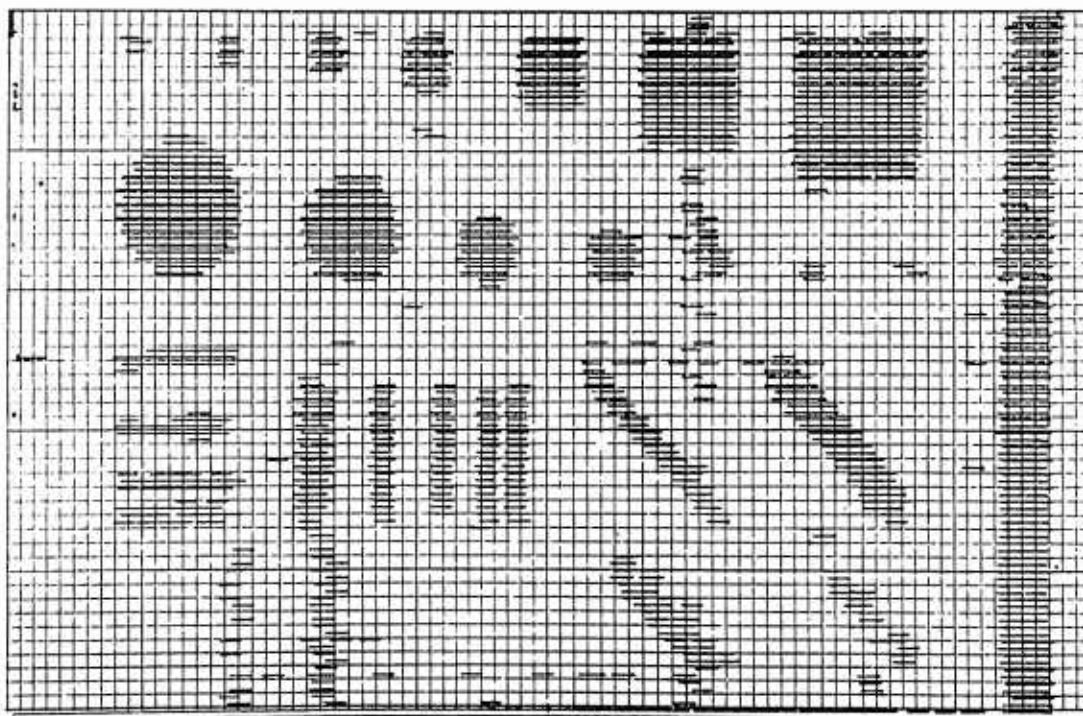


FIGURE 75. ULTRASONIC INSPECTION OF
VOID PANEL B-30

readily than in the 16-ply panel. Some unplanned apparent thickness discontinuity areas are also apparent in this panel. The ultrasonic thru-scan and radiograph inspection records for adherend panels B-12 through B-28 are shown in Appendix D.

Marking and machining of the 16 X 20-in. boron composite adherend panels into lap shear assembly details is shown in Figure 76. A 15/16-in. wide strip was cut from the long edges of each panel. Two 9-in. long tensile test specimens were cut from each strip (four per panel). These had glass-fabric/epoxy (1581/5505) load pads bonded (with AF 126-2) to the ends for the monotonically loaded tension test which provided the complete stress-strain curve for strength and modulus determination of each panel*. Standard constituent properties of boron/epoxy laminates are presented in Appendix B.

Fiber content of each panel was determined by the fiber count method using from two to six specimens cut at each end, and the center of each of the strips to be used for tensile test specimens. Figure 76 shows the location of the strips and individual specimens relative to the panel and adherend pieces

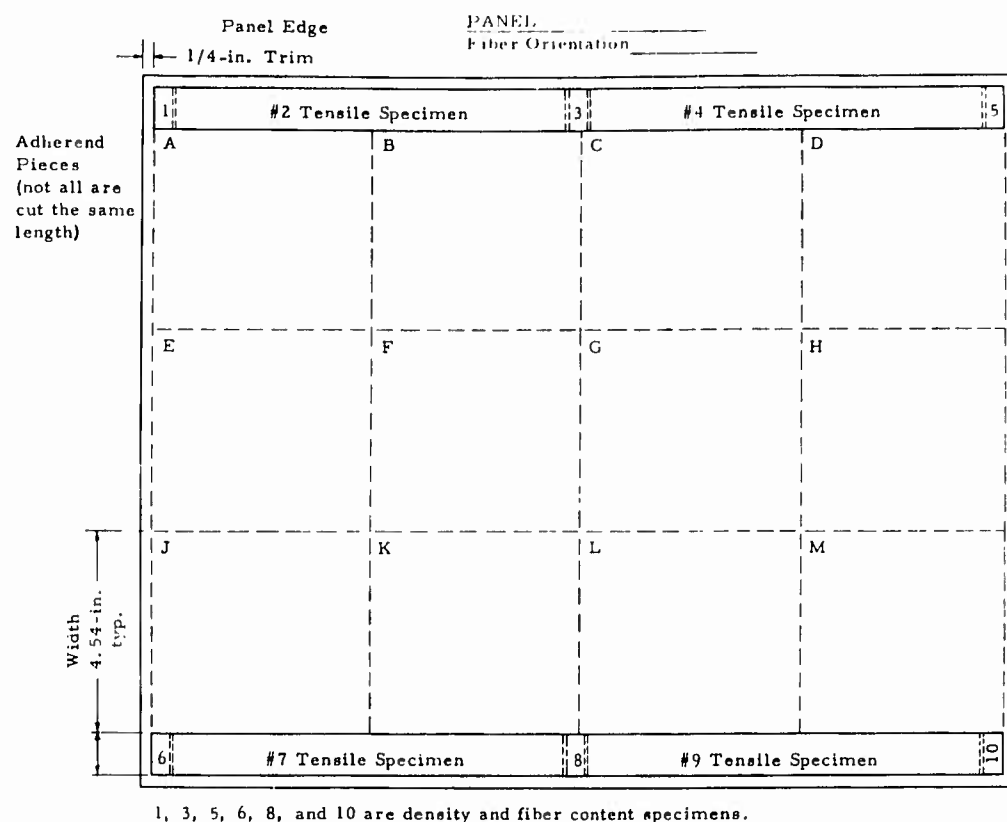


FIGURE 76. QUALITY CONTROL AND TENSILE STRENGTH TEST SPECIMENS

*See Appendix C for Test Method, Appendix E for typical data.

SECTION VII

LAMINATE AND TITANIUM ADHEREND TEST RESULTS

VII.1. GENERAL

Section VII is devoted to summarizing and discussing the results obtained from testing composite and titanium adherend materials. Section VII.2 analyzes the Laminate Adherend Experimental Results whereas Section VII.3 summarizes the Titanium Adherend Experimental Results.

VII.2. LAMINATE ADHEREND EXPERIMENTAL RESULTS

Selected typical tensile test data on the N-5505 boron/epoxy laminates are given in Appendix E. There are typical stress-strain curves and cross-section photomicrograph is presented for each different material batch/orientation group of four tensile specimens. A summary of the key properties has been made from the detailed data and is shown in Table IX. Typical, representative failed specimens are covered in Figures 77 and 78.

VII.2.a. Laminate Performance

It becomes obvious after study of this data that laminate tensile specimen performance was not up to par with 2nd Edition Design Guide data.* In an attempt to establish the magnitude of the discrepancy from the normal or expected values the unidirectional data were analyzed. Panels B-12, 13 and 18 from material Batch No. 373 and Panels B-21 and 25 from material Batch No. 381 were $[0]_{11T}$ laminates from which tensile specimens and adherend materials were cut with their longitudinal axis parallel to the fibers. The method used for properties prediction was originally proposed by Tsai⁽¹⁷⁾ based on the "rule of mixtures" technique. The "k" (and k') factor used by Tsai was called a fiber misalignment factor. In the analysis here it shall be called the "void factor" and based on an empirically developed mathematical form of the laminate decimal void-volume (V.V.). The results of this study along with the formulas are presented in Table X. These formulas give results which are strongly dependent on the fiber volume (F.V.). In addition, the factor K_0 (and K'_0) is a function of the matrix/fiber modulus or strength ratio. Here another deviation was used. Both the matrix modulus and strength were utilized as being the average of the matrix material and a 104 glass scrim laminate.† Since the tensile stress-strain curve of this boron/epoxy material is linearly elastic‡ almost to failure it was felt satisfactory to use the rule of mixtures technique to predict ultimate strength as well as modulus.

A study of the photomicrographs of Appendix E will reveal that all the reinforcing fibers in the laminates were badly cracked but fully encased in resin throughout the crack spaces. Therefore, it must be assumed that the fibers were cracked prior to laminating the prepreg material in the hot platen press. It also is assumed that the extensive amount of cracked and broken fibers visible in the photomicrographs had not occurred at the time of impregnating them with resin. This assumption is based on the judgment that impregnating such extensively cracked and broken fibers would have been impossible by present methods. There is the possibility of course that the breakage could have occurred immediately after impregnating due to handling of the prepreg manufacturer or due to subsequent handling by the laminator.** In the author's judgment the latter two possibilities are remote

* $F_L^{T'} = 188$ ksi, $E_L^{T'} = 30 \times 10^6$ psi.

†See Appendix B.

‡Sometimes in two stages.

**SwRI.

TABLE IX
LAMINATE MECHANICAL/PHYSICAL PROPERTIES DATA SUMMARY

Panel Number	N-5505 Broomfield Panel No.														
	B-12	B-13	B-14	B-15	B-16	B-17	B-18	B-19	B-21	B-22	B-23	B-24	B-25	B-26	B-28
Orientation Parameters	[0]°/3°	[0]°/6°	[0]°/90°/45°/0°/1°	[0]°/90°/45°/0°/1°	[0]°/45°/0°/45°/0°/1°	[0]°/45°/0°/45°/0°/1°	[0]°/45°/0°/45°/0°/1°	[0]°/90°/45°/0°/1°	[0]°/90°/45°/0°/1°	[0]°/45°/0°/45°/0°/1°	[0]°/45°/0°/45°/0°/1°	[0]°/45°/0°/45°/0°/1°	[0]°/45°/0°/45°/0°/1°	[0]°/45°/0°/45°/0°/1°	[0]°/45°/0°/45°/0°/1°
No. of Plys	3	6	9	1°	9	1°	6	17	9	17	16	9	8	16	9
σ_u , ksi	122.539	146.738	59.972	52.876	90.036	88.009	147.726	15.110	177.387	109.665	40.005	99.790	177.850	93.524	92.989
ϵ_{u1} , $\mu\text{in./in.}$	4.727	5.382	3.658	3.577	5.110	5.558	5.370	3.622	6.068	6.246	3.140	6.382	6.255	5.614	5.342
ϵ_{u2} , $\mu\text{in./in.}$	964	1.145	1.29	1.04	3.435	3.665	1.059	92	1.208	4.588	98	4.129	1.391	4.020	3.548
σ_{ϕ} , ksi	97.753	127.960	34.861	27.476	61.824	64.571	120.053	33.012	174.564	64.500	24.772	73.155	166.735	71.190	77.930
$\epsilon_{\phi 1}$, $\mu\text{in./in.}$	3.656	4.638	1.902	1.692	3.355	3.874	4.282	1.940	5.944	3.515	1.626	4.333	5.808	4.186	4.404
$\epsilon_{\phi 2}$, $\mu\text{in./in.}$	744	975	85	65	2.205	2.570	923	67	1.190	2.532	60	2.929	1.289	2.975	2.952
E_p , ksi	26.767	27.682	18.095	15.967	18.435	16.880	28.312	17.041	29.535	18.476	15.356	16.873	28.701	17.027	17.705
E_z , ksi	22.062	25.314	14.390	13.113	16.440	14.588	13.365	13.365	16.832	16.832	15.654	15.654	15.654	15.654	15.654
ν_p	0.2134	0.2087	0.0427	0.0395	0.6578	0.8528	0.2015	0.0342	0.1956	0.7212	0.0370	0.6625	0.2112	0.7195	0.6790
ν_z	0.2165	0.2065	0.0334	0.330	0.6466	0.6503	0.0310	0.0310	0.520	0.7314	0.505	0.6648	0.2112	0.7160	0.6790
F.V. Fraction	0.536	0.498	0.476	0.508	0.468	0.520	0.501	0.512	0.520	0.496	0.505	0.506	0.505	0.484	0.495
V.V. Fraction	0.160	0.014	0.004	0	0	0	0.0490	0	0.018	0	0	0	0	0	0
Density, lb/in. ³	0.0643	0.0688	0.0681	0.0710	0.0683	0.0708	0.0678	0.0712	0.0697	0.0713	0.0712	0.0704	0.0698	0.0713	0.0721
% Cracked Filaments	94.5	96.0	89.8	94.0	93.0	96.5	80.0	60.5	97.0	82.0	91.0	91.7	100	94.5	82.0
Thickness per ply, in.	0.00551	0.00554	0.00546	0.00535	0.00547	0.00572	0.00528	0.00514	0.00528	0.00536	0.00519	0.00537	0.00516	0.00531	0.00499
Total Thickness, in.	0.01655	0.03325	0.04918	0.09098	0.04925	0.09150	0.03167	0.09027	0.04760	0.09117	0.08308	0.04835	0.04126	0.0488	0.04494
Material Batch/Lot	373/1	373/1	373/1	373/1 & 2	373/2	373/3	373/3	373/3	381/30	381/30 & 31	381/30 & 31	381/30 & 31	381/31	381/31 & 32	381/73

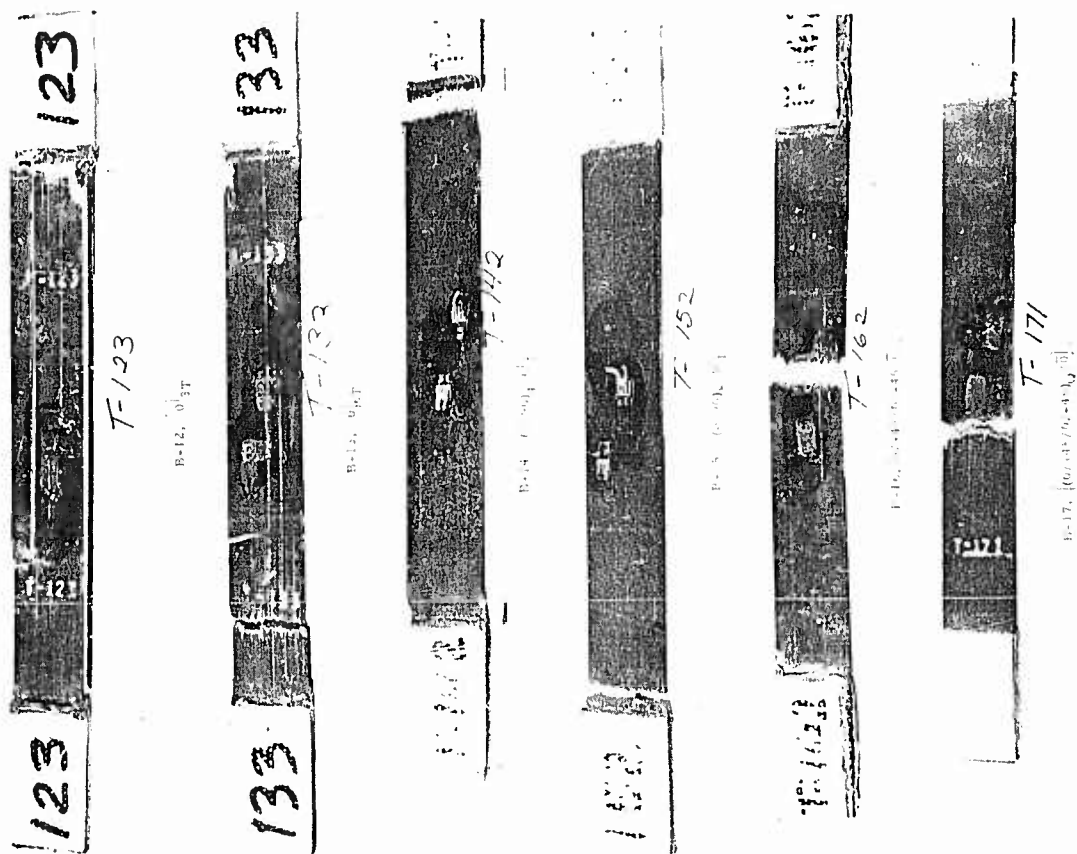


FIGURE 77. TYPICAL FAILED COMPOSITE TENSILE SPECIMENS, MATERIAL BATCH 373

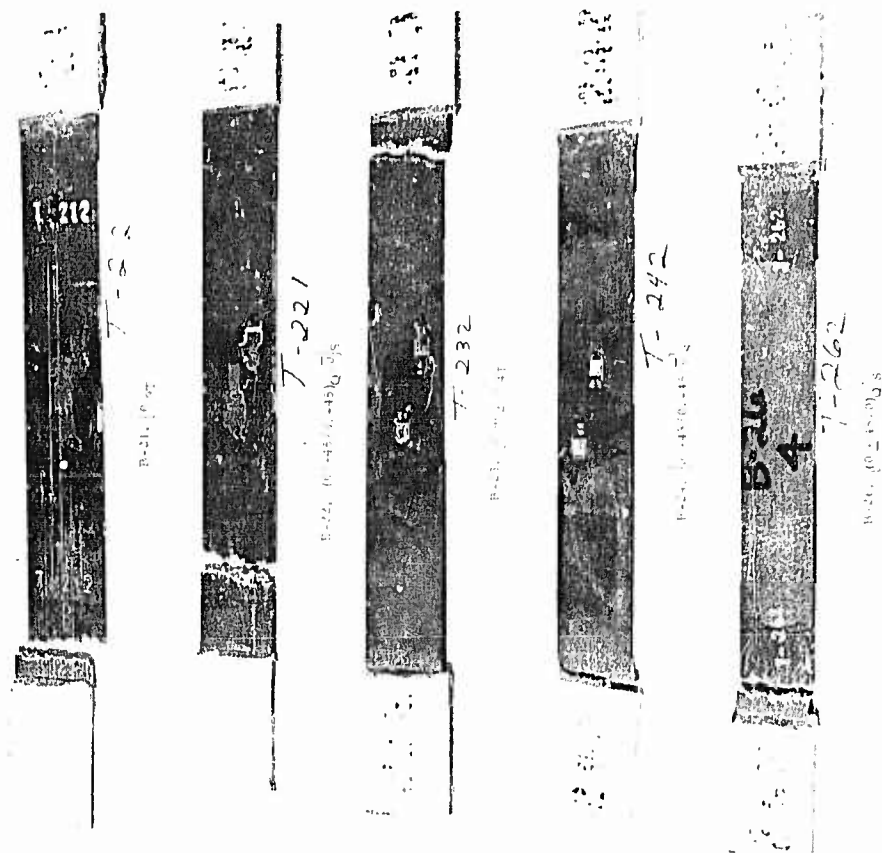


FIGURE 78. TYPICAL FAILED COMPOSITE TENSILE SPECIMENS, MATERIAL BATCH 381

TABLE X
UNIDIRECTIONAL LAMINATE PERFORMANCE

Batch	Panel No.	Panel F.V.	Panel V.V.	Panel Density, lb/in. ³	Exper. E_p , 10 ⁶ psi	Calc. E_q , 10 ⁶ psi	$E_p/E_q \times 100$, %	Exper. σ_u , ksi	Calc. F_{tu} , ksi	$\sigma_u/F_{tu} \times 100$, %
373	B-12	0.536	0.160	0.0643	26.767	31.140	85.96	122.539	168.739	72.62
	B-13	0.498	0.014	0.0688	27.682	29.752	93.04	146.738	184.934	79.34
	B-18	0.501	0.040	0.0678	28.312	29.938	94.57	147.726	181.090	81.58
381	B-21	0.520	0.018	0.0697	29.535	31.021	95.21	177.387	191.608	92.58
	B-25	0.505	0	0.0698	28.701	30.218	94.98	177.856	190.080	93.57
Formulas										
Modulus					Strength					
$E_q = kE_f [1 - K_0(1 - F.V.)]$					$F_{tu} = k'E_f [1 - K'_0(1 - F.V.)]$					
$k = 1 - (V.V.)^2$					$k' = 0.80(1 - V.V.)$					
$K_0 = 1 - \frac{E_m}{E_f} = 0.9682$					$K'_0 = 1 - \frac{F_m}{F_f} = 0.9534$					
Properties										
$E_m = \frac{(3.2 + 0.487) \times 10^6}{2} = 1.844 \times 10^6 \text{ psi}$					$E_f = 58.0 \times 10^6 \text{ psi}$					
$F_m = \frac{37.8 + 4.184}{2} = 20.992 \text{ ksi}$					$F_f = 450.0 \text{ ksi}$					

because (1) handling the material after impregnating does not usually involve severe mechanical impingements and (2) making flat laminates does not normally induce such damage. Since this fiber was one of the first batches delivered after the twisted fiber episode with the fiber makers was solved, the fiber manufacture appears to be at fault. It is the authors' judgment that built-in residual stresses in the boron fibers caused cracking and breaking at some time after impregnation but before curing.

What is amazing about this problem is that only the tensile tests and photomicrographs uncovered the phenomena and the flexure tests and ultrasonic and radiograph inspections on the cured panels did not reveal the problem.

For Material Batch 373 in Table X it can be seen that Panel B-12 had a very high void volume (16%) with a resultant substantial reduction in the tensile properties from that of the low void volume laminate of Panels B-13 and B-18. Panel B-12 exhibited properties realization percentages of 85.96% for modulus of elasticity and 72.62% for strength whereas the average of Panels B-13 and B-18 gave 93.80% for modulus and 80.46% for strength. This illustrates the reduction caused by a high void content. Longitudinal flexure acceptance tests showed this material passed the minimum strength required (225 ksi) by 9% while the modulus failed by 5%. Transverse flexural strength was 42% above requirements (10 ksi) whereas interlaminar shear strength exceeded minimum requirements (13 ksi) by

only 3%. While the flexure acceptance test predicted closely what would happen to the tensile modulus the flexural strength was not even close as a predictor of tensile strength.

Material Batch 381, received later, was substantially better than 373 as indicated by both the acceptance tests and the tensile tests. However, the modulus and strength realization percentages* are still only 95.10% and 93.08%, respectively, as shown by the average of Panels B-21 and B-25. This compares with longitudinal flexural strength and modulus values which exceeded the requirements by 21% and 5%, respectively. Transverse flexural strength exceeded that required by 41% whereas horizontal shear strength exceeded that required by 20%.

All this indicates that the flexure and interlaminar shear tests for acceptance are not good measures of cracked or broken fibers even though they may be good checks on impregnation and lamination processing variables.

Because of the fiber breakage problem, which was detected from photomicrographs on all panels regardless of orientation, all of the longitudinal tensile properties are somewhat low. However, it is doubtful that the transverse tension and shear tests of $[0]_nT$ laminates would show any reduction, although transverse tests on the angleply ones would probably exhibit some degradation.

VII.2.b. Laminate Orientation Sequence vs Performance

An interesting phenomena is the variation of properties with laminate orientation sequence. For the general crossply (0/90) orientation type the following comparison illustrates this point.

Item	Panel Nos.	F.V.	Orientation	V.V.	σ_U , ksi	E_P , 10^6 psi	Batch
1	B-15/B-19	0.510	$[(0/90)_8/0]_T$	0	53.993	16.504	373
2	B-23	0.505	$[0/90_2/0]_4T$	0	40.005	15.356	381
					13.988	1.144	
					Diff.	Diff.	

The $[0/90_2/0]_4T$ orientation exhibits a 26% reduction in strength and a 7% reduction in modulus compared to the $[(0/90)_8/0]_T$ one. This occurred in spite of the fact that the $[0/90_2/0]_4T$ orientation laminate was made from a substantially superior batch (381) of material. While the 12-1/2% more 0° plies in the first one over the second one may account for the modulus change it does not account for all of the strength change.

Another comparison can be made with the general $0/\pm 45^\circ$ orientation as shown in the following table.

Item	Panel Nos.	F.V.	Orientation	V.V.	σ_U , ksi	E_P , 10^6 psi	Batch
1	B-16	0.468	$[0/+45/0/-45/\bar{0}]_S$	0	90.036	18.435	373
2	B-24/B-28	0.500	$[0/+45/0/-45/\bar{0}]_S$	0	96.390	17.289	381
					6.354	1.146	
					Diff.	Diff.	
3	B-17	0.520	$[(0/+45/0/-45)_Q/\bar{0}]_S$	0	88.009	16.880	373
4	B-22	0.496	$[(0/+45/0/-45)_Q/\bar{0}]_S$	0	109.669	18.476	381
					21.660	1.596	
					Diff.	Diff.	
5	B-22	0.496	$[(0/+45/0/-45)_Q/\bar{0}]_S$	0	109.669	18.476	381
6	B-26	0.484	$[(0/\pm 45/0)_Q]_S$	0	93.524	17.027	381
					16.145	1.449	
					Diff.	Diff.	

*As measured in tension.

In Items 1 and 2, identical nine-ply orientations are compared for the two different material batches. Items 3 and 4 compare identical seventeen-ply orientations of the two different material batches. The strength values of Material Batch 381 show 7% and 25% improvement, respectively, over those of Batch 373 while the modulus values are about the same for the two pair of items. Comparison of the $[(0/+45/0/-45)_2/0]_S$ orientation with the $[(0/\pm45/0)_2]_S$ one is shown in Items 5 and 6. The first orientation shows an improvement of 17% in strength and 9% in modulus over the second one with both laminates being of the same batch of material. Again the strength increase is greater than would be indicated by the 12-1/2% increase in 0° plies whereas the modulus increase could be accounted for by this difference.

A direct comparison of Panels B-23, B-15/B-19, B-26, and B-22 is made below showing the trend of improvement with change of basic orientation and sequence.

Item	Panel Nos.	F.V.	Orientation	V.V.	σ_U , ksi	E_P , 10^6 psi	Batch
1	B-23	0.505	$[0/90_2/0]_4T$	0	40.005	15.356	381
2	B-15/B-19	0.510	$[(0/90)_8/0]_T$	0	53.993	16.504	373
3	B-26	0.484	$[(0/\pm45/0)_2]_S$	0	93.524	17.027	381
4	B-22	0.496	$[(0/+45/0/-45)_2/0]_S$	0	109.669	18.476	381

From these comparisons it appears that the general $0/\pm45^\circ$ orientation is stronger and stiffer than the general $0/90^\circ$ orientation and that further improvement can be made by separating either the plus and minus 45° plies or the 90° plies by 0° plies.

The orientations and thicknesses selected for adherend materials are believed to be representative of those used in the aerospace industry. They cover ten orientation/thickness combinations in the fifteen 16×20 -in. flat panels made, from which adherends were cut for the bonded joint program.

VII.3. TITANIUM ADHEREND EXPERIMENTAL RESULTS

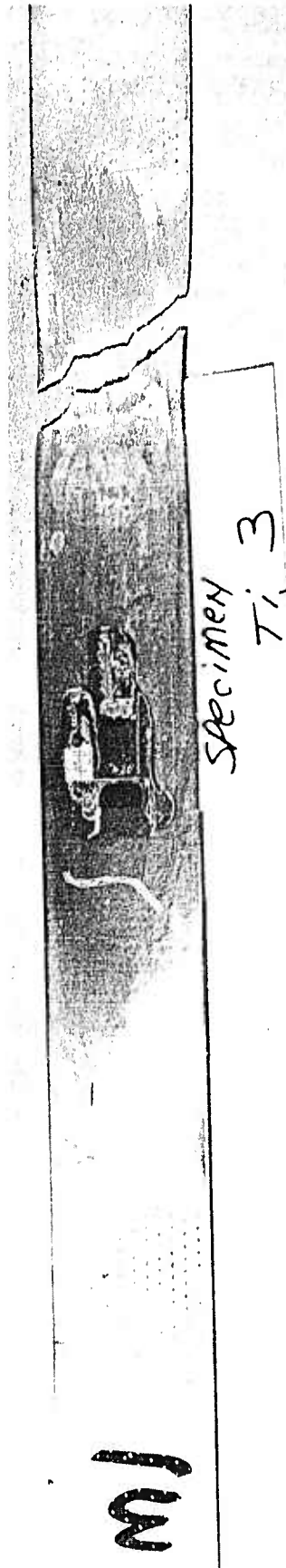
The other adherend material was 6Al-4V annealed titanium sheet purchased from Titanium Metals Corp. (TMC). Four nominal thicknesses were used. These were 0.016, 0.032, 0.045 and 0.090 in. Two straight-sided tensile specimens were tested from each thickness with the same equipment and instrumentation used to test the composite tensile specimens and the bonded joints. Average stress-strain curves for each thickness are contained in Appendix E. A summary of these properties is presented in Table XI whereas Figure 79 presents typical, representative tensile specimen failures. These average curves of Appendix E were used to obtain the Ramberg-Osgood parameters for use in the nonlinear analysis of bonded joints with at least one of the adherends made of titanium. Properties measured compared reasonably well with TMC and handbook typical properties. It can be observed from these data that the titanium becomes far more nonlinear than the composite materials studied in this bonded joint investigation.

TABLE XI
6AL-4V TITANIUM SHEET PROPERTIES SUMMARY

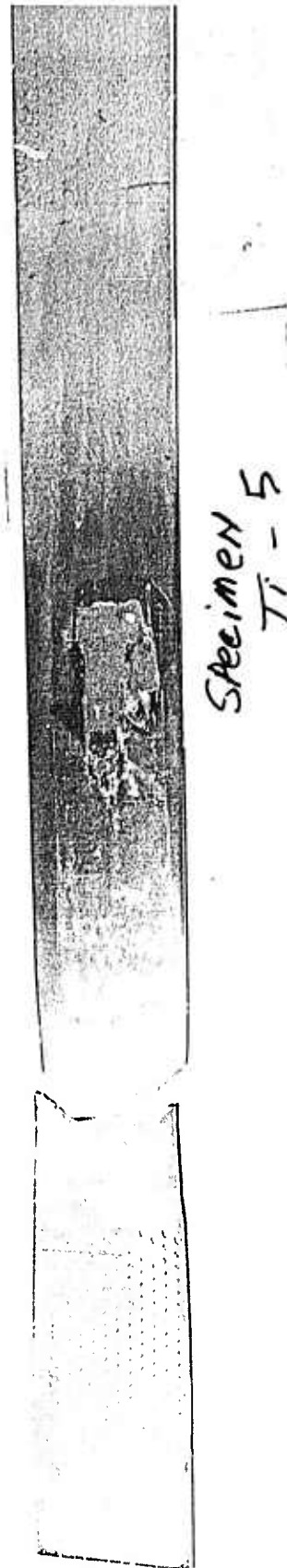
Parameter	Nom. Sheet Thickness, in.			
	0.016	0.032	0.045	0.090
t_{ACT} , in.	0.0165	0.0315	0.0455	0.0925
σ_u , ksi	146.026	129.607	137.523	134.860
σ_y , ksi	136.500	128.850	135.200	131.400
σ_{pe} , ksi	116.834	125.356	123.584	112.700
ν_p	0.3074	0.3086	0.3184	0.2902
$E_p \times 10^{-6}$	17.756	15.514	17.251	16.096
$\epsilon_{1y} \times 10^{-6}$ in./in.	9,575	10,225	9,750	9,985
$\epsilon_{2y} \times 10^{-6}$ in./in.	2,700	5,750	2,800	2,907
$\epsilon_{1pe} \times 10^6$ in./in.	6,590	8,074	7,171	7,004
$\epsilon_{2pe} \times 10^6$ in./in.	2,012	2,575	2,312	2,038
$\epsilon_{1u} \times 10^6$ in./in.	46,636	20,934	38,260	21,300
$\epsilon_{2u} \times 10^6$ in./in.	9,120	7,885	14,362	3,735
TMC-Typ. F_{tu} , ksi	146.200	138.000	137.500	138.400
TMC-Heat No.	G-9075	G-9072	G-9520	K-3793
*Properties were obtained by use of straight sided "composite configuration" tensile specimen one inch wide; gripping tensile specimens was by direct contact.				



0.016 in. Nom. Thick.



0.032 in. Nom. Thick.



0.045 in. Nom. Thick.

FIGURE 79. TYPICAL FAILURE OF Ti-6Al-4V ANNEALED TENSILE SPECIMENS

SECTION VIII

BONDED JOINT PROCESSING

VIII.1. GENERAL

This section covers the processing and fabrication of the simple specimen bonded joints. Section VIII.2 presents the Adhesive Acceptance Test Results whereas Section VIII.3 covers the Simple Specimen Joint Fabrication.

VIII.2. ADHESIVE ACCEPTANCE TEST RESULTS

A summary of the last acceptance test results for both the old and new batches of the two adhesive systems (AF-126 and MB-329) used in this program is presented in Tables XII and XIII. These tests were run on 29 October 1970. Earlier acceptance tests were run on the first Batch (724) of Scotchweld®* AF-126-2 adhesive on 15 March 1970. The later Batch (739) of AF-126 adhesive was first tested on 24 July 1970. Initial acceptance tests on the Metlbond®† 329 adhesive batches were performed on (1) the first Batch 345/47 on 15 March 1970 and (2) the later Batch 360/40 on 24 July 1970. Batch 739 of AF-126 and Batch 360/40 of Metlbond 329 were used in fabricating the lap shear assemblies for this program. The data from these tables (XII and XIII) indicate that some degradation occurred with aging, however, all tests passed the MMM-A-132 specification requirements.

VIII.3. SIMPLE SPECIMEN JOINT FABRICATION

Single and double lap shear assemblies were fabricated in accordance with Figures 80 and 81 covering both boron/epoxy to boron/epoxy and boron/epoxy to titanium joints with each adhesive system. A detailed listing of the single and double lap shear assemblies for single and double lap joints with boron/epoxy to boron/epoxy adherends utilizing both adhesive systems is shown in Table XIV. The boron/epoxy to titanium single and double lap shear assemblies with both adhesive systems are shown in Table XV. Fiberglass tabs were bonded on the boron/epoxy adherends with Eastman 910. Tabs were not used on the titanium adherends.

It was originally intended that three-step lap joints would be made by machining steps into the boron/epoxy laminates and titanium with subsequent matching and bonding as shown in Figure 82. Machining such steps in boron/epoxy proved nearly impossible with state-of-the-art diamond tools and cutting equipment. In consulting the Design Guide and several recent research investigations on machining boron/epoxy composites, nothing was found to guide our efforts on machining steps. After contacting the manufacturing experts of several aerospace companies it was found that most organizations lay-up and mold in the steps, usually in combination with bonding. However, several ideas were obtained on how step machining in boron/epoxy materials might be done. One idea was tried. Several diamond cup cutting wheels were tried with little success. After cutting the three steps in two different boron/epoxy laminate adherend materials and starting on a third, the tools were worn out. The manhour expenditure and the cutting tool wear rate on fabricating the steps that were made were prohibitive.

One machined step lap joint was made as shown in Figure 83. All other step lap joints were made from the unmachined details that were originally scheduled to be used in the machined step lap program. Three types of multiple-laminate step lap joints were made. The first was a single step lap joint shown in Figure 84 and the second was a double step lap joint shown in Figure 85. Figure 86 presents the triple step lap joint design.

Because of the large overlap involved some volatiles were trapped in the step lap joints‡ bonded with MB-329 and as a result they had multiple small voids in the bondlines which gave lower than desirable results. The voids were visible, unmagnified on the edges of the bondlines. All AF-126 step lap joints performed well.

*Registered trade name of the 3M Company

†Registered trade name of the Whittaker Corporation

‡LSA-11, -13, -24 (see Fig. 84)

TABLE XII. ACCEPTANCE TEST* RESULTS ON
AF-126 ADHESIVE (LS-HE)

Batch No.	Specimen No.	Single Overlap Length†	Shear Strength, psi	Failure Mode	Previous Results, psi	Date of Previous Results	Min. Req. Value,* psi
724	A-1	0.500	4,662	Cohesive			
	A-2	0.500	4,802	Cohesive			
	A-3	0.500	4,845	Cohesive			
	A-4	0.500	4,780	Cohesive			
	A-5	0.500	4,421	Cohesive			
	Average		4,702		5,690	4/15/70	2,500
724	B-1	0.500	5,625	Cohesive			
	B-2	0.500	5,627	Cohesive			
	B-3	0.500	4,995	Cohesive			
	B-4	0.500	5,666	Cohesive			
	B-5	0.500	5,160	Cohesive			
	Average		5,415		5,993	4/15/70	2,500
724	Average		5,059		5,842	4/15/70	2,500
739	A-1	0.500	4,818	Cohesive			
	A-2	0.500	4,941	Cohesive			
	A-3	0.500	5,015	Cohesive			
	A-4	0.500	4,995	Cohesive			
	A-5	0.500	5,147	Cohesive			
	Average		4,983		5,772‡	7/24/70	2,500
739	B-1	0.500	5,266	Cohesive			
	B-2	0.500	5,029	Cohesive			
	B-3	0.500	5,327	Cohesive			
	B-4	0.500	5,117	Cohesive			
	B-5	0.500	5,267	Cohesive			
	Average		5,201		5,092	7/24/70	2,500
739	Average		5,092		5,432	7/24/70	2,500
*Per MMM-A-132, Type I, Class 3 except 10 specimens instead of 6 were tested.							
†Inches.							
‡Probably used wrong primer on these.							

TABLE XIII. ACCEPTANCE TEST* RESULTS ON
MB-329 ADHESIVE (HS-LE)

Batch No.	Specimen No.	Single Overlap Length†	Shear Strength, psi	Failure Mode	Previous Results, psi	Date of Previous Results	Min. Req. Value,* psi
345/47	A-1	0.500	2,566	Adhesive			
	A-2	0.500	2,488	Adhesive			
	A-3	0.500	2,488	Adhesive			
	A-4	0.500	2,356	Adhesive			
	A-5	0.500	2,410	Adhesive			
	Average		2,471		2,577‡	4/15/70	2,250
345/47	B-1	0.500	2,674	Adhesive			
	B-2	0.500	2,517	Adhesive			
	B-3	0.500	2,371	Adhesive			
	B-4	0.500	2,371	Adhesive			
	B-5	0.500	2,203	Adhesive			
	Average		2,464		2,730‡	4/15/70	2,250
345/47	Average		2,468		2,653‡	4/15/70	2,250
360/40	A-1	0.500	2,628	Adhesive			
	A-2	0.500	2,660	Adhesive			
	A-3	0.500	2,699	Adhesive			
	A-4	0.500	2,717	Adhesive			
	A-5	0.500	2,663	Adhesive			
	Average		2,673		2,574‡	7/24/70	2,250
360	B-1	0.500	2,972	Adhesive			
	B-2	0.500	2,833	Adhesive			
	B-3	0.500	2,914	Adhesive			
	B-4	0.500	2,826	Adhesive			
	B-5	0.500	2,650	Adhesive			
	Average		2,839		2,262‡	7/24/70	2,250
360	Average		2,756		2,418‡	7/24/70	2,250
*Per MMM-A-132, Type II except 10 specimens instead of 6 were tested.							
†Inches.							
‡No primer used.							

Originally, the program's scope covered the manufacture of scarf joints for tests. These were designed to be made as shown in Figure 87. However, a reorientation of the program eliminated their fabrication.

All lap shear assemblies were cut into one-inch wide strips for simple specimen coupon testing.

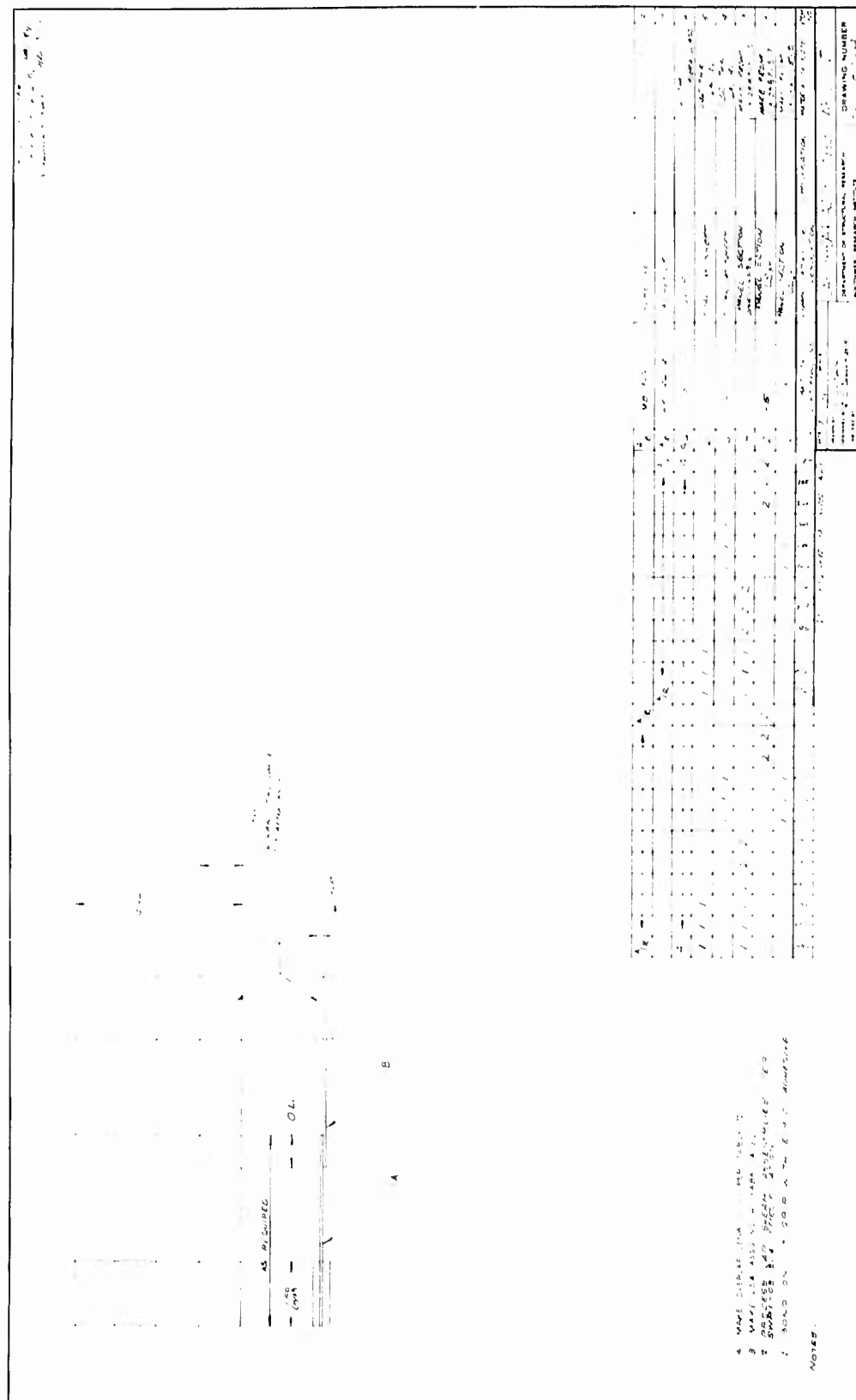


FIGURE 80. LAP SHEAR ASSEMBLY SINGLE LAP JOINT

TABLE XIV

SINGLE AND DOUBLE LAP SHEAR ASSEMBLIES - BORON/BORON

L.S.A. No.	Type Adhesive	Adherend No.	Adherend Thickness	Joint Thickness	Bond-Line Thickness	Primer	Cure Temp., °F	Cure Time, min
1	AF-126	B-21-A B-21-D	0.044 0.044	0.0925	0.0045	Blue EC-2320	50	275
14	AF-126	B-21-F B-21-H	0.042 0.043	0.091	0.006	Dry at 150° for 30 min		
27	AF-126	B-21-C B-21-J	0.043 0.043	0.093	0.007			
2	AF-126	B-24-A B-24-B	0.045 0.047	0.0955	0.0035			
15	AF-126	B-28-C B-28-G	0.044 0.042	0.0935	0.0075			
28	AF-126	B-24-D B-24-H	0.046 0.047	0.096	0.003			
3	AF-126	B-12-A B-12-D B-13-K	0.016 0.016 0.032	0.065	0.0005			
16	AF-126	B-12-G B-12-L B-13-F	0.015 0.015 0.032	0.067	0.0025			
29	AF-126	B-12-H B-12-M B-13-M	0.015 0.015 0.032	0.0675	0.00275			
4	AF-126	B-14-J B-14-K B-15-K	0.048 0.046 0.088	0.1845	0.00125			
17	AF-126	B-14-B B-14-F B-15-L	0.046 0.047 0.088	0.184	0.0015			
30	AF-126	B-14-L B-14-M B-19-K	0.047 0.047 0.087	0.184	0.0015			
5	AF-126	B-24-J B-24-K B-17-A	0.046 0.045 0.091	0.1845	0.00125			
18	AF-126	B-24-F B-24-F B-17-B	0.04 0.046 0.088	0.1845	0.00175			
31	AF-126	B-16-A B-16-G B-22-I	0.047 0.045 0.089	0.192	0.0055	Blue EC-2320		275
40	MB-329	B-25-F B-25-J	0.040 0.042	0.086	0.004	Red MB-329 Type II Air dry for 15 min Force dry for 30 min at 235°F		350
53	MB-329	B-25-F B-25-K	0.041 0.041	0.089	0.007			
66	MB-329	B-25-G B-25-L	0.041 0.041	0.0895	0.0075			
41	MB-329	B-28-B B-28-K	0.042 0.042	0.095	0.011			
54	MB-329	B-28-D B-28-H	0.045 0.043	0.099	0.011			
67	MB-329	B-16-C B-16-L	0.048 0.048	0.1025	0.0065			
42	MB-329	B-12-F B-12-K B-13-B	0.016 0.016 0.032	0.0715	0.00375			
55	MB-329	B-12-B B-12-C B-13-J	0.016 0.016 0.032	0.071	0.0035		50	350
68	MB-329	B-12-J B-12-N B-13-L	0.017 0.016 0.033	0.0755	0.00475	Red MB-Bond 329	50	350
43	MB-329	B-14-A B-14-F B-15-J	0.049 0.049 0.088	0.196	0.005			
56	MB-329	B-14-C B-14-G B-19-A	0.047 0.047 0.088	0.192	0.005			
69	MB-329	B-14-D B-14-H B-15-D	0.047 0.049 0.090	0.1935	0.00375			
44	MB-329	B-28-A B-28-F B-17-J	0.046 0.044 0.090	0.1955	0.00775			
57	MB-329	B-24-C B-24-L B-22-K	0.047 0.046 0.087	0.1945	0.00725			
70	MB-329	B-16-B B-16-H B-17-C	0.047 0.047 0.087	0.1945	0.00675		50	350

TABLE XV

SINGLE AND DOUBLE LAP SHEAR ASSEMBLIES—BORON/TITANIUM

L.S.A. No.	Type Adhesive	Adherend No.	Adherend Thickness	Joint Thickness	Bond-Line Thickness*	Primer	Cure Pressure, psi	Cure Temp., °F
6	AF-126	B-18-C Ti	0.031 0.032	0.0655	0.0025	Blue EC-2320	50	275
19	AF-126	B-18-K Ti	0.029 0.032	0.0695	0.0085			↓
32	AF-126	B-18-J Ti	0.031 0.032	0.068	0.005			275
45	MB-329	B-18-H Ti	0.031 0.032	0.0655	0.0025	Red M-Bond 329 Type		350
58	MB-329	B-13-D Ti	0.031 0.032	0.070	0.007			↓
71	MB-329	B-18-E Ti	0.031 0.032	0.068	0.005			350
7	AF-126	B-16-D Ti	0.047 0.045	0.0915	0	Blue EC-2320		275
20	AF-126	B-16-E Ti	0.047 0.045	0.0955	0.0035			↓
33	AF-126	B-24-M Ti	0.047 0.045	0.099	0.007			275
46	MB-329	B-28-F Ti	0.043 0.045	0.091	0.003	Red M-Bond 329		350
59	MB-329	B-28-M Ti	0.044 0.045	0.093	0.004			↓
72	MB-329	B-16-J Ti	0.048 0.045	0.1445	0.0065			350
8	AF-126	B-18-A Ti	0.031 0.016	0.064	0.001	Blue EC-2320		275
21	AF-126	B-18-F Ti	0.031 0.016	0.063	0			↓
34	AF-126	B-13-H Ti	0.031 0.016	0.0605	0			275
47	MB-329	B-18-D Ti	0.031 0.016	0.074	0.055	Red M-Bond 329		350
60	MB-329	B-13-C Ti	0.032 0.016	0.074	0.005			↓
73	MB-329	B-18-B Ti	0.031 0.016	0.0725	0.0045			350
9	AF-126	B-15-A Ti	0.090 0.045	0.178	0	Blue EC-2320		275
22	AF-126	B-15-C Ti	0.087 0.045	0.178	0.0005			↓
35	AF-126	B-19-B Ti	0.086 0.045	0.175	0	Red M-Bond 329		275
48	MB-329	B-15-B Ti	0.087 0.045	0.1875	0.00525			350
61	MB-329	B-19-J Ti	0.090 0.045	0.193	0.0065			↓
74	MB-329	B-15-M Ti	0.087 0.045	0.190	0.0065	Red M-Bond 329		350
10	AF-126	B-22-J Ti	0.089 0.045	0.180	0.0005	Blue EC-2320	50	275
23	AF-126	B-17-K Ti	0.088 0.045	0.1815	0.00175	Blue EC-2320	50	275
36	AF-126	B-22-C Ti	0.089 0.045	0.1805	0.00075			↓
49	MB-329	B-22-A Ti	0.089 0.045	0.1945	0.00775	Red M-Bond 329		275
62	MB-329	B-22-B Ti	0.089 0.045	0.1975	0.00925			350
75	MB-329	B-17-L Ti	0.089 0.045	0.195	0.008		50	350

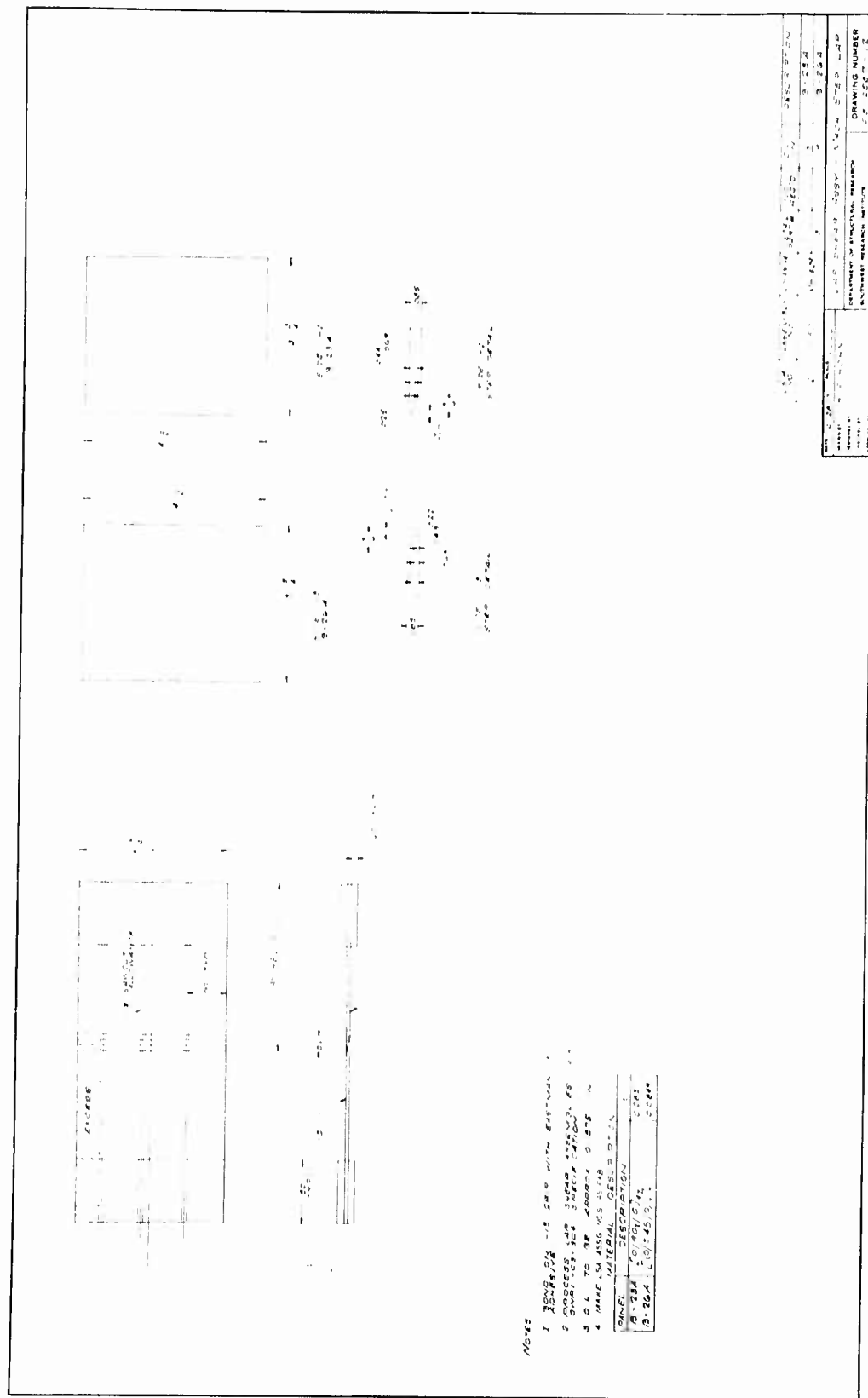
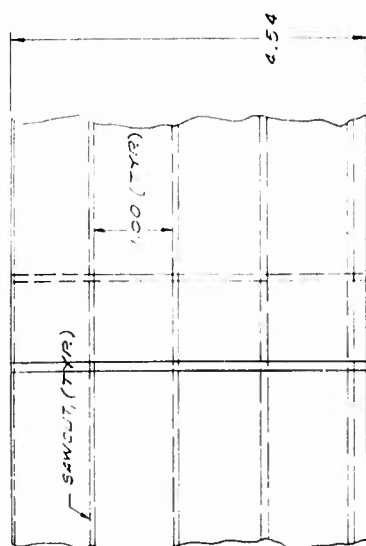


FIGURE 83. LAP SHEAR ASSEMBLY - MACHINED STEP LAP JOINT



MATERIAL	DESCRIPTION
1	...
2	...
3	...
4	...
5	...
6	...
7	...
8	...
9	...
10	...
11	...
12	...
13	...
14	...
15	...
16	...
17	...
18	...
19	...
20	...
21	...
22	...
23	...
24	...
25	...
26	...
27	...
28	...
29	...
30	...

PANEL	DESCRIPTION	?
B-23	[0/90/0] ₄	00891
B-25	[0] ₄	00913
B-26	[0/±45/0] ₄	00949

1. BOND FIBERGLASS STRIPS ON TO CARBON FIBER
ADHEREND, ONLY WITH EASTMAN 970
2. PROCESS LAP SHEAR ASSEMBLER PER
SWR/1-03-304 SPECIFICATION
3. MAKE LSA ASSG NO. 45 FAB

0522	3/4/57	2	1	1	0.53-1.14	5
0523	3/4/57	2	1	1	0.53-1.14	5
0524	3/4/57	2	1	1	0.53-1.14	5
0525	3/4/57	2	1	1	0.53-1.14	5
0526	3/4/57	2	1	1	0.53-1.14	5
0527	3/4/57	2	1	1	0.53-1.14	5
0528	3/4/57	2	1	1	0.53-1.14	5
0529	3/4/57	2	1	1	0.53-1.14	5
0530	3/4/57	2	1	1	0.53-1.14	5
0531	3/4/57	2	1	1	0.53-1.14	5
0532	3/4/57	2	1	1	0.53-1.14	5
0533	3/4/57	2	1	1	0.53-1.14	5
0534	3/4/57	2	1	1	0.53-1.14	5
0535	3/4/57	2	1	1	0.53-1.14	5
0536	3/4/57	2	1	1	0.53-1.14	5
0537	3/4/57	2	1	1	0.53-1.14	5
0538	3/4/57	2	1	1	0.53-1.14	5
0539	3/4/57	2	1	1	0.53-1.14	5
0540	3/4/57	2	1	1	0.53-1.14	5
0541	3/4/57	2	1	1	0.53-1.14	5
0542	3/4/57	2	1	1	0.53-1.14	5
0543	3/4/57	2	1	1	0.53-1.14	5
0544	3/4/57	2	1	1	0.53-1.14	5
0545	3/4/57	2	1	1	0.53-1.14	5
0546	3/4/57	2	1	1	0.53-1.14	5
0547	3/4/57	2	1	1	0.53-1.14	5
0548	3/4/57	2	1	1	0.53-1.14	5
0549	3/4/57	2	1	1	0.53-1.14	5
0550	3/4/57	2	1	1	0.53-1.14	5
0551	3/4/57	2	1	1	0.53-1.14	5
0552	3/4/57	2	1	1	0.53-1.14	5
0553	3/4/57	2	1	1	0.53-1.14	5
0554	3/4/57	2	1	1	0.53-1.14	5
0555	3/4/57	2	1	1	0.53-1.14	5
0556	3/4/57	2	1	1	0.53-1.14	5
0557	3/4/57	2	1	1	0.53-1.14	5
0558	3/4/57	2	1	1	0.53-1.14	5
0559	3/4/57	2	1	1	0.53-1.14	5
0560	3/4/57	2	1	1	0.53-1.14	5
0561	3/4/57	2	1	1	0.53-1.14	5
0562	3/4/57	2	1	1	0.53-1.14	5
0563	3/4/57	2	1	1	0.53-1.14	5
0564	3/4/57	2	1	1	0.53-1.14	5
0565	3/4/57	2	1	1	0.53-1.14	5
0566	3/4/57	2	1	1	0.53-1.14	5
0567	3/4/57	2	1	1	0.53-1.14	5
0568	3/4/57	2	1	1	0.53-1.14	5
0569	3/4/57	2	1	1	0.53-1.14	5
0570	3/4/57	2	1	1	0.53-1.14	5
0571	3/4/57	2	1	1	0.53-1.14	5
0572	3/4/57	2	1	1	0.53-1.14	5
0573	3/4/57	2	1	1	0.53-1.14	5
0574	3/4/57	2	1	1	0.53-1.14	5
0575	3/4/57	2	1	1	0.53-1.14	5
0576	3/4/57	2	1	1	0.53-1.14	5
0577	3/4/57	2	1	1	0.53-1.14	5

DATE 11-1-22 Y = 70 / 540 A. E. 2012 10/10/22

ON 10/10/10

AMERICAN

100

DATE: 12-22-79 / 10:00 AM - 12:00 PM

On the 14th of May 1900

INDEX

Figure 1

W-200-2444-2

DEPARTMENT OF STRUCTURAL RESEARCH

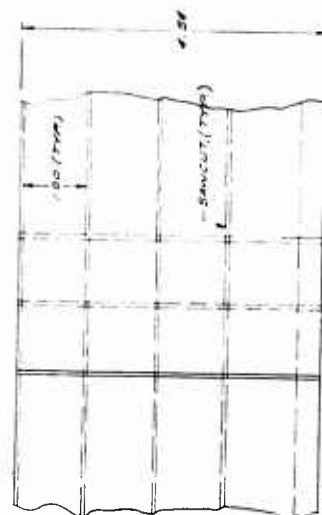
SOUTHWEST RESEARCH INSTITUTE

77 STEP LAB JOINT

DRAWING NUMBER

65-2597 - 7

FIGURE 84. MULTIPLE-LAMINATE SINGLE-STEP LAP JOINT.



MATERIAL	DESCRIPTION
1	...
2	...
3	...
4	...
5	...
6	...
7	...
8	...
9	...
10	...
11	...
12	...
13	...
14	...
15	...
16	...
17	...
18	...
19	...
20	...
21	...
22	...
23	...
24	...
25	...
26	...
27	...
28	...
29	...
30	...

DATE	DESCRIPTION	
8-28	1000/000	1000
8-29	1000/000	1000

- PROCESS LAB - CHEMISTS - 10/1/53
MAKE - 5A ASSY NO AS FAB

[illegible][illegible]

FIGURE 85. MULTIPLE-LAMINATE TWO-STEP LAP JOINT

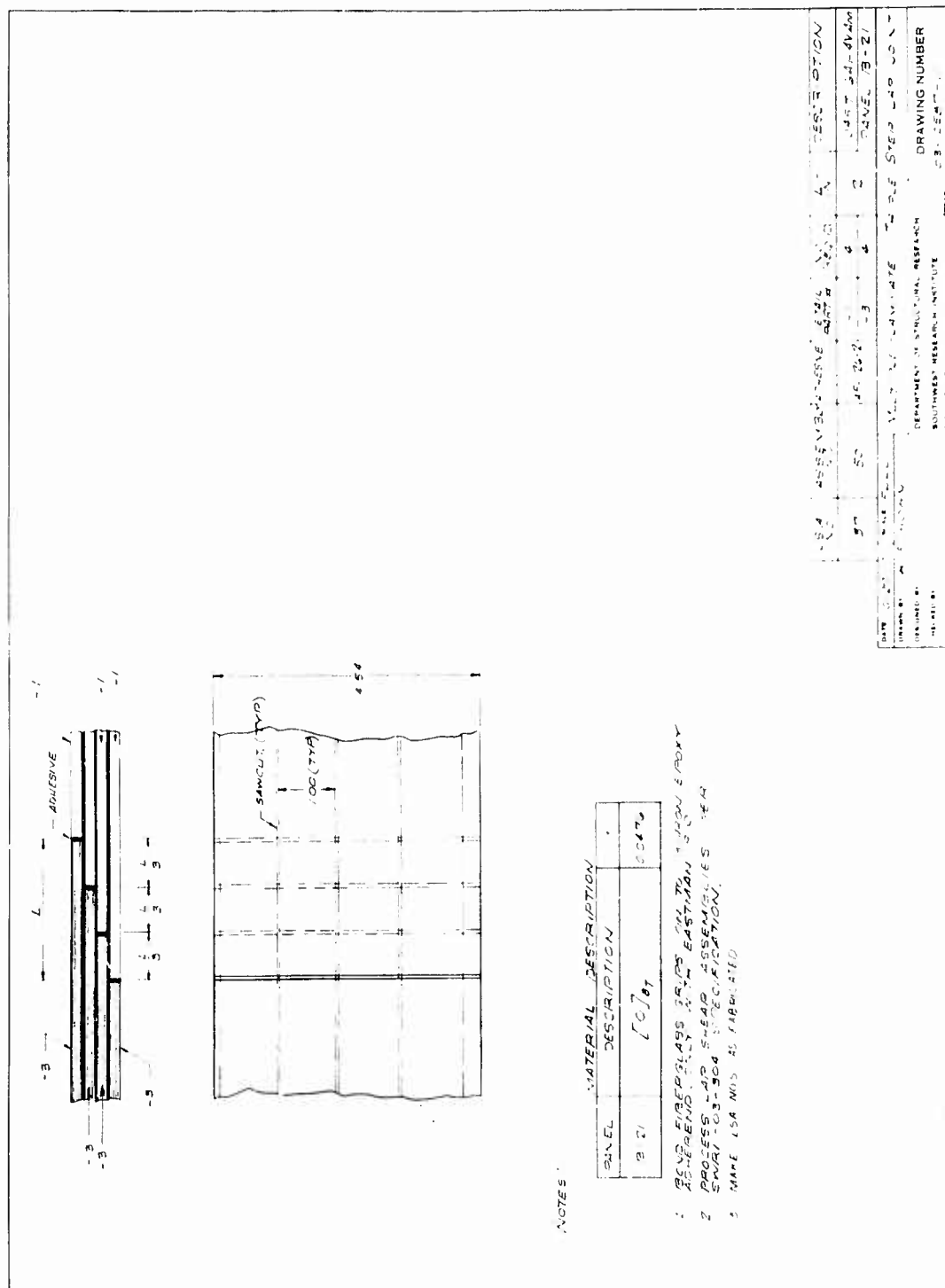
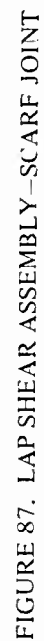


FIGURE 86. MULTIPLE-LAMINATE TRIPLE STEP LAP JOINT



SECTION IX

BONDED JOINT TEST RESULTS

IX.1. GENERAL

This Section presents the experimental results of the simple specimen bonded joint testing conducted in this program. Two hundred and three specimens covering two adhesives, three lap configurations, three basic composite adherend fiber orientations, and two adherend material combinations were tested. Six representative samples of these specimens were extensively strain gaged and tested for detailed behavior study.

Section IX.2 presents the Simple Specimen Data Summary based on the detailed data covered in Appendix F. Section IX.3 gives the results of the Special Joint Investigation Data Summary covering the six joints which were extensively strain gaged.

IX.2. SIMPLE SPECIMEN DATA SUMMARY

A summary of all the simple specimen lap joint tests is contained in Tables XVI through XXIV along with the failed specimen photographs presented in Figures 88 through 103. Each lap shear assembly number identified in these tables represents an average of three or four specimens taken from it and tested. The total number of simple specimens tested was 203 and the detailed data tables are located in Appendix F. There were 72 single lap, 108 double lap, and 23 step lap joints tested covering composite/composite and composite/titanium bonded joints utilizing two adhesive systems: a nitrile-epoxy low stiffness-high elongation (LS-HE) system* and an epoxy-novolak high stiffness-low elongation (HS-LE) system.† Selectively covered were three basic orientations of the boron/epoxy adherend materials with sequence variations on two of these. The titanium adherend materials were the 6A1-4V alloy in the annealed condition. Data on the adherend materials was previously covered in Section VII.

From Tables XVI and XVIII, the graph in Figure 104 summarizes the single lap composite/composite joint data on the two adhesives whereas the graph in Figure 105 (taken from Tables XVII and XIX) presents the data on the double lap composite/composite joints with the same two adhesives. In Figure 104 on load transfer capability of single lap composite/composite joints it can be noted that the curve slope increases with increased adherend stiffness, decreased adhesive stiffness, and increased adhesive elongation. By contrast the change in slope due to these same property variables is much less in double lap joints as shown in Figure 105. In fact all other slopes except one are close to being the same. For this exception it appears that the high Poisson's ratio of the basic $0/\pm 45^\circ$ orientation adherend is detrimental when used with the high stiffness-low elongation epoxy-novolak adhesive. Also presented in Figure 105 are slopes of data points which represent poor quality specimens, illustrating the deleterious effects of interface region failure.

On the composite/titanium joints summarized in Tables XX and XXII the graph in Figure 106 presents the data on the single lap joints with both adhesive systems whereas the graph in Figure 107 (taken from Tables XXI and XXIII) give them for the double lap joints utilizing the two adhesives. The same sort of trend in load transfer capability exhibited in Figure 104 for the single lap joints is evident in Figure 106. Higher slopes result from higher adherend stiffnesses and adhesive elongations plus lower adhesive moduli. Figure 107 also exhibits the same trends as were shown in Figure 105. In fact all but one of the adherend/adhesive combinations plot on the same line; this one with the $0/\pm 45^\circ$ orientation adherends bonded together with the high stiffness low elongation epoxy novolak adhesive gives a slightly lower slope, probably because of Poisson's ratio effects. Again, poor quality specimen results are shown. These had poor adhesive materials quality in the bondline. Also the slopes of the double lap joint curves are generally higher than those of the single lap graphs.

*3M Company's AF-126-2.

†Narmco's Metlbond 329.

TABLE XVI

COMPOSITE/COMPOSITE SINGLE LAP JOINT DATA SUMMARY (LS-HE)
AF-126-2, Nominal Width--1.000 In.

Assembly Number	Measured Length Between Tabs, in.	Measured Adhesive Thickness, in.	Composite Adherent Fiber Orientation	Composite Adherent Panel Number	Measured Composite Adherent Thickness, in.	Measured Overlap Length, in.	F/t	Failure Load, lb/in.	Adherent Stress at Failure, psi	Adhesive Stress at Failure, psi	Load Transfer at Failure, lb/in. ply	Failure Type*, %						General Comments
												1	2	3	4	5	6	
LSA 1	4-1/8	0.0010	[0]q _T	B-21A/D	0.047/0.045	0.250	5.556	1,063	23,629	4,247	118	15		78	6	1		
LSA 14	5-1/4	0.0043	[0]q _T	B-21E/H	0.0423/0.045	1.250	29.551	5,668	131,928	4,466	630	2		27	52	19	1	
LSA 27	7-5/8	0.0043	[0]q _T	B-21C/J	0.0463/0.046	1.7357	37.733	7,873	164,928	4,361	875			5	5	23	67	
LSA 2	4-1/8	0.0030	[0/+45/0/-45/0] _g	B-24A/B	0.047/0.047	0.250	5.319	1,147	24,945	4,593	127	27		70	3			
LSA 15	3-1/4	0.0060	[0/+45/0/-45/0] _g	B-28C/G	0.0433	1.250	24.868	3,938	89,611	3,106	438	70			26	4		
LSA 28	6-7/8	0.0042	[0/+45/0/-45/0] _g	B-24D/H	0.046	2.000	43.478	4,758	102,770	2,365	529	1		2			1	96**

*1 % adhesive to boron/epoxy composite
2 % adhesive to titanium (6 Al-4V)
3 % cohesive
4 % surface resin
5 % interlaminar
6 % other

† Longitudinal splitting

‡ Net section tension and longitudinal splitting composite

** Net section tension composite

TABLE XVII

COMPOSITE/COMPOSITE DOUBLE LAP JOINT DATA SUMMARY (LS-HE)
AF-126-2, Nominal Width = 1.000 In.

Assembly Number	Measured Length Between Tabs, in.	Measured Adhesive Thickness, in.	Composite Adherent Fiber Orientation	Composite Adherent Panel Number	Measured Composite Adherent Thickness, in.	Measured Overlap Length, in.	F/t	Failure Load, lb/in.	Adherent Stress at Failure, psi	Adhesive Stress at Failure, psi	Load Transfer at Failure, lb/in. ply	Failure Type*, %						General Comments
												1	2	3	4	5	6	
LSA 3	4-1/4	0.0023	2 x [0]q _T [0] _{6J}	B-12A/D, B-13K	2 x 0.016/0.0273	0.250	9.158	1,783	65,262	3,510	297	50		46	3	1		
LSA 16	4-3/16	0.0048	2 x [0]q _T [0] _{6J}	B-12G/I, B-13J	2 x 0.015/0.0113	0.500	16.667	4,000	131,982	3,958	667	18		17	5		60†	
LSA 29	4-5/8	0.0033	2 x [0]q _T [0] _{6J}	B-12H/M, B-13M	2 x 0.015/0.0313	0.750	25.00	4,150	136,807	2,736	692						100†	
LSA 4	4-1/8	0.0018	2 x [(0/90) _q /0] _T , [(0/90) _q /0] _J	B-14J/K, B-15K	2 x 0.046/0.088	0.218	2.477	1,520	17,015	3,439	89	58		32	10			
LSA 17	4-13/32	0.0027	2 x [(0/90) _q /0] _T , [(0/90) _q /0] _J	B-14B/J, B-15I	2 x 0.046/0.0867	0.437	5.040	4,782	54,445	5,197	281	21		59	3		17**	
LSA 30	4-5/8	0.0009	2 x [(0/90) _q /0] _T , [(0/90) _q /0] _J	B-14I/M, B-15L	2 x 0.047/0.0897	0.729	8.379	5,898	66,977	4,090	347						100**††	
LSA 5	4-1/4	0.0033	2 x [0/+45/0/-45/0] _g , [(0/+45/0/-45/0) _g] _g	B-24J/K, B-17A	2 x 0.045/0.088	0.250	2.841	2,295	25,820	4,523	135	31		54	15			
LSA 18	4-17/32	0.0020	2 x [0/+45/0/-45/0] _g , [(0/+45/0/-45/0) _g] _g	B-24I/J, B-17B	2 x 0.046/0.0877	0.750	8.552	7,018	78,988	4,614	413	18		55	25	2		
LSA 31	5-3/16	0.0037	2 x [0/+45/0/-45/0] _g , [(0/+45/0/-45/0) _g] _g	B-16A/G, B-22I	2 x 0.045/0.0897	1.250	13.935	8,715	95,621	3,443	513						100**††	

*1 bond

† Net section tension and longitudinal splitting composite

‡ Failure in double adherend partially over and/or adjacent the bond area

** Net section tension composite

†† Failure in single adherend away from the bond area

‡‡ Failure in double adherend away from the bond area

TABLE XVIII

COMPOSITE/COMPOSITE SINGLE LAP JOINT DATA SUMMARY (HS-LE)
MB-329, Nominal Width—1.000 In.

Assembly Number	Measured Length Between Tabs, in.	Measured Adhesive Thickness, in.	Composite Adherend Fiber Orientation	Composite Adherend Panel Number	Measured Composite Adherend Thickness, in.	Measured Overlap Length, in.	T/t	Failure Load, lb/in.	Adherend Stress at Failure, psi	Adhesive Stress at Failure, psi	Load Transfer at Failure, lb/in./ply	Failure Type*, %						General Comments
												1	2	3	4	5	6	
ISA 40	4.5/16	0.0043	[0] _{KT}	B-25I/J	0.0407/0.040	0.250	6.250	1,075	26,348	4,218	114	8	43	49				
ISA 53	5.5/16	0.0073	[0] _{KT}	B-25I/K	0.0403/0.0403	1.250	31.017	3,045	74,482	2,403	381	28		8	55	9		
ISA 66	6	0.0063	[0] _{KT}	B-25G/I	0.041/0.0403	2.250	55.831	4,902	120,486	2,160	613			18	70	12		
ISA 41	4.9/16	0.0070	[0/+45/0/-45/0] _S	B-28B/K	0.043/0.043	0.500	11.628	880	20,578	1,755	98	86		10	4			
ISA 54	5.5/8	0.0117	[0/+45/0/-45/0] _S	B-28D/H	0.044/0.043	1.500	34.884	2,157	49,502	1,418	240	75		7	18			
ISA 67	6.3/8	0.0087	[0/+45/0/-45/0] _S	B-16C/I	0.047/0.0477	2.500	53.191	3,043	64,311	1,209	338	85			12	3		

*Bad

TABLE XIX

COMPOSITE/COMPOSITE DOUBLE LAP JOINT DATA SUMMARY (HS-LE)
MB-329, Nominal Width—1.000 In.

Assembly Number	Measured Length Between Tabs, in.	Measured Adhesive Thickness, in.	Composite Adherend Fiber Orientation	Composite Adherend Panel Number	Measured Composite Adherend Thickness, in.	Measured Overlap Length, in.	T/t	Failure Load, lb/in.	Adherend Stress at Failure, psi	Adhesive Stress at Failure, psi	Load Transfer at Failure, lb/in./ply	Failure Type*, %						General Comments
												1	2	3	4	5	6	
ISA 42	4.1/4	0.0034	2 × [0] _{3T} , [0] _{6T}	B-12I/K B-13B	2 × 0.016/ 0.016	0.250	7.812	2,165	66,615	4,266	361	27		16	57			
ISA 55	4.3/8	0.0055	2 × [0] _{3T} , [0] _{6T}	B-12F/K B-13A	2 × 0.016/ 0.016	0.500	16.667	4,300	132,716	4,248	717	23		8	1		55	
ISA 68	4.7/8	0.0082	2 × [0] _{3T} , [0] _{6T}	B-12I/K B-13A	2 × 0.016/ 0.030	1.000	33.333	4,012	123,816	1,981	569	11		7	25	5*	1	
ISA 43	4.1/4	0.0076	2 × [(0/90) ₄ /0] _T , [(0/90) ₈ /0] _I	B-14A B-15J	2 × 0.049/ 0.090	0.250	2.778	1,718	18,800	3,383	101	17		36	46	1		
ISA 56	4.1/2	0.0046	2 × [(0/90) ₄ /0] _T , [(0/90) ₈ /0] _I	B-14C/G B-19A	2 × 0.047/ 0.088	0.750	8.523	5,048	56,657	3,322	297	15		12	52	4	1***	
ISA 69	5.5/16	0.0069	2 × [(0/90) ₄ /0] _T , [(0/90) ₈ /0] _I	B-14D/H B-15D	2 × 0.047/ 0.083	1.500	16.988	4,907	54,869	1,617	789	56		5	21	18		
ISA 44	4.5/16	0.0087	2 × [0/+45/0/-45/0] _S , [(0/+45/0/-45/0) ₂] _S	B-28A/I, B-17I	2 × 0.044/ 0.091	0.229	2.602	2,010	22,508	4,423	118	57		10	32	1		
ISA 57	4.7/8	0.0081	2 × [0/+45/0/-45/0] _S , [(0/+45/0/-45/0) ₂] _S	B-24C/I, B-22K	2 × 0.046/ 0.086	1.000	11.628	5,077	60,611	2,874	309	35		9	55	1		
ISA 70	5.1/2	0.0065	2 × [0/+45/0/-45/0] _S , [(0/+45/0/-45/0) ₂] _S	B-16B/H, B-17C	2 × 0.047/ 0.088	1.750	19.886	5,073	57,407	1,436	298	58		2	38	2		

*Bad

**Not section tension and longitudinal splitting composite

† Failure in double adherend partially over and/or adjacent the bond area

***Not section tension composite

TABLE XX

COMPOSITE/TITANIUM SINGLE LAP JOINT DATA SUMMARY (HS-LE)
AF-126-2, Nominal Width—1.000 In.

Assembly Number	Measured Length Between Tabs, in	Measured Adhesive Thickness, in	Composite Adherent Fiber Orientation	Composite Adherent Panel Number	Measured Composite Adherent Thickness, in	Measured Titanium Adherent Thickness, in	Measured Overlap Length, in	L/t	Failure Load, lb/in	Adherent Stress at Failure, psi	Adhesive Stress at Failure, psi	Load Transfer at Failure, lb/in /ply	Failure Type*, %						General Comments
													1	2	3	4	5	6	
LSA-6	2 1/4	0.0022	[0] _{6T}	B-18C	0.030	0.032	0.250	8.13	995	33,166(B)	3948	166	1	15	64	18			
LSA-19	3 3/16	0.0058	[0] _{6T}	B-18K	0.031	0.032	1.250	40.323	4197	133,366(B) 129,258(T)	3307	700			13	13	13	12	491
LSA-32	3 5/8	0.0042	[0] _{6T}	B-18J	0.0313	0.032	1.687	53.898	4168	133,061(B) 130,260(T)	2470	695							1001
LSA-7	2 3/8	0.0027	[0/+45/0/-45/0] ₅	B-16D	0.045	0.045	0.239	5.313	1133	25,185(B)	4497	126	55	11	32	2			
LSA-20	3 1/4	0.0028	[0/+45/0/-45/0] ₅	B-16I	0.0467	0.045	1.250	27.778	4255	89,979(B) 93,241(T)	3351	473		2	3	15	13	67**	
LSA-33	3 7/8	0.0032	[0/+45/0/-45/0] ₅	B-24M	0.0467	0.045	2.000	46.444	5087	109,325(B) 112,537(T)	2531	565							100**
*Ibid †Net section tension and longitudinal splitting—composite ‡Net section tension in titanium **Net section tension in composite General Note: Each assembly represents the average of 3 or 4 tests																			

TABLE XXI

COMPOSITE/TITANIUM DOUBLE LAP JOINT DATA SUMMARY (LS-HE)
AF-126-2, Nominal Width—1.000 In.

Assembly Number	Measured Length Between Tabs, in	Measured Adhesive Thickness, in	Composite Adherent Fiber Orientation	Composite Adherent Panel Number	Measured Composite Adherent Thickness, in	Measured Titanium Adherent Thickness, in	Measured Overlap Length, in	L/t	Failure Load, lb/in	Adherent Stress at Failure, psi	Adhesive Stress at Failure, psi	Load Transfer at Failure, lb/in /ply	Failure Type*, %						General Comments
													1	2	3	4	5	6	
LSA-8	2 5/16	0.0008	[0] _{6T}	B-18A	0.029	2 x 0.016	0.239	8.241	2,592	88,943(B) 79,743(T)	5,373	432		8	23	47	22		
LSA-21	2 1/2	0.0003	[0] _{6T}	B-18F	0.030	2 x 0.016	0.500	16.667	3,497	129,825(B) 121,689(T)	3,893	583		2	2	7	7		821†
LSA-34	2 5/8	0.0002	[0] _{6T}	B-13H	0.030	2 x 0.016	0.750	25.000	3,353	111,037(B) 104,141(T)	2,222	558							100*
LSA-9	2 1/4	0.0002	[0/90] ₆ [0] _{1T}	B-15A	0.088	2 x 0.045	0.250	2.841	1,873	30,920(B)	3,681	110	23	18	39	18	2		
LSA-22	2 1/2	0.0019	[0/90] ₆ [0] _{1T}	B-15C	0.0847	2 x 0.045	0.500	5.903	5,220	60,464(B)	5,119	307		8	23	22	11		34**
LSA-35	2 11/16	0.0009	[0/90] ₆ [0] _{1T}	B-19B	0.0847	2 x 0.045	0.750	8.855	5,930	69,564(B)	3,927	348							100**
LSA-10	2 1/4	0.0010	[0/+45/0/-45/0] ₅	B-22I	0.088	2 x 0.045	0.250	2.841	2,368	26,557(B)	4,669	139	7	32	38	21	2		
LSA-23	2 11/16	0.0030	[0/+45/0/-45/0] ₅	B-17K	0.087	2 x 0.045	0.687	7.897	7,450	86,348(B)	5,457	438		8	28	35	29		
LSA-36	3 1/8	0.0018	[0/+45/0/-45/0] ₅	B-22C	0.089	2 x 0.045	1.250	14.045	9,780	109,111(B) 107,907(T)	3,883	575							100†
*Ibid †Net section tension and longitudinal splitting—composite ‡Net section tension in Ti **Net section tension—composite																			

TABLE XXII

COMPOSITE/TITANIUM SINGLE LAP JOINT DATA SUMMARY (HS-LE)
MB-329, Nominal Width—1,000 In.

Assembly Number	Measured Length Between Tabs, in.	Measured Adhesive Thickness, in.	Composite Adhesive Fiber Orientation	Composite Adhesive Panel Number	Measured Composite Adhesive Thickness, in.	Measured Titanium Adhesive Thickness, in.	Measured Overlap Length, in.	L/t	Failure Load, lb/in.	Adhesive Stress at Failure, psi	Load Transfer at Failure, lb/in.	Failure Type*, %						General Comments
												1	2	3	4	5	6	
LSA-45	2-5/16	0.0050	[0] ₆₇	B-18H	0.030	0.012	0.250	8.433	77*	25,625(B)	3,076	5				86	9	
LSA-58	5-3/16	0.0052	[0] ₆₇	B-130	0.0317	0.032	1.250	38.432	1.957	61,079(B)	1,548	10	32	15	41	2		
LSA-71	4-1/4	0.0048	[0] ₆₇	B-14F	0.032	0.032	2.250	70.312	2.788	87,135(B)	1,240	465	3	42	10	38	7	
LSA-46	3-1/16	0.0045	[0/-45/0/-45/0] ₁₅	B-201	0.043	0.045	0.500	11.628	0.73	22,445(B)	1,930	108	62		5	32	1	
LSA-59	5-7/16	0.0037	[0/-45/0/-45/0] ₁₅	B-204	0.043	0.045	1.437	33.419	2.093	48,048(B)	1,438	233	4	4	8	66	18	
LSA-72	4-9/16	0.0107	[0/-45/0/-45/0] ₁₅	B-16J	0.048	0.045	2.500	52.083	2.215	46,270(B)	882	246	48	5		42	5	

*Ibid

TABLE XXIII

COMPOSITE/TITANIUM DOUBLE LAP JOINT DATA SUMMARY (HS-LE)
MB-329, Nominal Width—1,000 In.

Assembly Number	Measured Length Between Tabs, in.	Measured Adhesive Thickness, in.	Composite Adhesive Fiber Orientation	Composite Adhesive Panel Number	Measured Composite Adhesive Thickness, in.	Measured Titanium Adhesive Thickness, in.	Measured Overlap Length, in.	L/t	Failure Load, lb/in.	Adhesive Stress at Failure, psi	Load Transfer at Failure, lb/in.	Failure Type*, %						General Comments
												1	2	3	4	5	6	
LSA-47	2-1/4	0.0059	[0] ₆₇	B-18D	0.0397	2 x 0.016	0.250	8.418	2.945	86,671(B)	5,212	441	5	5	8	60	2	
LSA-40	3-3/8	0.0053	[0] ₆₇	B-134	0.031	2 x 0.016	0.500	16.129	1.330	42,161(B)	1,326	222		22	57	1*	4	
LSA-73	2-3/4	0.0056	[0] ₆₇	B-18B	0.0303	2 x 0.016	1.000	33.003	4.393	143,923(B) 136,439(Ti)	2,183	732	5	3	2	20	37	33*
LSA-48	2-1/4	0.0054	[0/90/0/0] ₁₇	B-15B	0.086	2 x 0.045	0.250	2.907	2.508	38,682(B)	4,930	148	13		4	63	20	
LSA-61	2-13/16	0.0067	[0/90/0/0] ₁₇	B-9J	0.0897	2 x 0.045	0.708	7.893	4.703	52,392(B)	3,310	277	2	18	3	22	55	
LSA-74	3-7/16	0.0058	[0/90/0/0] ₁₇	B-15M	0.0887	2 x 0.045	1.500	16.911	4.997	56,126(B)	1,632	294	20	3	3	24	20	30*
LSA-49	2-5/16	0.0060	[0/-45/0/-45/0] ₁₅	B-22A	0.0893	2 x 0.045	0.250	2.890	1.587	17,564(B)	3,212	93	17	11	71	1		
LSA-62	3	0.0099	[0/-45/0/-45/0] ₁₅	B-22B	0.068*	2 x 0.045	1.040	11.274	4.191	38,267(B)	2,483	505	7	5	84	4		
LSA-75	3-11/16	0.0065	[0/-45/0/-45/0] ₁₅	B-17I	0.069*	2 x 0.045	1.69*	18.919	3.98*	44,027(B)	1,104	235	2	34	1	57	6	

*Ibid

*Net section titanium Ti

*Net section titanium composite

TABLE XXIV

STEP LAP JOINT DATA SUMMARY
(Nominal Width - 1.000 In.)

Assembly Number	No. of Steps	Fabrication Steps	Length Between Tabs, in.	Adherend Comb Type	Adhesive Thickness, in.	Composite Adherend Fiber Orientation	Composite Adherend Panel Number	Net Composite Adherend Thickness, in.	Net Titanium Adherend Thickness, in.	Total Overlap, in.	L/t	Failure Load, lb/in.	Adherend Stress at Failure, psi	Adhesive Stress at Failure, psi	Load Transfer at Failure, lb/in./ply	Failure Type*, %						General Comments
																1	2	3	4	5	6	
LSA-13	1	L	7-1/2	B-T	0.0017	2 x [0] 8T	B-25C/M	0.086	0.085	2.006	23.600	2,650	30,550(B)	1,325	166	-	30	9	55	6	-	
LSA-11	1	L	6-7/16	B-T	0.0160	2 x [0; +45; 0] 9T	B-26E/G	0.1662	0.1762	2.051	2.341	1,745	10,443(B)	847	55	2	22	11	55	1	9+	
LSA-24	1	L	5-7/8	B-T	0.0130	2 x [0/90; 0] 14T	B-23/L	0.1727	0.1767	2.010	1.639	1,492	8,628(B)	741	47	3	42	1	27	2	25+	
LSA-25	2	L	4-7/8	B-T	0.0010	3 x [0/90; 0] 14T	B-23	0.2637	0.265	3.689	3.989	5,403	20,474(B)	1,462	113	-	-	-	-	-	-	100+
LSA-26	2	L	5-11/16	B-T	0.0058	3 x [0; +45; 0] 9T	B-26	0.262	0.264	3.879	4.805	11,146	42,401(B)	2,864	232	10	-	1	19	44	26+	
LSA-37	3	L	6-7/16	B-T	0.0059	4 x [0] 9T	B-21	0.1797	0.1743	1.969	1.297	11,783	65,437(B)	5,966	327	10	22	15	34	-	19+	
LSA-12	3	M	4-3/16	B-B	0.0070	[0/90; 0] 14T [0; +45; 0] 9T	B-23A B-26A	0.0863 0.0857	-	0.267	3.116	900	10,474(B)	3,376	56	7	-	31	36	26	-	

Note: L = Laminating by bonding up prefabricated laminates
M = Machining

*Ibid

† Net section tension and longitudinal splitting - composite

‡ Net section tension - composite

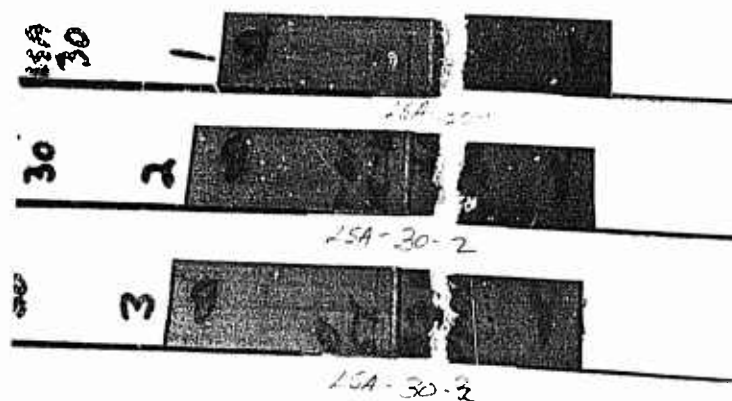
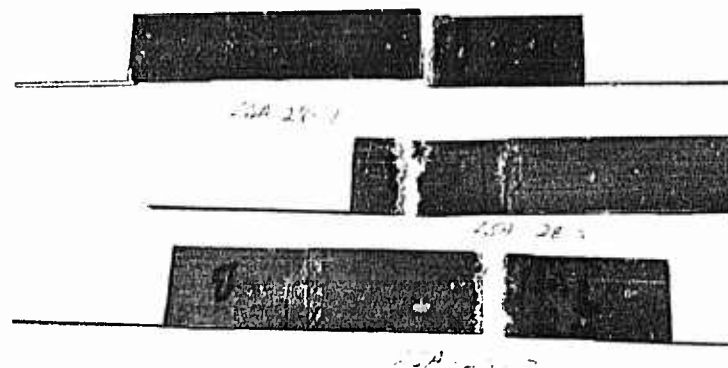


FIGURE 90. LSA-30 FAILED SPECIMENS

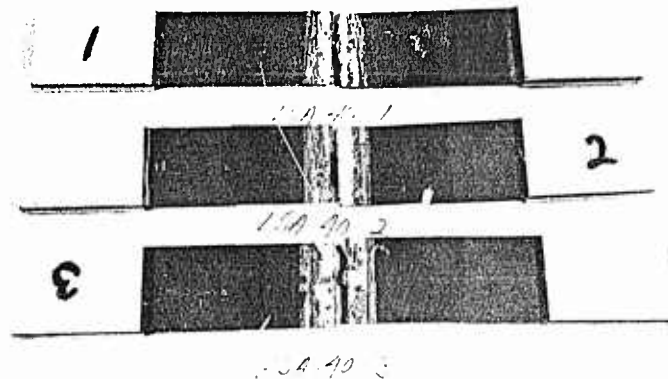


FIGURE 91. LSA-40 FAILED SPECIMENS

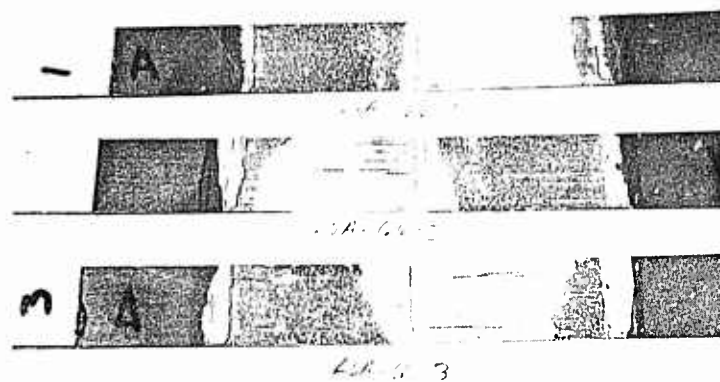


FIGURE 92. LSA-66 FAILED SPECIMENS



FIGURE 93. LSA-57 FAILED SPECIMENS

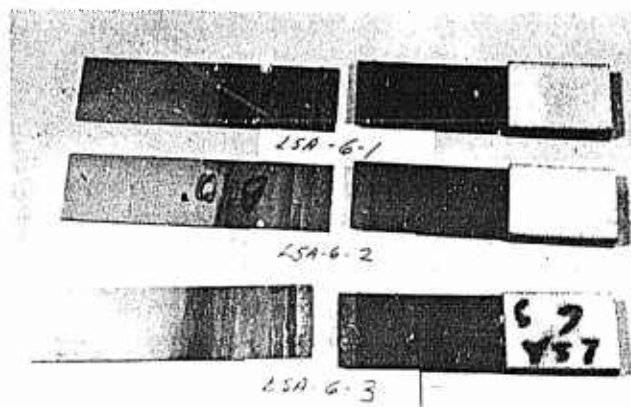


FIGURE 94. LSA-6 FAILED SPECIMENS

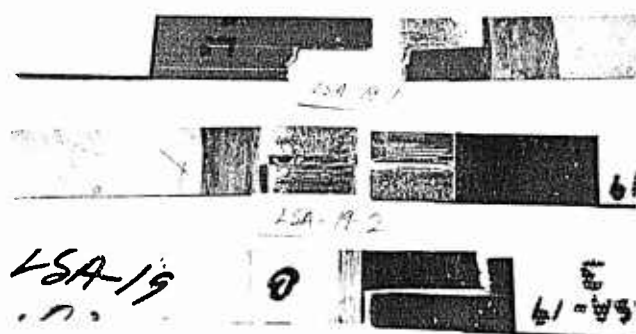


FIGURE 95. LSA-19 FAILED SPECIMENS

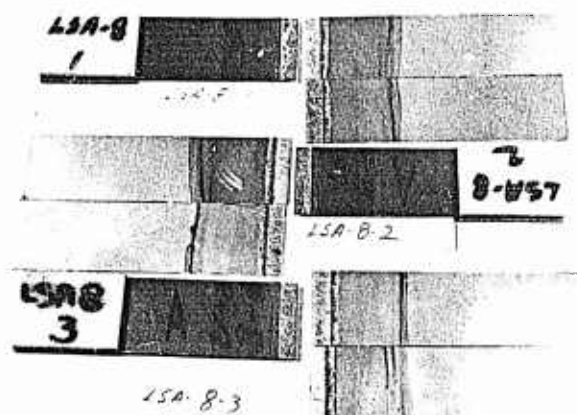


FIGURE 96. LSA-8 FAILED SPECIMENS

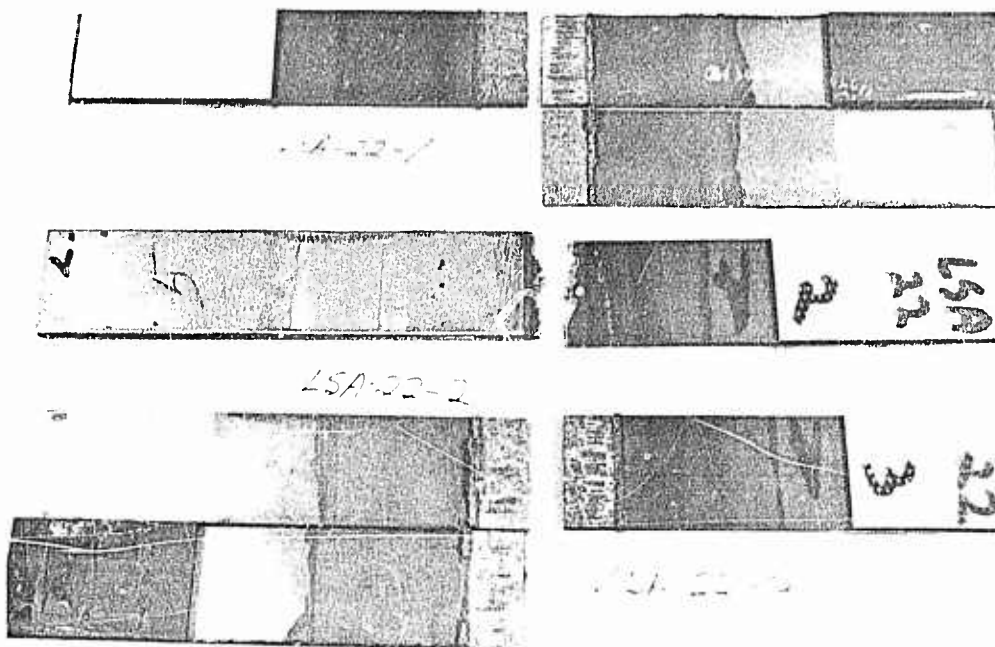


FIGURE 97. LSA-22 FAILED SPECIMENS

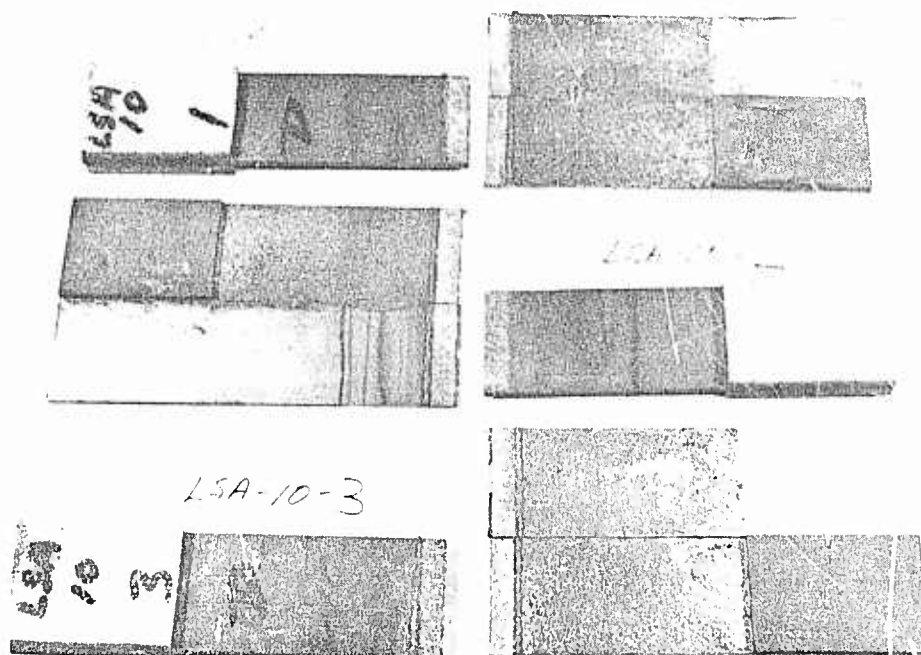


FIGURE 98. LSA-10 FAILED SPECIMENS

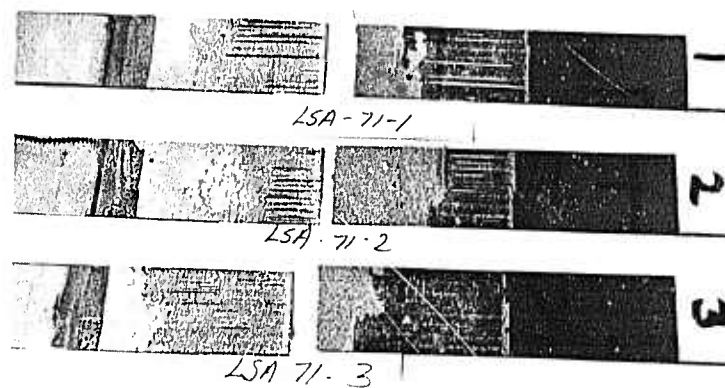


FIGURE 99. LSA-71 FAILED SPECIMENS

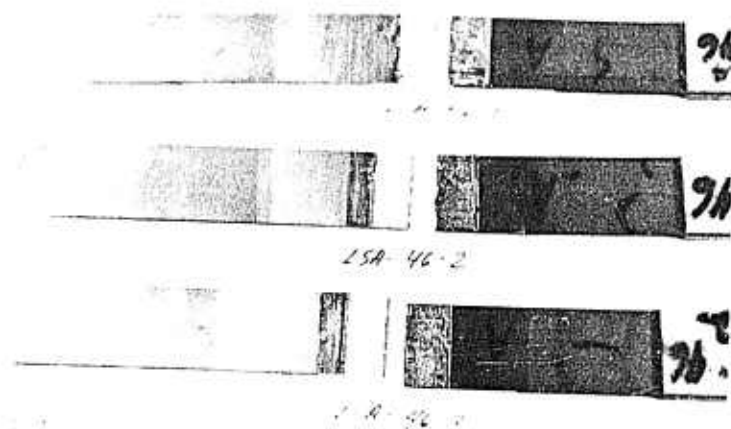


FIGURE 100. LSA-46 FAILED SPECIMENS

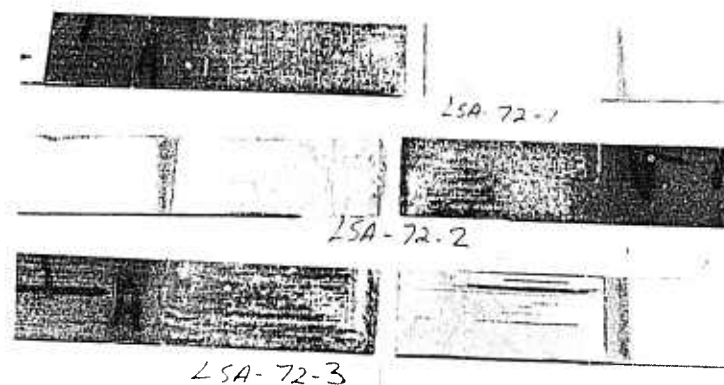


FIGURE 101. LSA-72 FAILED SPECIMENS

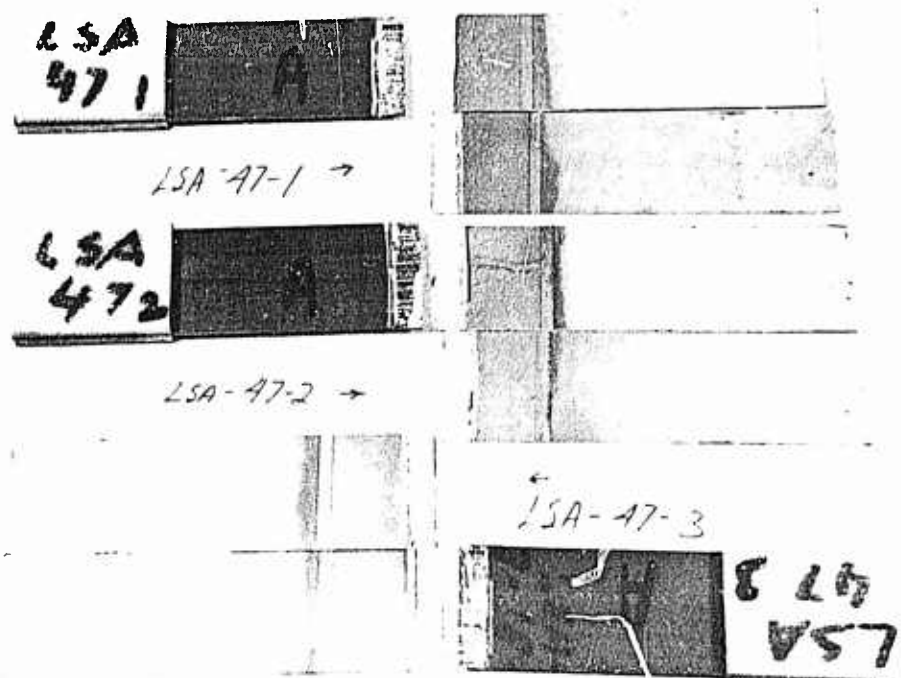


FIGURE 102. LSA-47 FAILED SPECIMENS

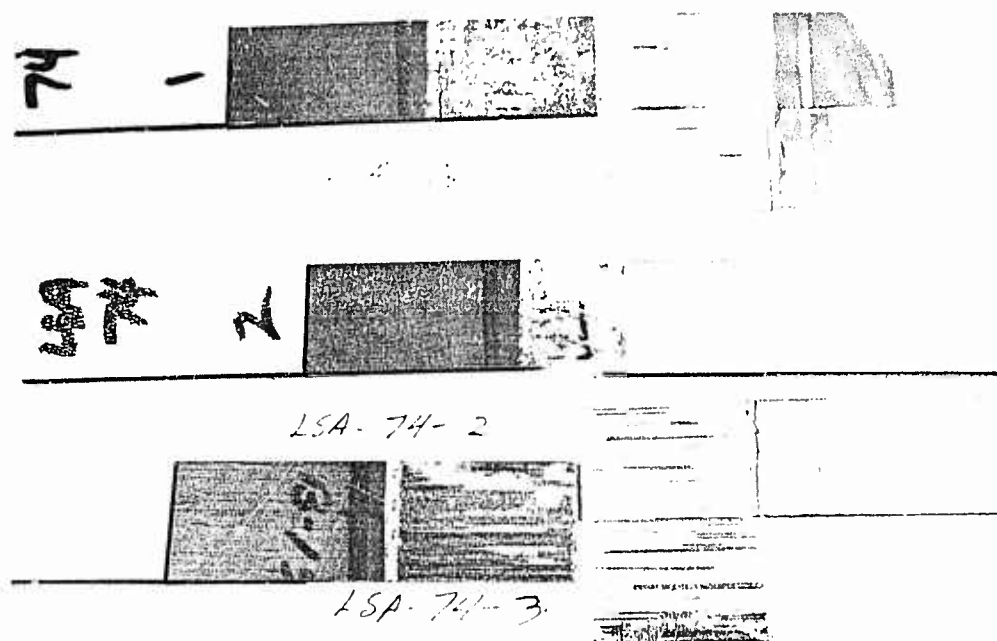


FIGURE 103. LSA-74 FAILED SPECIMENS

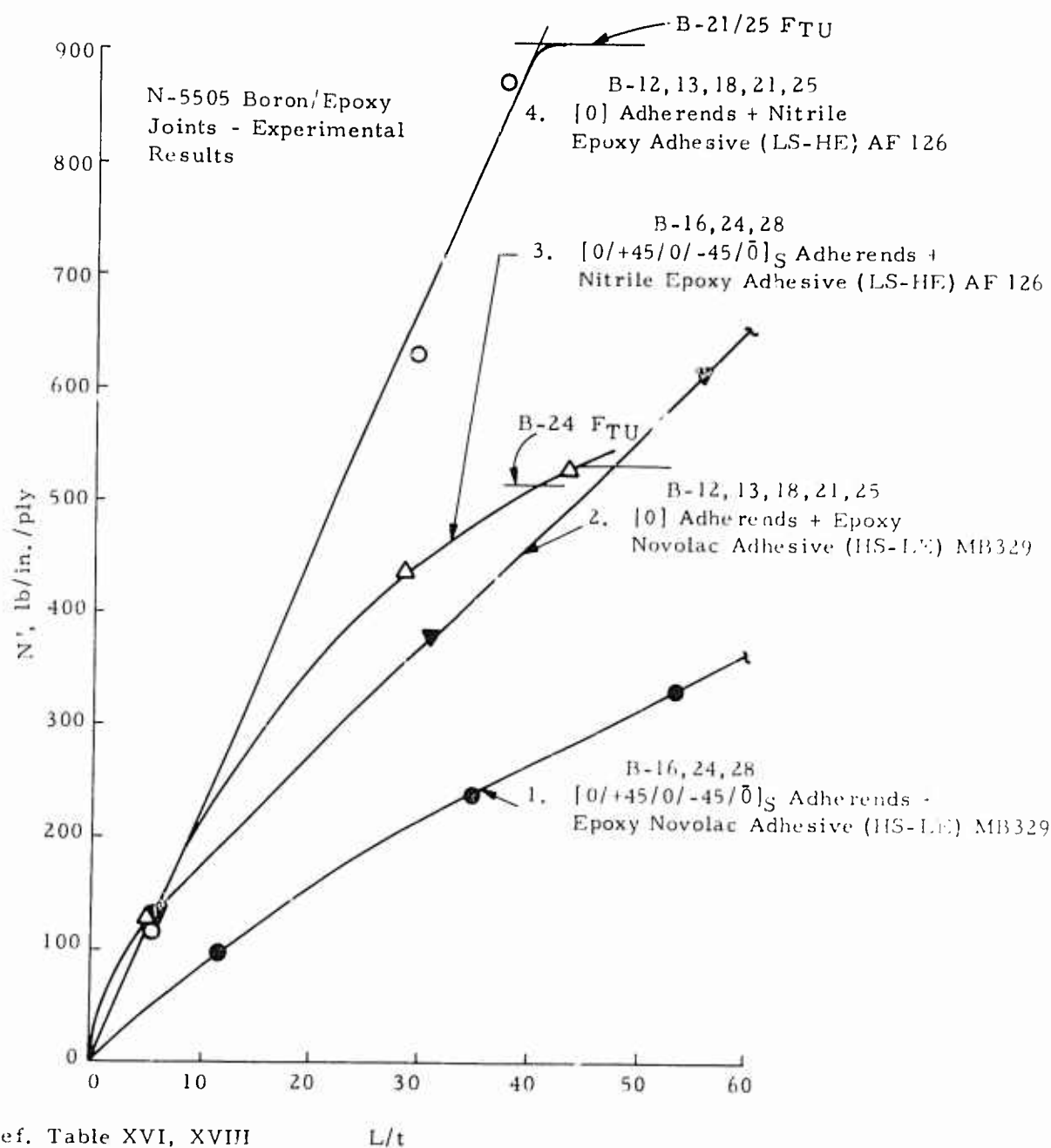


FIGURE 104. SINGLE LAP COMPOSITE/COMPOSITE JOINTS
LOAD TRANSFER CAPABILITY

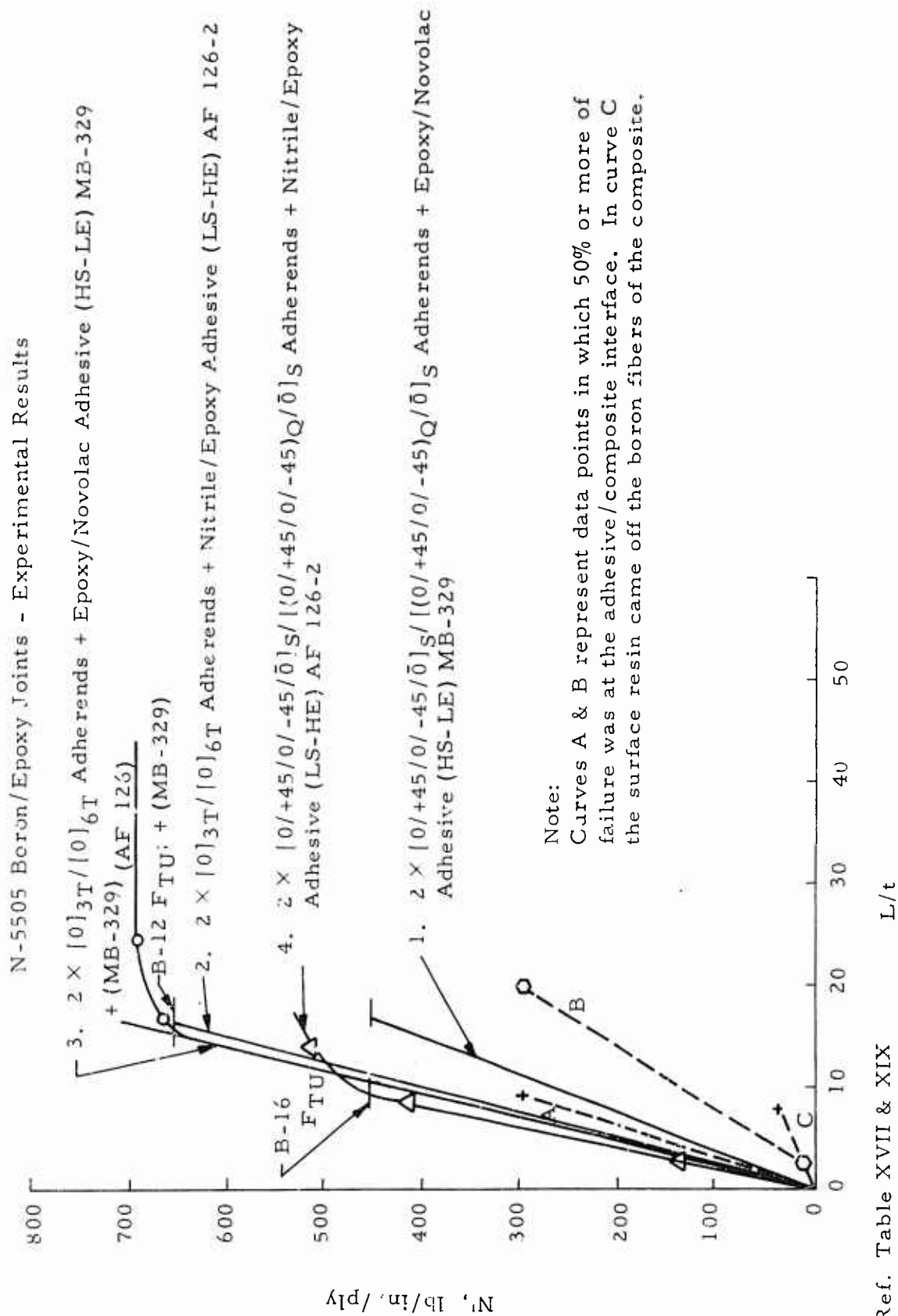


FIGURE 105. DOUBLE LAP COMPOSITE/COMPOSITE JOINTS LOAD TRANSFER CAPABILITY

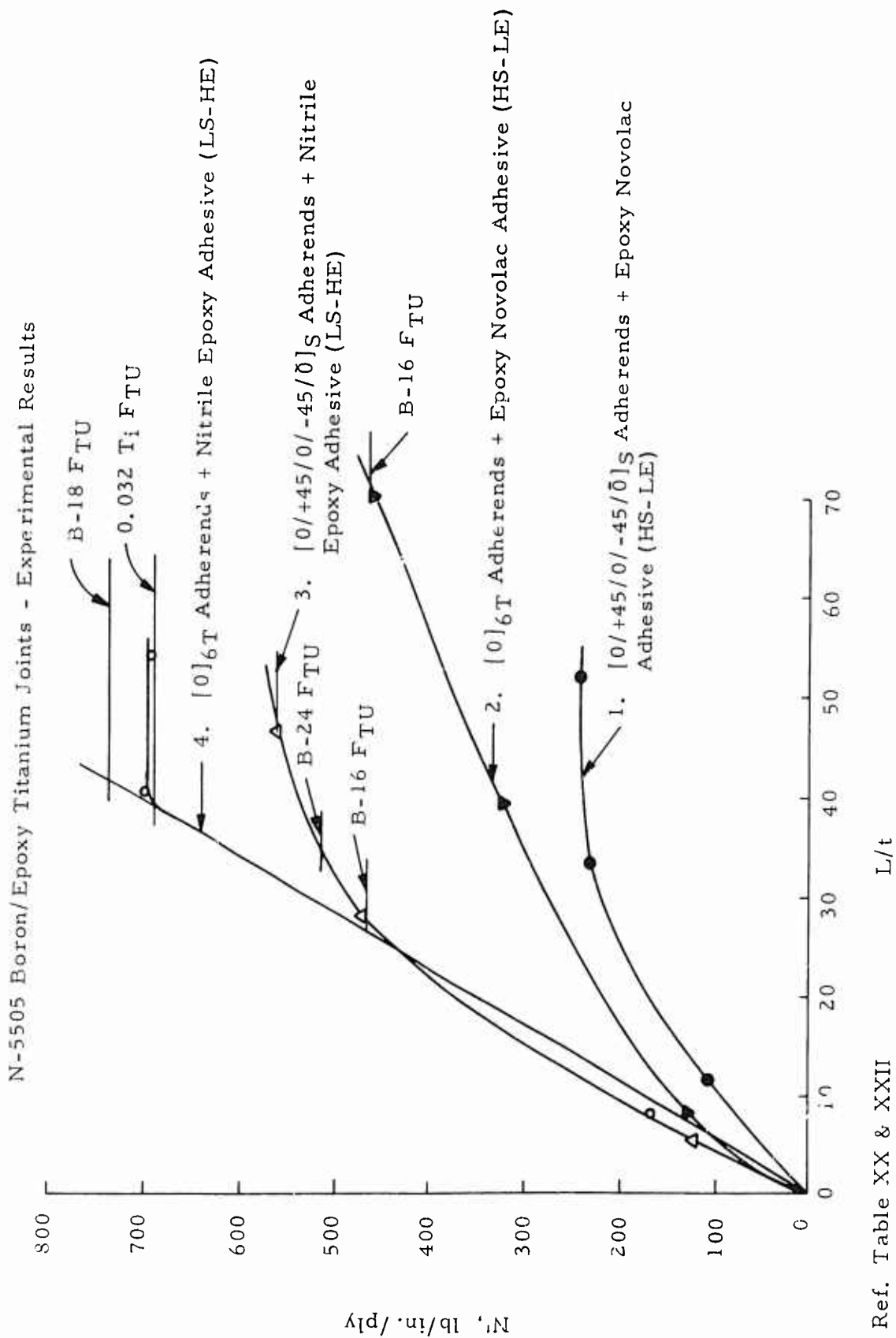


FIGURE 106. SINGLE LAP COMPOSITE/TITANIUM JOINTS LOAD TRANSFER CAPABILITY

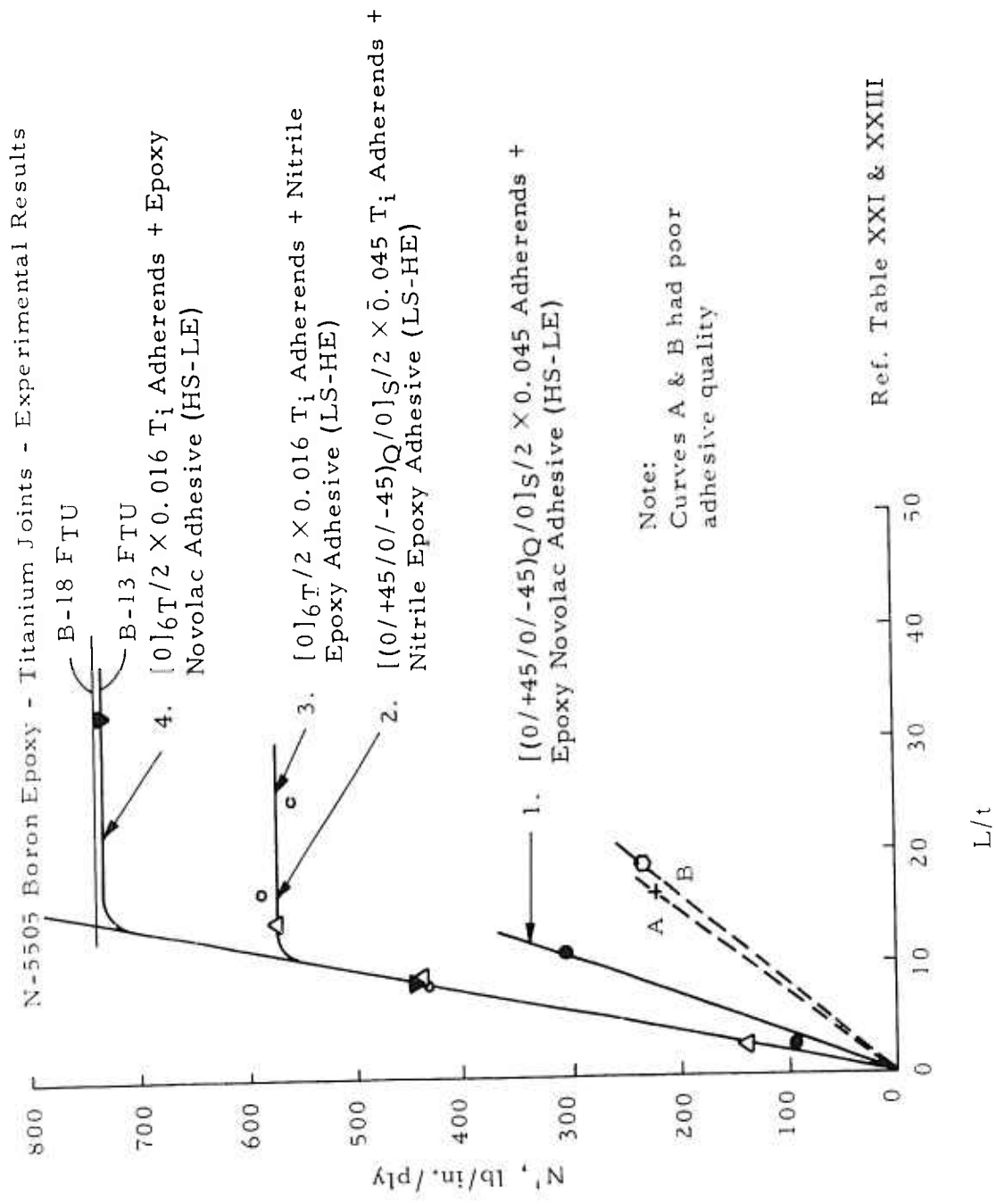


FIGURE 107. DOUBLE LAP COMPOSITE/TITANIUM JOINTS LOAD TRANSFER CAPABILITY

Limited step lap test data were obtained in this program and are summarized in Figure 108 (taken from Table XXIV). Examination of Figure 108 will reveal that the same trends are in effect as with the single lap joints with the addition of one new trend. This is that the slope also increases as the number of steps are increased from one to three. It should be noted, as shown in Section VIII, that these are single step-lap joints. This configuration is probably more related to single lap joints than the double lap ones, as slope comparisons with Figures 104 and 106 will show. The load transfer shown for these joints is that of the "gross section" rather than the "net section," therefore, this capability looks low for the one step-lap joint. However, net section calculations would double it. Curve 3 does give a higher slope than the best of the single lap data but not quite as good as the best of the double lap data. These trends probably indicate that an even higher number of steps would further increase the slope as would changing the configuration to that of a double step lap. In this case, the low quality specimens had voids in the bondline.

It should be brought to the readers attention that the above graphical analysis was performed only on the composite/composite and composite/titanium joints utilizing the 0° and $0^\circ/\pm 45^\circ$ general adherend orientations with both adhesives. Data utilizing both adherend combinations and both adhesive selections were also obtained using the $0/90^\circ$ orientation, but not as extensively. Only double lap and step lap data were obtained with this orientation.

Testing of the tensile lap shear simple specimens was performed in a Multirange Baldwin Test Machine at a constant deflection rate of 0.0025 in./min (over a 2-in. gage length over the bond area).^{*} An autographically recorded load deflection curve was obtained to failure on each specimen over this 2-in. gage length with a multi-range TSMD extensometer. Temperature and humidity during testing were $70^\circ \pm 4^\circ\text{F}$ and $50\% \pm 10\%$, respectively.

Figures 109 and 110 are characteristic of the type of load/deflection[†] curves that were obtained from the joint specimens, the characteristic difference being that the joint with the low stiffness-high elongation adhesive has a curve which exhibits some nonlinearity while the high stiffness-low elongation adhesive curve is linear to failure. The LS-HE adhesive joint is stronger but gives a slightly lower curve slope compared to the HS-LE joint. A detailed description of these two example joints follows:

Figure 109 represents a 1-in. wide double lap joint with 0.045-in. thick 6A1-4V annealed Ti double adherends and a $[(0/+45/0/-45)Q/0]_S$ 17-ply boron epoxy single adherend 0.087 in. thick. The overlap length was 0.687 in. with the AF-126-2 nitrile epoxy low modulus, high elongation adhesive bond. Failure was predominately cohesive and surface resin fracture at a bondline average shear stress of 5,444 psi. Adherend average tensile stress was 86,023 psi. The load transfer capability of joints made with this adhesive system were very high, regardless of adherend stiffness lap length, or lap type.

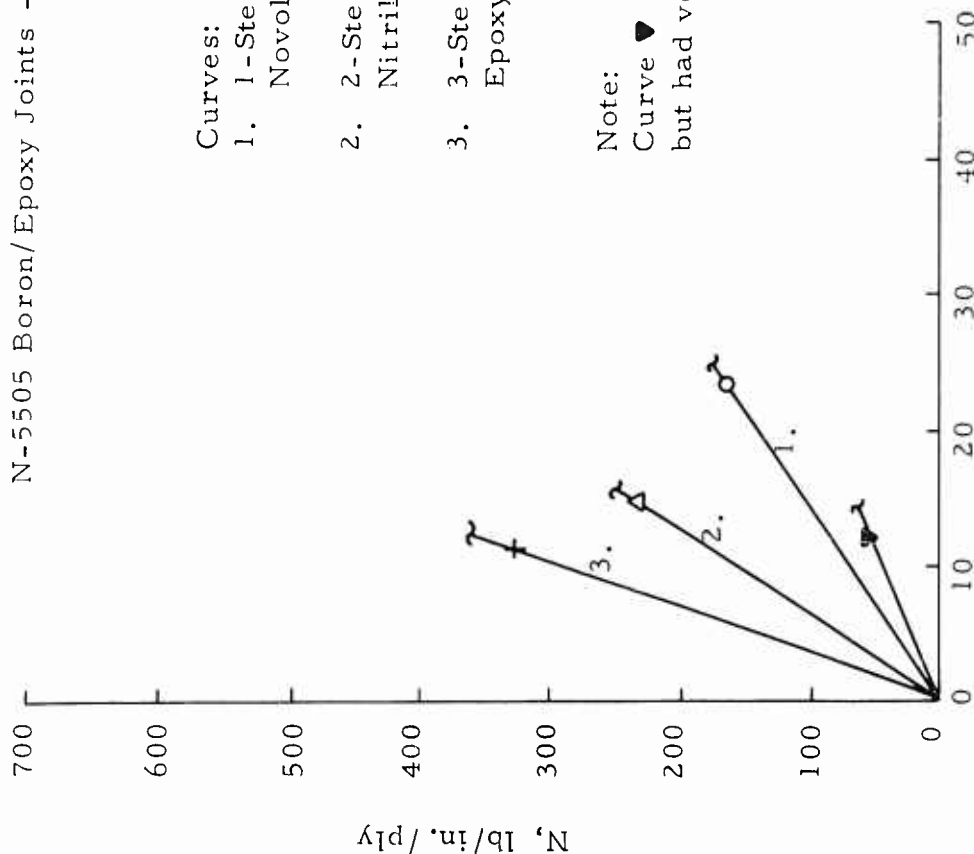
Figure 110 presents a 1-in. wide double lap joint with 0.047-in. thick $[0/+45/0/-45/0]_S$ 9-ply boron/epoxy double adherends and a 0.087-in. thick $[(0/+45/0/-45)Q/0]_S$ 17-ply boron/epoxy single adherend. Overlap length was 1.75 in. using the Metlbond-329 high modulus, low elongation adhesive system. Failure was predominately at the interface region between the laminate and the adhesive at a bondline shear stress of 1,154 psi and an adherend average tensile stress of 45,384 psi. The load transfer capability of these joints range from very high to very low depending on adherend stiffness, lap length and type.

By contrast Figure 109 represents a high quality, high performance joint and Figure 110 illustrates a low quality, low performance joint. Their characteristic failures are the key to their quality differences, although the adhesive shear stresses will always be lower with larger overlaps on high modulus, low elongation bondline materials. It has been found that the type of failure typified by the joint whose mechanical behavior curve is shown in Figure 109 has a predictable failing load with the nonlinear bonded joint analysis techniques developed in this program using a maximum stress adhesive failure criterion (i.e., for the low modulus, high elongation adhesive). Failures in the HS-LE adhesive joint can also be predicted by this criterion when failures are cohesive or surface resin fracture.

^{*}i.e., strain rate is 0.00125 in./in./min.

[†]Deflection divided by the 2-in. gage length gives gross strain.

N-5505 Boron/Epoxy Joints - Experimental Results



- Curves:
- 1-Step, $2 \times [0]_{gT}$ C. Adherends + Epoxy Novolac Adhesive (HS-LE)
 - 2-Step, $3 \times [(0/\pm 45/0)Q]_S$ C. Adherends + Nitrile Epoxy Adhesive (LS-HE)
 - 3-Step, $4 \times [0]_{gT}$ C. Adherends + Nitrile Epoxy Adhesive (LS-HE)

Note:
Curve \blacktriangledown joints were like those of No. 1 but had voids in bond line

Ref. Table XXIV L/t

FIGURE 108. STEP LAP COMPOSITE/TITANIUM JOINTS LOAD TRANSFER CAPABILITY

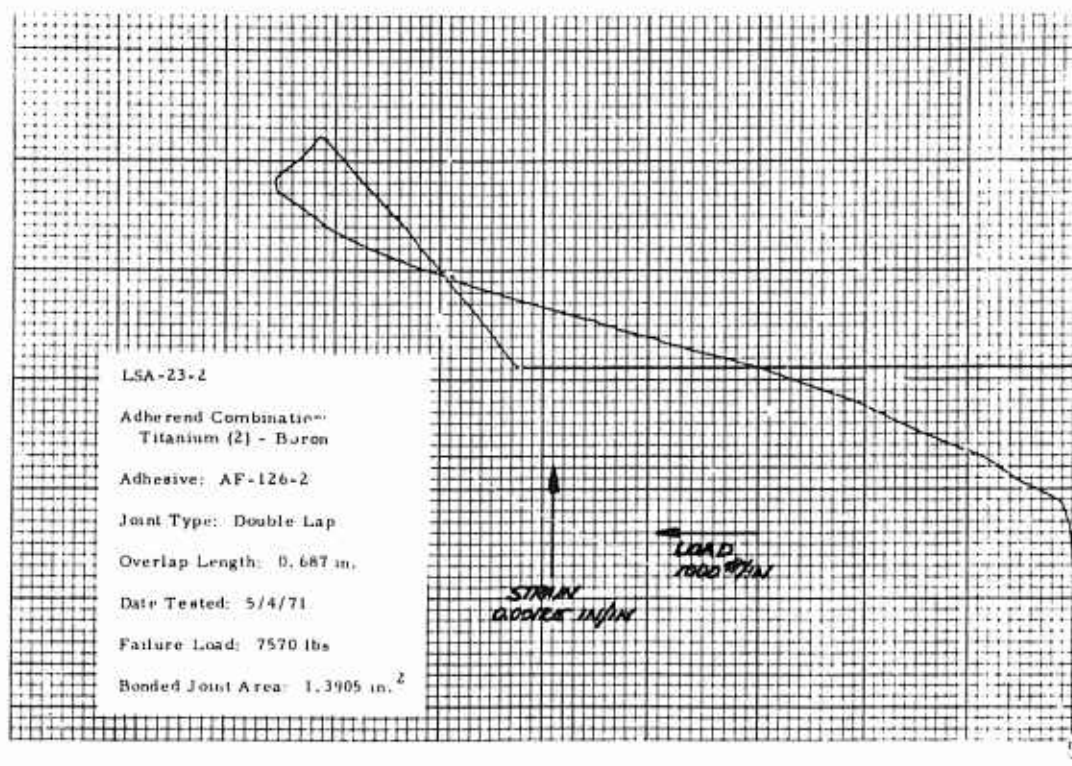


FIGURE 109. LOAD/STRAIN CURVE FOR DOUBLE LAP AF-126-2 BONDED JOINT
(Two Inch Gage Length Over Joint Area)

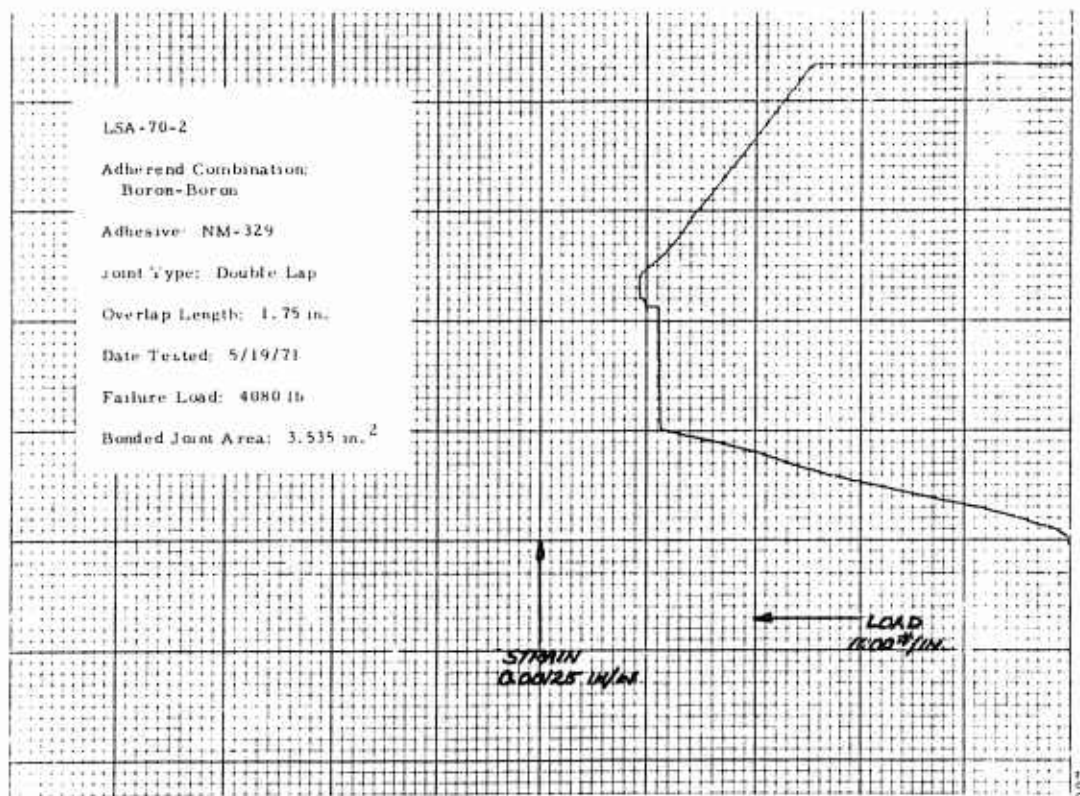


FIGURE 110. LOAD/STRAIN CURVE FOR MB-329 BONDED JOINT
(Two Inch Gage Length Over Joint Area)

However, failures cannot be predicted for either adhesive system when failures occur like the one on the specimen whose mechanical behavior is described in Figure 110. This illustrates that a lack of adhesion exists at the interface region and results in behavior which is not predictable by current nonlinear orthotropic mechanics methods without empirical modification. It is suspected that this is a materials and processes quality problem and therefore should not be considered in design/analysis. Whenever such a condition cannot be prevented it should at least be identified and isolated as was done herein in order for the results to be analyzed in a meaningful manner.

The types of failure observed in the simple joint program can be generally divided into the following classes:

- A. Adhesive/Adherend Interface Adhesion Failure
- B. Adherend Surface Resin/Reinforcing Fiber Interface Adhesion Failure
- C. Cohesive Fracture of the Bondline
- D. Cohesive Fracture of the Adherend Surface Resin
- E. Delamination, Splitting
- F. Adherend Net Section Tension

The first two types (A and B) almost always occur as a result of materials or process quality being low. Failures of this type usually occur at lower joint load transfer magnitudes than those failing by other means. The nonlinear bonded joint analytical methods will not predict these failure types or load magnitudes.

Failure modes C and D represent high quality specimens which have predictable failure modes and magnitudes with the nonlinear joint analysis techniques. The maximum stress failure surface can be used to predict the C and D failure types with the nonlinear theory. Occasionally poor adhesive (or matrix resin) material or improper cure will result in low magnitude test values with the C or D failure type.

Delamination and splitting type failure* is associated with laminate behavior, probably emanating from some sort of micro-mechanical damage occurring during non-failure loading. However, this has not been proven for boron/epoxy laminates. Large differences in modulus, Poisson's ratio, or thermal coefficient of expansion of the two adherend materials could be a contributing factor as well as a low quality laminate. In any case the present nonlinear techniques cannot predict these failure types or magnitudes without further modification.

Adherend net section tension failures† were observed on those specimens designed to fail in this fashion and the failure stress magnitudes were approximately equal to the experimentally measured tensile strength of the composite and titanium materials. Failure predictions can be accomplished with the nonlinear techniques using maximum strain failure criteria for the composite adherends and maximum stress failure criteria for the titanium adherends.

IX.3. SPECIAL JOINT INVESTIGATION DATA SUMMARY

Six composite/titanium bonded joints were selected from the simple specimen program reported in Section IX.2 for in-depth experimental behavior study. These "special" joints cover the single, double and step-lap configurations with both adhesive systems and one composite material orientation category ($0 \pm 45^\circ$). The joints chosen for study were:

No.	Joint Type	Adhesive	No. of Strain Gages
LSA-20-1	S.L.	AF-126-2	4
LSA-23-1	D.L.	AF-126-2	4
LSA-59-1	S.L.	MB-329	2
LSA-62-1	D.L.	MB-329	6
LSA-11-4	1-St.L.	MB-329	5
LSA-26-4	2-St.L.	AF-126-2	6

Detail experimental data at failure on these joints appear in Appendix F.

*Type E.

†Type F.

The method used for presenting the experimental data is the familiar stress-strain curve. Stresses used were the average calculated values based on the adherend cross-section area outside the joint overlap. Strains were those measured directly on the adherend surfaces at selected longitudinal centerline locations.

Data on LSA-20-1 are presented in Figure 111. A map of these strains vs overlap location are shown in Figure 112. Strains at four composite adherend stress levels were mapped: 10, 60, 80 and 92.437 (failure) ksi. The first stress level (10 ksi) was picked so that both the average adherend and adhesive behavior were still in the linear range. The second stress level (60 ksi) was picked so that the average adherend behavior would still be linear (just below the P.L.) but the adhesive would be nonlinear. At the third stress level (80 ksi) both the adherend and the adhesive average stress levels are in the nonlinear range. Failure stress level (92.437 ksi) was selected as the fourth one with fracture occurring by net section tension in the composite at about the same stress as the average tensile strength data on panel B-16 would indicate. Transverse composite adherend strains were high, as would be expected with the high Poisson's ratio of the $0/\pm 45^\circ$ orientation.

Figure 113 gives the LSA-23-1 joint strain behavior as a function of average adherend stress level. Failure characteristics of this series of joints (covering also LSA-23-2 and 23-3) is shown in Figure 114. Primary failure was caused by cohesive fracture of the adhesive and composite surface resin. Strain maps of both the composite and titanium adherend are shown in Figure 115. Again the four adherend stress levels were picked for the same reasons given above. They are as shown below:

Avg. Adherend Stress Level (ksi)	Estimated Adherend Behavior Range	Estimated Bondline Behavior Range
10	linear	linear
50	linear	nonlinear
80	nonlinear	nonlinear
90.203	failure	failure

The higher transverse strains of the composite adherend can be seen clearly in Figure 115.

Specimen LSA 59-1 strain data are shown in Figure 116 with typical failures shown in Figure 117. The primary mode was failure at the interface of the surface resin and the boron fibers of the composite adherend under the bondline. Results are considered to be low. The strain distribution map is shown in Figure 118. The high transverse strains in the composite adherend can be noted. Three adherend stresses were selected at which to evaluate the strain distribution: 10, 30 and 44.954 (F) ksi. All are in the linear range for the adherend, but the second one could cause nonlinear behavior in the adhesive. The third (failure) adherend stress level selected is definitely such that the adhesive behavior will be in the nonlinear range.

Figure 119 presents the strain data on LSA-62-1 and Figure 120 shows the cohesive fracture of the adhesive as the primary failure mode. Strain map curves covering both the composite and titanium adherends are shown in Figure 121. Since the adherend net section stress vs joint surface strain plots are all linear (with some minor knees evident) only two stress levels were investigated in the strain distribution study: 25 and 56.648 (F) ksi. While the longitudinal (X-dir.) strains in the composites are only slightly higher than those in the titanium at locations just outside the joint, the transverse strains in the composite are substantially higher (than those in the titanium) at all locations.

Strain distribution on joint LSA-11-4 is shown in Figure 122 with a strain map at four adherend stress levels given in Figure 123. Primary failure was by cohesive fracture of the surface resin of the composite with secondary failure at the interface between the adhesive and the composite surface resin. Some cohesive fracture of the adhesive was also evident. Results are considered to be low. All adherend and adhesive stress levels up to failure, which were investigated, are considered to be in the linear behavior range.

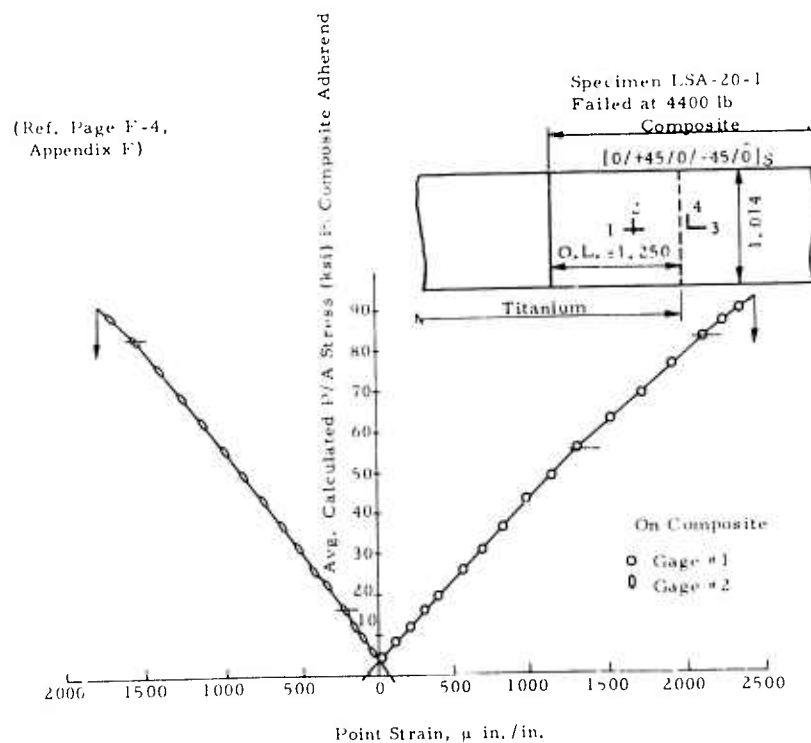
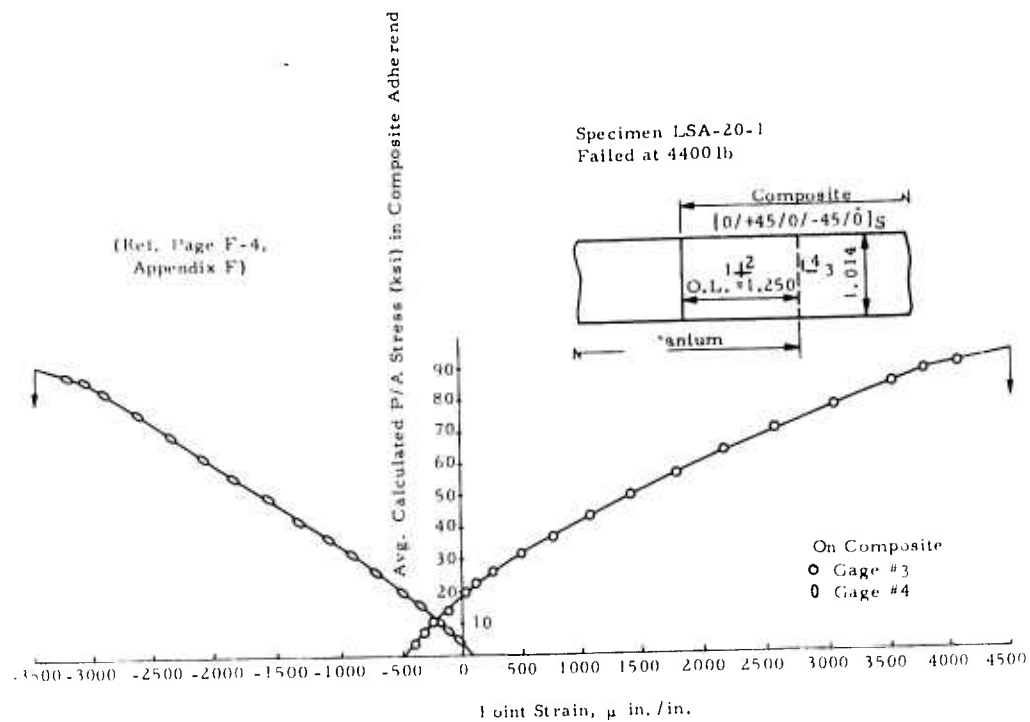


FIGURE 111. SINGLE LAP COMPOSITE/TITANIUM JOINT WITH NITRILE EPOXY ADHESIVE (LS-HE)

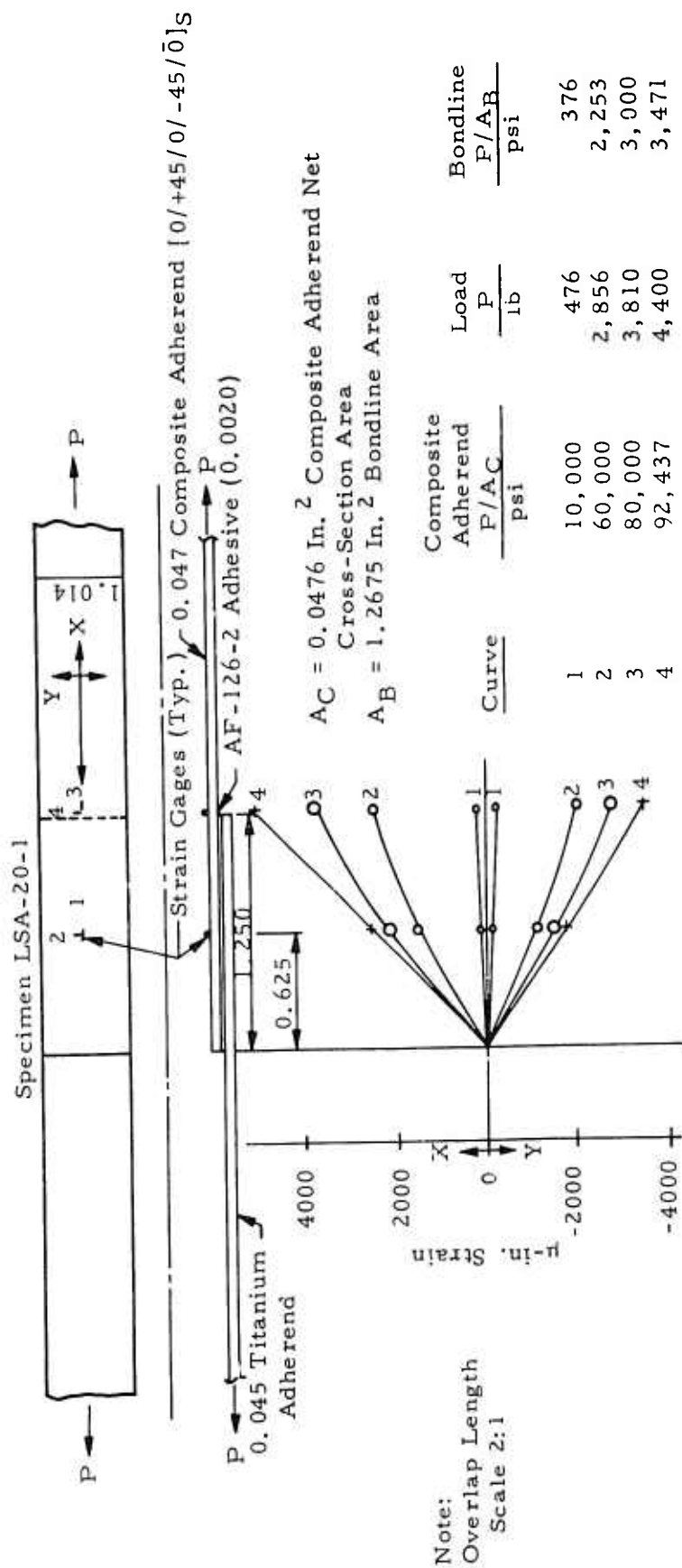


FIGURE 112. SINGLE LAP C/T-LSHE JOINT, COMPOSITE ADHEREND STRAIN DISTRIBUTION

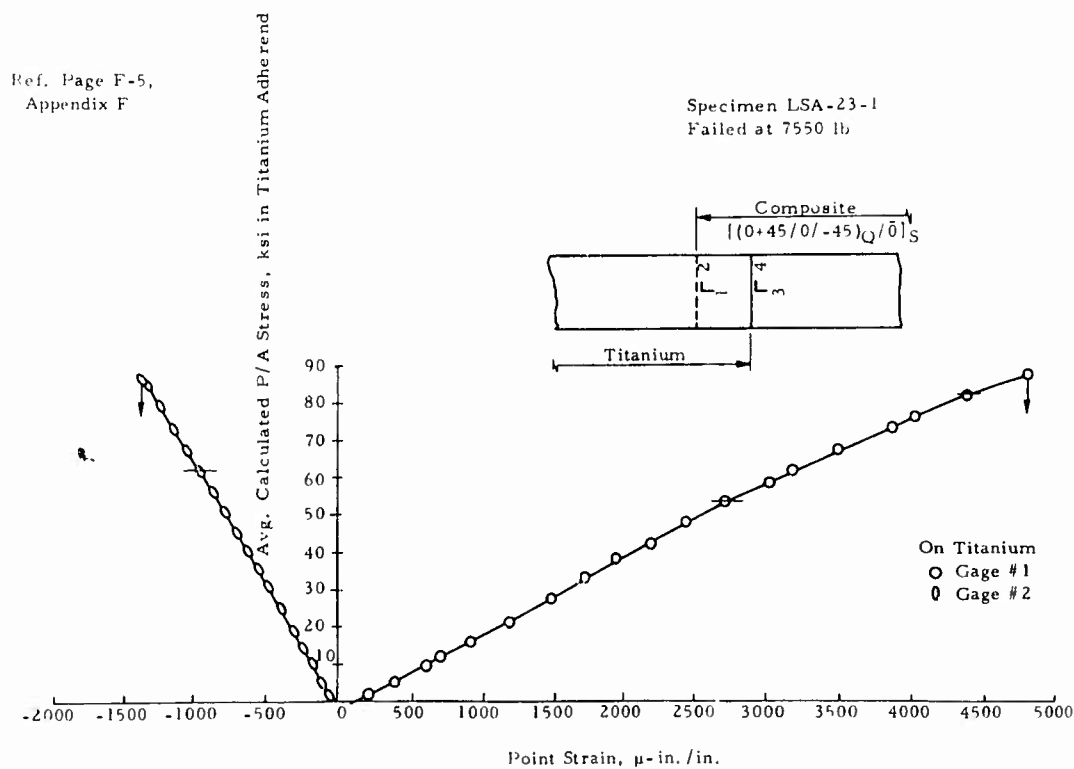
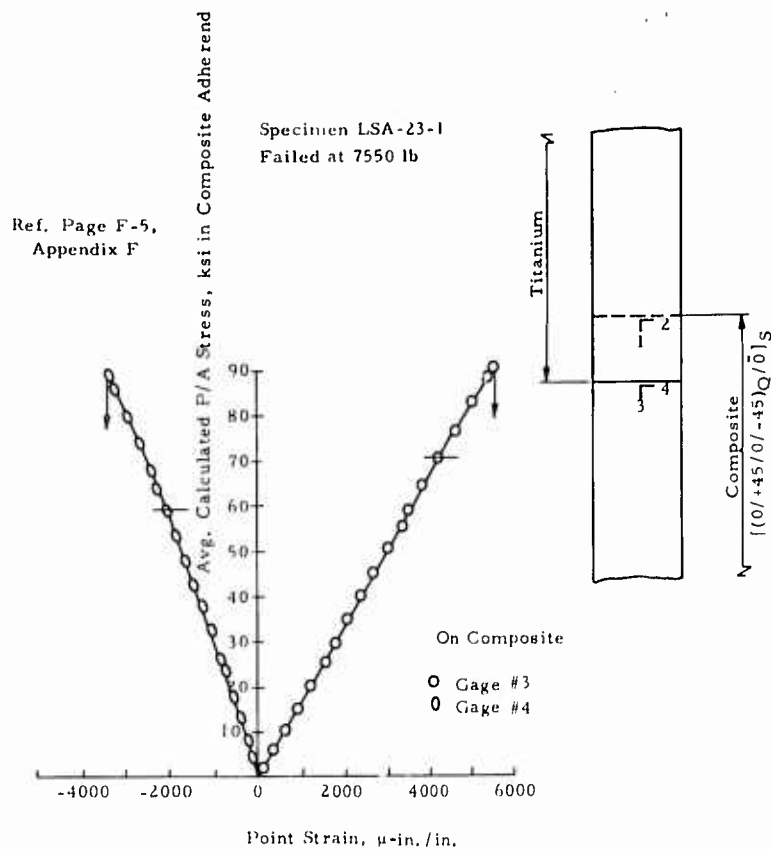


FIGURE 113. DOUBLE LAP COMPOSITE/TITANIUM JOINT WITH NITRILE EPOXY ADHESIVE (LS-HE)



FIGURE 114. LSA-23 FAILURE PHOTOGRAPHS

(Ref. Page F-9,
Appendix F)

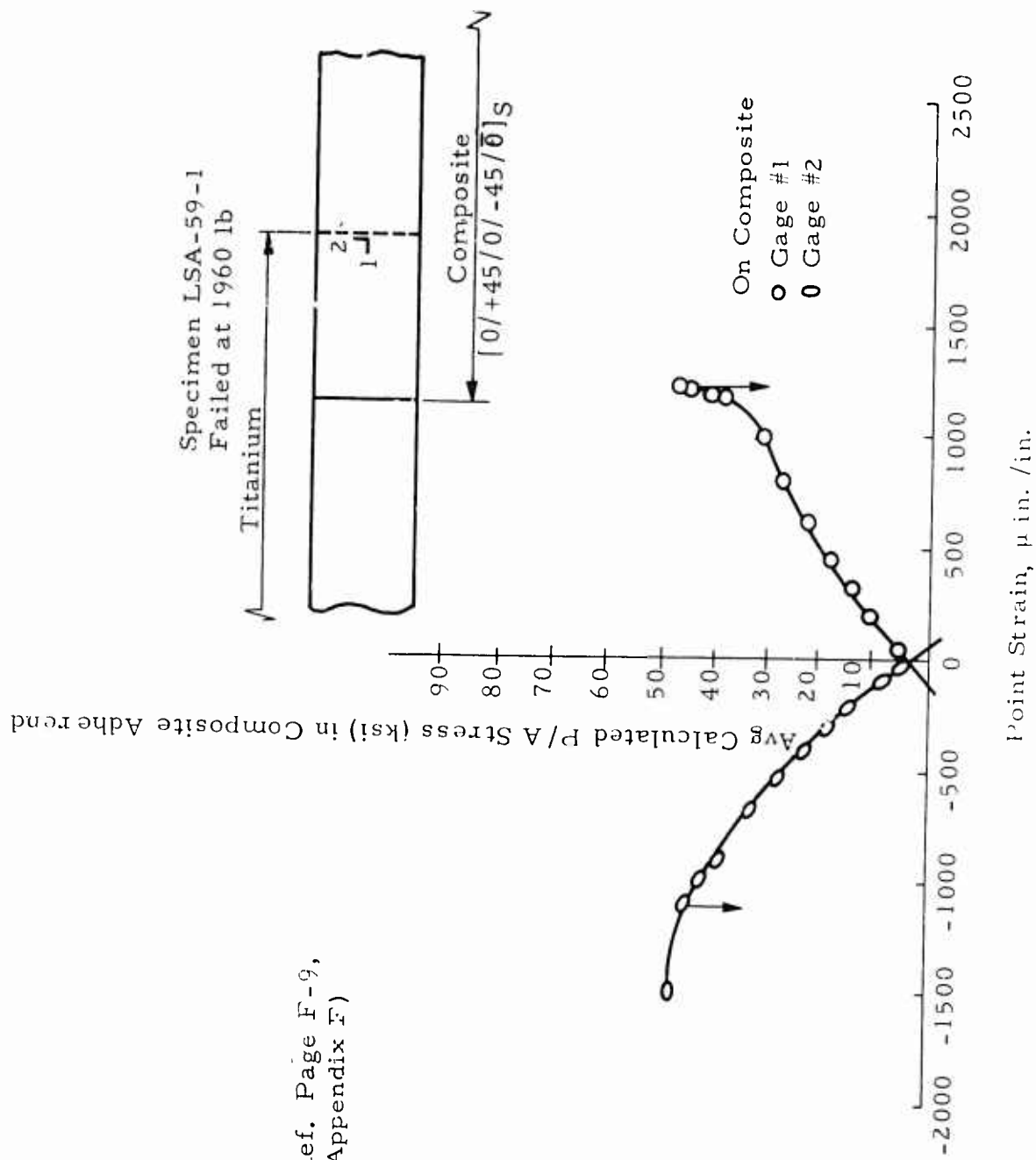


FIGURE 116. SINGLE LAP COMPOSITE TITANIUM JOINT WITH EPOXY NOVOOLAK ADHESIVE (HS-LE)



LSA-59-1



LSA-59-2



LSA-59-1

FIGURE 117. LSA-59 FAILURE PHOTOGRAPHS

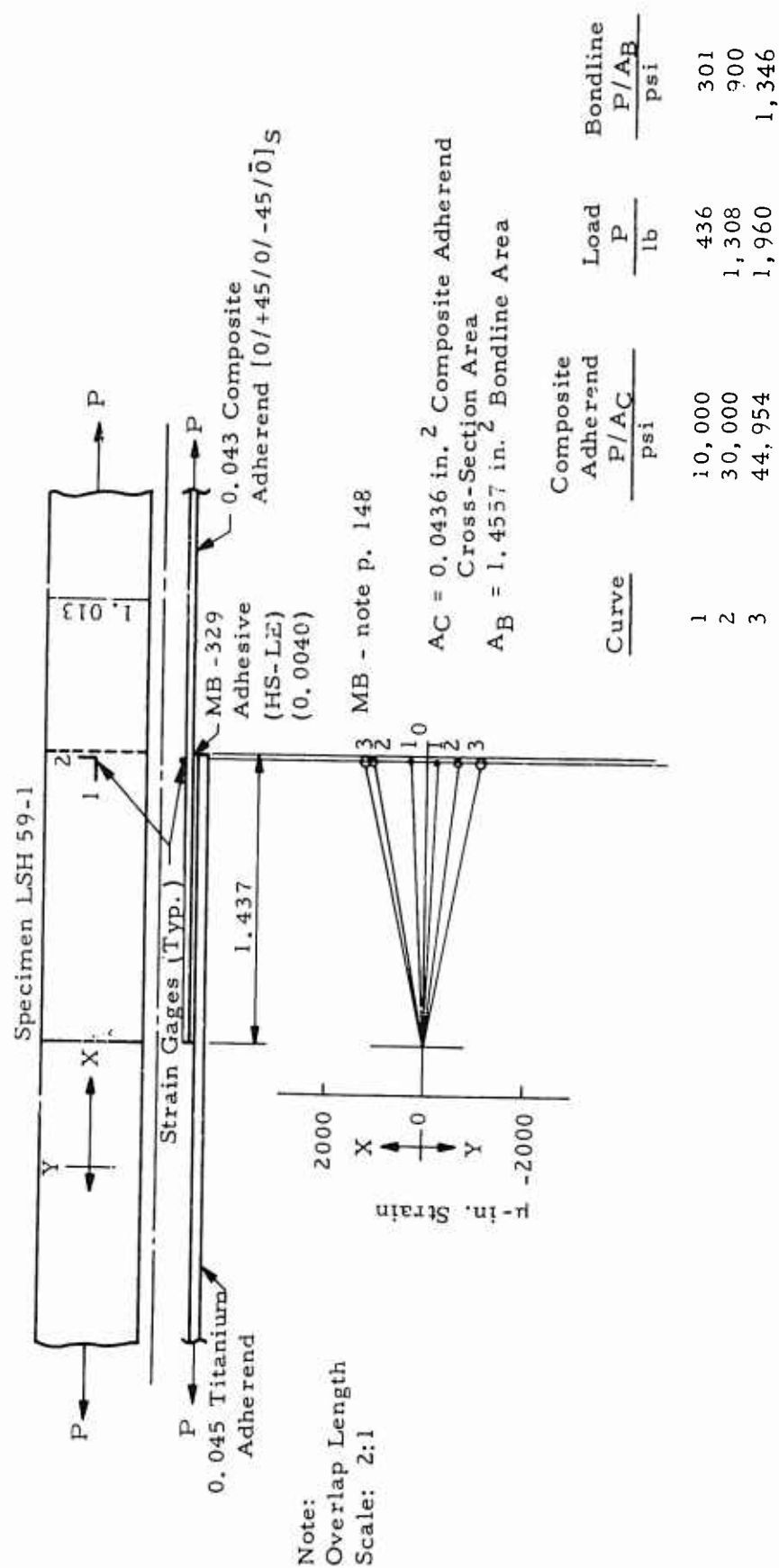


FIGURE 118. SINGLE LAP C/T-HSLE JOINT COMPOSITE ADHEREND STRAIN DISTRIBUTION

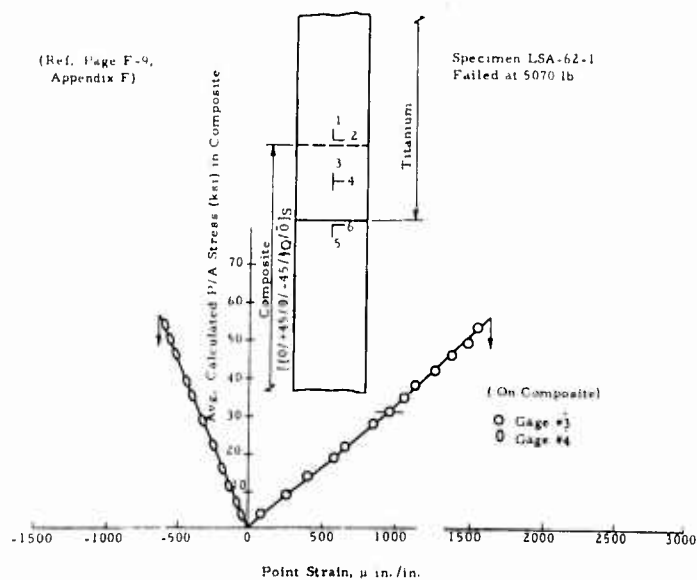
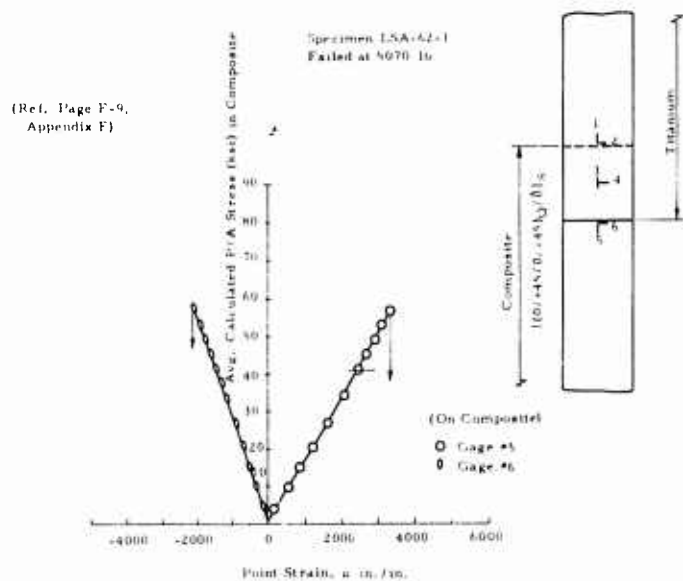
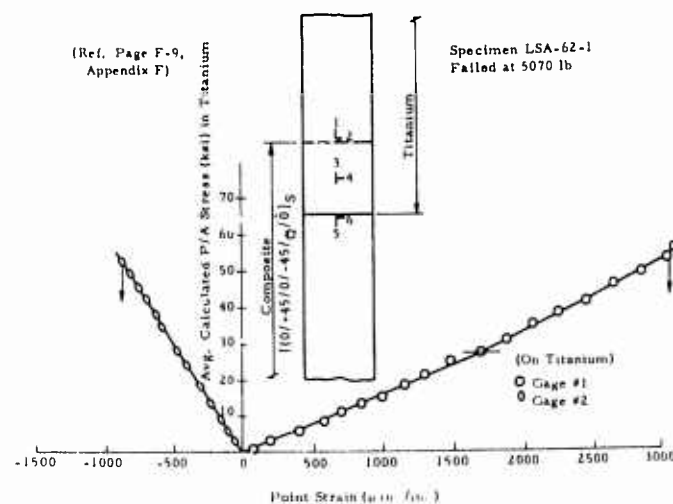


FIGURE 119. DOUBLE LAP COMPOSITE/TITANIUM JOINT WITH EPOXY NOVOLAK ADHESIVE (HS-LE)

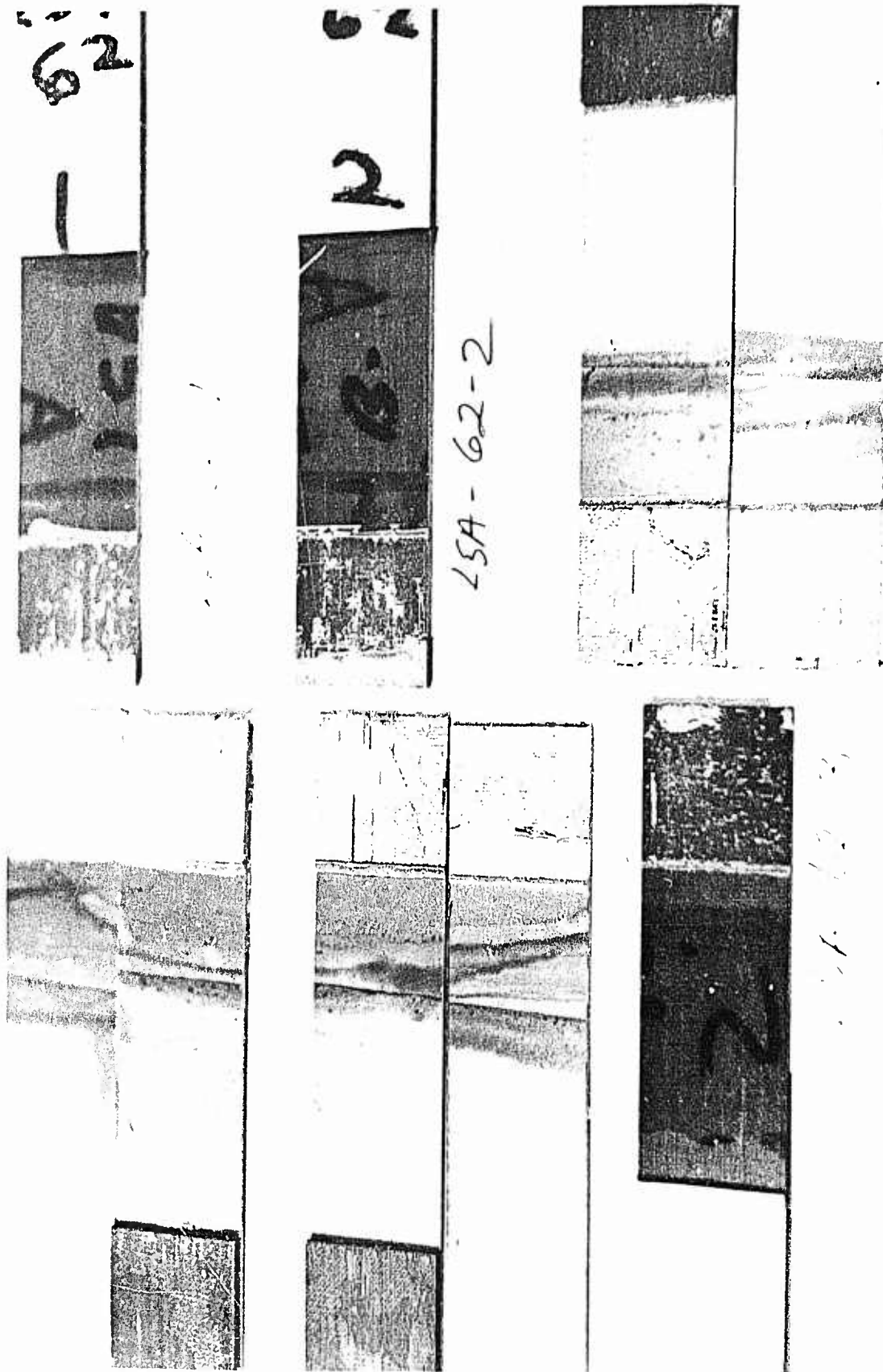
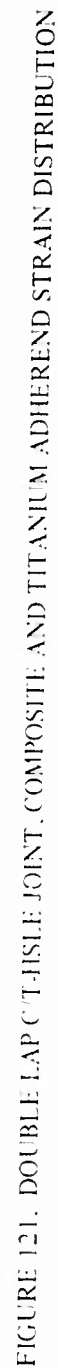


FIGURE 120. LSA-62 FAILURE PHOTOGRAPHS



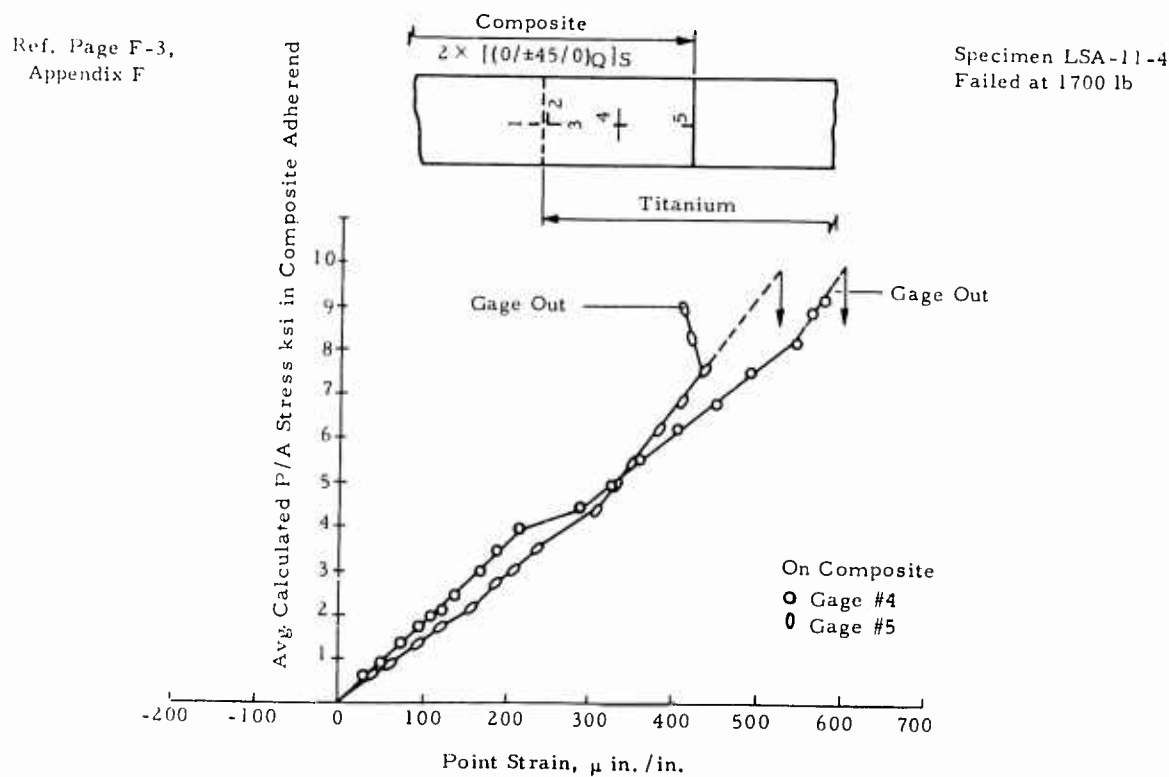
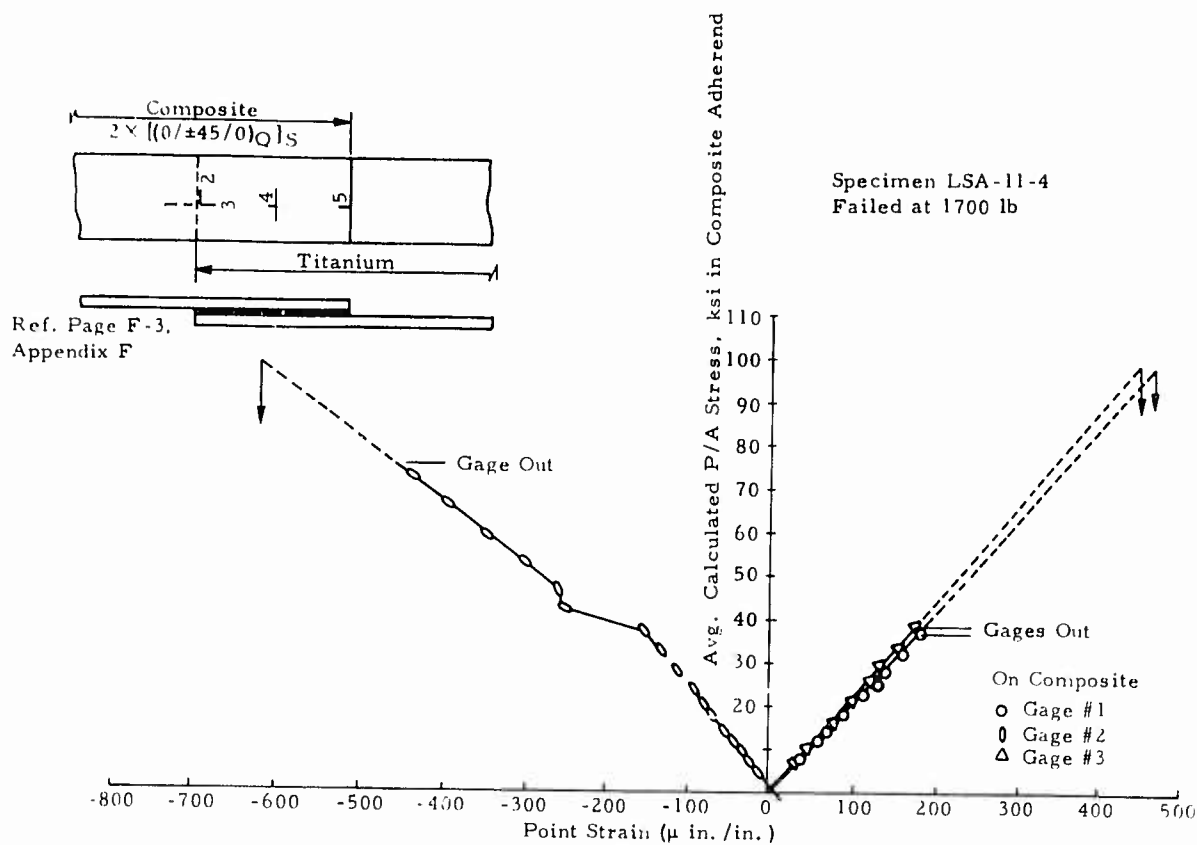


FIGURE 122. ONE-STEP LAP COMPOSITE/TITANIUM JOINT WITH EPOXY NOVOLAK ADHESIVE (HS-LE)

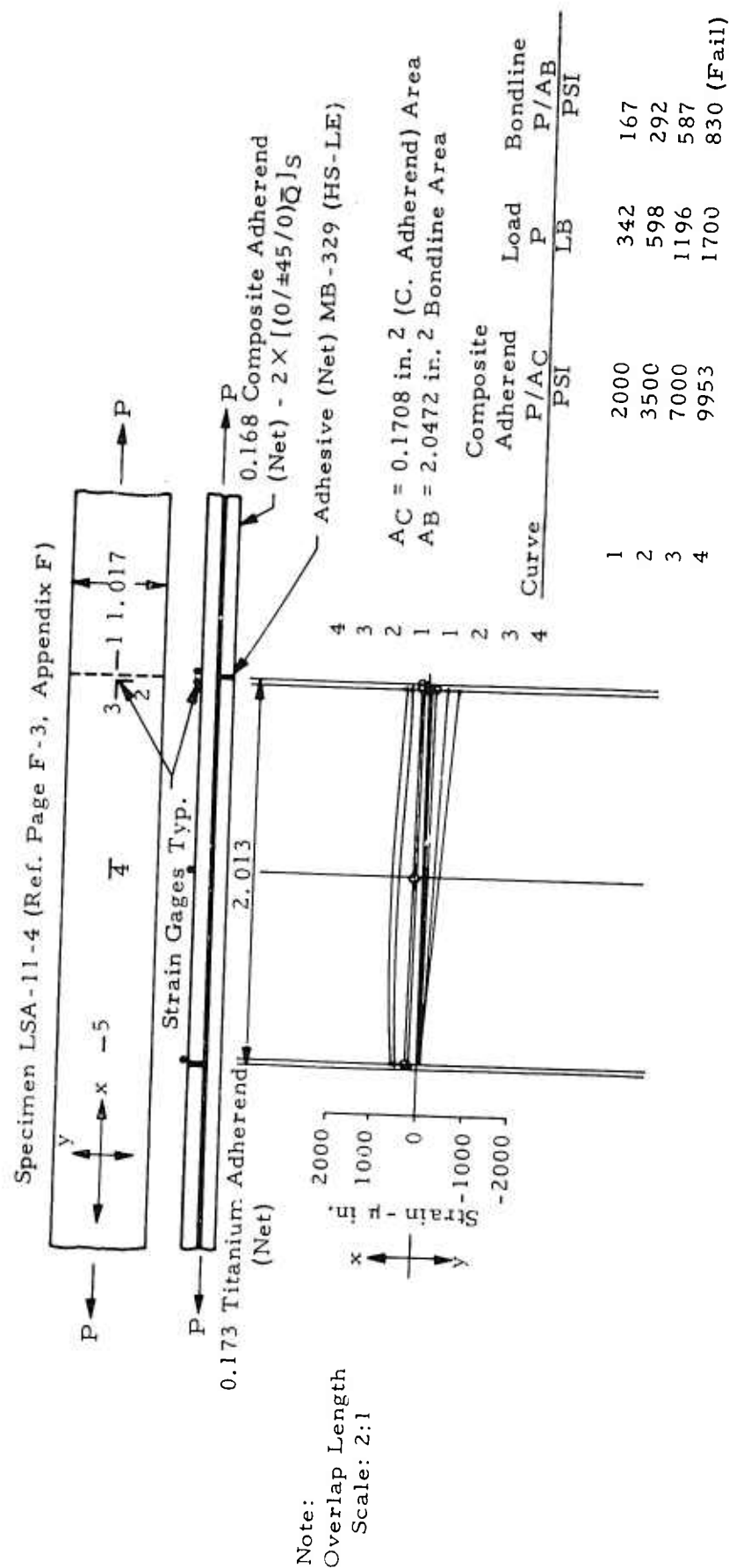


FIGURE 123. ONE-STEP LAP C/T-HSLE JOINT, COMPOSITE ADHEREND STRAIN DISTRIBUTION

LSA-26-4 specimen strain distribution is given in Figure 124. Failure mode was cohesive fracture of both the adhesive and the surface resin of the composite. Figure 125 shows the strain distribution map for the four adherend stress levels investigated and can be categorized as follows:

Avg. Adherend Stress Level (ksi)	Estimated Adherend Behavior Range	Estimated Adhesive Behavior Range
5	linear	linear
15	linear	nonlinear
30	linear	nonlinear
36.969(F)	linear	nonlinear

The adherend strain map shows that the strain distribution for the two-step-lap joint deviates substantially from that of the single and double lap joints. Maximum adherend surface strains occur in the middle of the joint on this two-step-lap configuration while those on the single and double lap ones are located at the start of the overlap. A sudden change in strain also occurs over the middle riser where the middle layer is changing from composite to titanium. Transverse strains of the composite adherend are relatively high.

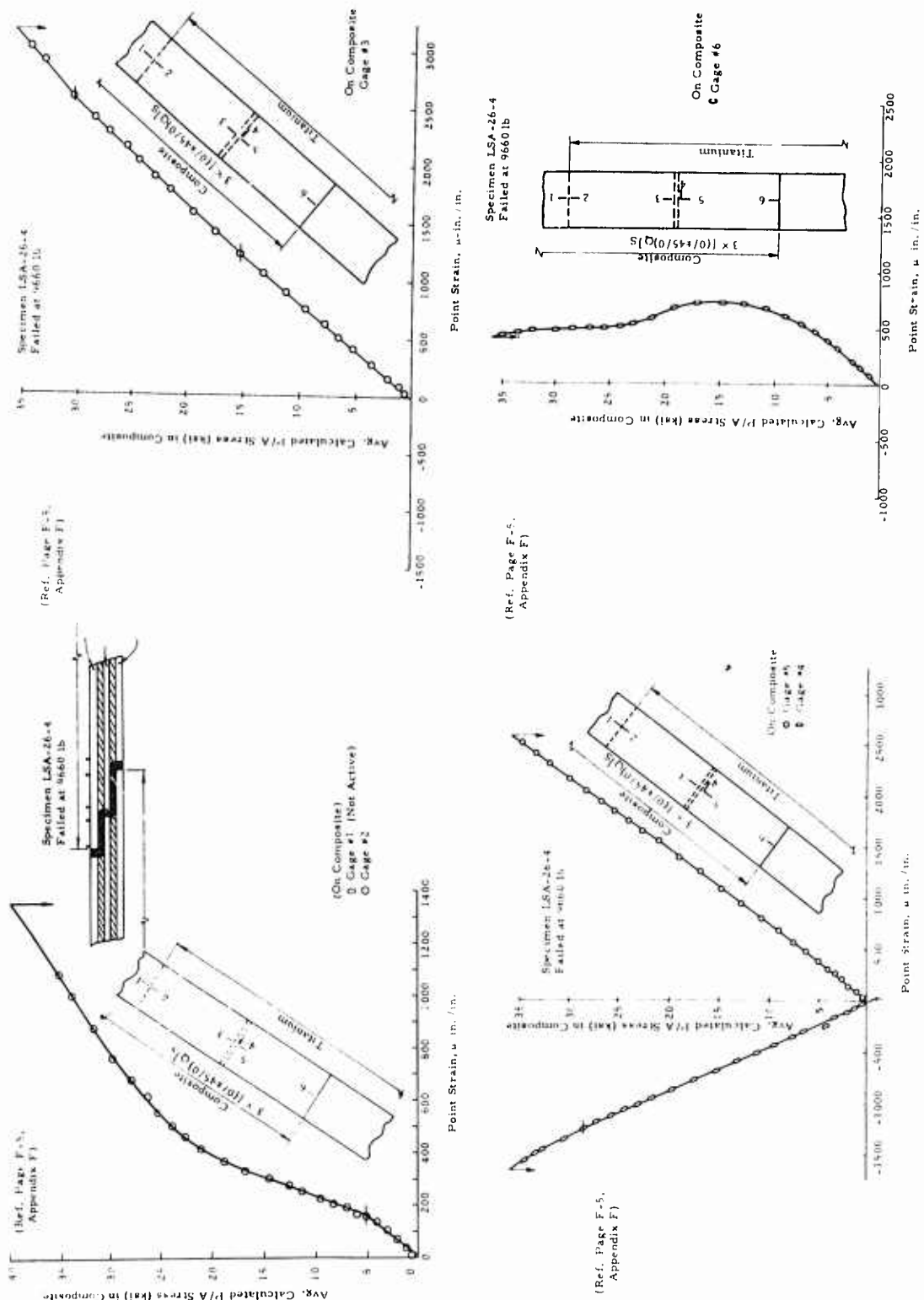
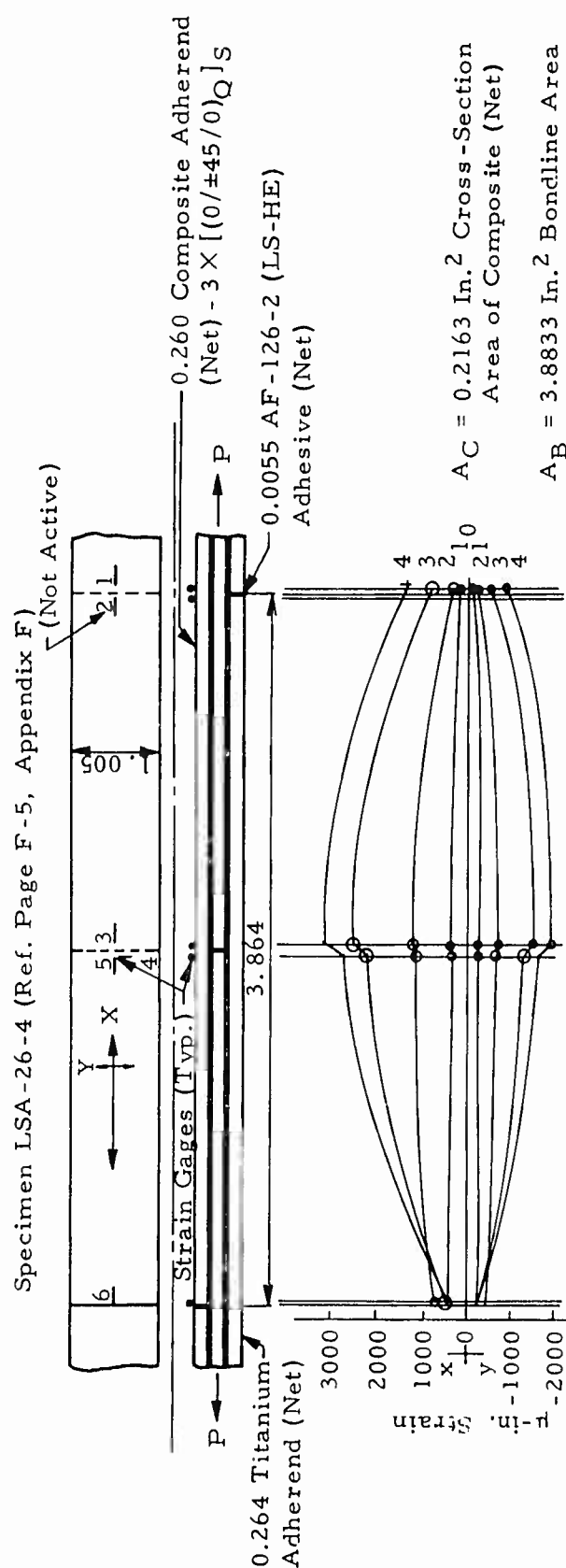


FIGURE 124. TWO-STEP LAP COMPOSITE/TITANIUM JOINT WITH NITRILE EPOXY ADHESIVE (LS-HE)



Notes:

1. Overlap Length Scale 2:1
2. Y-Points on Curve Denoted by • Were Calculated by Using the ν of the 4/5 Gages at Each Load Level, with the X-Strains

Curve	Composite Adherend		Load		Bondline	
	P/A/C	PSI	P	LB	P/AB	PSI
1	5,000		1,308			333
2	15,000		3,903			1,025
3	30,000		7,860			2,060
4	36,969		9,660 (Fail.)			2,488 (Cohesive)

FIGURE 125. TWO-STEP LAP C/T-LSHE JOINT, COMPOSITE ADHEREND STRAIN DISTRIBUTION

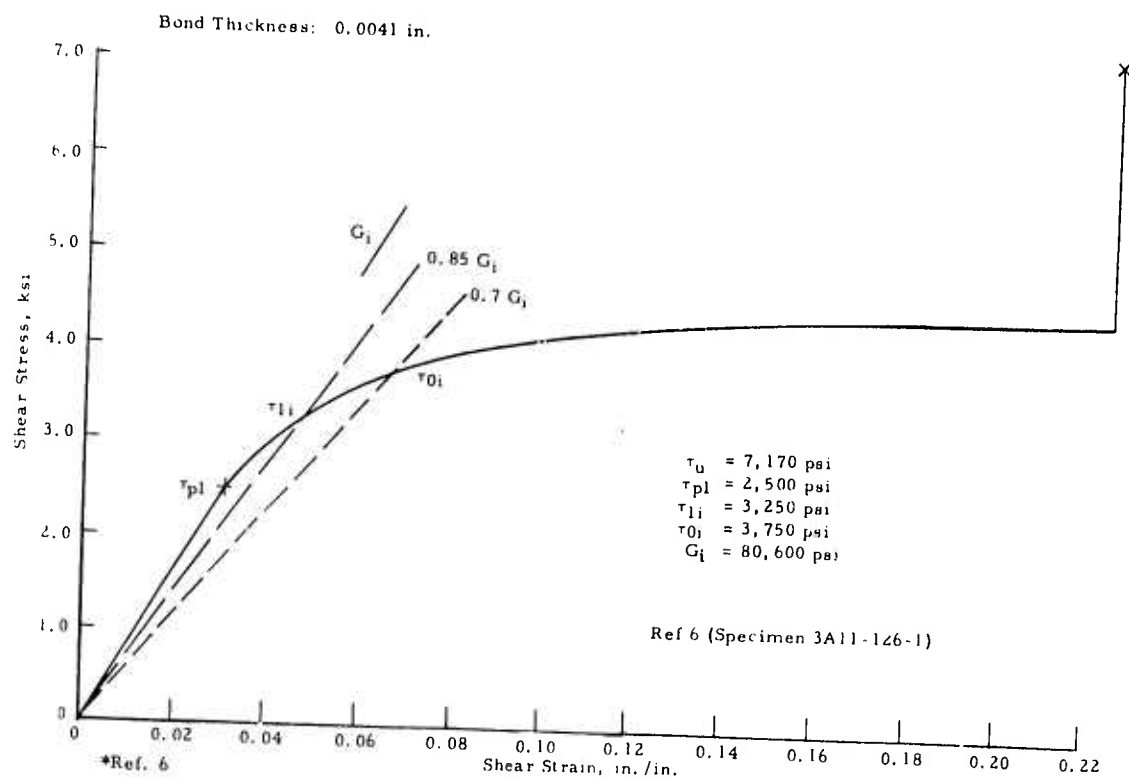


FIGURE 126. SHEAR STRESS-STRAIN CURVE OF AF126-2 ADHESIVE, SPECIMEN 3A11-126-1* (Typical)

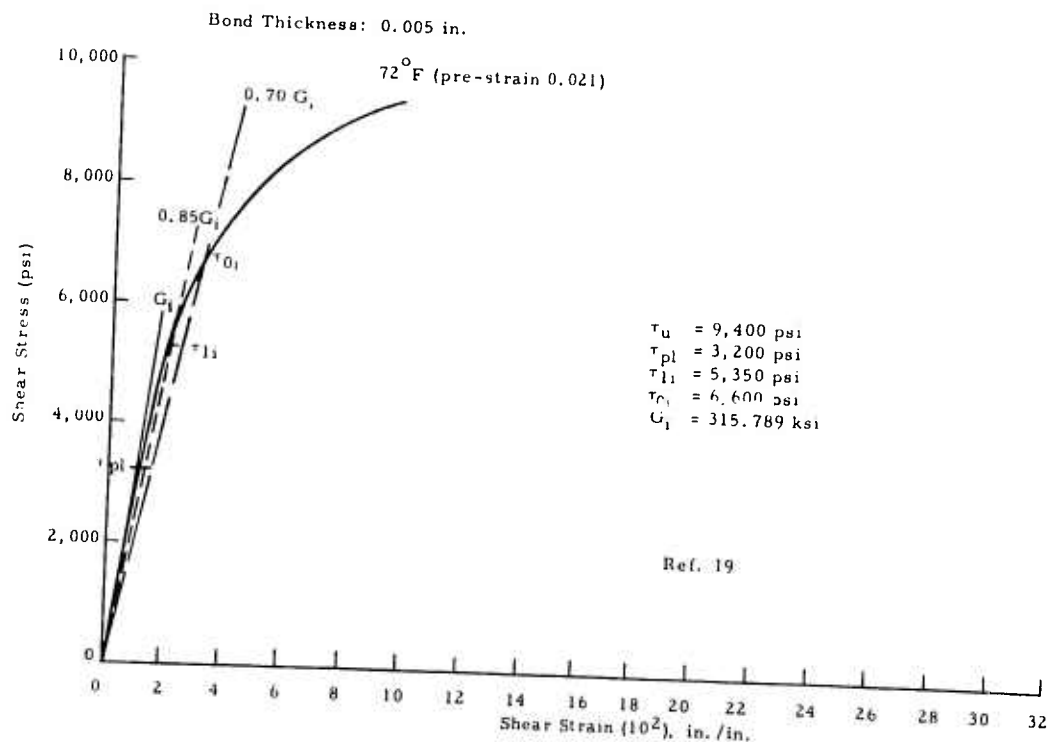


FIGURE 127. TYPICAL SHEAR STRESS-STRAIN CURVE OF METLBOND 329 ADHESIVE* (Typical)

SECTION X

THEORETICAL/EXPERIMENTAL BEHAVIOR COMPARISONS AND "EFFECTIVE" PROPERTIES

X.1. GENERAL

The purpose of this section is to show the correlation between the theoretically predicted joint behavior (including failure loads) and the experimental results on both small simple specimens and larger complex assemblies. Section X.2 covers the Addition of Effective Bending to the theory developed earlier and Section X.3 covers the Analytical/Experimental Behavior Comparison on Simple and Special Joints. Section X.4 presents the Design Analysis of Complex Joints. In Section X.5 Complex Joint Test Data Correlation with Predictive Methods is given.

X.2. ADDITION OF EFFECTIVE BENDING

The theory outlined in Section II was used to predict the failure loads of several of the experimental joint configurations. Maximum stress theory was used for the adhesive and isotropic adherends. Maximum strain theory was used for the composite adherends. These theories were incorporated into the computer program.

Early investigation indicated that the theory as presented predicted excessively low failure loads. Attempts were made to bring theory into agreement with experiment by an effective properties approach, e.g., modifying the adhesive modulus appropriately. Such attempts were not entirely successful.*

Comparison of analytical and experimental strains indicated the theory predicted excessively high bending strains. For example, the theory of Section II predicted *compressive* strains in adherend 2 of the single lap at x equal zero, y_2 equal to $t_2/2$ (refer to Figure 2). This was never observed in the experimental data. Similar inconsistencies arose in the double and step lap. The primary cause of the high predicted bending stresses is the small deflection assumption for the derivation of the equilibrium equations. As the axial load is increased, the eccentricity of the joint is reduced and, therefore, the bending due to the axial load is also reduced. (The reverse occurs in the familiar beam-column problem.) Thus, the moment in adherend 2 of the single lap at x equal zero is significantly less than $P\bar{t}(1 - c/a)/2$ as would be predicted by Equation (9). The plane sections remain plane assumption also exaggerates the bending since in the vicinity of the adherend-adhesive interface shear deformations are significant.

In order to remedy this situation without revising the entire theory, an effective bending factor, k_e , was introduced. This factor reduced all the computed bending moments in the joint by k_e . The quantity k_e was introduced into the equations of Section II in the following form:

Single Lap

$$\begin{aligned} M_1 &= \frac{1}{2} \left[\theta + \frac{P\bar{t}}{a} \left(x - \frac{c}{2} \right) - \frac{t_1}{2} \phi \right] k_e \\ M_2 &= \frac{1}{2} \left[\theta - \frac{P\bar{t}}{a} \left(x - \frac{c}{2} \right) + \frac{t_2}{2} \phi \right] k_e \end{aligned} \quad (12M)$$

*While "effective G " could be used in shear distribution and ultimate load prediction, when the normal stresses and the failure theories were introduced, the approach became useless. Large changes (by a factor of 2 to 4) in effective G resulted in only small changes in the predicted failing load.

$$p_1 = \frac{E}{t(1-\nu^2)} \left(\frac{1}{D_1} + \frac{1}{D_2} \right) k_e$$

$$p_2 = \frac{E}{2t(1-\nu^2)} \left(\frac{t_1}{D_1} - \frac{t_2}{D_2} \right) k_e$$

$$p_3 = \frac{G}{t} \left(\frac{1}{A_1} + \frac{1}{A_2} + \frac{t_1^2 k_e}{4D_1} + \frac{t_2^2 k_e}{4D_2} \right)$$

$$p_4 = \frac{G}{2t} \left(\frac{t_1}{D_1} - \frac{t_2}{D_2} \right) k_e$$

(71M)

$$q_1 = -\frac{PE\bar{t}k_e}{at(1-\nu^2)} \left(\frac{1}{D_1} - \frac{1}{D_2} \right) \left(x - \frac{c}{2} \right) - \frac{2E}{t(1-\nu^2)} \left(\frac{M_1 p}{D_1} + \frac{M_2 p}{D_2} \right)$$

$$q_3 = \frac{PG}{t} \left[\frac{1}{A_1} - \frac{1}{A_2} + \frac{k_e t}{2a} \left(\frac{t_1}{D_1} + \frac{t_2}{D_2} \right) \left(\frac{c}{2} - x \right) \right] + \frac{G}{t} \left[\frac{2N_1 p}{A_1} - \frac{2N_2 p}{A_2} - \frac{t_1 M_1 p}{D_1} + \frac{t_2 M_2 p}{D_2} \right]$$

Double Lap

$$M_1 = \frac{1}{2} \left(\theta - \frac{t_1}{2} \phi \right) k_e$$

(81M)

$$p_1 = \frac{Ek_e}{(1-\nu^2)tD_1}$$

$$p_2 = \frac{Et_1 k_e}{2(1-\nu^2)tD_1}$$

$$p_3 = \frac{G}{t} \left(\frac{1}{A_1} + \frac{2}{A_2} + \frac{t_1^2 k_e}{4D_1} \right)$$

$$p_4 = \frac{Gt_1 k_e}{2tD_1}$$

(83M)

Step Lap

$$M_1 = \frac{1}{2} \left[\theta + \frac{P}{4} (t_1 - t_2) - \frac{t_1}{2} \phi \right] k_e$$

$$M_2 = \frac{1}{2} \left[\theta - \frac{P}{4} (t_1 - t_2) + \frac{t_2}{2} \phi \right] k_e$$

(91M)

$$\begin{aligned}
p_1 &= \frac{E}{t(1-\nu^2)} \left(\frac{1}{D_1} + \frac{1}{D_2} \right) k_e \\
p_2 &= \frac{E}{2t(1-\nu^2)} \left(\frac{t_1}{D_1} - \frac{t_2}{D_2} \right) k_e \\
p_3 &= \frac{G}{t} \left(\frac{1}{A_1} + \frac{1}{A_2} + \frac{t_1^2 k_e}{4D_1} + \frac{t_2^2 k_e}{4D_2} \right) \\
p_4 &= \frac{G}{2t} \left(\frac{t_1}{D_1} - \frac{t_2}{D_2} \right) k_e \\
q_1 &= -\frac{PEk_e}{t(1-\nu^2)} \left(\frac{t_1 - t_2}{4} \right) \left(\frac{1}{D_1} - \frac{1}{D_2} \right) - \frac{2E}{t(1-\nu^2)} \left(\frac{M_1 p}{D_1} + \frac{M_2 p}{D_2} \right)
\end{aligned} \tag{93M}$$

where the equation numbers of Section II are referred to with the suffix M to indicate Modified. The following values of k_e were found to give reasonable analytical/experimental correlation:

	k_e
Single Lap	0.01
Double Lap	0.02
Step Lap	0.10

X.3. ANALYTICAL/EXPERIMENTAL BEHAVIOR COMPARISON ON SIMPLE AND SPECIAL JOINTS

X.3.a. Simple Specimen Joints

For correlation purposes the averaged results from sixteen lap shear assemblies* were chosen as representative samples of the 67† investigated in this research program. Seven single lap (S.L.), seven double lap (D.L.), and two step lap (St.L.) joints were chosen, covering both adhesive systems and adherend combinations, selectively. Within these categories the choices were made, based on a study of the quality of the experimental data. Bad data points were judged by the failure mode (interface or interlaminar) and/or whether the points fell on or near the majority data test curves (N' vs L/t) as shown in the previous section.

Adherend properties were obtained from Section VII and the literature for use in the computer prediction program. Adhesive properties, taken from the literature, are presented in Table XXV and Figures 126 and 127. A summary of all the properties used in the computer program is given in Table XXVI.

The nonlinear joint behavior equations were programmed for failure by (1) cohesive fracture of the adhesive by the maximum stress theory, (2) tensile failure of the composite adherend by maximum strain theory, and (3) tensile failure of the titanium adherend by maximum stress theory. The experimental/theoretical correlation is presented in Table XXVII. The predicted low values of item 6 may have been caused by the inaccuracy of the unidirectional lamina Ramberg-Osgood three parameter predicted stress-strain curve for the 0/90° orientation laminate that was used for all three adherends. Observe that the experimental value in parenthesis correlates reasonably well with that

*Each assembly represents 3 or 4 specimens.

†Totaling 203 individual specimens.

TABLE XXV
AVERAGE ADHESIVE MECHANICAL
PROPERTIES

Property	Material	
	AF 126-2 (LSHE)*	MB-329 (HSLE)†
σ_u	5513 psi	7300 psi
$E‡$	0.22568×10^6 psi	0.96847×10^6 psi
$\nu‡$	0.40	0.4284
τ_u	7170 psi	8970 psi
G	0.0806×10^6 psi	0.399×10^6 psi
*See References (6) and (18).		
†See References (18) and (19).		
‡These values are calculated. Such calculations are based on experimentally measured G and E^* (constrained) values assuming an isotropic-elastic relationship among E , G and ν . See Reference (19).		

predicted. It represents the proportional limit average value for this group of joints and was taken from the 2-in. gage length (over the bondline) autographically recorded load/deflection curves. Item 6 (lap shear assembly 56) load/deflection curves are shown in Figure 128. Apparently, the shape of the three parameter stress-strain curves used to derive the 0/90° orientation adherend behavior resulted in adhesive stresses high enough to cause joint failure prediction at the loads indicated. In the actual test adherend proportional limits* were exceeded and a redistribution of stresses in the adhesive was brought on by the sudden drop in adherend modulus, allowing the bondline to go to a much higher stress, i.e., the joint to transfer much higher loads. It is felt that the proper choice of unidirectional lamina Ramberg-Osgood parameters would give derived 0/90° stress-strain curves which would allow accurate prediction of failure loads. Item 13 (lap shear assembly 61) apparently was less affected by this phenomenon because only the single adherend was 0/90 composite with the double adherends being titanium. The limiting factor in these three parameter stress-strain curves' accuracy could be the lack of 90° lamina experimental data.†

As pointed out in the previous section, values of the bending factor were selected for reasonable correlation with each joint type (BF-JT) and are listed in Table XXVII. Table XXVIII gives a more explicit listing of the BF-JT factors relating them to the item nos. of Table XXVII.

Figure 129 shows the experimental/analytical correlation with these bending factors by joint type. A limited amount of effort was devoted to further refining the values of the bending factor for various adhesive types and failure types within the joint types (BF-JT, AT, FT). The selected bending factors are shown in Table XXIX and Figure 130 shows the corresponding correlation. This latter approach could be extended to other joint configurations. The refinement of the bending factor definition is limited only by the amount of experimental data available.

Typical failure types are shown photographically in Figures 130 through 135. Figures 131, 132 and 133 show the composite net section tension failure of the LSA-31, -33 and -36 specimens, respectively. Figures 134 and 135 show the cohesive fracture of the composite surface resin and bondline of LSA-56 and -58, respectively. In Figure 136 specimens LSA-61 show primary composite adherend delamination and secondary surface resin fracture.

Five typical computer printouts on the joint predictive techniques are given in Appendix G. These are on items 7 (LSA-20), 9 (LSA-23), and 15 (LSA-26) from Table XXVII. The printouts cover shear (TAU) and normal (SIGMA) stresses at various stations along the joint overlap length for ultimate loads in Appendix G.1. The individual ply stresses at intermediate loads are also presented in Appendix G.2 for items 7 (LSA-20), 14 (LSA-62), and 15 (LSA-26). Correlation of the predicted surface ply stresses on the special test specimens with the experimentally measured strains is given in the next subsection.

*See Appendix E for appropriate experimental laminate tensile specimen stress-strain curves.

†This research effort generated only 0° unidirectional lamina axial test data, the 90° axial data were taken from the literature, as were the in-plane shear values.

TABLE XXVI
THREE PARAMETER STRESS-STRAIN CURVE VALUES

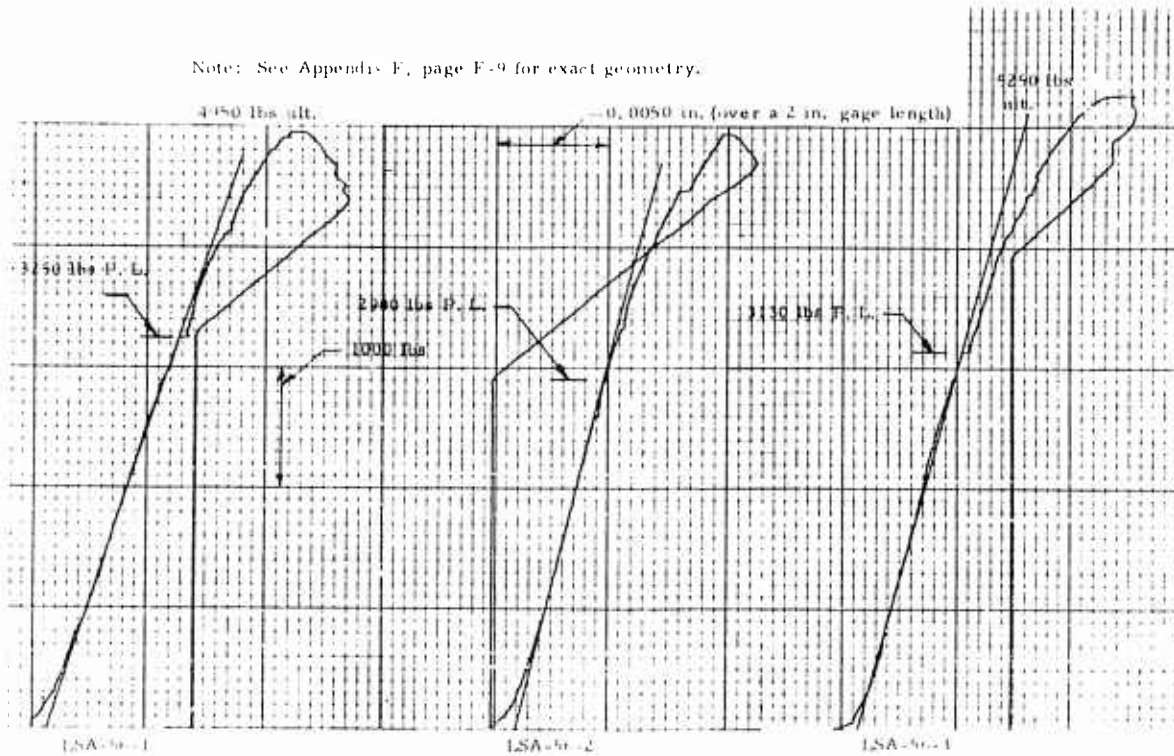
Item	Curve	ADHEREND PROPERTIES													
		σ_{0i} , ksi	σ_{1i} , ksi	$E_i \times 10^{-6}$ psi	n_i	σ_{0i} , ksi	σ_{1i} , ksi	$E_i \times 10^{-6}$ psi	n_i	σ_{0i} , ksi	σ_{1i} , ksi	$E_i \times 10^{-6}$ psi	n_i		
		Composite Adherends Panels B-12 (B-12 only)				Composite Adherends Panels B-13, B-18 Avg (B-13 thru B-19)				Composite Adherends Panels B-21, B-21 Avg (B-21 thru B-28)					
1	(σ_Q vs ϵ_Q) _A	-	122.539	25.923	-	-	147.232	27.489	-	-	177.622	28.825	-		
2	(σ_Q vs ϵ_I) _A	-	122.539	127.115	-	-	147.232	133.604	-	-	177.622	136.632	-		
3	(σ_I vs ϵ_I) _L	11.910		2.750	2.541	11.910		2.750	2.541	11.910		2.750	2.541		
4	(τ_{QI} vs γ_{QI}) _L	7.950		0.933	2.991	7.950		0.933	2.991	7.950		0.933	2.991		
5	(σ vs ϵ) _A	0.016 Sheet Ti 6Al-4V Annealed				0.032 Sheet Ti 6Al-4V Annealed				0.045 Sheet Ti 6Al-4V Sheet				0.090 Sheet Ti 6Al-4V Sheet	
		137.7	134.5	17.756	38.741	129.5	128.2	15.514	75.438	136.6	133.3	17.251	37.246	134.0	130.5
		ADHESIVE PROPERTIES													
		τ_{0i} , ksi	τ_{1i} , ksi	$G_i \times 10^{-6}$ psi	n_i	τ_{0i} , ksi	τ_{1i} , ksi	$G_i \times 10^{-6}$ psi	n_i						
		Adhesive-Nitrile/Epoxy (LSHE) AF 126-2				Adhesive-Epoxy/Novolak (HSLE) MB-329									
6	(τ vs γ) _L	3.75	3.25	0.0806	6.318	6.60	5.35	0.3158	4.227						
7	(τ vs γ) _C	3.32		0.1750	2.684										
Subscripts:															
		A - experimental values obtained in the program (see Section VII)													
		L - experimental values taken from the literature													
		C - calculated values taken from literature													

TABLE XXVII

SUMMARY OF EXPERIMENTAL/THEORETICAL CORRELATION

Item	Joint No and Type	Adhesive Thickness	Adherend	General Comp. Adher. Orient. Code	Ultimate Load						Failure Type†**	Experimental Failure Description		
					Experimental, lb	Bending Factor-JT*		Bending Factor-JT, AT, FT†						
						B.F.	Predicted, lb	Exp./Pred.	B.F.	Predicted, lb			Exp./Pred.	
1	14 (SL)	0.0043	B (C)	B (C)	[0]c	5.668	0.01	6.420	0.883	0.01	6.420	0.883	4, 3	Cohesive fracture of composite surface resin and bondline
2	27 (SL)	0.0043	B (C)	B (C)	[0]c	7.873	0.01	7.132	1.104	0.01	7.132	1.104	6††, 5	Composite adherend tension, longitudinal splitting, and delamination
3	18 (DL)	0.0020	B (C)	B (C)	[0/±45]c	7.018	0.02	8.486	0.827	0.20	6.986	1.005	3, 4	Cohesive fracture of bondline and composite surface resin
4	31 (DL)	0.0037	B (C)	B (C)	[0/±45]c	8.715	0.02	9.042	0.964	0.02	9.042	0.964	6††***	Adherend tension
5	53 (SL)	0.0073	B (C)	B (C)	[0]c	3.045	0.01	2.622	1.161	0.01	2.622	1.161	4, 1	Cohesive fracture of composite surface resin and composite/adhesive interface
6	56 (DL)	0.0046	B (C)	B (C)	[0/90]c	5.048	0.02	3.272	1.543	0.02	3.272†††	1.543	4, 6†††††	Cohesive fracture of composite surface resin and adherend tension
7	20**** (SL)	0.0028	B (C)	T (C)	[0/±45]c	4.255	0.01	4.677	(0.945)†††††	0.01	4.677	0.910	6††.4	Adherend tension and surface resin cohesive fracture
8	33 (SL)	0.0032	B (C)	T (C)	[0/±45]c	5.087	0.01	5.548	0.917	0.01	5.548	0.917	6††	Adherend tension
9	23***** (DL)	0.0030	T (C)	B (C)	[0/±45]c	7.450	0.02	8.326	0.895	0.20	7.474	0.997	4, 5, 3	Composite surface resin cohesive fracture, delamination, cohesive fracture of bondline
10	36 (DL)	0.0018	T (C)	B (C)	[0/±45]c	9.780	0.02	9.430	1.037	0.02	9.430	1.037	6††	Adherend tension and longitudinal splitting
11	58 (SL)	0.0052	B (C)	T (C)	[0]c	1.957	0.01	1.446	1.353	0.01	1.446	1.353	4, 2, 3	Cohesive fracture of composite surface resin and bondline and composite/adhesive interface
12	59***** (SL)	0.0037	B (C)	T (C)	[0/±45]c	2.093	0.01	1.615	1.300	0.01	1.615	1.300	4, 5	Cohesive fracture of composite surface resin and delamination
13	61 (DL)	0.0067	T (C)	B (C)	[0/90]c	4.703	0.02	3.958	1.182	0.02	3.958	1.188	5, 4	Composite delamination and surface resin cohesive fracture
14	62***** (DL)	0.0099	T (C)	B (C)	[0/±45]c	5.193	0.02	5.792	0.900	0.02	5.792	0.900	4	Cohesive fracture of composite surface resin
15	26***** (2 St. L.)	0.0058	B (C)	T (C)	[0/±45]c	11.146	0.10	11.181†††††	0.997	0.10	11.181†††††	0.997	5, 6††	Composite delamination and tension
16	37 (3 St. L.)	0.0059	B (C)	T (C)	[0]c	11.783	0.10	9.296	1.268	0.01	11.124	1.058	4, 2, 6††	Cohesive fracture of surface resin of composite, titanium/bondline interface, composite tension, and splitting

Note: See Appendix F, page F-9 for exact geometry.



Note: See Appendix F-9 for exact geometry.

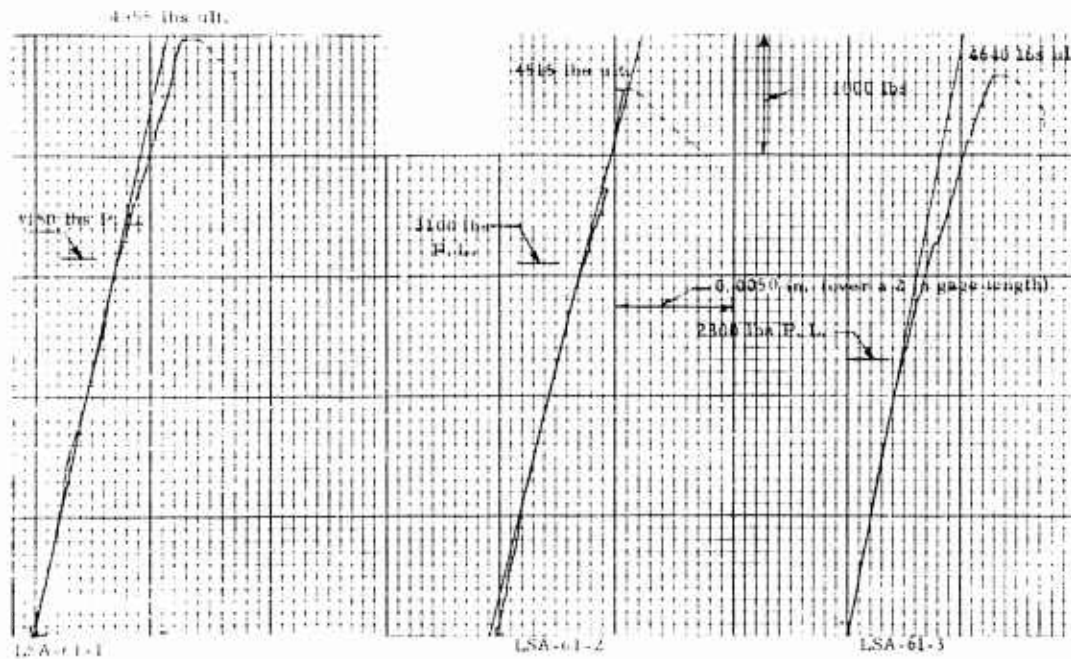


FIGURE 128. JOINT LOAD/DEFLECTION CURVES
FOR LSA-56 (D.L.-HISLE)

TABLE XXVIII
VARIABLE BENDING FACTOR
SELECTIONS: BE/JT
(Based on Joint Type Only)

Joint Type	Bending Factor	Item Numbers, Table XXVII
Single Lap	0.01	1, 2, 5, 7, 8, 11, 12
Double Lap	0.02	3, 4, 6, 9, 10, 13, 14
Step Lap	0.10	15, 16

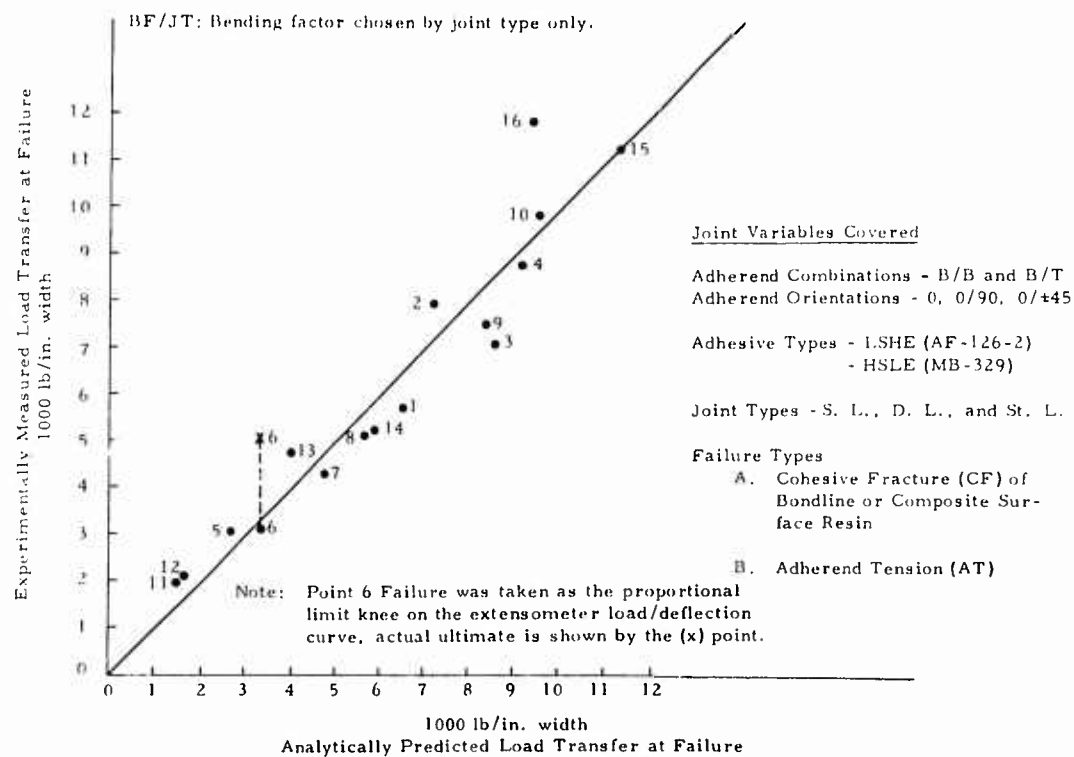


FIGURE 129. CORRELATION CURVE ON BONDED JOINTS FOR BF/JT

TABLE XXIX

BEST BENDING FACTOR SELECTIONS: BF/JT-AT-FT
(Based on Joint Type, Adhesive Type, and Failure Type)

Joint Type	Adhesive Type	Primary Failure Type	Bending Factor	Item Numbers, Table XXVII
S.L.	LSHE or HSLE	AT or CF	0.01	1, 2, 5, 7, 8, 11, 12
D.L.	LSHE	CF	0.20	3, 9
D.L.	LSHE	AT	0.02	4, 10
D.L.	HSLE	CF	0.02	6, 13, 14
2-St.L.	LSHE	AT	0.10	15
3-St.L.	LSHE	CF	0.01	16

Legend: S.L. - Single Lap
D.L. - Double Lap
St.L. - Step Lap
LSHE - Low stiffness/high elongation (AF-126-2)
HSLE - High stiffness/low elongation (MB-329)
AT - Adherend Tension
CF - Cohesive Fracture (Bondline or Composite Surface Resin)

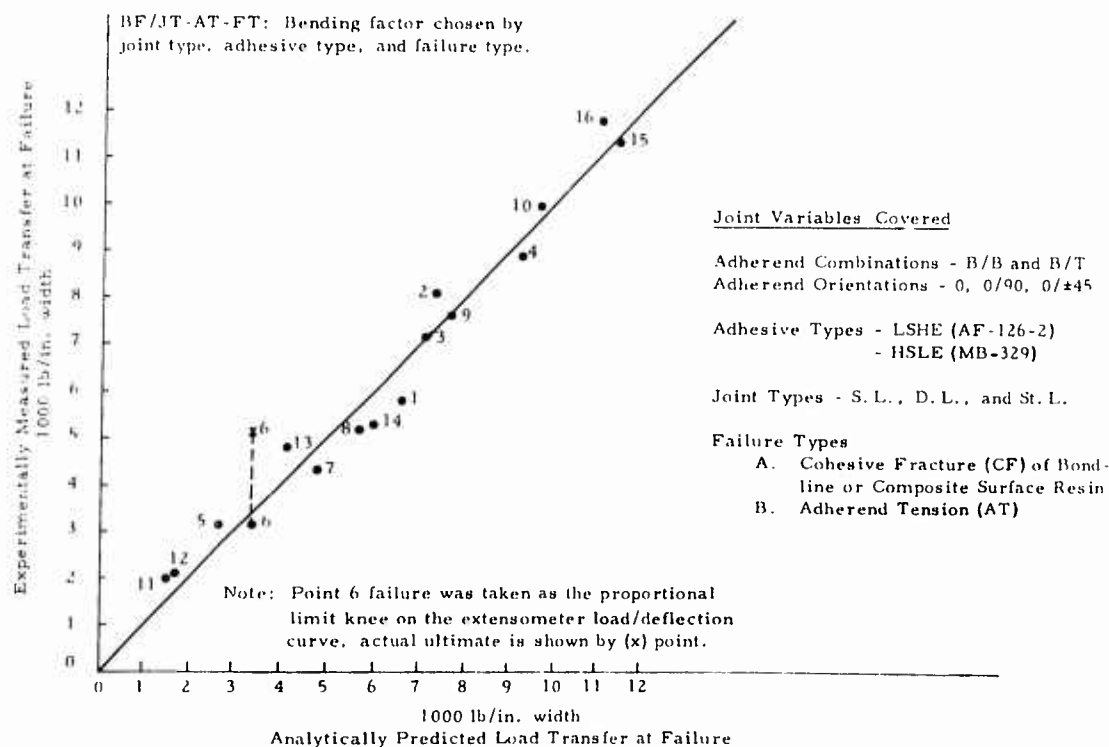


FIGURE 130. CORRELATION CURVE ON BONDED JOINTS FOR BF/JT-AT-FT

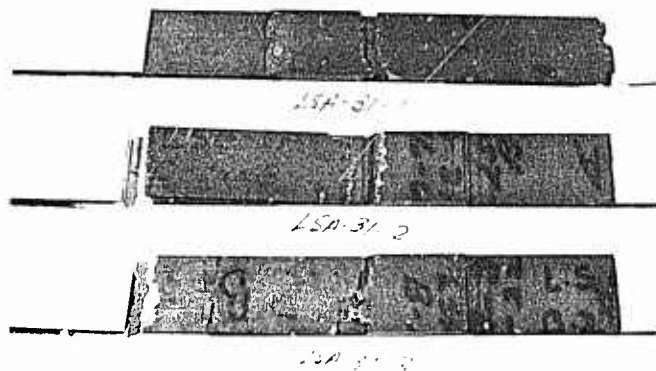


FIGURE 131. LSA-31 FAILURE

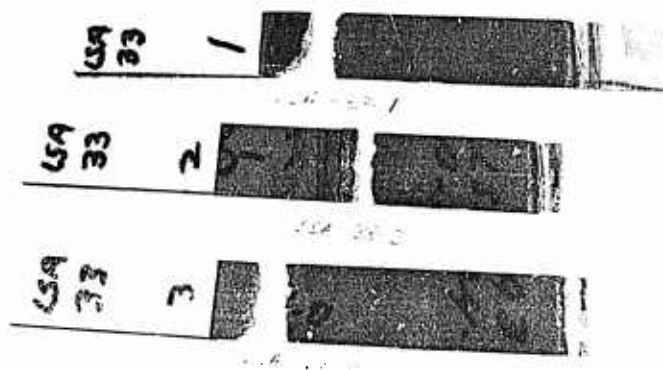


FIGURE 132. LSA-33 FAILURE

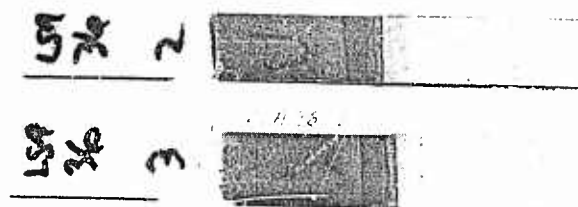


FIGURE 133. LSA-36 FAILURE

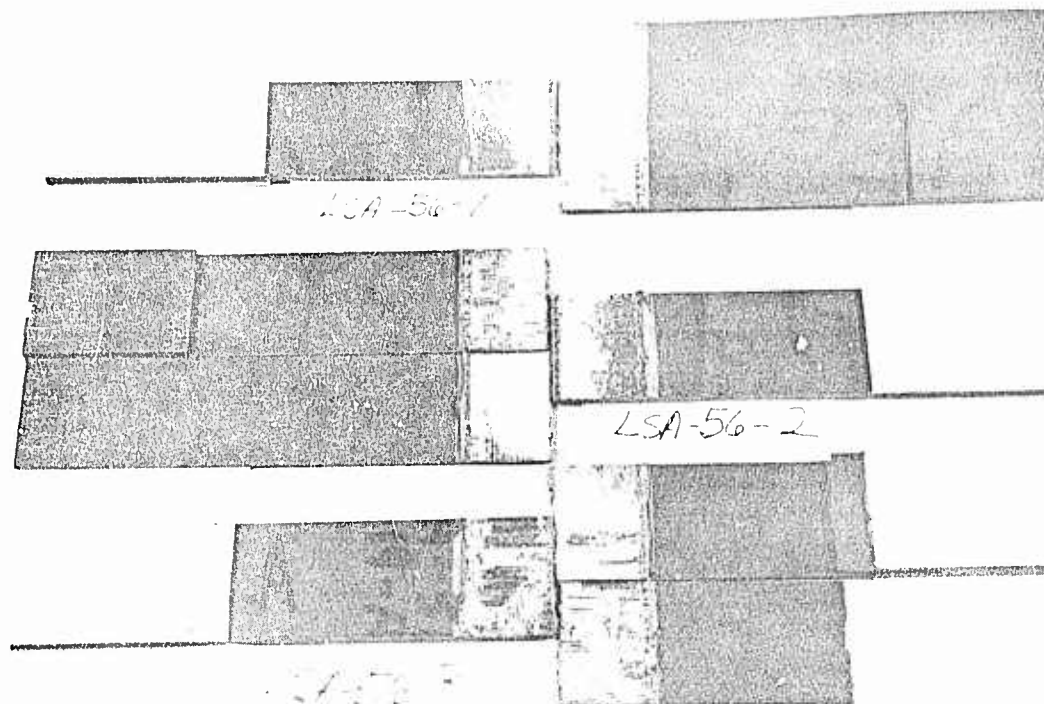


FIGURE 134. LSA-56 FAILURE

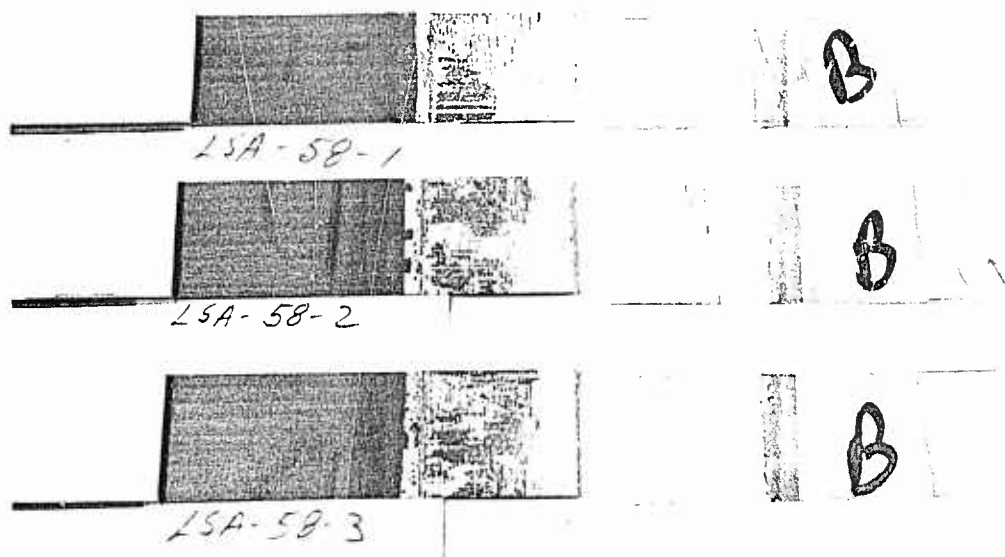


FIGURE 135. LSA-58 FAILURE

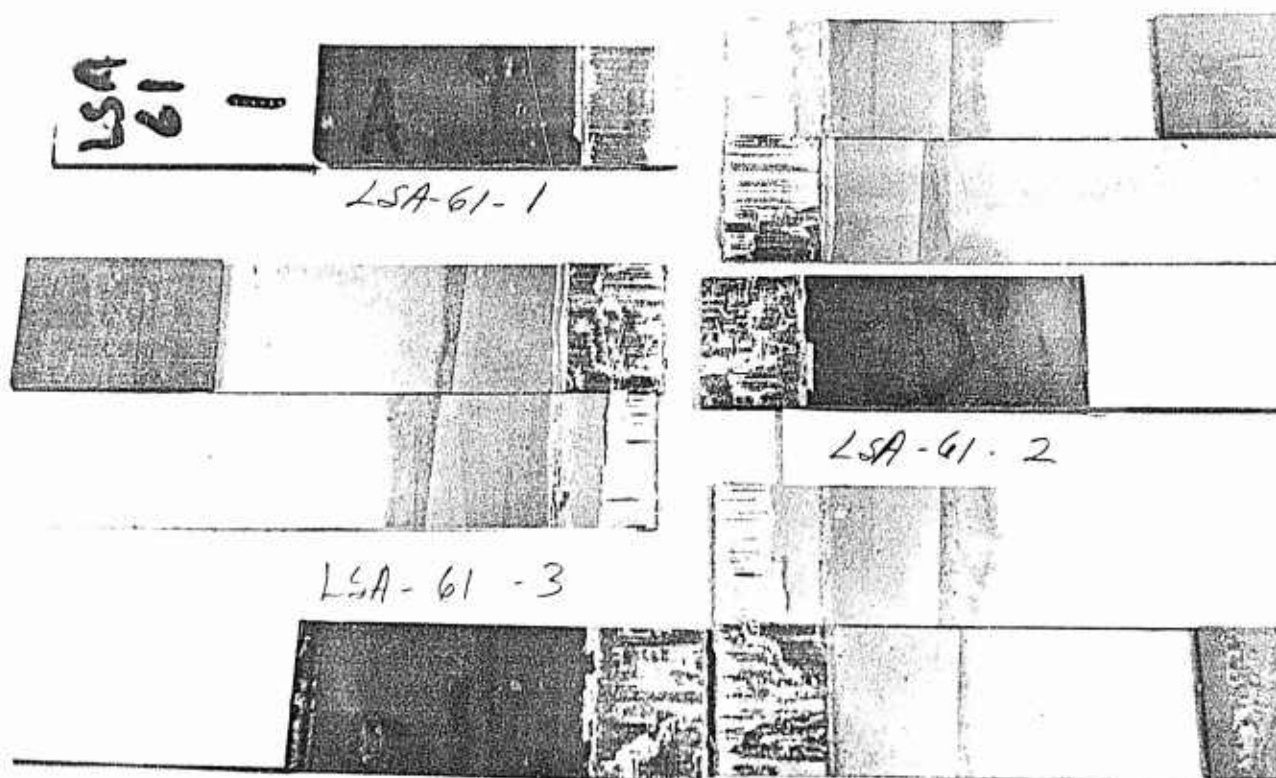


FIGURE 136. LSA-61 FAILURE

X.3.b. Special Joint Correlations

Figure 137 shows the plots of the predicted surface strains in the overlap area of specimen LSA-20-1 at one load level with the experimentally measured values superimposed. Figure 138 presents the predicted surface strains in the overlap area of specimen LSA-62-1 at one load level with the experimental points superimposed. Correlation is good enough to further verify the nonlinear analysis and design techniques developed herein.

Note that the experimentally measured longitudinal surface strain values correlate very closely to those predicted for both composite and titanium adherends. The experimentally measured transverse strains on the composite are also shown. Since the plane strain assumption is used in the program the predicted transverse strains are zero.

X.4. DESIGN ANALYSIS OF COMPLEX JOINTS

A more complex* joint was designed to evaluate the size effects which can be anticipated when designing larger joints. A basic composite/titanium double lap joint configuration, five inches wide, was chosen for evaluation. Eight of these joints were designed as shown in Figure 139 (Dwg. No. 03-2587-13), varying overlap length, adhesive, and laminate orientation. Of these, two were chosen for test: the -501 and -509 assemblies. These two joints are analyzed in Table XXX. This empirical analysis considers the possibility of failure in the titanium adherends, the composite adherend, and the bondline. Experimentally determined titanium (Table XI) and composite (Table IX) strength are used along with simple specimen bonded joint (Figs. 107 and 140) test data. Design was based on average test

Type Bending Factor: BF-JT
Bending Factor, $K_e=0.010$

Specimen LSA-20-1, Single Lap
 $P=4400$ lbs at Failure

(Ref. Fig. 111)

- Theoretically Predicted Long. Strain
- Experimentally Measured Long. Strain
- ▲ Experimentally Measured Trans. Strain

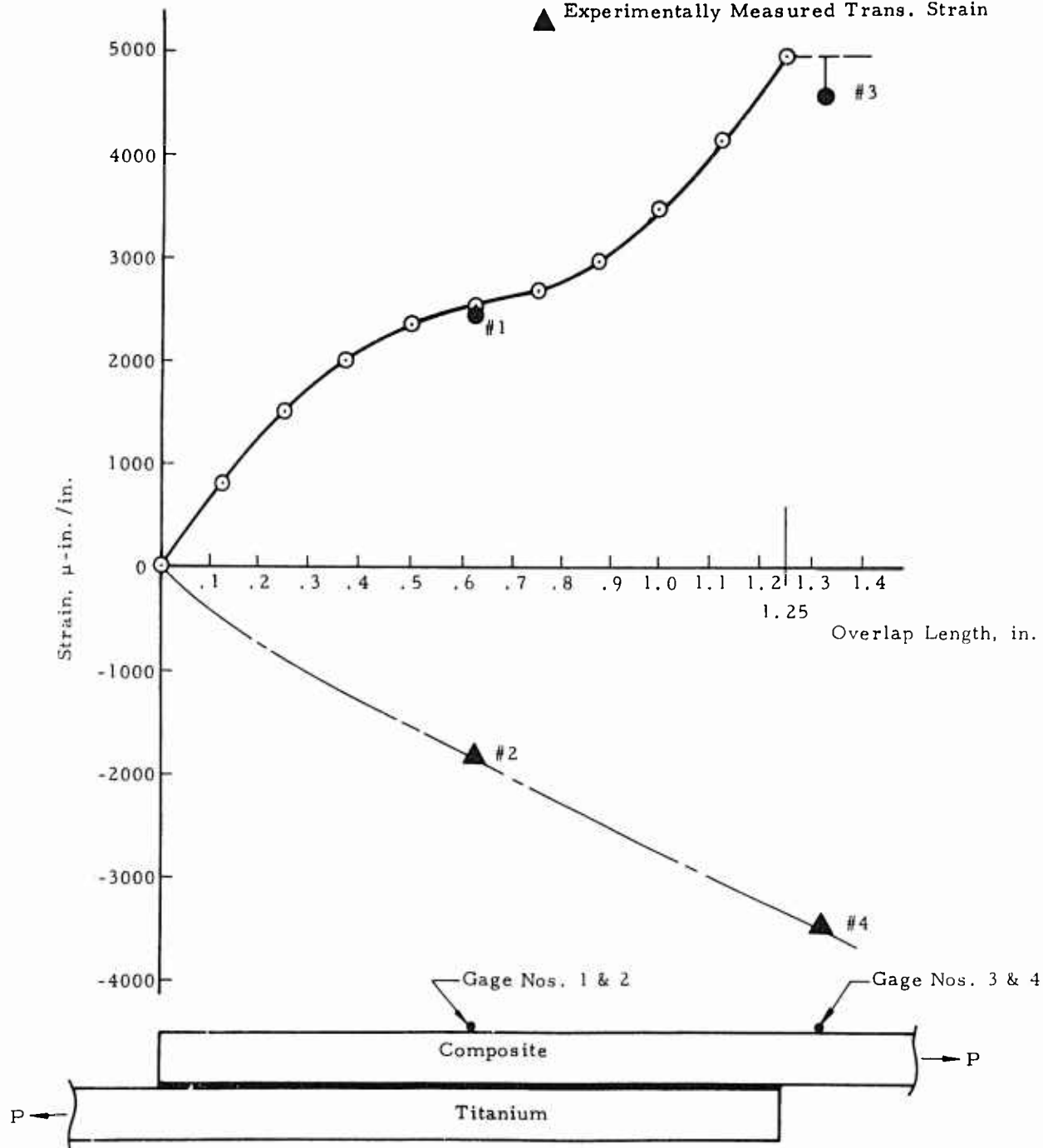
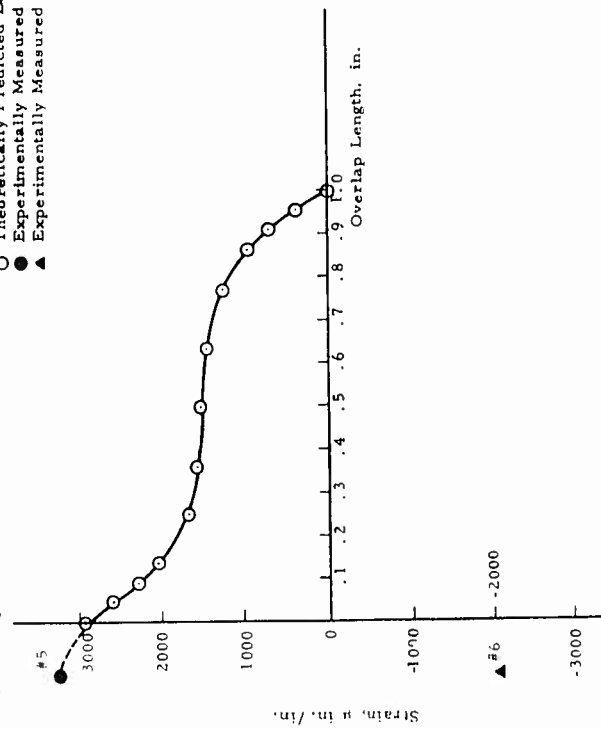


FIGURE 137. THEORETICAL/EXPERIMENTAL CORRELATION OF SINGLE LAP JOINT SURFACE STRAINS

Specimen LSA 62-1, Double Lap
P=2535 lb at Failure Composite
Adherend

○ Theoretically Predicted Long. Strain
● Experimentally Measured Long. Strain
▲ Experimentally Measured Trans. Strain

(Ref. Fig. 119)

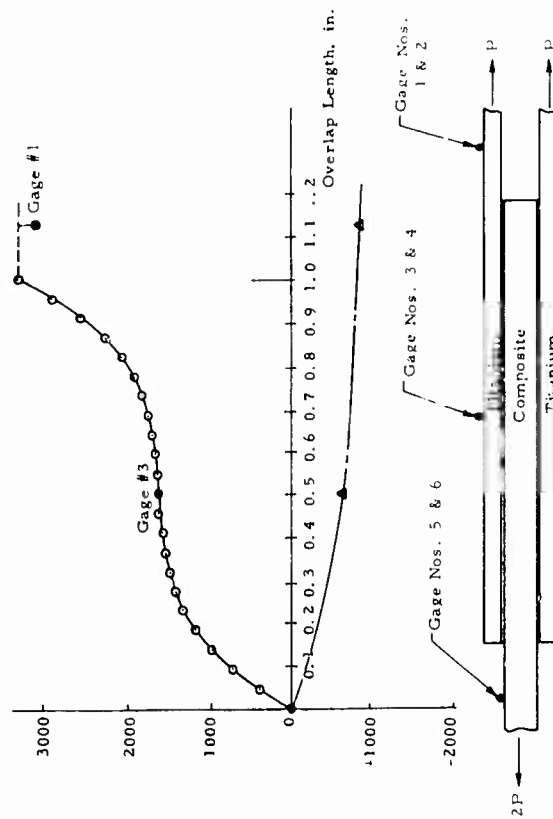


Specimen LSA 62-1, Double Lap
P = 2535 lb at Failure

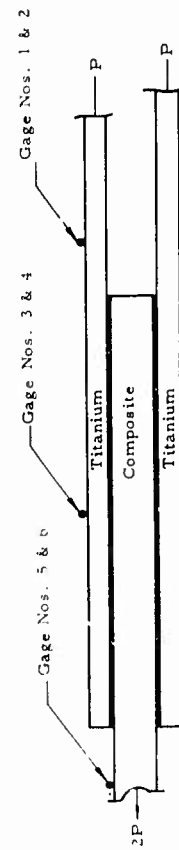
Titanium Adherend
○ Theoretically Predicted Long. Strain
● Experimentally Measured Long. Strain
▲ Experimentally Measured Trans. Strain

Type Bending Factor, BF-JT
 $k_e = 0.020$

(Ref. Fig. 119)



(a) Titanium Adherend



(b) Composite Adherend

FIGURE 138. THEORETICAL/EXPERIMENTAL CORRELATION OF DOUBLE LAP JOINT SURFACE STRAINS

TABLE XXX

COMPLEX JOINT ANALYSIS

Titanium				Boron/Epoxy															
1		2		3		4		5		6		7		8		9		10	
No. Plies	L	Adhesive	Ass'y No.	Sheet Thick., t_2 , in.	Test F_{7T} , ksi	$1 \times 3 =$ Unit Load Strength N_1 , kips/in.	Panel No.	Fiber Orientation	t_1 , in. (each adher.)	Thick.	Test F_{7T} , ksi	$2 \times 6 \times 7 =$ Unit Load Strength, N_2 , kips/in. (2 adherends)	Unit Load per Ply Strength, N_2 , kips/in./ply	l/t					
2 x 16	1.5	LSHF	501	0.090	134.86*	12.137	B-27†	[0]/±45/0)Q1S	0.085		93,524‡	15.899	0.944	16.67(Ti) 17.65(B)					
2 x 16	2.5	HSLE	509	0.090	134.86*	12.137	B-27†	[0]/±45/0)Q1S	0.085		93,524‡	15.899	0.944	27.9(Ti) 29.5(B)					
				11	12	13	14	15											
				Simple Joint Data			Simple Joint Data												
Ass'y No.	Test Avg.‡ Unit Load per Ply for L/t , N_3 , kips/in./ply (2 adherends)	Test Avg.‡ Unit Load N_3 , kips/in. (2 adherends)	Avg. Bondline Shear Stress at N_{min} , ksi**	Avg. Bondline Shear Strength‡‡ at L/t , ksi	Avg. Allowable Unit Load for Bondline Strength, N , kips/in.	Type Failure Predicted													
501	0.572	18,304	4,044	3,110	9,330	Bondline (or surface resin) cohesive fracture													
509	0.572	18,304	2,427	1,250	6,250	Bondline (or surface resin) cohesive fracture													
* See Table XI																			
† Panel B-27 identical to Panel B-26, B-26 properties used (see Table IX)																			
‡ See Figure 107																			
** The smallest of 3, 8 or 12 divided by overlap length l																			
‡‡ See Figure 140																			

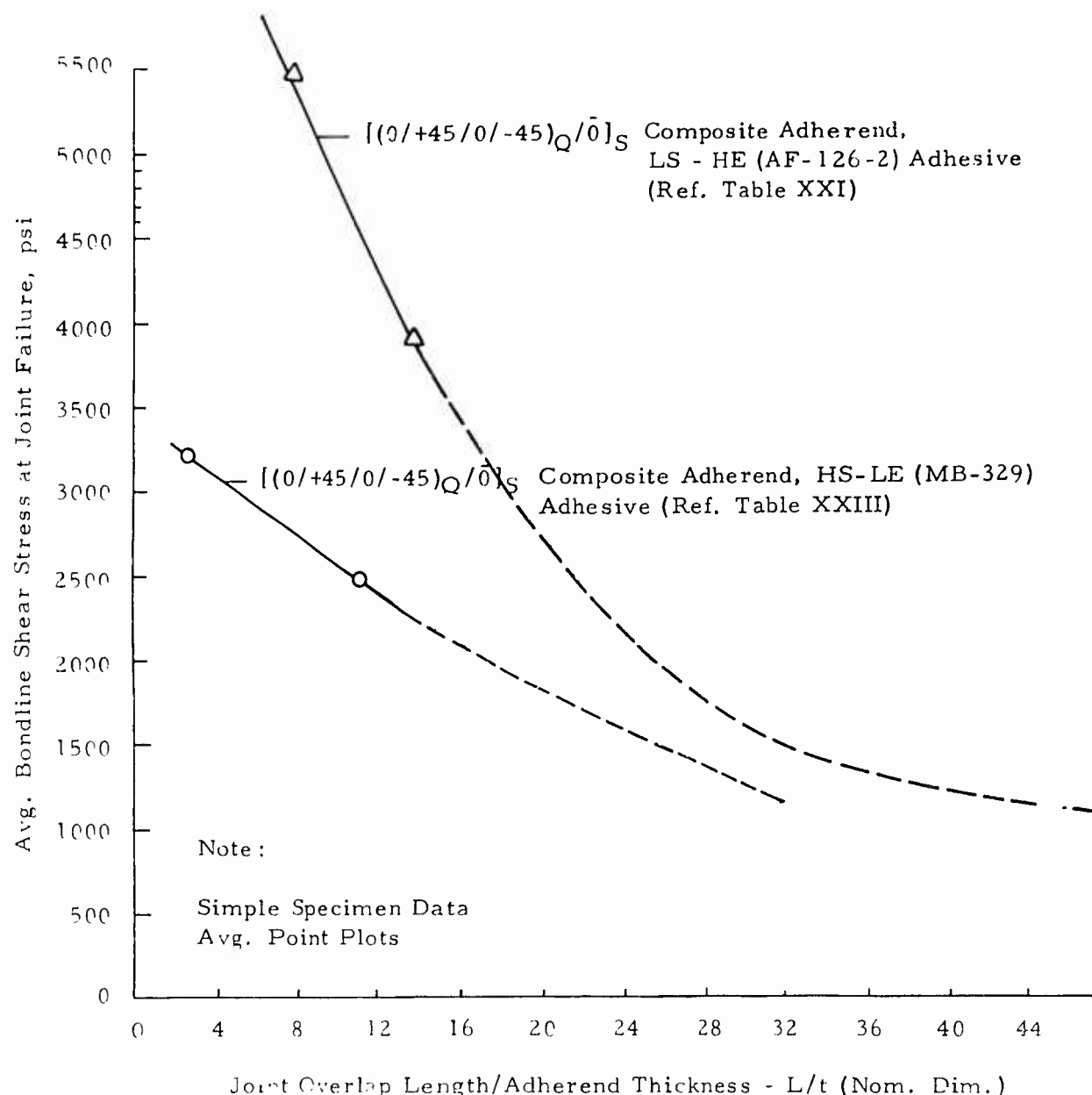


FIGURE 140. BONDLINE SHEAR STRESS VS L/t FOR COMPOSITE/TITANIUM DOUBLE LAP JOINTS

data using no safety factors. Unit failure load is predicted to be cohesive fracture of the bondline or composite surface resin.

Loading of the complex joint was to be done through four 1/2-in. diameter steel bolts at each end which are loaded via two 3/8-in. steel plates. These steel plates are loaded through a clevis by a 2-1/2-in. diameter steel pin (see Fig. 141).^{*} This setup was mounted in a Baldwin Universal Test Machine for loading. Load introduction analysis follows for the 03-2587-13 Dwg.-501 and -509 complex joints:

^{*}Dwg. No. 03-2587-14.

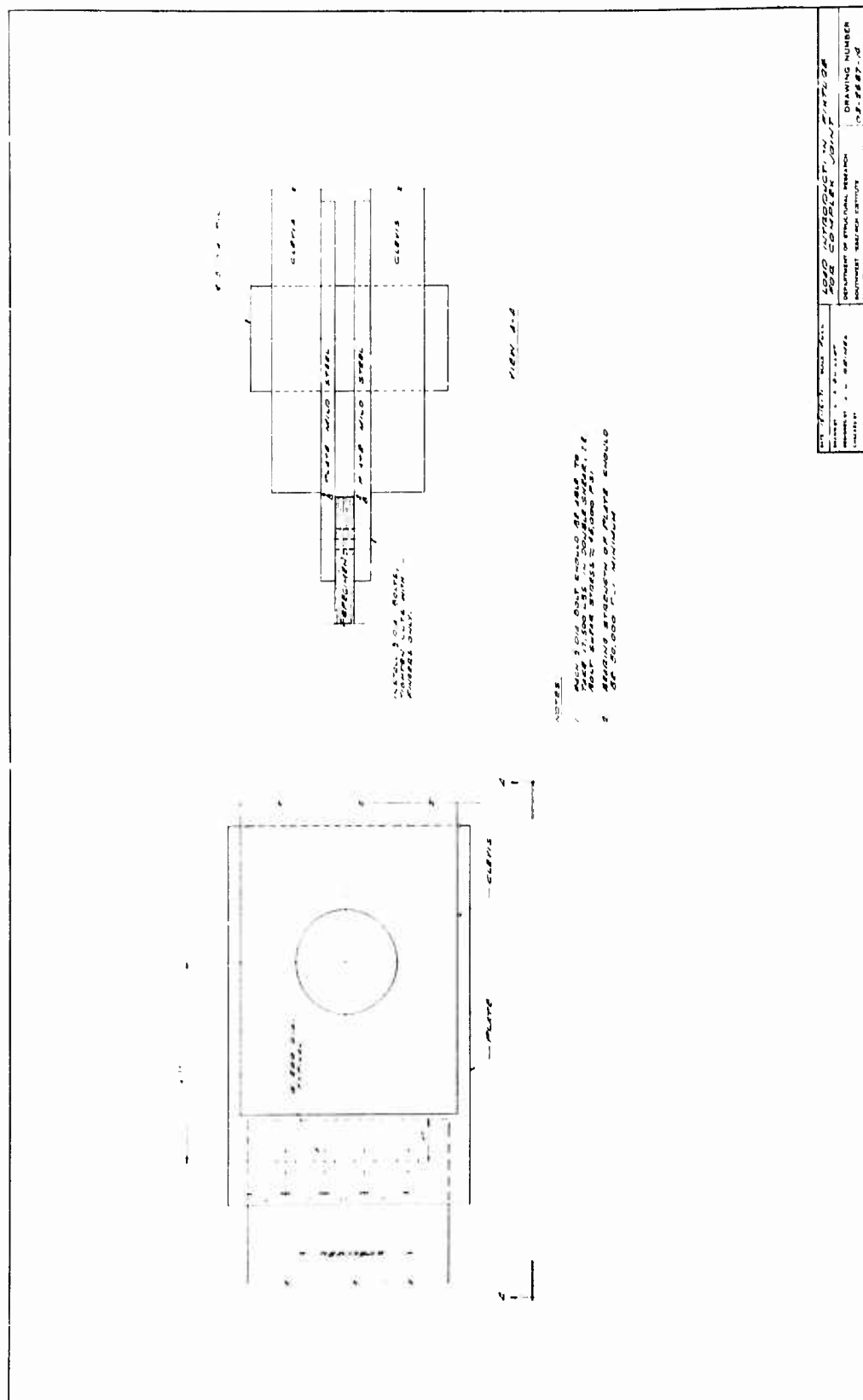


FIGURE 141. LOAD INTRODUCTION FIXTURE FOR COMPLEX JOINT

-509 Assembly

$V_{\text{max}} = 9,330 \text{ lb in.}$ (from Table XXX)

$V_{\text{max}} \times S = 46,650 \text{ lb}$ estimated failure load

$P = 1.5 \times 46,650 = 69,975 \text{ lb}$ (load intro. des. ld.)

Load Bolt = $P/4 = \frac{69,975}{4} = 17,494 \text{ lb/bolt}$

Since moduli of Ti and 0/±45° orientation B/E are approximately equal, from Figure 139 let $T_1^* = 3 \times 0.090 = 0.270 \text{ in.}$ for the single adherend all Ti end and $T_2^* = 3 \times 0.090 + 2 \times 0.085 = 0.440 \text{ in.}$ for the composite double adherend end.

Using the double adherend end T_2 .

$$CF_{BR} = \frac{P}{dT_2} = \frac{17,494}{1/2(0.440)} = 79,500 \text{ psi}$$

$TiF_{BRU} = 245,000 \text{ psi}$ (Fig. 3.0362, Page 21, Code 3707, AFML-TR-68-115 Vol. II, Jan. 1968)

0/±45 B/E $F_{BRU} = 43,000 \text{ psi}$ (Fig. 6.2.2.20, Design Guide)⁽²⁰⁾

i.e.,

if the B/E fails in bearing, this amount of load will be picked up by the Ti insert and grip plates and all the load would be transferred to the boron through the four bondlines. This then results in the same bearing condition as the single adherend end, i.e.,

$$F_B = \frac{17,494}{1/2(0.270)} = 130,000 \text{ psi bearing in Ti}$$

i.e., bearing in Ti ok when compared with allowable. Bondline stress then becomes P/AB :

from above $P = 69,975 \text{ lb}$

$AB = 4 \times 5 \times 4 = 80 \text{ in.}^2$

$$F_S = \frac{69,975}{80} = 875 \text{ psi}$$

This stress is lower than the lowest value obtained from all the lap joint data, i.e., bond line is ok.

Another check using Figure 107 gives 572 lb/in. ply composite joint allowable (18,304 lb/in.) or 91,520 lb total load allowable.

Therefore load introduction joint is safe with the bondline being most critical. -509 assembly will not transmit as much load, i.e., it is ok.

* $T_1 = T_2 = 2T_3$ (from Fig. 139)
 $T_1 = T_2 = T_3 = 2T_3$

5. COMPLEX JOINT TEST DATA CORRELATION WITH PREDICTIVE METHODS

The two complex (double lap) joints, assemblies -501 and -509, of SwRI Dwg. 03-2587-13 (see Fig. 139) were fabricated and tested to further check out the nonlinear theoretical predictive techniques developed in this research effort. These joints represented larger, wider bonded joint structures which can be more easily instrumented for behavior measurement. Twenty-four strain gages were laid on the front and back faces of the joint in the pattern shown in Figure 142. Test setup for the -501 complex joint assembly with the LSHE* adhesive is shown in Figure 143 whereas Figure 144 shows the -509 assembly with the HSLE† adhesive.

Load rate was 0.00125 in./min over a two-inch gage length in the joint area and strain gage readings were taken automatically at each 1,000 pound increment of load to failure. Load introduction tabs of 6A1-4V annealed titanium were bonded to the specimens, initially with a room temperature setting, two-part epoxy.

Assembly -501 was loaded to 32,200 lb on first loading, at which the load introduction tabs on the bottom became unbonded. New tabs were made, cleaned, and rebonded with AF-126-2 film adhesive. On second loading failure of the tab bond at the top occurred at 48,100 lb. New tabs were made, cleaned and rebonded with AF-126 adhesive. On third loading the failure occurred in the joint by cohesive fracture of the bondline at 56,800 lb (11,340 lb/in.). A summary of the strain gage readings is given in Table XXXI for each of the three loadings.

Assembly -509 was loaded first to 30,675 lb at which failure occurred simultaneously at both ends in the load introduction tab/specimen bondline. New tabs were made, cleaned, and rebonded with AF-126-2 adhesive. The second loading resulted in cohesive fracture of the joint bondline at 33,000 lb (6,590 lb/in.). Table XXXII presents a summary of the strain gage data for each of these loadings.

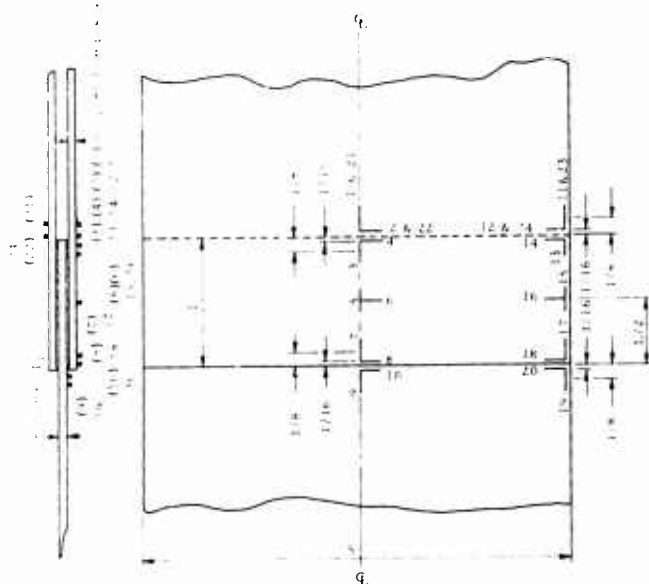


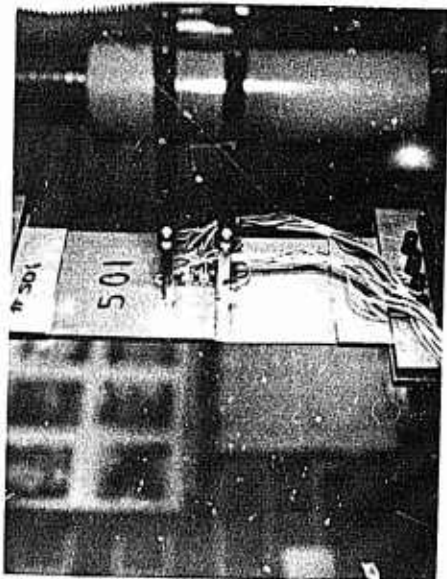
FIGURE 142. COMPLEX JOINT STRAIN GAGE LOCATIONS

Using the actual measured joint dimensions the nonlinear predictive program was used to predict the failure load and mode of each of the joints. For the -501 joint, failure was predicted at 12,144 lb/in. whereas for the -509 joint, failure was predicted at 5,188 lb/in. Both failure mode predictions were for a cohesive fracture of the adhesive. Observed mode of failure was cohesive fracture of bondline in both cases starting near the ends of the composite adherends. Table XXXIII summarizes the measured and predicted values. Complete printouts of these predictions and their related adhesive and adherend stresses are presented in Appendix H. Composite surface strains taken from these predicted failure data are included above the measured strains in Tables XXX and XXXII.

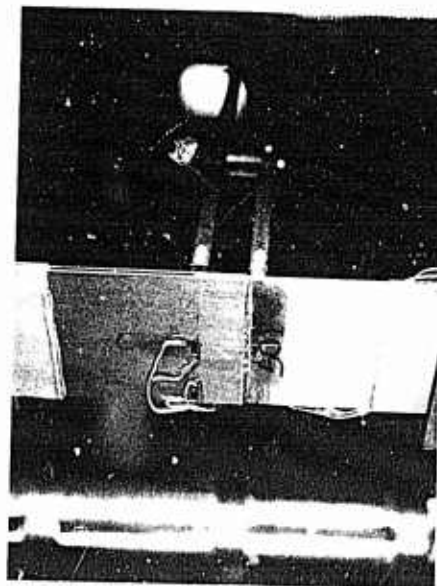
Observed that the longitudinal strains predicted at gages 1, 3, 5 and 9 (see Fig. 142) on both joints for all loadings correlated well with the measured strains at that load level. Also, observe that the predicted strains at gage 7 do not correlate the measured strains. With gage 7 located near the end of the bondline

*LSHE: Low Stiffness, High Elongation (AF-126-2).

†HSLE: High Stiffness, Low Elongation (MB-329).

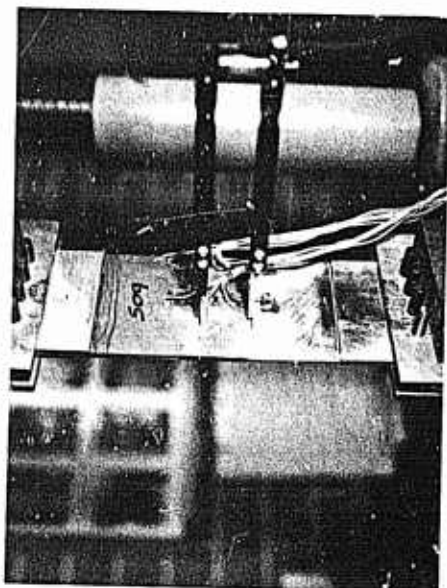


(a) Front

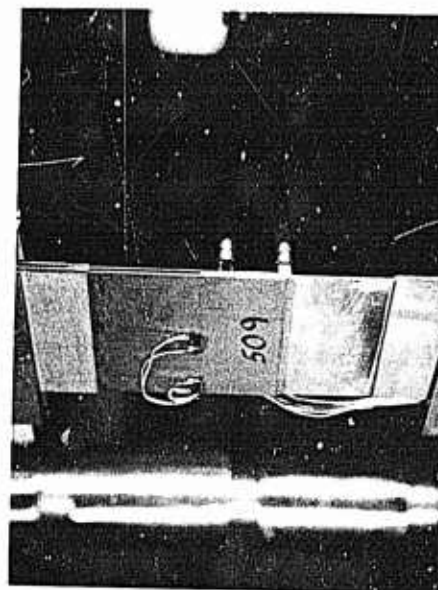


(b) Back

FIGURE 143. COMPLEX JOINT -501 TEST SET-UP



(a) Front



(b) Back

FIGURE 144. COMPLEX JOINT -509 TEST SET-UP

TABLE XXXI

COMPLEX JOINT EXPERIMENTAL DATA WITH HSLE ADHESIVE

Ass. No. of Dwg. No. of 0.5" x 8" x 1.5"	Loading Magnitude kips	Loading Rate in./min.	Composite Adherent Net Sec. Tens. Stress, ksi	T. Adherent Net Sec. Tens. Stress, ksi	Joint Unit Load Transfer N./sq. in.	Unit Load Transfer N./sq. in.	Strains, μ in./in. (0.0001 in./in. = 1 μ)																						
							Adherent Surface Strains, μ in./in. (0.0001 in./in. = 1 μ)																						
1	2	3	4	5	6	7	8	9	10	11	12	13	14	15	16	17	18	19	20										
501	8		9.56	17.8	2.92	2.92	2.92	2.92	2.92	2.92	2.92	2.92	2.92	2.92	2.92	2.92	2.92	2.92	2.92	2.92	2.92	2.92	2.92	2.92	2.92	2.92	2.92	2.92	2.92
	16		19.1	35.6	5.84	5.84	5.84	5.84	5.84	5.84	5.84	5.84	5.84	5.84	5.84	5.84	5.84	5.84	5.84	5.84	5.84	5.84	5.84	5.84	5.84	5.84	5.84	5.84	5.84
	24		28.7	53.4	8.76	8.76	8.76	8.76	8.76	8.76	8.76	8.76	8.76	8.76	8.76	8.76	8.76	8.76	8.76	8.76	8.76	8.76	8.76	8.76	8.76	8.76	8.76	8.76	8.76
	32		38.2	71.1	11.7	11.7	11.7	11.7	11.7	11.7	11.7	11.7	11.7	11.7	11.7	11.7	11.7	11.7	11.7	11.7	11.7	11.7	11.7	11.7	11.7	11.7	11.7	11.7	11.7
	40		47.8	88.8	14.6	14.6	14.6	14.6	14.6	14.6	14.6	14.6	14.6	14.6	14.6	14.6	14.6	14.6	14.6	14.6	14.6	14.6	14.6	14.6	14.6	14.6	14.6	14.6	14.6
502	8		9.56	17.8	2.92	2.92	2.92	2.92	2.92	2.92	2.92	2.92	2.92	2.92	2.92	2.92	2.92	2.92	2.92	2.92	2.92	2.92	2.92	2.92	2.92	2.92	2.92	2.92	2.92
	16		19.1	35.6	5.84	5.84	5.84	5.84	5.84	5.84	5.84	5.84	5.84	5.84	5.84	5.84	5.84	5.84	5.84	5.84	5.84	5.84	5.84	5.84	5.84	5.84	5.84	5.84	5.84
	24		28.7	53.4	8.76	8.76	8.76	8.76	8.76	8.76	8.76	8.76	8.76	8.76	8.76	8.76	8.76	8.76	8.76	8.76	8.76	8.76	8.76	8.76	8.76	8.76	8.76	8.76	8.76
	32		38.2	71.1	11.7	11.7	11.7	11.7	11.7	11.7	11.7	11.7	11.7	11.7	11.7	11.7	11.7	11.7	11.7	11.7	11.7	11.7	11.7	11.7	11.7	11.7	11.7	11.7	11.7
	40		47.8	88.8	14.6	14.6	14.6	14.6	14.6	14.6	14.6	14.6	14.6	14.6	14.6	14.6	14.6	14.6	14.6	14.6	14.6	14.6	14.6	14.6	14.6	14.6	14.6	14.6	14.6
503	8		9.56	17.8	2.92	2.92	2.92	2.92	2.92	2.92	2.92	2.92	2.92	2.92	2.92	2.92	2.92	2.92	2.92	2.92	2.92	2.92	2.92	2.92	2.92	2.92	2.92	2.92	2.92
	16		19.1	35.6	5.84	5.84	5.84	5.84	5.84	5.84	5.84	5.84	5.84	5.84	5.84	5.84	5.84	5.84	5.84	5.84	5.84	5.84	5.84	5.84	5.84	5.84	5.84	5.84	5.84
	24		28.7	53.4	8.76	8.76	8.76	8.76	8.76	8.76	8.76	8.76	8.76	8.76	8.76	8.76	8.76	8.76	8.76	8.76	8.76	8.76	8.76	8.76	8.76	8.76	8.76	8.76	8.76
	32		38.2	71.1	11.7	11.7	11.7	11.7	11.7	11.7	11.7	11.7	11.7	11.7	11.7	11.7	11.7	11.7	11.7	11.7	11.7	11.7	11.7	11.7	11.7	11.7	11.7	11.7	11.7
	40		47.8	88.8	14.6	14.6	14.6	14.6	14.6	14.6	14.6	14.6	14.6	14.6	14.6	14.6	14.6	14.6	14.6	14.6	14.6	14.6	14.6	14.6	14.6	14.6	14.6	14.6	14.6
504	8		9.56	17.8	2.92	2.92	2.92	2.92	2.92	2.92	2.92	2.92	2.92	2.92	2.92	2.92	2.92	2.92	2.92	2.92	2.92	2.92	2.92	2.92	2.92	2.92	2.92	2.92	2.92
	16		19.1	35.6	5.84	5.84	5.84	5.84	5.84	5.84	5.84	5.84	5.84	5.84	5.84	5.84	5.84	5.84	5.84	5.84	5.84	5.84	5.84	5.84	5.84	5.84	5.84	5.84	5.84
	24		28.7	53.4	8.76	8.76	8.76	8.76	8.76	8.76	8.76	8.76	8.76	8.76	8.76	8.76	8.76	8.76	8.76	8.76	8.76	8.76	8.76	8.76	8.76	8.76	8.76	8.76	8.76
	32		38.2	71.1	11.7	11.7	11.7	11.7	11.7	11.7	11.7	11.7	11.7	11.7	11.7	11.7	11.7	11.7	11.7	11.7	11.7	11.7	11.7	11.7	11.7	11.7	11.7	11.7	11.7
	40		47.8	88.8	14.6	14.6	14.6	14.6	14.6	14.6	14.6	14.6	14.6	14.6	14.6	14.6	14.6	14.6	14.6	14.6	14.6	14.6	14.6	14.6	14.6	14.6	14.6	14.6	14.6
505	8		9.56	17.8	2.92	2.92	2.92	2.92	2.92	2.92	2.92	2.92	2.92	2.92	2.92	2.92	2.92	2.92	2.92	2.92	2.92	2.92	2.92	2.92	2.92	2.92	2.92	2.92	2.92
	16		19.1	35.6	5.84	5.84	5.84	5.84	5.84	5.84	5.84	5.84	5.84	5.84	5.84	5.84	5.84	5.84	5.84	5.84	5.84	5.84	5.84	5.84	5.84	5.84	5.84	5.84	5.84
	24		28.7	53.4	8.76	8.76	8.76	8.76	8.76	8.76	8.76	8.76	8.76	8.76	8.76	8.76	8.76	8.76	8.76	8.76	8.76	8.76	8.76	8.76	8.76	8.76	8.76	8.76	8.76
	32		38.2	71.1	11.7	11.7	11.7	11.7	11.7	11.7	11.7	11.7	11.7	11.7	11.7	11.7	11.7	11.7	11.7	11.7	11.7	11.7	11.7	11.7	11.7	11.7	11.7	11.7	11.7
	40		47.8	88.8	14.6	14.6	14.6	14.6	14.6	14.6	14.6	14.6	14.6	14.6	14.6	14.6	14.6	14.6	14.6	14.6	14.6	14.6	14.6	14.6	14.6	14.6	14.6	14.6	14.6
506	8		9.56	17.8	2.92	2.92	2.92	2.92	2.92	2.92	2.92	2.92	2.92	2.92	2.92	2.92	2.92	2.92	2.92	2.92	2.92	2.92	2.92	2.92	2.92	2.92	2.92	2.92	2.92
	16		19.1	35.6	5.84	5.84	5.84	5.84	5.84	5.84	5.84	5.84	5.84	5.84	5.84	5.84	5.84	5.84	5.84	5.84	5.84	5.84	5.84	5.84	5.84	5.84	5.84	5.84	5.84
	24		28.7	53.4	8.76	8.76	8.76	8.76	8.76	8.76	8.76	8.76	8.76	8.76	8.76	8.76	8.76	8.76	8.76	8.76	8.76	8.76	8.76	8.76	8.76	8.76	8.76	8.76	8.76
	32		38.2	71.1	11.7	11.7	11.7	11.7	11.7	11.7	11.7	11.7	11.7	11.7	11.7	11.7	11.7	11.7	11.7	11.7	11.7	11.7	11.7	11.7	11.7	11.7	11.7	11.7	11.7
	40		47.8	88.8	14.6	14.6	14.6	14.6	14.6	14.6	14.6	14.6	14.6	14.6	14.6	14.6	14.6	14.6	14.6	14.6	14.6	14.6	14.6	14.6	14.6	14.6	14.6	14.6	14.6
507	8		9.56	17.8	2.92	2.92	2.92	2.92	2.92	2.92	2.92	2.92	2.92	2.92	2.92	2.92	2.92	2.92	2.92	2.92	2.92	2.92	2.92	2.92	2.92	2.92	2.92	2.92	2.92
	16		19.1	35.6	5.84	5.84	5.84	5.84	5.84	5.84	5.84	5.84	5.84	5.84	5.84	5.84	5.84	5.84	5.84	5.84	5.84	5.84	5.84	5.84	5.84	5.84	5.84	5.84	5.84
	24		28.7	53.4	8.76	8.76	8.76	8.76	8.76	8.76	8.76	8.76	8.76	8.76	8.76	8.76	8.76	8.76	8.76	8.76	8.76	8.76	8.76	8.76	8.76	8.76	8.76	8.76	8.76
	32		38.2	71.1	11.7	11.7	11.7	11.7	11.7	11.7	11.7	11.7	11.7	11.7	11.7	11.7	11.7	11.7	11.7	11.7	11.7	11.7	11.7	11.7	11.7	11.7	11.7	11.7	11.7
	40		47.8	88.8	14.6	14.6	14.6	14.6	14.6	14.6	14.6	14.6	14.6	14.6	14.6	14.6	14.6	14.6	14.6	14.6	14.6	14.6	14.6	14.6	14.6	14.6	14.6	14.6	14.6
508	8		9.56	17.8	2.92	2.92	2.92	2.92	2.92	2.92	2.92	2.92	2.92	2.92	2.92	2.92	2.92	2.92	2.92	2.92	2.92	2.92	2.92	2.92	2.92	2.92	2.92	2.92	2.92
	16		19.1	35.6	5.84	5.84	5.84	5.84	5.84	5.84	5.84	5.84	5.84	5.84	5.84	5.84	5.84	5.84	5.84	5.84	5.84	5.84	5.84	5.84	5.84	5.84	5.84	5.84	5.84
	24		28.7	53.4	8.76	8.76	8.76	8.76	8.76	8.76	8.76	8.76	8.76	8.76	8.76	8.76	8.76	8.76	8.76	8.76	8.76	8.76	8.76	8.76	8.76	8.76	8.76	8.76	8.76
	32		38.2	71.1	11.7	11.7	11.7	11.7	11.7	11.7	11.7	11.7	11.7	11.7	11.7	11.7	11.7	11.7	11.7	11.7	11.7	11.7	11.7	11.7	11.7	11.7	11.7	11.7	11.7
	40		47.8	88.8	14.6	14.6	14.6	14.6	14.6	14.6	14.6	14.6	14.6	14.6	14.6	14.6	14.6	14.6	14.6	14.6	14.6	14.6	14.6	14.6	14.6	14.6	14.6	14.6	14.6
509	8		9.56	17.8	2.92	2.92	2.92	2.92	2.92	2.92	2.92	2.92	2.92	2.92	2.92	2.92	2.92	2.92	2.92	2.92	2.92	2.92	2.92	2.92	2.92	2.92	2.92	2.92	2.92
	16		19.1	35.6	5.84	5.84	5.84	5.84	5.84	5.84	5.84	5.84	5.84	5.84	5.84	5.84	5.84	5.84	5.84	5.84	5.84	5.84	5.84	5.84	5.84	5.84	5.84	5.84	5.84
	24		28.7	53.4	8.76	8.76	8.76	8.76	8.76	8.76	8.76	8.76	8.76	8.76	8.76	8.76	8.76	8.76	8.76	8.76	8.76	8.76	8.76	8.76	8.76	8.76	8.76	8.76	8.76
	32		38.2	71.1	11.7	11.7	11.7	11.7	11.7	11.7	11.7	11.7	11.7	11.7	11.7	11.7	11.7	11.7	11.7	11.7	11.7	11.7	11.7	11.7	11.7	11.7	11.7	11.7	11.7
	40		47.8	88.8	14.6	14.6	14.6	14.6	14.6	14.6	14.6	14.6	14.6	14.6	14.6	14.6	14.6	14.6	14.6	14.6	14.6	14.6	14.6	14.6	14.6	14.6	14.6	14.6	14.6
510	8		9.56	17.8	2.92	2.92	2.92	2.92	2.92	2.92	2.92	2.92	2.92	2.92	2.92	2.92	2.92	2.92	2.92	2.92	2.92	2.92	2.92	2.92	2.92	2.92	2.92	2.92	2.92

Failure of bond indicated from tab. specimen boundary

A - Actual strain measurement

P - Predicted strain measurement

Strain values below line are calculated on the basis of

TABLE XXXII

COMPLEX JOINT EXPERIMENTAL DATA WITH HSLE ADHESIVE

Ass. No. of Dwg. No. of 03-2867-13	Loading No.	Loading Magnitude, kips	Composite Adherend Net Sect. Ten Stress, ksi	Tr. Adherend Net Sect. Ten Stress, ksi	Joint Unit Load Transfer, N./In. ²	Composite, per Ply Unit Load Transfer (Both PLY)	Titanium Single and Composite Double Adherend Surface Strains at Gage No. Indicated																					
							1	2	3	4	5	6	7	8	9	10	11	12	13	14	15	16	17	18	19	20		
504	1	8	9.40	17.8	1600	50	-541	273	-454	236	-373	208	-189	213	-1288	227	-518	285	-511	236	-447	-209	-188	244	-136	329		
		16	18.8	35.6	3200	100	-1081	517	-876	462	-519	398	-343	410	-2473	457	-1024	545	-973	459	-874	383	-330	459	-2476	626		
		21	24.7	46.6	4200	131	-1404	663	-1151	594	-933	499	-422	498	-3035	563	-1385	725	-1241	597	-1130	493	-398	580	-3147	905		
							P	0	0	-10.5	0	-8.2	0	-4.25	0	0	0	0	0	0	0	0	0	0	0	0		
	2	24	28.2	53.3	4800	150	-1504	-46	-1325	675	-1065	569	-449	588	-3481	623	-1592	846	-1449	693	-1306	566	-388	696	-3630	935		
		30	35.2	66.6	6000	185	-2040	985	-1715	906	-1307	772	-148	82	-4449	829	-2008	1114	-1883	916	-1703	761	-14	888	-4789	1156		
		30 (30.6-50)	36.0	68.1	6130	192	-536	214	-380	204	-323	169	2	181	-1196	222	-536	243	-420	183	-410	-168	75	205	-1272	316		
		16	18.8	35.6	3200	100	-1057	469	-834	446	-509	380	26	403	-2408	465	-1035	526	-909	413	-864	370	119	443	-2501	618		
		21	24.7	46.6	4200	131	-1395	632	-1127	601	-942	515	-45	54	-3172	620	-1341	702	-1210	578	-1145	497	137	585	-3228	800		
							P	0	0	-10.5	0	-8.2	0	-4.25	0	0	0	0	0	0	0	0	0	0	0	0		
		24	28.2	53.3	4800	150	-1509	-31	-1305	695	-1089	597	62	617	-3629	714	-1522	809	-1398	645	-1311	573	141	674	-3650	946		
		30	35.2	66.6	6000	185	-2040	951	-1605	908	-1414	805	113	803	-4617	905	-1916	1033	-1768	834	-1663	-746	189	817	-4508	1128		
		32	37.6	71.1	6400	200	-2276	1080	-1906	1038	-1453	937	12	940	-5079	1012	-2116	1137	-1934	931	-1752	826	231	814	-4804	1207		
		33 (33.0-43)	38.8	73.3	6500	206	-2587	1229	-2156	1198	-1726	1218	-19	973	-5285	1060	-2324	1216	-2076	1001	-1429	-798	191	874	-5074	1301		

A Actual strains
P Predicted strains

Failure of load into tab specimen bonding

* A Actual strains

P Predicted strains

† Failure of load intro. tab specimen bondline

TABLE XXXIII. LARGE JOINT ANALYSIS/TEST COMPARISON

Joint Assembly	Standard Stress Analysis Prediction		Nonlinear Design Prediction		Actual Experimental Failure	
	P_u , lb/in.	Type Failure	P_u , lb/in.	Type Failure	P_u , lb/in.	Type Failure
-501	9,330	C.F.	12,144	C.F.	11,340*	C.F.
-509	6,250	C.F.	5,188	C.F.	6,590†	C.F.
*Ref. Table XXXI						
†Ref. Table XXXII						

overlap on the composite adherend over the area where failure is supposed to occur, this difference in predicted vs actual strains is critical. On -501, note, gage 7 shows a 22% reduction in measured strain from the first loading to the third one, an indication that bondline shear and normal stress peaking has been reduced at this point by the repeated loadings beyond the adhesives' proportional limit. A more vivid indication of this is shown by the behavior of gage 17 in the corner of the composite adherend. On the first loading the strain at gage 17 was exactly 50% of that of gage 7, on second loading 17 was 77% of 7, while on third loading gage 17 was reading 169% of gage 7. For -509 a different redistribution phenomena occurred. On first loading the strain reading of gage 17 lagged those of gage 7 only slightly as the loading increased through 24,000 lb and then started dropping as the load was increased to 30,000 lb. Gage 17 strain dropped faster than 7 and it was reading about 10% of 17 at 30,000 lb load. On second loading both 7 and 17 were reading decreasing magnitudes of minus strain. Gage 7 read decreasing small minus strains to 30,000 lb while gage 17 read decreasing small minus strains to 32,000 lb before they started increasing again.

Plots of the predicted longitudinal strains along the joint overlap length for predicted failure load are shown for -501 in Figure 145 and for -509 in Figure 146. Actual strains at this load level are superimposed on these figures for the last (or failure) loading test sequence and they correlate well with those predicted. Transverse strain predictions are zero due to the plane strain assumption; however, actual transverse strain measurements are shown to be relatively large. This is caused by the large Poisson's ratio exhibited by the $0/\pm 45^\circ$ composite adherends.

A redistribution of the surface ply strains of the composite adherend at or near the ends and corners, apparently resulting from multiple load cycles before failure, is probably caused by a redistribution of the adhesive strains (stresses) at those points. Such a redistribution could cause the test article to fail at higher loads than predicted since peak adhesive stresses (strains) would not be reached as soon. This could be offset by preload damage to the adhesive, thereby reducing its strength. The exact phenomena causing surface strain redistribution and its resulting effects are unknown.

At this point it can be said that there is a substantial amount of correlation of the predicted mechanical behavior with the experimental results on the complex joints with accurately predicted failure loads obtained when using maximum stress theory cohesive fracture of the adhesive. Adherend failure prediction in the joint was not checked experimentally in the complex joints.

Failed specimen photographs for -501 are shown in Figures 147 and 148 whereas Figures 149 and 150 show the -509 failures.

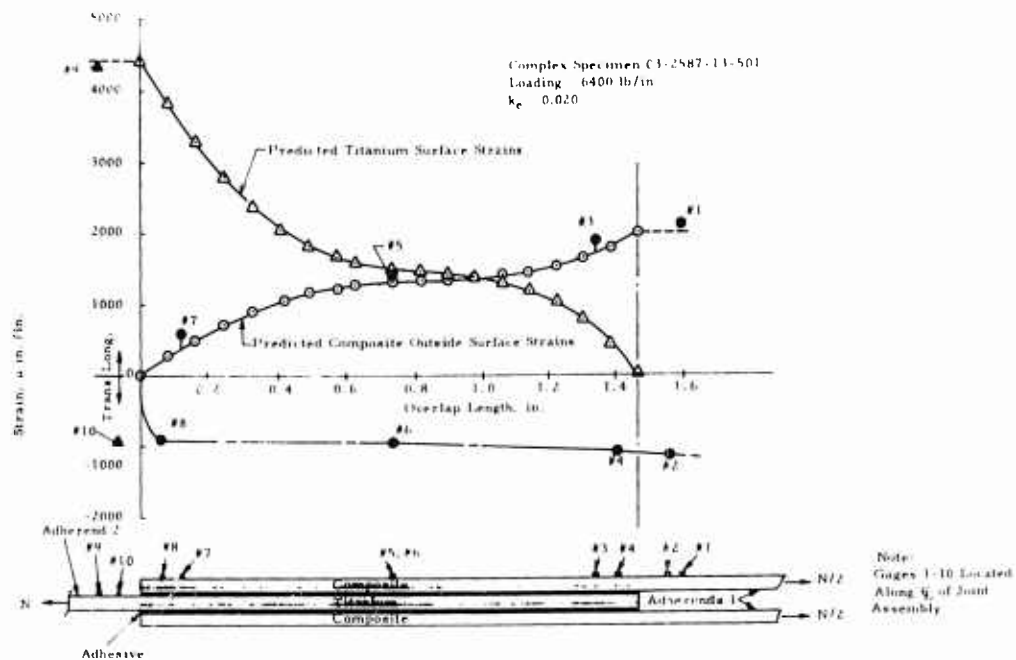


FIGURE 145. C/T COMPLEX JOINT-PREDICTED VS EXPERIMENTAL ADHEREND SURFACE STRAINS. LS-HE ADHESIVE

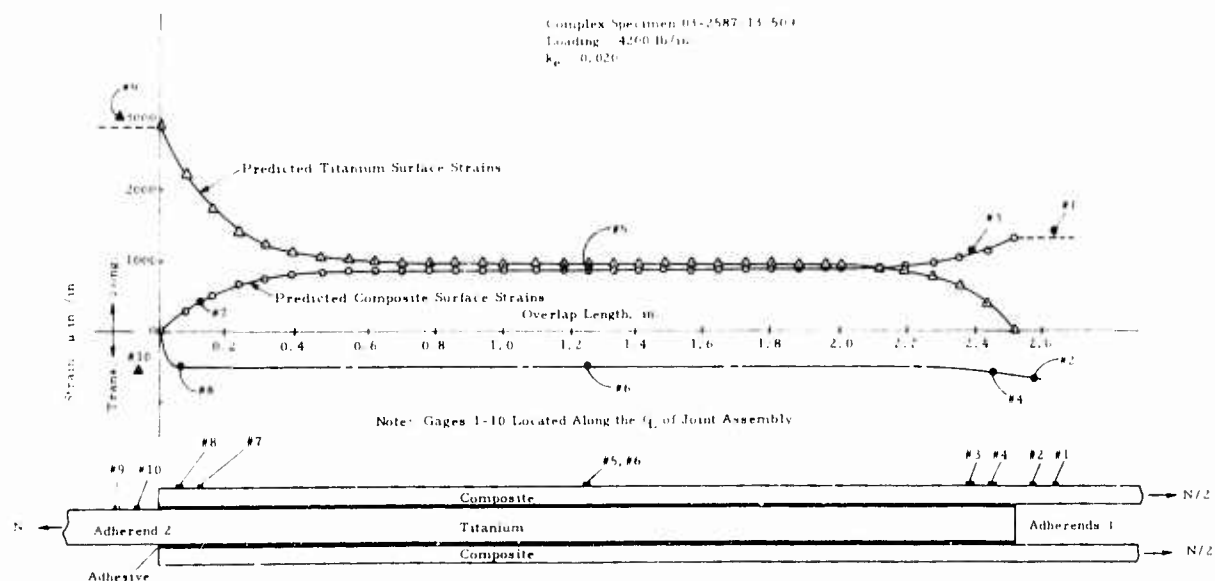
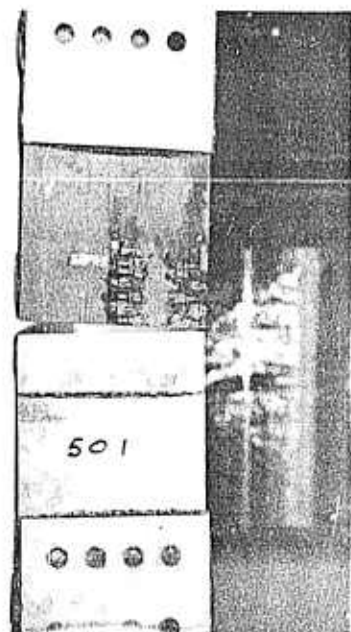
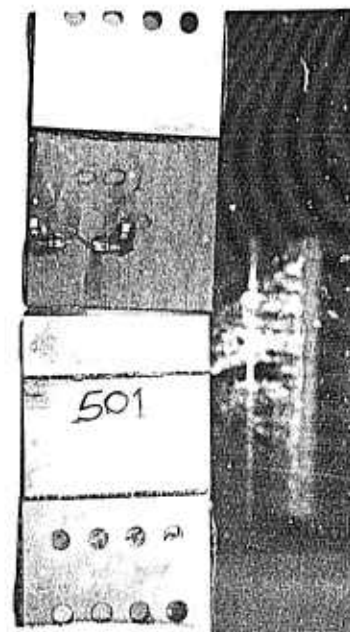


FIGURE 146. C/T COMPLEX JOINT-PREDICTED VS EXPERIMENTAL ADHEREND SURFACE STRAINS. HS-LE ADHESIVE

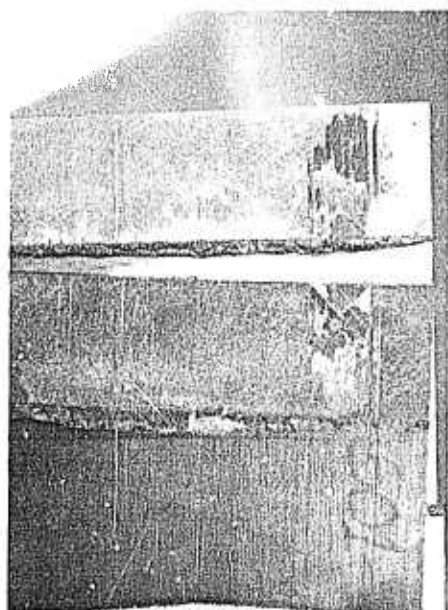


(a) Front



(b) Back

FIGURE 147. COMPLEX JOINT -501 AFTER FAILURE



(a) Front

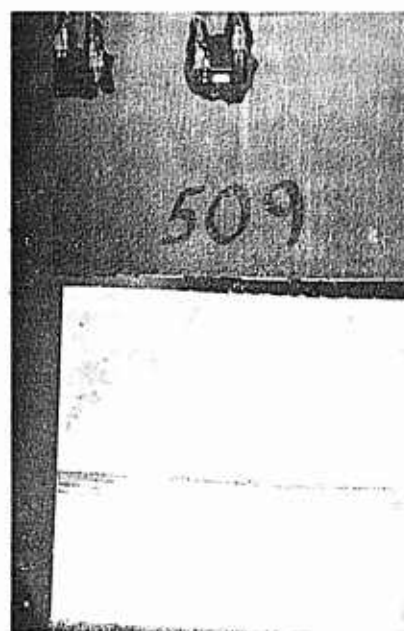


(b) Back

FIGURE 148. FAILURE MODE OF -501 COMPLEX JOINT

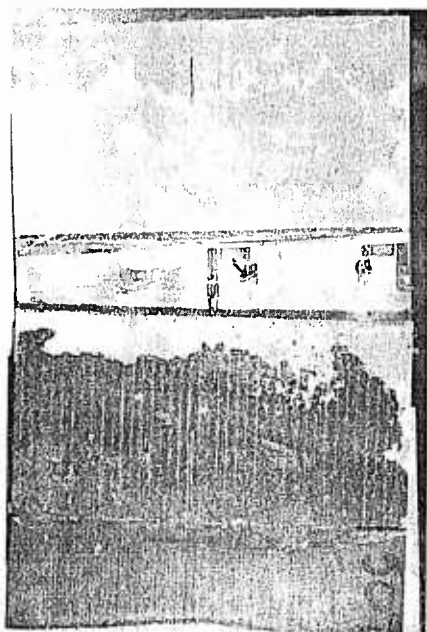


(a) Front

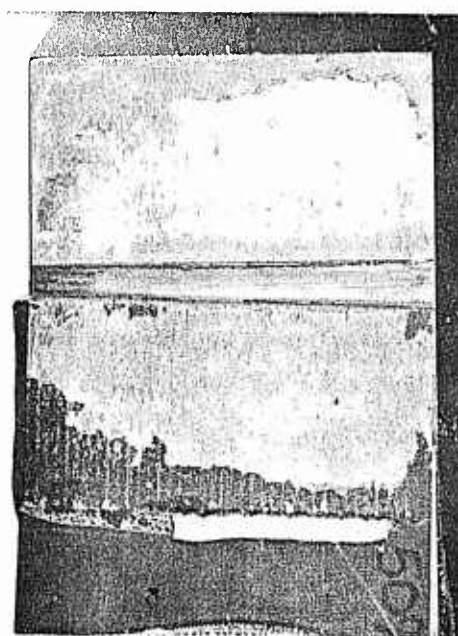


(b) Back

FIGURE 149. COMPLEX JOINT -509 AFTER FAILURE



(a) Front



(b) Back

FIGURE 150. FAILURE MODE OF -509 COMPLEX JOINT

SECTION XI

BONDED JOINT DESIGN CURVES

XI.1. GENERAL

The purpose of this section is to illustrate how the nonlinear design/analysis techniques developed in this program can be used to generate useful design curves on bonded joints. Section XI.2 presents a Discussion of Approach whereas Section XI.3 gives the Design Curves and how to use them.

XI.2. DISCUSSION OF APPROACH

Design oriented experimental data curves for composite adherend joints can be generated by plotting failure loads vs the geometric parameter L/t . For each composite orientation a plot of running load/ply vs L/t is recommended. The running loads at joint failure in lb/in. are divided by the number of plies to get the running load/ply (N') in lb/in./ply. The L/t parameter may be obtained by dividing the bondline overlap length by the adherend thickness. Always use the smaller of the two adherend thicknesses.

For this project, data from selected, representative joints were picked from Table XXVII for use in design oriented experimental data curve generation. Table XXXIV summarizes the experimental/analytical data on nine joint groups* which were used as a basis for design curve prediction along with pertinent, related geometric parameters. These predicted failure load values and the use of $N' = 0$ when $L/t = 0$ define these curves (or lines) up to laminate failure. Laminate failure then becomes a cut off at $N' = \text{laminate failure load (constant)}$. This cutoff value may be predicted or plugged in from experimental data on laminates. While the cutoff shown here is based on laminate adherend failure it could just as easily be based on titanium adherend failure (for composite/titanium joints) where this is critical.

XI.3. DESIGN CURVES

The design oriented average experimental data curves generated fall on or very close to the nonlinear analytically predicted joint failure load values as shown in Figure 151. All predicted and actual failure modes correspond except one, that being No. 36. Actual failure of this joint was by laminate adherend tension while its predicted failure was by cohesive fracture of the adhesive†. Experimentally measured tensile ultimate strength is used as the horizontal cutoffs for these curves with the points 31, 33, and 36 used for correlation.

Use of such design oriented experimental data curves which allow prediction of average test values for any L/t (or vice-versa) is one method of allowables determination. Statistically based formulas can be applied with such data to obtain reduced values for use as design allowables. Such formulas were developed in Section V on Experimental Design. The 95% confidence design ultimate allowables may be calculated using the general formula (given by equation 172, page) in which the average (mean) value can be taken from the Figure 151 curves. The other parameters are known or can be determined from the detail data tabulation of Appendix F.

Once the nonlinear analytical formulas have been checked out with simple lap joint tests utilizing the joint configuration and material combination desired, they can be used to generate a family of curves for design allowables purposes as was done herein. Or the computerized formulas could be used to predict failure loads and types of failure for any specific joint design which could be modeled as single, double, or step lap. If it is desired to use the type

*Each joint group is made up of the avg of 3 or 4 test specimens taken from one lap shear assembly.

†Changing the bending factor k_b , from 0.02 to 0.05 predicts adherend tension failure mode but at a somewhat lower failure load.

TABLE XXXIV.

BONDED JOINT ANALYTICAL/EXPERIMENTAL DESIGN DATA SUMMARY FOR 0/±45 COMPOSITE ADHERENDS

Avg. Data Item No.*	Description of Joint*	Experimental Data			N*, lb/in. ply	Analytically Predicted Values					Bending Factor†	Actual Failure Type**	L/††
		Unit Load Transfer, N, lb/in.*	Unit Load Transfer/ply, Stress, lb/in./ply	Average Adherend Stress, f_A , ksi		Average Bondline Stress, τ_B , psi	f_A , ksi	τ_B , psi	Max. Bondline Shear Stress, τ_{max} , psi†	Corresponding Max. Bondline Normal Stress, σ_{max} , psi†			
7(S.L.)	20-LSHE-B/T-0/±45	4,255	473	89.28(B) 93.24(Tt)	3,357	4,677(A.T.)	98.8(B) 102.5(Tt)	3,590	5,926(1)	1,737(1)	A.T.	27.778	
8(S.L.)	33-LSHE-B/T-0/±45	5,087	562	109.32(B) 112.54(Tt)	2,531	5,548(A.T.)	119.5(B) 123.0(Tt)	2,750	6,339(2)	1,469(2)	A.T.	46.444	
12(S.L.)	59-HSLE-B/T-0/±45	2,093	232	48.05(B)	1,438	1,615(C.F.)	37.0	1,105	7,477(3)	3,921(3)	C.F.	33.419	
3(D.L.)	18-LSHE-B/B-0/±45	7,018	413	78.99(B)	4,614	6,986(C.F.)	78.8(B)	4,600	5,910(4)	2,214(4)	C.F.	8.552	
4(D.L.)	31-LSHE-B/B-0/±45	8,715	512	96.62(B)	3,443	9,047(A.T.)	99.2(B)	3,580	5,802(5)	-961(5)	A.T.	13.935	
9(D.L.)	23-LSHE-B/T-0/±45	7,450	438	86.35(B)	5,457	7,474(C.F.)	86.5(B)	5,480	5,993(6)	2,156(6)	C.F.	7.897	
10(D.L.)	36-LSHE-B/T-0/±45	9,780	575	109.11(B) 107.91(Tt)	3,883	9,430(C.F.)††	105.2(B) 104.3(Tt)	3,750	6,501(7)	-1,153(7)	A.T./L.S.	14.045	
14(D.L.)	62-HSLE-B/T-0/±45	5,193	305	58.27(B)	2,483	5,792(C.F.)	64.9(B)	2,870	8,171(8)	-1,676(8)	C.F.	11.274	
15(St.L.)	26-2-LSHE-B/T-0/±45	11,146	232	42.40(B)	2,864	11,181(C.F.)	42.5(B)	2,880	(S-1)5,524(E) 4,425(M) (S-2)4,436(M) 5,432(E)	+3,018(E) -458(M) -455(M) +3,067(E)	A.T.	14.805	

Notes:
(1) Other end has $\tau_{max} = 5877$ psi, $\sigma_{max} = 1594$ psi
(2) Other end has $\tau_{max} = 6183$ psi, $\sigma_{max} = 1388$ psi
(3) Other end has $\tau_{max} = 7435$ psi, $\sigma_{max} = 4267$ psi
(4) At other end $\tau_{max} = 5684$ psi, $\sigma_{max} = 2205$
(5) At other end $\tau_{max} = 5771$ psi, $\sigma_{max} = 957$ psi
(6) At other end $\tau_{max} = 5910$ psi, $\sigma_{max} = 2161$
(7) At other end $\tau_{max} = 6492$ psi, $\sigma_{max} = 1152$
(8) At other end $\tau_{max} = 8164$ psi, $\sigma_{max} = +1672$

*From Table XXVII
†S1: step 1
S2: step 2
E: end of joint overlap
M: middle of joint overlap (end of step 1, start of step 2)
† Bending factor is based on types of joint, adhesive, and failure, Ref. Table XXVII
** Failure Type
A.T. - Adherend net section tension
C.F. - Cohesive fracture of bondline or surface resin or both
L.S. - Longitudinal splitting
†† Ref. Appendix F
††† A bending factor of $k_e = 0.05$ was used the predicted failure type was A.T. but failure load was only 9144 lb/in.

Notes:

- (1) Other end has $\tau_{max} = 5877$ psi, $\sigma_{max} = 1594$ psi
 (2) Other end has $\tau_{max} = 6183$ psi, $\sigma_{max} = 1388$ psi
 (3) Other end has $\tau_{max} = 7435$ psi, $\sigma_{max} = 4267$ psi
 (4) At other end $\tau_{max} = 5684$ psi, $\sigma_{max} = 2205$
 (5) At other end $\tau_{max} = 5771$ psi, $\sigma_{max} = 957$ psi
 (6) At other end $\tau_{max} = 5910$ psi, $\sigma_{max} = 2161$
 (7) At other end $\tau_{max} = 6492$ psi, $\sigma_{max} = +1152$
 (8) At other end $\tau_{max} = 8164$ psi, $\sigma_{max} = +1672$

*From Table XXVII

†S-1: step 1

S-2: step 2

E: end of joint overlap

M: middle of joint overlap (end of step 1, start of step 2)

†Bending factor is based on types of joint, adhesive, and failure, Ref. Table XXVII

**Failure Type

A.T. - Adherent net section tension

C.F. - Cohesive fracture of bondline or surface resin or both

L.S. - Longitudinal splitting

††Ref. Appendix F

†††If a bending factor of $k_F = 0.05$ was used the predicted failure type was A.T. but failure load was only 9144 lb/in.

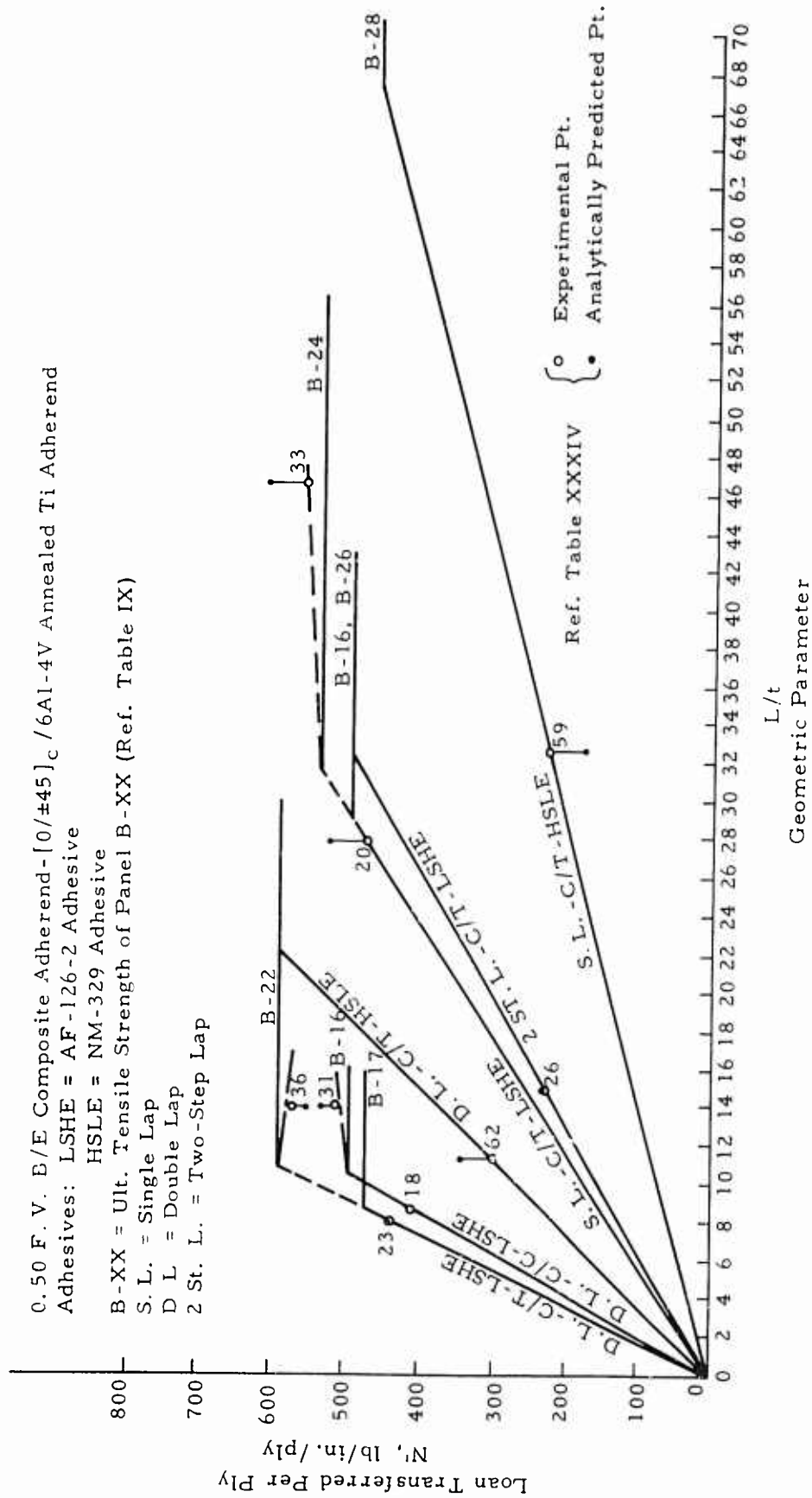


FIGURE 151. DESIGN CURVES FOR SINGLE, DOUBLE, AND STEP-LAP JOINTS

of allowable curves generated above directly in design it will be necessary to use a design factor K which would be

$$K = \frac{(DA)}{f_s} = \frac{N'_D}{N'_f} \quad (173)$$

where

(DA) = Design allowable value, N'_D lb/in./ply (use eq. 172)

f_s = Mean value of strength N'_f lb/in./ply

To use the curve in this fashion the design load in lb/in./ply would be input on the ordinate to curve intersection and the L/t value read on the abscissa at that point. This L/t value would then have to be adjusted as follows:

$$(L/t)_D = \frac{1}{K} (L/t)_f = \frac{N'_f}{N'_D} (L/t)_f \quad (174)$$

where

$(L/t)_D$ = Design value

$(L/t)_f$ = Mean value read from curve

If the input load is above the horizontal cutoff line (as in Fig. 151) a stronger orientation or composite material must be used.

When using the design predictive formulas or computer programs, the distance between assumed zero bending moment points on the adherend on each side of the joint (quantity a) must be known or very large† as compared to the overlap length c . That is, the ratio c/a must be known or small† (in the latter case it can be assumed to be zero).

Design ultimate allowables can be calculated based on the nonlinear design/analysis formulae prediction values. These values are used as mean strength values and can be applied to most any joint design which is or can be broken into single, double, or step lap configurations. If the users then have a large backlog of lap joint test data, typical experimentally based statistical parameters will also be available. These can be used with the predicted mean strength to calculate bonded joint design ultimate allowables for most any adherend/adhesive and configuration combination.

Where insufficient basic adherend or adhesive material properties are known, the use of these formulas will be advantageous. This can be done by using assumed "effective" properties‡, chosen on a trial and error basis to predict failure loads and correlate them with the results from a few simple lap joint tests. Such a procedure will provide a powerful technique for mean joint strength prediction. However, such "effective" properties may be substantially different from the real ones.

Since the predicted mean strength and type of failure of the complex joints (see Section X.5) is reasonably accurate when compared with experimental results, design allowables calculated from such mean strength predictions should also be accurate. Therefore, the use of the standard 1.5 factor of safety on design limit loads to obtain design ultimate loads should be sufficient to provide ample operational safety for static load conditions at room temperature.

*This would also be the N'_f value used in equation 172 to obtain the N'_D value.

† a should be 1/50 or smaller.

‡In the form of the Ramberg-Osgood three parameter stress-strain curve values for the adherend orthotropic lamina or isotropic material and the adhesive.

SECTION XII

RESULTS, CONCLUSIONS AND RECOMMENDATIONS

XII.1. GENERAL

The purpose of this section is to provide a brief summary of the results and conclusions which have become evident in the completion of the research and in addition to delineate problem areas which were identified. Recommendations for future research along lines related to this effort but further advanced are also covered. Results and Conclusions are covered in Section XII.2, whereas Section XII.3 covers the Recommendations.

XII.2. RESULTS AND CONCLUSIONS

In brief, the results of this research have been the development and verification of nonlinear design/analysis techniques for certain types of bonded joints covering static failure in several principal modes at room temperature. The methods developed have proven to be accurate when using basic material behavior characteristics and appropriate empirical bending factors.* The use of assumed adhesive properties in these formulae can be a reasonably accurate technique as long as some simple joint experimental data are available for use in calculating "effective" properties for comparison. Through the use of appropriate failure criteria for the adherend and adhesive in the nonlinear joint formulae the analytical methods become design-predictive equations which can be used to predict joint mean strength, failure type, and as a basis for average strength curves. Example curves have been generated and their design use explained.

Bonded single, double, and step lap, and scarf joints were studied resulting in nonlinear design/analysis techniques being developed for the first three types of joints, whereas only the differential equations were set up for the scarf joint. Comparative results based on typical joint models were generated by both the theoretical methods and the standard nonlinear discrete element techniques. The latter took considerably more computer time to run than the former one. After the theory was developed to the point where good agreement was obtained with the discrete element method, an experimental effort was initiated to provide final verification of the nonlinear analysis methods.

For the three lap configurations, composite adherends of three fiber orientations with two adhesive systems were utilized in the test program along with two adherend material combinations. A total of 203 simple specimen joints were made and tested along with the necessary characterization tests on the composite and titanium adherend materials. In addition, six of these simple specimens were selected for "special" investigation and were extensively strain gauged in the joint overlap area. Data from these special specimens were correlated with the theoretical behavior prediction methods. The large quantity of simple specimen results allowed the theory to be checked out against many geometric, configuration, and material parameter variations as well as failure mode changes. Finally, two larger, complex joints were designed, built, instrumented, and tested as a final check on the analytical methods. These complex specimens were extensively strain gauged for study of the joint behavior under loading. Experimental verification was successful.

Every effort was made to achieve high quality repeatable processing, inspection, and testing. Existing specifications were utilized as much as possible with new specifications written as required. Basically the philosophy was to (1) rigidly monitor and control the incoming material and its subsequent storage, (2) provide complete traceability records on all materials, processing, and testing, and (3) inspect the fabricated materials and joints as necessary with visual and automatic ultrasonic and radiographic methods. Specimen fabrication and instrumentation was accomplished using the same rigid processing and inspection controls utilized in laminate and joint manufacture. Testing was accomplished in accordance with appropriate specifications with all testing conducted at a constant strain rate and with load and strain data automatically recorded both digitally and with autographic continuous plots. Data reduction and analyses were designed to fit the analytical method verification requirements, causing many details to

*Necessary because the small deflection assumption was inadequate.

be recorded and analyzed which have not usually been considered important in the past. The detailed traceability records were extremely useful in the data analysis task.

A survey and statistical study of bonded lap joint data in the literature was made early in the program to provide guidance on the experimental effort and insight into the generation of design information.

Problem areas encountered were (1) low and variable boron fiber quality from one prepreg batch to the next, (2) inability to machine steps into boron laminate adherends in preparation for step lap joint fabrication and (3) the difficulty of developing rigorous scarf joint analysis equations. Another small problem was that a closely controlled bondline thickness was not achieved in the experimental effort. Tools for achieving lap shear assemblies with controlled, consistent, and repeatable bondline thicknesses were designed but not fabricated and used because of program economic limitations.

In summary, the above research program accomplished all objectives delineated in Section I. The goal of being able to predict all principal failure modes was only partially achieved, however. Cohesive fracture of the bondline or composite surface resin and adherend net section tension failure are the principal modes predictable by the nonlinear equations developed herein. Interlaminar shear (or longitudinal splitting) failure is not predictable by these methods. Neither is interface (adhesive/adherend or composite surface resin/fiber) failure but it is doubtful that this should be considered an acceptable primary mode of failure since it is related to poor materials and processing quality.

The nonlinear joint analysis techniques developed utilize the Ramberg-Osgood three-parameter stress-strain curves on the adhesive and adherend materials as inputs into program in order that behavior may be predicted throughout the elastic and inelastic range to failure. Maximum stress theory was used for both adhesive and titanium adherend failure prediction, whereas maximum strain theory was used for laminate adherend failure prediction. When these were input the analysis computer programs became design predictive programs for mean strength estimation. At predicted failure load the program prints out the bondline adhesive shear and normal stresses at numerous stations along the overlap length along with individual lamina and isotropic adherend stresses at these points. This provides a complete stress map of the overlap area in digital form. Such information will be useful in joint design analysis as well as post-failure critiques.

XII.3. RECOMMENDATIONS

The areas which need further study are (1) the adaptation of these nonlinear techniques to predict interlaminar shear (and longitudinal splitting) failure*, (2) modification of the nonlinear formulas to predict interface failure and correlate it with some materials or processing property which depicts quality level, (3) modification of plane strain assumption used in the formulas to predict correct transverse composite adherend lamina strains for various orientations and (4) determination of the small deflection theory's adequacy for nonlinear analysis developed herein. The equations need experimental verification for compressive and combined loadings and for other composite materials which exhibit different behavior patterns such as graphite/epoxy, glass/epoxy, and metal matrix composites. Design analysis application studies need to be made which would check out these formulas against typical airframe component structural joints which have been or could be experimentally evaluated.

A need for experimental study of the detailed joint behavior under repeated loadings† is also indicated from the test results of this program. Such loadings, expanded into time and temperature dependent spectrums and or environmental exposures typical of airframe applications would yield much information on the time-temperature dependent and/or environmental effects change of bonded joint behavior under various loadings. It might also be

*Ref (21) presents methods of predicting interlaminar shear bonded joint failure in the elastic range, however, report was received too late for consideration in present program.

†Ref (21) also presents considerable fatigue data on bonded joints but was received too late for consideration herein.

possible to relate these behavior changes to a pattern of changes in "effective" input properties and then use the nonlinear formulae as predictive methods.

An effort to complete development of the nonlinear analysis equations for the scarf joint is also needed along with the necessary discrete element and experimental checks. This effort would round out the nonlinear methods available to cover all the basic types of load transfer joints used in airframe structures.

LIST OF REFERENCES

1. Jensen, W. R., Falby, W. E., and Prince, N., "Matrix Analysis Methods for Anisotropic Inelastic Structures," Technical Report AFFDL-TR-65-770, April, 1966.
2. Ramberg, W. and Osgood, W. R., "Description of Stress-Strain Curves by Three Parameters," NACA TN 902, July 1943.
3. Spiegel, M. R., *Applied Differential Equations*, Prentice-Hall, 1958.
4. Salmon, M., Berke, L., and Sandhu, R., "An Application of the Finite Element Method to Elastic-Plastic Problems of Plane Stress," AFFDL-TR-68-39, May 1970.
5. Dastin, S., "Joining and Machining Techniques," from Lubin, G., *Handbook of Fiberglass and Advanced Plastic Composites*, Van Nostrand Reinhold, p 581 (1969).
6. Imrie, G. C. and Bell, J. E., "Test Techniques for Determination of Adhesive and Interlaminar Properties," Interim Technical Report 3 to AFFDL, Contract F33615-70-C-1292 by Boeing, December 1970.
7. Lackman, L. M., "Aircraft Structural Design Manual," AFML Advanced Composites Division, WPAFB Report NA-68-321-9, December 1968, pp 26, 38 and Report NA-68-321-12, pp 57, 74, 84, March 1969.
8. Dastin, et al., "Advanced Composite Wing Structures-Materials Qualitative Properties, Final Report," Grumman T. R. AC-ME-ST 8082, October 1968.
9. Lehman, G. M., et al, Quarterly Reports Nos. 1-7, "Investigation of Joints and Cutouts in Advanced Fibrous Composites of Aircraft Structures," June 1967-January 1969, McDonnell-Douglas.
10. Chessin, N. and Curran, V., "Preparation of Aluminum Surfaces for Bonding" in Bodnar, M., *Applied Polymer Symposium No. 3, Structural Adhesive Bonding*, 1966.
11. Kutscha, D. and Hofer, K. E., "Feasibility of Joining Advanced Composite Flight Vehicle Structure," AFML-TR-68-391, January 1969-IITRI.
12. Grimes, G. C., et al, "Investigation of Structural Design Concepts for Fibrous Aircraft Structures," AFFDL-TR-67-29, Volumes I and III, February 1968 and November 1967 - SwRI.
13. ASTM-E-178-68, "Recommended Practice for Dealing With Outlying Observations," 1971.
14. Grimes, Glenn C., "Stress Distribution in Adhesive Bonded Lap Joints," SAE Paper 710107, January 1971 (SAE Congress Paper), also published in 1971 SAE *Transactions*.
15. Final Draft and First Edition, *Structural Design Guide for Advanced Composite Applications*.
16. Sessler and Weiss, AFML-TR-68-115, Vol. II, "Non-Ferrous Light Metal Alloys," January 1968.
17. Tsai, S. W., "Structural Behavior of Composite Materials," NASA-CR-71, July 1964.
18. Gehring, R. W. and Hughes, E. J., et al, "Evaluation of Environmental and Service Conditions on Filamentary Reinforced Composite Structural Joints and Attachments," Technical Management Report No. 4, May 1970, Cn F33615-69-C-1436.

LIST OF REFERENCES (Cont'd)

19. Rutherford, J. L., et al, "Analysis of Mechanical Properties of Metlbond 329," Final Report on Grumman P. O. No. 9-84247.
20. 2nd Edition. **Structural Design Guide for Advanced Composite Applications.**
21. Fehrle, Albert C., et al, "Development of an Understanding of the Fatigue Phenomena of Bonded and Bolted Joints in Advanced Filamentary Composites," AFFDL-TR-71-44, June 1971.

APPENDICES

	Page
A Scarf Joint Equations	A-1
B Standard Constituent Properties of Boron-Epoxy Laminates	B-1
C Specifications	C-1
D Ultrasonic Thru-Scan and Radiograph Inspection Records on Boron/Epoxy Adherend Panels	D-1
E Selected Typical Adherend Material Tensile Stress-Strain Curves and Photomicrographs	E-1
F Complete Experimental Data on Bonded Joints	F-1
G Nonlinear Design/Analysis Program Failure/Behavior Prediction Results on Simple Joints	G-1
H Nonlinear Formula Predictions of Complex Joint Failure Loads/Behavior	H-1

APPENDIX A
SCARF JOINT EQUATIONS

SCARF JOINT EQUATIONS

The scarf joint is idealized as shown in Fig. A.1, the cement thickness being exaggerated for clarity.

We take the coordinate axes, x and z , as shown. The displacement $\bar{u}_0 = \bar{u}_0(x, z)$ is the x displacement of the right face of the adhesive and $\bar{u}_1 = \bar{u}_1(x, z)$ is the x displacement of the left face.

The displacements u_0 and u_1 are the x displacements of the centroids of the upper and lower adherends, as shown. The z displacements of the upper and lower adherends are w_0 and w_1 taken positive in the positive z directions. The displacements w_0 and w_1 are the usual "bending deflections" of the adherends.

For the present, we shall assume the material to be elastic-isotropic and consider conditions of plane strain.

Consider the free body of Fig. A.2. Equilibrium of the upper element requires that

$$V_U + dV_U - V_U + \frac{\tau dx}{\cos \frac{\theta}{2}} \sin \frac{\theta}{2} - \frac{\sigma dx}{\cos \frac{\theta}{2}} \cos \frac{\theta}{2} = 0$$

or

$$\frac{dV_U}{dx} = \sigma - \tau \tan \frac{\theta}{2} \quad (1)$$

and

$$dN_U - \frac{\tau dx}{\cos \frac{\theta}{2}} \cos \frac{\theta}{2} - \frac{\sigma dx \sin \frac{\theta}{2}}{\cos \frac{\theta}{2}} = 0$$

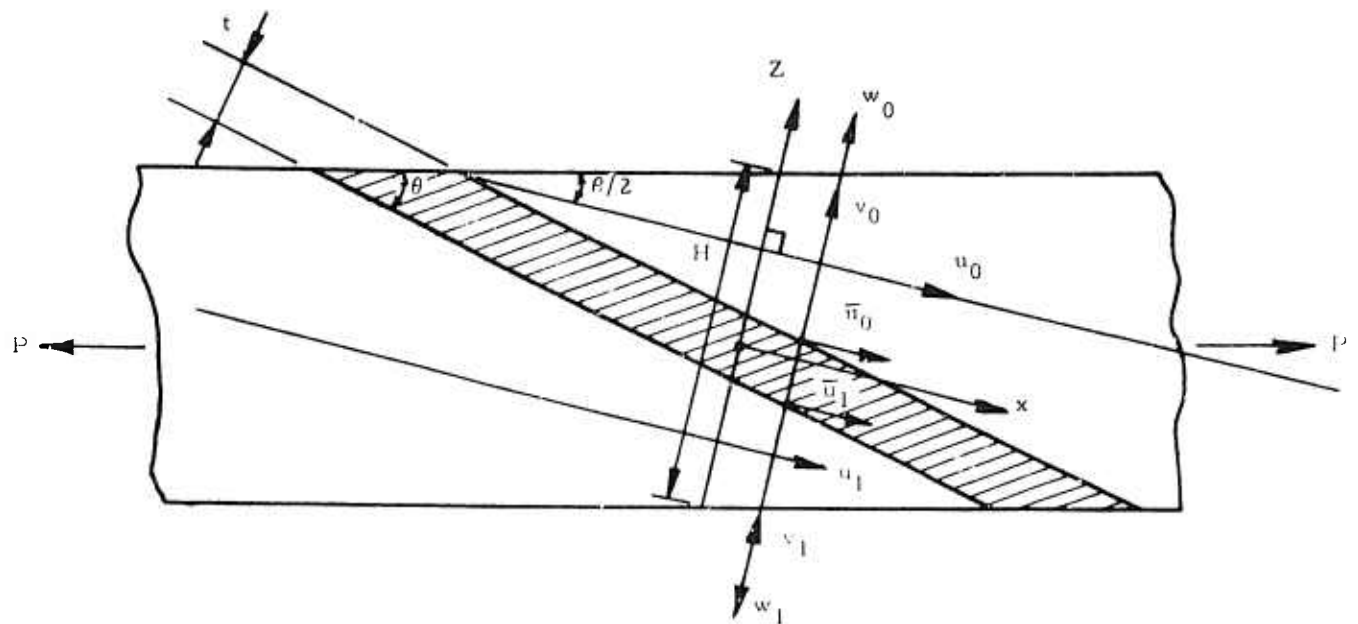


FIGURE A. 1. SCHEMATIC OF SCARF

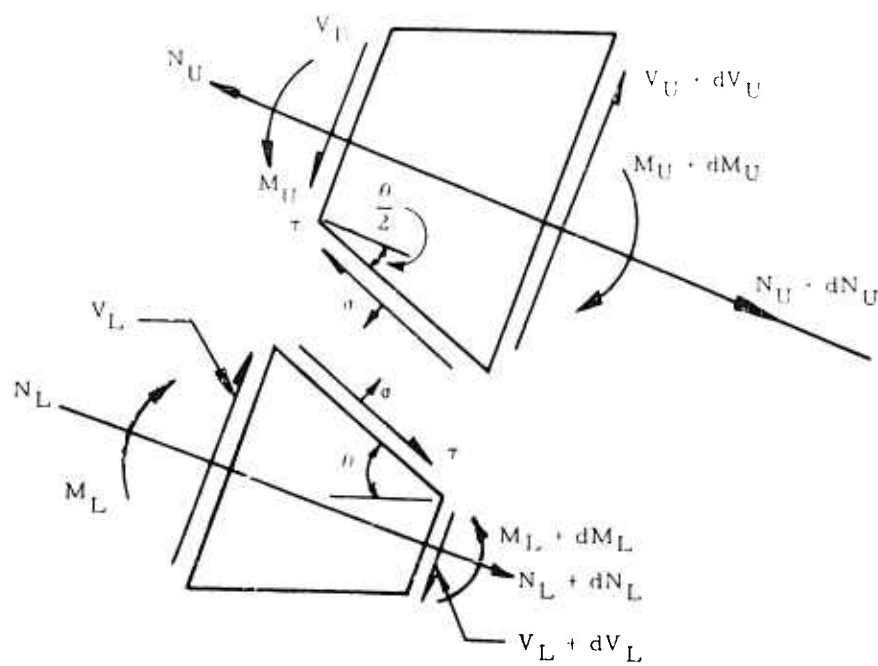


FIGURE A. 2. FREE BODY OF SCARF

or

$$\frac{dN_U}{dx} = \tau + \sigma \tan \frac{\theta}{2} \quad (2)$$

Similarly, for the lower element we have

$$\frac{dV_L}{dx} = \sigma - \tau \tan \frac{\theta}{2} \quad (3)$$

$$\frac{dN_L}{dx} = - \left(\tau + \sigma \tan \frac{\theta}{2} \right) \quad (4)$$

Equations (1) and (3) give

$$\frac{d}{dx} (V_U - V_L) = 0$$

So

$$V_U - V_L = \text{constant} \quad (5)$$

If we take moments about a transverse section, that is, a section normal to the x axis, we get

$$M_U + N_U \frac{h_U}{2} - M_L - N_L \frac{h_L}{2} - P \frac{(h_U - h_L)}{2} \cos \frac{\theta}{2} = 0$$

or

$$M_U - M_L + \frac{(N_U h_U - N_L h_L)}{2} - 2Px \sin \frac{\theta}{2} = 0 \quad (6)$$

Considering the deformation of the cement, we have

$$\tau = \frac{G}{t} \cos \frac{\theta}{2} \left[(\bar{u}_0 - \bar{u}_1) - (v_0 - v_1) \tan \frac{\theta}{2} \right] \quad (7)$$

$$\sigma = \frac{E_C}{t} \cos \frac{\theta}{2} \left[(\bar{u}_0 - \bar{u}_1) \tan \frac{\theta}{2} + (v_0 - v_1) \right] \quad (8)$$

where G and E_C are the shear and tensile moduli of the cement. Noting that

$$h_U = \frac{H}{2} + 2x \tan \frac{\theta}{2}, \quad h_L = \frac{H}{2} - 2x \tan \frac{\theta}{2}$$

or

$$\frac{dh_U}{dx} = - \frac{dh_L}{dx} = 2 \tan \frac{\theta}{2} \quad (9)$$

and

$$u_0 = u_0 + \frac{h_U}{2} \frac{dw_0}{dx}, \quad \bar{u}_1 = u_1 + \frac{h_L}{2} \frac{dw_1}{dx}, \quad (10)$$

$$v_0 = w_0, \quad v_1 = w_1$$

we get

$$\tau = \frac{G}{t} \cos \frac{\theta}{2} \left[(u_0 - u_1) + \frac{h_U}{2} \frac{dw_0}{dx} - \frac{h_L}{2} \frac{dw_1}{dx} - (w_0 + w_1) \tan \frac{\theta}{2} \right] \quad (11)$$

$$\sigma = \frac{E_C}{t} \cos \frac{\theta}{2} \left[(u_0 - u_1) \tan \frac{\theta}{2} + \left(\frac{h_U}{2} \frac{dw_0}{dx} - \frac{h_L}{2} \frac{dw_1}{dx} \right) \tan \frac{\theta}{2} + (w_0 + w_1) \right] \quad (12)$$

Differentiation gives

$$\frac{d\tau}{dx} = \frac{G}{t} \cos \frac{\theta}{2} \left[\frac{d}{dx} (u_0 - u_1) + \frac{1}{2} \left\{ h_U \frac{d^2 w_0}{dx^2} - h_L \frac{d^2 w_1}{dx^2} \right\} \right] \quad (13)$$

$$\frac{d\sigma}{dx} = \frac{E_C}{t} \cos \frac{\theta}{2} \left[\frac{d}{dx} (u_0 - u_1) \tan \frac{\theta}{2} + \frac{1}{2} \tan \frac{\theta}{2} \left\{ h_U \frac{d^2 w_0}{dx^2} - h_L \frac{d^2 w_1}{dx^2} \right\} + \sec^2 \frac{\theta}{2} \frac{d}{dx} (w_0 + w_1) \right] \quad (14)$$

We assume the following strain-displacement and moment curvature relations for the adherend

$$N_U = \frac{Eh_U}{1 - \nu^2} \frac{du_0}{dx} \quad (15)$$

$$N_L = \frac{Eh_L}{1 - \nu^2} \frac{du_1}{dx} \quad (16)$$

$$M_U = - \frac{Eh_U^3}{12(1 - \nu^2)} \frac{d^2w_0}{dx^2}, \quad M_L = - \frac{Eh_L^3}{12(1 - \nu^2)} \frac{d^2w_1}{dx^2} \quad (17)$$

where E is the elastic modulus of the adherend and ν is Poisson's ratio.

From Equations (15), (16), and (17), we get

$$\frac{du_0}{dx} - \frac{du_1}{dx} = \frac{(1 - \nu^2)}{E} \left(\frac{N_U}{h_U} - \frac{N_L}{h_L} \right)$$

$$h_U \frac{d^2w_0}{dx^2} - h_L \frac{d^2w_1}{dx^2} = - \frac{12(1 - \nu^2)}{E} \left(\frac{M_U}{h_U^2} - \frac{M_L}{h_L^2} \right) \quad (18)$$

$$\frac{d^2w_0}{dx^2} + \frac{d^2w_1}{dx^2} = - \frac{12(1 - \nu^2)}{E} \left(\frac{M_U}{h_U^3} + \frac{M_L}{h_L^3} \right)$$

Substitution into Equations (13) and (14) gives

$$\frac{d\tau}{dx} = \frac{(1 - \nu^2)G}{Et} \cos \frac{\theta}{2} \left[\left(\frac{N_U}{h_U} - \frac{N_L}{h_L} \right) - 6 \left(\frac{M_U}{h_U^2} - \frac{M_L}{h_L^2} \right) \right] \quad (19)$$

$$\frac{d\sigma}{dx} = \frac{(1 - \nu^2)E_C}{Et} \sin \frac{\theta}{2} \left[\left(\frac{N_U}{h_U} - \frac{N_L}{h_L} \right) - 6 \left(\frac{M_U}{h_U^2} - \frac{M_L}{h_L^2} \right) + \frac{2E \operatorname{cosec} \theta}{(1 - \nu^2)} \frac{d}{dx} (w_0 + w_1) \right] \quad (20)$$

Differentiation of Equation (20) and substitution from the third of Equations (18) gives

$$\frac{d^2\sigma}{dx^2} = \frac{(1 - v^2)E_C}{Et} \sin \theta \left[\frac{d}{dx} \left(\frac{N_U}{h_U} - \frac{N_L}{h_L} \right) - 6 \frac{d}{dx} \left(\frac{M_U}{h_U^2} - \frac{M_L}{h_L^2} \right) - 6 \operatorname{cosec} \theta \left(\frac{M_U}{h_U^3} + \frac{M_L}{h_L^3} \right) \right] \quad (21)$$

From Equations (1) and (3), we get

$$\sigma - \tau \tan \frac{\theta}{2} = \frac{1}{2} \frac{d}{dx} (V_U + V_L) \quad (22)$$

and, from Equations (2) and (4), there results

$$\tau + \sigma \tan \frac{\theta}{2} = \frac{1}{2} \frac{d}{dx} (N_U - N_L) \quad (23)$$

Solving Equations (22) and (23) for σ and τ , there results

$$\tau \sec^2 \frac{\theta}{2} = \frac{1}{2} \left[\frac{d}{dx} (V_U + V_L) + \tan \frac{\theta}{2} \frac{d}{dx} (N_U - N_L) \right] \quad (24)$$

$$\tau \sec^2 \frac{\theta}{2} = \frac{1}{2} \left[\frac{d}{dx} (N_U - N_L) - \tan \frac{\theta}{2} \frac{d}{dx} (V_U + V_L) \right] \quad (25)$$

Since

$$V_U = \frac{dM_U}{dx}, \quad V_L = \frac{dM_L}{dx}$$

these equations may be written in the form

$$\sigma = \frac{1}{2} \cos^2 \frac{\theta}{2} \left[\frac{d^2}{dx^2} (M_U + M_L) + \tan \frac{\theta}{2} \frac{d}{dx} (N_U - N_L) \right] \quad (26)$$

$$\tau = \frac{1}{2} \cos^2 \frac{\theta}{2} \left[\frac{d}{dx} (N_U - N_L) - \tan \frac{\theta}{2} \frac{d^2}{dx^2} (M_U + M_L) \right] \quad (27)$$

We note the following identities:

$$\frac{N_U}{h_U} - \frac{N_L}{h_L} = \left(\frac{1}{h_U} - \frac{1}{h_L} \right) (N_U + N_L) + (N_U - N_L) \left(\frac{1}{h_U} + \frac{1}{h_L} \right) \quad (28)$$

$$\frac{M_U}{h_U^2} - \frac{M_L}{h_L^2} = \left(\frac{1}{h_U^2} - \frac{1}{h_L^2} \right) (M_U + M_L) + (M_U - M_L) \left(\frac{1}{h_U^2} + \frac{1}{h_L^2} \right) \quad (29)$$

Since

$$N_U + N_L = P \cos \frac{\theta}{2} \quad (30)$$

and, from Equation (6),

$$\begin{aligned} M_U - M_L &= 2Px \sin \frac{\theta}{2} + \frac{1}{4} [(N_U + N_L)(h_U + h_L) + (N_U - N_L)(h_U - h_L)] \\ &= 3Px \sin \frac{\theta}{2} + (N_U - N_L) \frac{H}{4} \end{aligned} \quad (31)$$

Equations (28) and (29) give

$$\begin{aligned} \frac{N_U}{h_U} - \frac{N_L}{h_L} &= \left[-4Px \sin \frac{\theta}{2} + (N_U - N_L)H \right] \frac{1}{h_U h_L} \\ \frac{M_U}{h_U^2} - \frac{M_L}{h_L^2} &= \frac{1}{h_U^2 h_L^2} \left\{ -4x \tan \frac{\theta}{2} (M_U + M_L) + \left[3Px \sin \frac{\theta}{2} + (N_U - N_L) \frac{H}{4} \right] \right. \\ &\quad \left. \times (h_U^2 + h_L^2) \right\} \end{aligned}$$

Substitution of these results in Equations (19) and (21) gives

$$\begin{aligned} \frac{d\tau}{dx} &= \frac{(1 - \nu^2)G}{Et h_U h_L} \cos \frac{\theta}{2} \left[-4Px \sin \frac{\theta}{2} + H(N_U - N_L) \right. \\ &\quad \left. - \frac{6}{h_U h_L} \left\{ -4Hx \tan \frac{\theta}{2} (M_U + M_L) + 3Px(h_U^2 + h_L^2) \sin \frac{\theta}{2} \right. \right. \\ &\quad \left. \left. + \frac{H}{4} (h_U^2 + h_L^2)(N_U - N_L) \right\} \right] \end{aligned}$$

$$= \frac{(1 - \nu^2)G}{Et h_U h_L} \cos \frac{\theta}{2} \left\{ - \left[2 + \frac{9(h_U^2 + h_L^2)}{h_U h_L} \right] P_x \sin \frac{\theta}{2} \right. \\ \left. + \left[1 - \frac{3}{2} \frac{(h_U^2 + h_L^2)}{h_U h_L} \right] H(N_U - N_L) + \frac{24Hx}{h_U h_L} \tan \frac{\theta}{2} (M_U + M_L) \right\} \quad (32)$$

$$\frac{d^2 \sigma}{dx^2} = \frac{(1 - \nu^2)E_C}{Et} \sin \frac{\theta}{2} \left[\frac{d}{dx} \left\{ - \frac{4P_x}{h_U h_L} \sin \frac{\theta}{2} + \frac{H}{h_U h_L} (N_U - N_L) \right\} \right] \\ - 6 \frac{d}{dx} \left\{ - \frac{4xH}{h_U^2 h_L^2} \tan \frac{\theta}{2} (N_U + M_L) + \frac{(h_U^2 + h_L^2)}{h_U^2 h_L^2} \left(3P_x \sin \frac{\theta}{2} \right. \right. \\ \left. \left. + (N_U - N_L) \frac{H}{4} \right) \right\} - 3 \operatorname{cosec} \theta \left\{ \left(\frac{1}{h_U^3} + \frac{1}{h_L^3} \right) (M_U + M_L) \right. \\ \left. + \left(\frac{1}{h_U^3} - \frac{1}{h_L^3} \right) \left[3P_x \sin \frac{\theta}{2} + \frac{H}{4} (N_U - N_L) \right] \right\} \quad (33)$$

Differentiation of Equations (26) and (27) and introduction into Equations (32) and (33) yield

$$\frac{1}{2} \cos^2 \frac{\theta}{2} \left[\frac{d^2}{dx^2} (N_U - N_L) - \tan \frac{\theta}{2} \frac{d^3}{dx^3} (M_U + M_L) \right] \\ = \frac{(1 - \nu^2)G}{Et h_U h_L} \cos \frac{\theta}{2} \left\{ - \left[2 + \frac{9(h_U^2 + h_L^2)}{h_U h_L} \right] P_x \sin \frac{\theta}{2} \right. \\ \left. + \left[1 - \frac{3}{2} \frac{(h_U^2 + h_L^2)}{h_U h_L} \right] H(N_U - N_L) + \frac{24Hx}{h_U h_L} \tan \frac{\theta}{2} (M_U + M_L) \right\} \quad (34)$$

$$\begin{aligned}
& \frac{1}{2} \cos^2 \frac{\theta}{2} \left[\frac{d^4}{dx^4} (M_U + M_L) + \tan \frac{\theta}{2} \frac{d^3}{dx^3} (N_U - N_L) \right] \\
&= \frac{(1 - v^2) E_C}{Et} \sin \frac{\theta}{2} \left\{ \frac{d}{dx} \left[- \frac{4Px}{h_U h_L} \sin \frac{\theta}{2} + \frac{H}{h_U h_L} (N_U - N_L) \right] \right. \\
&\quad - 6 \frac{d}{dx} \left[- \frac{4xH}{h_U^2 h_L^2} \tan \frac{\theta}{2} (M_U + M_L) + \frac{(h_U^2 + h_L^2)}{h_U^2 h_L^2} \left(3Px \sin \frac{\theta}{2} \right. \right. \\
&\quad \left. \left. + (N_U - N_L) \frac{H}{4} \right) \right] - 3 \operatorname{cosec} \theta \left[\left(\frac{1}{h_U^3} + \frac{1}{h_L^3} \right) (M_U + M_L) \right. \right. \\
&\quad \left. \left. + \left(\frac{1}{h_U^3} - \frac{1}{h_L^3} \right) \left\{ 3Px \sin \frac{\theta}{2} + \frac{H}{4} (N_U - N_L) \right\} \right] \right\} \quad (35)
\end{aligned}$$

Equations (34) and (35) represent the two basic differential equations in $(M_U + M_L)$ and $(N_U - N_L)$ that are to be integrated. The coefficients in the equations are variable, being functions of the coordinate x . The integral of these equations is not known.

BIBLIOGRAPHY

Lubkin, J. L., J. Appl. Mech., 9A, Vol. 24, p. 255.

Lubkin, J. L. and Reissner, E., Transactions ASME, Vol. 78, pp. 1213-1221, August 1956.

"Aircraft Structural Design Manual--Advanced Composites," First Quarterly Progress Report, Contract F33615-68-C-1489, L. A. Div. N. A. R. Corp., June 1968.

APPENDIX B
STANDARD CONSTITUENT PROPERTIES
OF BORON-EPOXY LAMINATES*

*Taken from 1st Edition Structural Design Guide for Advanced Composite Applications, August 1969.

TABLE B.1. BORON FIBER PROPERTIES (RT)

<u>Property</u>	<u>Value</u>
Diameter	0.004275 in.
Density	0.100 lb/in. ³
α	2.7×10^{-6} in./in./°F
ν	0.20
F_{tu}	450.0 ksi
E^t	58.0×10^6 psi
G	24.2×10^6 psi

TABLE B.2. 104 GLASS SCRIM/5505 LAMINATE PROPERTIES (RT)

Property	Value
Density	
α_T	9.5×10^{-6} in./in./°F
α_L	5.8×10^{-6} in./in./°F
F_L^{tu}	37.8 ksi
$F_L^{tp\ell}$	33.3 ksi
E_L^t	3.2×10^6 psi
ν_{LT}^t	0.151 (at 5000 μ -in./in. strain)
F_T^{tu}	13.41 ksi
$F_T^{tp\ell}$	9.00 ksi
E_T^t	1.7×10^6 psi
ν_{TL}^t	0.120 (at 5000 μ -in./in. strain)
F_L^{cu}	45.36 ksi
$F_L^{cp\ell}$	8.88 ksi
E_L^c	4.69×10^6 psi
ν_{LT}^c	0.32 (at 5000 μ -in./in. strain)
F^{su}	11.11 ksi
$F^{sp\ell}$	2.10 ksi
G	0.933×10^6 psi

TABLE B. 3. 2387 EPOXY-NOVOLAK RESIN MATRIX (RT)

<u>Property</u>	<u>Value</u>
Density	0.044 lb/in. ³
α	27×10^{-6} in./in./°F
F^{tu}	4.184 ksi
$F^{tp\ell}$	2.92 ksi
E^t	0.487×10^6 psi
ν^t	0.31 (at 5000 μ -in./in. strain)
F^{cu}	23.52 ksi
$F^{cp\ell}$	8.88 ksi
E^c	0.560×10^6 psi
ν^c	0.387 (at 5000 μ -in./in. strain)
F^{su}	1.54 ksi
G	0.191 ksi

APPENDIX C
SPECIFICATIONS

SwRI-S3-101

GENERAL SPECIFICATION LAMINATE ORIENTATION CODE

Date: March 19, 1970
Prepared by: G. Wolfe
Approved by: J. Grimes

SwRI-S3-101
GENERAL SPECIFICATION

Laminate Orientation Code

1.0 Purpose

The purpose of this specification is to establish a Standard Laminate Code that will provide the user with a clear, concise, and common notation when dealing with Laminated Composite Materials.

2.0 Applicable Documents

"Structural Design Guide for Advanced Composite Applications,"
First Edition, Section 1.5.

3.0 Scope

This specification presents only the sections of the Standard Laminate Code that are applicable to the work being done presently at the Institute. For the complete code and a condensed code, see the document referenced above.

Note: This specification is intended to be used in specifying laminate orientation. It does not imply any preferred laminate design.

4.0 Standard Laminate Code

The Standard Laminate Code is used to describe a specific laminate uniquely. It is most simply defined by the following detailed description of its features.

4.1 Standard Code Elements

- a. Each lamina is denoted by a number representing its orientation in degrees between its filament direction and the X-axis (principal axis).
- b. Individual adjacent laminae are separated in the code by a slash, if their angles are different.
- c. The laminae are listed in sequence from one laminate face to the other, with brackets indicating the beginning and end of the code.
- d. Adjacent laminae of the same angle are denoted by a numerical subscript.
- e. A subscript T to the bracket indicates that the total laminate is shown.

<u>Laminate</u>	<u>Code</u>
45	$[45/0/90_2/30]_T$
0	
90	
90	
30	

4.2 Positive and Negative Angles

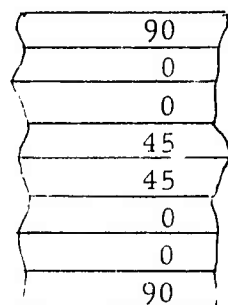
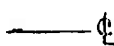
When adjacent laminae are of the same angle but opposite in sign, the appropriate use of + and - signs is employed. Each + or - sign represents one lamina and supersedes the use of the numerical subscript, which is used only when the directions are identical. Positive angles are assumed clockwise:

<u>Laminate</u>	<u>Code</u>
<div>45</div> <div>0</div> <div>-60</div> <div>-60</div> <div>30</div>	$[45/0/-60_2/30]_T$
<div>45</div> <div>-45</div> <div>-30</div> <div>+30</div> <div>0</div>	$[\pm 45/\mp 30/0]_T$
<div>45</div> <div>45</div> <div>-45</div> <div>-45</div> <div>0</div>	$[45_2/-45_2/0]_T$
<div>45</div> <div>-45</div> <div>45</div> <div>-45</div> <div>0</div>	$[(+45)_2/0]_T$, or $[\pm 45/\pm 45/0]_T$
<div>45</div> <div>-45</div> <div>-45</div> <div>45</div> <div>0</div>	$[\pm \mp 45/0]_T$
<div>45</div> <div>-45</div> <div>-45</div> <div>45</div> <div>45</div> <div>45</div> <div>-45</div> <div>-45</div> <div>45</div>	$[+-++--++45]_T$ or $[\pm \mp ++\pm \mp 45]_T$

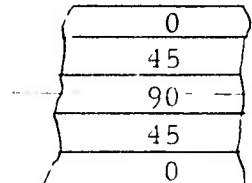
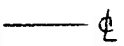
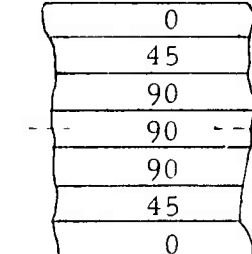
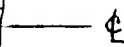
Note that, in condensing signs, the sign of the center lamina of an odd number is left uncombined.

4.3 Symmetric Laminates

Symmetric laminates with an even number of laminae still list the laminae in sequence, starting at one face, but stopping at the plane of symmetry instead of continuing to the other face. A bracket subscript S indicates only one-half of the laminate is shown:

<u>Laminate</u>		<u>Code</u>
		$[90/0_2/45]_S$

Symmetric laminates with an odd number of laminae are coded the same as even symmetric laminates, except that the center lamina, listed last, is overlined to indicate that half of it lies on either side of the plane of symmetry:

<u>Laminate</u>		<u>Code</u>
		$[0/45/\overline{90}]_S$
		$[0/45/90/\overline{90}]_S$

4.4 Sets

Repeating sequences of laminae are called sets and are enclosed in parentheses. A set is coded in accordance with the same rules which apply to a single lamina:

<u>Laminate</u>		<u>Code</u>
45		
0	SET	
90		$\left[(45/0/90)_2 \right]_S$
45	SET	
0		
90	SYM	or
90		
0	SET	
45		
90		$\left[45/0/90 \right]_{2S}$
0	SET	
45		

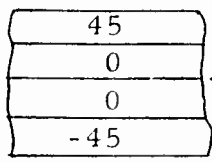
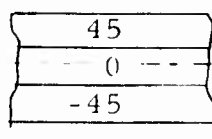
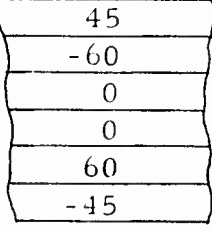
on the other hand:

45		
0	SET	
90		$\left[(45/0/90)_4 \right]_T$
45	SET	
0		
90	NOT	or
45	SYM	
0	SET	
90		
45		$\left[45/0/90 \right]_{4T}$
0	SET	
90		

Laminates are often composed of a single repeated set. When it is desired to refer to the laminate in a generic sense, or when the number of sets has yet to be determined, as in the sizing stages of design, the coefficient n will be used with the bracket subscripts T and S instead of a numerical coefficient.

4.5 Quasi-Symmetric Laminates

Laminates which would be symmetrical about the center plane, except that the halves of corresponding pairs of laminae are of different sign, are said to exhibit quasi-symmetry. These are coded in the same manner as symmetrical laminates except for the introduction of the bracket subscript Q in place of the subscript S. The direction of the positive angle is assumed clockwise:

<u>Laminate</u>	<u>Code</u>
	$\left[45/0 \right]_Q$
	$\left[45/\bar{0} \right]_Q$
	$\left[45/-60/0 \right]_Q$

SwRI 03-301

PROCESS STANDARD FOR BORON/RESIN
COMPOSITE LAMINATE FABRICATION

SwRI 03-301

PROCESS STANDARD FOR BORON/RESIN
COMPOSITE LAMINATE FABRICATION

SUBJECT: Manufacture and Quality Control of Advanced Composite Laminate -
Fiber Glass/Epoxy and Boron/Epoxy.

SCOPE: This process standard establishes the procedures for the fabrication and quality control of laminates of fiber glass/epoxy and boron/epoxy composites to be used in the evaluation of simple bonded joints.

REFERENCES:

- (1) Division X "Processes and Effects," Structural Design Guide for Advanced Composite Applications, Final Draft, November 1968.
- (2) "Structural Airframe Application of Advanced Composite Materials," Volume VII, Manufacturing Methods, by B. E. Chitwood and J. R. Stovall, The Fort Worth Division of General Dynamics, Technical Report AFML-TR-69-101, May 1969.
- (3) "Advanced Composite Wing Structure," Grumman Aircraft Engineering Corporation, AF Contract F33615-68-C-1301, First Quarterly Progress Report, May 1968.

MATERIALS AND EQUIPMENT:

- (1) NARMCO 1581-5505 preimpregnated glass fabric.
- (2) NARMCO Boron/5505 epoxy preimpregnated material.
- (3) 181 and 120 dry glass fabric.
- (4) TX-1040 glass fabric (TeflonTM treated) - Pallflex Corporation.

- (5) 0.001-inch Mylar® film - duPont.
- (6) Coroprene (rubber-asbestos) - Armstrong Cork.
- (7) Herblease (EXL-1894/10% Vydax AR) - Mitchell Rand/duPont.
- (8) M and N 50-ton Hydraulic Press (350°F).
- (9) Air-circulating oven (500°F).
- (10) Molds.

PROCEDURE:

A. General - Requirements for fabrication of glass fabric/epoxy and boron/epoxy composites are as follows:

- (1) Temperature and Humidity Control - the layup area shall be maintained at $70^{\circ}\text{F} \pm 5^{\circ}\text{F}$ and humidity shall be 65 percent or less.
- (2) The number and orientation of plies in each panel shall be as specified in process instructions. The ply orientation shall be accurate to $\pm 0.50^{\circ}$. Butt joints of 3-in. boron tape shall be staggered 0.500 in. \pm 0.030 in. between plies. During layup, the fiber spacing of the tape shall be inspected. Loose fibers, crossovers, and gaps greater than 0.030 in. wide shall be repaired. All discrepancies shall be noted and approval for further use must be obtained from the project leader.
- (3) To avoid penetration of boron filaments into the flesh or clothing, the following safety precautions must be used:
 - (a) A coat of nylon or equivalent tight-weave, smooth surface fabric must be worn at all times when working with boron/epoxy materials.

- (b) Safety glasses or eye shield shall be worn when cutting boron filaments.
- (c) Immediately remove any filament which penetrates the flesh to prevent the filament from breaking off or penetrating deeper.

B. Laminating Requirements

- (1) Preparation - The steel tooling plate shall have two coats of EXL/10 percent Vydax, each coat allowed to dry at least 10 min, followed by buffing. If steel restraining dams are to be used for boundary supports, they should also be coated with two applications of EXL/10 percent Vydax. Steel dams shall be 1/2 in. in width and within +0.005/-0.000 in. of the final laminate thickness. If Coroprene dams are used, 1/8-in. thick Coroprene shall be used for 8 through 19 plies of boron/epoxy or half that number of glass fiber/epoxy plies.
- (2) Laminates to be subsequently bonded shall have a peel ply which is to be placed on the tool surface. If a partial peel ply is to be used, the remainder of the tool surface shall be covered with Teflon[®] film of the same thickness. Weight of the peel ply shall be recorded.
- (3) The lot number and roll number of the boron/epoxy or fiber glass epoxy used for the layup shall be recorded. Panel weight before and after curing shall be entered on the quality control sheet for each panel. The preimpregnated materials shall be maintained in

0°F storage until ready for use. The material is then removed from storage and allowed to warm to room temperature while sealed in the polyethylene bag.

- (4) Hand layup shall use Mylar[®] templates for each ply of material. Each template is scribed with the panel size, shape, and fiber orientation. It will be identified with the panel number, dash number, and ply number counting from the tool. Tooling pin holes will locate the template on the tool. Boron or fiber-glass material is laid up on each template, trimmed to the trim lines, and covered with transparent polyethylene film. The material is taped in place and inspected with template layup. If the panel is not laid up immediately, the material is returned to 0°F storage until ready for layup. Templates are allowed to come to room temperature before protective sheet is removed. The Mylar[®] template is placed (material down) on the tool next to the tooling pins. The template is rubbed over the layup to create intimate contact with the tool or preimpregnated peel ply. The template is removed by rolling from one corner with the axis of the roll perpendicular to the fiber direction. Each subsequent ply is located in the same way. The exposed material is inspected after each template is removed.
- (5) When the last ply of material has been laid up on the tool, a boundary support is located around the periphery of the panel. This boundary must be within 0.06 in. (maximum) of the edge of

the panel. It must be slightly thicker than the cured panel.

Resin (liquid and at 85 psi) must not be able to leak under the boundary support or through the corners. All resin loss must be vertical. The layup is then covered with one ply of TX-1040 trimmed to fit within the boundary support. The required number of bleeder plies are trimmed to fit within the boundary support and are placed on the TX-1040. (One-ply, 120-dry glass fabric bleeder should be used for each 4 to 5 plies boron; one ply of 181 preimpregnated glass fabric is equal to the thickness of two plies of boron.) The entire layup is covered with thin Mylar[®] (0.0075 in. thick) which extends over the boundary support and is taped to the tool on two opposite sides. The Mylar[®] film is perforated on 2-in. centers which allow escape of gas, but prevent excessive loss of resin. The layup is then covered with one ply of 181-dry glass fabric large enough to completely cover the layup and overhang the tool by at least 4 in. on at least one side. This ply permits gas in the panel to vent to the atmosphere. A press plate (or upper tool plate) is placed over the layup and the panel is cured in the hot platen press. See Figure 30 on the following page.

- (6) The panel is cured at a pressure of 85 psi with temperature cycle as follows:

- (a) 200°F for 2 hr

1. Separator Cloth (TX1040) or Peel Ply
2. Boron or Glass Fabric Laminate
3. Separator Cloth (TX1040)
4. Bleeder Plies (120 Glass Fabric - -1 ply per 4 plies Boron or 2 plies Glass Fabric)
5. Mylar Film (Overlaps Boundary Support)
6. 181 Vent Ply (Overlaps Tool)
7. Boundary Support

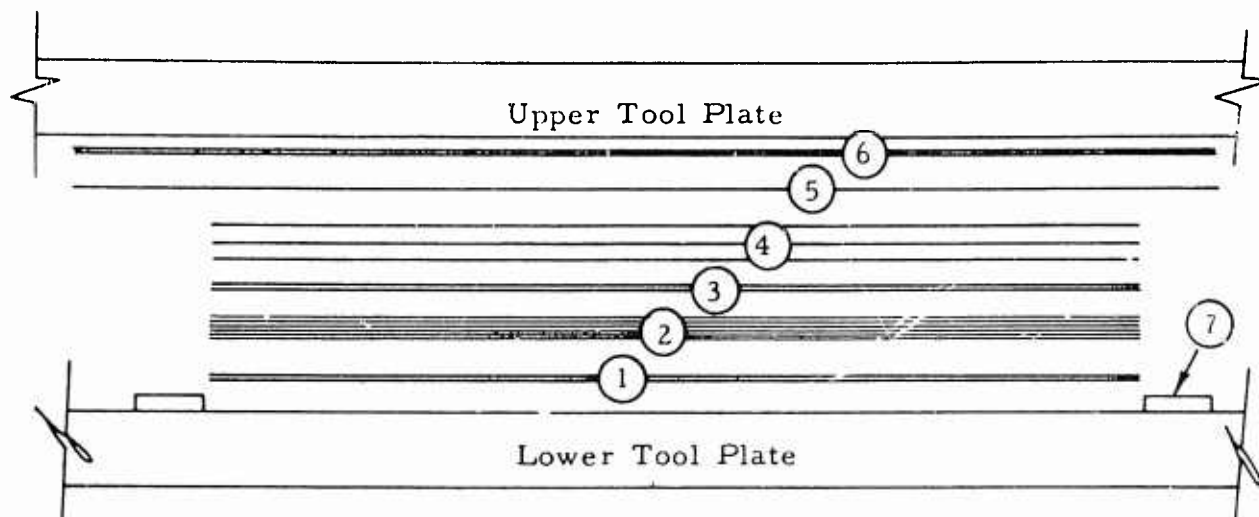


FIGURE 30. LAYOUT PROCEDURE

(b) 300°F for 2 hr

(c) 350°F for 2 hr

Allow panel to cool in press under 85-psi pressure until cooled to 125°F. If postcure is required, this may be accomplished in the air circulating oven.

- (7) Trim laminate to remove resin flash and record panel weight. Calculate and record the retained resin content on the quality control sheet.

Quality Assurance Provisions

- (1) Receiving - All materials shall be inspected upon receipt and before use in layup in accordance with provisions outlined in The Structural Design Guide for Advanced Composite Applications.

- (2) Process Control - A quality control sheet shall be maintained for each panel to verify compliance to the requirements of this specification.
- (3) Process Verification Panels - A 15-ply, 3×9 in., 0° orientation process verification tab shall be molded simultaneously with each panel using the same lot of material unless excess (cutoff) panel material is available. The process verification tab shall be submitted for testing for flexural strength and horizontal shear strength at room temperature prior to machining of the test specimen laminate.
- (4) Nondestructive Test Requirements - Each laminate, including test tabs, shall be inspected ultrasonically for voids, delaminations, and missing plies and results recorded on the quality control sheet. Each machined detail shall be visually inspected for filament orientation (or other nondestructive inspection) and results recorded on the quality control sheet.

SwRI 03-304

PROCESS STANDARD FOR ADHESIVE BONDING OF ADVANCED
COMPOSITE LAMINATES AND METAL ATTACHMENTS

PROCESS STANDARD FOR ADHESIVE BONDING OF ADVANCED
COMPOSITE LAMINATES AND METAL ATTACHMENTS

SUBJECT: Bonding Techniques for Preparation of Physical Test Specimens and Bonded Joints from Fiber Glass/Epoxy or Boron/Epoxy Composite Laminates and Metal Attachments.

SCOPE: This process standard establishes the procedures for surface preparation of composite laminates and metal attachments and adhesive bonding and cure of joints or other attachments.

REFERENCES:

- (1) ASTM-2093-62T Preparation of Surfaces of Plastic for Adhesive Bonding.
- (2) ASTM-2651-67T Preparation of Metal Surfaces for Adhesive Bonding
- (3) "Investigation of Structural Design Concepts for Fibrous Aircraft Structures," by G. C. Grimes, B. J. Pape, and J. H. Ferguson, Southwest Research Institute, Technical Report AFFDL-TR-67-29-Vol. III, November 1967.

MATERIALS AND EQUIPMENT:

- (1) 3M Company - AF-126-2-0.06 Film Adhesive
- (2) NARMCO Materials Division, Whittaker Corporation - Metlbond - 329 Film Adhesive
- (3) 7075-T6 Clad Aluminum Alloy
- (4) 6Al-4V Titanium Alloy

- (5) 1581 Glass Fabric/5505 Epoxy Laminate
- (6) Boron/5505 Epoxy Laminate
- (7) Constant Temperature Bath (150 to 650° F)
- (8) Air-Circulating Oven (RT-500° F)
- (9) M&N 50-Ton Hydraulic Press/Heated Platens (RT-600° F).

CLEANING PROCEDURES:

A. Aluminum Alloy - Aluminum alloys are to be cleaned prior to applying the adhesive bonding agent by the following procedure:

- (1) Wipe with solvent (MEK)
- (2) Immerse in Oakite 61B (6 to 8 oz/gal) at 160 to 180° F for 5 min
- (3) Rinse with R. T. running tap water for 1 min
- (4) Immerse in Oakite 34M (8 to 16 oz/gal) at R. T. for 10 min
- (5) Rinse with R. T. running tap water for 2 min
- (6) Dry in air-circulating oven at 200° F for 5 to 10 min.

B. Titanium Alloy - Titanium alloys are to be cleaned prior to applying the adhesive bonding agent by the following procedure:

- (1) Grit blast with fine grit
- (2) Immerse in Oakite 31 (1 part Oakite to 2 parts water) at R. T. for 5 min
- (3) Rinse with R. T. running tap water for 3 min
- (4) Immerse in the following solution at R. T. for 2 min
 - (a) 841 ml HCL acid (Reagent Grade, 37 to 38 percent)
 - (b) 89 ml Orthophosphoric acid (Reagent Grade, 85 to 87 percent)

- (c) 63 ml HF acid (Reagent Grade, 60 percent)
- (d) Rinse with R. T. running tap water for 3 min
- (e) Air dry for 1 hr at less than 60 percent R. H. and above 65°F or oven dry for 15 min at 180° to 200°F.

C. 1581 Glass Fabric or Boron/5505 Epoxy Laminates - Glass fabric or boron laminates in epoxy matrix are cleaned for application of adhesive bonding agents as follows:

- (1) Wipe with solvent (MEK or acetone)
- (2) Sand with emery paper or sandpaper, fine grit, no larger than No. 400
- (3) Wipe with clean, dry cloth
- (4) Wipe with solvent (MEK or acetone).

BONDING PROCEDURES

A. AF-126-2-0.06 Film Adhesive - The AF-126 adhesive is a nitrile-epoxy, unsupported B-stage film adhesive manufactured by the 3M Company. It is used with EC-2320 Primer according to the following procedure

- (1) Clean parts to be bonded (see Cleaning Procedures above)
- (2) Apply EC-2320 Primer to bonding area by spray, brush or dip method
- (3) Dry primer in air-circulating oven at 150°F for 30 min
- (4) Cut film to be used from roll with separating liner in place
- (5) Place film on primed part using the separating liner as a protective cover

- (6) Roll film onto part with a rubber roller insuring that no air is trapped between surface and film
- (7) Remove protective cover
- (8) Assemble parts
- (9) Cure bond at 50 psi and 275°F for 1 hr. Heat-up rate should not exceed 10°F/min and cool down under pressure to 200°F or below. Temperature should be monitored at glue line.

B. Metlbond - 329 Film Adhesive - The MB-329 adhesive is modified epoxy, nylon cloth supported, B-stage film adhesive manufactured by NARMCO Materials Division, Whittaker Corporation. The bonding procedure is as follows

- (1) Clean parts to be bonded (see Cleaning Procedures above)
- (2) Apply primer to bonding area
- (3) Dry primer
- (4) Cut film adhesive to be used from roll with protective liners in place
- (5) Remove paper separator and place film on part using plastic liner as a protective cover
- (6) Roll film onto part with a rubber roller to insure that no air is trapped between surface and film
- (7) Remove plastic protective cover
- (8) Assemble parts

- (9) Cure bond at 50 psi and 350°F for 1 hr. Heat-up rate should not exceed 10°F/min and cool down under pressure to 200°F or below. Temperature should be monitored at glue line.

SwRI S3-401

TEST STANDARD FOR FIBROUS COMPOSITE TENSILE SPECIMENS

TEST STANDARD FOR FIBROUS COMPOSITE TENSILE SPECIMENS

1.0 PURPOSE

It is the purpose of this standard to provide a standardized technique for measuring the static tensile properties of boron/epoxy and graphite/epoxy composites subjected to a monotonically increasing load to failure.

2.0 APPLICABLE DOCUMENTS

"Structural Design Guide for Advanced Composite Applications,
2nd Edition, Sections 7.3.1 and 7.3.2.

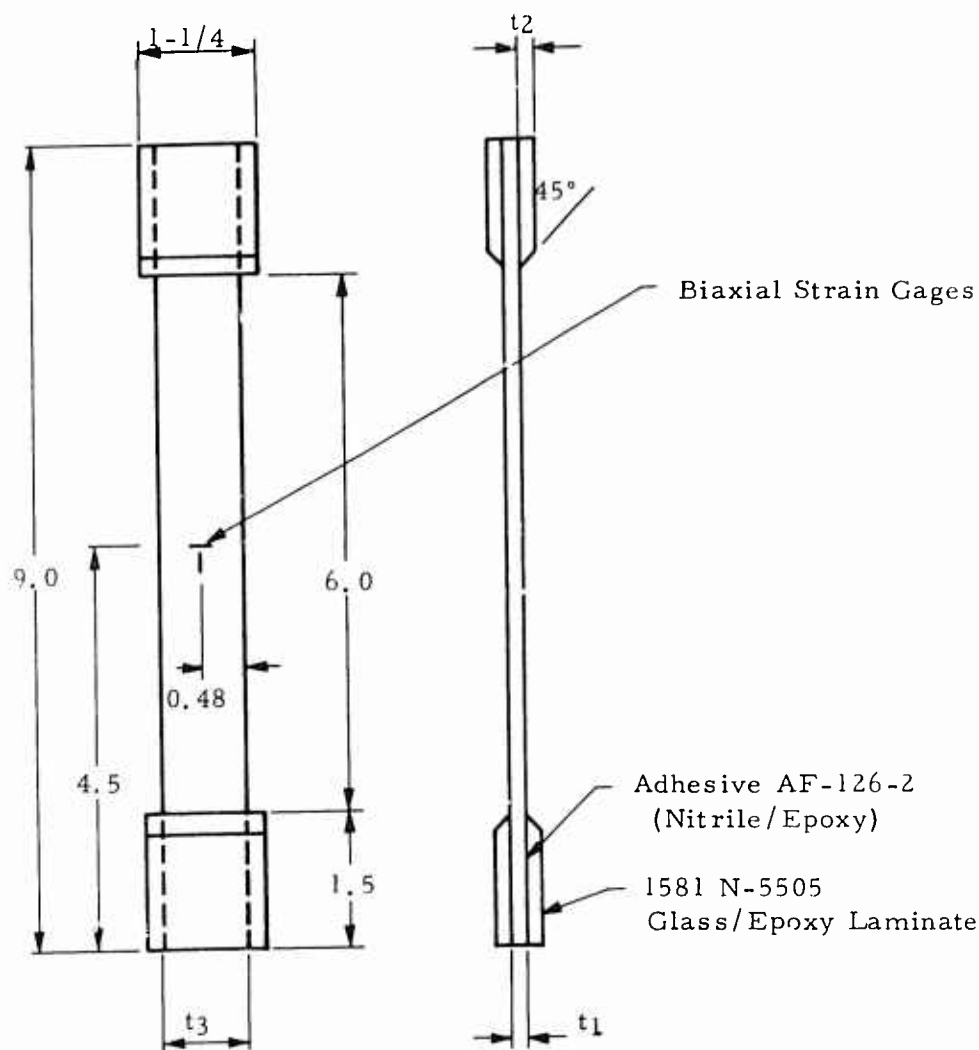
3.0 SCOPE

This standard covers both boron/epoxy and graphite/epoxy materials up to 18 plies thick. Measurements shall include load/biaxial strain data to obtain biaxial stress-strain curves to failure under constant strain rate conditions.

4.0 SPECIMEN PREPARATION AND INSTRUMENTATION

Specimens are to be laid out and cut from a suitable size panel to the dimensions shown on the drawing below. Subsequent to cutting out the specimens, tabs are bonded onto the specimens in groups of three or more (see drawing below). Strain gages are to be as described on the drawing.

SwRI Standard Tensile Specimen for Composites



Notes:

1. t_1 - boron/epoxy or graphite/epoxy specimen ≤ 18 plies thick unidirectional or angleply
2. t_2 - fiberglass/epoxy tabs 0.100 ± 0.01 in. thick (approximately 12 plies 1581)
3. Strain gages - Micro-Measurements 06-250BF-350
4. Tolerances: $X \pm 0.1$
 $XX \pm 0.04$
 Fractions $\pm 1/16$ } unless noted otherwise
5. t_3 - boron/epoxy 0.96 in. wide } sides to be smooth, splinter free and
 - graphite/epoxy 0.75 in. wide } flat and parallel within 0.015
6. Diamond cutoff wheel to be used in sizing specimens from panel
7. Tabs are bonded on in groups of three specimens or more at time with strip tabs leaving 3/8-in. spacing between specimens. Individual specimens are then sliced off by cutting through tab material.
8. Use stand Instron wedge grips with fine serrations.
9. Tab bonding: cure adhesive 1 hr at 275°F at 50 psi in heated platen press.

5.0 TESTING

In addition to the strain gages, a clamp on extensometer with a 2-in. gage length will be used on each specimen in order to control the strain rate during test and to provide back-up load-deflection curves should they be needed. Loading should be on a monotonically increasing basis at a constant strain rate of 0.00125 in./min. Load and strain shall be recorded automatically, either continuously or at known automatically spaced time intervals.

6.0 FAILURE ANALYSIS

All specimens shall be categorized as to failure type, such as (1) net section tension, (2) delamination, (3) diagonal shear, (4) brooming net section tension delamination, or (5) any combination thereof. Location of the failure shall be measured and recorded.* Any type failure between tabs is acceptable. Any type failure under the tabs is unacceptable. Complete failure description, type and location shall be recorded.

7.0 DATA REDUCTION

Raw data shall be appropriately processed to yield stress-strain data from which biaxial stress-strain curves may be plotted. Proportional limits, knees, moduli, Poisson's ratio, and ultimate strengths shall be

*Photographs of typical failures shall be made for record.

located, calculated, and tabulated along with related strains. Complete computerized data reduction, plotting, and the tabulation of data is acceptable.

APPENDIX D

ULTRASONIC THRU-SCAN AND RADIOGRAPH INSPECTION
RECORDS ON BORON/EPOXY ADHIEREND PANELS

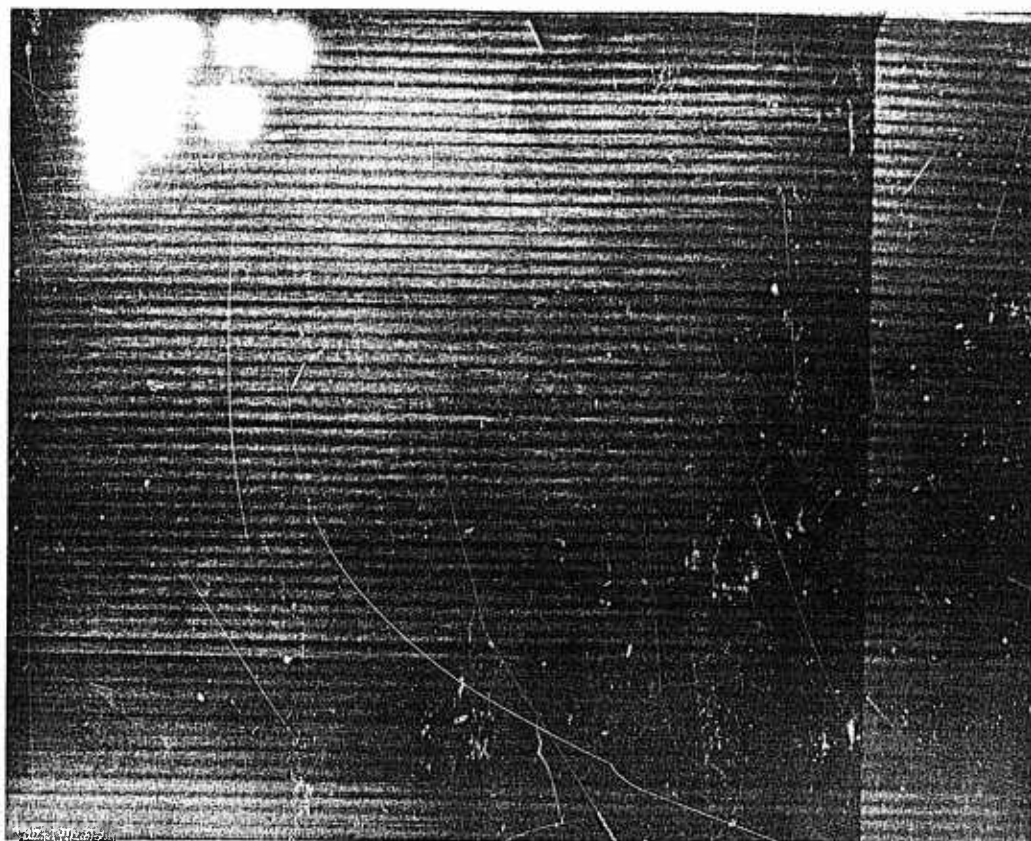
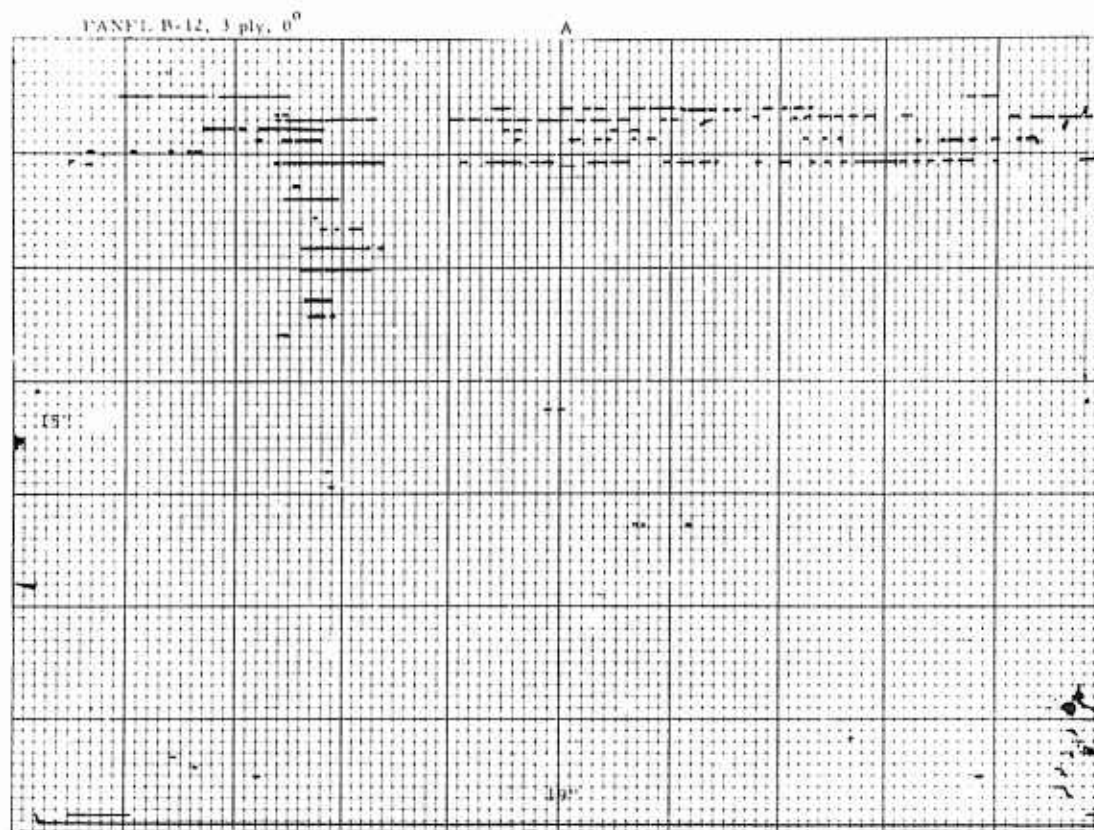
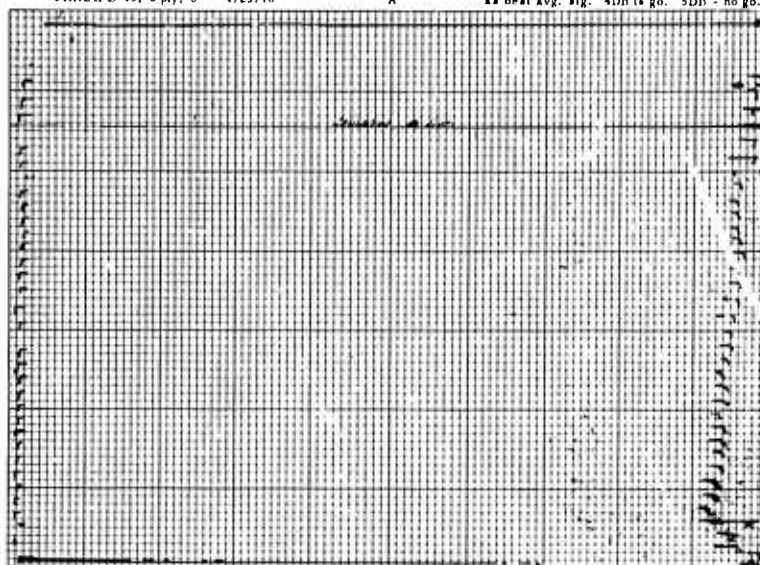


FIGURE D.1 INSPECTION RECORD, B-12

PANEL B-13, 6 ply, 0° 4/23/70

A

Sensitivity set so that any defect below 50%
will show as a mark on graph. 100% is set
as beat avg. sig. 4DB is go. 5DB - no go.



TEST OPERATOR WK
DATE 12/8/70

B
PANEL NUMBER B-13

PRINCIPAL FIBER
ORIENTATION: ←
SENSITIVITY SETTING: 4 DB

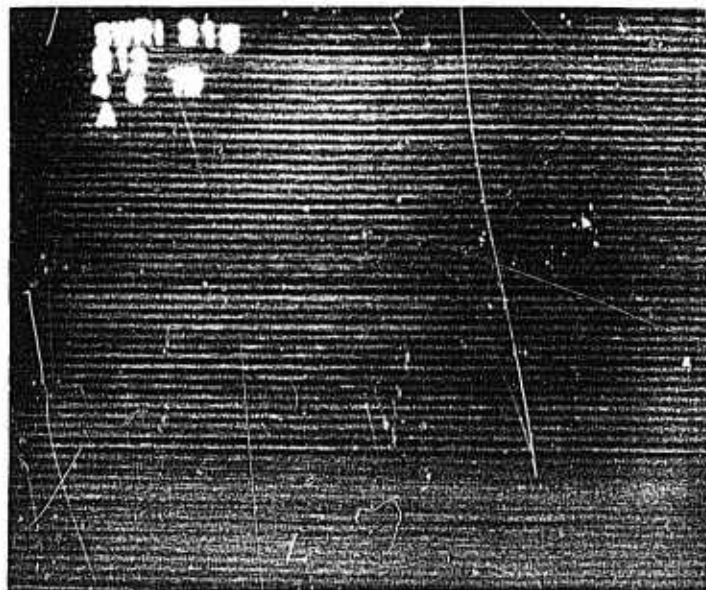
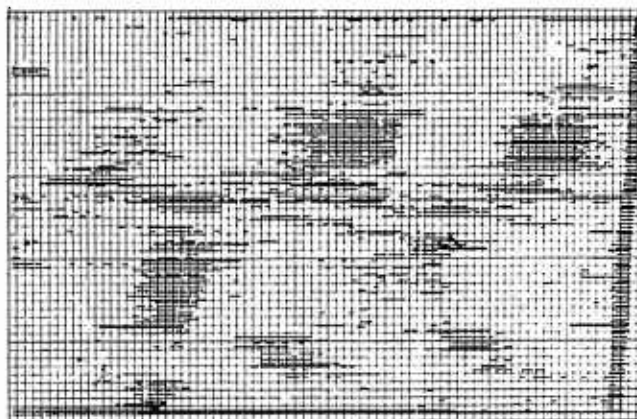


FIGURE D,2 INSPECTION RECORD, B-13

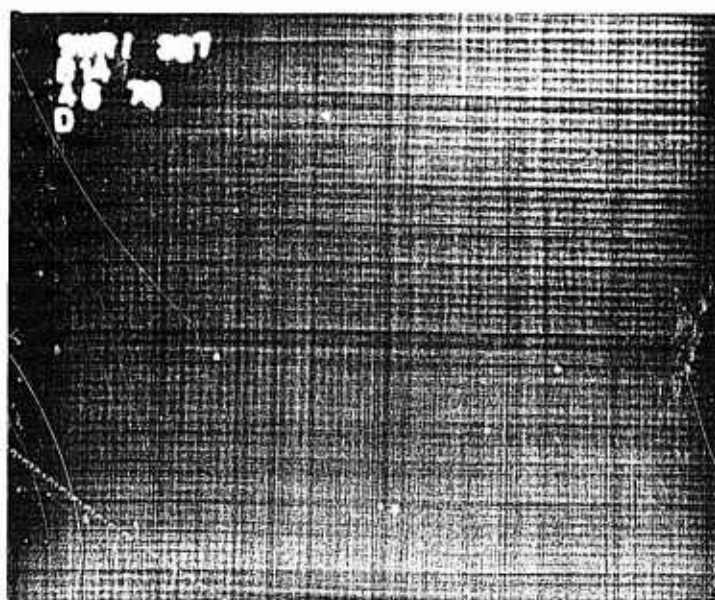
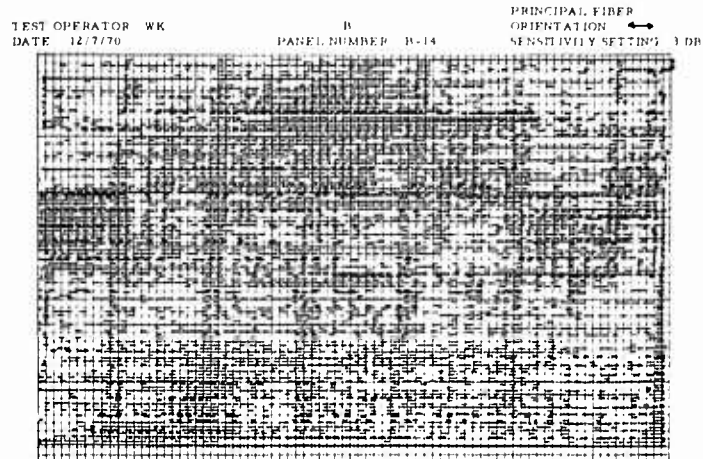
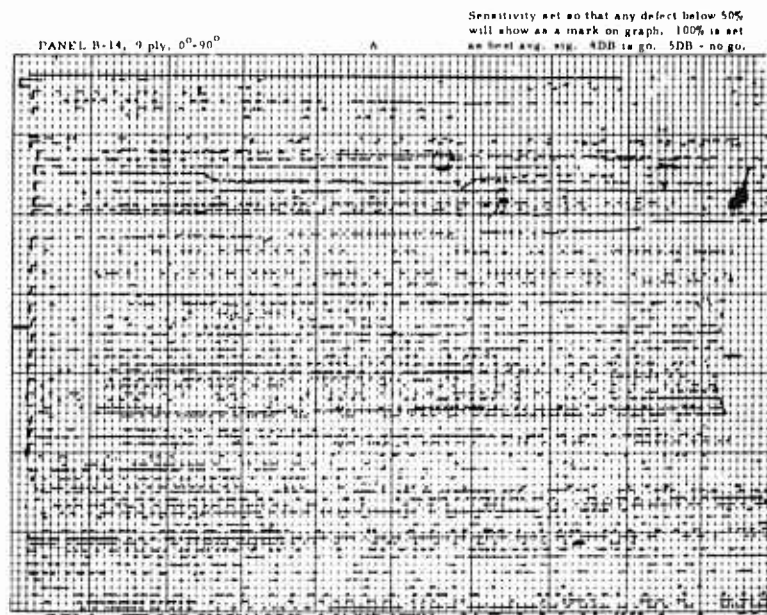


FIGURE D.3 INSPECTION RECORD, B-14

PANEL B-15, 1 ply, 0°-90° 4/23/70

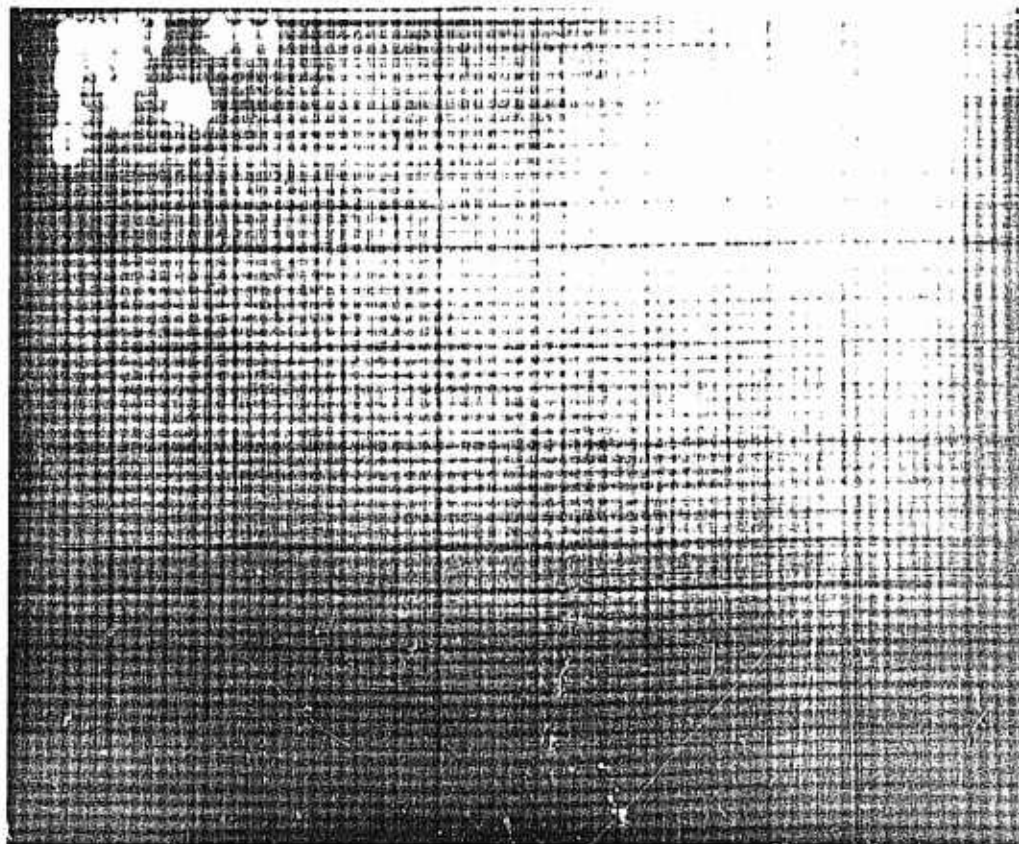


FIGURE D.4 INSPECTION RECORD, B-15

PANEL B-16, 9 ply, $0^0 \pm 45^0$

4 DB go, 5 DB no go

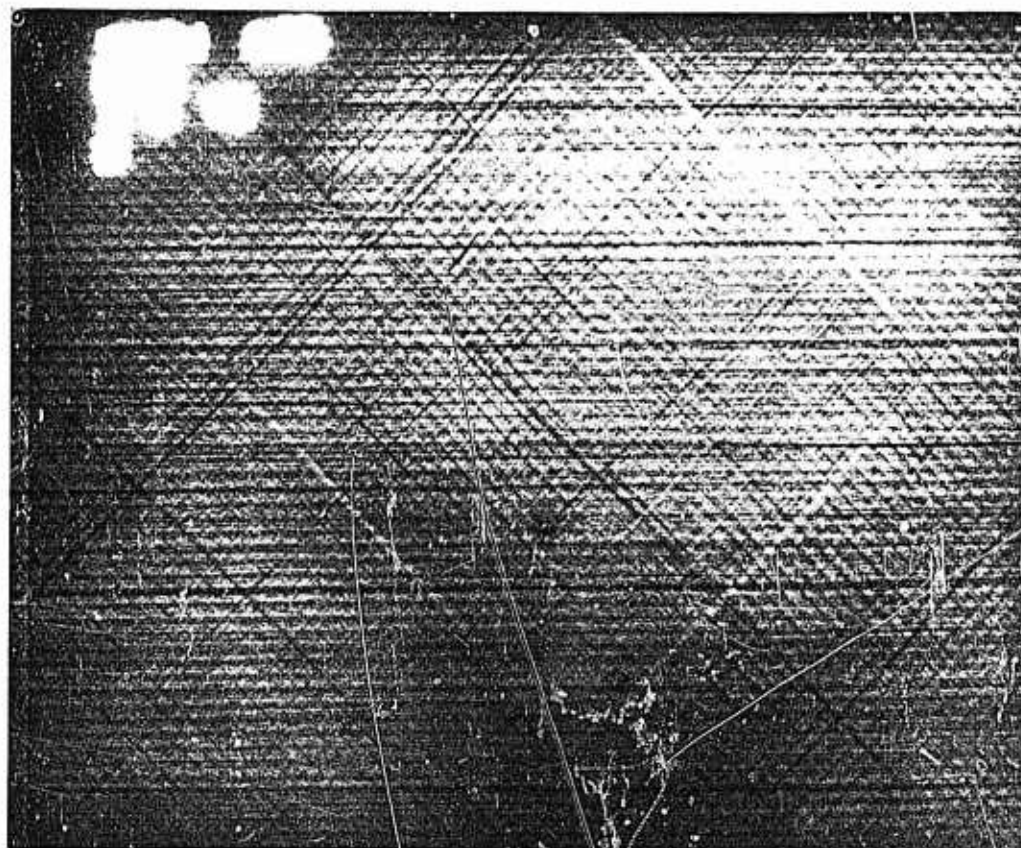
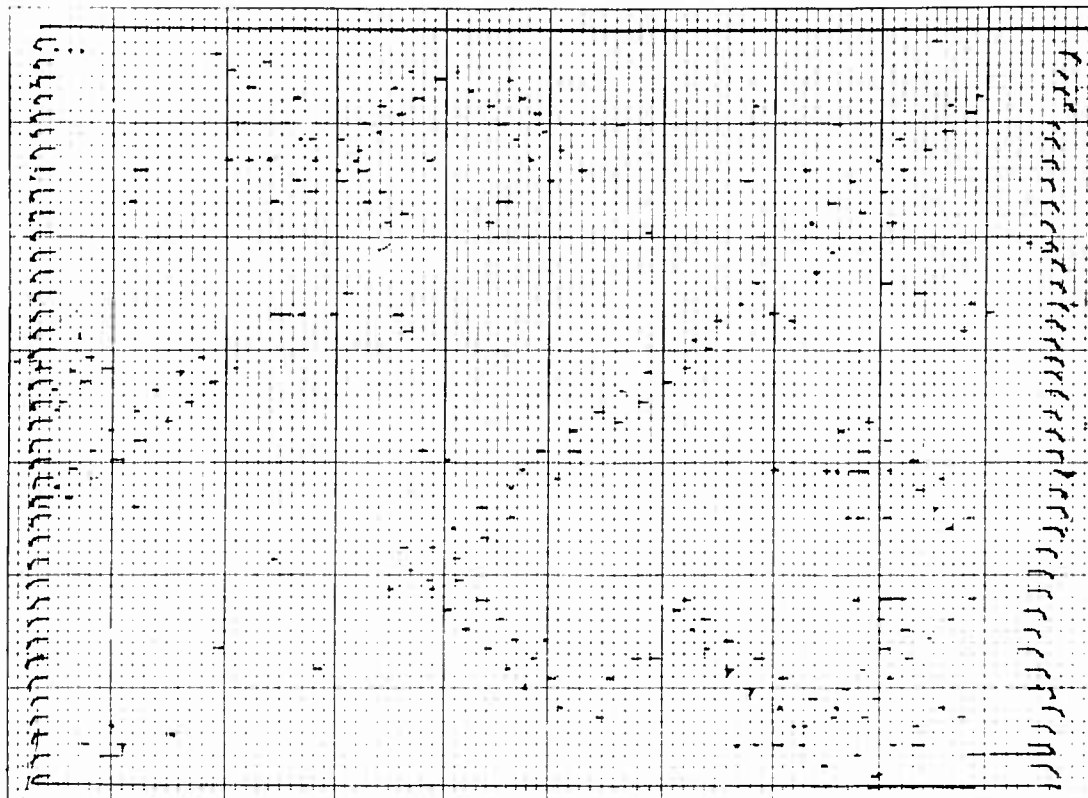


FIGURE D.5 INSPECTION RECORD, B-16

PANE: B-17, 17 ply, 0⁰ ± 4⁰ 4/30/70

4 DB go, 5 DB no go

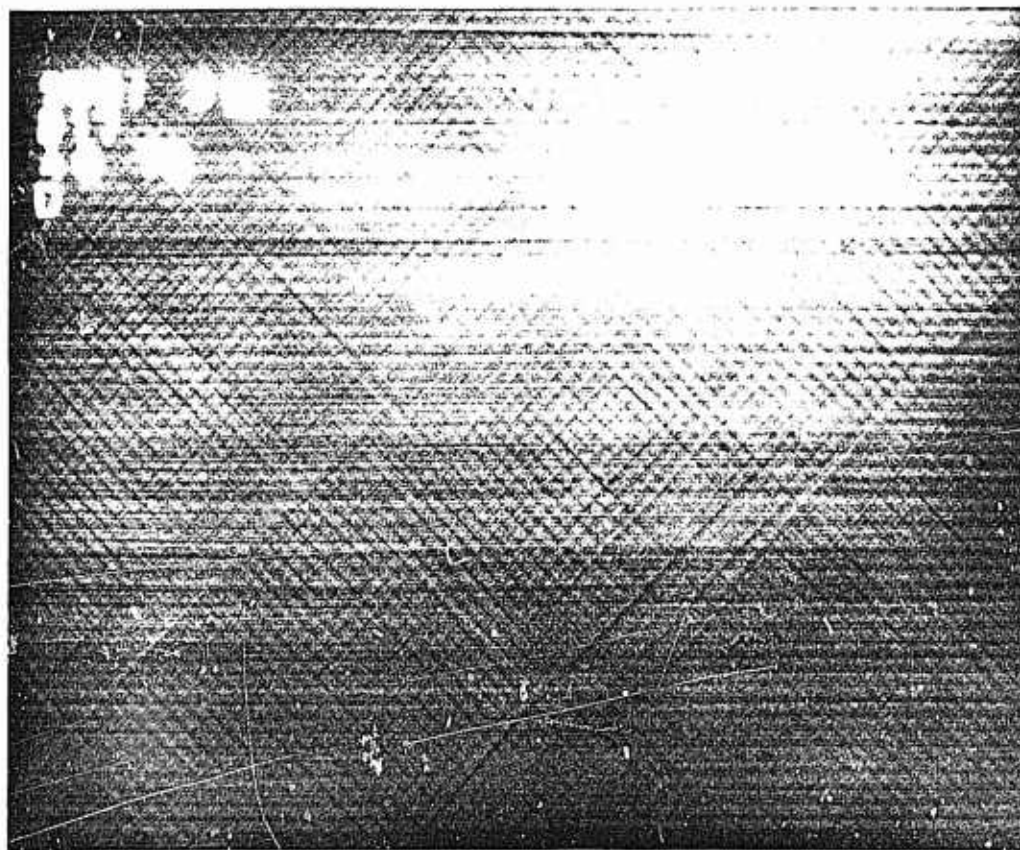
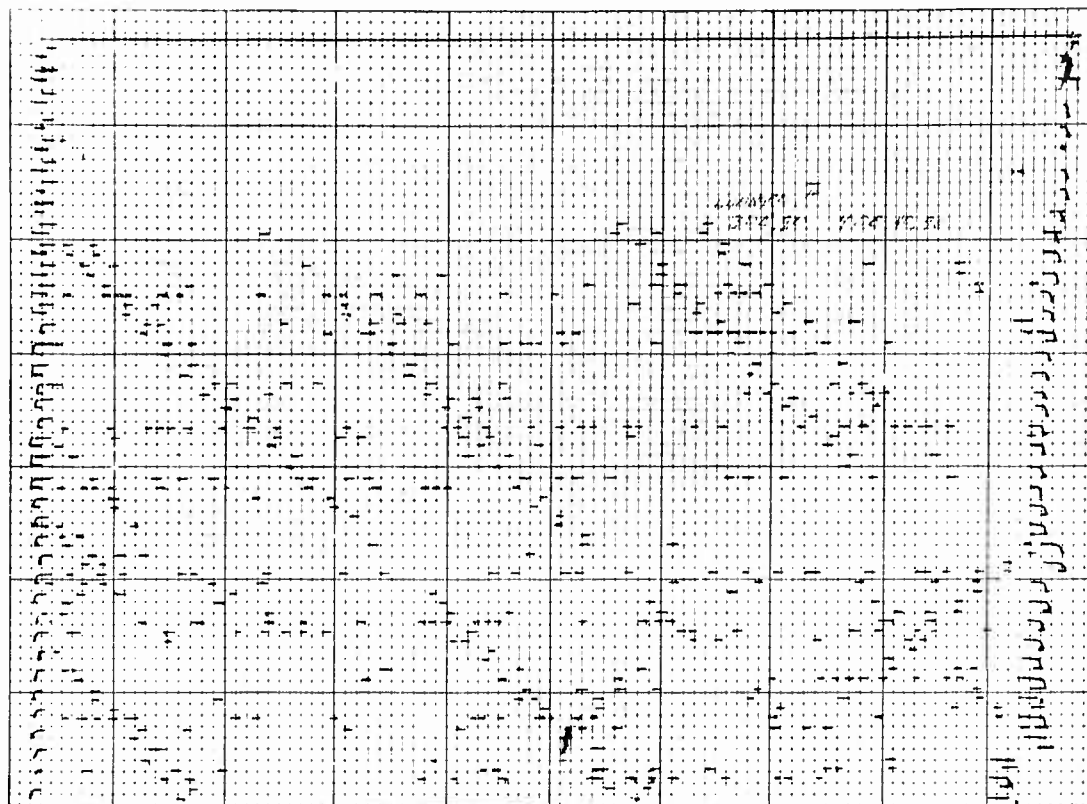
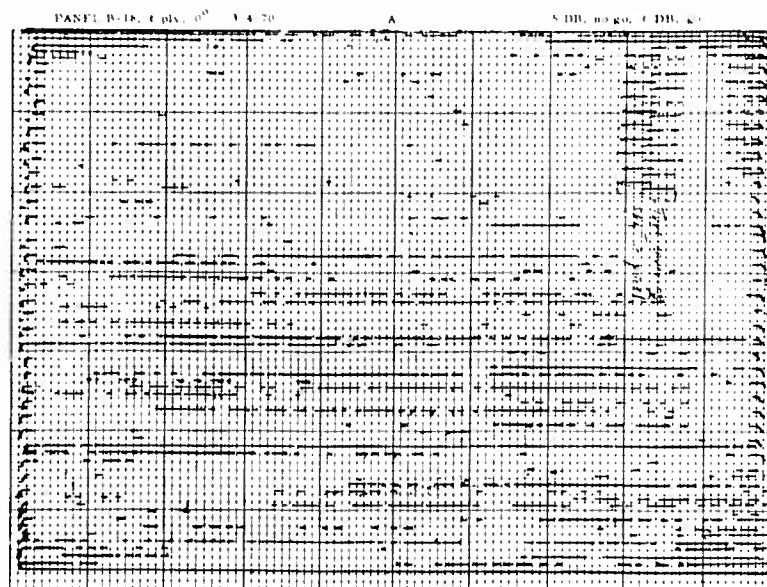


FIGURE D.6 INSPECTION RECORD, B-17



TEST OPERATOR WK
DATE 12/4/70

PANEL NUMBER 1 70

PRINCIPAL FIBER
ORIENTATION
SENSITIVITY SETTING 4 DB



Crack
Crack

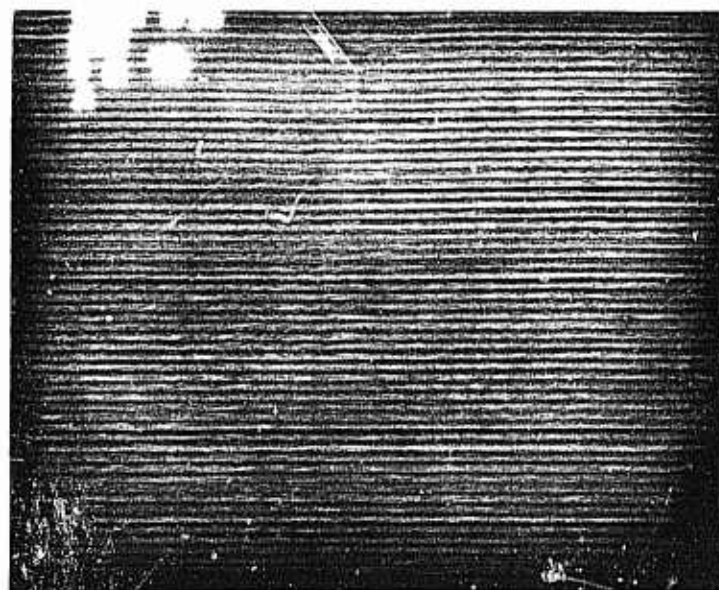
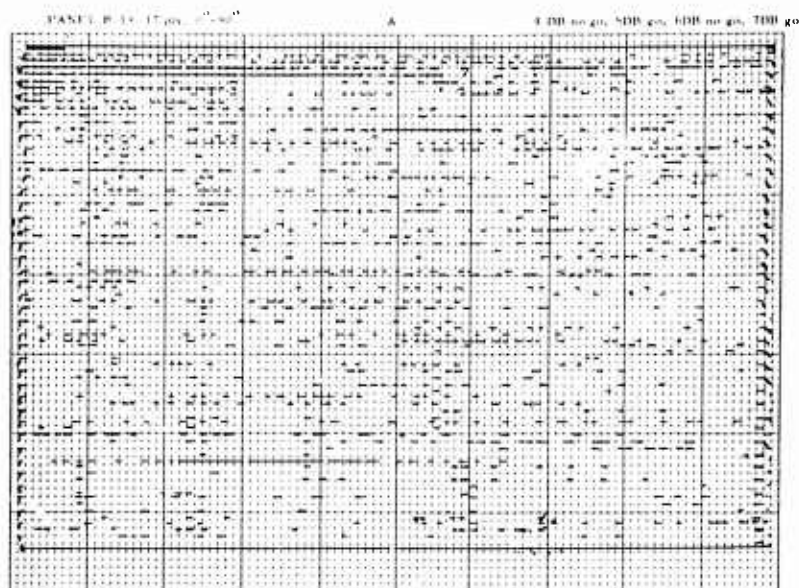


FIGURE D.7 INSPECTION RECORD, B-18



TEST OPERATOR WK
DATE 12/1/70

PANEL NUMBER B-19

PRINCIPAL FIBER
ORIENTATION
SENSITIVITY SETTING 0.0R

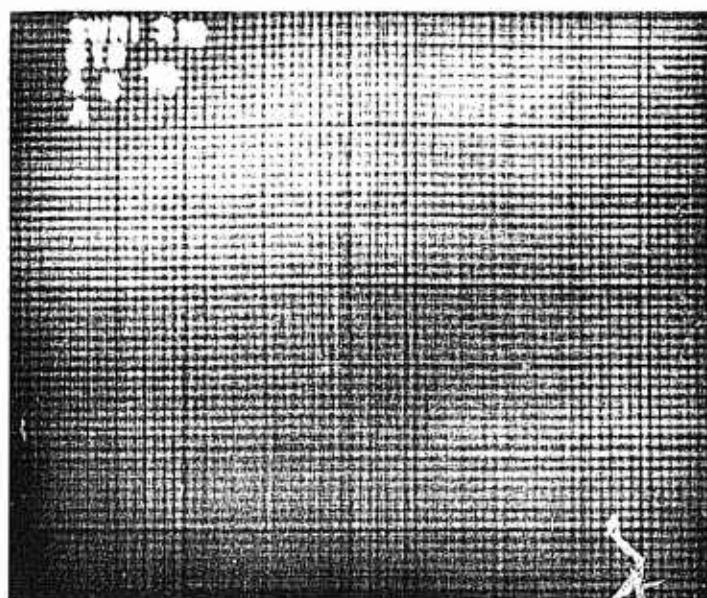
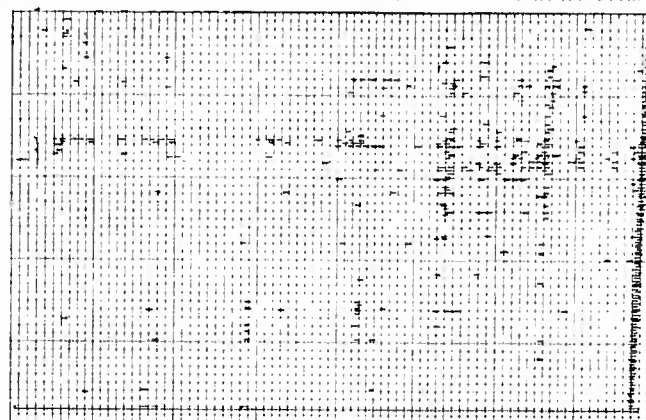
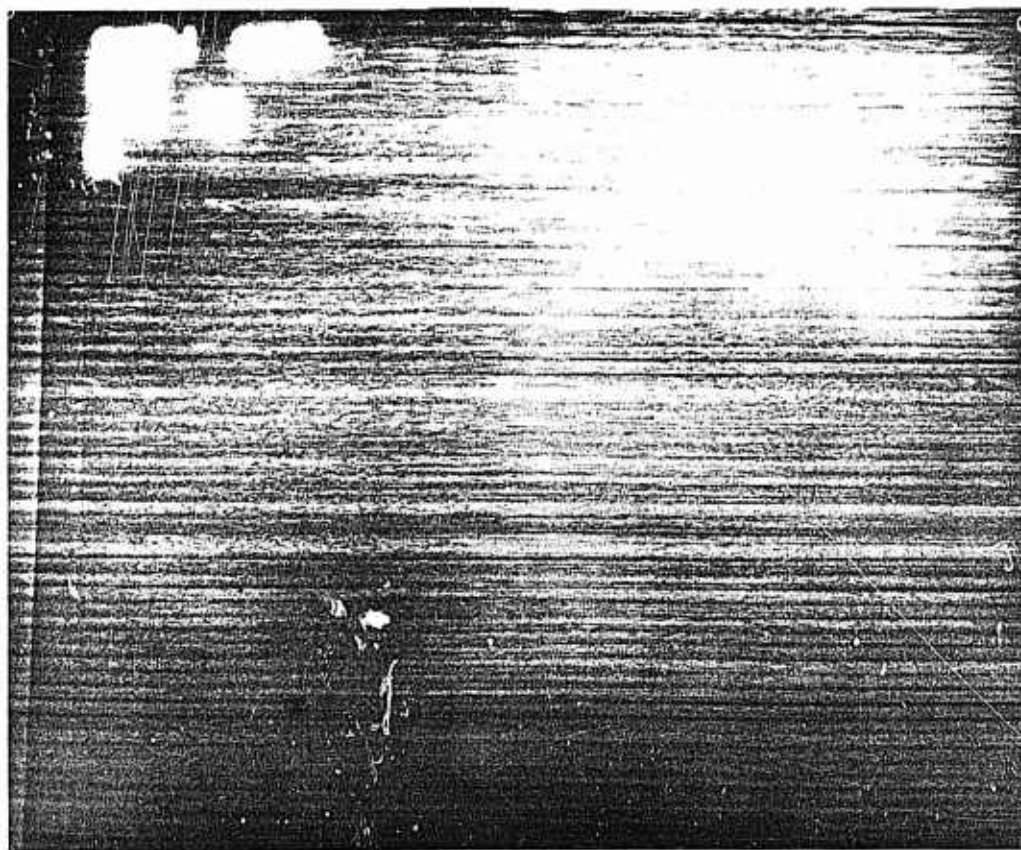
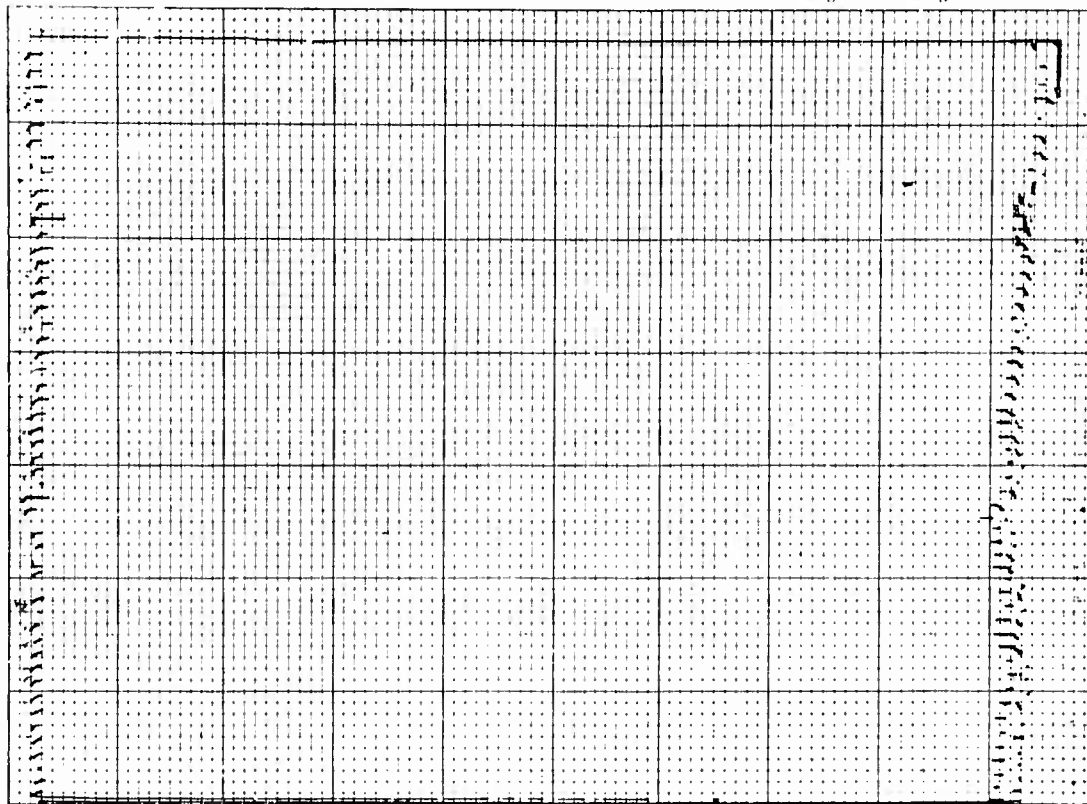


FIGURE D.8 INSPECTION RECORD, B-19

3DB go, 4DB no go



D-10

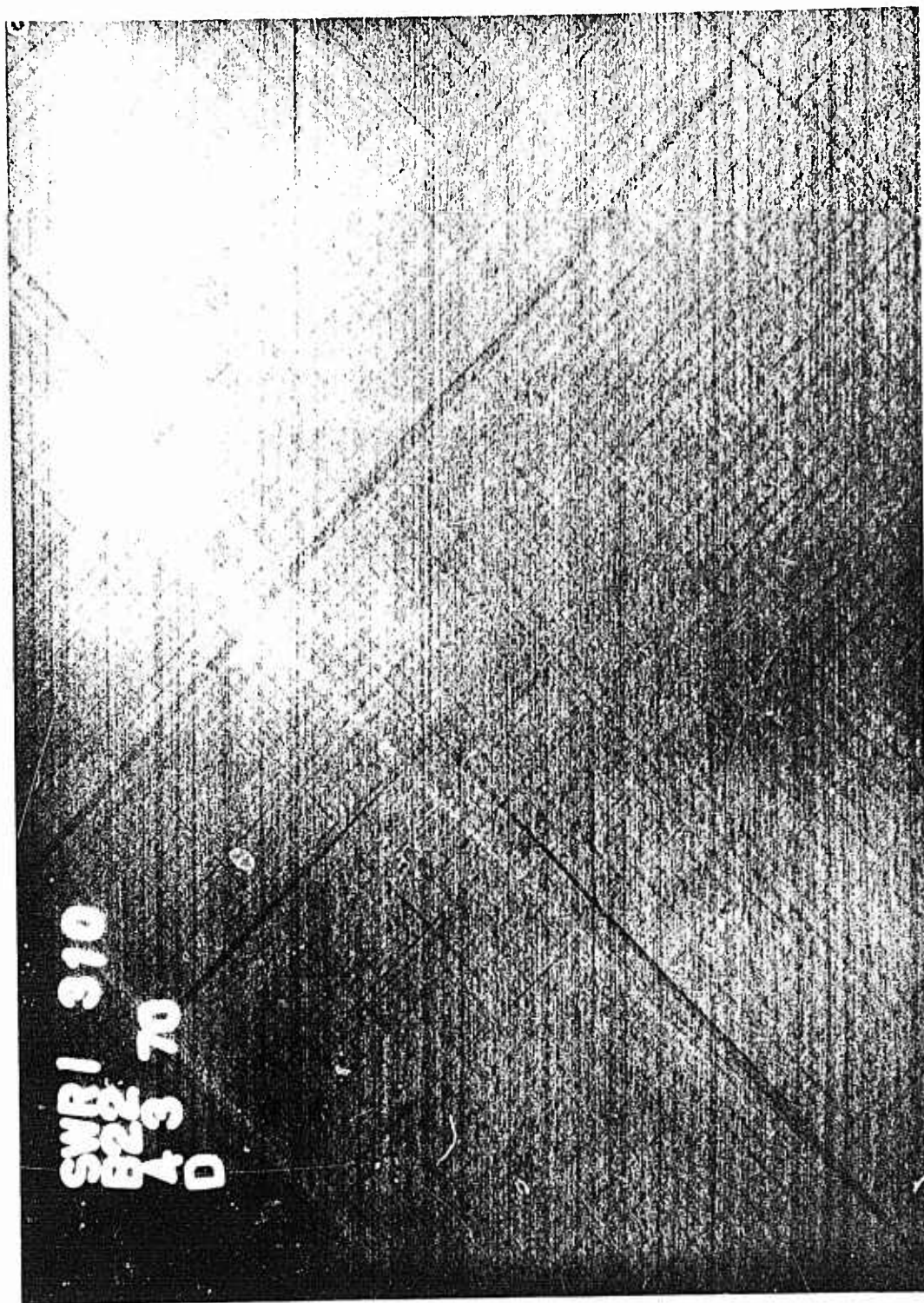


FIGURE D. 10 INSPECTION RECORD, B-22

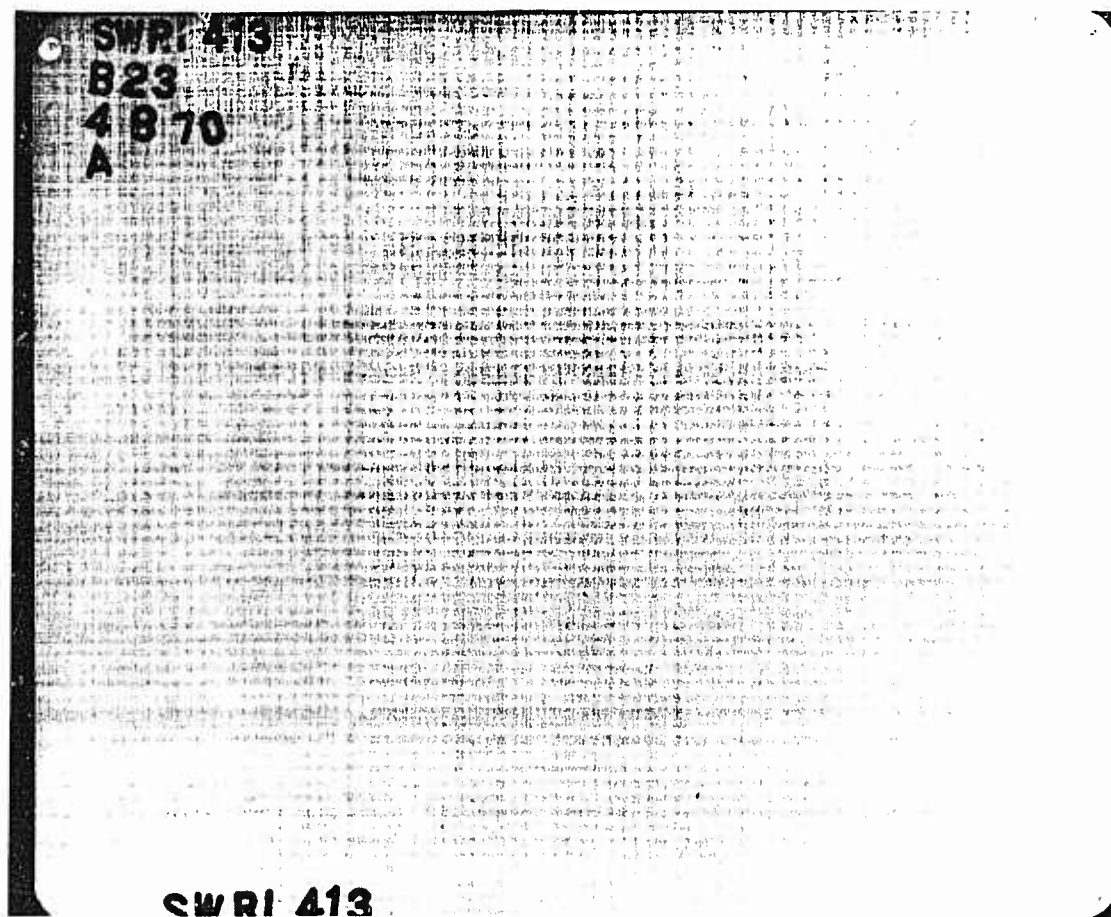
[illegible]

FIGURE D.11 INSPECTION RECORD, B-23

PANEL B-24, 9 ply, 0/±45°

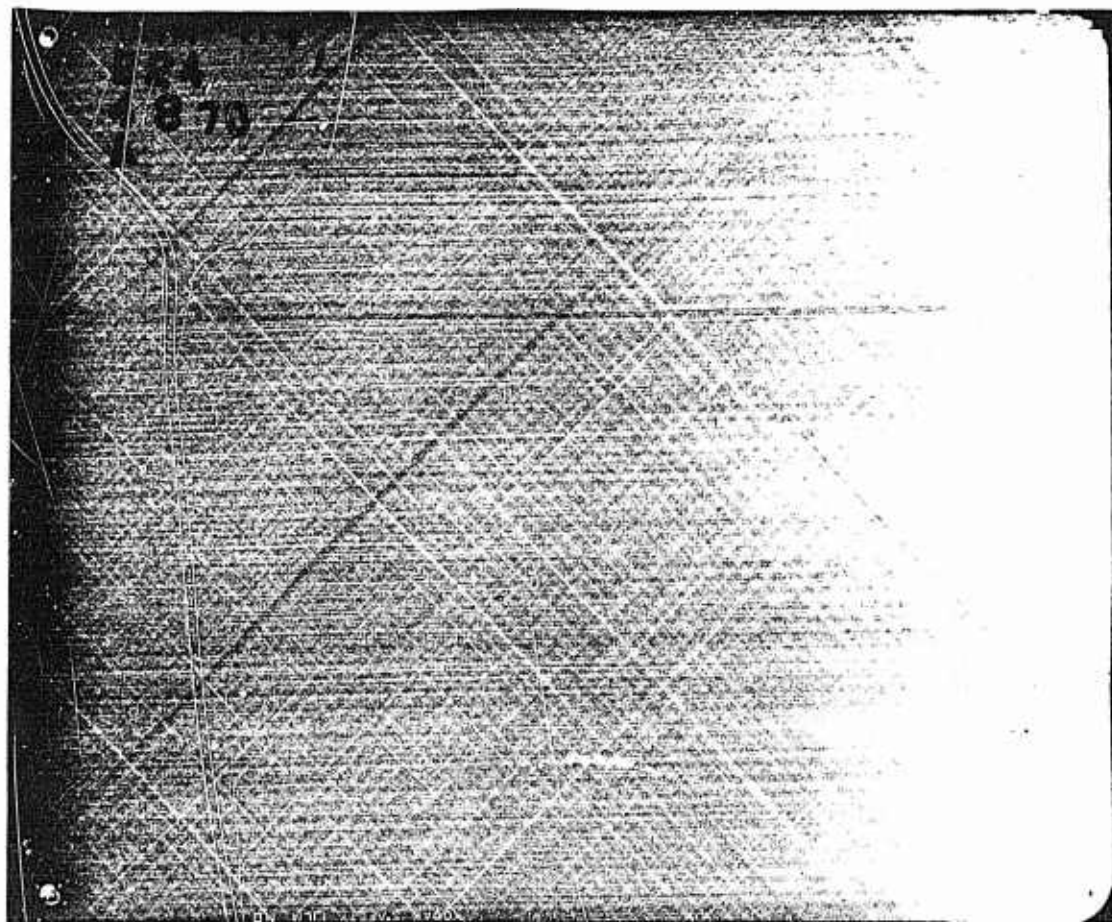
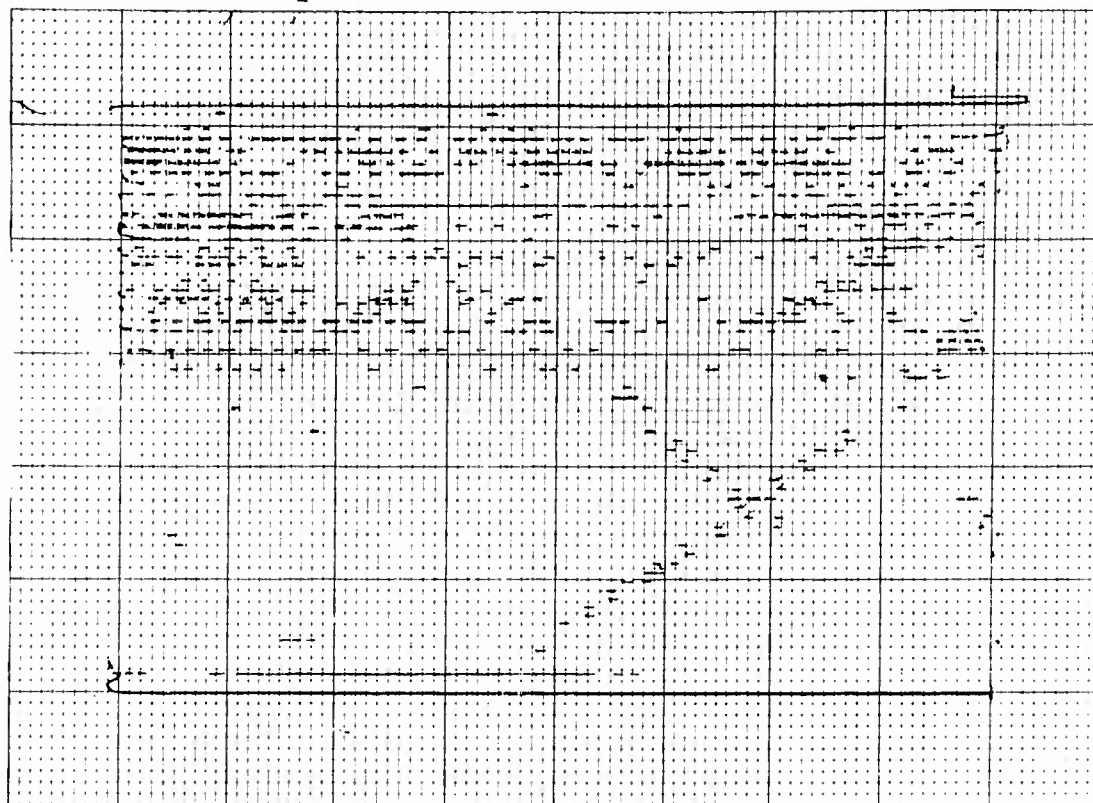


FIGURE D. 12 INSPECTION RECORD, B-24

PANEL B-25, 8 ply 16" x 20"

6 DB below maximum figure

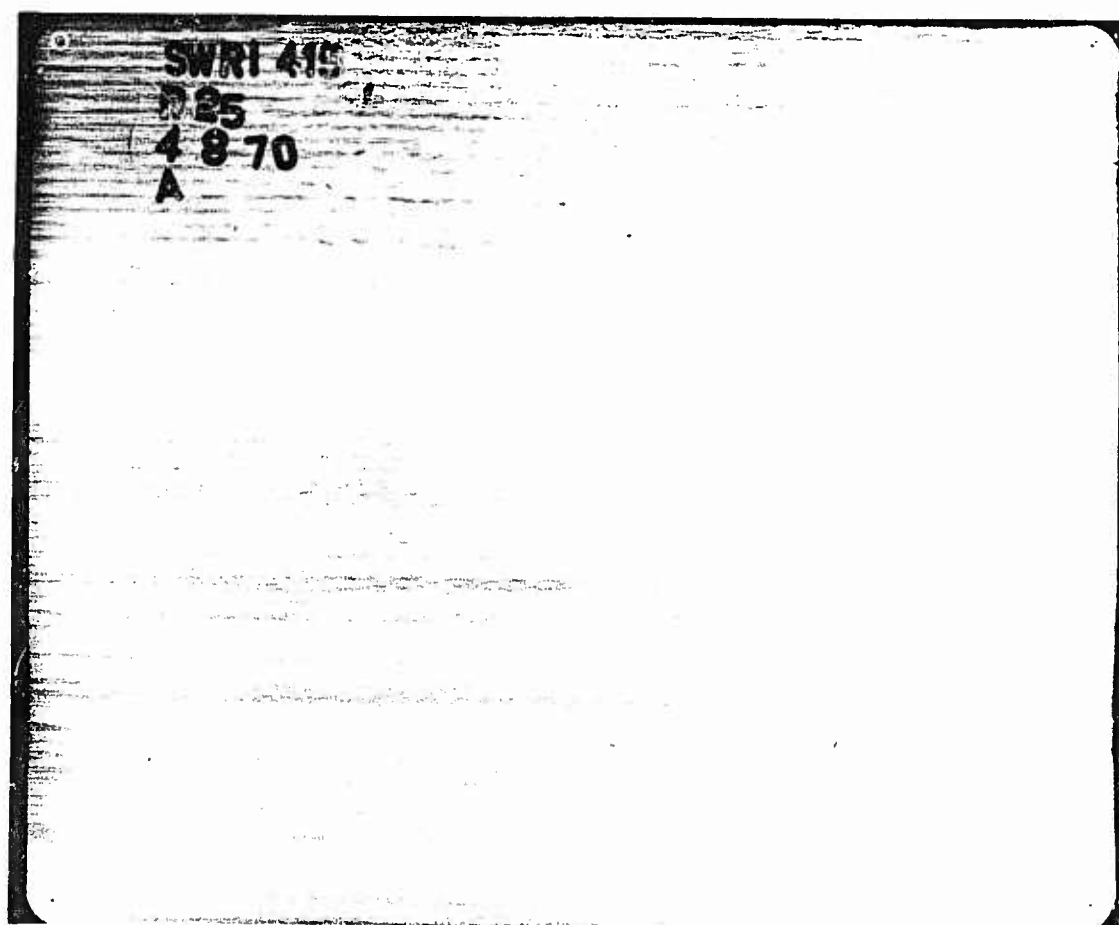
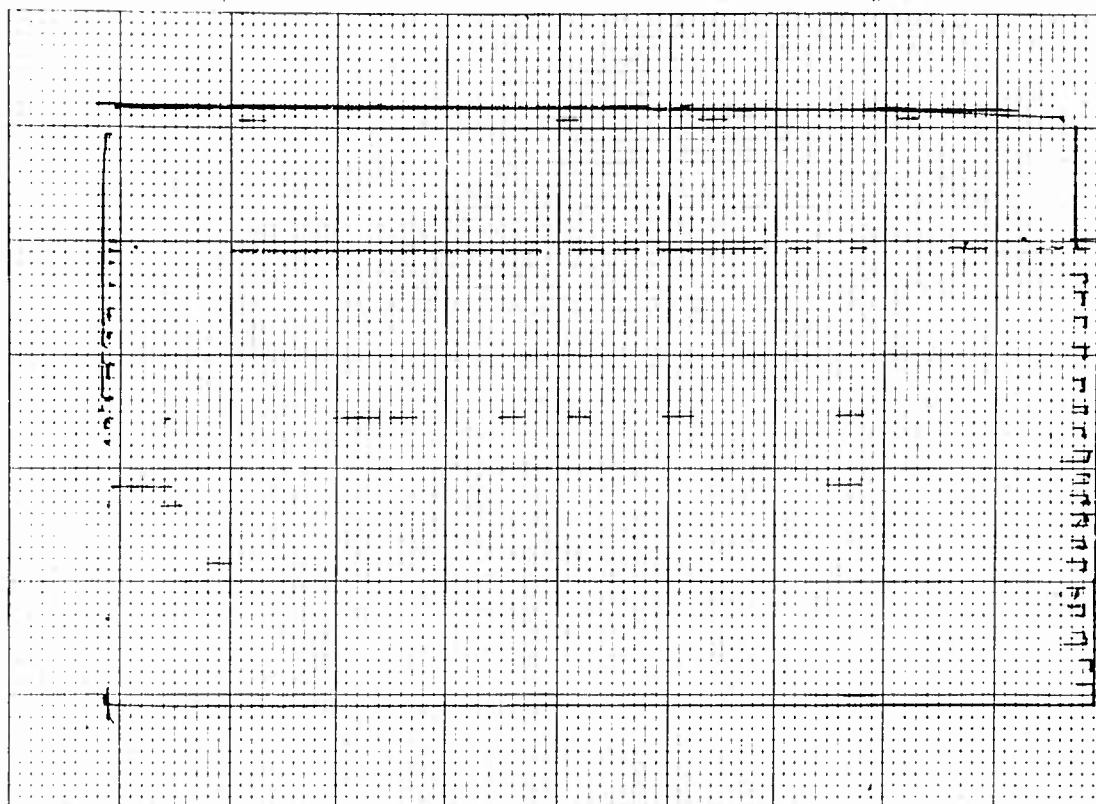


FIGURE D. 13 INSPECTION RECORD, B-25

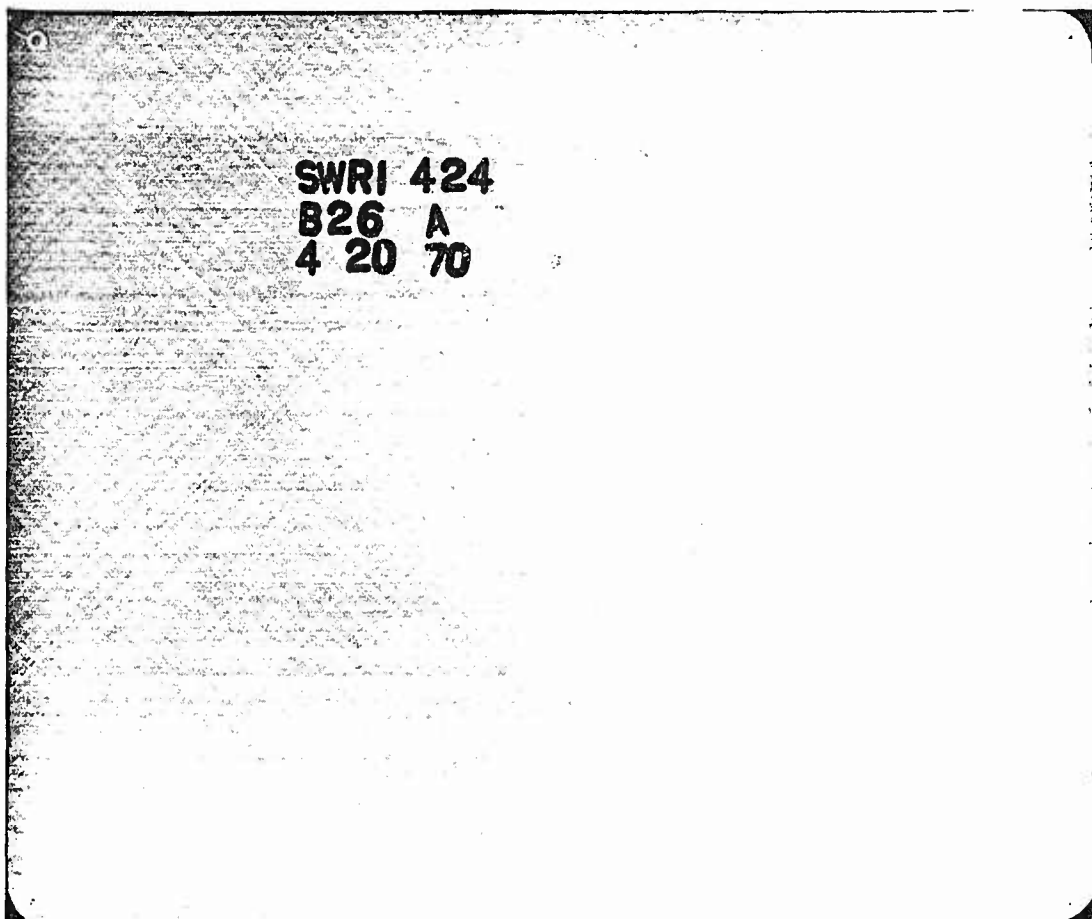
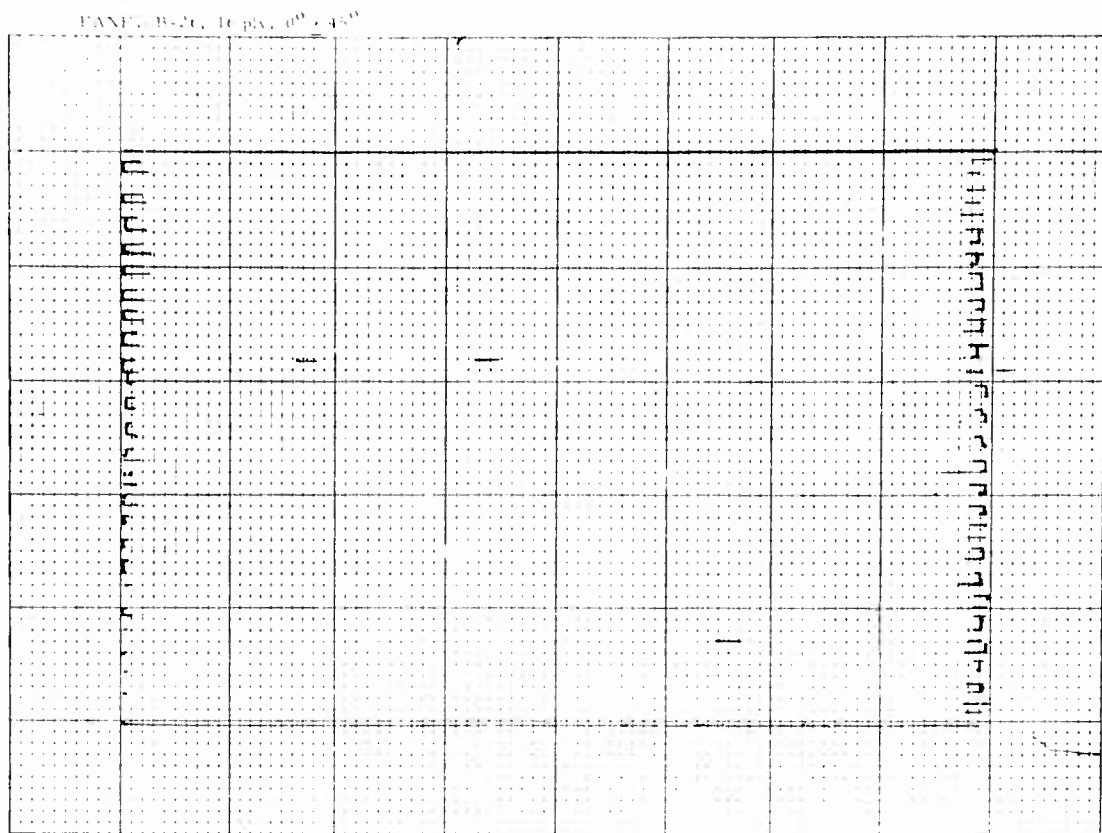


FIGURE D. 14 INSPECTION RECORD, B-26

PAGE B-27, 14 pgs., 45° 10/12/70

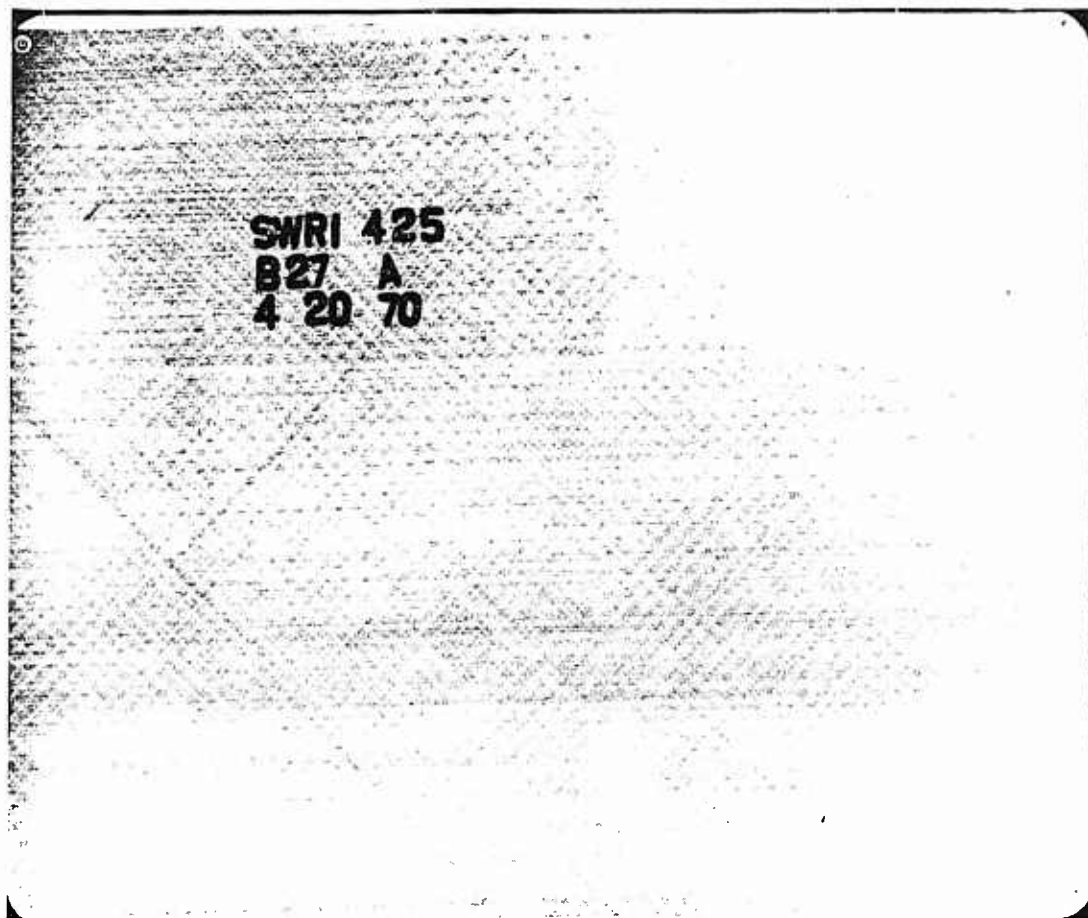
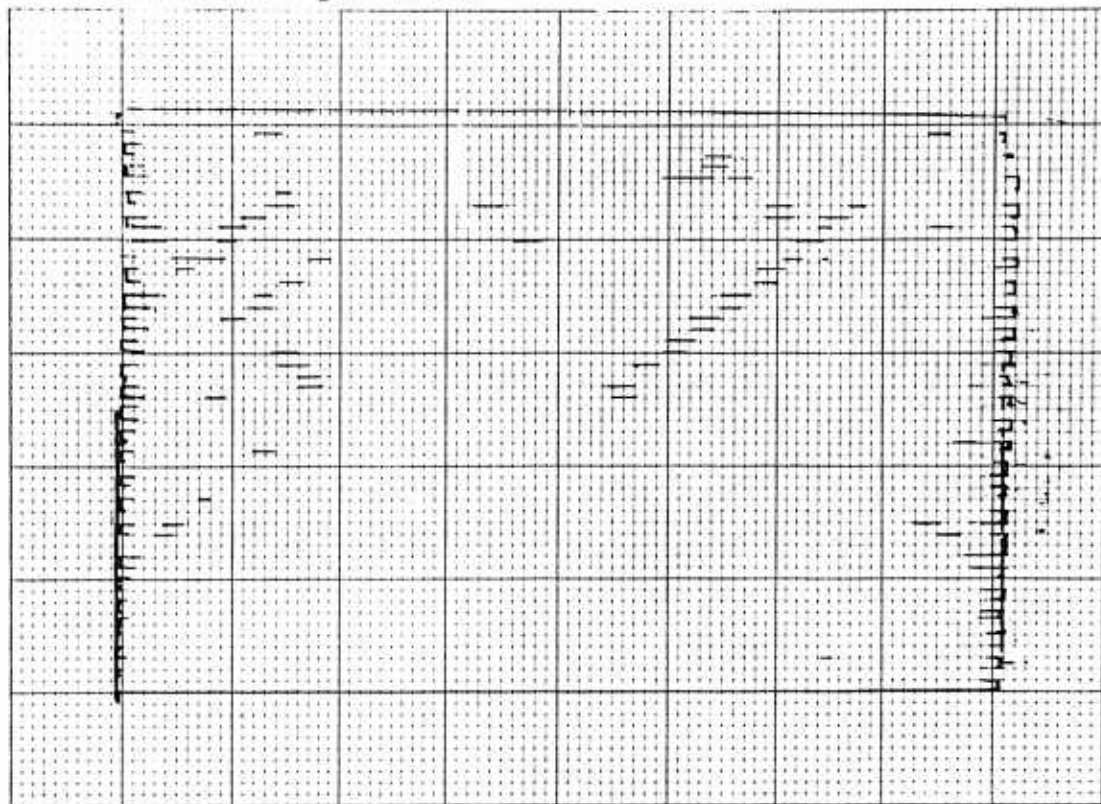


FIGURE D.15 INSPECTION RECORD, B-27

PANEL B-28, 9 ply, 0 + 45° 10/30/70

DB-3

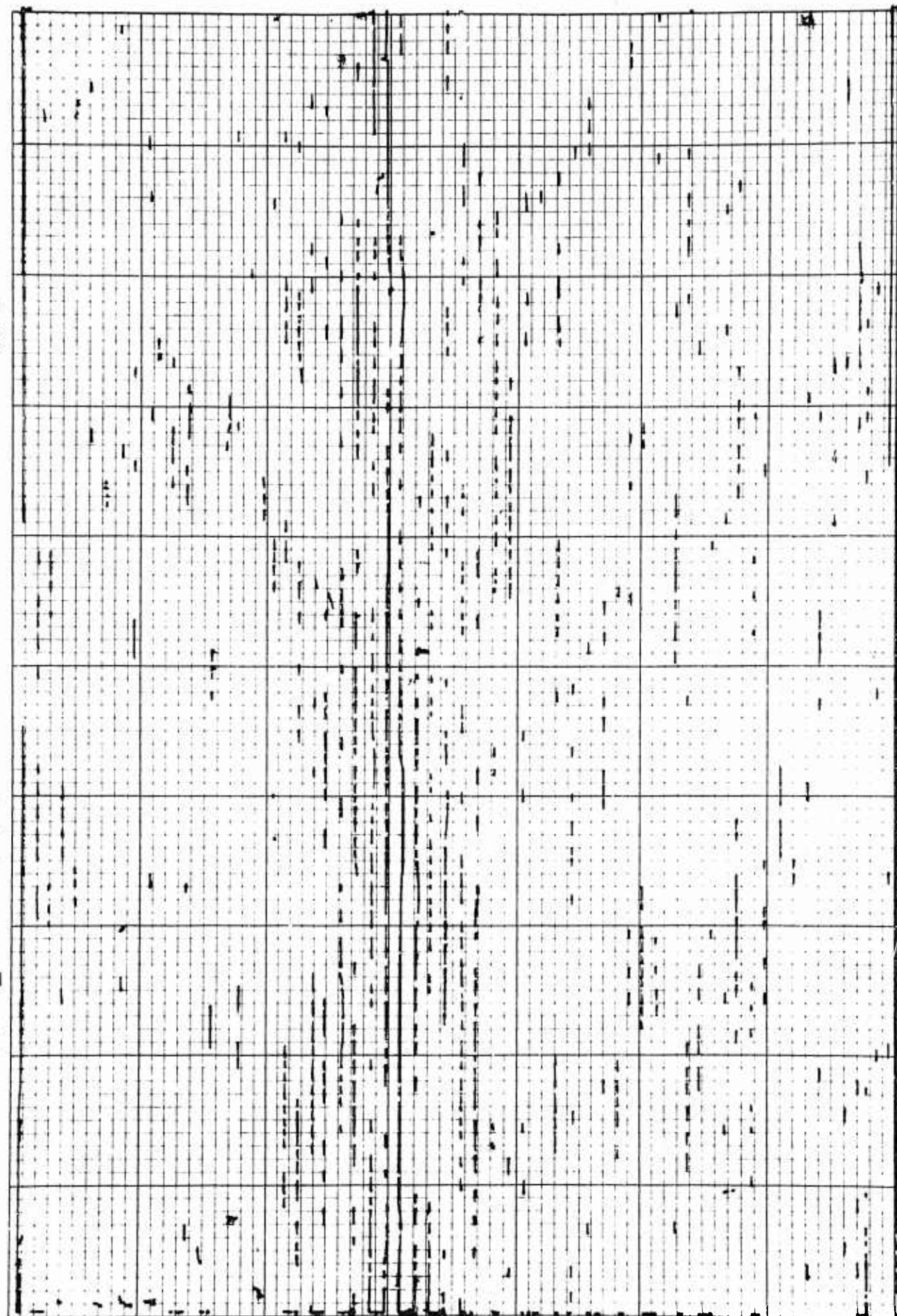


FIGURE D. 16 INSPECTION RECORD, B-28

APPENDIX E

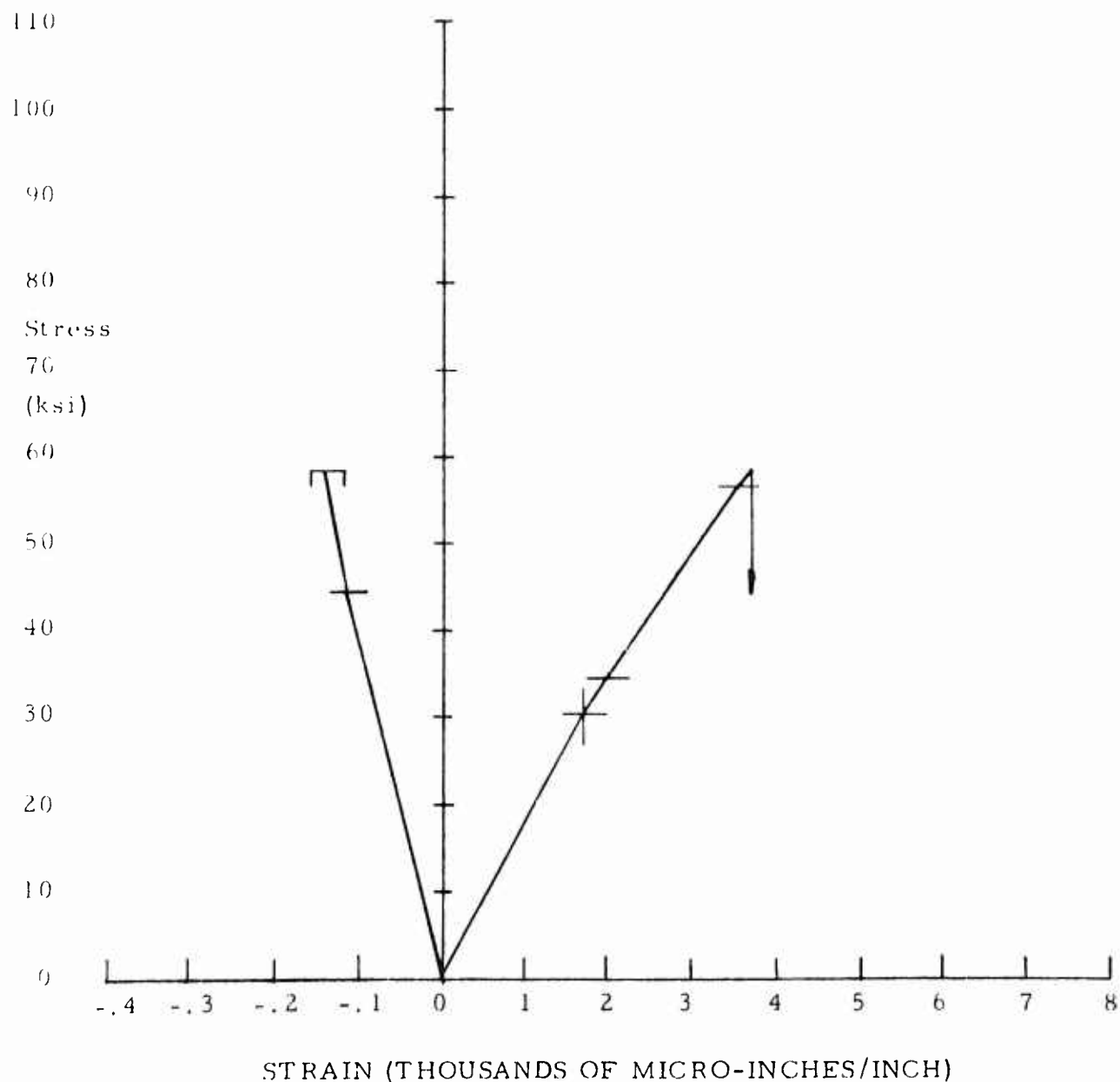
SELECTED TYPICAL ADHEREND MATERIAL TENSILE
STRESS-STRAIN CURVES AND PHOTOMICROGRAPHS

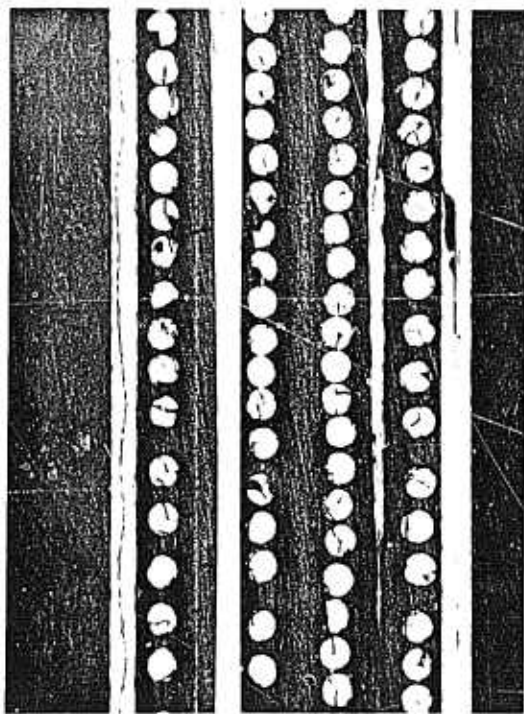
SPECIMEN T-142
(Tension)

$[(0/90)_4/0]_T$

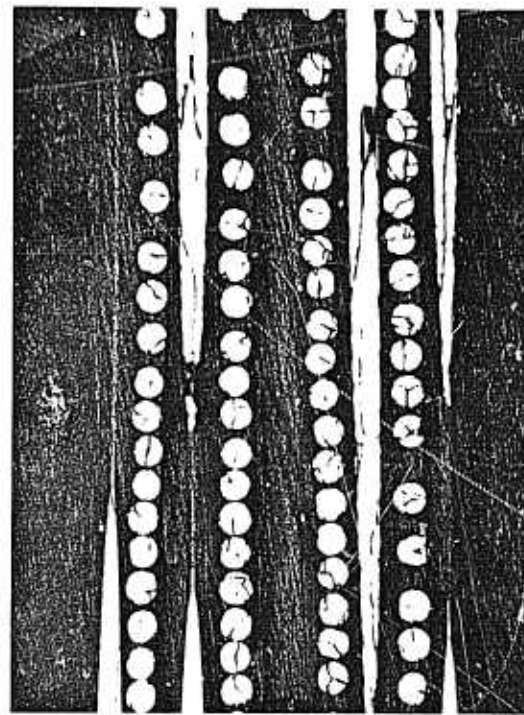
FIGURE E.1
STRESS VS STRAIN

$\sigma_u = 58,454 \text{ psi}$
 $\epsilon_u = 3,692 \times 10^{-6} \text{ in./in.}$
 $\nu_p = 0.0435$
 $\nu_s = 0.0394$
 $\sigma_{pl} = 30,096 \text{ psi}$
 $\epsilon_{pl} = 1,691 \times 10^{-6} \text{ in./in.}$
 $E_p = 17.798 \times 10^6 \text{ psi}$
 $E_s = 14.270 \times 10^6 \text{ psi}$

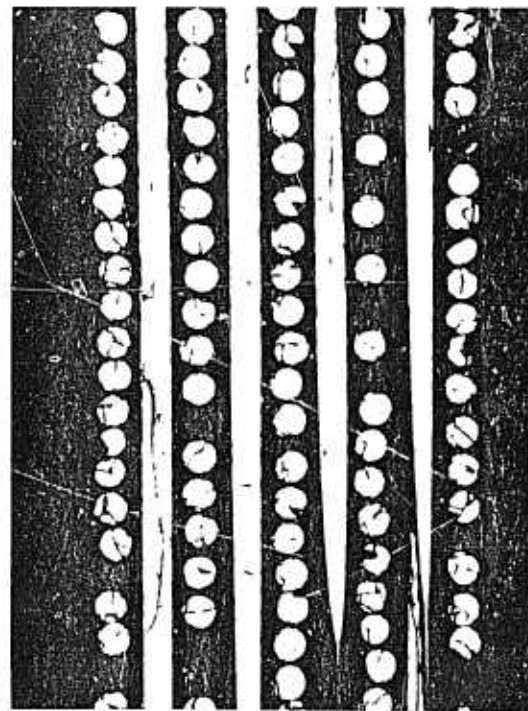




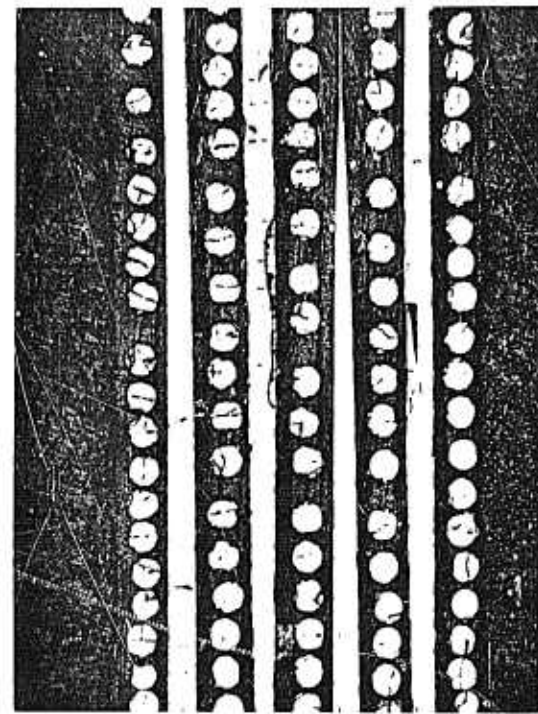
(a) 50X 0° Photo No. 15305



(b) 50X 0° Photo No. 15298



(c) 50X 90° Photo No. 15259



(d) 50X 90° Photo No. 15306

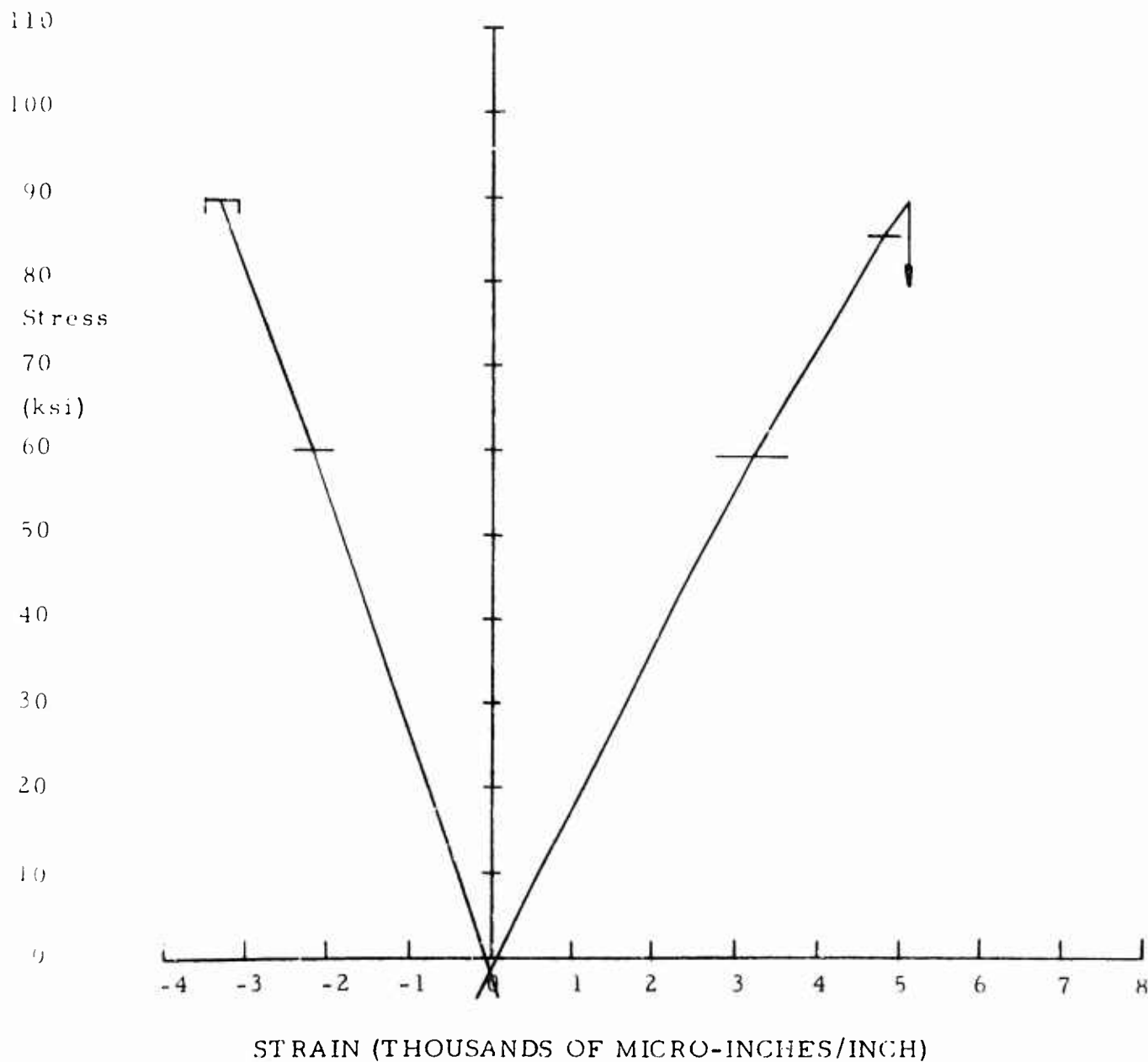
FIGURE E.2 PANEL B-14 PHOTOMICROGRAPHS

SPECIMEN T-163
(Tension)

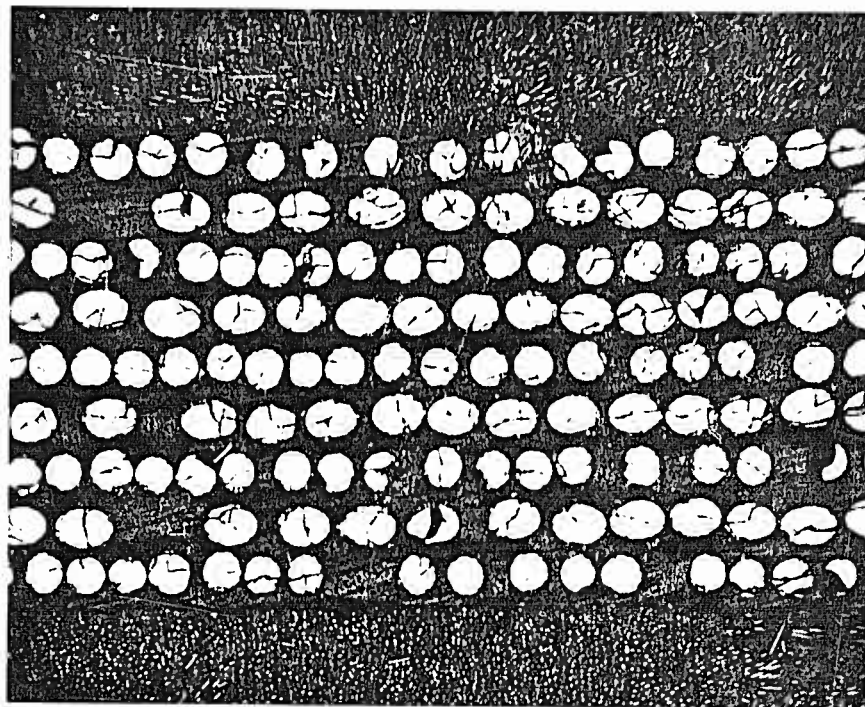
$[0/+45/0/-45/\bar{0}]_s$

FIGURE E.3
STRESS VS STRAIN

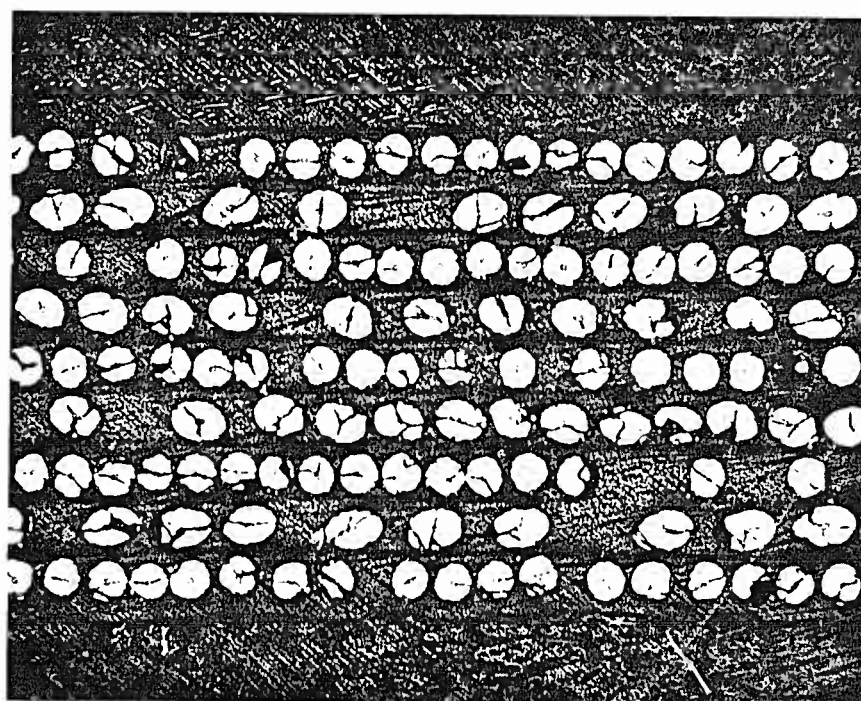
$\sigma_u = 89,287 (91,087)* \text{ psi}$
 $\epsilon_u = 5,090 \times 10^{-6} \text{ in./in.}$
 $\nu_p = 0.6561$
 $\nu_s = 0.6700$
 $\sigma_{pl} = 59,426 (61,226)* \text{ psi}$
 $\epsilon_{pl} = 3,209 \times 10^{-6} \text{ in./in.}$
 $E_F = 18.518 \times 10^6 (19.079)* \text{ psi}$
 $E_s = 16.673 \times 10^6 (17.009)* \text{ psi}$



*1bid



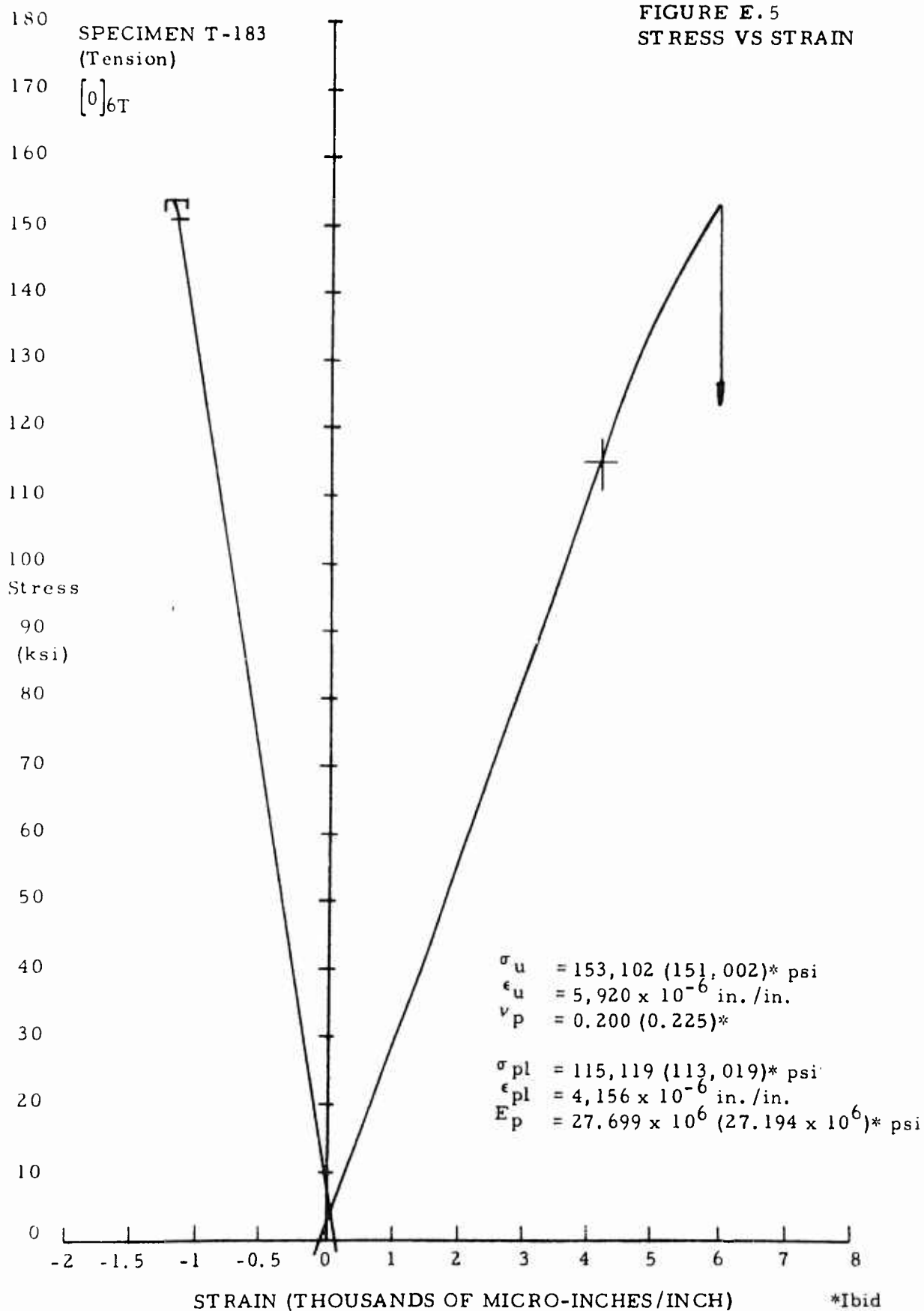
(a) 50X 90° Photo No. 15303



(b) 50X 90° Photo No. 15260

SPECIMEN T-183
(Tension)
[0]₆T

FIGURE E. 5
STRESS VS STRAIN



SPECIMEN T-223

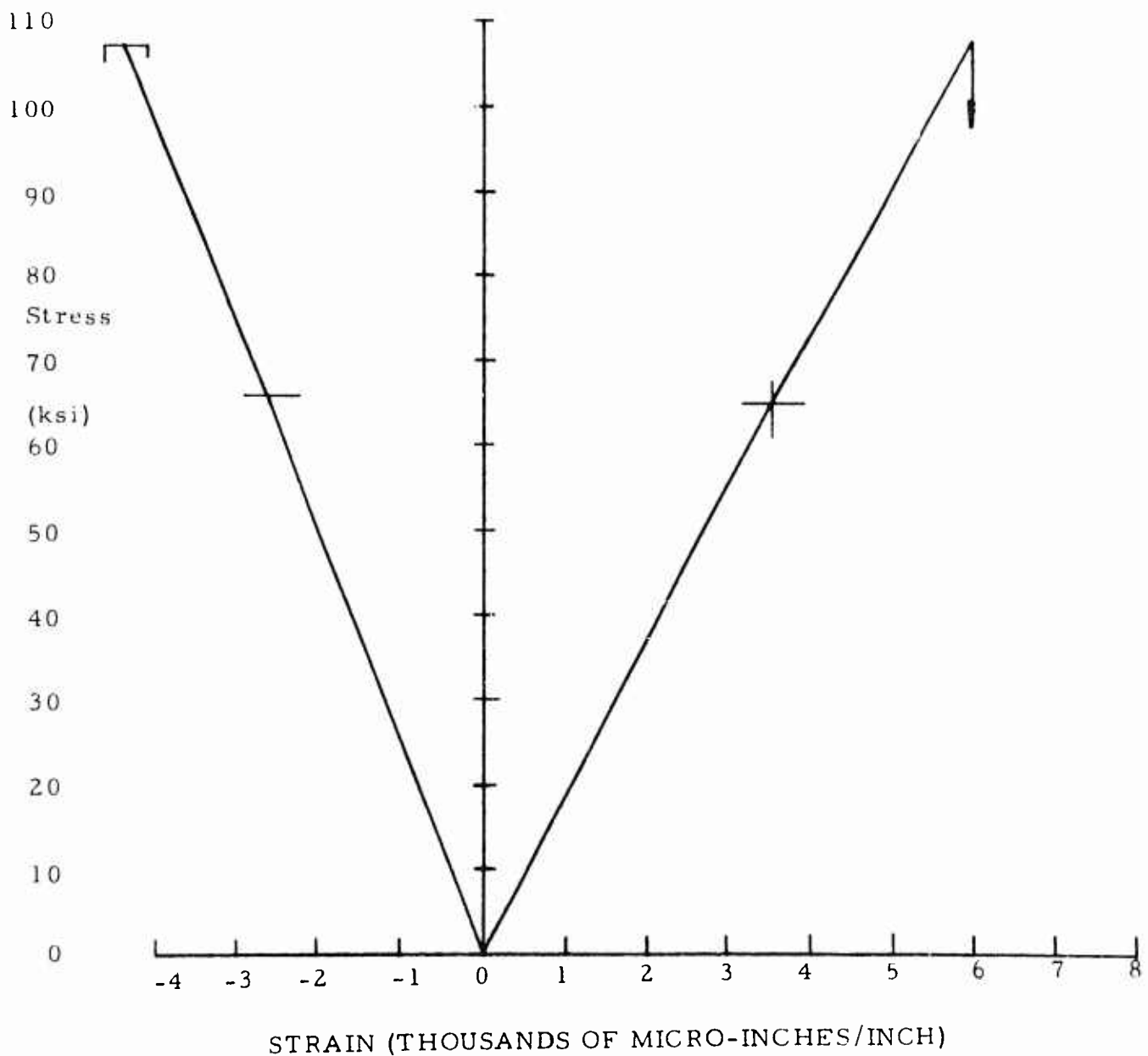
(Tension)

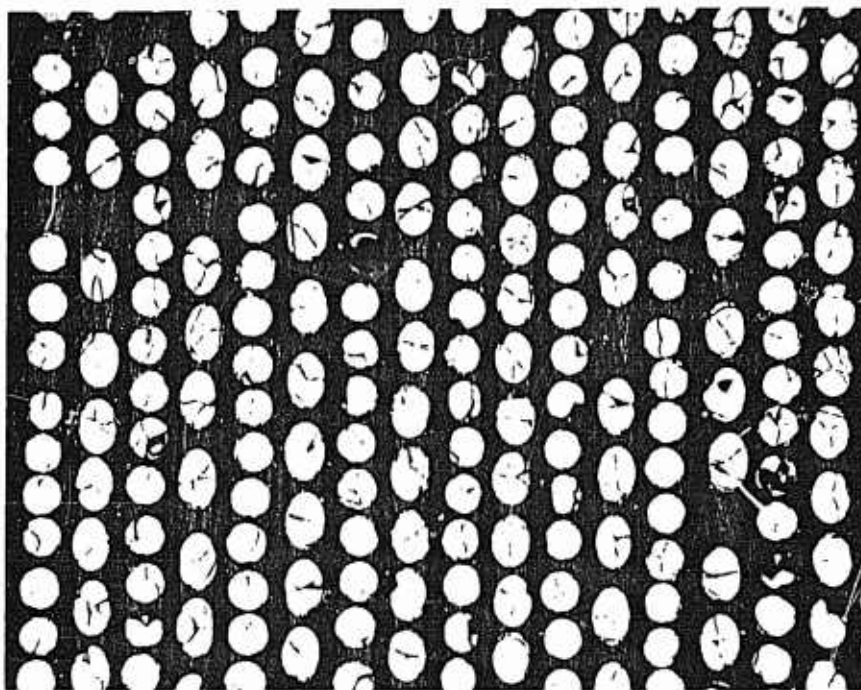
$\left[(0/+45/0/-45)_Q/\bar{0}\right]_s$

FIGURE E.6

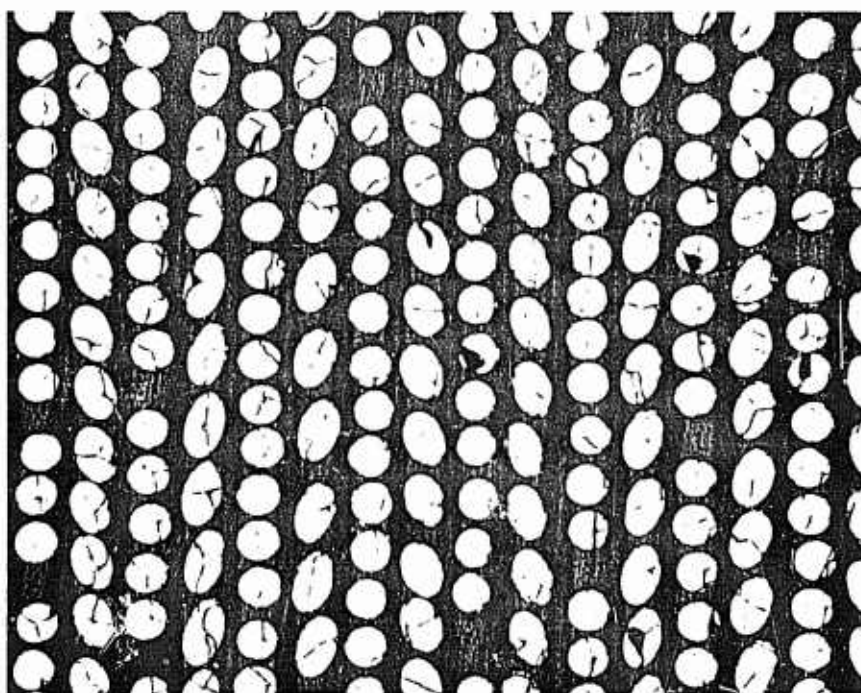
STRESS VS STRAIN

$\sigma_u = 107,150 \text{ psi}$
 $\epsilon_u = 5,954 \times 10^{-6} \text{ in./in.}$
 $\nu_p = 0.7200$
 $\nu_s = 0.7344$
 $\sigma_{pl} = 64,875 \text{ psi}$
 $\epsilon_{pl} = 3,525 \times 10^{-6} \text{ in./in.}$
 $E_p = 18.404 \times 10^6 \text{ psi}$
 $E_s = 17.399 \times 10^6 \text{ psi}$





(a) 50X 90° Photo No. 15308



(b) 50X 90° Photo No. 15296

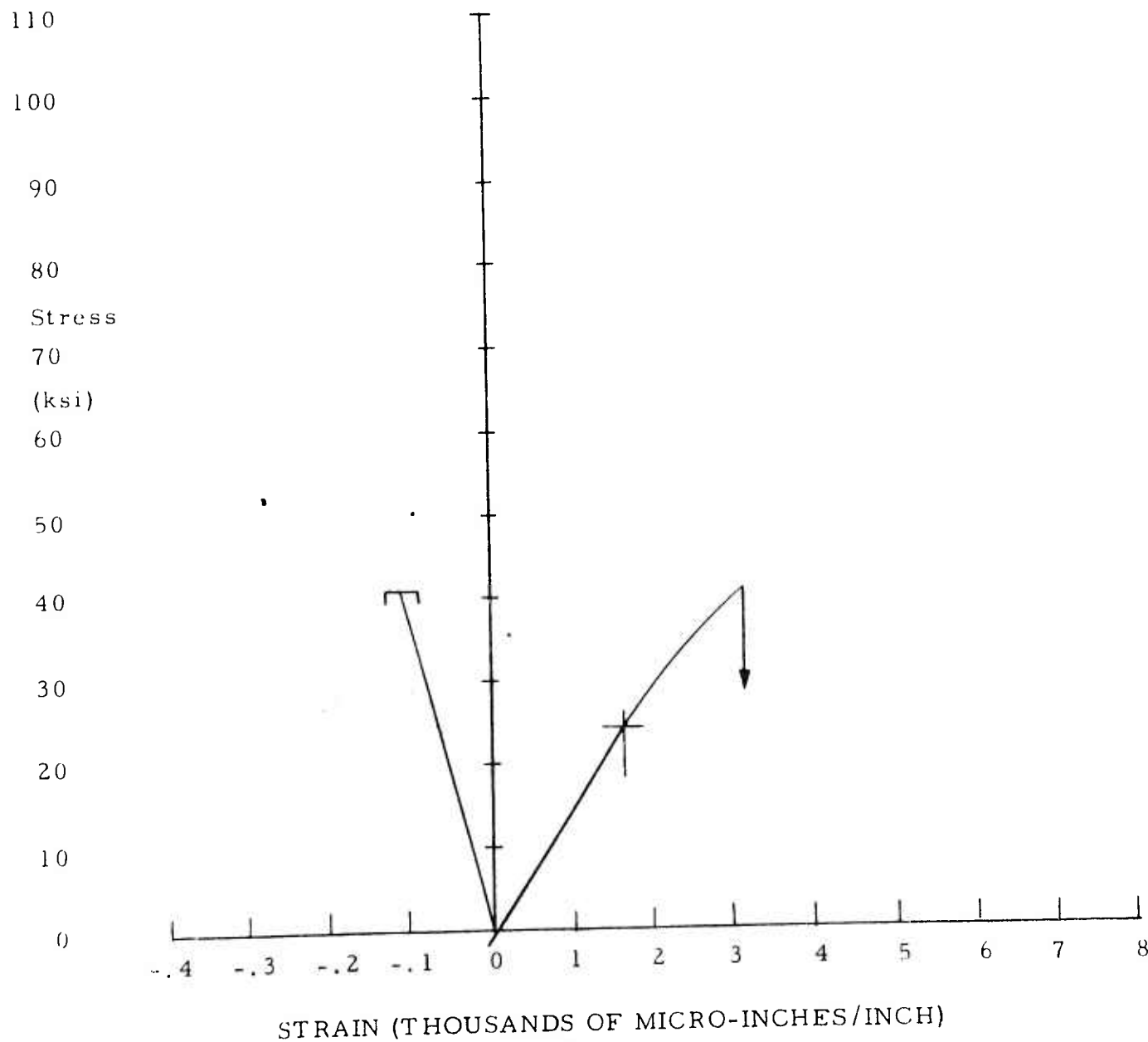
SPECIMEN T-233
(Tension)

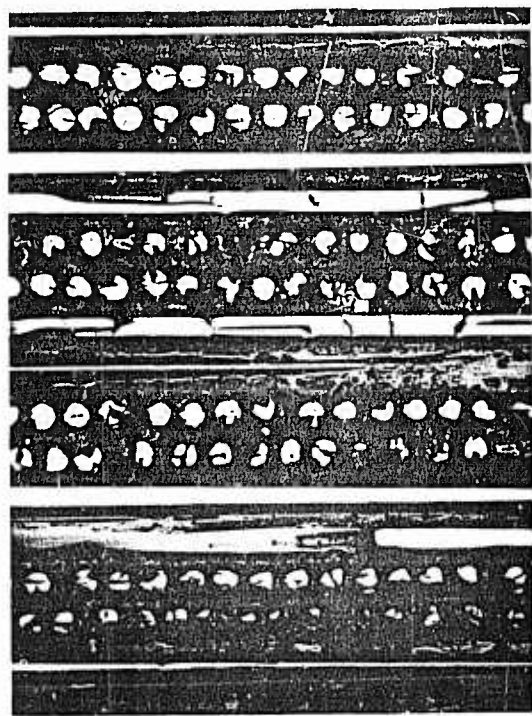
$[0/90_2/0]_{4T}$

FIGURE E.8
STRESS VS STRAIN

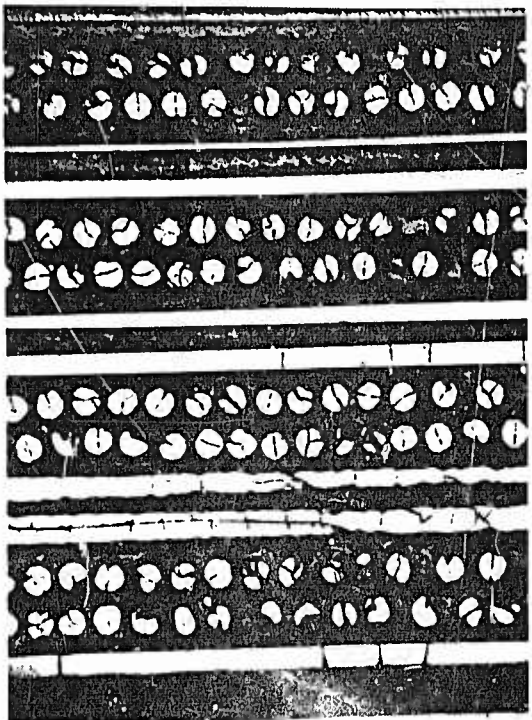
$$\begin{aligned}\sigma_u &= 40,872 (41,672)* \text{ psi} \\ \epsilon_u &= 3,200 \times 10^{-6} \text{ in./in.} \\ \nu &= 0.0377 (0.0400)*\end{aligned}$$

$$\begin{aligned}\sigma_{pl} &= 24,183 (24,983)* \text{ psi} \\ \epsilon_{pl} &= 1,634 \times 10^{-6} \text{ in./in.} \\ E &= 14.800 \times 10^6 (15.289 \times 10^6)* \text{ psi}\end{aligned}$$

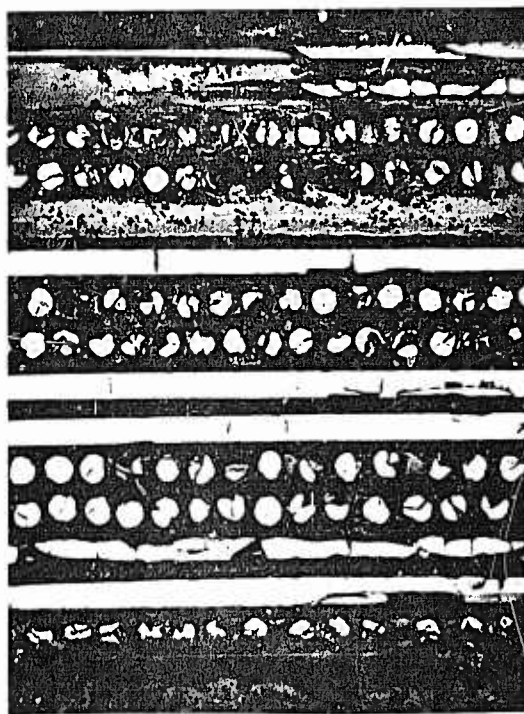




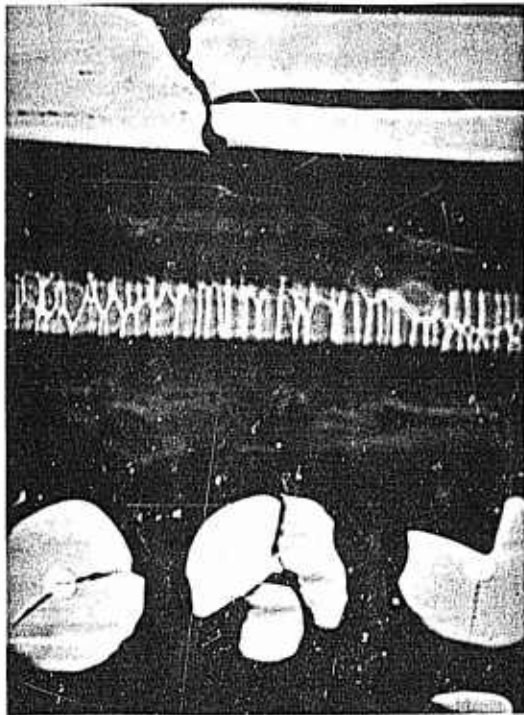
(a) 50X 0° Photo No. 14860



(b) 50X 0° Photo No. 14988



(c) 50X 90° Photo No. 14879

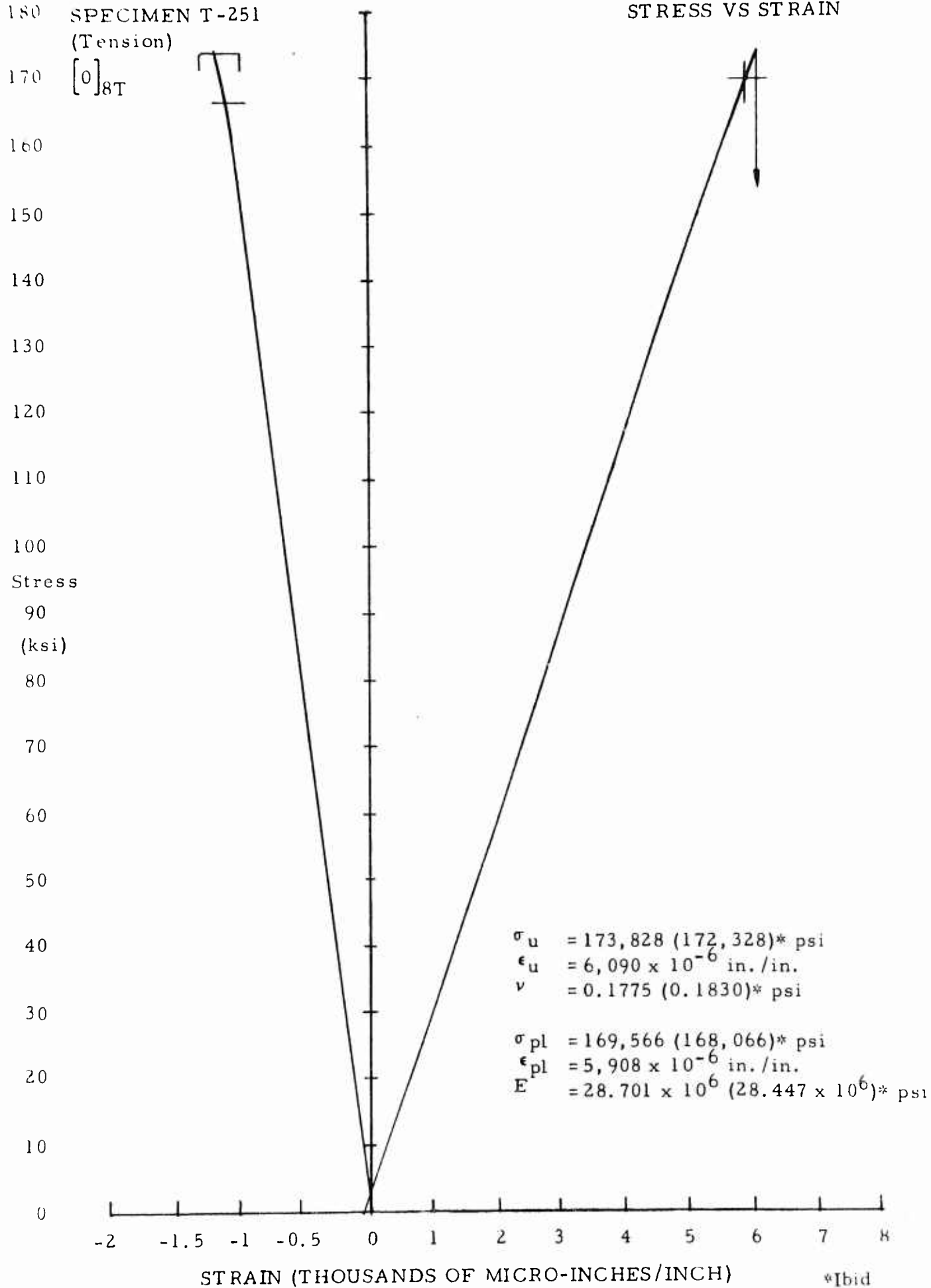


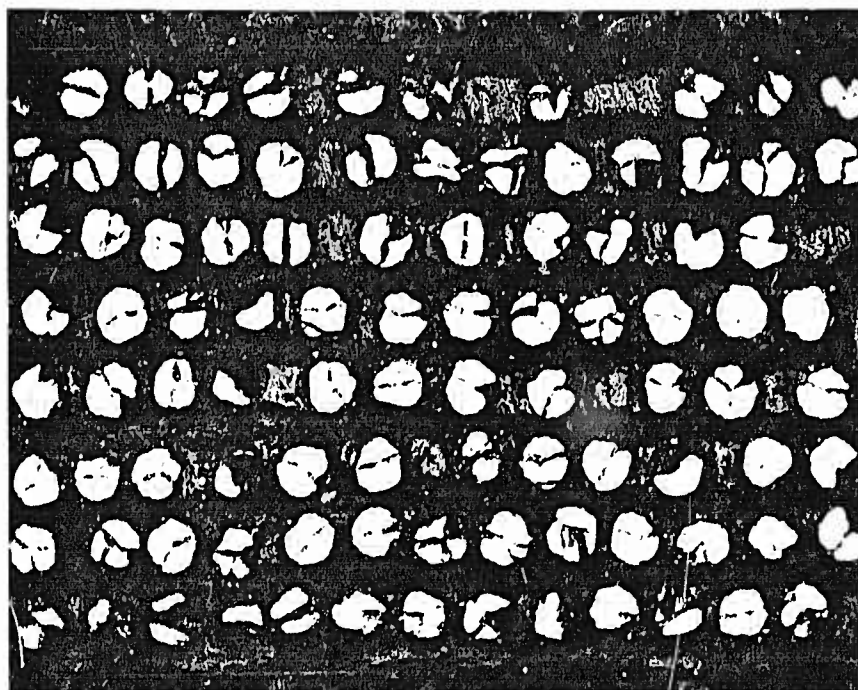
(d) 300X 0° Photo No. 14861

FIGURE E. 9 PANEL B-23 PHOTO MICROGRAPHS

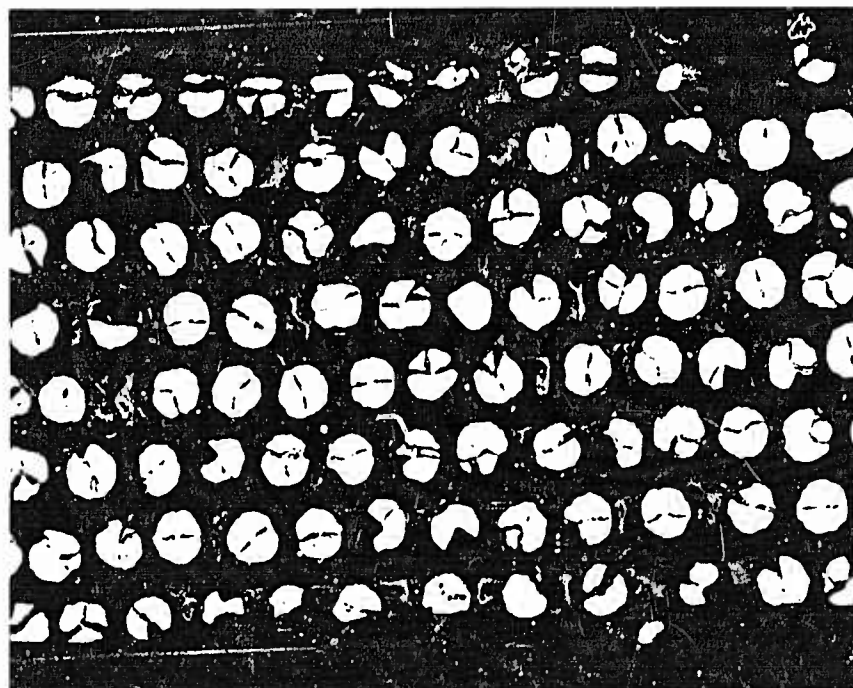
FIGURE E. 10
STRESS VS STRAIN

SPECIMEN T-251
(Tension)
[0]_{8T}





(a) 75X 90° Photo No. 14881



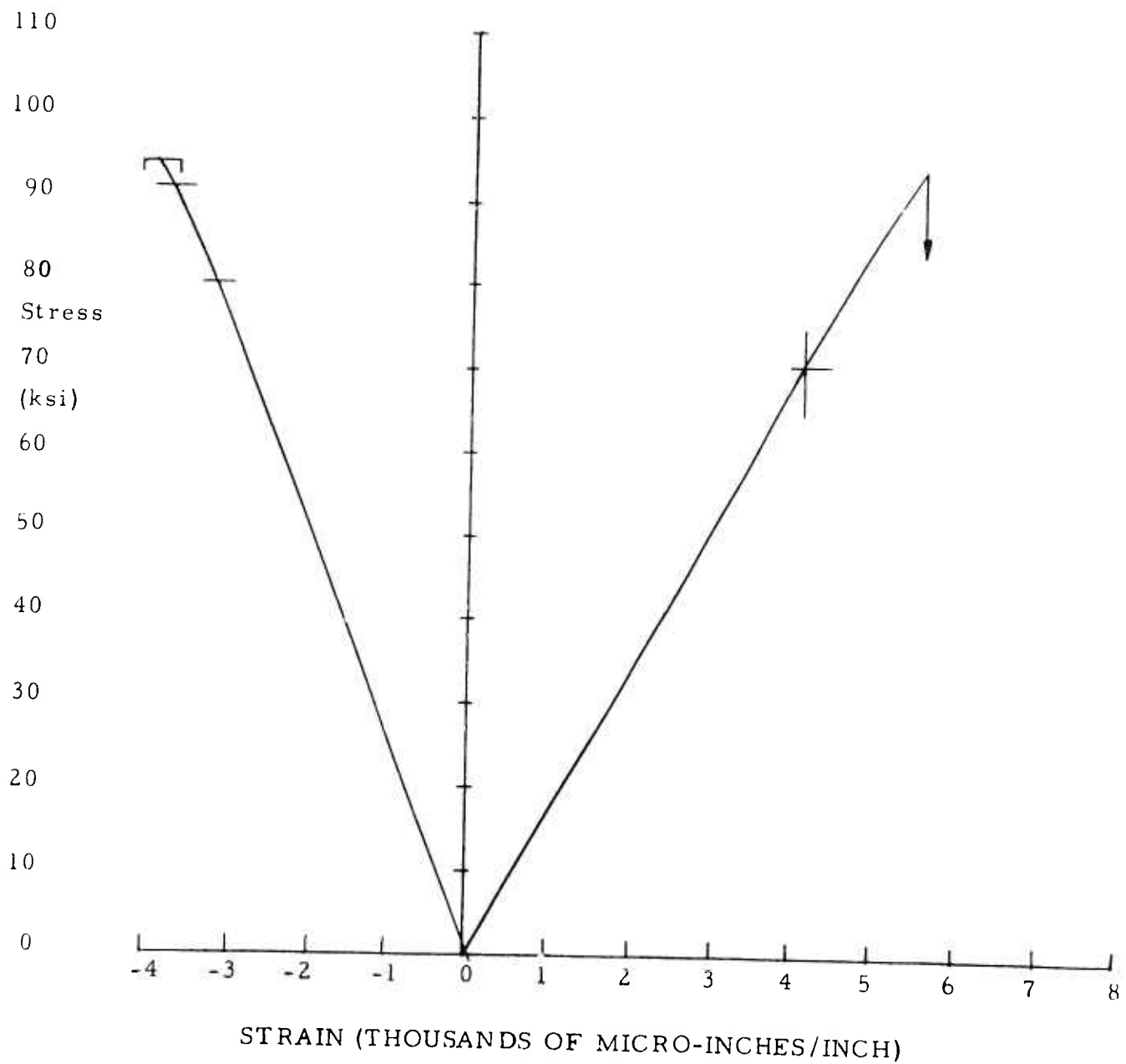
(b) 75X 90° Photo No. 14984

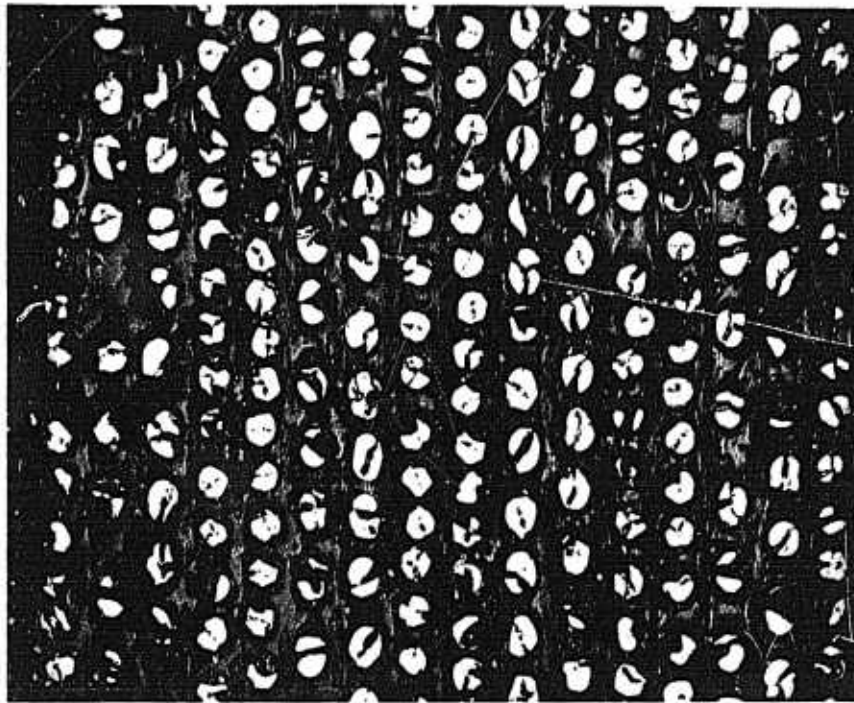
SPECIMEN T-264
(Tension)

$\left[(0/+45/0)_q \right]_s$

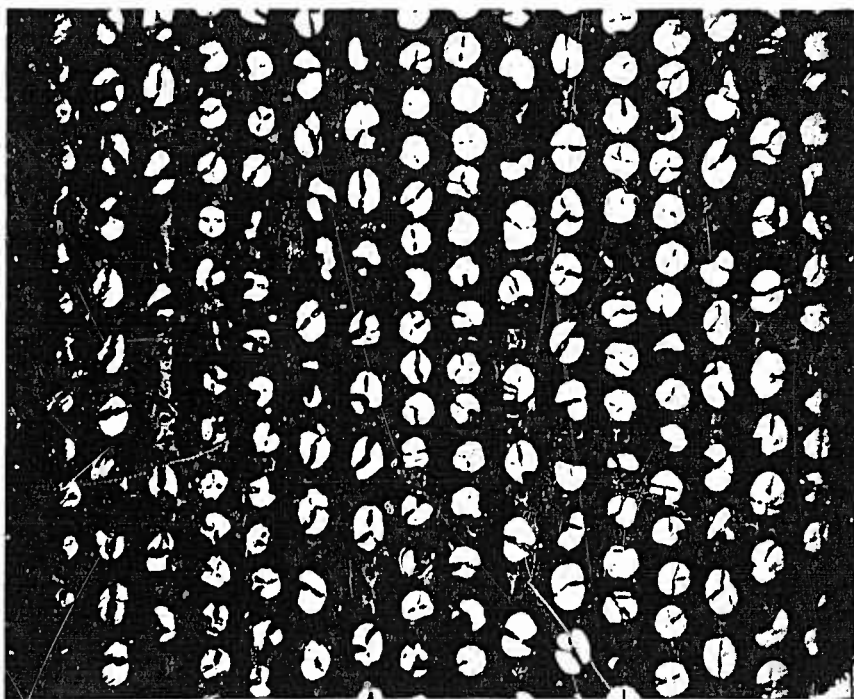
FIGURE E. 12
STRESS VS STRAIN

$\sigma_u = 94,134 \text{ psi}$
 $\epsilon_u = 5,561 \times 10^{-6} \text{ in./in.}$
 $\nu_p = 0.6849 (0.7138)^*$
 $\nu_s = 0.6914 (0.6944)^*$
 $\sigma_{pl} = 70,691 \text{ psi}$
 $\epsilon_{pl} = 4,087 \times 10^{-6} \text{ in./in.}$
 $E_p = 17.296 \times 10^6 \text{ psi}$
 $E_s = 16.284 \times 10^6 \text{ psi}$





(a) 50X 90° Photo No. 14986



(b) 50X 90° Photo No. 14987

FIGURE E.13 PANEL B-26 PHOTOMICROGRAPHS

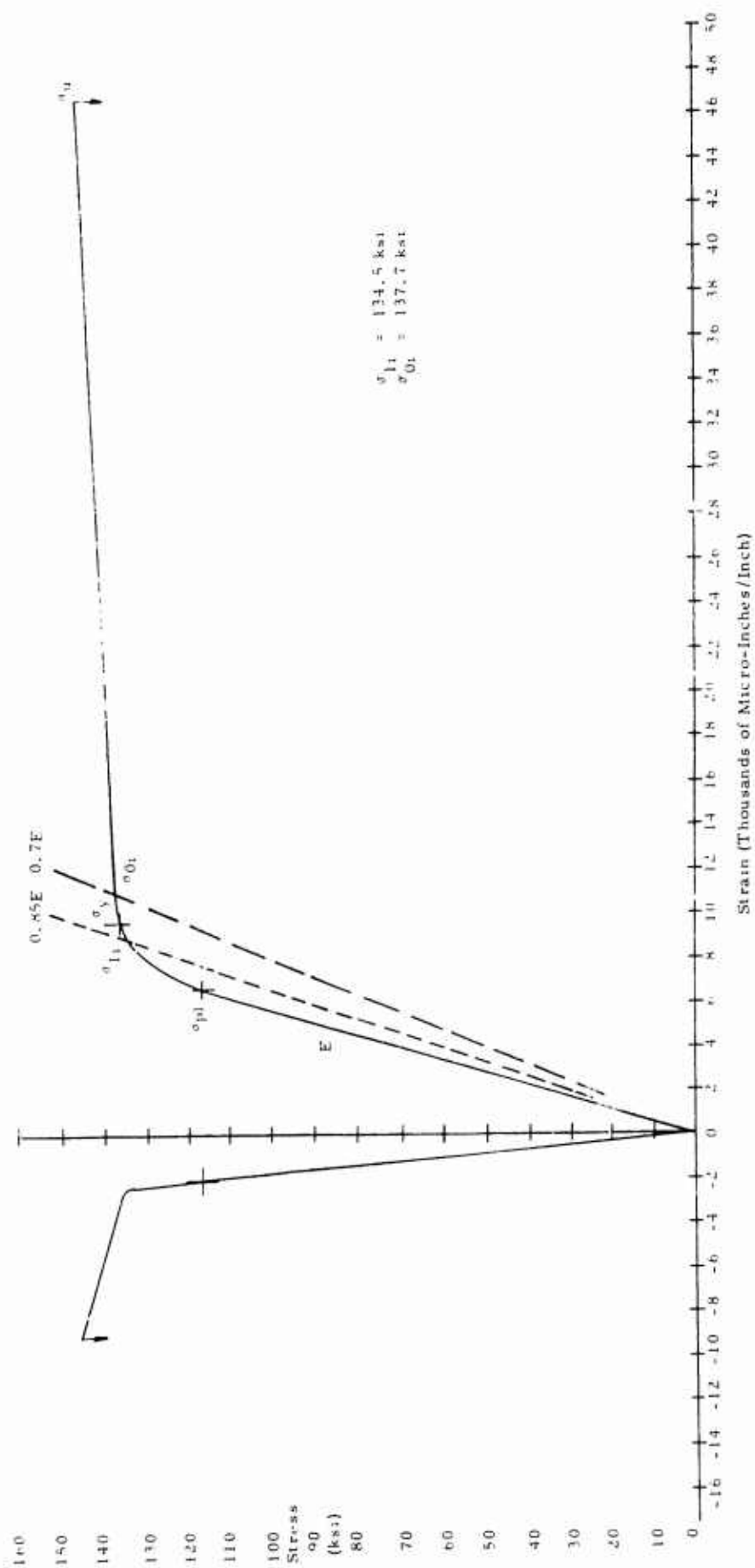


FIGURE E. 14 AVERAGE DATA STRESS VS STRAIN CURVE - 0.016 Ti 6Al-4V ANNEALED SHEET

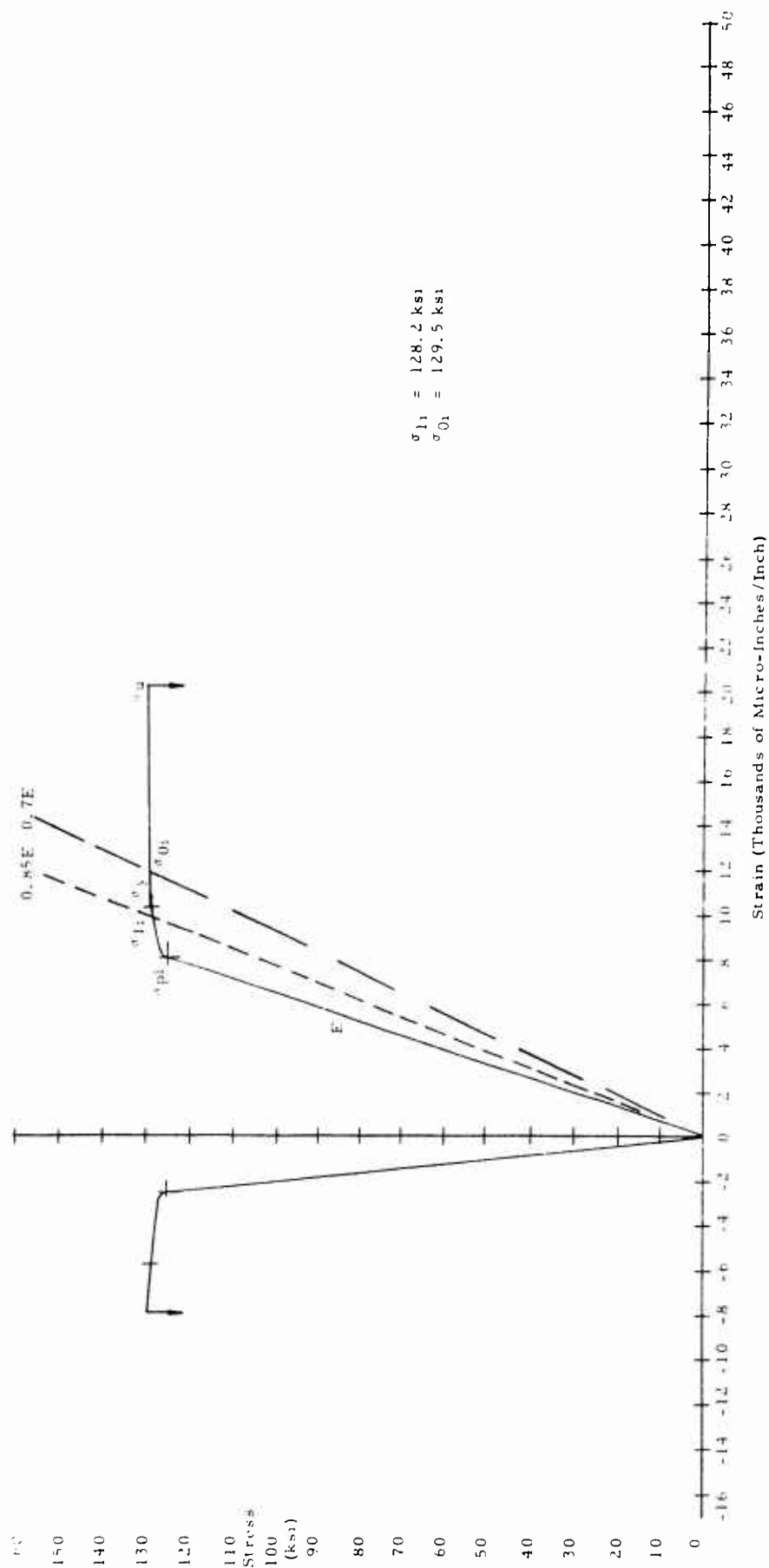


FIGURE E. 15 AVERAGE DATA STRESS VS STRAIN CURVE - 0.032 Ti 6Al-4V ANNEALED SHEET

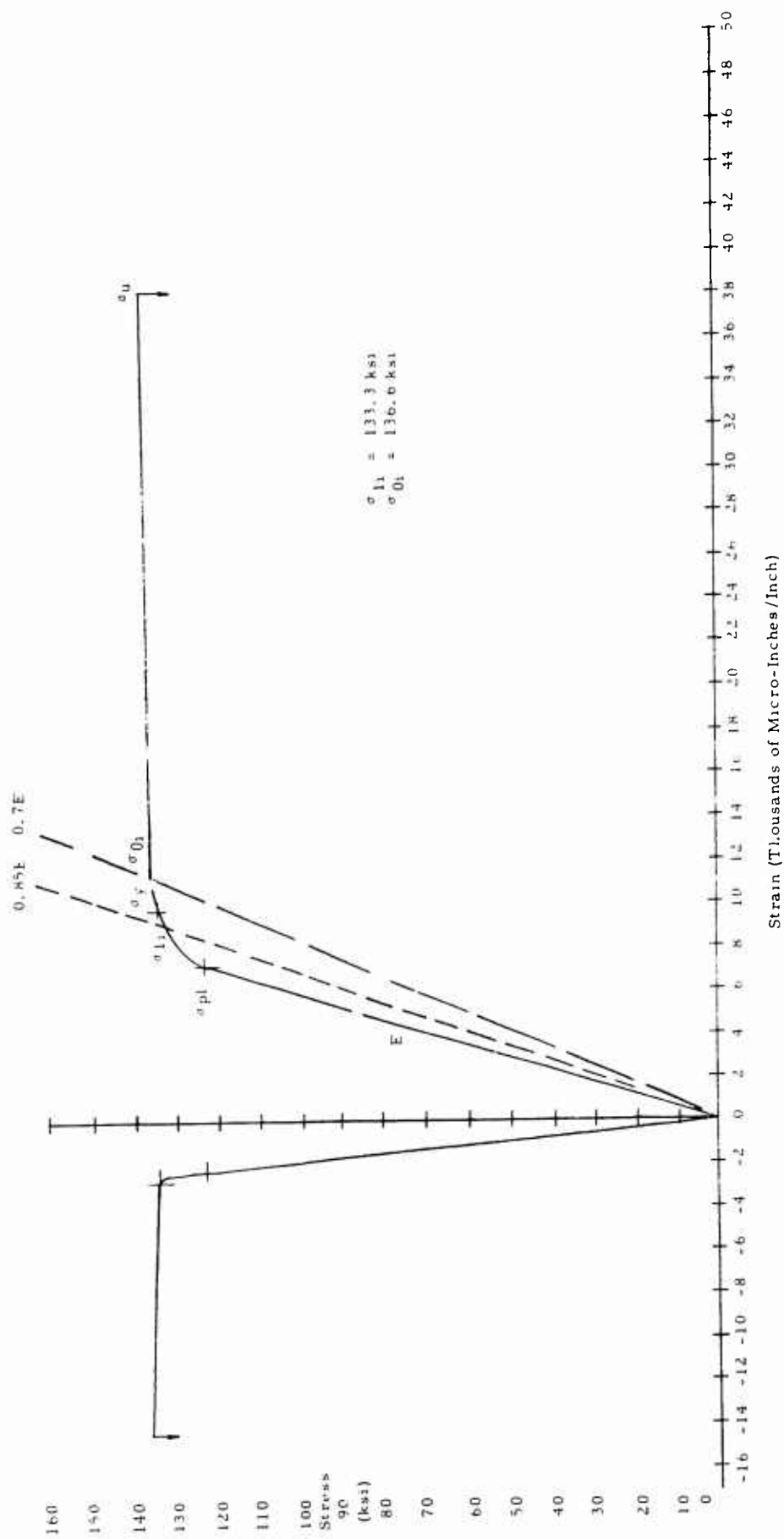


FIGURE E.16 AVERAGE DATA STRESS VS STRAIN CURVE - 0.045 Ti 6Al-4V ANNEALED SHEET

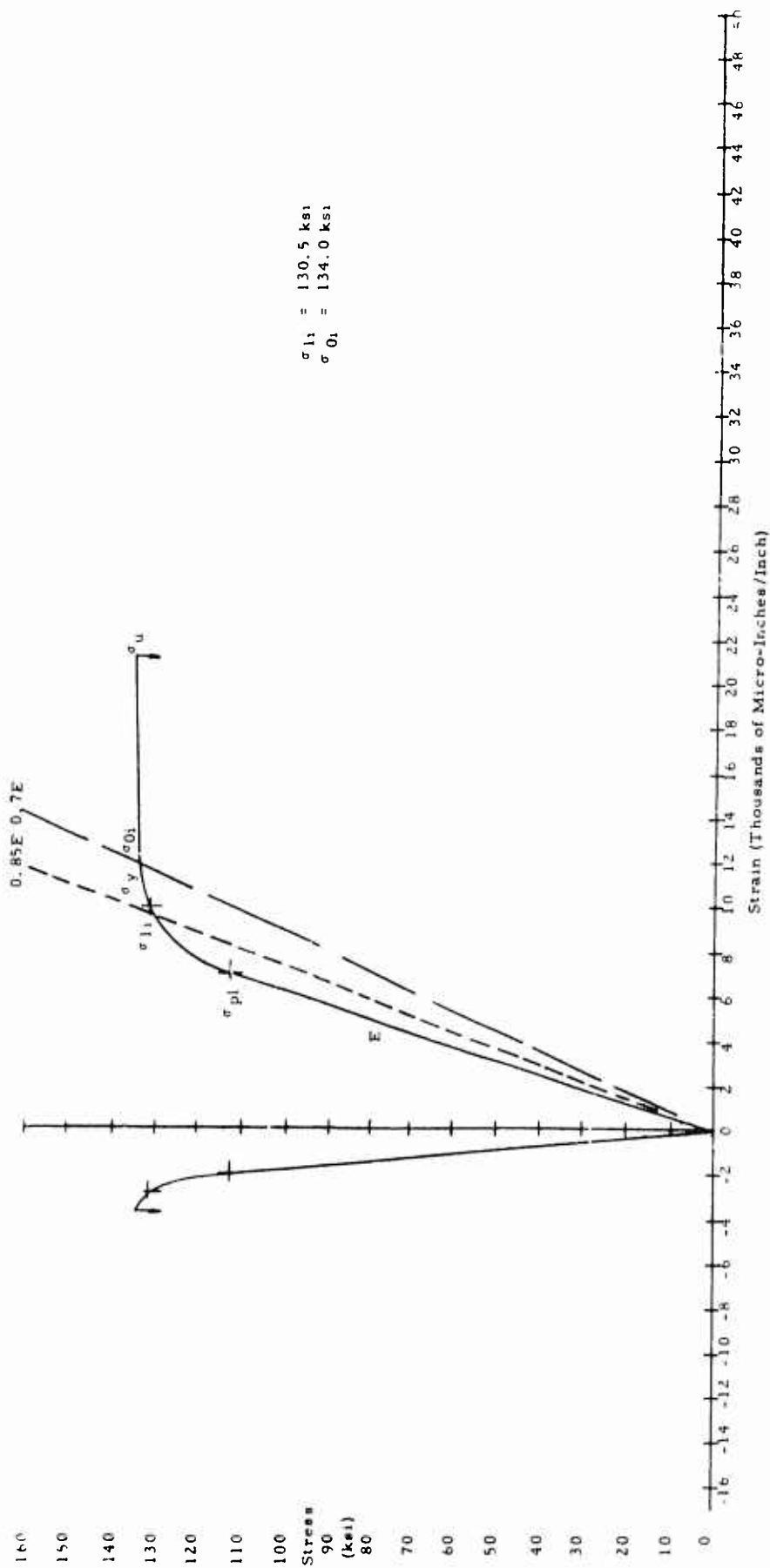


FIGURE E. 17 AVERAGE DATA STRESS VS STRAIN CURVE - 0.090 Ti 6Al-4V ANNEALED SHEET

APPENDIX F
COMPLETE EXPERIMENTAL DATA ON BONDED JOINTS

TABLE F.1

DETAILED TEST DATA ON BONDED JOINTS

Specification Number	Joint Type	Length Between Tabs	Adhesive Thickness	Adherend Combination	Composite Adherend Fiber Orientation	Composite Adherend Panel Number	Composite Adherend Thickness (Net)	Adherend Width	II Adherend Thickness, in	Adherend Cross Section Area, in ²	Overlap Length, in	Bonded Joint Area, in ²	Failure Load, (lb/in)	Adherend Stress at Failure, psi	Adhesive Stress at Failure, psi	Failure Type
LSA-1.1	S-L	4.18	AI-126.2	B-B	[0]0T	B-21A-D	0.047 ± 0.045	1.000		0.045	0.250	0.250	1.120	24,888	4,480	20
LSA-1.2	S-L	4.18	AI-126.2	B-B	[0]0T	B-21A-D	0.047 ± 0.045	1.003		0.045	0.250	0.251	1.100	24,444	4,382	15
LSA-1.3	S-L	4.18	AI-126.2	B-B	[0]0T	B-21A-D	0.047 ± 0.045	1.003		0.045	0.250	0.250	970	21,556	3,880	80
LSA-1.4	S-L	4.18	AI-126.2	B-B	[0]0T	B-21A-D	0.047 ± 0.045	1.003		0.045	0.250	0.250	1.063	23,620(B)	4,247	15
LSA-2.1	S-L	4.18	AI-126.2	B-B	[0/-45/0/-45/0]S	B-24A-B	0.047 ± 0.047	0.909		0.047	0.250	0.250	1.105	23,511	4,420	15
LSA-2.2	S-L	4.18	AI-126.2	B-B	[0/-45/0/-45/0]S	B-24A-B	0.047 ± 0.047	1.000		0.046	0.250	0.250	1.170	25,415	4,680	25
LSA-2.3	S-L	4.18	AI-126.2	B-B	[0/-45/0/-45/0]S	B-24A-B	0.047 ± 0.048	0.996		0.045	0.250	0.250	1.165	25,889	4,679	40
LSA-2.4	S-L	4.18	AI-126.2	B-B	[0/-45/0/-45/0]S	B-24A-B	0.047 ± 0.047	0.998		0.046(B)	0.250	0.250	1.147	24,945(B)	4,593	20
LSA-3.1	D-L	4.14	AI-126.2	B-B	2 × [0]3T/[0]6T	B-12A-D, B-13K	2 × 0.016 ± 0.026	1.015		0.026	2 × 0.250	0.508	1.785	63,750	3,514	60
LSA-3.2	D-L	4.14	AI-126.2	B-B	2 × [0]3T/[0]6T	B-12A-D, B-13K	2 × 0.016 ± 0.027	1.015		0.027	2 × 0.250	0.508	1.740	64,444	3,425	50
LSA-3.3	D-L	4.14	AI-126.2	B-B	2 × [0]3T/[0]6T	B-12A-D, B-13K	2 × 0.016 ± 0.027	1.015		0.027	2 × 0.250	0.508	1.825	67,592	3,592	40
LSA-3.4	D-L	4.14	AI-126.2	B-B	2 × [0]3T/[0]6T	B-12A-D, B-13K	2 × 0.016 ± 0.027	1.015		0.027(B)	2 × 0.250	0.508	1.783	65,262(B)	3,510	50
LSA-4.1	D-L	4.16	AI-126.2	B-B	2 × [0/-45/0/-45/0]S	B-14J-K, B-15K	2 × 0.046 ± 0.088	1.013		0.089	2 × 0.218	0.442	1.595	17,921	3,608	50
LSA-4.2	D-L	4.16	AI-126.2	B-B	2 × [0/-45/0/-45/0]S	B-14J-K, B-15K	2 × 0.046 ± 0.088	1.014		0.089	2 × 0.218	0.442	1.430	16,067	3,235	70
LSA-4.3	D-L	4.18	AI-126.2	B-B	2 × [0/-45/0/-45/0]S	B-14J-K, B-15K	2 × 0.046 ± 0.087	1.014		0.090	2 × 0.218	0.442	1.535	17,056	3,473	55
LSA-4.4	D-L	4.18	AI-126.2	B-B	2 × [0/-45/0/-45/0]S	B-14J-K, B-15K	2 × 0.046 ± 0.088	1.014		0.090(B)	2 × 0.218	0.442	1.520	17,015(B)	3,439	55
LSA-5.1	D-L	4.14	AI-126.2	B-B	2 × [0/-45/0/-45/0]S	B-24J/K, B-17A	2 × 0.045 ± 0.089	1.014		0.090	2 × 0.250	0.508	2.410	26,778	4,744	38
LSA-5.2	D-L	4.14	AI-126.2	B-B	2 × [0/-45/0/-45/0]S	B-24J/K, B-17A	2 × 0.045 ± 0.088	1.013		0.089	2 × 0.250	0.506	2.225	25,000	4,397	25
LSA-5.3	D-L	4.14	AI-126.2	B-B	2 × [0/-45/0/-45/0]S	B-24J/K, B-17A	2 × 0.045 ± 0.087	1.015		0.088	2 × 0.250	0.508	2.250	25,681	4,429	30
LSA-5.4	D-L	4.14	AI-126.2	B-B	2 × [0/-45/0/-45/0]S	B-24J/K, B-17A	2 × 0.045 ± 0.088	1.014		0.089(B)	2 × 0.250	0.507	2.295	25,820(B)	4,523	31
LSA-6.1	S-L	2.14	AI-126.2	B-T	[0]6T	B-18C	0.030	1.010	0.032	0.030	0.250	0.252	1.000	33,333	3,968	5
LSA-6.2	S-L	2.14	AI-126.2	B-T	[0]6T	B-18C	0.030	1.009	0.032	0.030	0.250	0.252	820	27,333	3,254	10
LSA-6.3	S-L	2.14	AI-126.2	B-T	[0]6T	B-18C	0.030	1.008	0.032	0.030	0.250	0.252	1.165	38,833	4,623	10
LSA-6.4	S-L	2.14	AI-126.2	B-T	[0]6T	B-18C	0.030	1.009	0.032	0.030(B)	0.250	0.252	995	33,166(B)	3,948	3
LSA-7.1	S-L	2.18	AI-126.2	B-T	[0/-45/0/-45/0]S	B-16D	0.045	1.008	0.045	0.045	0.250	0.252	1.215	27,000	4,821	40
LSA-7.2	S-L	2.18	AI-126.2	B-T	[0/-45/0/-45/0]S	B-16D	0.045	1.010	0.045	0.045	0.250	0.252	1.140	25,333	4,524	80
LSA-7.3	S-L	2.18	AI-126.2	B-T	[0/-45/0/-45/0]S	B-16D	0.045	1.010	0.045	0.045	0.218	0.252	1.045	23,222	4,147	45
LSA-7.4	S-L	2.18	AI-126.2	B-T	[0/-45/0/-45/0]S	B-16D	0.045	1.009	0.045	0.045(B)	0.239	0.252	1.133	25,155(B)	4,497	55

TABLE F.1 (Cont'd)

Specimen Number	Joint Type	Length Between Joints	Adhesive Thickness	Adhesive Combination	Composite Adhesive Fiber Orientation	Composite Adhesive Panel Number	Composite Adhesive Thickness (mm)	Adhesive Width	Adhesive Thickness	Adhesive Cross Section Area, in ²	Overlap Length, in	Bonded Area, in ²	Failure Load, lb/in	Adhesive Stress at Failure, psi	Failure Type					
															1	2	3	4	5	6
LSA 8.1	D1	2.5 16	AI 126.2	B1	[0/6]	B 18A	0.029	1.01	2 × 0.016	0.0295 (B)	2 × 0.250	0.5084	2.685	91,017 (B)	5	10	50	36		
LSA 8.2	D1	2.5 16	AI 126.2	B1	[0/6]	B 18A	0.029	1.016	2 × 0.016	0.0295 (B)	2 × 0.250	0.5080	2.620	88,814 (B)	5	25	45	25		
LSA 8.3	D1	2.5 16	AI 126.2	B1	[0/6]	B 18A	0.028	1.015	2 × 0.016	0.0284 (B)	2 × 0.218	0.4426	2.470	86,972 (B)	5	30	45	10		
LSA 8.4	D1	2.5 16	AI 126.2	B1	[0/6]	B 18A	0.029	1.016	2 × 0.016	0.0291 (B)	2 × 0.239	0.4863	2.592	88,944 (B)	5	23	47	22		
LSA 9.1	D1	2.1 4	AI 126.2	B1	[0/90/0/0]	B 15A	0.088	1.019	2 × 0.045	0.0887	2 × 0.250	0.5095	1.350	15,050	38	10	37	15		
LSA 9.2	D1	2.1 4	AI 126.2	B1	[0/90/0/0]	B 15A	0.089	1.018	2 × 0.045	0.0896	2 × 0.250	0.5090	2.055	22,682	15	25	43	1		
LSA 9.3	D1	2.1 4	AI 126.2	B1	[0/90/0/0]	B 15A	0.088	1.017	2 × 0.045	0.0885	2 × 0.250	0.5085	2.215	25,028	15	20	38	20		
LSA 9.4	D1	2.1 4	AI 126.2	B1	[0/90/0/0]	B 15A	0.088	1.018	2 × 0.045	0.0896 (B)	2 × 0.250	0.5090	1.873	20,920 (B)	23	18	39	18		
LSA 10.1	D1	2.1 4	AI 126.2	B1	[0/45/0/45]	B 221	0.087	1.002	2 × 0.045	0.0872	2 × 0.250	0.5090	2.260	25,917	10	45	33	12		
LSA 10.2	D1	2.1 4	AI 126.2	B1	[0/45/0/45]	B 221	0.088	1.020	2 × 0.045	0.0898	2 × 0.250	0.5100	2.360	26,281	4	25	60	15		
LSA 10.3	D1	2.1 4	AI 126.2	B1	[0/45/0/45]	B 221	0.088	1.021	2 × 0.045	0.0898	2 × 0.250	0.5100	2.485	27,473	4	25	30	35		
LSA 10.4	D1	2.1 4	AI 126.2	B1	[0/45/0/45]	B 221	0.088	1.014	2 × 0.045	0.0899 (B)	2 × 0.250	0.5072	2.368	26,557 (B)		32	38	21		
LSA 11.1	S1	6.7 16	MB 329	B1	2 × [0/45/0/45]	B 261 G	0.168	1.017	0.172	0.1708	2.013	2.0472	1.700	9,953	8	20	15	65		
LSA 11.2	S1	6.7 16	MB 329	B1	2 × [0/45/0/45]	B 261 G	0.168	1.018	0.172	0.1683	2.024	2.0159	1.740	10,526	8	30	9	60		
LSA 11.3	S1	6.7 16	MB 329	B1	2 × [0/45/0/45]	B 261 G	0.165	1.008	0.172	0.1665	2.050	2.0284	1.710	10,526	5	20	14	45		
LSA 11.4	S1	6.7 16	MB 329	B1	2 × [0/45/0/45]	B 261 G	0.1662	1.008	0.172	0.1662	2.051	2.0619	1.745	10,438 (B)	8	20	6	60		
LSA 12.1	S1	4.3 16	MB 329	B1	[0/90/0/41]	B 23A B 26A	0.086	1.003		0.0863	0.269	0.2698	850	9,849	3	50	22	2		
LSA 12.2	S1	4.3 16	MB 329	B1	[0/90/0/41]	B 23A B 26A	0.086	1.004		0.0863	0.284	0.2851	935	10,834	3	28	45	1		
LSA 12.3	S1	4.3 16	MB 329	B1	[0/90/0/41]	B 23A B 26A	0.087	1.002		0.0852	0.24	0.2475	915	10,739	3	14	16	30	40	
LSA 12.4	S1	4.3 16	MB 329	B1	[0/90/0/41]	B 23A B 26A	0.0863	1.003		0.0859 (B)	0.26	0.267	900	10,474 (B)	3	31	36	26		
LSA 13.1	S1	7.1 2	MB 329	B1	2 × [0/81]	B 250 M	0.088	0.997	0.087	0.0877	2.008	2.0020	2.835	32,326	1	25	13	60	2	
LSA 13.2	S1	7.1 2	MB 329	B1	2 × [0/81]	B 250 M	0.088	0.996	0.083	0.0856	2.008	1.9970	2.205	25,750	1	14	50	10	35	
LSA 13.3	S1	7.1 2	MB 329	B1	2 × [0/81]	B 250 M	0.087	0.997	0.085	0.0867	2.005	1.9990	2.910	33,564	1	15	5	70	10	
LSA 13.4	S1	7.1 2	MB 329	B1	2 × [0/81]	B 250 M	0.086	0.996	0.085	0.0867 (B)	2.006	1.9993	2.850	30,550 (B)	1	30	4	55	6	
LSA 14.1	S1	5.1 4	AI 126.2	B1	[0/91]	B 211 H	0.043	1.016		0.0437	1.560	1.5700	5,754	131,579	5	10	55	20		
LSA 14.2	S1	5.1 4	AI 126.2	B1	[0/91]	B 211 H	0.042	1.015		0.0426	1.550	1.5688	5,358	129,930	4	362	30	50	20	
LSA 14.3	S1	5.1 4	AI 126.2	B1	[0/91]	B 211 H	0.042	1.015		0.0426	1.550	1.5688	5,720	134,774	4	508	40	50	10	
LSA 14.4	S1	5.1 4	AI 126.2	B1	[0/91]	B 211 H	0.042	1.015		0.04296 (B)	1.550	1.568	5,668	131,928 (B)	2	27	52	19		

TABLE F. I (Cont'd)

Specification Number	Joint Type	Length between Tabs	Adhesive Thickness	Adhesive Combination	Composite Adhesive Thickness (in)	Composite Adhesive Thickness (mm)	Adhesive Width	Adhesive Thickness (in)	Adhesive Thickness (mm)	Overlap Length (in)	Bonded Joint Area (in ²)	Failure Load (lb/in)	Adherent Failure (psi)	Adhesive Failure (psi)	Failure Type	Failure Type
LSA 15.1	S1	3.9 32	AI-126.2	0.0065	BB	10-45 0.45 0.5	0.043	1.013	0.043	1.250	1.2662	4.109	94,037	3,236	65	30
LSA 15.2	S1	3.1 4	AI-126.2	0.0040	BB	10-45 0.45 0.5	0.043	1.013	0.043	1.250	1.2662	3.815	85,347	3,007	70	25
LSA 15.3	S1	3.1 4	AI-126.2	0.0075	BB	10-45 0.45 0.5	0.043	1.013	0.043	1.250	1.2662	3.990	89,450	3,074	75	25
LSA 15.4	S1	3.1 4	AI-126.2	0.0060	BB	10-45 0.45 0.5	0.043	1.013	0.043	1.250	1.2662	3.938	89,611	3,106	70	26
LSA 16.1	D1	4.3 16	AI-126.2	0.0050	BB	25-10-45 0.45 0.5	0.043	1.013	0.043	2.5 0.500	1.0100	4.070	132,673	3,960	30	15
LSA 16.2	D1	4.3 16	AI-126.2	0.0050	BB	25-10-45 0.45 0.5	0.043	1.013	0.043	2.5 0.500	1.0100	4.085	134,018	4,040	30	15
LSA 16.3	D1	4.3 16	AI-126.2	0.0045	BB	25-10-45 0.45 0.5	0.043	1.013	0.043	2.5 0.500	1.0100	3.905	126,454	3,655	30	15
LSA 16.4	D1	4.3 16	AI-126.2	0.0048	BB	25-10-45 0.45 0.5	0.043	1.013	0.043	2.5 0.500	1.0100	4.093	131,082	3,936	30	15
LSA 17.1	D1	4.13 32	AI-126.2	0.0035	BB	25-10-45 0.45 0.5	0.043	1.013	0.043	2.5 0.500	1.0100	4.000	126,226	3,824	30	15
LSA 17.2	D1	4.13 32	AI-126.2	0.0025	BB	25-10-45 0.45 0.5	0.043	1.013	0.043	2.5 0.500	1.0100	4.000	126,226	3,824	30	15
LSA 17.3	D1	4.3 8	AI-126.2	0.0020	BB	25-10-45 0.45 0.5	0.043	1.013	0.043	2.5 0.500	1.0100	4.000	126,226	3,824	30	15
LSA 17.4	D1	4.13 32	AI-126.2	0.0027	BB	25-10-45 0.45 0.5	0.043	1.013	0.043	2.5 0.500	1.0100	4.000	126,226	3,824	30	15
LSA 18.1	D1	4.3 8	AI-126.2	0.0022	BB	25-10-45 0.45 0.5	0.043	1.013	0.043	2.5 0.500	1.0100	4.000	126,226	3,824	30	15
LSA 18.2	D1	4.5 5	AI-126.2	0.0018	BB	25-10-45 0.45 0.5	0.043	1.013	0.043	2.5 0.500	1.0100	4.000	126,226	3,824	30	15
LSA 18.3	D1	4.5 8	AI-126.2	0.0020	BB	25-10-45 0.45 0.5	0.043	1.013	0.043	2.5 0.500	1.0100	4.000	126,226	3,824	30	15
LSA 18.4	D1	4.13 32	AI-126.2	0.0020	BB	25-10-45 0.45 0.5	0.043	1.013	0.043	2.5 0.500	1.0100	4.000	126,226	3,824	30	15
LSA 19.1	S1	3.3 16	AI-126.2	0.0050	BB	10-45 0.45 0.5	0.043	1.013	0.043	1.250	1.2662	4.109	94,037	3,236	65	30
LSA 19.2	S1	3.3 16	AI-126.2	0.0035	BB	10-45 0.45 0.5	0.043	1.013	0.043	1.250	1.2662	3.815	85,347	3,007	70	25
LSA 19.3	S1	3.3 16	AI-126.2	0.0070	BB	10-45 0.45 0.5	0.043	1.013	0.043	1.250	1.2662	3.990	89,450	3,074	75	25
LSA 19.4	S1	3.3 16	AI-126.2	0.0058	BB	10-45 0.45 0.5	0.043	1.013	0.043	1.250	1.2662	3.938	89,611	3,106	70	26
LSA 20.1	S1	3.1 4	AI-126.2	0.0020	BB	10-45 0.45 0.5	0.043	1.013	0.043	1.250	1.2662	4.109	94,037	3,236	65	30
LSA 20.2	S1	3.1 4	AI-126.2	0.0020	BB	10-45 0.45 0.5	0.043	1.013	0.043	1.250	1.2662	3.815	85,347	3,007	70	25
LSA 20.3	S1	3.1 4	AI-126.2	0.0045	BB	10-45 0.45 0.5	0.043	1.013	0.043	1.250	1.2662	3.990	89,450	3,074	75	25
LSA 20.4	S1	3.1 4	AI-126.2	0.0025	BB	10-45 0.45 0.5	0.043	1.013	0.043	1.250	1.2662	3.938	89,611	3,106	70	26

TABLE F.1 (Cont'd)

Specification Number	Joint Type	Length Between Tabs	Adhesive Thickness	Adhesive Combination	Composite Adhesive Fiber Orientation	Composite Adhesive Panel Number	Composite Adhesive Thickness (in.)	Adhesive Width	II Adhesive Thickness (in.)	Adhesive Cross-Section Area, in. ²	Overlap Length, in.	Bonded Joint Area, in. ²	Failure Load, lb (N)	Adhesive Stress at Failure, psi (MPa)	Adhesive Stress at Failure, psi (MPa)	Failure Type, %	6	5	4	3	2	1
LSA 21.1	D1	2.12	AI 126.2	0.0005	B-I	[0/61	0.030	1.013	2 × 0.016	0.0304(B)	2 × 0.500	1.013	3.990	131,250(B)	3,939	131,148(B)	50					
LSA 21.2	D1	2.12	AI 126.2	0.0006	B-I	[0/61	0.030	1.013	2 × 0.016	0.0304(B)	2 × 0.500	1.013	4.010	131,908(B)	3,958	132,765(B)	100					
LSA 21.3	D1	2.12	AI 126.2	0.0002	B-I	[0/61	0.030	1.015	2 × 0.016	0.0304(B)	2 × 0.500	1.015	3.840	126,316(B)	3,783	128,154(B)	100					
LSA 21.4	D1	2.12	AI 126.2	0.0003	B-I	[0/61	0.030	1.014	2 × 0.016	0.0304(B)	2 × 0.500	1.014	3.947	129,825(B)	3,893	121,689(B)	82					
LSA 22.1	D1	2.12	AI 126.2	0.0020	B-I	[0/90/0/0/1	0.088	1.020	2 × 0.048	0.086	2 × 0.500	1.020	5.250	60,554	5,14	60,554	30					
LSA 22.2	D1	2.12	AI 126.2	0.0020	B-I	[0/90/0/0/1	0.088	1.019	2 × 0.048	0.086	2 × 0.500	1.019	5.200	60,046	5,103	60,046	100					
LSA 22.3	D1	2.12	AI 126.2	0.0018	B-I	[0/90/0/0/1	0.084	1.020	2 × 0.048	0.085	2 × 0.500	1.020	5.210	60,793	5,108	60,793	10					
LSA 22.4	D1	2.12	AI 126.2	0.0019	B-I	[0/90/0/0/1	0.084	1.020	2 × 0.048	0.085	2 × 0.500	1.020	5.220	60,464(B)	5,119	60,464(B)	13					
LSA 23.1	D1	2.116	AI 126.2	0.0032	B-I	[0/45/0/45/0/0/8	0.08	0.962	2 × 0.048	0.083	2 × 0.687	1.318	2.550	90,203	5,685	90,203	13					
LSA 23.2	D1	2.116	AI 126.2	0.0032	B-I	[0/45/0/45/0/0/8	0.08	0.962	2 × 0.048	0.083	2 × 0.687	1.318	2.550	90,203	5,685	90,203	13					
LSA 23.3	D1	2.116	AI 126.2	0.0028	B-I	[0/45/0/45/0/0/8	0.08	0.962	2 × 0.048	0.083	2 × 0.687	1.318	2.550	90,203	5,685	90,203	13					
LSA 23.4	D1	2.116	AI 126.2	0.0030	B-I	[0/45/0/45/0/0/8	0.08	0.962	2 × 0.048	0.083	2 × 0.687	1.318	2.550	90,203	5,685	90,203	13					
LSA 24.1	D1	5.78	MB 320	0.010	B-I	[0/90/0/0/1	0.175	1.001	0.180	0.175	2.012	2.012	1.591	9,075	789	9,075	40					
LSA 24.2	D1	5.78	MB 320	0.013	B-I	[0/90/0/0/1	0.175	1.002	0.176	0.175	2.009	2.010	1.405	8,154	698	8,154	25					
LSA 24.3	D1	5.78	MB 320	0.015	B-I	[0/90/0/0/1	0.175	1.000	0.174	0.175	2.008	2.008	1.480	8,655	737	8,655	25					
LSA 24.4	D1	5.78	MB 320	0.011	B-I	[0/90/0/0/1	0.175	1.001	0.176	0.175	2.010	2.011	1.492	8,655	741	8,655	25					
LSA 25.1	D1	4.78	AI 126.2	0.0005	B-I	[0/90/0/0/1	0.264	1.003	0.265	0.264	3.686	3.686	5.845	22,073	1,581	22,073	100					
LSA 25.2	D1	4.78	AI 126.2	0.0010	B-I	[0/90/0/0/1	0.264	1.003	0.265	0.264	3.686	3.686	5.845	22,073	1,581	22,073	100					
LSA 25.3	D1	4.78	AI 126.2	0.0010	B-I	[0/90/0/0/1	0.264	1.003	0.265	0.264	3.686	3.686	5.845	22,073	1,581	22,073	100					
LSA 25.4	D1	4.78	AI 126.2	0.0010	B-I	[0/90/0/0/1	0.264	1.003	0.265	0.264	3.686	3.686	5.845	22,073	1,581	22,073	100					
LSA 26.1	D1	5.116	AI 126.2	0.0055	B-I	[0/45/0/45/0/0/8	0.260	1.005	0.264	0.260	3.504	3.504	9.600	36,969	2,488	36,969	50					
LSA 26.2	D1	5.116	AI 126.2	0.0050	B-I	[0/45/0/45/0/0/8	0.260	1.005	0.264	0.260	3.504	3.504	9.600	36,969	2,488	36,969	50					
LSA 26.3	D1	5.116	AI 126.2	0.0055	B-I	[0/45/0/45/0/0/8	0.260	1.005	0.264	0.260	3.504	3.504	9.600	36,969	2,488	36,969	50					
LSA 26.4	D1	5.116	AI 126.2	0.0058	B-I	[0/45/0/45/0/0/8	0.260	1.005	0.264	0.260	3.504	3.504	9.600	36,969	2,488	36,969	50					
LSA 27.1	D1	5.58	AI 126.2	0.0030	B-I	[0/90/0/0/1	0.042	0.946	0.042	0.042	1.714	1.714	7.600	106,901	4,383	106,901	100					
LSA 27.2	D1	5.58	AI 126.2	0.0070	B-I	[0/90/0/0/1	0.042	0.946	0.042	0.042	1.714	1.714	7.600	106,901	4,383	106,901	100					
LSA 27.3	D1	5.58	AI 126.2	0.0030	B-I	[0/90/0/0/1	0.042	0.946	0.042	0.042	1.714	1.714	7.600	106,901	4,383	106,901	100					
LSA 27.4	D1	5.58	AI 126.2	0.0043	B-I	[0/90/0/0/1	0.042	0.946	0.042	0.042	1.714	1.714	7.600	106,901	4,383	106,901	100					
LSA 28.1	D1	6.78	AI 126.2	0.0040	B-I	[0/45/0/45/0/0/8	0.046	1.002	0.046	0.046	2.000	2.000	4.715	102,278	2,353	102,278	2					
LSA 28.2	D1	6.78	AI 126.2	0.0045	B-I	[0/45/0/45/0/0/8	0.046	1.006	0.046	0.046	2.000	2.000	4.715	102,278	2,353	102,278	2					
LSA 28.3	D1	6.78	AI 126.2	0.0040	B-I	[0/45/0/45/0/0/8	0.046	1.006	0.046	0.046	2.000	2.000	4.715	102,278	2,353	102,278	2					
LSA 28.4	D1	6.78	AI 126.2	0.0042	B-I	[0/45/0/45/0/0/8	0.046	1.006	0.046	0.046	2.000	2.000	4.715	102,278	2,353	102,278	2					
LSA 29.1	D1	4.58	AI 126.2	0.0030	B-I	[0/90/0/0/1	0.046	1.000	0.046	0.046	2.000	2.000	4.715	102,278	2,353	102,278	2					
LSA 29.2	D1	4.58	AI 126.2	0.0035	B-I	[0/90/0/0/1	0.046	1.000	0.046	0.046	2.000	2.000	4.715	102,278	2,353	102,278	2					
LSA 29.3	D1	4.58	AI 126.2	0.0035	B-I	[0/90/0/0/1	0.046	1.000	0.046	0.046	2.000	2.000	4.715	102,278	2,353	102,278	2					
LSA 29.4	D1	4.58	AI 126.2	0.0033	B-I	[0/90/0/0/1	0.046	1.000	0.046	0.046	2.000	2.000	4.715	102,278	2,353	102,278	2					
LSA 29.5	D1	4.58	AI 126.2	0.0033	B-I	[0/90/0/0/1	0.046	1.000	0.046	0.046	2.000	2.000	4.715	102,278	2,353	102,278	2					

TABLE F.1 (Cont'd)

Specimen Name	Joint Type	Length Between Tabs	Adhesive Thickness	Adhesive Combination	Composite Adherent Fiber Orientation	Composite Adherent Panel Number	Composite Thickness (Net)	Adherent Width	H Adhesive Thickness	Bonded Joint Area, in ²	Failure Load, lb (in)	Adherent Stress at Failure, psi	Failure Type				
													1	2	3	4	
LSA-30-1	D.L	4.5/8	AI-126-2	B-B	2 x [0/90/0/0]T [0/90/0/0]T	B-141 M, B-19K	2 x 0.042" 0.08"	1.011		0.0880	2 x 0.750	1.5165	70,454				100%
LSA-30-2	D.L	4.5/8	AI-126-2	B-B	2 x [0/90/0/0]T [0/90/0/0]T	B-141 M, B-19K	2 x 0.042" 0.08"	1.013		0.0881	2 x 0.750	1.5195	65,266				100%
LSA-30-3	D.L	4.5/8	AI-126-2	B-B	2 x [0/90/0/0]T [0/90/0/0]T	B-141 M, B-19K	2 x 0.042" 0.08"	1.013		0.0881	2 x 0.68"	1.3919	65,210				100%
LSA-31 Avg	D.L	4.5/8	AI-126-2	B-B	2 x [0/90/0/0]T [0/90/0/0]T	B-141 M, B-19K	2 x 0.042" 0.08"	1.012		0.0880 (B)	2 x 0.729	1.4760	66,977 (B)				100%
LSA-31-1	D.L	5.3/16	AF-126-2	B-B	2 x [0/+45/0/-45/0]S [0/+45/0/-45/0]S	B-16A G, B-22L	2 x 0.045 0.089	1.013		0.0912	2 x 1.250	2.5322	97,478				100%
LSA-31-2	D.L	5.3/16	AF-126-2	B-B	2 x [0/+45/0/-45/0]S [0/+45/0/-45/0]S	B-16A G, B-22L	2 x 0.045 0.090	1.011		0.0910	2 x 1.250	2.5275	94,560				100%
LSA-31-3	D.L	5.3/16	AF-126-2	B-B	2 x [0/+45/0/-45/0]S [0/+45/0/-45/0]S	B-16A G, B-22L	2 x 0.045 0.089	1.013		0.912	2 x 1.250	2.5325	104,834				100%
LSA-31 Avg	D.L	5.3/16	AF-126-2	B-B	2 x [0/+45/0/-45/0]S [0/+45/0/-45/0]S	B-16A B, B-22L	2 x 0.045 0.0897	1.012		0.0911 (B)	2 x 1.250	2.5308	95,621 (B)				100%
LSA-32-1	S.L	3.5/8	AI-126-2	B-T	[0]6T	B-18J	0.032	1.005	0.042	0.0320 (B)	1.687	1.6870	130,312 (B)				100%
LSA-32-2	S.L	3.5/8	AI-126-2	B-T	[0]6T	B-18J	0.031	1.001	0.042	0.0320 (B)	1.687	1.6887	134,516 (B)				100%
LSA-32-3	S.L	3.5/8	AI-126-2	B-T	[0]6T	B-18J	0.031	1.000	0.042	0.0320 (B)	1.687	1.6870	130,312 (T)				100%
LSA-32 Avg	S.L	3.5/8	AI-126-2	B-T	[0]6T	B-18J	0.0313	1.000	0.042	0.0313 (B)	1.687	1.6876	133,081 (B)				100%
LSA-33-1	S.L	3.7/8	AI-126-2	B-T	[0/+45/0/-45/0]S	B-24M	0.046	1.005	0.045	0.0462 (B)	2.000	2.0100	113,528 (B)				100%
LSA-33-2	S.L	3.7/8	AI-126-2	B-T	[0/+45/0/-45/0]S	B-24M	0.047	1.005	0.045	0.0472 (B)	2.000	2.0100	116,040 (T)				100%
LSA-33-3	S.L	3.7/8	AI-126-2	B-T	[0/+45/0/-45/0]S	B-24M	0.046	1.004	0.045	0.0462 (B)	2.000	2.0080	107,521 (B)				100%
LSA-33 Avg	S.L	3.7/8	AI-126-2	B-T	[0/+45/0/-45/0]S	B-24M	0.0467	1.005	0.045	0.0465 (B)	2.000	2.0093	112,278 (T)				100%

TABLE F. I (Cont'd)

Specification Number	Joint Type	Length Between Tabs	Adhesive Thickness	Adhesive Combination	Composite Adherend Fiber Orientation	Composite Adherend Thickness (Net)	Adherend Width	TI Adherend Thickness, in	Adherend Cross-Section Area, in ²	Overlap Length, in	Bonded Joint Area, in ²	Failure Load, lb (N)	Adherend Stress at Failure, psi	Adhesive Stress at Failure, psi	Failure Type %
															1 2 3 4 5 6
LSA 34.1	D1	2.5.8	AF-126.2	0.0015	B-T	[0/6T]	1.007	2 x 0.016	0.0322(B)	2 x 0.750	1.5105	3.340	110.596(B)	2,211	100 ²
LSA 34.2	D1	2.5.8	AF-126.2	0	B-T	[0/6T]	1.006	2 x 0.016	0.0302(B)	2 x 0.750	1.5090	3.360	111.258(B)	2,227	100 ²
LSA 34.3	D1	2.5.8	AF-126.2	0	B-T	[0/6T]	1.005	2 x 0.016	0.0302(B)	2 x 0.750	1.5075	3.360	111.258(B)	2,229	100 ²
LSA 34.4 Avg	D1	2.5.8	AF-126.2	0.0002	B-T	[0/6T]	1.006	2 x 0.016	0.0322(T)	2 x 0.750	1.5090	3.353	111.037(B)	2,222	100 ²
LSA 35.1	D1	2.11.16	AF-126.2	0.0015	B-T	[0/90/0]T	1.007	2 x 0.045	0.0856	2 x 0.750	1.5105	6.180	72.196	4,091	100
LSA 35.2	D1	2.11.16	AF-126.2	0.0012	B-T	[0/90/0]T	1.007	2 x 0.045	0.0846	2 x 0.750	1.5105	6.175	67.090	3,757	100
LSA 35.3	D1	2.11.16	AF-126.2	0.0010	B-T	[0/90/0]T	1.006	2 x 0.045	0.0855	2 x 0.750	1.5090	5.935	69.415	3,933	100
LSA 35.4 Avg	D1	2.11.16	AF-126.2	0.0009	B-T	[0/90/0]T	1.007	2 x 0.045	0.0852(B)	2 x 0.750	1.5100	5.930	59.564(B)	3,927	100
LSA 36.1	D1	3.1.8	AF-126.2	0.0015	B-T	[0/-45/0/-45/0]S	1.007	2 x 0.045	0.0896(B)	2 x 1.250	2.5175	10.250	114.397(B)	4,071	100
LSA 36.2	D1	3.1.8	AF-126.2	0.0020	B-T	[0/-45/0/-45/0]S	1.007	2 x 0.045	0.0896(B)	2 x 1.250	2.5175	9.280	102.571(B)	3,686	100 ²
LSA 36.3	D1	3.1.8	AF-126.2	0.0018	B-T	[0/-45/0/-45/0]S	1.008	2 x 0.045	0.0897(B)	2 x 1.250	2.5200	9.810	106.264(B)	3,893	100 ²
LSA 36.4 Avg	D1	3.1.8	AF-126.2	0.0018	B-T	[0/-45/0/-45/0]S	1.007	2 x 0.045	0.0896(T)	2 x 1.250	2.5183	9.780	109.111(B)	3,683	100 ²
LSA 37.1	3SL	6.7.16	AF-126.2	0.0053	B-T	4 x [0/9T]	1.003	0.176	0.1826	2.062	2.0682	12.150	66.575	5,875	10 27 20 36
LSA 37.2	3SL	6.7.16	AF-126.2	0.0063	B-T	4 x [0/9T]	1.003	0.173	0.1788	1.998	2.0040	12.450	69.748	6,212	10 20 6 40
LSA 37.3	3SL	6.7.16	AF-126.2	0.0060	B-T	4 x [0/9T]	1.001	0.174	0.1792	1.948	1.9496	10.750	59.969	5,811	10 20 20 25
LSA 37.4 Avg	3SL	6.7.16	AF-126.2	0.006	B-T	4 x [0/9T]	1.002	0.173	0.1811(B)	1.993	1.9740	11.783	65.477(B)	5,966	10 22 15 34
LSA 40.1	S1	4.5.16	MB-329	0.0051	B-B	[0/8T]	1.019	0.040	0.0408	0.250	0.2548	1.078	26.348	4,219	10 40 50
LSA 40.2	S1	4.5.16	MB-329	0.0040	B-B	[0/8T]	1.019	0.040	0.0408	0.250	0.2548	1.078	26.348	4,219	10 40 50
LSA 40.3	S1	4.5.16	MB-329	0.0040	B-B	[0/8T]	1.020	0.040	0.0408	0.250	0.2548	1.078	26.348	4,219	10 40 50
LSA 40.4 Avg	S1	4.5.16	MB-329	0.0043	B-B	[0/8T]	1.019	0.040	0.0408	0.250	0.2548	1.078	26.348	4,219	10 40 50
LSA 41.1	S1	4.0.16	MB-329	0.0065	B-B	[0/-45/0/-45/0]S	1.003	0.043	0.0431	0.500	0.5015	8.85	19.838	1,705	85 10 5
LSA 41.2	S1	4.0.16	MB-329	0.0080	B-B	[0/-45/0/-45/0]S	1.002	0.043	0.0421	0.500	0.5010	8.70	20.665	1,736	90 5 5
LSA 41.3	S1	4.0.16	MB-329	0.0068	B-B	[0/-45/0/-45/0]S	1.003	0.043	0.0421	0.500	0.5010	8.70	20.665	1,736	90 5 5
LSA 41.4 Avg	S1	4.0.16	MB-329	0.0070	B-B	[0/-45/0/-45/0]S	1.003	0.043	0.0425(B)	0.500	0.5013	8.60	20.578(B)	1,765	86 10 4
LSA 42.1	D1	4.1.4	MB-329	0.0025	B-B	2 x [0/AT] [0/6T]	1.015	0.016	0.0158	2 x 0.250	0.5012	1.410	58.764	3,764	10 15 74
LSA 42.2	D1	4.1.4	MB-329	0.0038	B-B	2 x [0/AT] [0/6T]	1.015	0.016	0.0158	2 x 0.250	0.5012	1.410	58.764	3,764	10 15 74
LSA 42.3	D1	4.1.4	MB-329	0.0038	B-B	2 x [0/AT] [0/6T]	1.015	0.016	0.0158	2 x 0.250	0.5012	1.410	58.764	3,764	10 15 74
LSA 42.4 Avg	D1	4.1.4	MB-329	0.0034	B-B	2 x [0/AT] [0/6T]	1.015	0.016	0.0158(B)	2 x 0.250	0.5012	1.410	58.764	3,764	10 15 74

TABLE F.1 (Cont'd)

Specification Number	Joint Type	Length Between Tabs	Adhesive Thickness	Adhesive Combination	Composite Adherend Fiber Orientation	Composite Adherend Panel Number	Composite Adherend Thickness (Net)	Adhering Width	TI Adhering Thickness, in	Adhering Cross Section Area, in ²	Overlap Length, in	Bonded Joint Area, in ²	Failure Load, lb (m.l)	Adhering Stress at Failure, psi	Adhesive Stress at Failure, psi	*Failure Type %				
																1	2	3	4	5
LSA-41.1	D-L	4.14	MB-329	B-B	2 × [0/90]±0.1° [0/90]±0.1°	B-14A-E-B-15J	2 × 0.049 (0.090)	1.015		0.0914	2 × 0.250	0.5075	1,715	18,764	3,379		20	28	50	2
LSA-41.2	D-L	4.14	MB-329	B-B	2 × [0/90]±0.1° [0/90]±0.1°	B-14A-E-B-15J	2 × 0.049 (0.090)	1.016		0.0914	2 × 0.250	0.5080	1,800	19,694	3,543		25	25	50	
LSA-41.3	D-L	4.14	MB-329	B-B	2 × [0/90]±0.1° [0/90]±0.1°	B-14A-E-B-15J	2 × 0.049 (0.090)	1.016		0.0914	2 × 0.250	0.5080	1,640	17,943	3,228		7	55	36	
LSA-41 Avg	D-L	4.14	MB-329	B-B	2 × [0/90]±0.1° [0/90]±0.1°	B-14A-E-B-15J	2 × 0.049 (0.090)	1.016		0.0914 (B)	2 × 0.250	0.5078	1,718	18,800 (B)	3,383		17	36	46	1
LSA-44.1	D-L	4.14	MB-329	B-B	2 × [0/-45/0/45]±0.1° [0/-45/0/45]±0.1°	B-28A-E-B-17J	2 × 0.044 (0.080)	1.015		0.0893	2 × 0.187	0.3796	2,090	23,404	5,506		50	10	40	
LSA-44.2	D-L	4.516	MB-329	B-B	2 × [0/-45/0/45]±0.1° [0/-45/0/45]±0.1°	B-28A-E-B-17J	2 × 0.044 (0.080)	1.015		0.0893	2 × 0.250	0.5075	1,770	19,821	3,488		45	10	40	5
LSA-44.3	D-L	4.516	MB-329	B-B	2 × [0/-45/0/45]±0.1° [0/-45/0/45]±0.1°	B-28A-E-B-17J	2 × 0.044 (0.080)	1.015		0.0893	2 × 0.250	0.5075	2,170	24,390	4,276		75	10	15	
LSA-44 Avg	D-L	4.516	MB-329	B-B	2 × [0/-45/0/45]±0.1° [0/-45/0/45]±0.1°	B-28A-E-B-17J	2 × 0.044 (0.080)	1.015		0.0893 (B)	2 × 0.229	0.4649	2,010	22,508	4,423		57	10	32	1
LSA-45.1	S-L	2.516	MB-329	B-T	[0/67]	B-18H	0.031	1.011	0.032	0.0313	0.250	0.2528	810	25,878	3,204		5	80	15	
LSA-45.2	S-L	2.516	MB-329	B-T	[0/67]	B-18H	0.031	1.009	0.032	0.0293	0.250	0.2522	740	25,236	2,934		5	93	2	
LSA-45.3	S-L	2.516	MB-329	B-T	[0/67]	B-18H	0.031	1.010	0.032	0.0303	0.250	0.2525	780	25,742	3,089		5	85	10	
LSA-45 Avg	S-L	2.516	MB-329	B-T	[0/67]	B-18H	0.031	1.010	0.032	0.0303 (B)	0.250	0.2525	777	25,625 (B)	3,076		5	86	9	
LSA-46.1	S-L	3.132	MB-329	B-T	[0/-45/0/45]±0.1° [0/-45/0/45]±0.1°	B-28F	0.043	1.008	0.045	0.0433	0.500	0.5040	1,020	23,556	2,024		30	5	60	5
LSA-46.2	S-L	3.116	MB-329	B-T	[0/-45/0/45]±0.1° [0/-45/0/45]±0.1°	B-28F	0.043	1.009	0.045	0.0434	0.500	0.5045	980	22,581	1,942		75	5	20	
LSA-46.3	S-L	3.116	MB-329	B-T	[0/-45/0/45]±0.1° [0/-45/0/45]±0.1°	B-28F	0.043	1.009	0.045	0.0434	0.500	0.5045	920	21,198	1,824		80	5	15	
LSA-46 Avg	S-L	3.116	MB-329	B-T	[0/-45/0/45]±0.1° [0/-45/0/45]±0.1°	B-28F	0.043	1.009	0.045	0.0434 (B)	0.500	0.5043	973	22,445 (B)	1,930		62	5	32	1
LSA-47.1	D-L	2.14	MB-329	B-T	[0/67]	B-18D	0.029	1.015	2 × 0.016	0.0294	2 × 0.250	0.5075	2,735	36,224	5,389		10	85	5	
LSA-47.2	D-L	2.14	MB-329	B-T	[0/67]	B-18D	0.029	1.016	2 × 0.016	0.0305	2 × 0.250	0.5075	2,430	39,672	4,783		10	10	5	75
LSA-47.3	D-L	2.14	MB-329	B-T	[0/67]	B-18D	0.029	1.014	2 × 0.016	0.0304	2 × 0.250	0.5075	2,770	91,115	5,464		5	5	19	80
LSA-47 Avg	D-L	2.14	MB-329	B-T	[0/67]	B-18D	0.029	1.015	2 × 0.016	0.0301 (B)	2 × 0.250	0.5075	2,645	85,671 (B)	5,212		5	8	80	2
LSA-48.1	D-L	2.14	MB-329	B-T	[0/90]±0.1° [0/90]±0.1°	B-15B	0.087	1.017	2 × 0.045	0.0845	2 × 0.250	0.5085	2,345	26,497	4,612		35	5	55	5
LSA-48.2	D-L	2.14	MB-329	B-T	[0/90]±0.1° [0/90]±0.1°	B-15B	0.087	1.014	2 × 0.045	0.0872	2 × 0.250	0.5075	2,410	27,638	4,753		3	52	45	
LSA-48.3	D-L	2.14	MB-329	B-T	[0/90]±0.1° [0/90]±0.1°	B-15B	0.087	1.012	2 × 0.045	0.0868	2 × 0.250	0.5075	2,770	31,912	5,426		8	82	10	
LSA-48 Avg	D-L	2.14	MB-329	B-T	[0/90]±0.1° [0/90]±0.1°	B-15B	0.087	1.017	2 × 0.045	0.0867 (B)	2 × 0.250	0.508	2,508	28,662 (B)	4,930		13	4	63	20
LSA-49.1	D-L	2.516	MB-329	B-T	[0/-45/0/45]±0.1° [0/-45/0/45]±0.1°	B-22A	0.059	1.017	2 × 0.045	0.0585	2 × 0.250	0.5085	1,625	11,326	2,016		20	18	60	2
LSA-49.2	D-L	2.516	MB-329	B-T	[0/-45/0/45]±0.1° [0/-45/0/45]±0.1°	B-22A	0.059	1.009	2 × 0.045	0.0585	2 × 0.250	0.5075	1,865	12,251	2,581		10	10	40	
LSA-49.3	D-L	2.516	MB-329	B-T	[0/-45/0/45]±0.1° [0/-45/0/45]±0.1°	B-22A	0.059	1.009	2 × 0.045	0.0585	2 × 0.250	0.5075	1,830	11,440	2,581		20	5	75	
LSA-49 Avg	D-L	2.516	MB-329	B-T	[0/-45/0/45]±0.1° [0/-45/0/45]±0.1°	B-22A	0.059	1.017	2 × 0.045	0.0585 (B)	2 × 0.250	0.508	1,787	11,969 (B)	2,212		17	11	71	1
LSA-53.1	S-L	5.516	MB-329	B-B	[0/67]	B-25I-K	0.041 (0.041)	1.015		0.0415	1.250	1.2662	1,260	77,531	2,551		10	45	5	
LSA-53.2	S-L	5.516	MB-329	B-B	[0/67]	B-25I-K	0.041 (0.041)	1.015		0.0415	1.250	1.2662	1,260	76,356	2,443		85	5	10	
LSA-53.3	S-L	5.516	MB-329	B-B	[0/67]	B-25I-K	0.041 (0.041)	1.013		0.0415	1.250	1.2662	1,260	69,249	2,215		10	40	10	
LSA-53 Avg	S-L	5.516	MB-329	B-B	[0/67]	B-25I-K	0.041 (0.041)	1.014		0.0415 (B)	1.250	1.2662	1,260	74,452	2,413		26	5	65	9
LSA-54.1	S-L	5.916	MB-329	B-B	[0/-45/0/45]±0.1° [0/-45/0/45]±0.1°	B-25I-H	0.042 (0.042)	1.012		0.0415	1.500	1.580	1,515	49,090	1,406		80	10	10	
LSA-54.2	S-L	5.516	MB-329	B-B	[0/-45/0/45]±0.1° [0/-45/0/45]±0.1°	B-25I-H	0.042 (0.042)	1.014		0.0415	1.500	1.580	1,515	49,144	1,410		60	10	30	
LSA-54.3	S-L	5.516	MB-329	B-B	[0/-45/0/45]±0.1° [0/-45/0/45]±0.1°	B-25I-H	0.042 (0.042)	1.014		0.0415	1.500	1.580	1,515	50,229	1,436		85	10	10	
LSA-54 Avg	S-L	5.516	MB-329	B-B	[0/-45/0/45]±0.1° [0/-45/0/45]±0.1°	B-25I-H	0.042 (0.042)	1.013		0.0415 (B)	1.500	1.576	1,515	49,592 (B)	1,418		75	10	10	15

TABLE F. I (Cont'd)

Specification Number	Joint Type	Length Between Tabs	Adhesive Thickness	Adhesive Combination	Composite Adherent Fiber Orientation	Composite Adherent Panel Number	Composite Adherent Thickness (in)	Adherent Width	II Adherent Thickness (in)	Adherent Cross Section Area (in ²)	Overlap Length (in)	Bonded Joint Area (in ²)	Failure Load (lb/in)	Adherent Stress at Failure (psi)	Adhesive Stress at Failure (psi)	Failure Type	Notes
LSA 55-1	D1	4.3/8	0.0052	B-B	2 × [0/31°/0/67°]	B-12B C, B-13J	2 × 0.016 (0.030)	1.013	0.0324	0.0324	2 × 0.500	1.0130	3.840	118,518	3,791	45	20
LSA 55-2	D1	4.3/8	0.0052	B-B	2 × [0/31°/0/67°]	B-12B C, B-13J	2 × 0.016 (0.030)	1.013	0.0324	0.0324	2 × 0.500	1.0130	4.845	143,364	4,585	25	25
LSA 55-3	D1	4.3/8	0.0060	B-B	2 × [0/31°/0/67°]	B-12B C, B-13J	2 × 0.016 (0.030)	1.012	0.0324	0.0324	2 × 0.500	1.0120	4.415	136,265	4,367	23	45
LSA 55-Avg	D1	4.3/8	0.0055	B-B	2 × [0/31°/0/67°]	B-12B C, B-13J	2 × 0.016 (0.030)	1.012	0.0324	0.0324	2 × 0.500	1.0120	4.300	132,716	4,248	23	55
LSA 56-1	D1	4.1/2	0.0048	B-B	2 × [0/40/0/71°]	B-14 C, B-19A	2 × 0.047 (0.094)	1.012	0.0890	0.0890	2 × 0.750	1.5180	4.950	55,617	3,261	18	10
LSA 56-2	D1	4.1/2	0.0045	B-B	2 × [0/40/0/71°]	B-14 C, B-19A	2 × 0.047 (0.094)	1.012	0.0890	0.0890	2 × 0.750	1.5180	4.945	55,562	3,258	18	15
LSA 56-3	D1	4.1/2	0.0045	B-B	2 × [0/40/0/71°]	B-14 C, B-19A	2 × 0.047 (0.094)	1.015	0.0893	0.0893	2 × 0.750	1.5225	5.250	58,791	3,448	10	10
LSA 56-Avg	D1	4.1/2	0.0046	B-B	2 × [0/40/0/71°]	B-14 C, B-19A	2 × 0.047 (0.094)	1.013	0.0891	0.0891	2 × 0.750	1.5195	5.048	56,657	3,322	15	12
LSA 57-1	D1	4.7/8	0.0085	B-B	2 × [0/45/0/45/0/5°]	B-24 C, B-22K	2 × 0.046 (0.092)	1.013	0.0881	0.0881	2 × 1.000	2.0260	4.750	53,916	2,344	35	13
LSA 57-2	D1	4.7/8	0.0065	B-B	2 × [0/45/0/45/0/5°]	B-24 C, B-22K	2 × 0.046 (0.092)	1.013	0.0861	0.0861	2 × 1.000	2.0260	5.510	63,095	2,720	35	5
LSA 57-3	D1	4.7/8	0.0092	B-B	2 × [0/45/0/45/0/5°]	B-24 C, B-22K	2 × 0.046 (0.092)	1.014	0.0862	0.0862	2 × 1.000	2.0280	5.510	63,021	2,717	35	10
LSA 57-Avg	D1	4.7/8	0.0081	B-B	2 × [0/45/0/45/0/5°]	B-24 C, B-22K	2 × 0.046 (0.092)	1.013	0.0860	0.0860	2 × 1.000	2.0267	5.257	60,611	2,594	35	9
LSA 58-1	D1	5.3/16	0.0050	B-1	[0/67°]	B-13D	0.032	1.009	0.032	0.0323	1.250	1.2612	1.905	58,978	1,510	15	40
LSA 58-2	D1	5.3/16	0.0055	B-1	[0/67°]	B-13D	0.032	1.012	0.032	0.0314	1.250	1.2650	1.915	60,987	1,514	10	30
LSA 58-3	D1	5.3/16	0.0065	B-1	[0/67°]	B-13D	0.032	1.012	0.032	0.0324	1.250	1.2650	2.050	63,272	1,620	5	25
LSA 58-Avg	D1	5.3/16	0.0052	B-1	[0/67°]	B-13D	0.032	1.011	0.032	0.0320	1.250	1.2617	1.957	61,079	1,548	10	22
LSA 59-1	D1	5.7/16	0.0050	B-1	[0/45/0/45/0/5°]	B-24M	0.043	1.013	0.045	0.0436	1.437	1.4557	1.960	44,954	1,346	5	35
LSA 59-2	D1	5.7/16	0.0040	B-1	[0/45/0/45/0/5°]	B-24M	0.043	1.012	0.045	0.0438	1.437	1.4542	2.070	47,586	1,423	5	10
LSA 59-3	D1	5.7/16	0.0070	B-1	[0/45/0/45/0/5°]	B-24M	0.043	1.013	0.045	0.0438	1.437	1.4557	2.250	51,606	1,544	7	10
LSA 59-Avg	D1	5.7/16	0.0057	B-1	[0/45/0/45/0/5°]	B-24M	0.043	1.013	0.045	0.0438	1.437	1.4557	2.083	48,070	1,433	4	8
LSA 60-1	D1	3.3/8	0.004	B-1	[0/67°]	B-13D	0.030	1.003	0.030	0.0301	2 × 0.500	1.0030	1.210	40,192	1,206	27	50
LSA 60-2	D1	3.3/8	0.006	B-1	[0/67°]	B-13D	0.030	1.003	0.030	0.0301	2 × 0.500	1.0030	1.350	43,408	1,446	30	60
LSA 60-3	D1	3.3/8	0.0063	B-1	[0/67°]	B-13D	0.030	1.003	0.030	0.0301	2 × 0.500	1.0030	1.430	44,548	1,426	20	60
LSA 60-Avg	D1	3.3/8	0.0053	B-1	[0/67°]	B-13D	0.030	1.003	0.030	0.0301	2 × 0.500	1.0030	1.330	42,718	1,326	22	57
LSA 61-1	D1	2.3/4	0.0060	B-1	[0/40/0/71°]	B-19A	0.090	1.007	0.045	0.0902	2 × 0.687	1.3767	4.985	54,053	3,599	15	5
LSA 61-2	D1	2.3/16	0.0072	B-1	[0/40/0/71°]	B-19A	0.090	1.008	0.045	0.0924	2 × 0.687	1.3804	4.815	50,503	3,276	20	55
LSA 61-3	D1	2.3/16	0.0068	B-1	[0/40/0/71°]	B-19A	0.090	1.002	0.045	0.0902	2 × 0.687	1.3804	4.640	51,441	3,087	5	20
LSA 61-Avg	D1	2.3/16	0.0067	B-1	[0/40/0/71°]	B-19A	0.090	1.003	0.045	0.0902	2 × 0.687	1.3767	4.703	52,292	3,319	2	18
LSA 62-1	D1	3	0.0088	B-1	[0/45/0/45/0/5°]	B-22B	0.080	1.006	0.045	0.0898	2 × 1.000	2.912	5.070	56,048	2,520	10	5
LSA 62-2	D1	3	0.0100	B-1	[0/45/0/45/0/5°]	B-22B	0.088	1.006	0.045	0.0898	2 × 1.000	2.912	5.300	59,218	2,634	10	5
LSA 62-3	D1	3	0.0105	B-1	[0/45/0/45/0/5°]	B-22B	0.088	1.004	0.045	0.0884	2 × 1.000	2.910	5.217	58,057	2,595	10	5
LSA 62-Avg	D1	3	0.0099	B-1	[0/45/0/45/0/5°]	B-22B	0.088	1.008	0.045	0.0891	2 × 1.000	2.911	5.193	58,268	2,483	10	5

TABLE F. I (Cont'd)

Specification Number	Joint Type	Length Between Tabs	Adhesive Thickness	Adherend Combination	Composite Adherend Fiber Orientation	Composite Adherend Panel Number	Composite Adherend Thickness (Net)	Adherend Width	TI Adherend Thickness, in	Adherend Cross-Section Area, in ²	Overlap Length, in	Bonded Joint Area, in ²	Failure Load (lb/in)	Adherend Stress at Failure, psi	Adhesive Stress at Failure, psi	Failure Type, %				
																1	2	3	4	5
LSA-66-1	S L	6	MB-329	B-B	[0/±1]	B-25G/L	0.041/0.040	1.008		0.0403	2.250	2.2680	5.150	127.792	2.271	20	75	5		
LSA-66-2	S L	6	MB-329	B-B	[0/±1]	B-25G/L	0.041/0.041	1.010		0.0414	2.250	2.2725	5.205	125.725	2.290	20	65	15		
LSA-66-3	S L	6	MB-329	B-B	[0/±1]	B-25G/L	0.041/0.040	1.007		0.0403	2.250	2.2658	4.350	107.940	1.920	15	70	15		
LSA-66 Avg	S L	6	MB-329	B-B	[0/±1]	B-25G/L	0.041/0.040	1.008		0.0407(B)	2.250	2.2688	4.902	120.486(B)	2.160	18	70	12		
LSA-67-1	S L	6-3/8	MB-329	B-B	[0/-45/0/-45/0/±1]	B-16C/F	0.047/0.048	1.008		0.0474	2.500	2.5200	2.760	68.228	1.095	95				
LSA-67-2	S L	6-3/8	MB-329	B-B	[0/-45/0/-45/0/±1]	B-16C/F	0.047/0.047	1.010		0.0475	2.500	2.5200	3.020	63.579	1.196	85				
LSA-67-3	S L	6-3/8	MB-329	B-B	[0/-45/0/-45/0/±1]	B-16C/F	0.047/0.048	1.003		0.0471	2.500	2.5075	3.350	71.125	1.336	75				
LSA-67 Avg	S L	6-3/8	MB-329	B-B	[0/-45/0/-45/0/±1]	B-16C/F	0.047/0.047	1.007		0.0471(B)	2.500	2.5175	3.043	64.311(B)	1.209	85				
LSA-68-1	D L	4-7/8	MB-329	B-B	2 x [0/±1] [0/±1]	B-12N, B-13L	2 x 0.016/0.030	1.013		0.0324	2 x 1.000	2.0260	3.555	109.722	1.755	30	10	55		
LSA-68-2	D L	4-7/8	MB-329	B-B	2 x [0/±1] [0/±1]	B-12N, B-13L	2 x 0.016/0.030	1.013		0.0324	2 x 1.000	2.0260	4.150	128.086	2.048	40	20	65		
LSA-68-3	D L	4-7/8	MB-329	B-B	2 x [0/±1] [0/±1]	B-12N, B-13L	2 x 0.016/0.030	1.011		0.0324	2 x 1.000	2.0220	4.330	133.641	2.141	40	20	65		
LSA-68 Avg	D L	4-7/8	MB-329	B-B	2 x [0/±1] [0/±1]	B-12N, B-13L	2 x 0.016/0.030	1.012		0.0324(B)	2 x 1.000	2.0247	4.012	127.816(B)	1.981	11		25		
LSA-69-1	D L	5-5/16	MB-329	B-B	2 x [0/90/±1] [0/90/±1]	B-14D H, B-15D	2 x 0.047/0.090	1.011		0.0910	2 x 1.500	3.0330	5.290	67.143	1.714	62	10	25		
LSA-69-2	D L	5-5/16	MB-329	B-B	2 x [0/90/±1] [0/90/±1]	B-14D H, B-15D	2 x 0.047/0.088	1.010		0.0889	2 x 1.500	3.0300	5.275	59.336	1.741	41	2	20		
LSA-69-3	D L	5-5/16	MB-329	B-B	2 x [0/90/±1] [0/90/±1]	B-14D H, B-15D	2 x 0.047/0.087	1.014		0.0882	2 x 1.500	3.0420	4.245	48.129	1.395	65	3	17		
LSA-69 Avg	D L	5-5/16	MB-329	B-B	2 x [0/90/±1] [0/90/±1]	B-14D H, B-15D	2 x 0.047/0.088	1.012		0.0884(B)	2 x 1.500	3.0350	4.907	54.869(B)	1.617	56	5	21		
LSA-70-1	D L	5-1/2	MB-329	B-B	2 x [0/-45/0/-45/0/±1]	B-16B H, B-17C	2 x 0.047/0.087	1.007		0.0876	2 x 1.750	3.5245	4.770	54.452	1.353	80				
LSA-70-2	D L	5-1/2	MB-329	B-B	2 x [0/-45/0/-45/0/±1]	B-16B H, B-17C	2 x 0.047/0.089	1.010		0.0899	2 x 1.750	3.5350	4.080	45.384	1.154	60	5	35		
LSA-70-3	D L	5-1/2	MB-329	B-B	2 x [0/-45/0/-45/0/±1]	B-16B H, B-17C	2 x 0.047/0.087	1.011		0.0880	2 x 1.750	3.5385	6.370	72.386	1.800	35				
LSA-70 Avg	D L	5-1/2	MB-329	B-B	2 x [0/-45/0/-45/0/±1]	B-16B H, B-17C	2 x 0.047/0.088	1.009		0.0885(B)	2 x 1.750	3.5327	5.073	57.407(B)	1.436	58	2	38		
LSA-71-1	S L	4-1/4	MB-329	B-T	[0/±1]	B-18	0.032	0.999		0.032	2.250	2.2478	3.665	95.781	1.364	35	10	45		
LSA-71-2	S L	4-1/4	MB-329	B-T	[0/±1]	B-18	0.032	1.000		0.032	2.250	2.2500	2.840	98.750	1.262	5	10	20		
LSA-71-3	S L	4-1/4	MB-329	B-T	[0/±1]	B-18	0.032	1.000		0.032	2.250	2.2500	2.660	76.525	1.093	5	10	50		
LSA-71 Avg	S L	4-1/4	MB-329	B-T	[0/±1]	B-18	0.032	1.000		0.032(B)	2.250	2.2493	2.788	87.135(B)	1.240	3	42	10	38	
LSA-72-1	S L	4-9/16	MB-329	B-T	[0/-45/0/-45/0/±1]	B-16J	0.047	1.009		0.0473	2.500	2.5000	1.870	39.758	748	90				
LSA-72-2	S L	4-9/16	MB-329	B-T	[0/-45/0/-45/0/±1]	B-16J	0.048	1.004		0.0482	2.500	2.5100	2.325	48.236	926	45	5			
LSA-72-3	S L	4-9/16	MB-329	B-T	[0/-45/0/-45/0/±1]	B-16J	0.048	1.007		0.0483	2.500	2.5175	2.450	50.725	973	10	10	70		
LSA-72 Avg	S L	4-9/16	MB-329	B-T	[0/-45/0/-45/0/±1]	B-16J	0.048	1.004		0.0478(B)	2.500	2.5092	2.215	46.249(B)	882	48	5			

TABLE F.1 (Cont'd)

Specification Number	Joint Type	Length Between Tabs	Adhesive Thickness	Adhesive Combination	Composite Adhesive Fiber Orientation	Composite Adhesive Panel Number	Composite Adhesive Thickness (Net)	Adherend Width	TI Adherend Thickness, in	Adherend Cross-Section Area, in ²	Overlap Length, in	Bonded Joint Area, in ²	Failure Load, (lb/in)	Adherend Stress at Failure, %	Adhesive Failure, psi		Failure Type					
															1	2	3	4	5	6		
LSA-73.1	D.L	2-3/4	MB-329	0.0058	B-T	[0] 6T	B-18B	1.005	2 × 0.016	0.0312(B) 0.0322(TI)	2 × 1.000	2.010	4.385	140.545(B) 136.180(TI)	2,181	5	10	30	5	50 ²		
LSA-73.2	D.L	2-3/4	MB-329	0.0055	B-T	[0] 6T	B-18B	1.007	2 × 0.016	0.0302(B) 0.0322(TI)	2 × 1.000	2.014	4.320	143.046(B) 134.161(TI)	2,145			100	4			
LSA-73.3	D.L	2-3/4	MB-329	0.0055	B-T	[0] 6T	B-18B	1.006	2 × 0.016	0.0302(B) 0.0322(TI)	2 × 1.000	2.012	4.475	148.179(B) 138.975(TI)	2,224	10	5	30	5	50 ²		
LSA-73 Avg	D.L	2-3/4	MB-329	0.0056	B-T	[0] 6T	B-18B	1.006	2 × 0.016	0.0303(B) 0.0322(TI)	2 × 1.000	2.012	4.393	143.933(B) 136.439(TI)	2,183	5	3	20	37	13 ²		
LSA-74.1	D.L	3-7/16	MB-329	0.0055	B-T	[0] 40/0 0 1 T	B-15M	1.007	2 × 0.045	0.0896	2 × 1.500	3.0210	4.205	46.931	1,392	40	5	37	13			
LSA-74.2	D.L	3-7/16	MB-329	0.0060	B-T	[0] 40/0 0 1 T	B-15M	1.009	2 × 0.045	0.0888	2 × 1.500	3.0270	5.740	64.640	1,896	16				90 ²		
LSA-74.3	D.L	3-7/16	MB-329	0.0060	B-T	[0] 40/0 0 1 T	B-15M	1.008	2 × 0.045	0.0888	2 × 1.500	3.0270	5.045	56.813	1,667	10	3	5	37	45		
LSA-74 Avg	D.L	3-7/16	MB-329	0.0058	B-T	[0] 40/0 0 1 T	B-15M	1.008	2 × 0.045	0.0891(B)	2 × 1.500	3.0250	4.997	56.128(B)	1,652	20	3	24	20	30 ²		
LSA-75.1	D.L	3-11/16	MB-329	0.0068	B-T	[0] 45/0 45/0 0 1 S	B-17I	1.009	2 × 0.045	0.0898	2 × 1.718	3.4660	3.715	41.370	1,022	42	3	30	5			
LSA-75.2	D.L	3-11/16	MB-329	0.0055	B-T	[0] 45/0 45/0 0 1 S	B-17I	1.010	2 × 0.045	0.0909	2 × 1.687	3.4077	4.365	48.240	1,287	5	37	55	3			
LSA-75.3	D.L	3-11/16	MB-329	0.0072	B-T	[0] 45/0 45/0 0 1 S	B-17I	1.010	2 × 0.045	0.0909	2 × 1.687	3.4077	3.860	42.464	1,133	25	34	65	10			
LSA-75 Avg	D.L	3-11/16	MB-329	0.0065	B-T	[0] 45/0 45/0 0 1 S	B-17I	1.010	2 × 0.045	0.0905(B)	2 × 1.687	3.4274	3.947	44.025(B)	1,164	2	34	1	57	6		

Note: Stipped adherends for step lap (SL) joints made by bonding up 2 or more laminates or T-joints.

- Failure Types
1. Adhesive to B/S
 2. Adhesive to TI
 3. Cohesive
 4. Surface Resin
 5. Interlaminar
 6. Other

- Adherend Section Tension
1. Net section tension
 2. Net section tension
 3. Net section tension
 4. Net section tension
 5. Net section tension
 6. Net section tension
 7. Net section tension
 8. Net section tension
 9. Net section tension
 10. Net section tension
 11. Net section tension
 12. Net section tension
 13. Net section tension
 14. Net section tension
 15. Net section tension
 16. Net section tension
 17. Net section tension
 18. Net section tension
 19. Net section tension
 20. Net section tension
 21. Net section tension
 22. Net section tension
 23. Net section tension
 24. Net section tension
 25. Net section tension
 26. Net section tension
 27. Net section tension
 28. Net section tension
 29. Net section tension
 30. Net section tension
 31. Net section tension
 32. Net section tension
 33. Net section tension
 34. Net section tension
 35. Net section tension
 36. Net section tension
 37. Net section tension
 38. Net section tension
 39. Net section tension
 40. Net section tension
 41. Net section tension
 42. Net section tension
 43. Net section tension
 44. Net section tension
 45. Net section tension
 46. Net section tension
 47. Net section tension
 48. Net section tension
 49. Net section tension
 50. Net section tension
 51. Net section tension
 52. Net section tension
 53. Net section tension
 54. Net section tension
 55. Net section tension
 56. Net section tension
 57. Net section tension
 58. Net section tension
 59. Net section tension
 60. Net section tension
 61. Net section tension
 62. Net section tension
 63. Net section tension
 64. Net section tension
 65. Net section tension
 66. Net section tension
 67. Net section tension
 68. Net section tension
 69. Net section tension
 70. Net section tension
 71. Net section tension
 72. Net section tension
 73. Net section tension
 74. Net section tension
 75. Net section tension
 76. Net section tension
 77. Net section tension
 78. Net section tension
 79. Net section tension
 80. Net section tension
 81. Net section tension
 82. Net section tension
 83. Net section tension
 84. Net section tension
 85. Net section tension
 86. Net section tension
 87. Net section tension
 88. Net section tension
 89. Net section tension
 90. Net section tension
 91. Net section tension
 92. Net section tension
 93. Net section tension
 94. Net section tension
 95. Net section tension
 96. Net section tension
 97. Net section tension
 98. Net section tension
 99. Net section tension
 100. Net section tension

APPENDIX G

NONLINEAR DESIGN/ANALYSIS PROGRAM

FAILURE/BEHAVIOR PREDICTION RESULTS ON SIMPLE JOINTS

APPENDIX G.1

FAILURE LOAD PREDICTION RESULTS ON SIMPLE JOINTS

LSA 20 SINGLE LAP COMPOSITE TO TITANIUM ADHERENDS, LSHE ADHESIVE

NONLINEAR ORTHOTROPIC ANALYSIS, SINGLE LAP JOINT

TOTAL LENGTH = 3.2500
 JOINT LENGTH = 1.2500
 ERROR TOLERANCE = .025
 MAXIMUM ITERATIONS = 20
 NUMBER OF STATIONS = 61
 EFFECTIVE K = .010

ADHESIVE
 THICKNESS = .0028
 POISSONS RATIO = .40
 RAMBERG USGOOD CONSTANTS (SHEAR STRESS-STRAIN CURVE)
 G = 80600
 SECANT S = 3740
 N VALUE = 6.318

ADHEREND NUMBER 1(ORTHOTROPIC)
 THICKNESS .0467
 NUMBER OF LAYERS 9
 RAMBERG USGOOD CONSTANTS E
 SL VS. EL 27489000 -0 -0.000
 SL VS. ET -133604000 -0 -0.000
 ST VS. ET 2750000 11910 2.541
 SLT VS. ELT 933000 7950 2.991
 ORIENTATIONS 0 45 0 -45 0 45 0

ADHEREND NUMBER 2(ISOTROPIC)
 THICKNESS .0450
 POISSONS RATIO .3062
 RAMBERG USGOOD CONSTANTS E
 S VS. E 17251000
 SECANT S 136600
 N 37.246

ULTIMATE LOAD PREDICTION BASED ON
 ADHESIVE - MX STRESS, SU = 7.17E+03
 ADHEREND 1 - MX STRAIN, SL = 5.76E-03, ST = 4.01E-03, SLT = 1.50E-02
 ADHEREND 2 - MX STRESS, SL = 1.38E+05

ALPHA = 7.3919E+00
 BETA = 7.3915E+00
 LAMDA = 8.2150E+00
 N RESET TO 31

```

ITERATION FOR ULTIMATE LOAD
LOAD = 1
  AT ITERATION 1 ERROR IS 2.69E-09
  MAXIMUM STRESS(STRAIN)/ALLOWABLE = .001 IN ADHESIVE
LOAD = 789
  AT ITERATION 1 ERROR IS 1.11E-01
  AT ITERATION 2 ERROR IS 7.24E-03
  MAXIMUM STRESS(STRAIN)/ALLOWABLE = .458 IN ADHESIVE
LOAD = 1255
  AT ITERATION 1 ERROR IS 2.51E-01
  AT ITERATION 2 ERROR IS 5.44E-02
  AT ITERATION 3 ERROR IS 1.64E-02
  MAXIMUM STRESS(STRAIN)/ALLOWABLE = .602 IN ADHESIVE
LOAD = 1699
  AT ITERATION 1 ERROR IS 3.44E-01
  AT ITERATION 2 ERROR IS 1.35E-01
  AT ITERATION 3 ERROR IS 6.56E-02
  AT ITERATION 4 ERROR IS 3.52E-02
  AT ITERATION 5 ERROR IS 1.68E-02
  MAXIMUM STRESS(STRAIN)/ALLOWABLE = .717 IN ADHESIVE
LOAD = 2688
  AT ITERATION 1 ERROR IS 3.87E-01
  AT ITERATION 2 ERROR IS 1.97E-01
  AT ITERATION 3 ERROR IS 1.20E-01
  AT ITERATION 4 ERROR IS 7.74E-02
  AT ITERATION 5 ERROR IS 5.11E-02
  AT ITERATION 6 ERROR IS 3.36E-02
  AT ITERATION 7 ERROR IS 2.22E-02
  MAXIMUM STRESS(STRAIN)/ALLOWABLE = .817 IN ADHESIVE
LOAD = 3915
  AT ITERATION 1 ERROR IS 3.54E-01
  AT ITERATION 2 ERROR IS 1.98E-01
  AT ITERATION 3 ERROR IS 1.35E-01
  AT ITERATION 4 ERROR IS 9.64E-02
  AT ITERATION 5 ERROR IS 7.13E-02
  AT ITERATION 6 ERROR IS 5.29E-02
  AT ITERATION 7 ERROR IS 3.93E-02
  AT ITERATION 8 ERROR IS 2.92E-02
  AT ITERATION 9 ERROR IS 2.17E-02
  MAXIMUM STRESS(STRAIN)/ALLOWABLE = .885 IN ADHESIVE
LOAD = 4032
  AT ITERATION 1 ERROR IS 3.15E-01
  AT ITERATION 2 ERROR IS 1.77E-01
  AT ITERATION 3 ERROR IS 1.26E-01
  AT ITERATION 4 ERROR IS 9.54E-02
  AT ITERATION 5 ERROR IS 7.42E-02
  AT ITERATION 6 ERROR IS 5.87E-02
  AT ITERATION 7 ERROR IS 4.65E-02
  AT ITERATION 8 ERROR IS 3.68E-02
  AT ITERATION 9 ERROR IS 2.92E-02
  AT ITERATION 10 ERROR IS 2.31E-02
  MAXIMUM STRESS(STRAIN)/ALLOWABLE = .935 IN ADHESIVE
LOAD = 4435
  AT ITERATION 1 ERROR IS 2.30E-01
  AT ITERATION 2 ERROR IS 1.27E-01
  AT ITERATION 3 ERROR IS 9.24E-02
  AT ITERATION 4 ERROR IS 7.17E-02
  AT ITERATION 5 ERROR IS 5.64E-02
  AT ITERATION 6 ERROR IS 4.65E-02
  AT ITERATION 7 ERROR IS 3.80E-02
  AT ITERATION 8 ERROR IS 3.11E-02

```

AT ITERATION 9 ERROR IS 2.55E-02
 AT ITERATION 10 ERROR IS 2.08E-02
 MAXIMUM STRESS(STRAIN)/ALLOWABLE = .962 IN ADHESIVE
 LOAD = 4718
 AT ITERATION 1 ERROR IS 1.73E-01
 AT ITERATION 2 ERROR IS 9.47E-02
 AT ITERATION 3 ERROR IS 6.96E-02
 AT ITERATION 4 ERROR IS 5.48E-02
 AT ITERATION 5 ERROR IS 4.42E-02
 AT ITERATION 6 ERROR IS 3.46E-02
 AT ITERATION 7 ERROR IS 3.05E-02
 AT ITERATION 8 ERROR IS 2.54E-02
 AT ITERATION 9 ERROR IS 2.12E-02
 MAXIMUM STRESS(STRAIN)/ALLOWABLE = 1.015 IN ADHESIVE
 LOAD = 4577
 AT ITERATION 1 ERROR IS 1.07E-02
 MAXIMUM STRESS(STRAIN)/ALLOWABLE = 1.006 IN ADHESIVE

THE PREDICTED ULTIMATE LOAD IS 4577

RESULTS FOR P = 4677

NUMBER OF ITERATIONS = 1 , MAXIMUM ERROR = .01071

X	TAU	SIGMA	NX1	MX1	NX2	MX2
0.0000	5.9256E+03	1.7368E+03	4.3656E-11	0.	4.6775E+03	-6.5988E-01
.0417	5.8000E+03	1.3236E+03	2.4441E+02	-4.3080E-02	4.4331E+03	-6.1838E-01
.0833	5.6403E+03	9.1784E+02	4.8254E+02	-6.1887E-02	4.1942E+03	-5.5552E-01
.1250	5.4482E+03	5.3614E+02	7.1359E+02	-6.2878E-02	3.9639E+03	-4.7807E-01
.1667	5.2246E+03	1.9437E+02	9.3584E+02	-5.2619E-02	3.7416E+03	-3.9340E-01
.2083	4.9690E+03	-4.4118E+01	1.1482E+03	-3.6442E-02	3.5292E+03	-3.0738E-01
.2500	4.6787E+03	-3.1844E+02	1.3492E+03	-1.9297E-02	3.3283E+03	-2.2554E-01
.2917	4.3479E+03	-4.7010E+02	1.5373E+03	-4.4852E-03	3.1401E+03	-1.5197E-01
.3333	3.9648E+03	-5.4357E+02	1.7106E+03	5.7277E-03	2.9669E+03	-8.4800E-02
.3750	3.5044E+03	-5.3580E+02	1.8665E+03	1.0687E-02	2.8109E+03	-4.0843E-02
.4167	2.9624E+03	-4.5285E+02	2.0017E+03	1.1327E-02	2.6758E+03	-5.7438E-03
.4583	2.3544E+03	-3.2064E+02	2.1124E+03	4.8413E-03	2.5651E+03	1.5046E-02
.5000	1.8157E+03	-1.8711E+02	2.1988E+03	8.5444E-03	2.4787E+03	2.5884E-02
.5417	1.4354E+03	-2.44817E+01	2.2660E+03	8.4125E-03	2.4115E+03	3.0046E-02
.5833	1.2143E+03	-2.3678E+01	2.3207E+03	9.6518E-03	2.3562E+03	2.8880E-02
.6250	1.1304E+03	-4.6158E+00	2.3641E+03	1.1887E-02	2.3082E+03	2.5806E-02
.6667	1.1765E+03	-2.6356E+01	2.4167E+03	1.4174E-02	2.2502E+03	2.2424E-02
.7083	1.3573E+03	-8.7043E+01	2.4402E+03	1.4846E-02	2.2082E+03	1.9580E-02
.7500	1.6894E+03	-3.3333E+02	2.5314E+03	1.1479E-02	2.1455E+03	1.7564E-02
.7917	2.1453E+03	-3.1055E+02	2.6121E+03	8.6256E-04	2.0654E+03	1.6201E-02
.8333	2.7677E+03	-4.2646E+02	2.7155E+03	-2.0503E-02	1.9620E+03	1.4761E-02
.8750	3.3600E+03	-5.0071E+02	2.8438E+03	-5.5004E-02	1.8337E+03	1.1604E-02
.9167	3.8398E+03	-5.0136E+02	2.9440E+03	-1.0319E-01	1.6834E+03	4.8030E-03
.9583	4.2403E+03	-4.2427E+02	3.1625E+03	-1.4422E-01	1.5150E+03	6.4746E-03
1.0000	4.5833E+03	-2.7493E+02	3.3464E+03	-2.3613E-01	1.3310E+03	-2.1558E-02
1.0417	4.8822E+03	-6.0639E+01	3.5436E+03	-3.1577E-01	1.1339E+03	-3.8288E-02
1.0833	5.1444E+03	2.0406E+02	3.7525E+03	-3.4421E-01	9.2492E+02	-5.3422E-02
1.1250	5.3749E+03	5.2322E+02	3.9716E+03	-4.8121E-01	7.0586E+02	-6.2483E-02
1.1667	5.5739E+03	8.6884E+02	4.1998E+03	-5.5635E-01	4.7771E+02	-6.0504E-02
1.2083	5.7416E+03	1.2310E+03	4.4359E+03	-6.1745E-01	2.4214E+02	-4.1618E-02
1.2500	5.8771E+03	1.5944E+03	4.6775E+03	-6.5489E-01	1.4555E+02	-1.5916E-14

L8A 23 DOUBLE LAP TITANIUM TO COMPOSITE ADHERENDS, LSHE ADHESIVE

NONLINEAR ORTHOTROPIC ANALYSIS, DOUBLE LAP JOINT

JOINT LENGTH = .6870
 ERROR TOLERANCE = .025
 MAXIMUM ITERATIONS = 20
 NUMBER OF STATIONS = 61
 EFFECTIVE K = .020

ADHESIVE
 THICKNESS = .0030
 POISSONS RATIO = .40
 RAMBERG OSGOOD CONSTANTS (SHEAR STRESS-STRAIN CURVE)
 G = 80600
 SECANT S = 3740
 N VALUE = 6.318

ADHEREND NUMBER 1 (ISOTROPIC)

THICKNESS .0450
 POISSONS RATIO .3062
 RAMBERG OSGOOD CONSTANTS
 S VS. E 17251000
 SECANT S 136600
 N 37.24%

ADHEREND NUMBER 2 (ORTHOTROPIC)

THICKNESS .0870
 NUMBER OF LAYERS 17
 RAMBERG OSGOOD CONSTANTS
 SL VS. EL 27489000
 SL VS. ET -133604000
 ST VS. ET 2750000
 SLT VS. ELT 933000
 ORIENTATIONS 0 45 0 -45 0 45 0 -45 0 45 0 45 0

ULTIMATE LOAD PREDICTION BASED ON

ADHESIVE - MX STRESS, SU = 7.17E+03
 ADHEREND 1 - MX STRESS, SL = 1.38E+05
 ADHEREND 2 - MX STRAIN, SL = 5.36E-03, ST = 4.01E-03, SLT = 1.50E-02

ALPHA = 7.4702E+00
 BETA = 7.4230E+00
 LAMDA = 8.0475E+00
 N RESET TO 15

```

ITERATION FOR ULTIMATE LOAD
LOAD = 1
AT ITERATION 1 ERROR IS 2.32E-09
MAXIMUM STRESS(STRAIN)/ALLOWABLE = .001 IN ADHESIVE
LOAD = 810
AT ITERATION 1 ERROR IS 1.15E-01
AT ITERATION 2 ERROR IS 8.15E-03
MAXIMUM STRESS(STRAIN)/ALLOWABLE = .456 IN ADHESIVE
LOAD = 1292
AT ITERATION 1 ERROR IS 2.56E-01
AT ITERATION 2 ERROR IS 6.03E-02
AT ITERATION 3 ERROR IS 2.11E-02
MAXIMUM STRESS(STRAIN)/ALLOWABLE = .600 IN ADHESIVE
LOAD = 1964
AT ITERATION 1 ERROR IS 3.52E-01
AT ITERATION 2 ERROR IS 1.51E-01
AT ITERATION 3 ERROR IS 7.60E-02
AT ITERATION 4 ERROR IS 3.99E-02
AT ITERATION 5 ERROR IS 2.14E-02
MAXIMUM STRESS(STRAIN)/ALLOWABLE = .712 IN ADHESIVE
LOAD = 2830
AT ITERATION 1 ERROR IS 4.04E-01
AT ITERATION 2 ERROR IS 2.25E-01
AT ITERATION 3 ERROR IS 1.47E-01
AT ITERATION 4 ERROR IS 1.02E-01
AT ITERATION 5 ERROR IS 7.32E-02
AT ITERATION 6 ERROR IS 5.38E-02
AT ITERATION 7 ERROR IS 4.03E-02
AT ITERATION 8 ERROR IS 3.05E-02
AT ITERATION 9 ERROR IS 2.34E-02
MAXIMUM STRESS(STRAIN)/ALLOWABLE = .812 IN ADHESIVE
LOAD = 3641
AT ITERATION 1 ERROR IS 3.78E-01
AT ITERATION 2 ERROR IS 2.32E-01
AT ITERATION 3 ERROR IS 1.75E-01
AT ITERATION 4 ERROR IS 1.43E-01
AT ITERATION 5 ERROR IS 1.22E-01
AT ITERATION 6 ERROR IS 1.06E-01
AT ITERATION 7 ERROR IS 9.41E-02
AT ITERATION 8 ERROR IS 8.42E-02
AT ITERATION 9 ERROR IS 7.60E-02
AT ITERATION 10 ERROR IS 6.90E-02
AT ITERATION 11 ERROR IS 6.30E-02
AT ITERATION 12 ERROR IS 5.77E-02
AT ITERATION 13 ERROR IS 5.30E-02
AT ITERATION 14 ERROR IS 4.89E-02
AT ITERATION 15 ERROR IS 4.51E-02
AT ITERATION 16 ERROR IS 4.18E-02
AT ITERATION 17 ERROR IS 3.89E-02
AT ITERATION 18 ERROR IS 3.60E-02
AT ITERATION 19 ERROR IS 3.35E-02
AT ITERATION 20 ERROR IS 3.12E-02
MAXIMUM STRESS(STRAIN)/ALLOWABLE = .914 IN ADHESIVE
LOAD = 3982
AT ITERATION 1 ERROR IS 2.07E-01
AT ITERATION 2 ERROR IS 1.29E-01
AT ITERATION 3 ERROR IS 1.04E-01
AT ITERATION 4 ERROR IS 9.21E-02
AT ITERATION 5 ERROR IS 8.42E-02
AT ITERATION 6 ERROR IS 7.83E-02
AT ITERATION 7 ERROR IS 7.35E-02

```

AT ITERATION 8 ERROR IS 6.93E-02
 AT ITERATION 9 ERROR IS 6.55E-02
 AT ITERATION 10 ERROR IS 6.21E-02
 AT ITERATION 11 ERROR IS 5.89E-02
 AT ITERATION 12 ERROR IS 5.60E-02
 AT ITERATION 13 ERROR IS 5.33E-02
 AT ITERATION 14 ERROR IS 5.07E-02
 AT ITERATION 15 ERROR IS 4.83E-02
 AT ITERATION 16 ERROR IS 4.61E-02
 AT ITERATION 17 ERROR IS 4.40E-02
 AT ITERATION 18 ERROR IS 4.20E-02
 AT ITERATION 19 ERROR IS 4.02E-02
 AT ITERATION 20 ERROR IS 3.84E-02
 MAXIMUM STRESS(STRAIN)/ALLOWABLE = .968 IN ADHESIVE
 LOAD = 4083
 AT ITERATION 1 ERROR IS 9.47E-02
 AT ITERATION 2 ERROR IS 6.67E-02
 AT ITERATION 3 ERROR IS 5.80E-02
 AT ITERATION 4 ERROR IS 5.35E-02
 AT ITERATION 5 ERROR IS 5.04E-02
 AT ITERATION 6 ERROR IS 4.80E-02
 AT ITERATION 7 ERROR IS 4.59E-02
 AT ITERATION 8 ERROR IS 4.40E-02
 AT ITERATION 9 ERROR IS 4.22E-02
 AT ITERATION 10 ERROR IS 4.05E-02
 AT ITERATION 11 ERROR IS 3.90E-02
 AT ITERATION 12 ERROR IS 3.75E-02
 AT ITERATION 13 ERROR IS 3.60E-02
 AT ITERATION 14 ERROR IS 3.47E-02
 AT ITERATION 15 ERROR IS 3.34E-02
 AT ITERATION 16 ERROR IS 3.22E-02
 AT ITERATION 17 ERROR IS 3.10E-02
 AT ITERATION 18 ERROR IS 2.99E-02
 AT ITERATION 19 ERROR IS 2.88E-02
 AT ITERATION 20 ERROR IS 2.78E-02
 MAXIMUM STRESS(STRAIN)/ALLOWABLE = .980 IN ADHESIVE
 LOAD = 4163
 AT ITERATION 1 ERROR IS 7.30E-02
 AT ITERATION 2 ERROR IS 5.09E-02
 AT ITERATION 3 ERROR IS 4.44E-02
 AT ITERATION 4 ERROR IS 4.11E-02
 AT ITERATION 5 ERROR IS 3.90E-02
 AT ITERATION 6 ERROR IS 3.73E-02
 AT ITERATION 7 ERROR IS 3.59E-02
 AT ITERATION 8 ERROR IS 3.46E-02
 AT ITERATION 9 ERROR IS 3.34E-02
 AT ITERATION 10 ERROR IS 3.23E-02
 AT ITERATION 11 ERROR IS 3.12E-02
 AT ITERATION 12 ERROR IS 3.02E-02
 AT ITERATION 13 ERROR IS 2.92E-02
 AT ITERATION 14 ERROR IS 2.82E-02
 AT ITERATION 15 ERROR IS 2.73E-02
 AT ITERATION 16 ERROR IS 2.64E-02
 AT ITERATION 17 ERROR IS 2.56E-02
 AT ITERATION 18 ERROR IS 2.48E-02
 MAXIMUM STRESS(STRAIN)/ALLOWABLE = .993 IN ADHESIVE

RESULTS FOR P = 4163

NUMBER OF ITERATIONS = 18 , MAXIMUM ERROR = .02477

X	TAU	SIGMA	NX1	MX1	NX2	MX2
0.0000	6.4967E+03	1.2150E+03	5.8208E-11	-4.0927E-14	8.3255E+03	0.
.0491	6.3522E+03	1.0501E+03	3.1611E+02	-1.1397E-01	7.6932E+03	0.
.0981	6.2239E+03	8.5956E+02	6.2342E+02	-1.7451E-01	7.0786E+03	0.
.1472	6.1024E+03	6.6138E+02	9.2588E+02	-1.9063E-01	6.4737E+03	0.
.1963	5.9970E+03	4.7138E+02	1.2219E+03	-1.7292E-01	5.8816E+03	0.
.2454	5.9130E+03	2.9868E+02	1.5138E+03	-1.2999E-01	5.2978E+03	0.
.2944	5.8565E+03	1.4446E+02	1.8020E+03	-7.1399E-02	4.7214E+03	0.
.3435	5.8319E+03	2.2870E+00	2.0883E+03	-4.7648E-03	4.1488E+03	0.
.3926	5.8416E+03	-1.3978E+02	2.3743E+03	6.2115E-02	3.5769E+03	0.
.4416	5.8849E+03	-2.4401E+02	2.6614E+03	1.2153E-01	3.0027E+03	0.
.4907	5.9567E+03	-4.6757E+02	2.9516E+03	1.6572E-01	2.4223E+03	0.
.5398	6.0527E+03	-6.5998E+02	3.2454E+03	1.8512E-01	1.8346E+03	0.
.5889	6.1671E+03	-8.6202E+02	3.5453E+03	1.7091E-01	1.2348E+03	0.
.6379	6.2941E+03	-1.0576E+03	3.8497E+03	1.1255E-01	5.2610E+02	0.
.6870	6.4304E+03	-1.2273E+03	4.1627E+03	2.2737E-14	2.6193E-10	0.

NONLINEAR ORTHOTROPIC ANALYSIS, STEP LAP JOINT

```

ERROR TOLERANCE = .025
MAXIMUM ITERATIONS = 20
NUMBER OF STATIONS = 31 PER TRFAD
EFFECTIVE K = .100

```

STEP	GEOMETRY	R	B
		.0873	2.0080
		.0873	1.8730
		.0880	

ADHESIVE
THICKNESS = .0058
POISSONS RATIO = .40
RAMBERG OSGOOD
G = 20600
SFCANT S = 3740
N VALUE = 6.318

ADHERED NUMBER 1 (ORTHOTROPIC)

THICKNESS					
NUMBER OF LAYERS					
RAMBERG OSGOOD CONSTANTS					
SL VS. EL			.2620		
SL VS. ET			*8	E	
ST VS. ET			28825000		
SLT VS. ELT			-136632000		
ORIENTATIONS	0	45	-45	0	45 -45
	0	-45	45	0	-45 45
ADHEREND NUMBER 2 (ISOTROPIC)					
THICKNESS					
POISSONS RATIO					
RAMBERG OSGOOD CONSTANTS					
S VS. E			.2640		
			.3062		
SECANT S N					
			16096000		
			134000		
			34		559

ULTIMATE LOAD PREDICTION BASED ON
 ADHESIVE - MX STRESS, SU = 7.17E+03
 ADHESIVE 1 - MX STRAIN, SL = 6.08E-03, ST = 4.01E-03, SLT = 1.50E-02
 ADHESIVE 2 - MX STRESS, SL = 1.35E+05

```

STEP 1
ALPHA = 5.9221E+00
HETA = 5.8758E+00
LAMBDA = 3.9374E+00
N RESET TO 23

```

```

5112 2
44510 =
10 T4 =
LAMBDA =
5.9898E+00
5.9347E+00
3.9519E+00

```

```

ITERATION FOR ULTIMATE LOAD
LOAD = 1
  AT ITERATION 1 ERROR IS 1.25E-09
  MAXIMUM STRESS(STRAIN)/ALLOWABLE = .000 IN ADHESIVE
LOAD = 2166
  AT ITERATION 1 ERROR IS 7.59E-02
  AT ITERATION 2 ERROR IS 3.61E-03
  MAXIMUM STRESS(STRAIN)/ALLOWABLE = .472 IN ADHESIVE
LOAD = 3377
  AT ITERATION 1 ERROR IS 2.05E-01
  AT ITERATION 2 ERROR IS 9.44E-02
  AT ITERATION 3 ERROR IS 7.70E-03
  MAXIMUM STRESS(STRAIN)/ALLOWABLE = .629 IN ADHESIVE
LOAD = 4903
  AT ITERATION 1 ERROR IS 2.72E-01
  AT ITERATION 2 ERROR IS 8.44E-02
  AT ITERATION 3 ERROR IS 3.34E-02
  AT ITERATION 4 ERROR IS 1.32E-02
  MAXIMUM STRESS(STRAIN)/ALLOWABLE = .744 IN ADHESIVE
LOAD = 5394
  AT ITERATION 1 ERROR IS 2.49E-01
  AT ITERATION 2 ERROR IS 1.28E-01
  AT ITERATION 3 ERROR IS 6.55E-02
  AT ITERATION 4 ERROR IS 3.47E-02
  AT ITERATION 5 ERROR IS 1.86E-02
  MAXIMUM STRESS(STRAIN)/ALLOWABLE = .833 IN ADHESIVE
LOAD = 7084
  AT ITERATION 1 ERROR IS 2.83E-01
  AT ITERATION 2 ERROR IS 1.37E-01
  AT ITERATION 3 ERROR IS 8.16E-02
  AT ITERATION 4 ERROR IS 5.03E-02
  AT ITERATION 5 ERROR IS 3.14E-02
  AT ITERATION 6 ERROR IS 1.98E-02
  MAXIMUM STRESS(STRAIN)/ALLOWABLE = .895 IN ADHESIVE
LOAD = 9140
  AT ITERATION 1 ERROR IS 2.46E-01
  AT ITERATION 2 ERROR IS 1.26E-01
  AT ITERATION 3 ERROR IS 8.06E-02
  AT ITERATION 4 ERROR IS 5.41E-02
  AT ITERATION 5 ERROR IS 3.67E-02
  AT ITERATION 6 ERROR IS 2.51E-02
  AT ITERATION 7 ERROR IS 1.72E-02
  MAXIMUM STRESS(STRAIN)/ALLOWABLE = .936 IN ADHESIVE
LOAD = 10108
  AT ITERATION 1 ERROR IS 1.94E-01
  AT ITERATION 2 ERROR IS 1.02E-01
  AT ITERATION 3 ERROR IS 6.86E-02
  AT ITERATION 4 ERROR IS 4.82E-02
  AT ITERATION 5 ERROR IS 3.44E-02
  AT ITERATION 6 ERROR IS 2.47E-02
  MAXIMUM STRESS(STRAIN)/ALLOWABLE = .972 IN ADHESIVE
LOAD = 10487
  AT ITERATION 1 ERROR IS 9.84E-02
  AT ITERATION 2 ERROR IS 5.19E-02
  AT ITERATION 3 ERROR IS 3.55E-02
  AT ITERATION 4 ERROR IS 2.55E-02
  AT ITERATION 5 ERROR IS 1.86E-02
  MAXIMUM STRESS(STRAIN)/ALLOWABLE = .978 IN ADHESIVE
LOAD = 11194
  AT ITERATION 1 ERROR IS 1.54E-01
  AT ITERATION 2 ERROR IS 8.05E-02

```

AT ITERATION 3 ERROR IS 5.58E-02
AT ITERATION 4 ERROR IS 4.08E-02
AT ITERATION 5 ERROR IS 3.04E-02
AT ITERATION 6 ERROR IS 2.28E-02
MAXIMUM STRESS(STRAIN)/ALLOWABLE = 1.001 IN ADHESIVE

NO CONVERGENCE AFTER TEN ITERATIONS - TERMINATED

THE PREDICTED ULTIMATE LOAD IS 11181

RESULTS FOR P = 11181

NUMBER OF ITERATIONS = 6 , MAXIMUM ERROR = .02282

X	TAU	SIGMA	NX1	NX1	NX2	NX2	MX1	MX2
STEP NUMBER	1							
0.0000	5.5244E+03	3.0180E+03	1.1642E-10	-9.0949E-14	1.1154E+04	-4.8943E+01		
0.0913	5.3996E+03	1.6675E+03	4.9963E+02	-1.1195E+00	1.0695E+04	-4.3412E+01		
0.1825	5.1850E+03	5.4372E+02	9.8257E+02	-7.6460E-01	1.0212E+04	-3.6707E+01		
0.2738	4.8998E+03	-2.3542E+02	1.4437E+03	1.8470E-01	9.7509E+03	-2.9699E+01		
0.3651	4.5644E+03	-6.4223E+02	1.8750E+03	1.0432E+00	9.3193E+03	-2.3144E+01		
0.4564	4.1799E+03	-7.4606E+02	2.2774E+03	1.5860E+00	8.4194E+03	-1.7369E+01		
0.5476	3.7254E+03	-6.5566E+02	2.6354E+03	1.6618E+00	8.5589E+03	-1.2544E+01		
0.6389	3.1635E+03	-4.7512E+02	2.9506E+03	1.7023E+00	8.2436E+03	-8.6601E+00		
0.7302	2.4905E+03	-2.9579E+02	3.2090E+03	9.4728E-01	7.9852E+03	-5.6669E+00		
0.8215	1.8417E+03	-1.6723E+02	3.4057E+03	6.1163E-01	7.7886E+03	-3.4663E+00		
0.9127	1.3576E+03	-9.3465E+01	3.5502E+03	3.1302E-01	7.6440E+03	-1.8649E+00		
1.0040	1.0424E+03	-5.1276E+01	3.6586E+03	9.3327E-02	7.5356E+03	-6.5844E-01		
1.0953	8.6522E+02	-1.8251E+01	3.7447E+03	-6.8671E-02	7.4496E+03	3.1024E-01		
1.1865	8.0267E+02	1.8361E+01	3.8200E+03	-1.9035E-01	7.3742E+03	1.1709E+00		
1.2778	8.4636E+02	6.3778E+01	3.8945E+03	-3.0619E-01	7.2998E+03	2.0424E+00		
1.3691	1.0008E+03	1.1744E+02	3.9779E+03	-3.9705E-01	7.2164E+03	3.0489E+00		
1.4604	1.2841E+03	1.5846E+02	4.0810E+03	-4.7644E-01	7.1132E+03	4.3264E+00		
1.5516	1.7244E+03	1.6179E+02	4.2170E+03	-5.6135E-01	6.9772E+03	6.0244E+00		
1.6429	2.3503E+03	7.2177E+01	4.4008E+03	-7.3842E-01	6.7934E+03	8.2699E+00		
1.7342	3.9961E+03	-1.1442E+02	4.6440E+03	-1.1098E+00	6.5503E+03	1.1107E+01		
1.8255	3.5706E+03	-3.7544E+02	4.9446E+03	-1.8498E+00	6.2494E+03	1.1504E+01		
1.9167	4.0333E+03	-5.5854E+02	5.2717E+03	-3.0178E+00	5.9026E+03	1.7631E+01		
2.0080	4.4254E+03	-4.5723E+02	5.5785E+03	-4.74019E+00	5.5157E+03	2.0908E+01		
STEP NUMBER	2							
0.0000	4.4355E+03	-4.5522E+02	5.6785E+03	1.9885E+01	5.5157E+03	-3.1685E+00		
0.0913	4.0835E+03	-3.6200E+02	6.0417E+03	1.5741E+01	5.1525E+03	-2.0360E+00		
0.1825	3.6705E+03	-1.5575E+02	6.3716E+03	1.2659E+01	4.8226E+03	-1.2727E+00		
0.2738	3.1467E+03	2.9004E+01	6.6433E+03	9.3137E+00	4.5310E+03	-7.9013E-01		
0.3651	2.5743E+03	1.6354E+02	6.9078E+03	6.3787E+00	4.2884E+03	-5.0034E-01		
0.4564	1.9466E+03	1.0705E+02	7.1012E+03	4.0184E+00	4.0931E+03	-3.2624E-01		
0.5476	1.5273E+03	1.2768E+02	7.2495E+03	2.1862E+00	3.9472E+03	-2.0360E-01		
0.6389	1.2205E+03	1.2482E+02	7.3454E+03	7.6496E-01	3.8289E+03	-1.0098E-01		
0.7302	1.0492E+03	7.3212E+01	7.4410E+03	-1.7636E-01	3.7332E+03	1.0505E-02		
0.8215	9.9704E+02	2.5328E+01	7.5473E+03	-1.3854E+00	3.6470E+03	1.3513E-01		
0.9127	1.0594E+03	-1.5806E+01	7.6340E+03	-2.3781E+00	3.5603E+03	2.8220E-01		
1.0040	1.2449E+03	-6.0522E+01	7.7311E+03	-3.4732E+00	3.4631E+03	4.6503E-01		
1.0953	1.5715E+03	-1.2041E+02	7.8449E+03	-4.7249E+00	3.3444E+03	7.0028E-01		
1.1865	2.0674E+03	-2.1943E+02	8.0030E+03	-6.5151E+00	3.1912E+03	9.4858E-01		
1.2778	2.6691E+03	-3.7066E+02	8.2036E+03	-8.8005E+00	2.9902E+03	1.3464E+00		
1.3691	3.2684E+03	-5.4545E+02	8.4567E+03	-1.1824E+01	2.7376E+03	1.6555E+00		
1.4604	3.7701E+03	-7.1083E+02	8.7567E+03	-1.5645E+01	2.4375E+03	1.7751E+00		
1.5516	4.1855E+03	-7.5504E+02	9.0954E+03	-2.0317E+01	2.0849E+03	1.5612E+00		
1.6429	4.5444E+02	-5.9444E+02	9.4670E+03	-2.5412E+01	1.7272E+03	9.5350E-01		
1.7342	4.8565E+03	-1.3465E+03	9.8668E+03	-3.1450E+01	1.3275E+03	7.1777E-02		
1.8255	5.1214E+03	6.6070E+02	1.0242E+04	-3.8413E+01	9.0242E+02	-8.0176E-01		
1.9167	5.3184E+03	1.7685E+03	1.0736E+04	-4.4526E+01	4.5824E+02	-1.0737E+00		
2.0080	5.4319E+03	3.0664E+03	1.1144E+04	-4.74474E+01	1.4555E-10	-1.8130E-13		

APPENDIX G.2

BEHAVIOR PREDICTION AT GIVEN
LOADS IN SIMPLE JOINTS

LSA 20 SINGLE LAP COMPOSITE TO TITANIUM ADHERENDS, LSHE ADHESIVE

NONLINEAR ORTHOTROPIC ANALYSIS, SINGLE LAP JOINT

TOTAL LENGTH = 3.2500
JOINT LENGTH = 1.2500
ERROR TOLERANCE = .025
MAXIMUM ITERATIONS = 20
NUMBER OF STATIONS = 51
EFFECTIVE K = .010

ADHESIVE
THICKNESS = .0028
POISSON'S RATIO = .40
HARDER'S USG000 CONSTANTS (SHEAR STRESS-STRAIN CURVE)
G = 80600
SECANT S = 3740
N VALUE = 6.319

ADHEREND NUMBER 1 (ORTHOTROPIC)

THICKNESS .0467
NUMBER OF LAYERS 9
HARDER'S USG000 CONSTANTS
SL VS. EL 27484000 E SECANT S N
SL VS. ET -133604000 -0 -0.000
ST VS. ET 2750000 11910 2.541
SLT VS. ELT 933000 7950 2.941
ORIENTATIONS 0 45 0 -45 0 45 0

ADHEREND NUMBER 2 (ISOTROPIC)

THICKNESS .0450
POISSON'S RATIO .3062 E SECANT S N
HARDER'S USG000 CONSTANTS
S VS. E 17251000 136600 37.246

ALPHA = 7.3914E+00
BETA = 7.3915E+00
LAMBDA = 8.2150E+00
N RESET TO 31

(LOAD = 4570
 AT ITERATION 1 ERROR IS 7.28E-01
 AT ITERATION 2 ERROR IS 4.77E-01
 AT ITERATION 3 ERROR IS 3.47E-01
 AT ITERATION 4 ERROR IS 2.67E-01
 AT ITERATION 5 ERROR IS 2.10E-01
 AT ITERATION 6 ERROR IS 1.66E-01
 AT ITERATION 7 ERROR IS 1.32E-01
 AT ITERATION 8 ERROR IS 1.06E-01
 AT ITERATION 9 ERROR IS 8.51E-02
 AT ITERATION 10 ERROR IS 6.86E-02
 AT ITERATION 11 ERROR IS 5.54E-02
 AT ITERATION 12 ERROR IS 4.48E-02
 AT ITERATION 13 ERROR IS 3.62E-02
 AT ITERATION 14 ERROR IS 2.93E-02
 AT ITERATION 15 ERROR IS 2.37E-02

NUMBER OF ITERATIONS = 15 , MAXIMUM ERROR = .02375

NUMBER OF ITERATIONS = 15 , MAXIMUM ERROR = .02375

X	LAYER	TAU	SIGMA	NX1	NX2	NX2
0.0000	1	5.9940E+03	1.7263E+03	4.3656E-11	-4.5475E-15	4.4000E+03
0.0017	2	5.8102E+03	1.2972E+03	2.4401E+02	-4.3575E-02	4.1540E+03
0.0033	3	5.6040E+03	8.8054E+02	4.8358E+02	-6.2873E-02	3.9164E+03
0.0050	4	5.3725E+03	4.9311E+02	7.1228E+02	-6.4563E-02	3.6877E+03
0.0067	5	5.1130E+03	1.5003E+02	9.3063E+02	-5.5372E-02	3.4634E+03
0.0083	6	4.8214E+03	-1.3514E+02	1.1376E+03	-4.0231E-02	3.2624E+03
0.0100	7	4.4931E+03	-3.5163E+02	1.3317E+03	-2.5383E-02	3.0643E+03
0.0117	8	4.1163E+03	-4.8987E+02	1.5112E+03	-1.2573E-02	2.8808E+03
0.0133	9	3.6741E+03	-5.4352E+02	1.6736E+03	-4.1834E-03	2.7264E+03
0.0150	10	3.1378E+03	-5.1006E+02	1.8158E+03	-3.6777E-04	2.5842E+03
0.0167	11	2.5117E+03	-2.6740E+02	1.9337E+03	4.0904E-04	2.4663E+03
0.0183	12	1.9116E+03	-1.4617E+02	2.1255E+03	3.0741E-04	2.3755E+03
0.0200	13	1.4507E+03	-5.8044E+01	2.1485E+03	7.5412E-04	2.3050E+03
0.0217	14	1.1443E+03	-5.4924E+00	2.1921E+03	2.3145E-03	2.2515E+03
0.0233	15	9.4705E+02	8.4211E+00	2.2307E+03	5.1551E-03	2.2074E+03
0.0250	16	4.0115E+02	-1.1441E+01	2.2866E+03	1.3062E-02	2.1643E+03
0.0267	17	1.0842E+02	-6.5019E+01	2.3103E+03	1.6045E-02	2.1314E+03
0.0283	18	1.3519E+03	-1.5047E+02	2.3604E+03	1.5782E-02	2.0947E+03
0.0300	19	1.7687E+03	-2.6244E+02	2.4250E+03	5.9515E-03	1.9750E+03
0.0317	20	2.3345E+03	-3.4524E+02	2.5101E+03	-5.9416E-03	1.8844E+03
0.0333	21	2.9712E+03	-4.8170E+02	2.6207E+03	-3.4147E-02	1.7793E+03
0.0350	22	3.5235E+03	-5.0720E+02	2.7566E+03	-7.6531E-02	1.6443E+03
0.0367	23	4.0485E+03	-4.4820E+02	2.9137E+03	-1.3250E-01	1.4463E+03
0.0383	24	4.53847E+03	-3.0977E+02	3.0886E+03	-2.0031E-01	1.3114E+03
0.0400	25	4.7291E+03	-1.0086E+02	3.2785E+03	-2.7687E-01	1.1215E+03
0.0417	26	5.0243E+03	1.6744E+02	3.4418E+03	-3.5824E-01	9.1818E+02
0.0433	27	5.2915E+03	4.8518E+02	3.6467E+03	-4.4929E-01	7.0332E+02
0.0450	28	5.5288E+03	8.3772E+02	3.8211E+03	-5.1445E-01	4.7786E+02
0.0467	29	5.7418E+03	1.2104E+03	4.1567E+03	-5.7701E-01	2.4330E+02
0.0483	30	5.9324E+03	1.5844E+03	4.4400E+03	-6.2074E-01	1.4552E-10

X	LAYER	STRSL 1	STRSL 2	STRSLT 1	STRSLT 2	STRSLT 2
0.0000	1	0.	0.	0.	9.6143E+04	2.9439E+04
	2	0.	0.	0.	9.6552E+04	2.9584E+04
	3	0.	0.	0.	9.6460E+04	2.9584E+04
	4	0.	0.	0.	9.7369E+04	2.9814E+04
	5	0.	0.	0.	9.7778E+04	2.9940E+04
	6	0.	0.	0.	9.8186E+04	3.0065E+04
	7	0.	0.	0.	9.8595E+04	3.0190E+04
	8	0.	0.	0.	9.9004E+04	3.0315E+04
	9	0.	0.	0.	9.9413E+04	3.0440E+04

X	LAYER	STRSL 1	STRSL 2	STRSLT 1	STRSLT 2	STRSLT 2
0.0017	1	7.4211E+03	1.5267E+02	0.	9.0790E+04	2.7800E+04
	2	3.8004E+03	4.4739E+02	-1.2258E+02	9.1170E+04	2.7916E+04
	3	7.4902E+03	1.5400E+02	0.	9.1551E+04	2.8033E+04
	4	3.4344E+03	4.5151E+02	1.2365E+02	9.1931E+04	2.8149E+04
	5	7.5544E+03	1.5551E+02	0.	9.2311E+04	2.8266E+04

X	LAYER	STRSL 1	STRST 1	STRSLT 1	STRSL 2	STRST 2	STRSLT 2
0.033	6	3.8745E+03	4.5561E+02	1.2472E+02	9.2691E+04	2.8382E+04	0.
	7	7.6284E+03	1.5693E+02	0.	9.3071E+04	2.8498E+04	0.
	8	3.9099E+03	4.5972E+02	-1.2579E+02	9.3451E+04	2.8615E+04	0.
	9	7.6476E+03	1.5835E+02	0.	9.3832E+04	2.8731E+04	0.
	1	1.4648E+04	3.0187E+02	0.	8.5679E+04	2.6235E+04	0.
	2	7.5177E+03	8.7534E+02	-2.2352E+02	8.6017E+04	2.6338E+04	0.
	3	1.4793E+04	3.0392E+02	0.	8.6355E+04	2.6442E+04	0.
	4	7.5648E+03	8.8120E+02	2.2473E+02	8.6693E+04	2.6546E+04	0.
	5	1.4988E+04	3.0597E+02	0.	8.7032E+04	2.6649E+04	0.
	6	7.6198E+03	8.8700E+02	2.2594E+02	8.7370E+04	2.6753E+04	0.
	7	1.4988E+04	3.0802E+02	0.	8.7708E+04	2.6856E+04	0.
	8	7.6701E+03	8.9280E+02	-2.2714E+02	8.8046E+04	2.6960E+04	0.
	9	1.5048E+04	3.1007E+02	0.	8.8384E+04	2.7063E+04	0.

X	LAYER	STRSL 1	STRST 1	STRSLT 1	STRSL 2	STRST 2	STRSLT 2
0.1250	1	2.1771E+04	4.4590E+02	0.	8.0800E+04	2.4741E+04	0.
	2	1.1129E+04	1.2812E+03	-2.4800E+02	8.1087E+04	2.4824E+04	0.
	3	2.1475E+04	4.4401E+02	0.	8.1375E+04	2.4917E+04	0.
	4	1.1192E+04	1.2871E+03	2.4893E+02	8.1662E+04	2.5005E+04	0.
	5	2.1475E+04	4.5112E+02	0.	8.1944E+04	2.5093E+04	0.
	6	1.1234E+04	1.2924E+03	2.4986E+02	8.2237E+04	2.5181E+04	0.
	7	2.2041E+04	4.5322E+02	0.	8.2524E+04	2.5269E+04	0.
	8	1.1287E+04	1.2987E+03	-3.0077E+02	8.2811E+04	2.5357E+04	0.
	9	2.2184E+04	4.5533E+02	0.	8.3098E+04	2.5445E+04	0.

X	LAYER	STRSL 1	STRST 1	STRSLT 1	STRSL 2	STRST 2	STRSLT 2
0.1667	1	2.8596E+04	5.8616E+02	0.	7.6168E+04	2.3323E+04	0.
	2	1.4602E+04	1.6623E+03	-3.5159E+02	7.6400E+04	2.3394E+04	0.
	3	2.8684E+04	5.8796E+02	0.	7.6632E+04	2.3465E+04	0.
	4	1.4647E+04	1.6472E+03	3.5219E+02	7.6855E+04	2.3536E+04	0.
	5	2.8773E+04	5.8976E+02	0.	7.7097E+04	2.3607E+04	0.
	6	1.4692E+04	1.6721E+03	3.5279E+02	7.7324E+04	2.3678E+04	0.
	7	2.8861E+04	5.9157E+02	0.	7.7562E+04	2.3749E+04	0.
	8	1.4732E+04	1.6770E+03	-3.5339E+02	7.7744E+04	2.3821E+04	0.
	9	2.8950E+04	5.9337E+02	0.	7.8026E+04	2.3892E+04	0.

X	LAYER	STRSL 1	STRST 1	STRSLT 1	STRSL 2	STRST 2	STRSLT 2
0.2043	1	3.5103E+04	7.1846E+02	0.	7.1788E+04	2.1981E+04	0.
	2	1.7909E+04	2.0176E+03	-3.9059E+02	7.1465E+04	2.2036E+04	0.
	3	3.5169E+04	7.1974E+02	0.	7.2142E+04	2.2040E+04	0.
	4	1.7442E+04	2.0211E+03	3.9044E+02	7.2320E+04	2.2144E+04	0.
	5	3.5244E+04	7.2110E+02	0.	7.2447E+04	2.2199E+04	0.
	6	1.7476E+04	2.0246E+03	3.9127E+02	7.2674E+04	2.2253E+04	0.
	7	3.5294E+04	7.2443E+02	0.	7.2851E+04	2.2307E+04	0.

X	LAYER	STRSL 1	STRST 1	STRSLT 1	STRSL 2	STRST 2	STRSLT 2
8	1.8009E+04	2.0282E+03	-3.9162E+02	7.3028E+04	2.2361E+04	0.	
9	3.5364E+04	7.2775E+02	0.	7.3206E+04	2.2416E+04	0.	
1	4.1221E+04	8.4236E+02	0.	6.7682E+04	2.0724E+04	0.	
2	2.1012E+04	2.3449E+03	-4.1436E+02	6.7807E+04	2.0763E+04	0.	
3	4.1242E+04	8.4318E+02	0.	6.7733E+04	2.0801E+04	0.	
4	2.1038E+04	2.3470E+03	4.1453E+02	6.8059E+04	2.0840E+04	0.	
5	4.1303E+04	8.4400E+02	0.	6.8184E+04	2.0878E+04	0.	
6	2.1058E+04	2.3492E+03	4.1470E+02	6.8310E+04	2.0916E+04	0.	
7	4.1344E+04	8.4483E+02	0.	6.8435E+04	2.0955E+04	0.	
8	2.1074E+04	2.3514E+03	-4.1486E+02	6.8561E+04	2.0993E+04	0.	
9	4.1345E+04	8.4565E+02	0.	6.8687E+04	2.1032E+04	0.	

X	LAYER	STRSL 1	STRST 1	STRSLT 1	STRSL 2	STRST 2	STRSLT 2
1	4.6884E+04	9.5654E+02	0.	6.3876E+04	1.9559E+04	0.	
2	2.3893E+04	2.6424E+03	-4.4079E+02	6.3955E+04	1.9583E+04	0.	
3	4.6904E+04	9.5694E+02	0.	6.4036E+04	1.9608E+04	0.	
4	2.3903E+04	2.6435E+03	4.4085E+02	6.4116E+04	1.9632E+04	0.	
5	4.6925E+04	9.570E+02	0.	6.4196E+04	1.9657E+04	0.	
6	2.3913E+04	2.6446E+03	4.4092E+02	6.4276E+04	1.9681E+04	0.	
7	4.6945E+04	9.5781E+02	0.	6.4356E+04	1.9706E+04	0.	
8	2.3923E+04	2.6456E+03	-4.4099E+02	6.4436E+04	1.9730E+04	0.	
9	4.6955E+04	9.5821E+02	0.	6.4516E+04	1.9755E+04	0.	

X	LAYER	STRSL 1	STRST 1	STRSLT 1	STRSL 2	STRST 2	STRSLT 2
1	5.2005E+04	1.0595E+03	0.	6.0416E+04	1.8499E+04	0.	
2	2.6494E+04	2.9073E+03	-4.5877E+02	6.0459E+04	1.8512E+04	0.	
3	5.2012E+04	1.0596E+03	0.	6.0501E+04	1.8525E+04	0.	
4	2.6497E+04	2.9077E+03	4.5879E+02	6.0544E+04	1.8538E+04	0.	
5	5.2014E+04	1.0598E+03	0.	6.0586E+04	1.8551E+04	0.	
6	2.6500E+04	2.9080E+03	4.5880E+02	6.0628E+04	1.8564E+04	0.	
7	5.2024E+04	1.0599E+03	0.	6.0671E+04	1.8577E+04	0.	
8	2.6504E+04	2.9084E+03	-4.5883E+02	6.0713E+04	1.8590E+04	0.	
9	5.2032E+04	1.0600E+03	0.	6.0756E+04	1.8603E+04	0.	

X	LAYER	STRSL 1	STRST 1	STRSLT 1	STRSL 2	STRST 2	STRSLT 2
1	5.6481E+04	1.1491E+03	0.	5.7370E+04	1.7587E+04	0.	
2	2.8767E+04	3.1357E+03	-4.6857E+02	5.7384E+04	1.7591E+04	0.	
3	5.6481E+04	1.1491E+03	0.	5.7398E+04	1.7595E+04	0.	
4	2.8768E+04	3.1358E+03	4.6857E+02	5.7412E+04	1.7580E+04	0.	
5	5.6482E+04	1.1491E+03	0.	5.7426E+04	1.7584E+04	0.	
6	2.8768E+04	3.1358E+03	4.6857E+02	5.7440E+04	1.7588E+04	0.	
7	5.6482E+04	1.1491E+03	0.	5.7454E+04	1.7592E+04	0.	
8	2.8768E+04	3.1358E+03	-4.6857E+02	5.7468E+04	1.7597E+04	0.	
9	5.6483E+04	1.1492E+03	0.	5.7482E+04	1.7601E+04	0.	

X	LAYER	STRSL 1	STRST 1	STRSLT 1	STRSL 2	STRST 2	STRSLT 2
.4167	1	6.0186E+04	1.2231E+03	0.	5.4826E+04	1.6788E+04	0.
	2	3.0650E+04	3.3226E+03	-4.7704E+02	5.4821E+04	1.6786E+04	0.
	3	6.0185E+04	1.2231E+03	0.	5.4816E+04	1.6785E+04	0.
	4	3.0650E+04	3.3226E+03	4.7704E+02	5.4811E+04	1.6783E+04	0.
	5	6.0184E+04	1.2230E+03	0.	5.4806E+04	1.6782E+04	0.
	6	3.0650E+04	3.3226E+03	4.7704E+02	5.4801E+04	1.6780E+04	0.
	7	6.0184E+04	1.2230E+03	0.	5.4796E+04	1.6779E+04	0.
	8	3.0649E+04	3.3225E+03	-4.7704E+02	5.4791E+04	1.6777E+04	0.
	9	6.0183E+04	1.2230E+03	0.	5.4786E+04	1.6775E+04	0.

X	LAYER	STRSL 1	STRST 1	STRSLT 1	STRSL 2	STRST 2	STRSLT 2
.4583	1	6.3069E+04	1.2805E+03	0.	5.2829E+04	1.6176E+04	0.
	2	3.2116E+04	3.4667E+03	-4.8293E+02	5.2813E+04	1.6171E+04	0.
	3	6.3069E+04	1.2805E+03	0.	5.2797E+04	1.6167E+04	0.
	4	3.2116E+04	3.4667E+03	4.8292E+02	5.2782E+04	1.6162E+04	0.
	5	6.3068E+04	1.2805E+03	0.	5.2766E+04	1.6157E+04	0.
	6	3.2116E+04	3.4667E+03	4.8292E+02	5.2750E+04	1.6152E+04	0.
	7	6.3068E+04	1.2805E+03	0.	5.2735E+04	1.6147E+04	0.
	8	3.2115E+04	3.4667E+03	-4.8291E+02	5.2719E+04	1.6143E+04	0.
	9	6.3067E+04	1.2805E+03	0.	5.2703E+04	1.6138E+04	0.

X	LAYER	STRSL 1	STRST 1	STRSLT 1	STRSL 2	STRST 2	STRSLT 2
.5100	1	6.5253E+04	1.3239E+03	0.	5.1302E+04	1.5709E+04	0.
	2	3.3226E+04	3.5751E+03	-4.8699E+02	5.1282E+04	1.5703E+04	0.
	3	6.5252E+04	1.3239E+03	0.	5.1263E+04	1.5697E+04	0.
	4	3.3225E+04	3.5750E+03	4.8699E+02	5.1243E+04	1.5690E+04	0.
	5	6.5251E+04	1.3238E+03	0.	5.1223E+04	1.5684E+04	0.
	6	3.3225E+04	3.5749E+03	4.8699E+02	5.1203E+04	1.5678E+04	0.
	7	6.5250E+04	1.3238E+03	0.	5.1183E+04	1.5672E+04	0.
	8	3.3224E+04	3.5749E+03	-4.8698E+02	5.1163E+04	1.5666E+04	0.
	9	6.5249E+04	1.3238E+03	0.	5.1143E+04	1.5660E+04	0.

X	LAYER	STRSL 1	STRST 1	STRSLT 1	STRSL 2	STRST 2	STRSLT 2
.5417	1	6.6942E+04	1.3574E+03	0.	5.0113E+04	1.5344E+04	0.
	2	3.4083E+04	3.6583E+03	-4.8993E+02	5.0093E+04	1.5338E+04	0.
	3	6.6939E+04	1.3573E+03	0.	5.0073E+04	1.5332E+04	0.
	4	3.4081E+04	3.6581E+03	4.8992E+02	5.0053E+04	1.5326E+04	0.
	5	6.6935E+04	1.3573E+03	0.	5.0033E+04	1.5320E+04	0.
	6	3.4079E+04	3.6579E+03	4.8992E+02	5.0012E+04	1.5314E+04	0.
	7	6.6931E+04	1.3572E+03	0.	4.9992E+04	1.5308E+04	0.
	8	3.4078E+04	3.6578E+03	-4.8991E+02	4.9972E+04	1.5302E+04	0.
	9	6.6927E+04	1.3571E+03	0.	4.9952E+04	1.5295E+04	0.

X LAYER
 .5473
 1 6.6321E+04 STRSL 1 STRSLT 1 STRSL 2 STRSLT 2
 2 3.7254E+03 0. 4.9137E+04 1.5046E+04 0.
 3 6.8313E+04 -4.9220E+02 4.9119E+04 1.5040E+04 0.
 4 3.4778E+04 0. 4.9101E+04 1.5035E+04 0.
 5 3.7255E+03 4.9219E+02 4.9083E+04 1.5029E+04 0.
 6 6.8304E+04 0. 4.9055E+04 1.5024E+04 0.
 7 3.4774E+04 4.9218E+02 4.9047E+04 1.5018E+04 0.
 8 6.8246E+04 0. 4.9028E+04 1.5013E+04 0.
 9 3.4770E+04 -4.9216E+02 4.9010E+04 1.5007E+04 0.
 1.3841E+03 0. 4.8992E+04 1.5001E+04 0.

X LAYER
 .6250
 1 6.9546E+04 STRSL 1 STRSLT 1 STRSL 2 STRSLT 2
 2 3.5403E+04 0. 4.8268E+04 1.4780E+04 0.
 3 6.9531E+04 -4.9413E+02 4.8253E+04 1.4775E+04 0.
 4 3.5396E+04 0. 4.8238E+04 1.4770E+04 0.
 5 6.9517E+04 4.9411E+02 4.8223E+04 1.4766E+04 0.
 6 3.5389E+04 0. 4.8208E+04 1.4761E+04 0.
 7 6.9502E+04 4.9408E+02 4.8193E+04 1.4757E+04 0.
 8 3.5381E+04 0. 4.8177E+04 1.4752E+04 0.
 9 6.9488E+04 -4.9406E+02 4.8162E+04 1.4747E+04 0.

X LAYER
 .6567
 1 7.0753E+04 STRSL 1 STRSLT 1 STRSL 2 STRSLT 2
 2 3.6015E+04 0. 4.7413E+04 1.4518E+04 0.
 3 7.0732E+04 -4.9594E+02 4.7401E+04 1.4514E+04 0.
 4 3.6004E+04 0. 4.7389E+04 1.4510E+04 0.
 5 7.0711E+04 4.9591E+02 4.7376E+04 1.4507E+04 0.
 6 3.5943E+04 0. 4.7364E+04 1.4503E+04 0.
 7 7.0690E+04 4.9588E+02 4.7352E+04 1.4499E+04 0.
 8 3.5933E+04 0. 4.7340E+04 1.4495E+04 0.
 9 7.0669E+04 -4.9585E+02 4.7327E+04 1.4492E+04 0.

X LAYER
 .7063
 1 7.2075E+04 STRSL 1 STRSLT 1 STRSL 2 STRSLT 2
 2 3.6485E+04 0. 4.6476E+04 1.4231E+04 0.
 3 7.2044E+04 -4.9784E+02 4.6466E+04 1.4228E+04 0.
 4 3.6672E+04 0. 4.6456E+04 1.4225E+04 0.
 5 7.2023E+04 4.9780E+02 4.6447E+04 1.4222E+04 0.
 6 3.6654E+04 0. 4.6437E+04 1.4219E+04 0.
 7 7.1948E+04 4.9777E+02 4.6427E+04 1.4216E+04 0.
 8 3.6646E+04 0. 4.6417E+04 1.4213E+04 0.
 9 7.1922E+04 -4.9773E+02 4.6408E+04 1.4210E+04 0.

X	LAYER	STRSL 1	STRST 1	STRSLT 1	STRSL 2	STRST 2	STRSLT 2
.2500	1	7.3656E+04	1.4901E+03	0.	4.5351E+04	1.3887E+04	0.
	2	3.7488E+04	3.4240E+03	-5.0000E+02	4.5343E+04	1.3887E+04	0.
	3	7.3630E+04	1.4494E+03	0.	4.5336E+04	1.3887E+04	0.
	4	3.7475E+04	3.4437E+03	4.9997E+02	4.5328E+04	1.3879E+04	0.
	5	7.3605E+04	1.4891E+03	0.	4.5320E+04	1.3875E+04	0.
	6	3.7462E+04	3.4825E+03	4.9993E+02	4.5312E+04	1.3875E+04	0.
	7	7.3579E+04	1.4884E+03	0.	4.5304E+04	1.3872E+04	0.
	8	3.7449E+04	3.4812E+03	-4.9990E+02	4.5289E+04	1.3870E+04	0.
	9	7.3553E+04	1.4881E+03	0.	4.5289E+04	1.3867E+04	0.

X	LAYER	STRSL 1	STKST 1	STRSLT 1	STRSL 2	STKST 2	STRSLT 2
1	7.5644E+04	1.5247E+03	0.	4.3912E+04	1.3446E+04	0.	
2	3.8510E+04	4.0811E+03	-5.0257E+02	4.3905E+04	1.3444E+04	0.	
3	7.5648E+04	1.5247E+03	0.	4.3400E+04	1.3442E+04	0.	
4	3.8503E+04	4.0810E+03	5.0255E+02	4.3844E+04	1.3440E+04	0.	
5	7.5633E+04	1.5247E+03	0.	4.3888E+04	1.3438E+04	0.	
6	3.8495E+04	4.0809E+03	5.0254E+02	4.3882E+04	1.3437E+04	0.	
7	7.5617E+04	1.5286E+03	0.	4.3876E+04	1.3435E+04	0.	
8	3.8487E+04	4.0746E+03	-5.0252E+02	4.3870E+04	1.3432E+04	0.	
9	7.5602E+04	1.5285E+03	0.	4.3863E+04	1.3431E+04	0.	

X	LAYER	STRSL 1	STRST 1	SIRSLT 1	SIRSL 2	STRST 2	SIRSLT 2
.8333	1	7.8271E+04	1.5813E+03	0.	4.2014E+04	1.2885E+04	0.
	2	3.9851E+04	4.2091E+03	-5.0567E+02	4.2011E+04	1.2884E+04	0.
	3	7.8301E+04	1.5815E+03	0.	4.2007E+04	1.2889E+04	0.
	4	3.9856E+04	4.2084E+03	5.0568E+02	4.2002E+04	1.2861E+04	0.
	5	7.8310E+04	1.5817E+03	0.	4.1998E+04	1.2880E+04	0.
	6	3.9861E+04	4.2084E+03	5.0569E+02	4.1993E+04	1.2888E+04	0.
	7	7.8320E+04	1.5819E+03	0.	4.1989E+04	1.2857E+04	0.
	8	3.9866E+04	4.2093E+03	-5.0571E+02	4.1984E+04	1.2866E+04	0.
	9	7.8329E+04	1.5821E+03	0.	4.1980E+04	1.2844E+04	0.

X	LAYER	STPSL 1	STIRST 1	STIRSLT 1	STIRSL 1	STIRST 2	STIRSLT 2	STIRSL 2
8-250	1	8.1684E+04	1.6479E+03	0.	3.9549E+04	1.2110E+04	0.	0.
	2	4.1585E+04	4.3698E+03	-5.0924E+02	3.9546E+04	1.2109E+04	0.	0.
	3	8.1739E+04	1.6489E+03	0.	3.9544E+04	1.2108E+04	0.	0.
	4	4.1613E+04	4.3724E+03	5.0930E+02	3.9542E+04	1.2108E+04	0.	0.
	5	8.1794E+04	1.6500E+03	0.	3.9539E+04	1.2107E+04	0.	0.
	6	4.1654E+04	4.3750E+03	5.0935E+02	3.9537E+04	1.2106E+04	0.	0.
	7	8.1844E+04	1.6511E+03	0.	3.9535E+04	1.2106E+04	0.	0.
	8	4.1669E+04	4.3726E+03	-5.0940E+02	3.9532E+04	1.2105E+04	0.	0.
	9	8.1904E+04	1.6522E+03	0.	3.9530E+04	1.2104E+04	0.	0.

X	LAYER	STRSL 1	STKST 1	STRSLT 1	STRSL 2	STKST 2	STRSLT 2
1	1						
2	2						
3	3						
4	4						
5	5						
6	6						
7	7						
8	8						
9	9						
10	10						
11	11						
12	12						
13	13						
14	14						
15	15						
16	16						
17	17						
18	18						
19	19						
20	20						
21	21						
22	22						
23	23						
24	24						
25	25						
26	26						
27	27						
28	28						
29	29						
30	30						
31	31						
32	32						
33	33						
34	34						
35	35						
36	36						
37	37						
38	38						
39	39						
40	40						
41	41						
42	42						
43	43						
44	44						
45	45						
46	46						
47	47						
48	48						
49	49						
50	50						
51	51						
52	52						
53	53						
54	54						
55	55						
56	56						
57	57						
58	58						
59	59						
60	60						
61	61						
62	62						
63	63						
64	64						
65	65						
66	66						
67	67						
68	68						
69	69						
70	70						
71	71						
72	72						
73	73						
74	74						
75	75						
76	76						

1.0417

LAYER	STRSL 1	STRSL 2	STRSLT 1	STRSLT 2
1	8.5828E+04	1.7288E+03	0.	1.1181E+04
2	4.3705E+04	4.5456E+03	-5.1301E+02	1.1181E+04
3	8.5951E+04	1.7312E+03	0.	1.1182E+04
4	4.3764E+04	4.5713E+03	5.1311E+02	1.1182E+04
5	8.6074E+04	1.7336E+03	0.	1.1183E+04
6	4.3831E+04	4.5771E+03	5.1320E+02	1.1183E+04
7	8.6147E+04	1.7360E+03	0.	1.1184E+04
8	4.3844E+04	4.5828E+03	-5.1331E+02	1.1184E+04
9	8.6321E+04	1.7384E+03	0.	1.1185E+04

X

LAYER

STRSL 1

STRSL 2

STRSLT 1

STRSLT 2

STRSLT 2

STRSLT 2

1.0417

LAYER	STRSL 1	STRSL 2	STRSLT 1	STRSLT 2
1	9.0549E+04	1.8217E+03	0.	1.0104E+04
2	4.6151E+04	4.7884E+03	-5.1661E+02	1.0106E+04
3	9.0813E+04	1.8258E+03	0.	1.0109E+04
4	4.6259E+04	4.7983E+03	5.1676E+02	1.0111E+04
5	9.1026E+04	1.8300E+03	0.	1.0114E+04
6	4.6367E+04	4.8081E+03	5.1690E+02	1.0116E+04
7	9.1240E+04	1.8341E+03	0.	1.0118E+04
8	4.6476E+04	4.8174E+03	-5.1704E+02	1.0121E+04
9	9.1454E+04	1.8382E+03	0.	1.0123E+04

G-24

X

LAYER

STRSL 1

STRSL 2

STRSLT 1

STRSLT 2

STRSLT 2

STRSLT 2

1.0417

LAYER	STRSL 1	STRSL 2	STRSLT 1	STRSLT 2
1	9.5897E+04	1.9242E+03	0.	8.9028E+03
2	4.8866E+04	5.0324E+03	-5.1984E+02	8.9074E+03
3	9.6220E+04	1.9305E+03	0.	8.9131E+03
4	4.9040E+04	5.0471E+03	5.2001E+02	8.9183E+03
5	9.6543E+04	1.9367E+03	0.	8.9235E+03
6	4.9144E+04	5.0617E+03	5.2017E+02	8.9286E+03
7	9.6866E+04	1.9430E+03	0.	8.9338E+03
8	4.9358E+04	5.0764E+03	-5.2035E+02	8.9390E+03
9	9.7188E+04	1.9492E+03	0.	8.9442E+03

X

LAYER

STRSL 1

STRSL 2

STRSLT 1

STRSLT 2

STRSLT 2

STRSLT 2

1.0417

LAYER	STRSL 1	STRSL 2	STRSLT 1	STRSLT 2
1	1.0114E+05	2.0349E+03	0.	7.5978E+03
2	5.1413E+04	5.2932E+03	-5.2254E+02	7.6061E+03
3	1.0209E+05	2.0435E+03	0.	7.6143E+03
4	5.2039E+04	5.3130E+03	5.2271E+02	7.6226E+03
5	1.0254E+05	2.0521E+03	0.	7.6308E+03
6	5.2266E+04	5.3329E+03	5.2284E+02	7.6391E+03
7	1.0218E+05	2.0607E+03	0.	7.6474E+03
8	5.2442E+04	5.3527E+03	-5.2307E+02	7.6556E+03
9	1.0343E+05	2.0692E+03	0.	7.6639E+03

X

LAYER

STRSL 1

STRSL 2

STRSLT 1

STRSLT 2

STRSLT 2

STRSLT 2

1.0417

LAYER	STRSL 1	STRSL 2	STRSLT 1	STRSLT 2
1	1.0740E+05	2.1526E+03	0.	6.2033E+03
2	5.4447E+04	5.5677E+03	-5.2445E+02	6.2144E+03

X	LAYER	STRSL 1	STRSL 2	STRSLT 1	STRSLT 2	STRSLT 2
1.1250	3	1.083RE+05	2.1438E+03	0.	2.0332E+04	6.2255E+03
	4	5.526NE+04	5.5929E+03	5.2482E+02	2.0368E+04	6.2366E+03
	5	1.0895E+05	2.1744E+03	0.	2.0404E+04	6.2477E+03
	6	5.5533E+04	5.6182E+03	5.2497E+02	2.0440E+04	6.2588E+03
	7	1.0453E+05	2.1859E+03	0.	2.0477E+04	6.2699E+03
	8	5.5846E+04	5.6433E+03	-5.2513E+02	2.0513E+04	6.2810E+03
	9	1.1011E+05	2.1969E+03	0.	2.0549E+04	6.2921E+03
	1	1.1432E+05	2.2770E+03	0.	1.5462E+04	4.7346E+03
	2	5.8304E+04	5.8533E+03	-5.2616E+02	1.5504E+04	4.7474E+03
	3	1.1503E+05	2.2904E+03	0.	1.5546E+04	4.7602E+03
	4	5.8667E+04	5.8837E+03	5.2628E+02	1.5588E+04	4.7729E+03
	5	1.1574E+05	2.3039E+03	0.	1.5629E+04	4.7857E+03
	6	5.9027E+04	5.9141E+03	5.2640E+02	1.5671E+04	4.7985E+03
	7	1.1644E+05	2.3173E+03	0.	1.5713E+04	4.8113E+03
	8	5.9386E+04	5.9444E+03	-5.2651E+02	1.5755E+04	4.8241E+03
	9	1.1714E+05	2.3307E+03	0.	1.5796E+04	4.8369E+03

X	LAYER	STRSL 1	STRSL 2	STRSLT 1	STRSLT 2	STRSLT 2
1.1667	1	1.2120E+05	2.4070E+03	0.	1.0458E+04	3.2023E+03
	2	6.1826E+04	6.1486E+03	-5.2707E+02	1.0498E+04	3.2146E+03
	3	1.2203E+05	2.4227E+03	0.	1.0539E+04	3.2269E+03
	4	6.2247E+04	6.1835E+03	5.2715E+02	1.0579E+04	3.2392E+03
	5	1.2287E+05	2.4383E+03	0.	1.0619E+04	3.2516E+03
	6	6.2668E+04	6.2184E+03	5.2720E+02	1.0659E+04	3.2639E+03
	7	1.2370E+05	2.4534E+03	0.	1.0700E+04	3.2752E+03
	8	6.3084E+04	6.2532E+03	-5.2726E+02	1.0740E+04	3.2895E+03
	9	1.2453E+05	2.4645E+03	0.	1.0780E+04	3.3008E+03

X	LAYER	STRSL 1	STRSL 2	STRSLT 1	STRSLT 2	STRSLT 2
1.2083	1	1.2844E+05	2.5424E+03	0.	5.2462E+03	1.6217E+03
	2	6.5507E+04	6.4515E+03	-5.2742E+02	5.3238E+03	1.6302E+03
	3	1.2935E+05	2.5594E+03	0.	5.3514E+03	1.6386E+03
	4	6.5974E+04	6.4900E+03	5.2743E+02	5.3791E+03	1.6471E+03
	5	1.3028E+05	2.5727E+03	0.	5.4067E+03	1.6555E+03
	6	6.6451E+04	6.5283E+03	5.2743E+02	5.4343E+03	1.6640E+03
	7	1.3121E+05	2.5946E+03	0.	5.4614E+03	1.6724E+03
	8	6.6922E+04	6.5666E+03	-5.2742E+02	5.4896E+03	1.6804E+03
	9	1.3214E+05	2.6120E+03	0.	5.5172E+03	1.6844E+03

X	LAYER	STRSL 1	STRSL 2	STRSLT 1	STRSLT 2	STRSLT 2
1.2500	1	1.3597E+05	2.6831E+03	0.	0.	0.
	2	6.9350E+04	6.7618E+03	-5.2726E+02	0.	0.
	3	1.3697E+05	2.7016E+03	0.	0.	0.
	4	6.9858E+04	6.8024E+03	5.2721E+02	0.	0.

5	1.3798E+05	2.7202E+03	0.	0.	0.
6	7.0366E+04	6.8427E+03	5.2714E+02	0.	0.
7	1.3848E+05	2.7388E+03	0.	0.	0.
8	7.0873E+04	6.8830E+03	-5.2708E+02	0.	0.
9	1.3998E+05	2.7573E+03	0.	0.	0.

LSA 62 DOUBLE LAP TITANIUM TO COMPOSITE ADHERENDS, HSLE ADHESIVE

NONLINEAR ORTHOTROPIC ANALYSIS, DOUBLE LAP JOINT

JOINT LENGTH = 1.0000
 FRIZR TOLERANCE = .025
 MAXIMUM ITERATIONS = 20
 NUMBER OF STATIONS = 61
 EFFECTIVE λ = .020

ADHESIVE

THICKNESS = .0099
 POISSON'S RATIO = .43
 RANGERS USG0000 CONSTANTS (SHEAR STRESS-STRAIN CURVE)
 S = 315400
 SECANT S = 6400
 N VALUE = 4.227

ADHEREND NUMBER 1 (ISOTROPIC)

THICKNESS .0450
 POISSON'S RATIO .3062
 RANGERS OS0000 CONSTANTS
 S VS. E 17251000
 SECANT S 136400
 N 37.246

ADHEREND NUMBER 2 (ORTHOTROPIC)

THICKNESS .0887
 NUMBER OF LAYERS 17
 RANGERS OS0000 CONSTANTS
 SL VS. EL 24425000
 SL VS. ET -136632000
 ST VS. ET 2750000
 SLI VS. ELT 933000
 ORIENTATIONS 0 45 0 -45 0 45 0 -45 0 45 0 -45 0 45 0

ALPHA = 7.8924E+00
 DELTA = 7.4407E+00
 LAMBDA = 8.6294E+00
 N RESET TO 23

1000 = 2.44			
AT ITERATION	1	ERROR IS	3.59E-01
AT ITERATION	2	ERROR IS	4.62E-02
AT ITERATION	3	ERROR IS	3.33E-02
AT ITERATION	4	ERROR IS	1.59E-02

RESULTS FOR P = 2535

NUMBER OF ITERATIONS = 4 , MAXIMUM ERROR = .01594

X	TAU	SIGMA	NX1	NX1	NX2	NX2
0.0000	2.5108E+03	1.5671E+03	2.9104E-11	-1.1369E-14	5.0700E+03	0.
0.055	6.4027E+03	1.0493E+03	3.1853E+02	-1.1352E-01	4.4324E+03	0.
0.110	5.1231E+03	5.3235E+02	5.8046E+02	-1.5264E-01	3.9711E+03	0.
0.165	3.8544E+03	3.0250E+01	7.8403E+02	-1.5279E-01	3.5019E+03	0.
0.220	2.7507E+03	-3.0414E+02	9.3312E+02	-1.2183E-01	3.2038E+03	0.
0.275	1.9125E+03	-4.5565E+02	1.0380E+03	-8.2704E-02	2.9434E+03	0.
0.330	1.3220E+03	-4.7405E+02	1.1107E+03	-4.7524E-02	2.8496E+03	0.
0.385	4.2114E+02	-3.1325E+02	1.1611E+03	-2.1612E-02	2.7479E+03	0.
0.440	6.5673E+02	-3.1563E+02	1.1465E+03	-5.9165E-03	2.6770E+03	0.
0.495	4.9132E+02	-2.0448E+02	1.2227E+03	1.0446E-13	2.6255E+03	0.
0.550	4.0125E+02	-1.0214E+02	1.2823E+03	1.9354E-03	2.5854E+03	0.
0.605	3.7355E+02	1.8716E+02	1.2597E+03	-1.3433E-04	2.5507E+03	0.
0.660	4.0457E+02	1.0513E+02	1.2771E+03	-2.2102E-03	2.5152E+03	0.
0.715	4.4444E+02	2.1399E+02	1.2974E+03	-1.1358E-03	2.4752E+03	0.
0.770	6.5447E+02	3.2131E+02	1.3236E+03	6.6549E-03	2.4225E+03	0.
0.825	4.3440E+02	4.1884E+02	1.3597E+03	2.2100E-03	2.3505E+03	0.
0.880	1.2494E+03	4.7924E+02	1.4111E+03	4.8420E-02	2.2472E+03	0.
0.935	1.4516E+03	4.5847E+02	1.4833E+03	8.4005E-02	2.0445E+03	0.
0.990	2.4001E+03	3.0438E+02	1.5623E+03	1.2333E-01	1.8854E+03	0.
1.045	3.9175E+03	-3.6544E+01	1.7441E+03	1.5436E-01	1.5814E+03	0.
1.100	5.1845E+03	-5.4230E+02	1.9505E+03	1.5975E-01	1.1634E+03	0.
1.155	7.4441E+03	-1.1028E+03	2.2150E+03	1.1404E-01	6.4003E+02	0.
1.210	7.5271E+03	-1.5724E+03	2.5350E+03	1.2642E-14	1.4555E-10	0.

X	LAYER	STRSL 1	STRST 1	STRSLT 1	STRSL 2	STRST 2	STRSLT 2
0.0000	1	0.	0.	0.	8.5033E+04	1.6871E+03	0.
	2	0.	0.	0.	4.3273E+04	4.4312E+03	-5.7180E+02
	3	0.	0.	0.	8.5033E+04	1.6871E+03	0.
	4	0.	0.	0.	4.3273E+04	4.4312E+03	5.7180E+02
	5	0.	0.	0.	8.5033E+04	1.6871E+03	0.
	6	0.	0.	0.	4.3273E+04	4.4312E+03	-5.7180E+02
	7	0.	0.	0.	8.5033E+04	1.6871E+03	0.
	8	0.	0.	0.	4.3273E+04	4.4312E+03	5.7180E+02
	9	0.	0.	0.	8.5033E+04	1.6871E+03	0.
	10	0.	0.	0.	4.3273E+04	4.4312E+03	5.7180E+02
	11	0.	0.	0.	8.5033E+04	1.6871E+03	0.
	12	0.	0.	0.	4.3273E+04	4.4312E+03	-5.7180E+02
	13	0.	0.	0.	8.5033E+04	1.6871E+03	0.
	14	0.	0.	0.	4.3273E+04	4.4312E+03	5.7180E+02
	15	0.	0.	0.	8.5033E+04	1.6871E+03	0.
	16	0.	0.	0.	4.3273E+04	4.4312E+03	-5.7180E+02
	17	0.	0.	0.	8.5033E+04	1.6871E+03	0.

X	LAYER	STRSL 1	STRST 1	STRSLT 1	STRSL 2	STRST 2	STRSLT 2
0.0000	1	5.7293E+03	2.0758E+03	0.	7.4234E+04	1.4768E+03	0.
	2	5.4541E+03	2.0447E+03	0.	3.7741E+04	1.9316E+03	-5.6686E+02
	3	6.4289E+03	2.1216E+03	0.	7.4234E+04	1.4768E+03	0.
	4	7.0032E+03	2.1445E+03	0.	3.7741E+04	1.9316E+03	5.6686E+02
	5	7.0784E+03	2.1574E+03	0.	7.4234E+04	1.4768E+03	0.

LAYER	STRSL 1	STRSLT 1	STRSL 2	STRSLT 2
6	7.1532E+03	2.1903E+03	3.7791E+04	3.9316E+03
7	7.2290E+03	2.2132E+03	7.4234E+04	1.4768E+03
8	7.3028E+03	2.2361E+03	3.7791E+04	3.9316E+03
9	7.3775E+03	2.2590E+03	7.4234E+04	1.4768E+03
10			3.7791E+04	3.9316E+03
11			7.4234E+04	1.4768E+03
12			3.7791E+04	3.9316E+03
13			7.4234E+04	1.4768E+03
14			3.7791E+04	3.9316E+03
15			7.4234E+04	1.4768E+03
16			3.7791E+04	3.9316E+03
17			7.4234E+04	1.4768E+03

LAYER	STRSL 1	STRSLT 1	STRSL 2	STRSLT 2
1	1.2484E+04	3.8226E+03	6.5380E+04	1.3033E+03
2	1.2548E+04	3.8544E+03	3.3293E+04	3.5090E+03
3	1.2692E+04	3.8842E+03	5.5380E+04	1.3033E+03
4	1.2795E+04	3.9174E+03	3.3293E+04	3.5090E+03
5	1.2894E+04	3.9477E+03	6.5380E+04	1.3033E+03
6	1.3007E+04	3.9815E+03	3.3293E+04	3.5090E+03
7	1.3107E+04	4.0133E+03	6.5380E+04	1.3033E+03
8	1.3211E+04	4.0451E+03	3.3293E+04	3.5090E+03
9	1.3314E+04	4.0768E+03	6.5380E+04	1.3033E+03
10			3.3293E+04	3.5090E+03
11			6.5380E+04	1.3033E+03
12			3.3293E+04	3.5090E+03
13			6.5380E+04	1.3033E+03
14			3.3293E+04	3.5090E+03
15			6.5380E+04	1.3033E+03
16			3.3293E+04	3.5090E+03
17			6.5380E+04	1.3033E+03

LAYER	STRSL 1	STRSLT 1	STRSL 2	STRSLT 2
1	1.7021E+04	5.2117E+03	5.8517E+04	1.1681E+03
2	1.7121E+04	5.2425E+03	2.9804E+04	3.1724E+03
3	1.7222E+04	5.2733E+03	5.8517E+04	1.1681E+03
4	1.7322E+04	5.3041E+03	2.9804E+04	3.1724E+03
5	1.7423E+04	5.3349E+03	5.8517E+04	1.1681E+03
6	1.7524E+04	5.3657E+03	2.9804E+04	3.1724E+03
7	1.7624E+04	5.3965E+03	5.8517E+04	1.1681E+03
8	1.7725E+04	5.4273E+03	2.9804E+04	3.1724E+03
9	1.7825E+04	5.4581E+03	5.8517E+04	1.1681E+03
10			2.9804E+04	3.1724E+03
11			5.8517E+04	1.1681E+03
12			2.9804E+04	3.1724E+03
13			5.8517E+04	1.1681E+03
14			2.9804E+04	3.1724E+03
15			5.8517E+04	1.1681E+03
16			2.9804E+04	3.1724E+03
17			5.8517E+04	1.1681E+03

X	LAYER	STRSL 1	STRSL 1	STRSLT 1	STRSL 2	STRSLT 2	STRSLT 2
1819	1	2.0415E+04	6.2511E+03	0.	5.3499E+04	1.0691E+03	0.
	2	2.0495E+04	6.2752E+03	0.	2.7253E+04	2.9222E+03	-5.3186E+02
	3	2.0576E+04	6.3002E+03	0.	5.3499E+04	1.0691E+03	0.
	4	2.0656E+04	6.3248E+03	0.	2.7253E+04	2.9222E+03	5.3186E+02
	5	2.0736E+04	6.3494E+03	0.	5.3499E+04	1.0691E+03	0.
	6	2.0816E+04	6.3734E+03	0.	2.7253E+04	2.9222E+03	-5.3186E+02
	7	2.0896E+04	6.3985E+03	0.	5.3499E+04	1.0691E+03	0.
	8	2.0976E+04	6.4231E+03	0.	2.7253E+04	2.9222E+03	5.3186E+02
	9	2.1057E+04	6.4476E+03	0.	5.3499E+04	1.0691E+03	0.
	10				2.7253E+04	2.9222E+03	5.3186E+02
	11				5.3499E+04	1.0691E+03	0.
	12				2.7253E+04	2.9222E+03	-5.3186E+02
	13				5.3499E+04	1.0691E+03	0.
	14				2.7253E+04	2.9222E+03	5.3186E+02
	15				5.3499E+04	1.0691E+03	0.
	16				2.7253E+04	2.9222E+03	-5.3186E+02
	17				5.3499E+04	1.0691E+03	0.

Y	LAYER	STRSL 1	STRSL 1	STRSLT 1	STRSL 2	STRSLT 2	STRSLT 2
2224	1	2.2844E+04	6.9965E+03	0.	4.9974E+04	9.9930E+02	0.
	2	2.2904E+04	7.0132E+03	0.	2.5450E+04	2.7435E+03	-5.2023E+02
	3	2.2958E+04	7.0292E+03	0.	4.9974E+04	9.9930E+02	0.
	4	2.3013E+04	7.0452E+03	0.	2.5460E+04	2.7435E+03	5.2023E+02
	5	2.3047E+04	7.0632E+03	0.	4.9974E+04	9.9930E+02	0.
	6	2.3125E+04	7.0794E+03	0.	2.5460E+04	2.7435E+03	-5.2023E+02
	7	2.3176E+04	7.0965E+03	0.	4.9974E+04	9.9930E+02	0.
	8	2.3231E+04	7.1132E+03	0.	2.5460E+04	2.7435E+03	5.2023E+02
	9	2.3285E+04	7.1244E+03	0.	4.9974E+04	9.9930E+02	0.
	10				2.5460E+04	2.7435E+03	-5.2023E+02
	11				4.9974E+04	9.9930E+02	0.
	12				2.5460E+04	2.7435E+03	5.2023E+02
	13				4.9974E+04	9.9930E+02	0.
	14				2.5460E+04	2.7435E+03	-5.2023E+02
	15				4.9974E+04	9.9930E+02	0.
	16				2.5460E+04	2.7435E+03	5.2023E+02
	17				4.9974E+04	9.9930E+02	0.

X	LAYER	STRSL 1	STRSL 1	STRSLT 1	STRSL 2	STRSLT 2	STRSLT 2
2227	1	2.4557E+04	7.5143E+03	0.	4.7534E+04	9.5095E+02	0.
	2	2.4588E+04	7.5288E+03	0.	2.4219E+04	2.6187E+03	-5.1083E+02
	3	2.4619E+04	7.5384E+03	0.	4.7534E+04	9.5095E+02	0.
	4	2.4651E+04	7.5480E+03	0.	2.4219E+04	2.6187E+03	5.1083E+02
	5	2.4682E+04	7.5576E+03	0.	4.7534E+04	9.5095E+02	0.
	6	2.4713E+04	7.5672E+03	0.	2.4219E+04	2.6187E+03	-5.1083E+02
	7	2.4744E+04	7.5768E+03	0.	4.7534E+04	9.5095E+02	0.
	8	2.4775E+04	7.5864E+03	0.	2.4219E+04	2.6187E+03	5.1083E+02
	9	2.4807E+04	7.5959E+03	0.	4.7534E+04	9.5095E+02	0.
	10				2.4219E+04	2.6187E+03	-5.1083E+02
	11				4.7534E+04	9.5095E+02	0.
	12				2.4219E+04	2.6187E+03	5.1083E+02
	13				4.7534E+04	9.5095E+02	0.
	14				2.4219E+04	2.6187E+03	-5.1083E+02
	15				4.7534E+04	9.5095E+02	0.
	16				2.4219E+04	2.6187E+03	5.1083E+02
	17				4.7534E+04	9.5095E+02	0.

X	LAYER	STRSL 1	STRST 1	STRSLT 1	STRSL 2	STRST 2	STRSLT 2
.3132	1	2.5744E+04	7.8824E+03	0.	4.5843E+04	9.1741E+02	0.
	2	2.5759E+04	7.8373E+03	0.	2.3359E+04	2.5316E+03	-5.0361E+02
	3	2.5773E+04	7.8416E+03	0.	4.5843E+04	9.1741E+02	0.
	4	2.5787E+04	7.8460E+03	0.	2.3359E+04	2.5316E+03	5.0361E+02
	5	2.5801E+04	7.8503E+03	0.	4.5843E+04	9.1741E+02	0.
	6	2.5815E+04	7.8547E+03	0.	2.3359E+04	2.5316E+03	-5.0361E+02
	7	2.5830E+04	7.8590E+03	0.	4.5843E+04	9.1741E+02	0.
	8	2.5844E+04	7.8634E+03	0.	2.3359E+04	2.5316E+03	5.0361E+02
	9	2.5858E+04	7.8678E+03	0.	4.5843E+04	9.1741E+02	0.
	10				2.3359E+04	2.5316E+03	5.0361E+02
	11				4.5843E+04	9.1741E+02	0.
	12				2.3359E+04	2.5316E+03	-5.0361E+02
	13				4.5843E+04	9.1741E+02	0.
	14				2.3359E+04	2.5316E+03	5.0361E+02
	15				4.5843E+04	9.1741E+02	0.
	16				2.3359E+04	2.5316E+03	-5.0361E+02
	17				4.5843E+04	9.1741E+02	0.

G-32

X	LAYER	STRSL 1	STRST 1	STRSLT 1	STRSL 2	STRST 2	STRSLT 2
.3535	1	2.6573E+04	8.1366E+03	0.	4.4655E+04	8.9382E+02	0.
	2	2.6577E+04	8.1378E+03	0.	2.2754E+04	2.4701E+03	-4.9817E+02
	3	2.6581E+04	8.1390E+03	0.	4.4655E+04	8.9382E+02	0.
	4	2.6585E+04	8.1402E+03	0.	2.2754E+04	2.4701E+03	4.9817E+02
	5	2.6589E+04	8.1414E+03	0.	4.4655E+04	8.9382E+02	0.
	6	2.6593E+04	8.1426E+03	0.	2.2754E+04	2.4701E+03	-4.9817E+02
	7	2.6597E+04	8.1438E+03	0.	4.4655E+04	8.9382E+02	0.
	8	2.6601E+04	8.1450E+03	0.	2.2754E+04	2.4701E+03	4.9817E+02
	9	2.6605E+04	8.1462E+03	0.	4.4655E+04	8.9382E+02	0.
	10				2.2754E+04	2.4701E+03	4.9817E+02
	11				4.4655E+04	8.9382E+02	0.
	12				2.2754E+04	2.4701E+03	-4.9817E+02
	13				4.4655E+04	8.9382E+02	0.
	14				2.2754E+04	2.4701E+03	4.9817E+02
	15				4.4655E+04	8.9382E+02	0.
	16				2.2754E+04	2.4701E+03	-4.9817E+02
	17				4.4655E+04	8.9382E+02	0.

X	LAYER	STRSL 1	STRST 1	STRSLT 1	STRSL 2	STRST 2	STRSLT 2
.4141	1	2.7164E+04	8.3176E+03	0.	4.3791E+04	8.7666E+02	0.
	2	2.7163E+04	8.3174E+03	0.	2.2314E+04	2.4252E+03	-4.9400E+02
	3	2.7162E+04	8.3172E+03	0.	4.3791E+04	8.7666E+02	0.
	4	2.7162E+04	8.3164E+03	0.	2.2314E+04	2.4252E+03	4.9400E+02
	5	2.7161E+04	8.3167E+03	0.	4.3791E+04	8.7666E+02	0.
	6	2.7160E+04	8.3165E+03	0.	2.2314E+04	2.4252E+03	-4.9400E+02
	7	2.7160E+04	8.3163E+03	0.	4.3791E+04	8.7666E+02	0.

X	LAYER	STASL 1	STASL 2	STRSLT 1	STRSLT 2	STRSLT 2
8		2.7159E+04	8.3161E+03	0.	2.2314E+04	2.4252E+03
9		2.7159E+04	8.3159E+03	0.	4.3791E+04	8.7666E+02
10				0.	2.2314E+04	2.4252E+03
11					4.3791E+04	8.7666E+02
12					2.2314E+04	2.4252E+03
13					4.3791E+04	8.7666E+02
14					2.2314E+04	2.4252E+03
15					4.3791E+04	8.7666E+02
16					2.2314E+04	2.4252E+03
17					4.3791E+04	8.7666E+02

X	LAYER	STASL 1	STASL 2	STRSLT 1	STRSLT 2	STRSLT 2
4515	1	2.7611E+04	8.4546E+03	0.	4.3119E+04	8.6332E+02
	2	2.7610E+04	8.4542E+03	0.	2.1973E+04	2.3902E+02
	3	2.7609E+04	8.4538E+03	0.	4.3119E+04	8.6332E+02
	4	2.7608E+04	8.4534E+03	0.	2.1973E+04	2.3902E+03
	5	2.7607E+04	8.4530E+03	0.	4.3119E+04	8.6332E+02
	6	2.7606E+04	8.4526E+03	0.	2.1973E+04	2.3902E+03
	7	2.7605E+04	8.4522E+03	0.	4.3119E+04	8.6332E+02
	8	2.7604E+04	8.4518E+03	0.	2.1973E+04	2.3902E+03
	9	2.7603E+04	8.4514E+03	0.	4.3119E+04	8.6332E+02
	10				1.473E+04	2.3902E+03
	11				4.114E+04	8.6332E+02
	12				2.1973E+04	2.3902E+03
	13				4.3119E+04	8.6332E+02
	14				2.1973E+04	2.3902E+03
	15				4.3119E+04	8.6332E+02
	16				2.1973E+04	2.3902E+03
	17				4.3119E+04	8.6332E+02

X	LAYER	STASL 1	STASL 2	STRSLT 1	STRSLT 2	STRSLT 2
5100	1	2.7992E+04	8.5712E+03	0.	4.2536E+04	8.5174E+02
	2	2.7991E+04	8.5713E+03	0.	2.1676E+04	2.3598E+03
	3	2.7990E+04	8.5713E+03	0.	4.2536E+04	8.5174E+02
	4	2.7989E+04	8.5713E+03	0.	2.1676E+04	2.3598E+03
	5	2.7988E+04	8.5713E+03	0.	4.2536E+04	8.5174E+02
	6	2.7987E+04	8.5714E+03	0.	2.1676E+04	2.3598E+03
	7	2.7986E+04	8.5714E+03	0.	4.2536E+04	8.5174E+02
	8	2.7985E+04	8.5714E+03	0.	2.1676E+04	2.3598E+03
	9	2.7984E+04	8.5715E+03	0.	4.2536E+04	8.5174E+02
	10				2.1676E+04	2.3598E+03
	11				4.2536E+04	8.5174E+02
	12				2.1676E+04	2.3598E+03
	13				4.2536E+04	8.5174E+02
	14				2.1676E+04	2.3598E+03
	15				4.2536E+04	8.5174E+02
	16				2.1676E+04	2.3598E+03
	17				4.2536E+04	8.5174E+02

X	LAYER	STRSL 1	STRST 1	STRSLT 1	STRSL 2	STRST 2	STRSLT 2
1	2.83775E+04	8.64884E+03	0.	4.1951E+04	8.4010E+02	0.	0.
2	2.83775E+04	8.6488E+03	0.	4.1951E+04	2.3292E+03	-4.8456E+02	-4.8456E+02
3	2.83775E+04	8.6488E+03	0.	4.1951E+04	8.4010E+02	0.	0.
4	2.83775E+04	8.6488E+03	0.	4.1951E+04	2.3292E+03	4.8456E+02	4.8456E+02
5	2.83775E+04	8.6488E+03	0.	4.1951E+04	8.4010E+02	0.	0.
6	2.83775E+04	8.6488E+03	0.	4.1951E+04	2.3292E+03	-4.8456E+02	-4.8456E+02
7	2.83775E+04	8.6488E+03	0.	4.1951E+04	8.4010E+02	0.	0.
8	2.83775E+04	8.6488E+03	0.	4.1951E+04	2.3292E+03	4.8456E+02	4.8456E+02
9	2.83775E+04	8.6488E+03	0.	4.1951E+04	8.4010E+02	0.	0.
10	2.83775E+04	8.6488E+03	0.	4.1951E+04	2.3292E+03	-4.8456E+02	-4.8456E+02
11	2.83775E+04	8.6488E+03	0.	4.1951E+04	8.4010E+02	0.	0.
12	2.83775E+04	8.6488E+03	0.	4.1951E+04	2.3292E+03	4.8456E+02	4.8456E+02
13	2.83775E+04	8.6488E+03	0.	4.1951E+04	8.4010E+02	0.	0.
14	2.83775E+04	8.6488E+03	0.	4.1951E+04	2.3292E+03	-4.8456E+02	-4.8456E+02
15	2.83775E+04	8.6488E+03	0.	4.1951E+04	8.4010E+02	0.	0.
16	2.83775E+04	8.6488E+03	0.	4.1951E+04	2.3292E+03	4.8456E+02	4.8456E+02
17	2.83775E+04	8.6488E+03	0.	4.1951E+04	8.4010E+02	0.	0.

X	LAYER	STRSL 1	STRST 1	STRSLT 1	STRSL 2	STRST 2	STRSLT 2
1	2.8828E+04	8.8277E+03	0.	4.1272E+04	8.2660E+02	0.	0.
2	2.8828E+04	8.8277E+03	0.	4.1272E+04	2.2936E+03	-4.8086E+02	-4.8086E+02
3	2.8828E+04	8.8277E+03	0.	4.1272E+04	8.2660E+02	0.	0.
4	2.8828E+04	8.8277E+03	0.	4.1272E+04	2.2936E+03	4.8086E+02	4.8086E+02
5	2.8828E+04	8.8277E+03	0.	4.1272E+04	8.2660E+02	0.	0.
6	2.8828E+04	8.8277E+03	0.	4.1272E+04	2.2936E+03	-4.8086E+02	-4.8086E+02
7	2.8828E+04	8.8277E+03	0.	4.1272E+04	8.2660E+02	0.	0.
8	2.8828E+04	8.8277E+03	0.	4.1272E+04	2.2936E+03	4.8086E+02	4.8086E+02
9	2.8828E+04	8.8277E+03	0.	4.1272E+04	8.2660E+02	0.	0.
10	2.8828E+04	8.8277E+03	0.	4.1272E+04	2.2936E+03	-4.8086E+02	-4.8086E+02
11	2.8828E+04	8.8277E+03	0.	4.1272E+04	8.2660E+02	0.	0.
12	2.8828E+04	8.8277E+03	0.	4.1272E+04	2.2936E+03	4.8086E+02	4.8086E+02
13	2.8828E+04	8.8277E+03	0.	4.1272E+04	8.2660E+02	0.	0.
14	2.8828E+04	8.8277E+03	0.	4.1272E+04	2.2936E+03	-4.8086E+02	-4.8086E+02
15	2.8828E+04	8.8277E+03	0.	4.1272E+04	8.2660E+02	0.	0.
16	2.8828E+04	8.8277E+03	0.	4.1272E+04	2.2936E+03	4.8086E+02	4.8086E+02
17	2.8828E+04	8.8277E+03	0.	4.1272E+04	8.2660E+02	0.	0.

X	LAYER	STRSL 1	STRST 1	STRSLT 1	STRSL 2	STRST 2	STRSLT 2
1	2.9429E+04	9.0112E+03	0.	4.0394E+04	8.0914E+02	0.	0.
2	2.9429E+04	9.0112E+03	0.	4.0394E+04	2.2475E+03	-4.7590E+02	-4.7590E+02
3	2.9429E+04	9.0112E+03	0.	4.0394E+04	8.0914E+02	0.	0.
4	2.9429E+04	9.0112E+03	0.	4.0394E+04	2.2475E+03	4.7590E+02	4.7590E+02
5	2.9429E+04	9.0112E+03	0.	4.0394E+04	8.0914E+02	0.	0.
6	2.9429E+04	9.0112E+03	0.	4.0394E+04	2.2475E+03	-4.7590E+02	-4.7590E+02
7	2.9429E+04	9.0112E+03	0.	4.0394E+04	8.0914E+02	0.	0.
8	2.9429E+04	9.0112E+03	0.	4.0394E+04	2.2475E+03	4.7590E+02	4.7590E+02
9	2.9429E+04	9.0112E+03	0.	4.0394E+04	8.0914E+02	0.	0.
10	2.9429E+04	9.0112E+03	0.	4.0394E+04	2.2475E+03	-4.7590E+02	-4.7590E+02
11	2.9429E+04	9.0112E+03	0.	4.0394E+04	8.0914E+02	0.	0.
12	2.9429E+04	9.0112E+03	0.	4.0394E+04	2.2475E+03	4.7590E+02	4.7590E+02
13	2.9429E+04	9.0112E+03	0.	4.0394E+04	8.0914E+02	0.	0.
14	2.9429E+04	9.0112E+03	0.	4.0394E+04	2.2475E+03	-4.7590E+02	-4.7590E+02
15	2.9429E+04	9.0112E+03	0.	4.0394E+04	8.0914E+02	0.	0.
16	2.9429E+04	9.0112E+03	0.	4.0394E+04	2.2475E+03	4.7590E+02	4.7590E+02

17

X	LAYER	STRSL 1	STRSL 2	STRSLT 1	STRSLT 2	STRSL 1	STRSL 2	STRSLT 1	STRSLT 2
.6918	1	3.0274E+04	3.9185E+04	0.	0.	9.2698E+03	3.9185E+04	0.	0.
	2	3.0259E+04	1.9470E+04	0.	0.	9.2654E+03	2.1838E+03	0.	-4.6873E+02
	3	3.0254E+04	3.9185E+04	0.	0.	9.2609E+03	7.8508E+02	0.	0.
	4	3.0230E+04	1.9470E+04	0.	0.	9.2565E+03	2.1838E+03	0.	4.6873E+02
	5	3.0216E+04	3.9185E+04	0.	0.	9.2520E+03	7.8508E+02	0.	0.
	6	3.0201E+04	1.9470E+04	0.	0.	9.2476E+03	2.1838E+03	0.	-4.6873E+02
	7	3.0187E+04	3.9185E+04	0.	0.	9.2431E+03	7.8508E+02	0.	0.
	8	3.0172E+04	1.9470E+04	0.	0.	9.2387E+03	2.1838E+03	0.	4.6873E+02
	9	3.0157E+04	3.9185E+04	0.	0.	9.2342E+03	7.8508E+02	0.	0.
	10						2.1838E+03		4.6873E+02
	11						7.8508E+02		0.
	12						2.1838E+03		-4.6873E+02
	13						7.8508E+02		0.
	14						2.1838E+03		4.6873E+02
	15						7.8508E+02		0.
	16						2.1838E+03		-4.6873E+02
	17						7.8508E+02		0.

0.

8.0914E+02

4.0394E+04

G-35

X	LAYER	STRSL 1	STRSL 2	STRSLT 1	STRSLT 2	STRSL 1	STRSL 2	STRSLT 1	STRSLT 2
.7773	1	3.1495E+04	3.7464E+04	0.	0.	9.6499E+03	3.7464E+04	0.	0.
	2	3.1454E+04	1.9044E+04	0.	0.	9.6311E+03	2.0426E+03	0.	-4.5785E+02
	3	3.1422E+04	3.7464E+04	0.	0.	9.6213E+03	7.8508E+02	0.	0.
	4	3.1390E+04	1.9044E+04	0.	0.	9.6115E+03	2.0426E+03	0.	4.5785E+02
	5	3.1358E+04	3.7464E+04	0.	0.	9.6018E+03	7.8508E+02	0.	0.
	6	3.1326E+04	1.9044E+04	0.	0.	9.5920E+03	2.0426E+03	0.	-4.5785E+02
	7	3.1294E+04	3.7464E+04	0.	0.	9.5822E+03	7.8508E+02	0.	0.
	8	3.1262E+04	1.9044E+04	0.	0.	9.5725E+03	2.0426E+03	0.	4.5785E+02
	9	3.1230E+04	3.7464E+04	0.	0.	9.5627E+03	7.8508E+02	0.	0.
	10						2.0426E+03		4.5785E+02
	11						7.8508E+02		0.
	12						2.0426E+03		-4.5785E+02
	13						7.8508E+02		0.
	14						2.0426E+03		4.5785E+02
	15						7.8508E+02		0.
	16						2.0426E+03		-4.5785E+02
	17						7.8508E+02		0.

0.

7.5082E+02

3.7464E+04

.7727

Y	LAYER	STRSL 1	STRSL 2	STRSLT 1	STRSLT 2	STRSL 1	STRSL 2	STRSLT 1	STRSLT 2
.7727	1	4.3227E+04	3.4482E+04	0.	0.	1.0174E+04	3.4482E+04	0.	0.
	2	4.3172E+04	1.7831E+04	0.	0.	1.0157E+04	7.8508E+02	0.	-4.4066E+02
	3	4.3117E+04	3.4482E+04	0.	0.	1.0140E+04	7.8508E+02	0.	0.
	4	4.3061E+04	1.7831E+04	0.	0.	1.0123E+04	2.0426E+03	0.	4.4066E+02
	5	4.3006E+04	3.4482E+04	0.	0.	1.0106E+04	7.8508E+02	0.	0.
	6	4.2951E+04	1.7831E+04	0.	0.	1.0090E+04	2.0426E+03	0.	-4.4066E+02
	7	4.2895E+04	3.4482E+04	0.	0.	1.0073E+04	7.8508E+02	0.	0.
	8	4.2840E+04	1.7831E+04	0.	0.	1.0056E+04	2.0426E+03	0.	4.4066E+02
	9	4.2784E+04	3.4482E+04	0.	0.	1.0039E+04	7.8508E+02	0.	0.

0.

7.8508E+02

3.4482E+04

X	LAYER	STRSL 1	STRST 1	STRSLT 1	STRSL 2	STRST 2	STRSLT 2
10		3.5709E+04	1.0934E+04	0.	1.7831E+04	1.9604E+03	4.4066E+02
11		3.5628E+04	1.0909E+04	0.	3.4482E+04	7.0137E+02	0.
12		3.5547E+04	1.0884E+04	0.	1.7831E+04	1.9604E+03	-4.4066E+02
13		3.5465E+04	1.0859E+04	0.	3.4482E+04	7.0137E+02	0.
14		3.5384E+04	1.0834E+04	0.	1.7831E+04	1.9604E+03	4.4066E+02
15		3.5303E+04	1.0809E+04	0.	3.4482E+04	7.0137E+02	0.
16		3.5222E+04	1.0784E+04	0.	1.7831E+04	1.9604E+03	-4.4066E+02
17		3.5141E+04	1.0759E+04	0.	3.4482E+04	7.0137E+02	0.

X	LAYER	STRSL 1	STRST 1	STRSLT 1	STRSL 2	STRST 2	STRSLT 2
1		3.5709E+04	1.0934E+04	0.	3.1404E+04	6.2999E+02	0.
2		3.5628E+04	1.0909E+04	0.	1.6009E+04	1.7678E+02	-4.1258E+02
3		3.5547E+04	1.0884E+04	0.	3.1404E+04	6.2999E+02	0.
4		3.5465E+04	1.0859E+04	0.	1.6009E+04	1.7678E+02	4.1258E+02
5		3.5384E+04	1.0834E+04	0.	3.1404E+04	6.2999E+02	0.
6		3.5303E+04	1.0809E+04	0.	1.6009E+04	1.7678E+02	-4.1258E+02
7		3.5222E+04	1.0784E+04	0.	3.1404E+04	6.2999E+02	0.
8		3.5141E+04	1.0759E+04	0.	1.6009E+04	1.7678E+02	4.1258E+02
9		3.5059E+04	1.0734E+04	0.	3.1404E+04	6.2999E+02	0.
10					1.6009E+04	1.7678E+02	4.1258E+02
11					3.1404E+04	6.2999E+02	0.
12					1.6009E+04	1.7678E+02	-4.1258E+02
13					3.1404E+04	6.2999E+02	0.
14					1.6009E+04	1.7678E+02	4.1258E+02
15					3.1404E+04	6.2999E+02	0.
16					1.6009E+04	1.7678E+02	-4.1258E+02
17					3.1404E+04	6.2999E+02	0.

X	LAYER	STRSL 1	STRST 1	STRSLT 1	STRSL 2	STRST 2	STRSLT 2
1		3.9163E+04	1.1942E+04	0.	2.6335E+04	5.2869E+02	0.
2		3.9062E+04	1.1916E+04	0.	1.3426E+04	1.4915E+03	-3.6572E+02
3		3.8961E+04	1.1890E+04	0.	2.6335E+04	5.2869E+02	0.
4		3.8859E+04	1.1864E+04	0.	1.3426E+04	1.4915E+03	3.6572E+02
5		3.8757E+04	1.1838E+04	0.	2.6335E+04	5.2869E+02	0.
6		3.8655E+04	1.1812E+04	0.	1.3426E+04	1.4915E+03	-3.6572E+02
7		3.8553E+04	1.1786E+04	0.	2.6335E+04	5.2869E+02	0.
8		3.8451E+04	1.1760E+04	0.	1.3426E+04	1.4915E+03	3.6572E+02
9		3.8349E+04	1.1734E+04	0.	2.6335E+04	5.2869E+02	0.
10					1.3426E+04	1.4915E+03	3.6572E+02
11					2.6335E+04	5.2869E+02	0.
12					1.3426E+04	1.4915E+03	-3.6572E+02
13					2.6335E+04	5.2869E+02	0.
14					1.3426E+04	1.4915E+03	3.6572E+02
15					2.6335E+04	5.2869E+02	0.
16					1.3426E+04	1.4915E+03	-3.6572E+02
17					2.6335E+04	5.2869E+02	0.

X	LAYER	STRSL 1	STRST 1	STRSLT 1	STRSL 2	STRST 2	STRSLT 2
1		4.3764E+04	1.3400E+04	0.	1.9448E+04	3.9080E+02	0.
2		4.3659E+04	1.3364E+04	0.	9.9171E+03	1.1097E+03	-2.8918E+02

X	LAYER	STASL 1	STAST 1	STRSLT 1	STRSL 2	STRST 2	STRSLT 2
3	4.3555E+04	1.3334E+04	0.	1.9448E+04	3.9080E+02	0.	0.
4	4.3450E+04	1.3304E+04	0.	4.9171E+03	1.1097E+03	2.8818E+02	0.
5	4.3455E+04	1.3272E+04	0.	1.9448E+04	3.9080E+02	0.	0.
6	4.3241E+04	1.3240E+04	0.	4.9171E+03	1.1097E+03	-2.8818E+02	0.
7	4.3146E+04	1.3208E+04	0.	1.9448E+04	3.9080E+02	0.	0.
8	4.3032E+04	1.3176E+04	0.	4.9171E+03	1.1097E+03	2.8818E+02	0.
9	4.2927E+04	1.3144E+04	0.	1.9448E+04	3.9080E+02	0.	0.
10				4.9171E+03	1.1097E+03	2.8818E+02	0.
11				1.9448E+04	3.9080E+02	0.	0.
12				4.9171E+03	1.1097E+03	-2.8818E+02	0.
13				1.9448E+04	3.9080E+02	0.	0.
14				4.9171E+03	1.1097E+03	2.8818E+02	0.
15				1.9448E+04	3.9080E+02	0.	0.
16				4.9171E+03	1.1097E+03	-2.8818E+02	0.
17				1.9448E+04	3.9080E+02	0.	0.

X	LAYER	STASL 1	STAST 1	STRSLT 1	STRSL 2	STRST 2	STRSLT 2
1	4.9522E+04	1.5164E+04	0.	1.0643E+04	2.1406E+02	0.	0.
2	4.9447E+04	1.5141E+04	0.	5.4274E+03	6.1187E+02	-1.6722E+02	0.
3	4.9372E+04	1.5118E+04	0.	1.0643E+04	2.1406E+02	0.	0.
4	4.9297E+04	1.5095E+04	0.	5.4274E+03	6.1187E+02	1.6722E+02	0.
5	4.9222E+04	1.5072E+04	0.	1.0643E+04	2.1406E+02	0.	0.
6	4.9147E+04	1.5049E+04	0.	5.4274E+03	6.1187E+02	-1.6722E+02	0.
7	4.9072E+04	1.5026E+04	0.	1.0643E+04	2.1406E+02	0.	0.
8	4.8997E+04	1.5003E+04	0.	5.4274E+03	6.1187E+02	1.6722E+02	0.
9	4.8922E+04	1.4980E+04	0.	1.0643E+04	2.1406E+02	0.	0.
10				5.4274E+03	6.1187E+02	1.6722E+02	0.
11				1.0643E+04	2.1406E+02	0.	0.
12				5.4274E+03	6.1187E+02	-1.6722E+02	0.
13				1.0643E+04	2.1406E+02	0.	0.
14				5.4274E+03	6.1187E+02	1.6722E+02	0.
15				1.0643E+04	2.1406E+02	0.	0.
16				5.4274E+03	6.1187E+02	-1.6722E+02	0.
17				1.0643E+04	2.1406E+02	0.	0.

X	LAYER	STASL 1	STAST 1	STRSLT 1	STRSL 2	STRST 2	STRSLT 2
1	5.6333E+04	1.7244E+04	0.	0.	0.	0.	0.
2	5.6333E+04	1.7244E+04	0.	0.	0.	0.	0.
3	5.6333E+04	1.7244E+04	0.	0.	0.	0.	0.
4	5.6333E+04	1.7244E+04	0.	0.	0.	0.	0.
5	5.6333E+04	1.7244E+04	0.	0.	0.	0.	0.
6	5.6333E+04	1.7244E+04	0.	0.	0.	0.	0.
7	5.6333E+04	1.7244E+04	0.	0.	0.	0.	0.
8	5.6333E+04	1.7244E+04	0.	0.	0.	0.	0.
9	5.6333E+04	1.7244E+04	0.	0.	0.	0.	0.
10							
11							
12							
13							
14							
15							
16							
17							

AOYPLINE49 ORTHOTROPIC ANALYSIS, STEP LAP JOINT

```

ERROR TOLERANCE = .025
MAXIMUM ITERATIONS = 20
NUMBER OF STATIONS = 31
EFFECTIVE K = .100

```

STEP	SEQUENTRY	R	R
		.0873	2.0080
		.0873	1.8720
		.0880	

ADHESIVE THICKNESS = .0058
POISSON'S RATIO = .40
RAYNBERG USGOND CONSTANTS (SHEAR STRESS-STRAIN CURVE)
G = 80600
SECANT S = 3740
N VALUE = 6.318

ADHESIVE: NO NUMBER 1 (ORTHOTROPIC)

THICKNESS	NUMBER OF LAYERS	RAMFORD OSGOOD CONSTANTS		
		SL VS. EL	28825000	.2620
		SL VS. ET	-136632000	+8
		ST VS. ET	2750000	E
		SLI VS. ELT	493000	
ORIENTATIONS		0 +S -+S	0 0 +S -+S	
		0 -+S +S	0 0 -+S	

ADHEREND NUMBER 2 (ISOTROPIC)

THICKNESS	.2640
POISSON'S RATIO	.3062
RAWMER'S GOOD CONSTANTS	E
S VS. E	16090000

```
STEP 1
ALPHA = 5.4221E+00
BETA = 5.8758E+00
LAMBDA = 3.9374E+00
N RESET TO 23
```

```
STEP 2
ALPHA = 5.9898E+00
BETA = 5.9347E+00
LAMBDA = 3.9519E+00
```

G-38

LOAD = 2340
 AT ITERATION 1 ERROR IS 6.02E-01
 AT ITERATION 2 ERROR IS 3.02E-01
 AT ITERATION 3 ERROR IS 1.92E-01
 AT ITERATION 4 ERROR IS 1.13E-01
 AT ITERATION 5 ERROR IS 7.34E-02
 AT ITERATION 6 ERROR IS 4.42E-02
 AT ITERATION 7 ERROR IS 2.89E-02
 AT ITERATION 8 ERROR IS 1.87E-02

33411

MAXIMUM ERROR = .01872

STEP NUMBER	X	Y	IAU	SIGMA	NXI	MX1	NX2	MX2	MX3
1	0.0000	5.0282E+03	2.7746E+04	1.1442E+10	-9.0949E+14	8.3940E+03	7.9378E+03	-3.1676E+01	1.0000
2	0.0001	4.8520E+03	1.4445E+02	4.5213E+02	-9.0993E+01	7.5078E+03	7.5078E+03	-3.1676E+01	1.0000
3	0.0002	4.5702E+03	3.4740E+02	8.8215E+02	-7.0043E+01	7.1069E+03	7.1069E+03	-1.1689E+00	1.0000
4	0.0003	4.1489E+03	-3.7089E+02	1.2831E+03	6.0000E+00	6.7442E+03	6.7442E+03	-1.1429E+00	1.0000
5	0.0004	3.7464E+03	-6.9223E+02	1.6458E+03	6.8813E+01	6.4267E+03	6.4267E+03	-9.8313E+00	1.0000
6	0.0005	3.1408E+03	-7.0194E+02	1.9633E+03	9.7387E+01	6.1658E+03	6.1658E+03	-6.4446E+00	1.0000
7	0.0006	2.5162E+03	-5.3475E+02	2.2247E+03	9.3247E+01	5.9679E+03	5.9679E+03	-4.4444E+00	1.0000
8	0.0007	1.8377E+03	-3.2774E+02	2.4221E+03	7.2659E+01	5.8257E+03	5.8257E+03	-2.4444E+00	1.0000
9	0.0008	1.2040E+03	-1.7846E+02	2.5647E+03	4.8743E+01	5.7247E+03	5.7247E+03	-1.2905E+00	1.0000
10	0.0009	6.4044E+02	-8.7784E+01	2.6659E+03	2.7534E+01	5.6503E+03	5.6503E+03	-4.4672E+01	1.0000
11	0.0010	4.0949E+02	-4.4444E+01	2.7474E+03	1.0944E+01	5.5944E+03	5.5944E+03	-4.4672E+01	1.0000
12	0.0011	5.4663E+02	-1.9325E+01	2.7459E+03	-1.3901E+02	5.5482E+03	5.5482E+03	1.3010E+01	1.0000
13	0.0012	4.4671E+02	-2.8471E+00	2.8444E+03	-1.0073E+02	5.5063E+03	5.5063E+03	6.7395E+01	1.0000
14	0.0013	4.5544E+02	1.2316E+01	2.8834E+03	-1.8393E+01	5.4633E+03	5.4633E+03	1.1124E+02	1.0000
15	0.0014	5.0116E+02	4.5144E+01	2.9426E+03	-2.4444E+01	5.4301E+03	5.4301E+03	1.1414E+02	1.0000
16	0.0015	8.0037E+02	8.2047E+01	3.0770E+03	-3.4470E+01	5.3940E+03	5.3940E+03	2.2140E+02	1.0000
17	0.0016	1.0977E+03	1.1635E+02	3.0410E+03	-3.5446E+01	5.2631E+03	5.2631E+03	4.0098E+02	1.0000
18	0.0017	1.0078E+03	1.3151E+02	3.1259E+03	-1.4747E+01	5.1444E+03	5.1444E+03	5.5712E+02	1.0000
19	0.0018	1.5244E+03	9.4152E+01	3.2445E+03	-4.4444E+01	4.9742E+03	4.9742E+03	7.5373E+02	1.0000
20	0.0019	2.1234E+03	-5.0045E+01	3.4104E+03	-5.4324E+01	4.7540E+03	4.7540E+03	9.1653E+02	1.0000
21	0.0020	2.8152E+03	-2.6349E+02	3.5380E+03	-1.2270E+02	4.4672E+03	4.4672E+03	1.2718E+03	1.0000
22	0.0021	3.4437E+03	-4.5412E+02	3.9222E+03	-2.2345E+02	4.1311E+03	4.1311E+03	1.5555E+03	1.0000
23	0.0022	3.9349E+03	-3.4925E+02	4.2584E+03	-3.7445E+02	4.1311E+03	4.1311E+03	1.5555E+03	1.0000
24	0.0023	3.9447E+03	-3.4413E+02	4.2584E+03	1.4744E+01	4.1311E+03	4.1311E+03	1.5555E+03	1.0000
25	0.0024	3.4447E+03	-2.4447E+02	4.5760E+03	1.1430E+01	3.8140E+03	3.8140E+03	1.4444E+02	1.0000
26	0.0025	2.4447E+03	-2.4447E+02	4.8500E+03	4.9521E+02	3.5030E+03	3.5030E+03	1.3966E+02	1.0000
27	0.0026	2.4447E+03	7.8472E+01	5.0742E+03	6.0712E+00	3.3158E+03	3.3158E+03	4.4747E+01	1.0000
28	0.0027	1.8004E+03	1.8004E+02	5.2444E+03	3.4934E+00	3.1034E+03	3.1034E+03	-2.4447E+02	1.0000
29	0.0028	1.5722E+03	1.5722E+02	5.3204E+03	2.4444E+00	3.0744E+03			

STEP NUMBER 1

X	LAYER	STRSL 1	STRST 1	STRSLT 1	STRSL 2	STRST 2	STRSLT 2
0.0000	1	0.	0.	0.	4.1822E+04	1.2806E+04	0.
	2	0.	0.	0.	4.4199E+04	1.3534E+04	0.
	3	0.	0.	0.	4.6576E+04	1.4261E+04	0.
	4	0.	0.	0.	4.8952E+04	1.4989E+04	0.
	5	0.	0.	0.	5.1329E+04	1.5717E+04	0.
	6	0.	0.	0.	5.3694E+04	1.6441E+04	0.
	7	0.	0.	0.			
	8	0.	0.	0.			
	9	0.	0.	0.			
	10	0.	0.	0.			
	11	0.	0.	0.			
	12	0.	0.	0.			
	13	0.	0.	0.			
	14	0.	0.	0.			
	15	0.	0.	0.			
	16	0.	0.	0.			

X	LAYER	STRSL 1	STRST 1	STRSLT 1	STRSL 2	STRST 2	STRSLT 2
0.0013	1	4.7808E+03	1.3642E+02	0.	4.0050E+04	1.2253E+04	0.
	2	3.5329E+03	3.4851E+02	-1.0930E+02	4.2105E+04	1.2493E+04	0.
	3	3.6076E+03	4.0687E+02	1.1150E+02	4.4151E+04	1.3222E+04	0.
	4	1.2199E+03	1.4524E+02	0.	4.6217E+04	1.4152E+04	0.
	5	7.3553E+03	1.4914E+02	0.	4.8273E+04	1.4781E+04	0.
	6	3.8315E+03	4.3149E+02	-1.1806E+02	5.0318E+04	1.5407E+04	0.
	7	3.4061E+03	4.4027E+02	1.2023E+02			
	8	7.8054E+03	1.5701E+02	0.			
	9	7.9517E+03	1.5495E+02	0.			
	10	4.1300E+03	4.6524E+02	1.2671E+02			
	11	4.2047E+03	4.7362E+02	-1.2885E+02			
	12	8.3400E+03	1.4874E+02	0.			
	13	8.5372E+03	1.7122E+02	0.			
	14	4.4265E+03	4.6460E+02	1.3524E+02			
	15	4.5032E+03	5.0642E+02	-1.3735E+02			
	16	8.9758E+03	1.8053E+02	0.			

X	LAYER	STRSL 1	STRST 1	STRSLT 1	STRSL 2	STRST 2	STRSLT 2
0.1425	1	1.4626E+04	2.4495E+02	0.	3.8566E+04	1.1809E+04	0.
	2	7.5104E+03	8.3849E+02	-2.1505E+02	4.0235E+04	1.2370E+04	0.
	3	7.5633E+03	8.4471E+02	2.1528E+02	4.1405E+04	1.2811E+04	0.
	4	1.4433E+04	3.0019E+02	0.	4.3574E+04	1.3342E+04	0.
	5	1.5040E+04	3.0227E+02	0.	4.5244E+04	1.3854E+04	0.
	6	7.7214E+03	8.5201E+02	-2.1989E+02	4.7405E+04	1.4362E+04	0.
	7	7.7247E+03	8.5724E+02	2.2110E+02			
	8	1.5352E+04	3.0451E+02	0.			
	9	1.5454E+04	3.1054E+02	0.			
	10	7.4333E+03	8.4507E+02	2.2449E+02			
	11	7.4961E+03	8.4903E+02	-2.2587E+02			
	12	1.5755E+04	3.1682E+02	0.			

X	LAYER	STRSL 1	STRSL 2	STRSLT 1	STRSLT 2	STRSL 2	STRSLT 2
.5475	9	3.4422E+04	6.8917E+02	0.	0.	3.4050E+04	1.0426E+04
	10	1.7466E+04	1.8426E+03	3.7604E+02	3.7604E+02	3.4468E+04	1.0554E+04
	11	1.7392E+04	1.8450E+03	-3.7524E+02	-3.7524E+02	3.4886E+04	1.0682E+04
	12	3.3998E+04	6.8054E+02	0.	0.	3.5304E+04	1.0810E+04
	13	3.3843E+04	6.7767E+02	0.	0.	3.5722E+04	1.0938E+04
	14	1.7171E+04	1.8623E+03	3.7282E+02	3.7282E+02	3.6139E+04	1.1065E+04
	15	1.7097E+04	1.8548E+03	-3.7201E+02	-3.7201E+02		
	16	3.3410E+04	6.6405E+02	0.	0.		
.6389	1	4.0170E+04	8.0312E+02	0.	0.	3.4050E+04	1.0426E+04
	2	2.0393E+04	2.1905E+03	-4.0453E+02	-4.0453E+02	3.4468E+04	1.0554E+04
	3	2.0323E+04	2.1834E+03	4.0390E+02	4.0390E+02	3.4886E+04	1.0682E+04
	4	3.9757E+04	7.4488E+02	0.	0.	3.5304E+04	1.0810E+04
	5	3.9614E+04	7.4213E+02	0.	0.	3.5722E+04	1.0938E+04
	6	2.0111E+04	2.1620E+03	-4.0201E+02	-4.0201E+02	3.6139E+04	1.1065E+04
	7	2.0040E+04	2.1548E+03	4.0138E+02	4.0138E+02		
	8	3.9148E+04	7.8389E+02	0.	0.		
	9	3.9059E+04	7.8113E+02	0.	0.		
	10	1.9628E+04	2.1134E+03	3.9946E+02	3.9946E+02		
	11	1.9758E+04	2.1242E+03	-3.9982E+02	-3.9982E+02		
	12	3.8643E+04	7.7288E+02	0.	0.		
	13	3.8504E+04	7.7013E+02	0.	0.		
	14	1.9546E+04	2.1048E+03	3.9686E+02	3.9686E+02		
	15	1.9475E+04	2.0976E+03	-3.9621E+02	-3.9621E+02		
	16	3.8088E+04	7.6184E+02	0.	0.		
.737	1	4.3459E+04	8.6817E+02	0.	0.	3.3311E+04	1.0200E+04
	2	2.2022E+04	2.3601E+03	-4.1846E+02	-4.1846E+02	3.3574E+04	1.0280E+04
	3	2.2027E+04	2.3546E+03	4.1803E+02	4.1803E+02	3.3836E+04	1.0361E+04
	4	4.3134E+04	8.6175E+02	0.	0.	3.4044E+04	1.0441E+04
	5	4.3024E+04	8.5461E+02	0.	0.	3.4361E+04	1.0521E+04
	6	2.1862E+04	2.3381E+03	-4.1672E+02	-4.1672E+02	3.4422E+04	1.0601E+04
	7	2.1807E+04	2.3326E+03	4.1629E+02	4.1629E+02		
	8	4.2702E+04	8.5420E+02	0.	0.		
	9	4.2593E+04	8.5106E+02	0.	0.		
	10	2.1642E+04	2.3160E+03	4.1497E+02	4.1497E+02		
	11	2.1587E+04	2.3105E+03	-4.1453E+02	-4.1453E+02		
	12	4.2264E+04	8.4444E+02	0.	0.		
	13	4.2168E+04	8.4250E+02	0.	0.		
	14	2.1421E+04	2.2940E+03	4.1314E+02	4.1314E+02		
	15	2.1366E+04	2.2884E+03	-4.1274E+02	-4.1274E+02		
	16	4.1833E+04	8.3409E+02	0.	0.		
.737	1	4.5721E+04	9.1282E+02	0.	0.	3.2766E+04	1.0033E+04
	2	2.3251E+04	2.4455E+03	-4.2720E+02	-4.2720E+02	3.2923E+04	1.0081E+04
	3	2.3214E+04	2.4421E+03	4.2693E+02	4.2693E+02	3.3080E+04	1.0124E+04
	4	4.5502E+04	9.0442E+02	0.	0.	3.3236E+04	1.0177E+04

X	LAYER	STRSL 1	STRSL 2	STRSLT 1	STRSLT 2	STRSL 1	STRSL 2	STRSLT 1	STRSLT 2
5		4.5431E+04	3.3393E+04	0.	0.	3.3393E+04	1.0225E+04	0.	0.
6		2.3107E+04	3.3549E+04	-4.2612E+02	0.	3.3549E+04	1.0273E+04	0.	0.
7		2.3066E+04		4.5820E+03	4.2585E+02				
8		4.5213E+04		9.0278E+02	0.				
9		4.5140E+04		9.0135E+02	0.				
10		2.2955E+04		2.4471E+03	4.2504E+02				
11		2.4182E+04		2.4435E+03	-4.2476E+02				
12		4.4422E+04		8.9704E+02	0.				
13		4.4444E+04		8.9561E+02	0.				
14		2.2407E+04		2.4324E+03	4.2395E+02				
15		2.2770E+04		2.4287E+03	-4.2368E+02				
16		4.4631E+04		8.9131E+02	0.				

X	LAYER	STRSL 1	STRSL 2	STRSLT 1	STRSLT 2	STRSL 1	STRSL 2	STRSLT 1	STRSLT 2
1		4.7293E+04	3.2370E+04	0.	0.	3.2370E+04	9.9117E+03	0.	0.
2		2.4054E+04	3.2454E+04	-4.3287E+02	0.	3.2454E+04	9.9373E+03	0.	0.
3		2.4045E+04	3.2537E+04	4.3275E+02	0.	3.2537E+04	9.9630E+03	0.	0.
4		4.7170E+04	3.2621E+04	0.	0.	3.2621E+04	9.9886E+03	0.	0.
5		4.7121E+04	3.2705E+04	4.4057E+02	0.	3.2705E+04	1.0014E+04	0.	0.
6		2.3483E+04	3.2788E+04	2.5491E+03	-4.3231E+02	3.2788E+04	1.0040E+04	0.	0.
7		2.3462E+04		2.5470E+03	4.3216E+02				
8		4.7004E+04		9.3415E+02	0.				
9		4.6465E+04		9.3734E+02	0.				
10		2.3844E+04		2.4408E+03	4.3173E+02				
11		2.3874E+04		2.5388E+03	-4.3159E+02				
12		4.6842E+04		9.3442E+02	0.				
13		4.6801E+04		9.3411E+02	0.				
14		2.3816E+04		2.5326E+03	4.3116E+02				
15		2.3795E+04		2.5305E+03	-4.3102E+02				
16		4.6678E+04		9.3169E+02	0.				

X	LAYER	STRSL 1	STRSL 2	STRSLT 1	STRSLT 2	STRSL 1	STRSL 2	STRSLT 1	STRSLT 2
1		4.8424E+04	3.2080E+04	0.	0.	3.2080E+04	9.8229E+03	0.	0.
2		2.4654E+04	3.2112E+04	-4.3674E+02	0.	3.2112E+04	9.8325E+03	0.	0.
3		2.4644E+04	3.2143E+04	4.3674E+02	0.	3.2143E+04	9.8422E+03	0.	0.
4		4.8375E+04	3.2174E+04	0.	0.	3.2174E+04	9.8518E+03	0.	0.
5		4.8358E+04	3.2206E+04	9.6478E+02	0.	3.2206E+04	9.8614E+03	0.	0.
6		2.4520E+04	3.2237E+04	2.6120E+03	-4.3657E+02	3.2237E+04	9.8710E+03	0.	0.
7		2.4512E+04		2.6112E+03	4.3651E+02				
8		4.8304E+04		9.6382E+02	0.				
9		4.8249E+04		9.6350E+02	0.				
10		2.4547E+04		2.6108E+03	4.3635E+02				
11		2.4529E+04		2.6107E+03	-4.3629E+02				
12		4.8244E+04		9.6254E+02	0.				
13		4.8228E+04		9.6221E+02	0.				
14		2.4554E+04		2.6055E+03	4.3612E+02				
15		2.4546E+04		2.6044E+03	-4.3607E+02				
16		4.8179E+04		9.6125E+02	0.				

X	LAYER	STRSL 1	STRST 1	STRSLT 1	STRSL 2	STRST 2	STRSLT 2
1.0040	1	4.9284E+04	9.8304E+02	0.	3.1860E+04	9.7555E+03	0.
	2	2.5101E+04	2.6593E+03	-4.3967E+02	3.1851E+04	9.7529E+03	0.
	3	2.5102E+04	2.6594E+03	4.3968E+02	3.1843E+04	9.7503E+03	0.
	4	4.9292E+04	9.8317E+02	0.	3.1835E+04	9.7477E+03	0.
	5	4.9292E+04	9.8321E+02	0.	3.1828E+04	9.7452E+03	0.
	6	2.5103E+04	2.6598E+03	-4.3969E+02	3.1818E+04	9.7426E+03	0.
	7	2.5102E+04	2.6597E+03	4.3969E+02			
	8	4.9301E+04	9.8334E+02	0.			
	9	4.9303E+04	9.8338E+02	0.			
	10	2.5110E+04	2.6602E+03	4.3971E+02			
	11	2.5111E+04	2.6603E+03	-4.3972E+02			
	12	4.9310E+04	9.8351E+02	0.			
	13	4.9312E+04	9.8355E+02	0.			
	14	2.5115E+04	2.6606E+03	4.3973E+02			
	15	2.5114E+04	2.6607E+03	-4.3974E+02			
	16	4.9314E+04	9.8358E+02	0.			

X	LAYER	STRSL 1	STRST 1	STRSLT 1	STRSL 2	STRST 2	STRSLT 2
1.0453	1	4.9998E+04	9.9705E+02	0.	3.1681E+04	9.7009E+03	0.
	2	2.5471E+04	2.6456E+03	-4.4147E+02	3.1640E+04	9.6881E+03	0.
	3	2.5474E+04	2.6444E+03	4.4202E+02	3.1598E+04	9.6754E+03	0.
	4	5.0047E+04	9.9800E+02	0.	3.1557E+04	9.6627E+03	0.
	5	5.0063E+04	9.9832E+02	0.	3.1515E+04	9.6500E+03	0.
	6	2.5503E+04	2.6488E+03	-4.4216E+02	3.1474E+04	9.6374E+03	0.
	7	2.5512E+04	2.6496E+03	4.4222E+02			
	8	5.0111E+04	9.9927E+02	0.			
	9	5.0127E+04	9.9949E+02	0.			
	10	2.5536E+04	2.7020E+03	4.4236E+02			
	11	2.5545E+04	2.7028E+03	-4.4241E+02			
	12	5.0176E+04	1.0005E+03	0.			
	13	5.0192E+04	1.0009E+03	0.			
	14	2.5569E+04	2.7052E+03	4.4256E+02			
	15	2.5572E+04	2.7060E+03	-4.4261E+02			
	16	5.0249E+04	1.0018E+03	0.			

X	LAYER	STRSL 1	STRST 1	STRSLT 1	STRSL 2	STRST 2	STRSLT 2
1.1465	1	5.0657E+04	1.0100E+03	0.	3.1520E+04	9.6515E+03	0.
	2	2.5812E+04	2.7290E+03	-4.4405E+02	3.1448E+04	9.6244E+03	0.
	3	2.5824E+04	2.7304E+03	4.4413E+02	3.1376E+04	9.6073E+03	0.
	4	5.0744E+04	1.0114E+03	0.	3.1304E+04	9.5852E+03	0.
	5	5.0758E+04	1.0122E+03	0.	3.1231E+04	9.5631E+03	0.
	6	2.5884E+04	2.7345E+03	-4.4437E+02	3.1160E+04	9.5411E+03	0.
	7	2.5882E+04	2.7358E+03	4.4446E+02			
	8	5.0850E+04	1.0138E+03	0.			
	9	5.0878E+04	1.0143E+03	0.			
	10	2.5924E+04	2.7400E+03	4.4470E+02			
	11	2.5938E+04	2.7413E+03	-4.4479E+02			
	12	5.0461E+04	1.0160E+03	0.			
	13	5.0484E+04	1.0165E+03	0.			
	14	2.5940E+04	2.7444E+03	4.4504E+02			
	15	2.5944E+04	2.7468E+03	-4.4511E+02			
	16	5.1071E+04	1.0181E+03	0.			

1.2729

LAYER	STRSL 1	STRSL 1	STRSLT 1	STRSL 2	STRSLT 2	STRSLT 2
1	5.1353E+04	1.0737E+03	0.	3.1356E+04	9.6012E+03	0.
2	2.6170E+04	2.7641E+03	-4.4617E+02	3.1251E+04	9.5691E+03	0.
3	2.6189E+04	2.7654E+03	4.4624E+02	3.1146E+04	9.5370E+03	0.
4	5.1456E+04	1.0254E+03	0.	3.1104E+04	9.5104E+03	0.
5	5.1503E+04	1.0266E+03	0.	3.0937E+04	9.4728E+03	0.
6	2.6214E+04	2.7715E+03	-4.4661E+02	3.0833E+04	9.4409E+03	0.
7	2.6265E+04	2.7733E+03	4.4672E+02			
8	5.1515E+04	1.0288E+03	0.			
9	5.1552E+04	1.0294E+03	0.			
10	2.6322E+04	2.7784E+03	4.4705E+02			
11	2.6341E+04	2.7808E+03	-4.4714E+02			
12	5.1764E+04	1.0318E+03	0.			
13	5.1828E+04	1.0325E+03	0.			
14	2.6348E+04	2.7853E+03	4.4748E+02			
15	2.6412E+04	2.7882E+03	-4.4754E+02			
16	5.1414E+04	1.0347E+03	0.			

1.3491

LAYER	STRSL 1	STRSL 1	STRSLT 1	STRSL 2	STRSLT 2	STRSLT 2
1	5.2187E+04	1.0401E+03	0.	3.1167E+04	9.5434E+03	0.
2	2.6548E+04	2.8058E+03	-4.4865E+02	3.1023E+04	9.4993E+03	0.
3	2.6622E+04	2.8081E+03	4.4878E+02	3.0879E+04	9.4552E+03	0.
4	5.2324E+04	1.0428E+03	0.	3.0735E+04	9.4111E+03	0.
5	5.2370E+04	1.0437E+03	0.	3.0591E+04	9.3670E+03	0.
6	2.6642E+04	2.8149E+03	-4.4916E+02	3.0448E+04	9.3232E+03	0.
7	2.6715E+04	2.8172E+03	4.4930E+02			
8	5.2508E+04	1.0444E+03	0.			
9	5.2554E+04	1.0473E+03	0.			
10	2.6785E+04	2.8240E+03	4.4969E+02			
11	2.6842E+04	2.8263E+03	-4.4982E+02			
12	5.2642E+04	1.0500E+03	0.			
13	5.2748E+04	1.0504E+03	0.			
14	2.6878E+04	2.8331E+03	4.5021E+02			
15	2.6902E+04	2.8354E+03	-4.5034E+02			
16	5.2876E+04	1.0536E+03	0.			

1.4504

LAYER	STRSL 1	STRSL 1	STRSLT 1	STRSL 2	STRSLT 2	STRSLT 2
1	5.3273E+04	1.0614E+03	0.	3.0932E+04	9.4713E+03	0.
2	2.7154E+04	2.8544E+03	-4.5175E+02	3.0736E+04	9.4415E+03	0.
3	2.7181E+04	2.8626E+03	4.5190E+02	3.0541E+04	9.3516E+03	0.
4	5.3433E+04	1.0645E+03	0.	3.0344E+04	9.2418E+03	0.
5	5.3484E+04	1.0655E+03	0.	3.0150E+04	9.2319E+03	0.
6	2.7262E+04	2.8704E+03	-4.5233E+02	2.9456E+04	9.1724E+03	0.
7	2.7290E+04	2.8730E+03	4.5247E+02			
8	5.3645E+04	1.0687E+03	0.			
9	5.3698E+04	1.0647E+03	0.			
10	2.7371E+04	2.8804E+03	4.5291E+02			
11	2.7342E+04	2.8835E+03	-4.5306E+02			
12	5.3854E+04	1.0722E+03	0.			
13	5.3911E+04	1.0739E+03	0.			
14	2.7474E+04	2.8414E+03	4.5344E+02			

15 2.7506E+04 -4.5364E+02
16 5.4070E+04 0.

X	LAYER	STRSL 1	STRST 1	STRSLT 1	STRSL 2	STRST 2	STRSLT 2
1.5516	1	5.4754E+04	1.0905E+03	0.	3.0619E+04	9.3754E+03	0.
	2	2.7913E+04	2.9334E+03	-4.5580E+02	3.0353E+04	9.2940E+03	0.
	3	2.7943E+04	2.9364E+03	-4.5595E+02	3.0087E+04	9.2125E+03	0.
	4	5.4437E+04	1.0440E+03	0.	2.9821E+04	9.1311E+03	0.
	5	5.4447E+04	1.0452E+03	0.	2.9555E+04	9.0496E+03	0.
	6	2.8034E+04	2.4451E+03	-4.5642E+02	2.9290E+04	8.9686E+03	0.
	7	2.8044E+04	2.4481E+03	-4.5657E+02			
	8	5.5175E+04	1.0447E+03	0.			
	9	5.5234E+04	1.0498E+03	0.			
	10	2.8155E+04	2.4554E+03	-4.5704E+02			
	11	2.8145E+04	2.4598E+03	-4.5714E+02			
	12	5.5414E+04	1.1033E+03	0.			
	13	5.5473E+04	1.1045E+03	0.			
	14	2.8276E+04	2.4685E+03	-4.5765E+02			
	15	2.8304E+04	2.4714E+03	-4.5781E+02			
	16	5.5552E+04	1.1090E+03	0.			

G-47

X	LAYER	STRSL 1	STRST 1	STRSLT 1	STRSL 2	STRST 2	STRSLT 2
1.5429	1	5.6778E+04	1.1300E+03	0.	3.0182E+04	9.2418E+03	0.
	2	2.8446E+04	3.0331E+03	-4.5099E+02	2.9821E+04	9.1311E+03	0.
	3	2.8492E+04	3.0366E+03	-4.6117E+02	2.9459E+04	9.0204E+03	0.
	4	5.6945E+04	1.1433E+03	0.	2.9097E+04	8.9097E+03	0.
	5	5.7064E+04	1.1457E+03	0.	2.8736E+04	8.7999E+03	0.
	6	2.4043E+04	3.0472E+03	-4.6170E+02	2.8376E+04	8.6484E+03	0.
	7	2.4130E+04	3.0508E+03	-4.6184E+02			
	8	5.7286E+04	1.1400E+03	0.			
	9	5.7358E+04	1.1414E+03	0.			
	10	2.9241E+04	3.0614E+03	-4.6240E+02			
	11	2.9274E+04	3.0650E+03	-4.6258E+02			
	12	5.7576E+04	1.1457E+03	0.			
	13	5.7649E+04	1.1471E+03	0.			
	14	2.9388E+04	3.0756E+03	-4.6310E+02			
	15	2.9425E+04	3.0791E+03	-4.6328E+02			
	16	5.7846E+04	1.1513E+03	0.			

X	LAYER	STRSL 1	STRST 1	STRSLT 1	STRSL 2	STRST 2	STRSLT 2
1.7342	1	5.9492E+04	1.1832E+03	0.	2.9559E+04	9.0510E+03	0.
	2	3.0343E+04	3.1670E+03	-4.6748E+02	2.9070E+04	8.9012E+03	0.
	3	3.0394E+04	3.1720E+03	-4.6771E+02	2.8541E+04	8.7515E+03	0.
	4	5.9808E+04	1.1843E+03	0.	2.8092E+04	8.6017E+03	0.
	5	5.9912E+04	1.1843E+03	0.	2.7603E+04	8.4514E+03	0.
	6	3.0555E+04	3.1871E+03	-4.6834E+02	2.7114E+04	8.3024E+03	0.
	7	3.0617E+04	3.1922E+03	-4.6863E+02			
	8	6.0224E+04	1.1474E+03	0.			
	9	6.0328E+04	1.1494E+03	0.			
	10	3.0755E+04	3.2073E+03	-4.6932E+02			

X	LAYER	STRSL 1	STRSLT 1	STRSL 2	STRSLT 2
11		3.0818E+04	-4.6954E+02		
12		6.0644E+04	0.		
13		6.0743E+04	0.		
14		3.0977E+04	4.7022E+02		
15		3.1037E+04	-4.7044E+02		
16		5.1055E+04	0.		

X	LAYER	STRSL 1	STRSLT 1	STRSL 2	STRSLT 2
1.8255	1	6.2920E+04	0.	2.8671E+04	8.7790E+03
	2	3.2123E+04	-4.7491E+02	2.8024E+04	8.5810E+03
	3	3.3361E+03	4.7527E+02	2.7378E+04	8.3830E+03
	4	3.3444E+03	0.	2.6731E+04	8.1850E+03
	5	6.3472E+04	0.	2.6084E+04	7.9870E+03
	6	6.3655E+04	-4.7634E+02	2.5441E+04	7.7901E+03
	7	3.2447E+04	4.7671E+02		
	8	3.2591E+04	0.		
	9	6.4207E+04	0.		
	10	6.4391E+04	4.7777E+02		
	11	3.2621E+04	-4.7812E+02		
	12	3.2464E+04	0.		
	13	6.4443E+04	0.		
	14	6.5127E+04	4.7415E+02		
	15	3.3245E+04	-4.7448E+02		
	16	3.3334E+04	0.		
	17	4.5674E+04			

X	LAYER	STRSL 1	STRSLT 1	STRSL 2	STRSLT 2
1.9167	1	6.6904E+04	0.	2.7488E+04	8.4167E+03
	2	3.4234E+04	-4.8261E+02	2.6652E+04	8.1540E+03
	3	3.4395E+04	4.8318E+02	2.5837E+04	7.9113E+03
	4	6.7410E+04	0.	2.5012E+04	7.6585E+03
	5	6.8245E+04	0.	2.4184E+04	7.4058E+03
	6	3.4436E+04	-4.8488E+02	2.3365E+04	7.1544E+03
	7	3.5074E+04	4.8544E+02		
	8	6.9251E+04	0.		
	9	6.9587E+04	0.		
	10	3.5587E+04	4.8706E+02		
	11	3.5752E+04	-4.8758E+02		
	12	7.0543E+04	0.		
	13	7.0428E+04	0.		
	14	3.6264E+04	4.8913E+02		
	15	3.6439E+04	-4.8964E+02		
	16	7.1933E+04	0.		

X	LAYER	STRSL 1	STRSLT 1	STRSL 2	STRSLT 2
2.0181	1	7.1175E+04	0.	2.6036E+04	7.4722E+03
	2	3.6513E+04	-4.8985E+02	2.5024E+04	7.6624E+03
	3	3.6802E+04	4.9064E+02	2.4013E+04	7.3527E+03
	4	7.2987E+04	0.	2.3001E+04	7.0430E+03
	5	7.3453E+04	0.	2.1440E+04	6.7333E+03
	6	3.7474E+04	-4.9312E+02	2.0443E+04	6.4251E+03

7	3.7459E+04	3.8792E+03	4.9384E+02
8	7.5142E+04	1.4872E+03	0.
9	7.5731E+04	1.4942E+03	0.
10	3.8226E+04	3.9585E+03	4.9612E+02
11	3.9115E+04	3.9848E+03	-4.9684E+02
12	7.7440E+04	1.5311E+03	0.
13	7.8009E+04	1.5420E+03	0.
14	3.9947E+04	4.0636E+03	4.9884E+02
15	4.0272E+04	4.0898E+03	-4.9955E+02
16	7.9714E+04	1.5748E+03	0.

X	LAYER	STRSL 1	STRST 1	STRSLT 1	STRSL 2	STRST 2	STRSLT 2
-1702	1	4.5249E+04	9.0352E+02	0.	3.9624E+04	1.2133E+04	0.
	2	2.2454E+04	2.4481E+03	-4.2526E+02	4.0034E+04	1.2258E+04	0.
	3	2.2890E+04	2.4348E+03	4.2465E+02	4.0444E+04	1.2384E+04	0.
	4	4.4756E+04	8.9379E+02	0.	4.0452E+04	1.2448E+04	0.
	5	4.4592E+04	8.9055E+02	0.			
	6	2.2629E+04	2.4148E+03	-4.2280E+02			
	7	2.2546E+04	2.4065E+03	4.2217E+02			
	8	4.4094E+04	8.8081E+02	0.			
	9	4.3934E+04	8.7757E+02	0.			
	10	2.2291E+04	2.3815E+03	4.2028E+02			
	11	2.2211E+04	2.3732E+03	-4.1964E+02			
	12	4.3441E+04	8.6783E+02	0.			
	13	4.3277E+04	8.6459E+02	0.			
	14	2.1941E+04	2.3481E+03	4.1771E+02			
	15	2.1872E+04	2.3397E+03	-4.1705E+02			
	16	4.2784E+04	8.5484E+02	0.			
	17	4.2614E+04	8.5110E+02	0.			
	18	2.1524E+04	2.3146E+03	-4.1508E+02			
	19	2.1543E+04	2.3063E+03	4.1441E+02			
	20	4.2126E+04	8.4185E+02	0.			
	21	4.1952E+04	8.3860E+02	0.			
	22	2.1292E+04	2.2811E+03	-4.1238E+02			
	23	2.1208E+04	2.2727E+03	4.1169E+02			
	24	4.1464E+04	8.2885E+02	0.			
	25	4.1304E+04	8.2560E+02	0.			
	26	2.0874E+04	2.2475E+03	4.0962E+02			
	27	2.0874E+04	2.2391E+03	-4.0892E+02			
	28	4.0811E+04	8.1585E+02	0.			
	29	4.0647E+04	8.1260E+02	0.			
	30	2.0623E+04	2.2138E+03	4.0674E+02			
	31	2.0539E+04	2.2154E+03	-4.0607E+02			
	32	4.0155E+04	8.0286E+02	0.			

X	LAYER	STRSL 1	STRST 1	STRSLT 1	STRSL 2	STRST 2	STRSLT 2
-2554	1	4.6478E+04	9.2776E+02	0.	3.7279E+04	1.1415E+04	0.
	2	2.3614E+04	2.5126E+03	-4.2988E+02	3.7500E+04	1.1495E+04	0.
	3	2.3555E+04	2.5058E+03	4.2946E+02	3.7736E+04	1.1555E+04	0.
	4	4.6172E+04	9.2044E+02	0.	3.7852E+04	1.1590E+04	0.

S	5	6	7	8	9	10	11	12	13	14	15	16	17	18	19	20	21	22	23	24	25	26	27	28	29	30	31	32
	4.6017E+04	2.3373E+04	2.3321E+04	4.5671E+04	4.5555E+04	2.3144E+04	2.3094E+04	4.5204E+04	4.5094E+04	2.2410E+04	2.2851E+04	4.4748E+04	4.4632E+04	2.2675E+04	2.2614E+04	4.4286E+04	4.4171E+04	2.2440E+04	2.2322E+04	4.3825E+04	4.3709E+04	2.2206E+04	2.2147E+04	4.3343E+04	4.3248E+04	2.1971E+04	2.1912E+04	4.2900E+04
	9.1866E+02	2.4394E+03	2.4335E+03	9.1184E+02	9.0954E+02	2.4561E+03	2.4502E+03	9.0273E+02	9.0044E+02	2.4427E+03	2.4369E+03	8.9363E+02	8.9135E+02	2.4194E+03	2.4135E+03	8.8452E+02	8.8224E+02	2.3460E+03	2.3401E+03	8.7541E+02	8.7313E+02	2.3726E+03	2.3667E+03	8.6624E+02	8.6401E+02	2.3491E+03	2.3432E+03	8.5719E+02
	0.	-4.2923E+02	4.2782E+02	0.	0.	4.2456E+02	4.2414E+02	0.	0.	4.2486E+02	4.2443E+02	0.	0.	4.2314E+02	4.2270E+02	0.	0.	4.2138E+02	4.2094E+02	0.	0.	4.1960E+02	4.1915E+02	0.	0.	4.1779E+02	4.1733E+02	0.

X	LAYER	STRSL 1	STRST 1	STRSLT 1	3TRSL 2	STRST 2	STRSLT 2
-3+04	1	4.7383E+04	9.4560E+02	0.	3.5436E+04	1.0850E+04	0.
	2	2.4094E+04	2.5601E+03	-4.3316E+02	3.5581E+04	1.0845E+04	0.
	3	2.4054E+04	2.5563E+03	4.3290E+02	3.5726E+04	1.0939E+04	0.
	4	4.7154E+04	9.4111E+02	0.	3.5800E+04	1.0962E+04	0.
	5	2.3940E+04	2.5444E+03	-4.3212E+02			
	6	2.3901E+04	2.5411E+03	4.3185E+02			
	7	2.3901E+04	2.5411E+03	0.			
	8	4.6852E+04	9.3513E+02	0.			
	9	4.6774E+04	9.3363E+02	0.			
	10	2.3784E+04	2.5246E+03	4.3106E+02			
	11	2.3747E+04	2.5258E+03	-4.3079E+02			
	12	4.6448E+04	9.2414E+02	0.			
	13	4.6473E+04	9.2765E+02	0.			
	14	2.3631E+04	2.5143E+03	4.2999E+02			
	15	2.3592E+04	2.5105E+03	-4.2972E+02			
	16	4.6245E+04	9.2316E+02	0.			
	17	4.6153E+04	9.2166E+02	0.			
	18	2.3477E+04	2.4490E+03	4.2892E+02			
	19	2.3438E+04	2.4492E+03	-4.2865E+02			
	20	4.5441E+04	9.1717E+02	0.			
	21	4.5865E+04	9.1548E+02	0.			
	22	2.3122E+04	2.4837E+03	-4.2782E+02			
	23	2.3284E+04	2.4749E+03	4.2755E+02			
	24	4.5434E+04	9.1118E+02	0.			
	25	4.5562E+04	9.0464E+02	0.			
	26	2.3164E+04	2.4644E+03	4.2673E+02			
	27	2.3124E+04	2.4646E+03	-4.2645E+02			
	28	4.5344E+04	9.0520E+02	0.			

X	LAYER	STRSL 1	STRST 1	STRSLT 1	STRSL 2	STRST 2	STRSLT 2
29		4.5259E+04	9.0370E+02	0.			
30		2.3113E+04	2.4530E+03	4.2561E+02			
31		2.2975E+04	2.4492E+03	-4.2533E+02			
32		4.5031E+04	8.4422E+02	0.			
255							
1		4.8044E+04	9.5860E+02	0.	3.4057E+04	1.0428E+04	0.
2		2.4445E+04	2.5948E+03	-4.3549E+02	3.4156E+04	1.0459E+04	0.
3		2.4422E+04	2.5925E+03	4.3534E+02	3.4236E+04	1.0484E+04	0.
4		4.7905E+04	9.5584E+02	0.	3.4307E+04	1.0505E+04	0.
5		4.7859E+04	9.5497E+02	0.			
6		2.4351E+04	2.5455E+03	-4.3488E+02			
7		2.4328E+04	2.5432E+03	4.3472E+02			
8		4.7721E+04	9.5224E+02	0.			
9		4.7675E+04	9.5134E+02	0.			
10		2.4258E+04	2.5763E+03	4.3425E+02			
11		2.4234E+04	2.5740E+03	-4.3410E+02			
12		4.7534E+04	9.4461E+02	0.			
13		4.7490E+04	9.4470E+02	0.			
14		2.4144E+04	2.5670E+03	4.3363E+02			
15		2.4140E+04	2.5647E+03	-4.3347E+02			
16		4.7352E+04	9.4494E+02	0.			
17		4.7306E+04	9.4407E+02	0.			
18		2.4070E+04	2.5577E+03	4.3294E+02			
19		2.4047E+04	2.5554E+03	4.3284E+02			
20		4.7162E+04	9.4134E+02	0.			
21		4.7121E+04	9.4043E+02	0.			
22		2.3976E+04	2.5485E+03	-4.3234E+02			
23		2.3953E+04	2.5462E+03	4.3227E+02			
24		4.6983E+04	9.4171E+02	0.			
25		4.6937E+04	9.3680E+02	0.			
26		2.3882E+04	2.5392E+03	4.3172E+02			
27		2.3859E+04	2.5369E+03	-4.3156E+02			
28		4.6748E+04	9.3407E+02	0.			
29		4.6725E+04	9.3315E+02	0.			
30		2.3744E+04	2.5244E+03	4.3108E+02			
31		2.3765E+04	2.5276E+03	-4.3091E+02			
32		4.6611E+04	9.3044E+02	0.			

X	LAYER	STRSL 1	STRST 1	STRSLT 1	STRSL 2	STRST 2	STRSLT 2
515							
1		4.8534E+04	9.6825E+02	0.	3.3027E+04	1.0113E+04	0.
2		2.4706E+04	2.6205E+03	-4.3719E+02	3.3045E+04	1.0134E+04	0.
3		2.4694E+04	2.6193E+03	4.3711E+02	3.3164E+04	1.0155E+04	0.
4		4.8463E+04	9.6685E+02	0.	3.3149E+04	1.0166E+04	0.
5		4.8439E+04	9.6638E+02	0.			
6		2.4652E+04	2.6157E+03	-4.3688E+02			
7		2.4644E+04	2.6145E+03	4.3680E+02			
8		4.8367E+04	9.6497E+02	0.			
9		4.8343E+04	9.6450E+02	0.			
10		2.4609E+04	2.6104E+03	4.3656E+02			
11		2.4592E+04	2.6092E+03	-4.3648E+02			
12		4.8272E+04	9.6310E+02	0.			
13		4.8249E+04	9.6243E+02	0.			
14		2.4551E+04	2.6062E+03	4.3625E+02			

X	LAYER	STRSL 1	STRSL 2	STRSLT 1	STRSLT 2	STRST 1	STRST 2	STRSLT 1	STRSLT 2
15		2.4549E+04		2.6050E+03		-4.3617E+02			
16		4.8172E+04		9.4122E+02		0.			
17		4.8153E+04		9.6075E+02		0.			
18		2.4512E+04		2.6014E+03		-4.3593E+02			
19		2.4510E+04		2.6002E+03		4.3585E+02			
20		4.8082E+04		9.5934E+02		0.			
21		4.8054E+04		9.5884E+02		0.			
22		2.4454E+04		2.5855E+03		-4.3561E+02			
23		2.4452E+04		2.5854E+03		4.3554E+02			
24		4.7985E+04		9.5747E+02		0.			
25		4.7962E+04		9.5700E+02		0.			
26		2.4415E+04		2.5914E+03		-4.3521E+02			
27		2.4403E+04		2.5905E+03		4.3522E+02			
28		4.7891E+04		9.5554E+02		0.			
29		4.7867E+04		9.5512E+02		0.			
30		2.4367E+04		2.5871E+03		-4.3498E+02			
31		2.4355E+04		2.5854E+03		4.3490E+02			
32		4.7796E+04		9.5372E+02		0.			

X	LAYER	STRSL 1	STRSL 2	STRSLT 1	STRSLT 2	STRST 1	STRST 2	STRSLT 1	STRSLT 2
-5956	1	4.8913E+04		9.7522E+02		0.			
	2	2.4407E+04		2.6403E+03		-4.3848E+02			
	3	2.4402E+04		2.6399E+03		4.3846E+02			
	4	4.8892E+04		9.7530E+02		0.			
	5	4.8852E+04		9.7516E+02		0.			
	6	2.4493E+04		2.6389E+03		-4.3834E+02			
	7	2.4489E+04		2.6385E+03		4.3837E+02			
	8	4.8663E+04		9.7774E+02		0.			
	9	4.8654E+04		9.7760E+02		0.			
	10	2.4474E+04		2.6374E+03		-4.3830E+02			
	11	2.4472E+04		2.6371E+03		4.3827E+02			
	12	4.8835E+04		9.7418E+02		0.			
	13	4.8828E+04		9.7404E+02		0.			
	14	2.4464E+04		2.6360E+03		-4.3820E+02			
	15	2.4460E+04		2.6356E+03		4.3818E+02			
	16	4.8806E+04		9.7362E+02		0.			
	17	4.8794E+04		9.7348E+02		0.			
	18	2.4444E+04		2.6346E+03		-4.3811E+02			
	19	2.4442E+04		2.6342E+03		4.3809E+02			
	20	4.8774E+04		9.7305E+02		0.			
	21	4.8771E+04		9.7291E+02		0.			
	22	2.4435E+04		2.6332E+03		-4.3802E+02			
	23	2.4431E+04		2.6328E+03		4.3800E+02			
	24	4.8750E+04		9.7249E+02		0.			
	25	4.8742E+04		9.7235E+02		0.			
	26	2.4420E+04		2.6317E+03		-4.3793E+02			
	27	2.4417E+04		2.6314E+03		4.3791E+02			
	28	4.8721E+04		9.7193E+02		0.			
	29	4.8714E+04		9.7174E+02		0.			
	30	2.4404E+04		2.6303E+03		-4.3783E+02			
	31	2.4402E+04		2.6300E+03		4.3781E+02			
	32	4.8694E+04		9.7137E+02		0.			

X	LAYER	STRSL 1	STRST 1	STRSLT 1	STRSL 2	STRST 2	STRSLT 2
25	9509	9.4907E+04	9.4527E+02	0.	0.	0.	0.
26		2.5425E+04	2.4311E+03	4.4172E+02	3.0605E+04	9.3714E+03	0.
27		2.5434E+04	2.4920E+03	-4.4179E+02	3.0521E+04	9.3455E+03	0.
28		4.9458E+04	9.4228E+02	0.	3.0437E+04	9.3197E+03	0.
29		4.9475E+04	9.4228E+02	0.	3.0394E+04	9.3064E+03	0.
30		2.5440E+04	2.4345E+03	4.4144E+02			
31		2.5458E+04	2.4345E+03	-4.4149E+02			
32		5.0024E+04	4.9741E+02	0.			
1		4.9769E+04	9.4544E+02	0.	3.0605E+04	9.3714E+03	0.
2		2.5360E+04	2.4647E+03	-4.4132E+02	3.0521E+04	9.3455E+03	0.
3		2.5374E+04	2.4647E+03	4.4141E+02	3.0437E+04	9.3197E+03	0.
4		4.9451E+04	9.4416E+02	0.	3.0394E+04	9.3064E+03	0.
5		4.9478E+04	9.4470E+02	0.			
6		2.5415E+04	2.4602E+03	-4.4167E+02			
7		2.5429E+04	2.4616E+03	4.4175E+02			
8		4.9461E+04	9.4432E+02	0.			
9		4.9488E+04	9.4484E+02	0.			
10		2.5471E+04	2.4657E+03	4.4201E+02			
11		2.5485E+04	2.4670E+03	-4.4210E+02			
12		5.0070E+04	9.4244E+02	0.			
13		5.0088E+04	9.4402E+02	0.			
14		2.5527E+04	2.7011E+03	4.4234E+02			
15		2.5541E+04	2.7025E+03	-4.4244E+02			
16		5.0180E+04	1.0004E+03	0.			
17		5.0208E+04	1.0012E+03	0.			
18		2.5523E+04	2.7066E+03	-4.4270E+02			
19		2.5547E+04	2.7080E+03	4.4274E+02			
20		5.0240E+04	1.0028E+03	0.			
21		5.0317E+04	1.0033E+03	0.			
22		2.5434E+04	2.7121E+03	-4.4304E+02			
23		2.5453E+04	2.7134E+03	4.4312E+02			
24		5.0400E+04	1.0050E+03	0.			
25		5.0427E+04	1.0055E+03	0.			
26		2.5494E+04	2.7176E+03	-4.4338E+02			
27		2.5708E+04	2.7184E+03	4.4346E+02			
28		5.0509E+04	1.0071E+03	0.			
29		5.0537E+04	1.0077E+03	0.			
30		2.5750E+04	2.7230E+03	-4.4372E+02			
31		2.5764E+04	2.7244E+03	4.4380E+02			
32		5.0614E+04	1.0043E+03	0.			

X	LAYER	STRSL 1	STRST 1	STRSLT 1	STRSL 2	STRST 2	STRSLT 2
1	9509	5.0063E+04	4.9833E+02	0.	3.0070E+04	9.2074E+03	0.
2		2.5515E+04	2.4949E+03	-4.4228E+02	2.4441E+04	9.1449E+03	0.
3		2.5534E+04	2.7019E+03	4.4240E+02	2.4742E+04	9.1224E+03	0.
4		5.0178E+04	1.0006E+03	0.	2.4722E+04	9.1008E+03	0.
5		5.0217E+04	1.0014E+03	0.			
6		2.5599E+04	2.7026E+03	-4.4274E+02			
7		2.5613E+04	2.7045E+03	4.4283E+02			
8		5.0332E+04	1.0036E+03	0.			
9		5.0421E+04	1.0044E+03	0.			
10		2.5614E+04	2.7143E+03	4.4324E+02			

X	LAYER	STRSL 1	STRSL 2	STRSLT 1	STRSLT 2	STRSLT 2
11	1	2.5691E+04	2.7172E+03	-4.4335E+02	-4.4335E+02	0.
12	2	5.0486E+04	1.0066E+03	0.	0.	0.
13	3	5.0524E+04	1.0074E+03	0.	0.	0.
14	4	2.5750E+04	2.7229E+03	4.4371E+02	4.4371E+02	0.
15	5	2.5749E+04	2.7249E+03	-4.4383E+02	-4.4383E+02	0.
16	6	5.0640E+04	1.0097E+03	0.	0.	0.
17	7	5.0678E+04	1.0104E+03	0.	0.	0.
18	8	2.5828E+04	2.7306E+03	-4.4418E+02	-4.4418E+02	0.
19	9	2.5847E+04	2.7325E+03	4.4430E+02	4.4430E+02	0.
20	10	5.0794E+04	1.0127E+03	0.	0.	0.
21	11	5.0832E+04	1.0135E+03	0.	0.	0.
22	12	2.5906E+04	2.7383E+03	-4.4465E+02	-4.4465E+02	0.
23	13	2.5926E+04	2.7402E+03	4.4477E+02	4.4477E+02	0.
24	14	5.0948E+04	1.0157E+03	0.	0.	0.
25	15	5.0986E+04	1.0165E+03	0.	0.	0.
26	16	2.5984E+04	2.7459E+03	4.4511E+02	4.4511E+02	0.
27	17	2.6004E+04	2.7478E+03	-4.4523E+02	-4.4523E+02	0.
28	18	5.1101E+04	1.0187E+03	0.	0.	0.
29	19	5.1140E+04	1.0195E+03	0.	0.	0.
30	20	2.6063E+04	2.7536E+03	4.4558E+02	4.4558E+02	0.
31	21	2.6082E+04	2.7555E+03	-4.4569E+02	-4.4569E+02	0.
32	22	5.1255E+04	1.0218E+03	0.	0.	0.
1021	1	5.0416E+04	1.0053E+03	0.	0.	0.
	2	2.5721E+04	2.7182E+03	-4.4342E+02	-4.4342E+02	0.
	3	2.5727E+04	2.7208E+03	4.4357E+02	4.4357E+02	0.
	4	5.0570E+04	1.0083E+03	0.	0.	0.
	5	5.0622E+04	1.0093E+03	0.	0.	0.
	6	2.5806E+04	2.7284E+03	-4.4405E+02	-4.4405E+02	0.
	7	2.5832E+04	2.7310E+03	4.4421E+02	4.4421E+02	0.
	8	5.0766E+04	1.0124E+03	0.	0.	0.
	9	5.0828E+04	1.0134E+03	0.	0.	0.
	10	2.5910E+04	2.7387E+03	4.4468E+02	4.4468E+02	0.
	11	2.5937E+04	2.7412E+03	-4.4484E+02	-4.4484E+02	0.
	12	5.0982E+04	1.0164E+03	0.	0.	0.
	13	5.1034E+04	1.0174E+03	0.	0.	0.
	14	2.6015E+04	2.7489E+03	4.4530E+02	4.4530E+02	0.
	15	2.6041E+04	2.7515E+03	-4.4546E+02	-4.4546E+02	0.
	16	5.1188E+04	1.0205E+03	0.	0.	0.
	17	5.1240E+04	1.0215E+03	0.	0.	0.
	18	2.6120E+04	2.7592E+03	-4.4592E+02	-4.4592E+02	0.
	19	2.6146E+04	2.7617E+03	4.4607E+02	4.4607E+02	0.
	20	5.1394E+04	1.0245E+03	0.	0.	0.
	21	5.1456E+04	1.0255E+03	0.	0.	0.
	22	2.6224E+04	2.7694E+03	-4.4653E+02	-4.4653E+02	0.
	23	2.6251E+04	2.7714E+03	4.4669E+02	4.4669E+02	0.
	24	5.1600E+04	1.0285E+03	0.	0.	0.
	25	5.1651E+04	1.0296E+03	0.	0.	0.
	26	2.6329E+04	2.7746E+03	4.4715E+02	4.4715E+02	0.
	27	2.6355E+04	2.7822E+03	-4.4730E+02	-4.4730E+02	0.
	28	5.1806E+04	1.0326E+03	0.	0.	0.
	29	5.1857E+04	1.0336E+03	0.	0.	0.
	30	2.6434E+04	2.7898E+03	4.4775E+02	4.4775E+02	0.
	31	2.6460E+04	2.7924E+03	-4.4791E+02	-4.4791E+02	0.
	32	5.2011E+04	1.0366E+03	0.	0.	0.

LAYER	STRSL 1	STRSL 1	STRSL 1	STRSL 2	STRSL 2	STRSLT 2
1	5.0445E+04	1.0141E+03	0.	2.8623E+04	8.7644E+03	0.
2	2.5949E+04	2.7714E+03	-4.4484E+02	2.8330E+04	8.4746E+03	0.
3	2.5422E+04	2.7449E+03	4.4505E+02	2.8137E+04	8.5848E+03	0.
4	5.0704E+04	1.0141E+03	0.	2.7888E+04	8.5393E+03	0.
5	5.1134E+04	1.0141E+03	0.			
6	2.6074E+04	2.7549E+03	-4.4565E+02			
7	2.5111E+04	2.7549E+03	4.4587E+02			
8	5.1342E+04	1.0235E+03	0.			
9	5.1410E+04	1.0244E+03	0.			
10	2.5215E+04	2.7649E+03	4.4648E+02			
11	2.6506E+04	2.7714E+03	-4.4669E+02			
12	5.1615E+04	1.0244E+03	0.			
13	5.1689E+04	1.0302E+03	0.			
14	2.6354E+04	2.7820E+03	4.4724E+02			
15	2.6388E+04	2.7854E+03	-4.4749E+02			
16	5.1804E+04	1.0342E+03	0.			
17	5.1455E+04	1.0355E+03	0.			
18	2.5442E+04	2.7455E+03	-4.4809E+02			
19	2.5727E+04	2.7494E+03	4.4824E+02			
20	5.2150E+04	1.0395E+03	0.			
21	5.2282E+04	1.0406E+03	0.			
22	2.6631E+04	2.8090E+03	-4.4888E+02			
23	2.6664E+04	2.8124E+03	4.4908E+02			
24	5.2332E+04	1.0449E+03	0.			
25	5.2503E+04	1.0442E+03	0.			
26	2.6770E+04	2.8225E+03	4.4975E+02			
27	2.6804E+04	2.8254E+03	-4.4986E+02			
28	5.2704E+04	1.0503E+03	0.			
29	5.2744E+04	1.0514E+03	0.			
30	2.6504E+04	2.8340E+03	4.5045E+02			
31	2.6443E+04	2.8344E+03	-4.5054E+02			
32	5.2472E+04	1.0554E+03	0.			

LAYER	STRSL 1	STRSL 1	STRSL 1	STRSL 2	STRSL 2	STRSLT 2
1	5.1456E+04	1.0252E+03	0.	2.7525E+04	8.4282E+03	0.
2	2.6200E+04	2.7714E+03	-4.4669E+02	2.7132E+04	8.3074E+03	0.
3	2.6294E+04	2.7649E+03	4.4696E+02	2.6739E+04	8.1875E+03	0.
4	5.1249E+04	1.0311E+03	0.	2.6540E+04	8.1265E+03	0.
5	5.1820E+04	1.0329E+03	0.			
6	2.6435E+04	2.7844E+03	-4.4776E+02			
7	2.6401E+04	2.7444E+03	4.4803E+02			
8	5.2093E+04	1.0382E+03	0.			
9	5.2184E+04	1.0400E+03	0.			
10	2.6420E+04	2.8080E+03	4.4842E+02			
11	2.6664E+04	2.8125E+03	-4.4904E+02			
12	5.2457E+04	1.0454E+03	0.			
13	5.2544E+04	1.0472E+03	0.			
14	2.6404E+04	2.8240E+03	4.4997E+02			
15	2.6516E+04	2.8305E+03	-4.5013E+02			
16	5.2621E+04	1.0523E+03	0.			
17	5.2412E+04	1.0533E+03	0.			
18	2.6444E+04	2.8440E+03	4.5041E+02			
19	2.6444E+04	2.8445E+03	-4.5112E+02			
20	5.3164E+04	1.0594E+03	0.			

X	LAYER	STRSL 1	STRSLT 1	STRSL 2	STRSLT 2	STRSLT 2
1.2744	1	5.3276E+04	1.0614E+03	0.	0.	0.
	2	2.7175E+04	2.4520E+03	-4.5193E+02	7.9603E+03	0.
	3	2.221E+04	2.8565E+03	4.5218E+02	7.8101E+03	0.
	4	5.3549E+04	1.0548E+03	0.	7.6600E+03	0.
	5	5.3644E+04	1.0586E+03	0.	7.5838E+03	0.
	6	2.7360E+04	2.8794E+03	4.5294E+02		
	7	2.7406E+04	2.8844E+03	-4.5319E+02		
	8	5.3913E+04	1.0734E+03	0.		
	9	5.4004E+04	1.0757E+03	0.		
	10	2.7545E+04	2.8979E+03	4.5394E+02		
	11	2.7591E+04	2.9024E+03	-4.5419E+02		
	12	5.4276E+04	1.0811E+03	0.		
	13	5.2236E+04	1.0410E+03	0.	2.5497E+04	
	14	2.6563E+04	2.8122E+03	-4.4907E+02	2.5507E+04	
	15	2.6726E+04	2.8183E+03	4.4943E+02	2.5016E+04	
	16	5.2404E+04	1.0493E+03	0.	2.4768E+04	
	17	5.2230E+04	1.0507E+03	0.		
	18	2.6414E+04	2.8356E+03	-4.5049E+02		
	19	2.6477E+04	2.8427E+03	4.5083E+02		
	20	5.3100E+04	1.0580E+03	0.		
	21	5.3223E+04	1.0604E+03	0.		
	22	2.7145E+04	2.8410E+03	4.5188E+02		
	23	2.7227E+04	2.8672E+03	-4.5222E+02		
	24	5.3593E+04	1.0677E+03	0.		
	25	5.3717E+04	1.0701E+03	0.		
	26	2.7416E+04	2.8693E+03	4.5325E+02		
	27	2.7478E+04	2.8714E+03	-4.5358E+02		
	28	5.4087E+04	1.0774E+03	0.		
	29	5.4210E+04	1.0798E+03	0.		
	30	2.7666E+04	2.9097E+03	-4.5459E+02		
	31	2.7724E+04	2.9157E+03	4.5493E+02		
	32	5.4540E+04	1.0870E+03	0.		
	33	5.4704E+04	1.0894E+03	0.		
	34	2.7917E+04	2.9334E+03	-4.5591E+02		
	35	2.7980E+04	2.9400E+03	4.5624E+02		
	36	5.5074E+04	1.0967E+03	0.		
	37	5.5147E+04	1.0991E+03	0.		
	38	2.8168E+04	2.9582E+03	4.5721E+02		
	39	2.8231E+04	2.9643E+03	-4.5754E+02		
	40	5.5457E+04	1.1064E+03	0.		
	41	5.5491E+04	1.1089E+03	0.		
	42	2.8414E+04	2.9824E+03	4.5850E+02		
	43	2.8492E+04	2.9885E+03	-4.5880E+02		
	44	5.6060E+04	1.1150E+03	0.		

X	LAYER	STRSL 1	STRSLT 1	STRSL 2	STRSLT 2	STRSLT 2
1.3315	1	5.3249E+04	1.0604E+03	0.	7.3077E+03	0.
	2	2.7201E+04	2.8045E+03	-4.5208E+02	7.1387E+03	0.
	3	2.7287E+04	2.8229E+03	4.5255E+02	6.9697E+03	0.
	4	5.3757E+04	1.0704E+03	0.	6.8841E+03	0.
	5	5.3427E+04	1.0742E+03	0.		
	6	2.7544E+04	2.8480E+03	-4.5344E+02		

	X	LAYER	STRSL 1	STRSL 2	STRSLT 1	STRSL 2	STRSLT 2	STRSLT 2
2			2.2632E+04	2.9063E+03	4.5441E+02			
3			5.4478E+04	1.0850E+03	0.	2.1023E+04	6.4371E+03	0.
4			2.7859E+04	2.4283E+03	-4.5559E+02	2.0506E+04	6.2788E+03	0.
5			2.7477E+04	2.9347E+03	-4.5521E+02	1.9989E+04	6.1205E+03	0.
6			5.5411E+04	1.0987E+03	0.	1.9727E+04	6.0403E+03	0.
7			2.6332E+04	1.1033E+03	0.			
8			2.4452E+04	2.9855E+03	-4.5804E+02			
9			5.6111E+04	1.1170E+03	4.5864E+02			
10			5.4345E+04	1.1216E+03	0.			
11			2.8426E+04	3.0198E+03	4.6041E+02			
12			4.7045E+04	3.0312E+03	-4.6100E+02			
13			5.7228E+04	1.1353E+03	0.			
14			2.9282E+04	1.1344E+03	0.			
15			2.9400E+04	3.0654E+03	4.6271E+02			
16			5.2978E+04	3.0748E+03	-4.6328E+02			
17			5.8211E+04	1.1535E+03	0.			
18			2.9755E+04	1.1581E+03	0.			
19			2.9877E+04	3.1104E+03	-4.6494E+02			
20			5.8411E+04	3.1223E+03	4.6549E+02			
21			5.9144E+04	1.1763E+03	0.			
22			3.0240E+04	3.1564E+03	-4.6710E+02			
23			3.0349E+04	3.1676E+03	4.6762E+02			
24			5.9844E+04	1.1400E+03	0.			
25			4.0078E+04	1.1446E+03	0.			
26			3.0204E+04	3.2015E+03	4.6919E+02			
27			3.0823E+04	3.2128E+03	-4.6970E+02			
28			4.1011E+04	1.2082E+03	0.			
29			3.1174E+04	3.2457E+03	4.7121E+02			
30								

X	LAYER	STRSL 1	STRST 1	STRSLT 1	STRSL 2	STRST 2	STRSLT 2
31		3.1297E+04	3.2579E+03	-4.7172E+02			
32		6.1709E+04	1.2264E+03	0.			
1.5315							
1		5.5863E+04	1.1121E+03	0.	1.7473E+04	5.3504E+03	0.
2		2.8604E+04	3.0002E+03	-4.5439E+02	1.7148E+04	5.2507E+03	0.
3		2.8764E+04	3.0156E+03	4.6018E+02	1.6822E+04	5.1509E+03	0.
4		5.6808E+04	1.1306E+03	0.	1.6657E+04	5.1004E+03	0.
5		5.7123E+04	1.1368E+03	0.			
6		2.9244E+04	3.0618E+03	-4.6251E+02			
7		2.9401E+04	3.0722E+03	4.6327E+02			
8		5.8068E+04	1.1553E+03	0.			
9		5.8383E+04	1.1615E+03	0.			
10		2.9485E+04	3.1232E+03	4.6551E+02			
11		3.0045E+04	3.1385E+03	-4.6624E+02			
12		5.4328E+04	1.1799E+03	0.			
13		5.9643E+04	1.1841E+03	0.			
14		3.0525E+04	3.1844E+03	4.6838E+02			
15		3.0685E+04	3.1947E+03	-4.6908E+02			
16		6.0588E+04	1.2045E+03	0.			
17		6.0903E+04	1.2107E+03	0.			
18		3.1165E+04	3.2454E+03	-4.7113E+02			
19		3.1325E+04	3.2606E+03	4.7180E+02			
20		6.1842E+04	1.2291E+03	0.			
21		6.2163E+04	1.2352E+03	0.			
22		3.1405E+04	3.3041E+03	-4.7377E+02			
23		3.1965E+04	3.3213E+03	4.7441E+02			
24		6.3104E+04	1.2536E+03	0.			
25		6.3424E+04	1.2598E+03	0.			
26		3.2446E+04	3.3446E+03	-4.7629E+02			
27		3.2606E+04	3.3617E+03	4.7690E+02			
28		6.4568E+04	1.2782E+03	0.			
29		6.4663E+04	1.2843E+03	0.			
30		3.3084E+04	3.4270E+03	-4.7871E+02			
31		3.3246E+04	3.4420E+03	4.7930E+02			
32		6.5626E+04	1.3024E+03	0.			

X	LAYER	STRSL 1	STRST 1	STRSLT 1	STRSL 2	STRST 2	STRSLT 2
1.5177							
1		5.7364E+04	1.1415E+03	0.	1.3335E+04	4.0833E+03	0.
2		2.9414E+04	3.0783E+03	-4.6331E+02	1.3343E+04	4.0856E+03	0.
3		2.9626E+04	3.0944E+03	4.6424E+02	1.3350E+04	4.0878E+03	0.
4		5.8600E+04	1.1557E+03	0.	1.3354E+04	4.0890E+03	0.
5		5.8612E+04	1.1737E+03	0.			
6		3.0254E+04	3.1545E+03	-4.6715E+02			
7		3.0443E+04	3.1785E+03	4.6808E+02			
8		6.0244E+04	1.1974E+03	0.			
9		6.0564E+04	1.2059E+03	0.			
10		3.1091E+04	3.2344E+03	-4.7079E+02			
11		3.1301E+04	3.2542E+03	4.7167E+02			
12		6.1896E+04	1.2400E+03	0.			
13		6.2302E+04	1.2441E+03	0.			
14		3.1929E+04	3.3178E+03	-4.7423E+02			
15		3.2138E+04	3.3376E+03	4.7505E+02			
16		6.3544E+04	1.2621E+03	0.			

3	3.1659E+04	3.2921E+03	4.7307E+02	5.1737E+03	1.5842E+03	0.
4	6.2811E+04	1.2787E+03	0.	5.4215E+03	1.6601E+03	0.
5	6.3434E+04	1.2500E+03	0.			
6	3.2609E+04	3.3814E+03	-4.7681E+02			
7	3.2424E+04	3.4117E+03	4.7800E+02			
8	6.5303E+04	1.2963E+03	0.			
9	6.5425E+04	1.3084E+03	0.			
10	3.3827E+04	3.5008E+03	4.8143E+02			
11	3.4190E+04	3.5304E+03	-4.8253E+02			
12	6.7794E+04	1.3747E+03	0.			
13	6.8416E+04	1.3548E+03	0.			
14	3.5139E+04	3.6184E+03	4.8567E+02			
15	3.5455E+04	3.6483E+03	-4.8668E+02			
16	7.0295E+04	1.3930E+03	0.			
17	7.0407E+04	1.4050E+03	0.			
18	3.6404E+04	3.7362E+03	-4.8952E+02			
19	3.6220E+04	3.7654E+03	4.9044E+02			
20	7.2776E+04	1.4412E+03	0.			
21	7.3398E+04	1.4532E+03	0.			
22	3.7664E+04	3.8526E+03	-4.9315E+02			
23	3.7485E+04	3.8316E+03	4.9400E+02			
24	7.5267E+04	1.4842E+03	0.			
25	7.5869E+04	1.5013E+03	0.			
26	3.8434E+04	3.9683E+03	4.9643E+02			
27	3.9250E+04	3.9471E+03	-4.9721E+02			
28	7.7758E+04	1.5372E+03	0.			
29	7.8380E+04	1.5492E+03	0.			
30	4.0198E+04	4.0832E+03	4.9944E+02			
31	4.0514E+04	4.1118E+03	-5.0014E+02			
32	8.0245E+04	1.5850E+03	0.			

X	LAYER	STRSL 1	STRSL 1	STRSL 2	STRSL 2	STRSLT 1	STRSLT 2
1.8720	1	6.3318E+04	1.2577E+03	0.	0.	0.	0.
	2	3.2599E+04	3.3304E+03	-4.7672E+02	0.	0.	0.
	3	3.2453E+04	3.4143E+03	4.7808E+02	0.	0.	0.
	4	6.5445E+04	1.2941E+03	0.	0.	0.	0.
	5	6.6154E+04	1.3124E+03	0.	0.	0.	0.
	6	3.4033E+04	3.5157E+03	-4.8196E+02	0.	0.	0.
	7	3.4394E+04	3.5494E+03	4.8319E+02	0.	0.	0.
	8	6.4281E+04	1.3541E+03	0.	0.	0.	0.
	9	6.4490E+04	1.3674E+03	0.	0.	0.	0.
	10	3.5474E+04	3.5500E+03	4.8670E+02	0.	0.	0.
	11	3.5834E+04	3.6834E+03	-4.8782E+02	0.	0.	0.
	12	7.1117E+04	1.4091E+03	0.	0.	0.	0.
	13	7.1824E+04	1.4228E+03	0.	0.	0.	0.
	14	3.6414E+04	3.7842E+03	4.9102E+02	0.	0.	0.
	15	3.7274E+04	3.8163E+03	-4.9203E+02	0.	0.	0.
	16	7.3951E+04	1.4634E+03	0.	0.	0.	0.
	17	7.4662E+04	1.4776E+03	0.	0.	0.	0.
	18	3.8354E+04	3.9154E+03	-4.9493E+02	0.	0.	0.
	19	3.8714E+04	3.9482E+03	4.9584E+02	0.	0.	0.
	20	7.5788E+04	1.5186E+03	0.	0.	0.	0.
	21	7.7497E+04	1.5322E+03	0.	0.	0.	0.
	22	3.9744E+04	4.0765E+03	-4.9844E+02	0.	0.	0.
	23	4.0154E+04	4.0741E+03	4.9923E+02	0.	0.	0.
	24	7.9621E+04	1.5731E+03	0.	0.	0.	0.
	25	8.0333E+04	1.5767E+03	0.	0.	0.	0.
	26	4.1244E+04	4.1766E+03	5.0166E+02	0.	0.	0.

27	4.1593E+04	4.2089E+02	-5.0241E+02
28	8.2460E+04	1.6275E+03	0.
29	8.3164E+04	1.6411E+03	0.
30	4.2673E+04	4.3057E+03	5.0455E+02
31	4.3032E+04	4.3378E+03	-5.0522E+02
32	8.5291E+04	1.6417E+03	0.

APPENDIX H

NONLINEAR FORMULA PREDICTIONS OF COMPLEX JOINT FAILURE LOADS/BEHAVIOR

APPENDIX H.1
FAILURE PREDICTION RESULTS
IN COMPLEX JOINTS

501 COMPLEX DOUBLE LAP JOINT TITANIUM TO BORON, LSHE ADHESIVE

NONLINEAR ORTHOTROPIC ANALYSIS, DOUBLE LAP JOINT

JOINT LENGTH = 1.4670
 ERROR TOLERANCE = .025
 MAXIMUM ITERATIONS = 20
 NUMBER OF STATIONS = 61
 EFFECTIVE K = .020

ADHESIVE
 THICKNESS = .0040
 POISSON'S RATIO = .40
 RAMBERG OSGOOD CONSTANTS (SHEAR STRESS-STRAIN CURVE)
 G = 40600
 SECANT S = 3740
 N VALUE = 6.318

ADHESIVE NUMBER 1 (ORTHOTROPIC)

THICKNESS .0850
 NUMBER OF LAYERS 16
 RAMBERG OSGOOD CONSTANTS
 SL VS. EL 28825000
 ST VS. EL -136632000
 SLT VS. ELT 2750000
 SECANT S 11910
 N 2.541
 SECANT S 7950
 N 2.991

ORIENTATIONS 0 45 -45 0 0 -45 45 0 0 -45 45 0

ADHESIVE NUMBER 2 (ISOTROPIC)

THICKNESS .0900
 POISSON'S RATIO .3062
 RAMBERG OSGOOD CONSTANTS
 S VS. E 16096000
 SECANT S 134000
 N 34.559

H-3

ULTIMATE LOAD PREDICTION BASED ON

ADHESIVE - MX STRESS, SU = 7.17E+03
 ADHESIVE 1 - MX STRAIN, SL = 6.08E-03, ST = 4.01E-03, SLT = 1.50E-02
 ADHESIVE 2 - MX STRESS, SL = 1.35E+05

ALPHA = 4.2813E+00
 BETA = 4.2813E+00
 LAMBDA = 6.1671E+00
 N RESET TO 19

```

ITERATION FOR ULTIMATE LOAD
LOAD = 1.00E-01
AT ITERATION 1 ERROR IS 1.10E-09
MAXIMUM STRESS(STRAIN)/ALLOWABLE = .001 IN ADHESIVE
LOAD = 818
AT ITERATION 1 ERROR IS 1.16E-01
AT ITERATION 2 ERROR IS 8.97E-03
MAXIMUM STRESS(STRAIN)/ALLOWABLE = .456 IN ADHESIVE
LOAD = 1246
AT ITERATION 1 ERROR IS 2.57E-01
AT ITERATION 2 ERROR IS 5.82E-02
AT ITERATION 3 ERROR IS 1.72E-02
MAXIMUM STRESS(STRAIN)/ALLOWABLE = .595 IN ADHESIVE
LOAD = 2017
AT ITERATION 1 ERROR IS 3.61E-01
AT ITERATION 2 ERROR IS 1.49E-01
AT ITERATION 3 ERROR IS 7.30E-02
AT ITERATION 4 ERROR IS 3.70E-02
AT ITERATION 5 ERROR IS 1.60E-02
MAXIMUM STRESS(STRAIN)/ALLOWABLE = .709 IN ADHESIVE
LOAD = 2922
AT ITERATION 1 ERROR IS 4.12E-01
AT ITERATION 2 ERROR IS 2.19E-01
AT ITERATION 3 ERROR IS 1.37E-01
AT ITERATION 4 ERROR IS 8.88E-02
AT ITERATION 5 ERROR IS 5.88E-02
AT ITERATION 6 ERROR IS 3.92E-02
AT ITERATION 7 ERROR IS 2.63E-02
AT ITERATION 8 ERROR IS 1.77E-02
MAXIMUM STRESS(STRAIN)/ALLOWABLE = .801 IN ADHESIVE
LOAD = 3406
AT ITERATION 1 ERROR IS 4.19E-01
AT ITERATION 2 ERROR IS 2.45E-01
AT ITERATION 3 ERROR IS 1.73E-01
AT ITERATION 4 ERROR IS 1.28E-01
AT ITERATION 5 ERROR IS 9.61E-02
AT ITERATION 6 ERROR IS 7.29E-02
AT ITERATION 7 ERROR IS 5.55E-02
AT ITERATION 8 ERROR IS 4.24E-02
AT ITERATION 9 ERROR IS 3.25E-02
AT ITERATION 10 ERROR IS 2.49E-02
MAXIMUM STRESS(STRAIN)/ALLOWABLE = .874 IN ADHESIVE
LOAD = 4557
AT ITERATION 1 ERROR IS 3.51E-01
AT ITERATION 2 ERROR IS 2.04E-01
AT ITERATION 3 ERROR IS 1.52E-01
AT ITERATION 4 ERROR IS 1.18E-01
AT ITERATION 5 ERROR IS 9.43E-02
AT ITERATION 6 ERROR IS 7.58E-02
AT ITERATION 7 ERROR IS 6.12E-02
AT ITERATION 8 ERROR IS 4.96E-02
AT ITERATION 9 ERROR IS 4.02E-02
AT ITERATION 10 ERROR IS 3.27E-02
AT ITERATION 11 ERROR IS 2.66E-02
AT ITERATION 12 ERROR IS 2.10E-02
MAXIMUM STRESS(STRAIN)/ALLOWABLE = .922 IN ADHESIVE
LOAD = 5555
AT ITERATION 1 ERROR IS 3.20E-01
AT ITERATION 2 ERROR IS 1.89E-01
AT ITERATION 3 ERROR IS 1.41E-01
AT ITERATION 4 ERROR IS 1.13E-01

```

AT ITERATION 5 ERROR IS 9.32E-02
 AT ITERATION 6 ERROR IS 7.75E-02
 AT ITERATION 7 ERROR IS 6.50E-02
 AT ITERATION 8 ERROR IS 5.46E-02
 AT ITERATION 9 ERROR IS 4.59E-02
 AT ITERATION 10 ERROR IS 3.87E-02
 AT ITERATION 11 ERROR IS 3.26E-02
 AT ITERATION 12 ERROR IS 2.75E-02
 AT ITERATION 13 ERROR IS 2.33E-02
 MAXIMUM STRESS(STRAIN)/ALLOWABLE = .960 IN ADHESIVE
 LOAD = 5727

AT ITERATION 1 ERROR IS 2.06E-01
 AT ITERATION 2 ERROR IS 1.17E-01
 AT ITERATION 3 ERROR IS 8.82E-02
 AT ITERATION 4 ERROR IS 7.17E-02
 AT ITERATION 5 ERROR IS 5.94E-02
 AT ITERATION 6 ERROR IS 5.07E-02
 AT ITERATION 7 ERROR IS 4.32E-02
 AT ITERATION 8 ERROR IS 3.64E-02
 AT ITERATION 9 ERROR IS 3.15E-02
 AT ITERATION 10 ERROR IS 2.71E-02
 AT ITERATION 11 ERROR IS 2.33E-02
 MAXIMUM STRESS(STRAIN)/ALLOWABLE = .978 IN ADHESIVE
 LOAD = 5959

AT ITERATION 1 ERROR IS 1.43E-01
 AT ITERATION 2 ERROR IS 8.24E-02
 AT ITERATION 3 ERROR IS 5.25E-02
 AT ITERATION 4 ERROR IS 5.10E-02
 AT ITERATION 5 ERROR IS 4.30E-02
 AT ITERATION 6 ERROR IS 3.67E-02
 AT ITERATION 7 ERROR IS 3.15E-02
 AT ITERATION 8 ERROR IS 2.73E-02
 AT ITERATION 9 ERROR IS 2.36E-02
 MAXIMUM STRESS(STRAIN)/ALLOWABLE = .989 IN ADHESIVE

NO CONVERGENCE AFTER TEN ITERATIONS - TERMINATED

THE PREDICTED ULTIMATE LOAD IS 6077

REF. NO. 100 P = 6077

NUMBER OF ITERATIONS = 9 , MAXIMUM ERROR = .02357

X	TAU	SIGMA	MX1	MX2	MX1	MX2	MX2
0.0000	6.5693E+03	1.0291E+03	1.1542E-10	1.9099E-13	1.9099E-13	1.1918E+04	0.
0.0125	6.3112E+03	9.2337E+02	5.2204E+02	-3.8053E-01	-3.8053E-01	1.0874E+04	0.
0.0250	6.0294E+03	7.7834E+02	1.0233E+03	-6.1671E-01	-6.1671E-01	9.8711E+03	0.
0.0375	5.7191E+03	5.9204E+02	1.5008E+03	-7.3254E-01	-7.3254E-01	8.9166E+03	0.
0.0500	5.3773E+03	3.8130E+02	1.9515E+03	-7.4790E-01	-7.4790E-01	8.0147E+03	0.
0.0625	4.9822E+03	1.5230E+02	2.3728E+03	-6.8744E-01	-6.8744E-01	7.1724E+03	0.
0.0750	4.5293E+03	-7.5601E+01	2.7598E+03	-5.7915E-01	-5.7915E-01	6.3482E+03	0.
0.0875	3.9668E+03	-2.2530E+02	3.1064E+03	-4.4598E-01	-4.4598E-01	5.7045E+03	0.
0.1000	3.3144E+03	-3.8745E+02	3.4046E+03	-3.0800E-01	-3.0800E-01	5.1085E+03	0.
0.1125	2.5365E+03	-3.5152E+02	3.6424E+03	-1.6804E-01	-1.6804E-01	4.6324E+03	0.
0.1250	1.9331E+03	-1.9781E+02	3.8223E+03	-2.4030E-02	-2.4030E-02	4.2732E+03	0.
0.1375	1.2222E+03	-2.1728E+01	3.9683E+03	1.2244E-01	1.2244E-01	3.9812E+03	0.
0.1500	1.9207E+03	9.4042E+01	4.1140E+03	5.5522E-01	5.5522E-01	3.6843E+03	0.
0.1625	2.5112E+03	9.6573E+01	4.2912E+03	3.9328E-01	3.9328E-01	3.3341E+03	0.
0.1750	3.2808E+03	-6.6522E+01	4.5278E+03	4.8190E-01	4.8190E-01	2.8522E+03	0.
0.1875	3.9353E+03	-3.2312E+02	4.8212E+03	5.1154E-01	5.1154E-01	2.2742E+03	0.
0.2000	4.4547E+03	-5.8046E+02	5.1676E+03	4.5673E-01	4.5673E-01	1.5865E+03	0.
0.2125	4.8663E+03	-7.8394E+02	5.5430E+03	2.9492E-01	2.9492E-01	8.3121E-02	0.
0.2250	5.2600E+03	-9.0840E+02	5.9582E+03	5.4570E-14	5.4570E-14	2.3283E-10	0.

APPENDIX II.2

BEHAVIOR PREDICTION FOR GIVEN LOADS
IN COMPLEX JOINTS

501 COMPLEX DOUBLE LAP JOINT TITANIUM TO BORON, LSHE ADHESIVE

NONLINEAR ORTHOTROPIC ANALYSIS, DOUBLE LAP JOINT

JOINT LENGTH = 1.4670
 ERROR TOLERANCE = .025
 MAXIMUM ITERATIONS = 20
 NUMBER OF STATIONS = 61
 EFFECTIVE K = .020

ADHESIVE
 THICKNESS = .0040
 POISSONS RATIO = .40
 RAMBERG OSGOOD CONSTANTS (SHEAR STRESS-STRAIN CURVE)
 G = 80600
 SECANT S = 3740
 N VALUE = 6.318

ADHEREND NUMBER 1 (ORTHOTROPIC)

THICKNESS .0850
 NUMBER OF LAYERS 16
 RAMBERG OSGOOD CONSTANTS
 SL VS. EL 28825000
 SL VS. ET -136632000
 ST VS. ET 2750000
 SLT VS. ELT 933000
 ORIENTATIONS 0 45 -45 0 0 -45 45 0

ADHEREND NUMBER 2 (ISOTROPIC)

THICKNESS .0900
 POISSONS RATIO .3062
 RAMBERG OSGOOD CONSTANTS
 S VS. E 16096000
 SECANT S 134000
 N 34.559

ALPHA = 4.2819E+00
 BETA = 4.2613E+00
 LAMBDA = 6.1671E+00
 N RESET TO 19

```

LOAD = 3200
AT ITERATION 1 ERROR IS 6.43E-01
AT ITERATION 2 ERROR IS 3.52E-01
AT ITERATION 3 ERROR IS 2.27E-01
AT ITERATION 4 ERROR IS 1.52E-01
AT ITERATION 5 ERROR IS 1.03E-01
AT ITERATION 6 ERROR IS 7.11E-02
AT ITERATION 7 ERROR IS 4.94E-02
AT ITERATION 8 ERROR IS 3.46E-02
AT ITERATION 9 ERROR IS 2.44E-02

```

0.0000 3200

ITERATIONS = 9 , MAXIMUM ERROR = .02437

X	TAU	SIGMA	NX1	NX1	NX1	NX2	NX2	MX2
0.0000	5.4550E+03	9.6791E+02	5.8208E-11	6.3665E-14	6.4000E+03	0.	0.	0.
0.0000	5.0799E+03	8.3612E+02	4.3029E+02	-3.0441E-01	5.5394E+03	0.	0.	0.
0.0000	4.6373E+03	6.1721E+02	8.2480E+02	-4.6820E-01	4.7504E+03	0.	0.	0.
0.0000	4.0929E+03	3.2049E+02	1.1810E+03	-5.1943E-01	4.0381E+03	0.	0.	0.
0.0000	3.3827E+03	-2.2252E+01	1.4862E+03	-4.8514E-01	3.4277E+03	0.	0.	0.
0.0000	2.0453E+03	-3.0928E+02	1.7244E+03	-3.9719E-01	2.9511E+03	0.	0.	0.
0.0000	1.5579E+03	-4.2933E+02	1.8855E+03	-2.8182E-01	2.6291E+03	0.	0.	0.
0.0000	9.7644E+02	-4.1449E+02	1.4866E+03	-1.7134E-01	2.4267E+03	0.	0.	0.
0.0000	6.3229E+02	-3.1857E+02	2.0510E+03	-8.3851E-02	2.2981E+03	0.	0.	0.
0.0000	4.4551E+02	-1.8455E+02	2.0940E+03	-1.9941E-02	2.2121E+03	0.	0.	0.
0.0000	3.6845E+02	-3.4940E+01	2.1265E+03	2.8143E-02	2.1464E+03	0.	0.	0.
0.0000	3.8405E+02	9.1242E+01	2.1566E+03	7.3030E-02	2.0868E+03	0.	0.	0.
0.0000	4.9451E+02	1.8422E+02	2.1417E+03	1.2536E-01	2.0166E+03	0.	0.	0.
0.0000	7.2757E+02	2.2912E+02	2.2405E+03	1.9032E-01	1.9177E+03	0.	0.	0.
0.0000	1.4140	1.8210E+02	2.3152E+03	2.6312E-01	1.7696E+03	0.	0.	0.
0.0000	1.8295E+03	1.5736E+01	2.4340E+03	3.2058E-01	1.5921E+03	0.	0.	0.
0.0000	2.7753E+03	-2.7484E+02	2.6204E+03	3.2205E-01	1.1593E+03	0.	0.	0.
0.0000	3.6049E+03	-5.7516E+02	2.8821E+03	2.2097E-01	6.3582E+02	0.	0.	0.
0.0000	4.2121E+03	-7.7046E+02	3.2000E+03	9.0944E-15	1.1642E-10	0.	0.	0.

X	LAYER	STRSL 1	STRST 1	STRSLT 1	STRSL 2	STRST 2	STRSLT 2
0.0000	1	0.	0.	0.	7.1111E+04	2.1774E+04	0.
	2	0.	0.	0.	7.1111E+04	2.1774E+04	0.
	3	0.	0.	0.	7.1111E+04	2.1774E+04	0.
	4	0.	0.	0.	7.1111E+04	2.1774E+04	0.
	5	0.	0.	0.	7.1111E+04	2.1774E+04	0.
	6	0.	0.	0.	7.1111E+04	2.1774E+04	0.
	7	0.	0.	0.	7.1111E+04	2.1774E+04	0.
	8	0.	0.	0.	7.1111E+04	2.1774E+04	0.
	9	0.	0.	0.	7.1111E+04	2.1774E+04	0.
	10	0.	0.	0.	7.1111E+04	2.1774E+04	0.
	11	0.	0.	0.	7.1111E+04	2.1774E+04	0.
	12	0.	0.	0.	7.1111E+04	2.1774E+04	0.
	13	0.	0.	0.	7.1111E+04	2.1774E+04	0.
	14	0.	0.	0.	7.1111E+04	2.1774E+04	0.
	15	0.	0.	0.	7.1111E+04	2.1774E+04	0.
	16	0.	0.	0.	7.1111E+04	2.1774E+04	0.

H-10

X	LAYER	STRSL 1	STRST 1	STRSLT 1	STRSL 2	STRST 2	STRSLT 2
0.0815	1	7.3462E+03	1.4778E+02	0.	6.1549E+04	1.8846E+04	0.
	2	3.7706E+03	4.2509E+02	-1.1624E+02	6.1549E+04	1.8846E+04	0.
	3	3.7946E+03	4.2772E+02	1.1649E+02	6.1549E+04	1.8846E+04	0.
	4	7.4872E+03	1.5062E+02	0.	6.1549E+04	1.8846E+04	0.
	5	7.5342E+03	1.5155E+02	0.	6.1549E+04	1.8846E+04	0.
	6	3.8664E+03	4.3501E+02	1.1903E+02	6.1549E+04	1.8846E+04	0.
	7	3.8904E+03	4.3844E+02	-1.1973E+02	6.1549E+04	1.8846E+04	0.
	8	7.5751E+03	1.5434E+02	0.	6.1549E+04	1.8846E+04	0.
	9	7.7221E+03	1.5534E+02	0.	6.1549E+04	1.8846E+04	0.
	10	3.4623E+03	4.4652E+02	-1.2181E+02	6.1549E+04	1.8846E+04	0.

X	LAYER	STRSL 1	STRST 1	STRSLT 1	STRSL 2	STRST 2	STRSLT 2
11		3.9862E+03	4.4920E+02	1.2251E+02			
12		7.8630E+03	1.5817E+02	0.			
13		7.9100E+03	1.5912E+02	0.			
14		4.0581E+03	4.5723E+02	1.2458E+02			
15		4.0820E+03	4.5990E+02	-1.2527E+02			
16		8.0510E+03	1.6195E+02	0.			

X	LAYER	STRSL 1	STRST 1	STRSLT 1	STRSL 2	STRST 2	STRSLT 2
1	1630	1.4242E+04	2.8625E+02	0.	5.2782E+04	1.6162E+04	0.
2		7.2989E+03	8.1568E+02	-2.0983E+02	5.2782E+04	1.6162E+04	0.
3		7.3359E+03	8.1973E+02	2.1070E+02	5.2782E+04	1.6162E+04	0.
4		1.4460E+04	2.9062E+02	0.	5.2782E+04	1.6162E+04	0.
5		1.4532E+04	2.9207E+02	0.	5.2782E+04	1.6162E+04	0.
6		7.4464E+03	8.3187E+02	2.1330E+02	5.2782E+04	1.6162E+04	0.
7		7.4839E+03	8.3592E+02	-2.1117E+02	5.2782E+04	1.6162E+04	0.
8		1.4750E+04	2.9644E+02	0.	5.2782E+04	1.6162E+04	0.
9		1.4823E+04	2.9790E+02	0.	5.2782E+04	1.6162E+04	0.
10		7.5450E+03	8.4805E+02	-2.1674E+02	5.2782E+04	1.6162E+04	0.
11		7.6320E+03	8.5204E+02	2.1759E+02			
12		1.5040E+04	3.0227E+02	0.			
13		1.5113E+04	3.0372E+02	0.			
14		7.7430E+03	8.6421E+02	2.2013E+02			
15		7.7800E+03	8.6825E+02	-2.2098E+02			
16		1.5331E+04	3.0809E+02	0.			

X	LAYER	STRSL 1	STRST 1	STRSLT 1	STRSL 2	STRST 2	STRSLT 2
1	2445	2.0611E+04	4.1384E+02	0.	4.4867E+04	1.3738E+04	0.
2		1.0549E+04	1.1675E+03	-2.7775E+02	4.4867E+04	1.3738E+04	0.
3		1.0590E+04	1.1719E+03	2.7850E+02	4.4867E+04	1.3738E+04	0.
4		2.0854E+04	4.1819E+02	0.	4.4867E+04	1.3738E+04	0.
5		2.0935E+04	4.2031E+02	0.	4.4867E+04	1.3738E+04	0.
6		1.0713E+04	1.1852E+03	2.8076E+02	4.4867E+04	1.3738E+04	0.
7		1.0755E+04	1.1896E+03	-2.8150E+02	4.4867E+04	1.3738E+04	0.
8		2.1178E+04	4.2516E+02	0.	4.4867E+04	1.3738E+04	0.
9		2.1259E+04	4.2678E+02	0.	4.4867E+04	1.3738E+04	0.
10		1.0878E+04	1.2028E+03	-2.8372E+02			
11		1.0920E+04	1.2072E+03	2.8445E+02			
12		2.1501E+04	4.3164E+02	0.			
13		2.1582E+04	4.3325E+02	0.			
14		1.1043E+04	1.2204E+03	2.8664E+02			
15		1.1084E+04	1.2248E+03	-2.8737E+02			
16		2.1825E+04	4.3811E+02	0.			

X	LAYER	STRSL 1	STRST 1	STRSLT 1	STRSL 2	STRST 2	STRSLT 2
1	3255	2.6182E+04	5.2513E+02	0.	3.8085E+04	1.1662E+04	0.
2		1.3383E+04	1.4684E+03	-3.2441E+02	3.8085E+04	1.1662E+04	0.
3		1.3422E+04	1.4725E+03	3.2498E+02	3.8085E+04	1.1662E+04	0.
4		2.6410E+04	5.2467E+02	0.	3.8085E+04	1.1662E+04	0.
5		2.6485E+04	5.2311E+02	0.	3.8085E+04	1.1662E+04	0.
6		1.3532E+04	1.4847E+03	3.2666E+02	3.8085E+04	1.1662E+04	0.

7	1.3576E+04	1.4897E+03	-3.2722E+02	3.8085E+04	1.1662E+04	0.
8	2.6713E+04	5.3571E+02	0.	3.8085E+04	1.1662E+04	0.
9	2.6789E+04	5.3722E+02	0.	3.8085E+04	1.1662E+04	0.
10	1.3692E+04	1.5009E+03	-3.2889E+02			
11	1.3731E+04	1.5049E+03	3.2944E+02			
12	2.7016E+04	5.4175E+02	0.			
13	2.7092E+04	5.4327E+02	0.			
14	1.3846E+04	1.5171E+03	3.3109E+02			
15	1.3885E+04	1.5211E+03	-3.3153E+02			
16	2.7319E+04	5.4780E+02	0.			

X	LAYER	STRSL 1	STRSL 2	STRSLT 1	STRSLT 2	STRSLT 2
.4075	1	3.0614E+04	6.1345E+02	0.	3.2790E+04	1.0040E+04
	2	1.5633E+04	1.7035E+03	-3.5484E+02	3.2790E+04	1.0040E+04
	3	1.5655E+04	1.7068E+03	3.5522E+02	3.2790E+04	1.0040E+04
	4	3.0801E+04	6.1717E+02	0.	3.2790E+04	1.0040E+04
	5	3.0863E+04	6.1840E+02	0.	3.2790E+04	1.0040E+04
	6	1.5759E+04	1.7166E+03	3.5639E+02	3.2790E+04	1.0040E+04
	7	1.5791E+04	1.7199E+03	-3.5678E+02	3.2790E+04	1.0040E+04
	8	3.1050E+04	6.2211E+02	0.	3.2790E+04	1.0040E+04
	9	3.1112E+04	6.2335E+02	0.	3.2790E+04	1.0040E+04
	10	1.5885E+04	1.7297E+03	-3.5793E+02	3.2790E+04	1.0040E+04
	11	1.5918E+04	1.7330E+03	3.5831E+02		
	12	3.1248E+04	6.2706E+02	0.		
	13	3.1361E+04	6.2830E+02	0.		
	14	1.6013E+04	1.7428E+03	3.5946E+02		
	15	1.6044E+04	1.7441E+03	-3.5984E+02		
	16	3.1547E+04	6.3201E+02	0.		

X	LAYER	STRSL 1	STRSL 2	STRSLT 1	STRSLT 2	STRSLT 2
.4890	1	3.3680E+04	6.7447E+02	0.	2.9212E+04	8.9447E+03
	2	1.7184E+04	1.8637E+03	-3.7302E+02	2.9212E+04	8.9447E+03
	3	1.7207E+04	1.8660E+03	3.7327E+02	2.9212E+04	8.9447E+03
	4	3.3813E+04	6.7706E+02	0.	2.9212E+04	8.9447E+03
	5	3.3857E+04	6.7794E+02	0.	2.9212E+04	8.9447E+03
	6	1.7224E+04	1.8730E+03	3.7401E+02	2.9212E+04	8.9447E+03
	7	1.7297E+04	1.8753E+03	-3.7426E+02	2.9212E+04	8.9447E+03
	8	3.3989E+04	6.8057E+02	0.	2.9212E+04	8.9447E+03
	9	3.4034E+04	6.8144E+02	0.	2.9212E+04	8.9447E+03
	10	1.7364E+04	1.8822E+03	-3.7499E+02		
	11	1.7386E+04	1.8845E+03	3.7524E+02		
	12	3.4166E+04	6.8408E+02	0.		
	13	3.4210E+04	6.8495E+02	0.		
	14	1.7454E+04	1.8914E+03	3.7596E+02		
	15	1.7476E+04	1.8937E+03	-3.7621E+02		
	16	3.4343E+04	6.8758E+02	0.		

X	LAYER	STRSL 1	STRSL 2	STRSLT 1	STRSLT 2	STRSLT 2
.5215	1	3.5653E+04	7.1361E+02	0.	2.6963E+04	8.2562E+03
	2	1.8179E+04	1.9655E+03	-3.8363E+02	2.6963E+04	8.2562E+03

X	LAYER	STRSL 1	STRST 1	STRSLT 1	STRSL 2	STRST 2	STRSLT 2
3	1.8193E+04	1.9671E+03	3.8378E+02	2.6963E+04	8.2562E+03	0.	
4	3.5734E+04	7.1520E+02	0.	2.6963E+04	8.2562E+03	0.	
5	3.5761E+04	7.1574E+02	0.	2.6963E+04	8.2562E+03	0.	
6	1.8234E+04	1.9713E+03	3.8419E+02	2.6963E+04	8.2562E+03	0.	
7	1.8248E+04	1.9727E+03	-3.8433E+02	2.6963E+04	8.2562E+03	0.	
8	3.5841E+04	7.1734E+02	0.	2.6963E+04	8.2562E+03	0.	
9	3.5868E+04	7.1787E+02	0.	2.6963E+04	8.2562E+03	0.	
10	1.8289E+04	1.9769E+03	-3.8475E+02	2.6963E+04	8.2562E+03	0.	
11	1.8302E+04	1.9783E+03	3.8489E+02	2.6963E+04	8.2562E+03	0.	
12	3.5949E+04	7.1947E+02	0.	2.6963E+04	8.2562E+03	0.	
13	3.5976E+04	7.2000E+02	0.	2.6963E+04	8.2562E+03	0.	
14	1.8343E+04	1.9825E+03	3.8531E+02	2.6963E+04	8.2562E+03	0.	
15	1.8357E+04	1.9839E+03	-3.8545E+02	2.6963E+04	8.2562E+03	0.	
16	3.6056E+04	7.2160E+02	0.	2.6963E+04	8.2562E+03	0.	

X	LAYER	STRSL 1	STRST 1	STRSLT 1	STRSL 2	STRST 2	STRSLT 2
1	3.6928E+04	7.3890E+02	0.	2.5534E+04	7.8186E+03	0.	
2	1.8821E+04	2.0312E+03	-3.9008E+02	2.5534E+04	7.8186E+03	0.	
3	1.8828E+04	2.0319E+03	3.9014E+02	2.5534E+04	7.8186E+03	0.	
4	3.6968E+04	7.3969E+02	0.	2.5534E+04	7.8186E+03	0.	
5	3.6981E+04	7.3995E+02	0.	2.5534E+04	7.8186E+03	0.	
6	1.8848E+04	2.0340E+03	3.9034E+02	2.5534E+04	7.8186E+03	0.	
7	1.8855E+04	2.0346E+03	-3.9041E+02	2.5534E+04	7.8186E+03	0.	
8	3.7020E+04	7.4073E+02	0.	2.5534E+04	7.8186E+03	0.	
9	3.7033E+04	7.4094E+02	0.	2.5534E+04	7.8186E+03	0.	
10	1.8875E+04	2.0367E+03	-3.9061E+02	2.5534E+04	7.8186E+03	0.	
11	1.8881E+04	2.0374E+03	3.9067E+02	2.5534E+04	7.8186E+03	0.	
12	3.7073E+04	7.4177E+02	0.	2.5534E+04	7.8186E+03	0.	
13	3.7086E+04	7.4203E+02	0.	2.5534E+04	7.8186E+03	0.	
14	1.8902E+04	2.0394E+03	3.9087E+02	2.5534E+04	7.8186E+03	0.	
15	1.8908E+04	2.0401E+03	-3.9093E+02	2.5534E+04	7.8186E+03	0.	
16	3.7125E+04	7.4291E+02	0.	2.5534E+04	7.8186E+03	0.	

X	LAYER	STRSL 1	STRST 1	STRSLT 1	STRSL 2	STRST 2	STRSLT 2
1	3.7789E+04	7.5594E+02	0.	2.4578E+04	7.5259E+03	0.	
2	1.9253E+04	2.0752E+03	-3.9425E+02	2.4578E+04	7.5259E+03	0.	
3	1.9255E+04	2.0754E+03	3.9427E+02	2.4578E+04	7.5259E+03	0.	
4	3.7797E+04	7.5613E+02	0.	2.4578E+04	7.5259E+03	0.	
5	3.7800E+04	7.5614E+02	0.	2.4578E+04	7.5259E+03	0.	
6	1.9260E+04	2.0758E+03	3.9431E+02	2.4578E+04	7.5259E+03	0.	
7	1.9261E+04	2.0760E+03	-3.9433E+02	2.4578E+04	7.5259E+03	0.	
8	3.7810E+04	7.5638E+02	0.	2.4578E+04	7.5259E+03	0.	
9	3.7813E+04	7.5644E+02	0.	2.4578E+04	7.5259E+03	0.	
10	1.9264E+04	2.0765E+03	-3.9438E+02	2.4578E+04	7.5259E+03	0.	
11	1.9268E+04	2.0767E+03	3.9439E+02	2.4578E+04	7.5259E+03	0.	
12	3.7822E+04	7.5663E+02	0.	2.4578E+04	7.5259E+03	0.	
13	3.7825E+04	7.5669E+02	0.	2.4578E+04	7.5259E+03	0.	
14	1.9273E+04	2.0771E+03	3.9444E+02	2.4578E+04	7.5259E+03	0.	
15	1.9274E+04	2.0771E+03	-3.9446E+02	2.4578E+04	7.5259E+03	0.	
16	3.7835E+04	7.5681E+02	0.	2.4578E+04	7.5259E+03	0.	

X	LAYER	STRSL 1	STRST 1	STRSLT 1	STRSL 2	STRST 2	STRSLT 2
.8150	1	3.8438E+04	7.6883E+02	0.	2.3855E+04	7.3043E+03	0.
	2	1.9591E+04	2.1084E+03	-3.9732E+02	2.3855E+04	7.3043E+03	0.
	3	1.9578E+04	2.1082E+03	3.9730E+02	2.3855E+04	7.3043E+03	0.
	4	3.8425E+04	7.6857E+02	0.	2.3855E+04	7.3043E+03	0.
	5	3.8420E+04	7.6848E+02	0.	2.3855E+04	7.3043E+03	0.
	6	1.9572E+04	2.1075E+03	3.9724E+02	2.3855E+04	7.3043E+03	0.
	7	1.9564E+04	2.1073E+03	-3.9722E+02	2.3855E+04	7.3043E+03	0.
	8	3.8407E+04	7.6822E+02	0.	2.3855E+04	7.3043E+03	0.
	9	3.8403E+04	7.6813E+02	0.	2.3855E+04	7.3043E+03	0.
	10	1.9563E+04	2.1046E+03	-3.9716E+02	2.3855E+04	7.3043E+03	0.
	11	1.9560E+04	2.1051E+03	3.9714E+02	2.3855E+04	7.3043E+03	0.
	12	3.8390E+04	7.6787E+02	0.	2.3855E+04	7.3043E+03	0.
	13	3.8385E+04	7.6778E+02	0.	2.3855E+04	7.3043E+03	0.
	14	1.9554E+04	2.1057E+03	3.9707E+02	2.3855E+04	7.3043E+03	0.
	15	1.9551E+04	2.1054E+03	-3.9705E+02	2.3855E+04	7.3043E+03	0.
	16	3.8372E+04	7.6752E+02	0.	2.3855E+04	7.3043E+03	0.

X	LAYER	STRSL 1	STRST 1	STRSLT 1	STRSL 2	STRST 2	STRSLT 2
.8265	1	3.9039E+04	7.8074E+02	0.	2.3187E+04	7.0998E+03	0.
	2	1.9883E+04	2.1390E+03	-4.0009E+02	2.3187E+04	7.0998E+03	0.
	3	1.9872E+04	2.1384E+03	4.0003E+02	2.3187E+04	7.0998E+03	0.
	4	3.9005E+04	7.8006E+02	0.	2.3187E+04	7.0998E+03	0.
	5	3.8993E+04	7.7983E+02	0.	2.3187E+04	7.0998E+03	0.
	6	1.9860E+04	2.1366E+03	3.9988E+02	2.3187E+04	7.0998E+03	0.
	7	1.9854E+04	2.1361E+03	-3.9983E+02	2.3187E+04	7.0998E+03	0.
	8	3.8959E+04	7.7915E+02	0.	2.3187E+04	7.0998E+03	0.
	9	3.8948E+04	7.7893E+02	0.	2.3187E+04	7.0998E+03	0.
	10	1.9836E+04	2.1333E+03	-3.9967E+02	2.3187E+04	7.0998E+03	0.
	11	1.9830E+04	2.1327E+03	3.9962E+02	2.3187E+04	7.0998E+03	0.
	12	3.8913E+04	7.7825E+02	0.	2.3187E+04	7.0998E+03	0.
	13	3.8902E+04	7.7802E+02	0.	2.3187E+04	7.0998E+03	0.
	14	1.9813E+04	2.1319E+03	3.9945E+02	2.3187E+04	7.0998E+03	0.
	15	1.9807E+04	2.1313E+03	-3.9941E+02	2.3187E+04	7.0998E+03	0.
	16	3.8867E+04	7.7734E+02	0.	2.3187E+04	7.0998E+03	0.

X	LAYER	STRSL 1	STRST 1	STRSLT 1	STRSL 2	STRST 2	STRSLT 2
.9280	1	3.9742E+04	7.9465E+02	0.	2.2407E+04	6.8609E+03	0.
	2	2.0236E+04	2.1747E+03	-4.0325E+02	2.2407E+04	6.8609E+03	0.
	3	2.0226E+04	2.1737E+03	4.0316E+02	2.2407E+04	6.8609E+03	0.
	4	3.9683E+04	7.9348E+02	0.	2.2407E+04	6.8609E+03	0.
	5	3.9663E+04	7.9310E+02	0.	2.2407E+04	6.8609E+03	0.
	6	2.0146E+04	2.1707E+03	4.0290E+02	2.2407E+04	6.8609E+03	0.
	7	2.0186E+04	2.1697E+03	-4.0281E+02	2.2407E+04	6.8609E+03	0.
	8	3.9604E+04	7.9193E+02	0.	2.2407E+04	6.8609E+03	0.
	9	3.9584E+04	7.9154E+02	0.	2.2407E+04	6.8609E+03	0.
	10	2.0156E+04	2.1666E+03	-4.0254E+02	2.2407E+04	6.8609E+03	0.
	11	2.0146E+04	2.1654E+03	4.0245E+02	2.2407E+04	6.8609E+03	0.
	12	3.9525E+04	7.9037E+02	0.	2.2407E+04	6.8609E+03	0.
	13	3.9506E+04	7.8994E+02	0.	2.2407E+04	6.8609E+03	0.
	14	2.0116E+04	2.1626E+03	4.0218E+02	2.2407E+04	6.8609E+03	0.
	15	2.0106E+04	2.1616E+03	-4.0210E+02	2.2407E+04	6.8609E+03	0.
	16	3.9447E+04	7.8841E+02	0.	2.2407E+04	6.8609E+03	0.

X	LAYER	STRSL 1	STRST 1	STRSLT 1	STRSL 2	STRST 2	STRSLT 2
1.0595	1	4.0709E+04	8.1379E+02	0.	2.1323E+04	6.5290E+03	0.
	2	2.0723E+04	2.2238E+03	-4.0747E+02	2.1323E+04	6.5290E+03	0.
	3	2.0708E+04	2.2238E+03	4.0734E+02	2.1323E+04	6.5290E+03	0.
	4	4.0619E+04	8.1201E+02	0.	2.1323E+04	6.5290E+03	0.
	5	4.0589E+04	8.1172E+02	0.	2.1323E+04	6.5290E+03	0.
	6	2.0662E+04	2.2177E+03	4.0695E+02	2.1323E+04	6.5290E+03	0.
	7	2.0647E+04	2.2161E+03	-4.0682E+02	2.1323E+04	6.5290E+03	0.
	8	4.0500E+04	8.0955E+02	0.	2.1323E+04	6.5290E+03	0.
	9	4.0470E+04	8.0905E+02	0.	2.1323E+04	6.5290E+03	0.
	10	2.0601E+04	2.2115E+03	-4.0643E+02			
	11	2.0585E+04	2.2100E+03	4.0630E+02			
	12	4.0380E+04	8.0722E+02	0.			
	13	4.0350E+04	8.0659E+02	0.			
	14	2.0540E+04	2.2054E+03	4.0590E+02			
	15	2.0525E+04	2.2039E+03	-4.0577E+02			
	16	4.0260E+04	8.0492E+02	0.			

X	LAYER	STRSL 1	STRST 1	STRSLT 1	STRSL 2	STRST 2	STRSLT 2
1.1410	1	4.2159E+04	8.4248E+02	0.	1.9662E+04	6.0204E+03	0.
	2	1.1555E+04	2.2947E+03	-4.1354E+02	1.9662E+04	6.0204E+03	0.
	3	2.1434E+04	2.4953E+03	4.1337E+02	1.9662E+04	6.0204E+03	0.
	4	4.2035E+04	8.4003E+02	0.	1.9662E+04	6.0204E+03	0.
	5	4.1944E+04	8.3921E+02	0.	1.9662E+04	6.0204E+03	0.
	6	2.1371E+04	2.2884E+03	4.1286E+02	1.9662E+04	6.0204E+03	0.
	7	2.1350E+04	2.2868E+03	-4.1269E+02	1.9662E+04	6.0204E+03	0.
	8	4.1870E+04	8.3675E+02	0.	1.9662E+04	6.0204E+03	0.
	9	4.1809E+04	8.3594E+02	0.	1.9662E+04	6.0204E+03	0.
	10	2.1287E+04	2.2835E+03	-4.1217E+02			
	11	2.1266E+04	2.2794E+03	4.1200E+02			
	12	4.1705E+04	8.3349E+02	0.			
	13	4.1663E+04	8.3267E+02	0.			
	14	2.1203E+04	2.2721E+03	4.1149E+02			
	15	2.1182E+04	2.2699E+03	-4.1131E+02			
	16	4.1539E+04	8.3022E+02	0.			

X	LAYER	STRSL 1	STRST 1	STRSLT 1	STRSL 2	STRST 2	STRSLT 2
1.2425	1	4.4397E+04	8.8657E+02	0.	1.7023E+04	5.2124E+03	0.
	2	2.2899E+04	2.4107E+03	-4.2236E+02	1.7023E+04	5.2124E+03	0.
	3	2.2836E+04	2.4081E+03	4.2217E+02	1.7023E+04	5.2124E+03	0.
	4	4.4246E+04	8.8369E+02	0.	1.7023E+04	5.2124E+03	0.
	5	4.4196E+04	8.8269E+02	0.	1.7023E+04	5.2124E+03	0.
	6	2.2496E+04	2.4005E+03	4.2159E+02	1.7023E+04	5.2124E+03	0.
	7	2.2450E+04	2.3979E+03	-4.2140E+02	1.7023E+04	5.2124E+03	0.
	8	4.4044E+04	8.7971E+02	0.	1.7023E+04	5.2124E+03	0.
	9	4.3945E+04	8.7872E+02	0.	1.7023E+04	5.2124E+03	0.
	10	2.2383E+04	2.3402E+03	-4.2082E+02			
	11	2.2359E+04	2.3377E+03	4.2062E+02			
	12	4.3843E+04	8.7523E+02	0.			

X	LAYER	STRSL 1	STRST 1	STRSLT 1	STRSL 2	STRST 2	STRSLT 2
13	4.3792E+04	8.7474E+02	0.	0.			
14	2.2281E+04	2.390CE+03	4.2004E+02	4.3981E+04			
15	2.2255E+04	2.3775E+02	-4.1484E+02	-4.1484E+02			
16	4.3541E+04	8.7175E+02	0.	0.			
1	4.7807E+04	9.539CE+02	0.	0.	1.2881E+04	3.9442E+03	0.
2	4.7233E+04	2.5826E+03	-4.3458E+02	-4.3458E+02	1.2881E+04	3.9442E+03	0.
3	2.4297E+04	2.5801E+03	4.341E+02	4.341E+02	1.2881E+04	3.9442E+03	0.
4	4.7265E+04	9.501E+02	0.	0.	1.2881E+04	3.9442E+03	0.
5	4.7605CE+04	9.4961E+02	0.	0.	1.2881E+04	3.9442E+03	0.
6	2.4220E+04	2.5725E+03	4.3384E+02	4.3384E+02	1.2881E+04	3.9442E+03	0.
7	2.4161E+04	2.5696CE+03	-4.3372E+02	-4.3372E+02	1.2881E+04	3.9442E+03	0.
8	4.7453E+04	9.4492E+02	0.	0.	1.2881E+04	3.9442E+03	0.
9	4.7402E+04	9.4562E+02	0.	0.	1.2881E+04	3.9442E+03	0.
10	2.4177E+04	2.5623E+03	-4.3320E+02	-4.3320E+02	1.2881E+04	3.9442E+03	0.
11	2.4091E+04	2.5597E+03	4.330CE+02	4.330CE+02	1.2881E+04	3.9442E+03	0.
12	4.72305E+04	9.4726E+02	0.	0.	1.2881E+04	3.9442E+03	0.
13	4.7169E+04	9.4616E+02	0.	0.	1.2881E+04	3.9442E+03	0.
14	2.4130E+04	2.5521E+03	4.3251E+02	4.3251E+02	1.2881E+04	3.9442E+03	0.
15	2.4082E+04	2.5495E+03	-4.3233E+02	-4.3233E+02	1.2881E+04	3.9442E+03	0.
16	4.7270E+04	9.4393E+02	0.	0.	1.2881E+04	3.9442E+03	0.

X	LAYER	STRSL 1	STRST 1	STRSLT 1	STRSL 2	STRST 2	STRSLT 2
1.255	1	5.2479E+04	1.0457E+03	0.	7.0646E+03	2.1632E+03	0.
	2	2.6705E+04	2.8163E+03	-4.4318E+02	7.0646E+03	2.1632E+03	0.
	3	2.6688E+04	2.8145E+03	4.4980E+02	7.0646E+03	2.1632E+03	0.
	4	5.2375E+04	1.0437E+03	0.	7.0646E+03	2.1632E+03	0.
	5	5.2340E+04	1.0430E+03	0.	7.0646E+03	2.1632E+03	0.
	6	2.6635E+04	2.8094E+03	4.4878E+02	7.0646E+03	2.1632E+03	0.
	7	2.6618E+04	2.8077E+03	-4.4888E+02	7.0646E+03	2.1632E+03	0.
	8	5.2236E+04	1.0410E+03	0.	7.0646E+03	2.1632E+03	0.
	9	5.2201E+04	1.0403E+03	0.	7.0646E+03	2.1632E+03	0.
	10	2.6565E+04	2.8025E+03	-4.4833E+02	7.0646E+03	2.1632E+03	0.
	11	2.6547E+04	2.8008E+03	4.4827E+02	7.0646E+03	2.1632E+03	0.
	12	5.2097E+04	1.0382E+03	0.	7.0646E+03	2.1632E+03	0.
	13	5.2062E+04	1.0375E+03	0.	7.0646E+03	2.1632E+03	0.
	14	2.6494E+04	2.7956E+03	4.4797E+02	7.0646E+03	2.1632E+03	0.
	15	2.6476E+04	2.7939E+03	-4.4787E+02	7.0646E+03	2.1632E+03	0.
	16	5.14957E+04	1.0355E+03	0.	7.0646E+03	2.1632E+03	0.

X	LAYER	STRSL 1	STRST 1	STRSLT 1	STRSL 2	STRST 2	STRSLT 2
1.	1	5.8044E+04	1.1547E+03	0.	0.	0.	0.
	2	2.9553E+04	3.0913E+03	-4.6382E+02	0.	0.	0.
	3	2.9553E+04	3.0913E+03	4.6382E+02	0.	0.	0.
	4	5.8044E+04	1.1547E+03	0.	0.	0.	0.
	5	5.8044E+04	1.1547E+03	0.	0.	0.	0.
	6	2.9553E+04	3.0913E+03	4.6382E+02	0.	0.	0.
	7	2.9553E+04	3.0913E+03	-4.6382E+02	0.	0.	0.
	8	5.8044E+04	1.1547E+03	0.	0.	0.	0.

9	5.8044E+04	1.1547E+03	0.	0.	0.
10	2.9553E+04	3.0913E+03	-4.6381E+02	0.	
11	4.03E+04	3.0913E+03	4.6381E+02	0.	
12	2.9553E+04	1.1547E+03	0.	0.	
13	5.8044E+04	1.1547E+03	0.	0.	
14	2.9553E+04	3.0913E+03	4.6382E+02	0.	
15	2.9553E+04	3.0913E+03	20+3288E9	0.	
16	5.8044E+04	1.1547E+03	-4.6382E+02	0.	

Unclassified
Security Classification

DOCUMENT CONTROL DATA - R & D		
<i>Security classification of title, body of abstract and indexing annotation must be entered when the overall report is classified</i>		
1. ORIGINATING ACTIVITY (Corporate author)		2a. REPORT SECURITY CLASSIFICATION
Southwest Research Institute		Unclassified
		2b. GROUP
		N/A
3. REPORT TITLE		
The Development of Nonlinear Analysis Methods for Bonded Joints in Advanced Filamentary Composite Structures		
4. DESCRIPTIVE NOTES (Type of report and inclusive dates)		
Final Technical Report (14 April 1969 to 30 Oct. 1971)		
5. AUTHOR(S) (First name, middle initial, last name)		
G.C. Grimes, L.F. Greimann, T. Wah, G.E. Commerford, W.R. Blackstone, G.K. Wolfe		
6. REPORT DATE	7a. TOTAL NO. OF PAGES	7b. NO. OF REFS
September 1972	182 plus 15 prelims & 173 app	21
8a. CONTRACT OR GRANT NO.	9a. ORIGINATOR'S REPORT NUMBER(S)	
F-33615-69-C-1641	AFFDL-TR-72-97	
b. PROJECT NO.	9b. OTHER REPORT NO(S) (Any other numbers that may be assigned this report)	
4364		
c. Task No.		
436403		
d.		
10. DISTRIBUTION STATEMENT		
Distribution limited to U.S. Government agencies only; test and evaluation; statement applied March 72. Other requests for this document must be referred to AF Flight Dynamics Laboratory, (FBC), Wright-Patterson AFB, Ohio 45433.		
11. SUPPLEMENTARY NOTES		12. SPONSORING MILITARY ACTIVITY
		Air Force Flight Dynamics Laboratory (FBC) WPAFB, Ohio 45433
13. ABSTRACT		
<p>Development of analysis methods for orthotropic adherend bonded lap joints which account for material nonlinearities at room temperature was the primary objective of the research reported herein. The use of these methods in predicting mechanical behavior, ultimate loads, and failure modes was the goal. In order to accomplish this, new analytical procedures were developed and successfully checked with discrete element techniques for single, double, and step lap adhesively bonded attachment configurations. Experimental verification of these nonlinear analyses was accomplished by the fabrication and evaluation of a variety of simple joint specimens under static monotonically increasing load. Failure loads and modes were used as the primary substantiation characteristics but the mechanical behavior of a small number of these simple joint specimens was observed at intermediate loadings and found to compare favorably with the analytically predicted behavior. Larger, more complex bonded joints were designed, fabricated, and evaluated under static monotonically increasing loads at room temperature utilizing these methods. Ultimate load, failure mode, and detailed strain behavior at any intermediate load were accurately predicted with the new analyses, as substantiated by experimental observations. These techniques were put into a computerized design/analysis program for structural application use and the program was used to generate bonded joint design allowable curves.</p>		

KEY WORDS	LINK A		LINK B		LINK C	
	ROLE	WT	ROLE	WT	ROLE	WT
Adhesives						
Joints						
Composites						
Nonlinear Behavior						
Design						
Analysis						
Testing						
Computer Programs (JTSDL & JTSTP)						
Boron/epoxy						
Titanium						
Adhesion						
Surface Preparation						
Polymer Processing						
Bonding						